

Influence of β -diiminato Ligand Design in Transition Metal Mediated E_4 (E = P, As) Activation



DISSERTATION
ZUR ERLANGUNG DES
DOKTORGRADES DER NATURWISSENSCHAFTEN
(DR. RER. NAT.)
DER FAKULTÄT CHEMIE UND PHARMAZIE
DER UNIVERSITÄT REGENSBURG

vorgelegt von
Fabian Spitzer
aus Regensburg
im Jahr 2017

Diese Arbeit wurde angeleitet von Prof. Dr. Manfred Scheer.

Promotionsgesuch eingereicht am: 19. Mai 2017

Tag der mündlichen Prüfung: 23. Juni 2017

Vorsitzender: Prof. Dr. Arnd Vogler

Prüfungsausschuss: Prof. Dr. Manfred Scheer

Prof. Dr. Henri Brunner

Prof. Dr. Frank-Michael Matysik



Universität Regensburg

Eidesstattliche Erklärung

Ich erkläre hiermit an Eides statt, dass ich die vorliegende Arbeit ohne unzulässige Hilfe Dritter und ohne Benutzung anderer als der angegebenen Hilfsmittel angefertigt habe; die aus anderen Quellen direkt oder indirekt übernommenen Daten und Konzepte sind unter Angabe des Literaturzitats gekennzeichnet.

Fabian Spitzer

This thesis was elaborated within the period from January 2014 until May 2017 in the Institute of Inorganic Chemistry at the University of Regensburg, under the supervision of Prof. Dr. Manfred Scheer.

Parts of this work have already been published:

- F. Spitzer, M. Sierka, M. Latronico, P. Mastrorilli, A. V. Virovets, M. Scheer.
'Fixation and Release of Intact E₄ Tetrahedra (E = P, As)'
Angew. Chem. Int. Ed. **2015**, *54*, 4392-4396;
Angew. Chem. **2015**, *127*, 4467-4472.
- F. Spitzer, C. Graßl, G. Balázs, E. M. Zolnhofer, K. Meyer, M. Scheer.
'Influence of the nacnac Ligand in Iron(I)-Mediated P₄ Transformations'
Angew. Chem. Int. Ed. **2016**, *55*, 4340-4344;
Angew. Chem. **2016**, *128*, 4412-4416.
- F. Spitzer, C. Graßl, G. Balázs, E. Mädl, M. Keilwerth, E. M. Zolnhofer, K. Meyer, M. Scheer.
'Nacnac-Cobalt-Mediated P₄ Transformations'
Chem. Eur. J. **2017**, *23*, 2716-2721.

dedicated to Susi

'In the middle of difficulty lies opportunity'

Albert Einstein

Preface

Some of the presented results have already been published during the preparation of this thesis (*vide supra*). The relevant content is reprinted with the permission of WILEY-VCH publishing. The corresponding citations and license number are given at the beginning of the respective chapters.

Each chapter includes a list of authors. At the beginning of each chapter the individual contribution of each author is described. Additionally, if some of the presented results have already been partly discussed in other theses, it is stated at the beginning of the respective chapters.

To ensure uniform design of this work, all chapters are subdivided into 'Introduction', 'Results and Discussion', 'Conclusion', 'References', and 'Supporting Information'. Furthermore, all chapters have the same text settings and the numeration of compounds, figures, schemes and tables begins anew. The depicted molecular structures may differ in their style. A general 'Introduction' and the 'Research Objectives' are given at the beginning of this thesis. In addition, a comprehensive 'Conclusion' of this work is presented at the end of this thesis.

Table of Contents

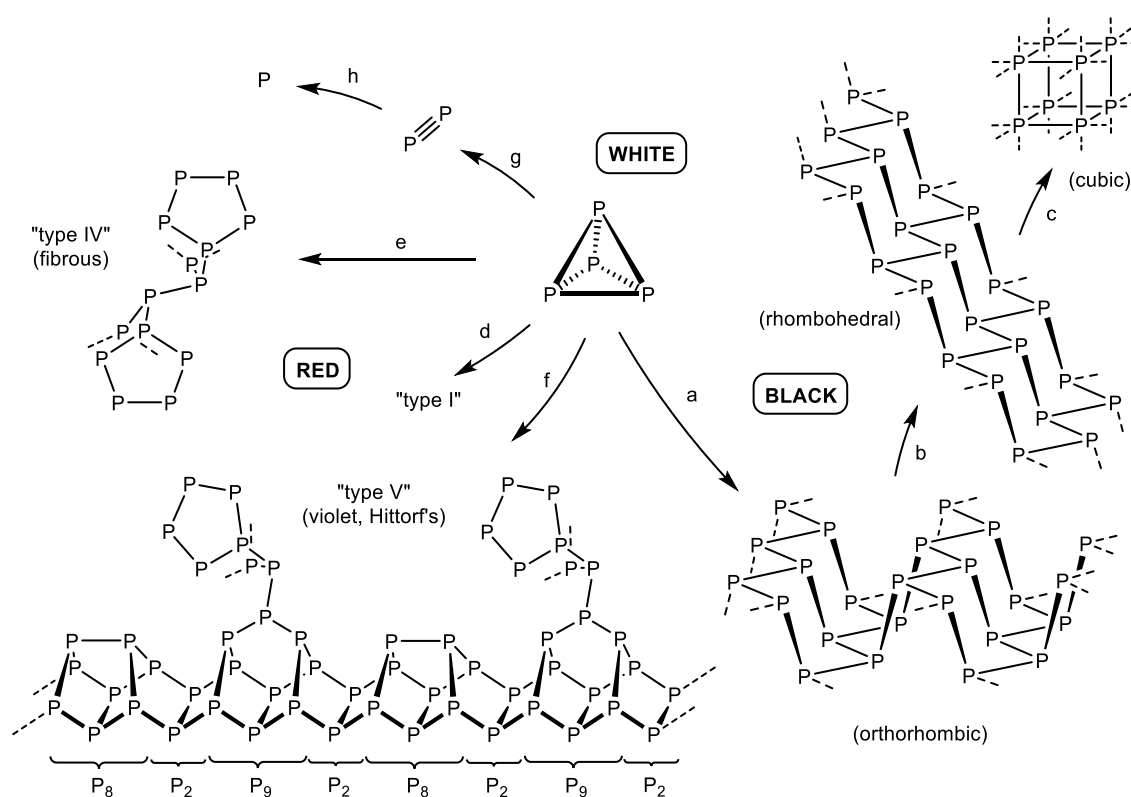
1. Introduction.....	1
1.1 Phosphorus – The Light Bearer	1
1.2 Arsenic – The Challenging Element.....	2
1.3 β -diiminato Ligands – A Manifold Ligand Class	4
1.4 Transformation, Degradation and Aggregation of E_4 (E = P, As).....	7
1.5 References.....	11
2. Research Objectives	15
3. Fixation and Release of Intact E_4 Tetrahedra (E = P, As).....	19
3.1 Introduction	19
3.2 Results and Discussion.....	21
3.3 Conclusion	28
3.4 References.....	28
3.5 Supporting Information	30
4. Influence of the nacnac Ligand in Iron(I)-Mediated P_4 Transformations	51
4.1 Introduction	51
4.2 Results and Discussion.....	52
4.3 Conclusion	58
4.4 References.....	59
4.5 Supporting Information	60
4.6 Addendum	85
5. Nacnac-Cobalt-Mediated P_4 Transformations.....	89
5.1 Introduction	89
5.2 Results and Discussion.....	91
5.3 Conclusion	99
5.4 References.....	99
5.5 Supporting Information	101

6. Influence of β-diketiminato Ligand Design and Solvates on the Solid State Structures of $[(\text{NacnacCu})_2(\mu\text{-}\eta^2\text{:}\eta^2\text{-E}_4)]$ (E = P, As)	132
6.1 Introduction.....	132
6.2 Results and Discussion.....	134
6.3 Conclusion	138
6.4 References	138
6.5 Supporting Information	139
7. Snapshots of As_4 Transformation - Degradation and Aggregation Induced by β-diiminato-M (M = Co, Fe) Fragments.....	146
7.1 Introduction.....	146
7.2 Results.....	149
7.2.1 Synthesis	149
7.2.2 LIFDI-MS and ^1H NMR Spectroscopy.....	151
7.2.3 Structural Characterization	151
7.3 Discussion.....	165
7.4 DFT Calculations.....	167
7.5 Conclusion	169
7.6 References	169
7.7 Supporting Information	172
8. Thesis Treasury.....	200
8.1 Reactivity of $[\text{L}^3\text{Cu}(\text{NCMe})]$ with Se_{red}	200
8.2 Reactivity of $[\text{L}^3\text{Cu}(\text{NCMe})]$ with P_4S_3	202
8.3 Reactivity of $[\text{L}^3\text{Cu}(\text{NCMe})]$ with As_4S_3	203
8.4 Synthesis of $[(\text{DAD})\text{Ni}(\text{COD})]$	205
8.5 Reactivity of $[(\text{DAD})\text{Ni}(\text{COD})]$ with P_4	206
8.6 Synthesis and Characterization of $[\text{L}^1\text{Na}(\text{thf})_2]$	207
8.7 References	208
9. Conclusion.....	217
10. Appendix.....	229
10.1 Thematic List of Abbreviations.....	229
10.2 Acknowledgements	231

1. Introduction

1.1 Phosphorus – The Light Bearer

Elemental phosphorus was discovered in 1669 by Hennig Brand in Hamburg.^[1] On account of the observed luminous properties, it was named 'phōsphōros' – the Greek word for 'light bearer'.^[1] Multiple allotropes are known, which are divided into three main classes: white, red and black phosphorus. At ambient conditions, the thermodynamic stability increases from white to red and black phosphorus (Scheme 1).^[2] They differ considerably in their molecular constitution (tetrahedral molecules, tubular units or layered structures), resulting in versatile chemical and physical properties.



Scheme 1. Main allotropes of phosphorus and selected formation conditions:^[3] a) Hg(cat.)/380 °C or 12 kbar/200 °C, b) 80 kbar c) 110 kbar, d) 200–400 °C, e) 500–600 °C, slow vapor deposition, f) 2 weeks, 550 °C, g) starting from 800 °C, h) $T > 2000$ °C.

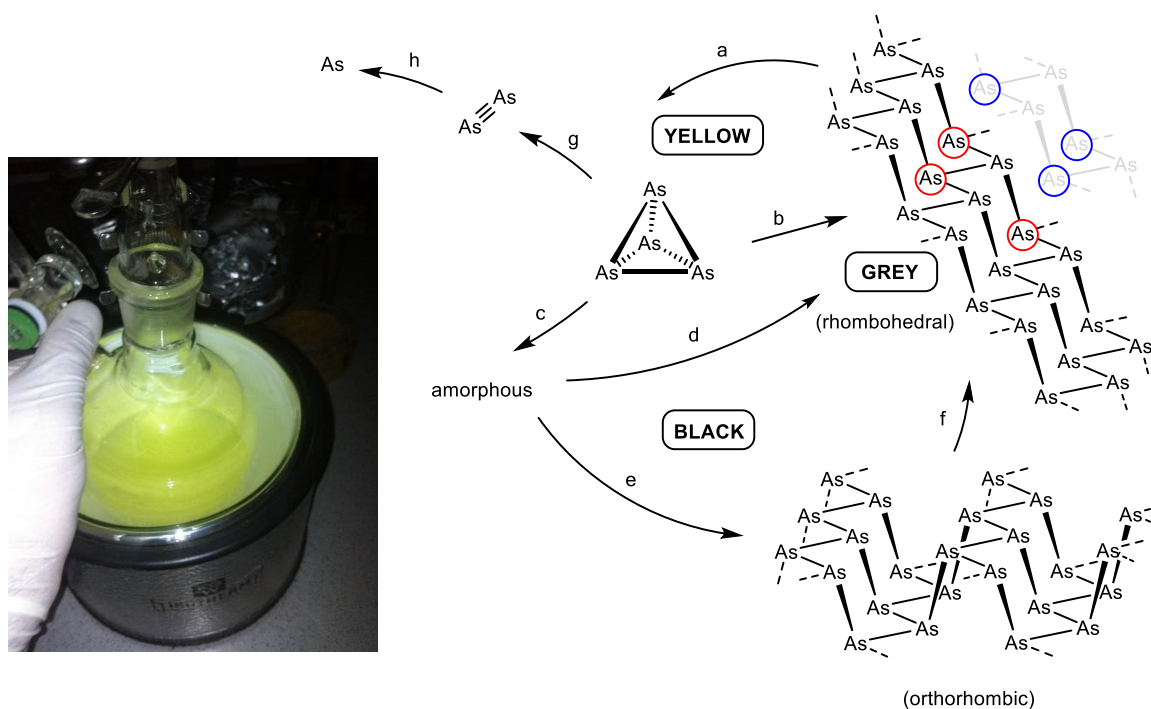
Black phosphorus was recognized as a new modification in 1914^[4] and its orthorhombic structure was described as consisting of condensed P₆ rings in 1935.^[5] Each ring adopts a chair conformation and contributes to a corrugated semi-conducting layer structure.^[6] In contrast, its rhombohedral, high-pressure modification resembles a 'flat' layer of joint P₆ units (arsenic type structure, vide infra). Further increasing the pressure results in a simple cubic, metallic modification (α -Po structure).^[7]

Commercially available red phosphorus is an amorphous solid composed of polymeric networks. According to Roth *et al.* this solid is named type I red phosphorus.^[8] By its stepwise annealing, the existence of four additional red phosphorus types II – V were proposed based on optical microscopy, powder diffraction and differential thermal analysis. The nature of type II and III red phosphorus is still unknown and their structures are still issue of discussion.^[9] The molecular structure of type IV was revealed in 2005 and was named fibrous red phosphorus due to its mechanical properties.^[10] It is composed of tubular polymer strands consisting of P_{21} ($=[P_8]P_2[P_9]P_2$)^[11] repeating units. They contain P_2 linked P_8 or P_9 moieties, which resemble α - P_4S_4 and β - P_4S_5 analogous structures.^[9a] Additionally, the P_9 cages are interlinked and arranged in pairs forming parallel double tubes (Scheme 1). The structure of type V red phosphorus was determined in 1969 and consists of analogous polymeric tubes, however linked in a crosswise orientation (Scheme 1).^[9a] It was identified as so-called violet or Hittorf's phosphorus, named after its discoverer in 1865.^[12] Based on theoretical studies, Häser and Böcker suggest that numerous different phosphorus repeating units display similar stability and are hypothesized to be involved in structurally unknown type II and III red phosphorus.^[11] This was supported by the discovery of polymeric phosphorus chains embedded in CuI matrixes, consisting of differently shaped P_{12} or P_{14} repeating units.^[13] After removing the CuI matrix, these nanorods were isolated as two new, red-brown phosphorus allotropes.^[14] Cylindric shaped nanotubes,^[15] as well as icosahedral or ring-shaped structures are predicted as further allotropes by calculations.^[16]

Finally, white phosphorus is the most reactive and only soluble phosphorus allotrope. Its tetrahedral P_4 constitution was identified in three modifications (α , β and γ).^[17] Single crystal diffraction, Raman spectroscopy^[18] and electron diffraction^[19] on gaseous P_4 reveal phosphorus distances of approximately 2.21 Å, which serve as a benchmark for P–P single bonds.

1.2 Arsenic – The Challenging Element

The discovery of elemental arsenic is attributed to Albertus Magnus in 1250,^[20] when he heated arsenolith with soap.^[21] Its name derives from 'arsenikón', the Greek term for 'yellow orpiment' (As_2S_3).^[20] Different allotropes of arsenic are known. With increasing thermodynamic stability, they are classified into yellow, black and grey arsenic.



Scheme 2. Left: Precipitation of As_4 , the yellow modification of arsenic, from a freshly prepared toluene solution. Right: Main allotropes of arsenic and selected formation conditions:^[22] a) 616 °C sublimation, b) r.t. (slow), increased by radiation, c) vapor deposition onto surface (100–200 °C), d) $T > 270$ °C, e) Hg/100–175 °C, f) 300 °C, g) starting from 800 °C, h) $T > 1700$ °C.

Yellow arsenic is a waxy solid, consisting of tetrahedral As_4 molecules.^[23] It is the only soluble allotrope of arsenic and is highly unstable: The metastable allotrope is not storable, as it slowly transforms into grey arsenic at room temperature. This conversion is strongly accelerated by radiation, even at lower temperatures (–180°C).^[24] Electron diffraction experiments on As_4 vapor reveal arsenic distances of approximately 2.43 Å, which serve as a benchmark for As–As single bonds.^[25] Yellow arsenic (Scheme 2, left picture) can be isolated by sublimation of grey arsenic and condensation of the arsenic vapor into cooled solutions,^[24] which was firstly reported by Bettendorff.^[26]

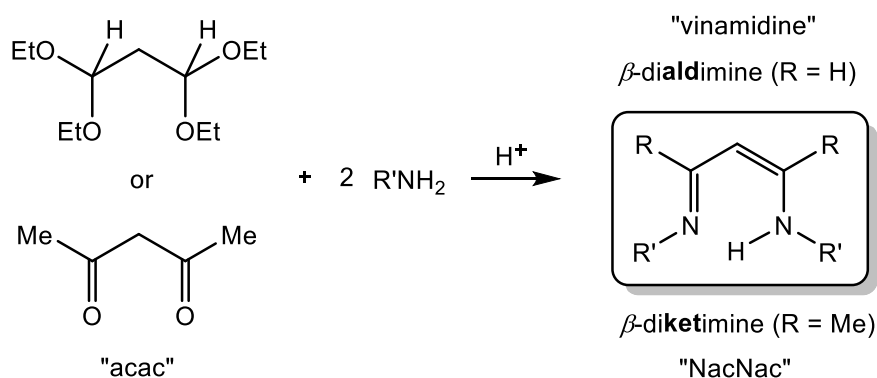
However, condensation of arsenic vapor onto heated surfaces results in formation of amorphous black arsenic,^[27] which is speculated to resemble red phosphorus in its amorphous structure.^[28] In addition, orthorhombic, black arsenic is reported.^[29] It is isostructural to black phosphorus in its orthorhombic, corrugated double layer structure. However, it was exclusively observed in solid solutions with ‘impurities’, such as phosphorus (up to 74% As atoms). Pure orthorhombic arsenic is metastable and could not be obtained, so far.^[30] Both the amorphous and orthorhombic black allotropes decompose to grey arsenic at elevated temperatures.

Grey arsenic is the thermodynamically most stable arsenic allotrope. Its rhombohedral structure consists of condensed As_6 rings, each in chair conformation, building densely

packed arsenic layers (analogous to rhombohedral, black phosphorus).^[31] Each arsenic atom is surrounded by three vicinal arsenic atoms of the same layer (highlighted by red rings, exemplified in Scheme 2) and three nearby atoms of the next layer (highlighted by blue rings, exemplified in Scheme 2). This distorted octahedral environment resembles a cubic packing, which is in line with the metallic character of grey arsenic.

1.3 β -diiminato Ligands – A Manifold Ligand Class

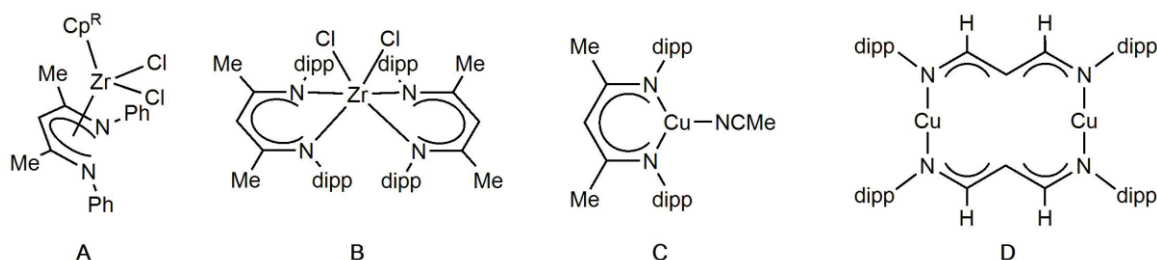
Since their first application in coordination chemistry in 1968, the β -aldiminato^[32] and β -ketiminato^[33] ligands gained increased attention and great popularity as exceptional tuneable spectator ligands with strong metal-ligand bonds. Various ligand combinations were created displaying different backbones ($R = \text{Ph}, \text{'Bu}, \text{Me}$ or H) and several imine substituents ($R' = \text{H}, \text{SiMe}_3$, various phenyl groups).^[34] The general structure of the β -diimine ligand class is depicted in Scheme 3 on the right hand side.



Scheme 3. Preparation of β -diimines from condensation reaction of ketones or acetals with primary amines.

However, the most attention has been received by $[\{\text{N}(\text{C}_6\text{H}_3\text{tPr}_2\text{-2,6})\text{C}(\text{Me})_2\text{CH}\}]^-$, which was reported in 1997^[35] and became a very popular and easily accessible auxiliary ligand in the following years.^[36] Its versatile applications in different research objectives ranges from stabilization of rare metal(I) oxidation states^[37] and homogeneous phase N_2 activation^[38] to the use as an active catalyst for e.g. C_2H_4 , CO_2 or lactide polymerization.^[39] Moreover, research groups started to study the influence of ligand design on the reaction outcome.^[34e] In this course, these ligands became well-established as 'NacNac' - owing to their relation with the 'acac' (acetylacetonato) ligand and emphasizing the incorporation of two 'N' atoms into the ligand backbone. Its preparation can be achieved by condensation reactions of ketones or acetals with two equivalents of a primary (aromatic) amine under acidic conditions (Scheme 3).^[36] The presented synthesis is simple, cheap and proceeds in high yields. Moreover, by variation of substituents R and R' , the ligands steric and electronic properties can be easily tuned.

After deprotonation of the β -diimine, the monoanionic β -diiminato ligand enables the stabilization of metal centers all over the periodic table. Manifold coordination modes are realized, which are influenced by factors like metal center, its ligand substituents and additional co-ligands. Selected examples are depicted in Scheme 4.



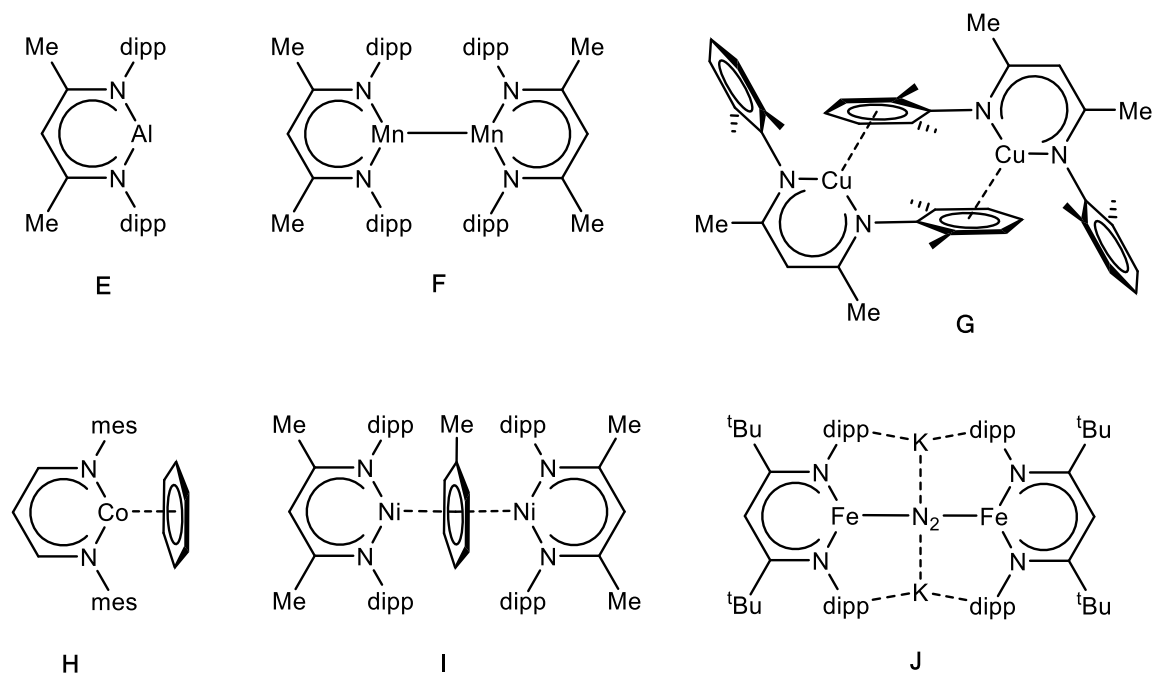
Scheme 4. Selected examples for β -diiminato complexes in different coordination modes. The substituent dipp stands for 2,6-diisopropylphenyl.

In the electron deficient zirconium complex **A** an η^5 -coordination mode of its π -conjugated backbone is observed, which explains the frequently referred similarity between β -diiminato ligands and the well-established cyclopentadienyl family ($6e^-$ π -donor).^[40] In envelope shaped coordination modes, like in complex **B**, the combination of a $4e^-$ σ - and $2e^-$ π -bonding mode is discussed,^[34b,40] whereas in **C** the ligand behaves as a terminal chelating ligand (terminal $4e^-$ σ -donor).^[40,41] Aforementioned ($16e^-$) compounds **A** and **B** exemplify the extent to which the donor properties of the other ligands bonded to the zirconium metal center modify the coordination mode of the β -diiminato ligand.^[40] Likewise, the properties of the ligand backbone affect the coordination fashion, which can be seen by comparison of complex **C** and **D**. The latter is exclusively obtained as a dinuclear (rather exotic) 12-membered metallacycle, though the supporting ligand only differs by its backbone substituents ($R = \text{Me}$ (**C**) vs. H (**D**)).^[42]

While the β -diiminato ligand family is commonly regarded as a robust spectator ligand, numerous publications describe it to participate in manifold unexpected reactivity or unwanted decomposition. This manifests in the non-innocent behavior of the ligand in oxidation and reduction reactions. The latter proceed with retention of the ligand constitution or under reductive (C–N) bond cleavage. Furthermore, oxidative coupling within the ligand backbone and C–H activation in the aromatic flanking group were found. Further details can be found in the recently published perspective article by Arnold *et al.*^[43] However, this thesis focuses on the application of sterically demanding, electronically flexible and particularly intact ancillary ligands.

In the last years, various low valent main group metals and transition metals could be stabilized by β -diiminato ligands. An overview is given in review articles by Lappert *et al.*^[36]

and Tsai.^[44] Selected examples of low coordinate metal centers in various bonding modes are depicted in Scheme 5.

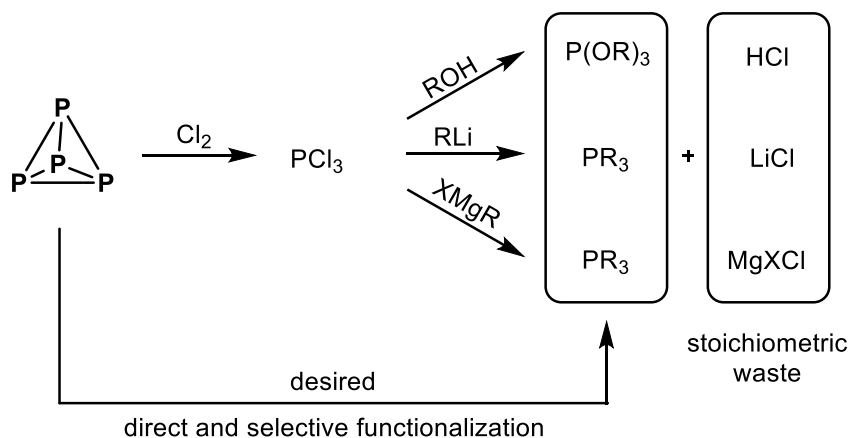


Scheme 5. Selected mononuclear or dinuclear low valent β -diiminato metal complexes.^[38,45-49] Definition of substituents: dipp = 2,6-diisopropylphenyl, mes = 2,4,6-methylphenyl.

In all these examples, the metal centers gain steric shielding by the aromatic flanking groups of the ligand, which stand almost orthogonal to the olefinic backbone plane. In case of group 13 metals, no further saturation is observed (type **E**).^[45] Other, open shell transition metal or main group compounds tend to form metal-metal bonds (type **F**).^[46] Additionally, the reactive metal fragment of transition metal systems can be saturated by either strongly binding co-ligands (e.g. CO) or weakly donating co-ligands (σ -donors: e.g. MeCN, Et₂O, THF; π -donors: e.g. phenyl groups). This is accomplished by the aggregation towards dimeric molecules via intermolecular coordination of the aromatic flanking groups (type **G**)^[47] or with additional co-ligands in mono- and dinuclear complexes (type **H**)^[48] and **I**)^[49]. Formal metal(0) compounds are obtained by intercalation of alkali metals between the aromatic flanking groups (type **J**).^[38] Those compounds dissociate in solution at ambient temperatures. Therefore, its weak co-ligands serve as labile leaving groups for subsequent reactions.

1.4 Transformation, Degradation and Aggregation of E₄ (E = P, As)

White phosphorus is the key starting material in industrial preparation of valuable organophosphorus derivatives. Those processes involve hazardous reagents like chlorine gas for the formation of PCl₃, PCl₅ or POCl₃ prior to metathesis reactions with alcohols, organolithium or Grignard reagents, respectively (Scheme 6). Thereby, stoichiometric amounts of waste are produced.^[50] The quest for replacing these processes by a sustainable, environmentally friendly and atom efficient approach is still open.

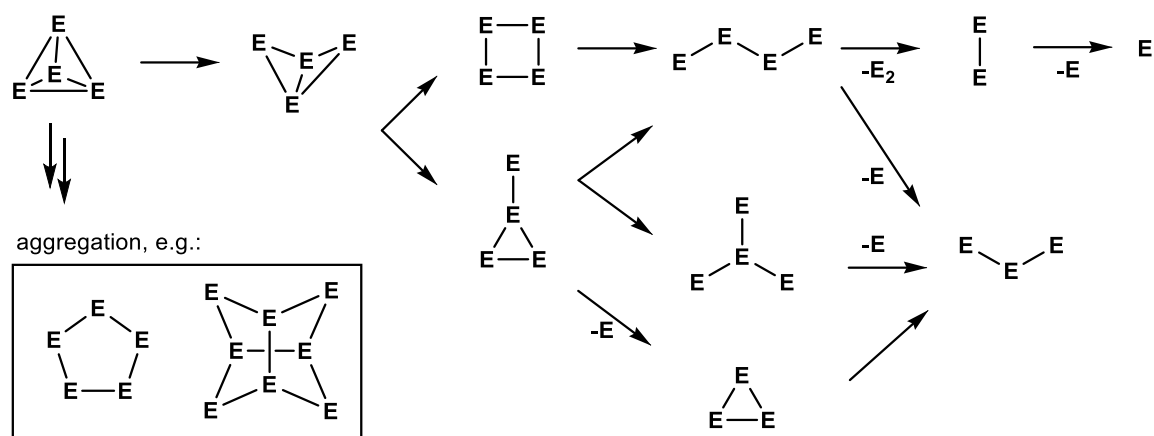


Scheme 6. General synthetic approach to organophosphorus compounds. The procedures involve halogenation of P₄ and subsequent metathesis reactions. The latter yield stoichiometric amounts of waste product.

When P₄ was recognized to coordinate transition metal complexes in the late 1970s,^[51] a period of intense investigation started including the activation of white phosphorus and its transformation. One successful synthetic approach is the reaction of P₄ with low valent transition metal complexes, which are stabilized by sterically demanding ligand systems and contain labile leaving groups. Some of the co-ligands (in particular CO or C₂H₄) can be detached under ambient, photolytic or thermolytic conditions and the generated electron deficient metal fragments readily react with white phosphorus in solution. Additionally, the reactivity of the isostructural, heavier congener yellow arsenic is an issue of academic research, which is often comparatively discussed.^[52] By means of this procedure, various substituent-free polyphosphorus or polyarsenic ligands, so-called 'E_n ligands' (E = P, As), have been prepared and were stabilized in the coordination sphere of transition metal complexes.

Numerous E_n ligand complexes are reported, especially containing well-established auxiliary ligand systems like Cp⁻ (cyclopentadiene) or multidentate phosphines like np₃ (tris(2-diphenylphosphinoethyl)amine) and dppe (1,2-bis(diphenylphosphino)ethane, Ph₂PCH₂CH₂PPh₂), among others. Different review articles sum up the versatile E_n ligand

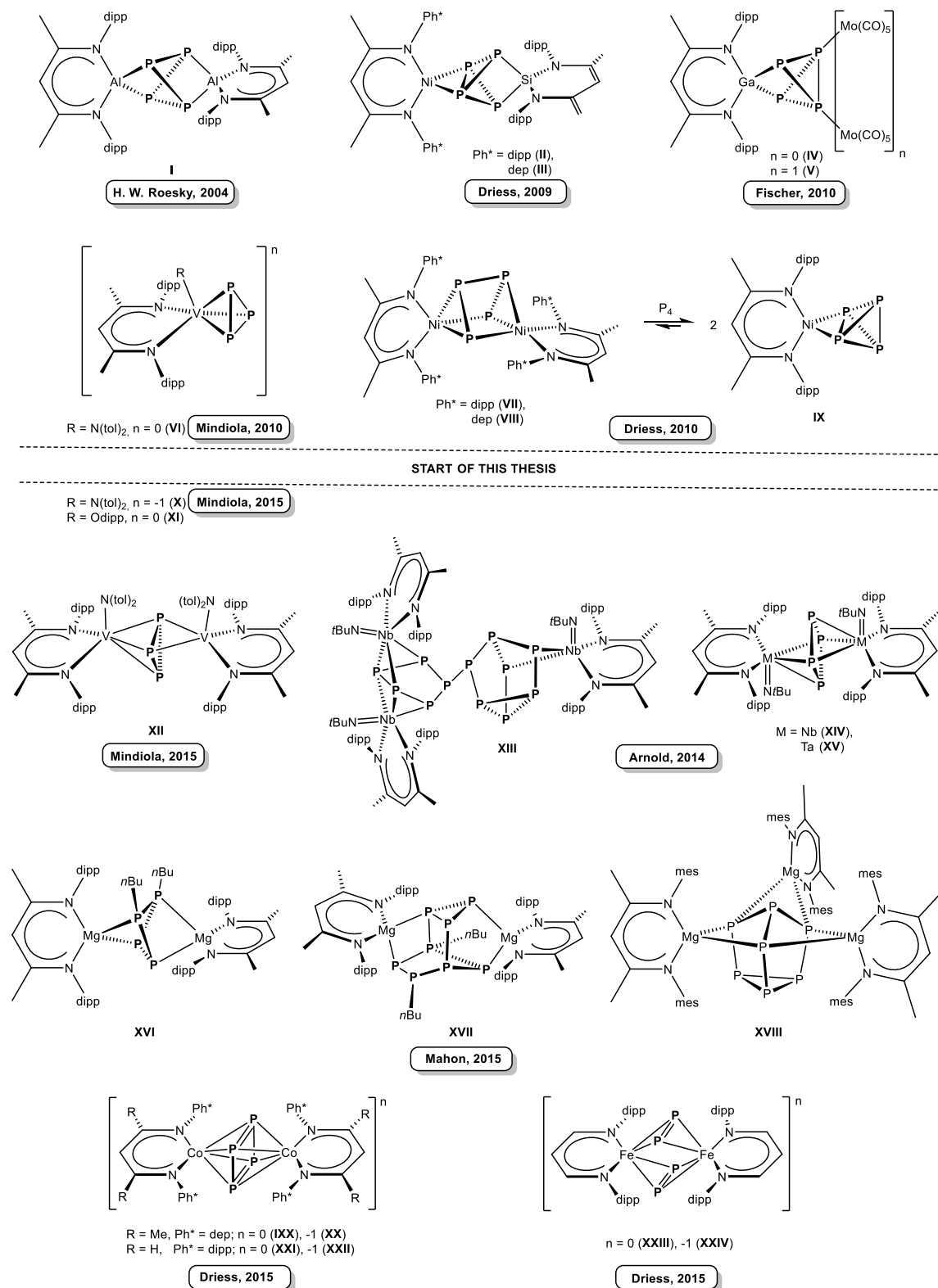
compounds containing early and late transition metals or main group metals.^[53] These elaborate investigations give insight into the main steps of gradual E_4 ($E = P, As$) degradation into fragmented E_n ligands ($n < 4$), which proceeds by successive (reductive) $E-E$ bond cleavage.^[53,54] Moreover, its aggregation towards polypnictogenide E_n ($n > 4$) ligands with more than four pnictogen atoms is observed (Scheme 7).



Scheme 7. Successive transformation and degradation of an intact E_4 ($E = P, As$) tetrahedron in the coordination sphere of transition metal fragments and possible aggregation products (in box). Bonding modes and charges are omitted.

In the last years, β -dialdiminato and most notably β -diketiminato systems found their entry into P_4 activation chemistry. Their low valent metal complexes are suitable precursors for small molecule activation and kinetic stabilization of the products obtained. This also applies for As_4 activation. However, to the best of our knowledge no As_4 activation has been reported using the β -diiminato ligand systems so far. An overview of substituent-free P_n ligand complexes obtained by P_4 activation with β -diiminato ligands involved is given in Scheme 8. In its upper part the literature until January 2014 (start of this PhD thesis) is covered and the second half depicts the results until May 2017.

As illustrated, several main group and transition metal systems were utilized. The first impulse was given by H. W. Roesky *et al.* in 2004, when they primarily reported the reaction of P_4 with a group 13 carbenoid: The reaction proceeds by reductive $P-P$ bond cleavage and a twofold edge opened $[P_4]^{4-}$ unit was obtained in the dinuclear aluminium complex **I**.^[55] In 2010, the reaction of the gallium analogue precursor with P_4 was reported leading to the mononuclear product **IV**, which was proven to behave Lewis basic in its adduct complex **V**.^[56] In the meantime, Driess *et al.* investigated the reactivity of P_4 with nickel(I) ‘NacNacs’ in presence of silylene species to form compounds **II** and **III**.^[57] The reaction of P_4 with the pure nickel(I) precursor was reported in 2010. The resulting dinuclear complexes **VII** and **VIII** display a so-called prismane-like $[Ni_2P_4]$ core motif. Compound **VII** is reported to be in equilibrium with its mononuclear equivalent **IX**.^[49]



Scheme 8. Overview of all reported P_n ligand complexes containing β -diiminato ligands. They are divided into publications before January 2014 (start of PhD thesis) and the research period until May 2017. Definition of substituents: dipp = 2,6-diisopropylphenyl, dep = 2,6-diethylphenyl, mes = 2,4,6-methylphenyl.

In 2010, Mindiola *et al.* prepared a neutral, mononuclear vanadium complex **VI** with a *cyclo*-P₃ moiety.^[58] Further contributions, reported in 2015, are the monoanionic species **X**, an additional neutral complex **XI**, and the dinuclear complex **XII**.^[59] In 2014, Arnold *et al.* reported complexes of the group V heavier congener tantalum and niobium systems containing *cyclo*-P₄ ligands, such as **XIV** and **XV**. The trinuclear product **XIII** with an unprecedented P₁₂ ligand was found among other uncharacterized side products.^[60] Advances in main group chemistry were provided by Mahon *et al.* in 2015. White phosphorus was shown to insert into Mg–C bonds of magnesium(II) ‘NacNac’ complexes to form compound **XVI** containing a P₄ ligand and complex **XVII** containing a P₈ ligand.^[61] The latter two complexes are exceptional, as they contain alkyl substituted phosphorus ligands and therefore do not fulfil the definition of ‘P_n ligand’ complexes. Substitution of the aromatic *dipp* (= 2,6-diisopropylphenyl) flanking groups by *mes* (= 2,4,6-methylphenyl) substituents lead to a reaction mixture with uncharacterized compounds. Exclusively, the trinuclear product **XVIII** with an incorporated [P₇]³⁻ moiety could be isolated. For late transition metals, Driess *et al.* reported on neutral cobalt (**IXX**, **XXI**) and iron (**XXIII**) compounds with *cyclo*-[P₄]⁰ or [P₂]²⁻ ligands, respectively.^[62] Additionally, their redox chemistry was investigated: In the iron complex **XXIV**, the reduction had no impact on the nature of the phosphorus ligands. However, for cobalt a transformation of the *cyclo*-[P₄]⁰ ligand into a twofold reduced *cyclo*-[P₄]²⁻ unit was observed in complexes **XX** and **XXII**.

As can be seen in this overview, only three ‘NacNac’ systems were applied as ancillary ligands so far: They differ in their *dipp*, *dep* or *mes* aromatic flanking groups. Furthermore, one β -dialdiminato ligand with *dipp* groups was used (e.g. in **XXIII**). It is striking that the variation of the used metal centers gives rise to various P_n ligand complexes. However, their different reaction conditions need to be emphasized.

The random choice of unequal preparation conditions and different metal centers as well as unsystematic application of ligand substituents prohibit a deeper understanding of the directing forces, which affect the reaction outcome of these P₄ activations. Therefore, a systematic reactivity study is desirable, which is performed under comparable reaction conditions, using distinct metal systems and systematically analysing the influence of ligand design on the activation of white phosphorus and yellow arsenic.

1.5 References

- [1] F. Krafft, *Angew. Chem. Int. Ed. Engl.* **1969**, *8*, 660-671.
- [2] A. F. Holleman, E. Wiberg, N. Wiberg in *Lehrbuch der Anorganischen Chemie*, 102. Auflage, de Gruyter, Berlin, **2007**, pp. 310; ISBN 978-3-11-017770-1.
- [3] a) Selected formation conditions from citation [2], pages 745-750; b) Initial idea for graphical set-up originates from: M. Serrano-Ruiz, A. Romerosa, P. Lorenzo-Luis, *Eur. J. Inorg. Chem.* **2014**, *2014*, 1587-1598.
- [4] P. W. Bridgman, *J. Am. Chem. Soc.* **1914**, *36*, 1344-1363.
- [5] R. Hultgren, N. S. Gingrich, B. E. Warren, *J. Chem. Phys.* **1935**, *3*, 351-355.
- [6] a) Refinement of crystal structure: A. Brown, S. Rundqvist, *Acta Cryst.* **1965**, *19*, 684-685; b) Semi-conducting properties: R. W. Keyes, *Phys. Rev.* **1953**, *92*, 580-584.
- [7] J. C. Jamieson, *Science* **1963**, *139*, 1291-1292.
- [8] W. L. Roth, T. W. DeWitt, A. J. Smith, *J. Am. Chem. Soc.* **1947**, *69*, 2881-2885.
- [9] a) H. Thurn, H. Krebs, *Acta Cryst. Section B* **1969**, *25*, 125-135; b) G. Fasol, M. Cardona, W. Hönle, H. G. von Schnering, *Solid State Commun.* **1984**, *52*, 307-310; c) S. R. Elliott, J. C. Dore, E. Marseglia, *J. Phys. Colloques*, **1985**, *46*, C8-349-C348-353.
- [10] M. Ruck, D. Hoppe, B. Wahl, P. Simon, Y. Wang, G. Seifert, *Angew. Chem. Int. Ed.* **2005**, *44*, 7616-7619.
- [11] Nomenclature accords to: S. Böcker, M. Häser, *Z. Anorg. Allg. Chem.* **1995**, *621*, 258-286.
- [12] W. Hittorf, *Ann. Phys.* **1865**, *202*, 193-228.
- [13] a) M. H. Möller, W. Jeitschko, *J. Solid State Chem.* **1986**, *65*, 178-189; b) A. Pfitzner, E. Freudenthaler, *Angew. Chem. Int. Ed. Engl.* **1995**, *34*, 1647-1649; c) A. Pfitzner, E. Freudenthaler, *Z. Naturforsch.* **1997**, *52 b*, 199-202.
- [14] A. Pfitzner, M. F. Bräu, J. Zweck, G. Brunklaus, H. Eckert, *Angew. Chem. Int. Ed.* **2004**, *43*, 4228-4231.
- [15] a) G. Seifert, E. Hernández, *Chem. Phys. Lett.* **2000**, *318*, 355-360; b) I. Cabria, J. W. Mintmire, *Europhys. Lett.* **2004**, *65*, 82-88.
- [16] A. J. Karttunen, M. Linnolahti, T. A. Pakkanen, *Chem. Eur. J.* **2007**, *13*, 5232-5237.
- [17] a) A. Simon, H. Borrmann, H. Craubner, *Phosphorus Sulfur Silicon Relat. Elem.* **1987**, *30*, 507; b) A. Simon, H. Borrmann, J. Horakh, *Chem. Ber.* **1997**, *130*, 1235-1240; c) H. Okudera, R. E. Dinnebier, A. Simon, *Z. Kristallogr.* **2005**, *220*, 259-264.
- [18] N. J. Brassington, H. G. M. Edwards, D. A. Long, *J. Raman Spectrosc.* **1981**, *11*, 346-348.
- [19] B. M. Cossairt, C. C. Cummins, A. R. Head, D. L. Lichtenberger, R. J. F. Berger, S. A. Hayes, N. W. Mitzel, G. Wu, *J. Am. Chem. Soc.* **2010**, *132*, 8459-8465.
- [20] See citation [2], page 822.
- [21] a) G. Süss-Fink, *Chem. Unserer Zeit* **2012**, *46*, 100-109; b) mentioned in 'De rebus metallicis et mineralibus' by Albertus Magnus.
- [22] Selected formation conditions from citation [2], pages 825-826.
- [23] J. Eiduss, R. Kalendarev, A. Rodionov, A. Sazonov, G. Chikvaidze, *Phys. Status Solidi B* **1996**, *193*, 3-23.
- [24] H. Erdmann, M. V. Unruh, *Z. anorg. Chem.* **1902**, *32*, 437-452.
- [25] a) Y. Morino, T. Ukaji, T. Ito, *Bull. Chem. Soc. Jpn.* **1966**, *39*, 64-71; b) L. R. Maxwell, S. B. Hendricks, V. M. Mosley, *J. Chem. Phys.* **1935**, *3*, 699-709.
- [26] A. Bettendorff, *Justus Liebigs Annalen der Chemie* **1867**, *144*, 110-114.
- [27] H. Stöhr, *Z. Anorg. Allg. Chem.* **1939**, *242*, 138-144.
- [28] a) See citation [2], page 826; b) G. N. Greaves, S. R. Elliott, E. A. Davis, *Adv. Phys.* **1979**, *28*, 49-141.
- [29] H. Krebs, W. Holz, K. H. Worms, *Chem. Ber.* **1957**, *90*, 1031-1037.
- [30] O. Osters, T. Nilges, F. Bachhuber, F. Pielhofer, R. Wehrich, M. Schöneich, P. Schmidt, *Angew. Chem. Int. Ed.* **2012**, *51*, 2994-2997.
- [31] See citation [2], page 824.
- [32] backbone exclusively = H, R' = o-, m- or p-Me-phenyl: C. L. Honeybourne, G. A. Webb, *Chem. Commun.* **1968**, 739-740.
- [33] a) S. G. McGeachin, *Can. J. Chem.* **1968**, *46*, 1903-1912; b) R. Bonnett, D. C. Bradley, K. J. Fisher, *Chem. Commun.*, **1968**, 886-887; c) J. E. Parks, R. H. Holm, *Inorg. Chem.* **1968**, *7*, 1408-1416.
- [34] a) P. B. Hitchcock, M. F. Lappert, D.-S. Liu, *J. Chem. Soc., Chem. Commun.* **1994**, 1699-1700; b) P. B. Hitchcock, M. F. Lappert, D.-S. Liu, *J. Chem. Soc., Chem. Commun.* **1994**, 2637-2638; c) M. F. Lappert, D.-S. Liu, *J. Organomet. Chem.* **1995**, *500*, 203-217; d) P. H. M. Budzelaar, A. B. van Oort, A. G. Orpen, *Eur. J. Inorg. Chem.* **1998**, *1998*, 1485-1494; e) D. J. E. Spencer, A. M. Reynolds, P. L. Holland, B. A.

- Jazdzewski, C. Duboc-Toia, L. Le Pape, S. Yokota, Y. Tachi, S. Itoh, W. B. Tolman, *Inorg. Chem.* **2002**, *41*, 6307-6321; f) R. Knorr, H. Hauer, A. Weiss, H. Polzer, F. Ruf, P. Löw, P. Dvortsák, P. Böhler, *Inorg. Chem.* **2007**, *46*, 8379-8390.
- [35] J. Feldman, S. J. McLain, A. Parthasarathy, W. J. Marshall, J. C. Calabrese, S. D. Arthur, *Organometallics* **1997**, *16*, 1514-1516.
- [36] L. Bourget-Merle, M. F. Lappert, J. R. Severn, *Chem. Rev.* **2002**, *102*, 3031-3066.
- [37] a) C. Cui, H. W. Roesky, H.-G. Schmidt, M. Noltemeyer, H. Hao, F. Cimpoesu, *Angew. Chem., Int. Ed.* **2000**, *39*, 4274-4276; b) N. J. Hardman, B. E. Eichler, P. P. Power, *Chem. Commun.*, **2000**, 1991-1992.
- [38] J. M. Smith, R. J. Lachicotte, K. A. Pittard, T. R. Cundari, G. Lukat-Rodgers, K. R. Rodgers, P. L. Holland, *J. Am. Chem. Soc.* **2001**, *123*, 9222-9223.
- [39] a) in combination with Et₂AlCl: V. C. Gibson, C. Newton, C. Redshaw, G. A. Solan, A. J. P. White, D. J. Williams, P. J. Maddox, *Chem. Commun.* **1998**, 1651-1652; b) M. Cheng, D. R. Moore, J. J. Reczek, B. M. Chamberlain, E. B. Lobkovsky, G. W. Coates, *J. Am. Chem. Soc.* **2001**, *123*, 8738-8749; c) A. P. Dove, V. C. Gibson, E. L. Marshall, A. J. P. White, D. J. Williams, *Chem. Commun.*, **2001**, 283-284; d) B. M. Chamberlain, M. Cheng, D. R. Moore, T. M. Ovitt, E. B. Lobkovsky, G. W. Coates, *J. Am. Chem. Soc.* **2001**, *123*, 3229-3238.
- [40] M. Rahim, N. J. Taylor, S. Xin, S. Collins, *Organometallics* **1998**, *17*, 1315-1323.
- [41] D. W. Randall, S. D. George, P. L. Holland, B. Hedman, K. O. Hodgson, W. B. Tolman, E. I. Solomon, *J. Am. Chem. Soc.* **2000**, *122*, 11632-11648.
- [42] C. Shimokawa, Y. Tachi, N. Nishiwaki, M. Ariga, S. Itoh, *Bull. Chem. Soc. Jpn.* **2006**, *79*, 118-125.
- [43] C. Camp, J. Arnold, *Dalton Trans.* **2016**, *45*, 14462-14498.
- [44] Y.-C. Tsai, *Coord. Chem. Rev.* **2012**, *256*, 722-758.
- [45] C. Cui, H. W. Roesky, H.-G. Schmidt, M. Noltemeyer, H. Hao, F. Cimpoesu, *Angew. Chem., Int. Ed.* **2000**, *39*, 4274-4276.
- [46] a) J. Chai, H. Zhu, A. C. Stückl, H. W. Roesky, J. Magull, A. Bencini, A. Caneschi, D. Gatteschi, *J. Am. Chem. Soc.* **2005**, *127*, 9201-9206; b) S. P. Green, C. Jones, A. Stasch, *Science* **2007**, *318*, 1754-1757.
- [47] L. D. Amisial, X. Dai, R. A. Kinney, A. Krishnaswamy, T. H. Warren, *Inorg. Chem.* **2004**, *43*, 6537-6539.
- [48] C. Chen, M. B. Hecht, A. Kavara, W. W. Brennessel, B. Q. Mercado, D. J. Weix, P. L. Holland, *J. Am. Chem. Soc.* **2015**, *137*, 13244-13247.
- [49] S. Yao, Y. Xiong, C. Milsman, E. Bill, S. Pfirrmann, C. Limberg, M. Driess, *Chem. Eur. J.* **2010**, *16*, 436-439.
- [50] Corbridge, D. E. *Phosphorus 2000*; Elsevier: Amsterdam, 2000.
- [51] First known P_n ligand complexes: a) A. P. Ginsberg, W. E. Lindsell, *J. Am. Chem. Soc.* **1971**, *93*, 2082-2084; b) P. Dapporto, S. Midollini, L. Sacconi, *Angew. Chem. Int. Ed. Engl.* **1979**, *18*, 469-469; c) A. P. Ginsberg, W. E. Lindsell, K. J. McCullough, C. R. Sprinkle, A. J. Welch, *J. Am. Chem. Soc.* **1986**, *108*, 403-416.
- [52] First known As_n ligand complex: a) A. S. Foust, M. S. Foster, L. F. Dahl, *J. Am. Chem. Soc.* **1969**, *91*, 5631-5633; b) A. S. Foust, M. S. Foster, L. F. Dahl, *J. Am. Chem. Soc.* **1969**, *91*, 5633-5635.
- [53] P_n ligand complexes: a) M. Caporali, L. Gonsalvi, A. Rossin, M. Peruzzini, *Chem. Rev.* **2010**, *110*, 4178-4235; b) B. M. Cossairt, N. A. Piro, C. C. Cummins, *Chem. Rev.* **2010**, *110*, 4164-4177; c) M. Scheer, G. Balázs, A. Seitz, *Chem. Rev.* **2010**, *110*, 4236-4256; d) N. A. Giffin, J. D. Masuda, *Coord. Chem. Rev.* **2011**, *255*, 1342-1359; e) S. Khan, S. S. Sen, H. W. Roesky, *Chem. Commun.*, **2012**, *48*, 2169-2179.
- As_n ligand complexes: f) O. J. Scherer, *Angew. Chem. Int. Ed. Engl.* **1985**, *24*, 924-943; g) O. J. Scherer, *Angew. Chem.* **1990**, *102*, 1137-1155; h) B. Rink, O. J. Scherer, G. Heckmann, G. Wolmershauser, *Chem. Ber.* **1992**, *125*, 1011-1016; i) O. J. Scherer, *Acc. Chem. Res.* **1999**, *32*, 751-762.
- [54] a) F. H. Stephens, M. J. A. Johnson, C. C. Cummins, O. P. Kryatova, S. V. Kryatov, E. V. Rybak-Akimova, J. E. McDonough, C. D. Hoff, *J. Am. Chem. Soc.* **2005**, *127*, 15191-15200; b) S. Dürr, D. Ertler, U. Radius, *Inorg. Chem.* **2012**, *51*, 3904-3909; c) B. Zarzycki, F. M. Bickelhaupt, U. Radius, *Dalton Trans.* **2013**, *42*, 7468-7481.
- [55] Y. Peng, H. Fan, H. Zhu, H. W. Roesky, J. Magull, C. E. Hughes, *Angew. Chem. Int. Ed.* **2004**, *43*, 3443-3445.
- [56] G. Prabusankar, A. Doddi, C. Gemel, M. Winter, R. A. Fischer, *Inorg. Chem.* **2010**, *49*, 7976-7980.
- [57] Y. Xiong, S. Yao, E. Bill, M. Driess, *Inorg. Chem.* **2009**, *48*, 7522-7524.
- [58] B. L. Tran, M. Singhal, H. Park, O. P. Lam, M. Pink, J. Krzystek, A. Ozarowski, J. Telsler, K. Meyer, D. J. Mindiola, *Angew. Chem. Int. Ed.* **2010**, *49*, 9871-9875.

- [59] B. Pinter, K. T. Smith, M. Kamitani, E. M. Zolnhofer, B. L. Tran, S. Fortier, M. Pink, G. Wu, B. C. Manor, K. Meyer, M.-H. Baik, D. J. Mindiola, *J. Am. Chem. Soc.* **2015**, *137*, 15247-15261.
- [60] C. Camp, L. Maron, R. G. Bergman, J. Arnold, *J. Am. Chem. Soc.* **2014**, *136*, 17652-17661.
- [61] M. Arrowsmith, M. S. Hill, A. L. Johnson, G. Kociok-Köhn, M. F. Mahon, *Angew. Chem.* **2015**, *127*, 7993-7996.
- [62] a) S. Yao, N. Lindenmaier, Y. Xiong, S. Inoue, T. Szilvási, M. Adelhardt, J. Sutter, K. Meyer, M. Driess, *Angew. Chem.* **2015**, *127*, 1266-1270; b) S. Yao, T. Szilvasi, N. Lindenmaier, Y. Xiong, S. Inoue, M. Adelhardt, J. Sutter, K. Meyer, M. Driess, *Chem. Commun.*, **2015**, *51*, 6153-6156.

2. Research Objectives

In the last decades, extensive progress was made in the activation of E_4 ($E = P, As$) by transition metal complexes. Classical synthetic routes to E_n ligand complexes involve the application of harsh thermolytic or photolytic conditions, which prevents the selective isolation of metastable intermediates, and rather favors their further degradation. In most examples, well-established cyclopentadienyl or phosphine based ligands were applied as ancillary ligands. Lately, the β -diiminato ligand class gained increased popularity due to its ability to stabilize metal(I) centers and in some cases to dissociate under mild conditions. Up to date, no example is reported for an As_4 activation with a β -diiminato ligand containing complex. Furthermore, only few examples for P_4 reactions are reported. However, they suffer from the lack of systematic investigations regarding the influence of reaction conditions, metal centers and ligand design on the reaction outcome.

The current work focuses on the reactivity of white phosphorus and yellow arsenic and the characterization of the E_n ligand complexes obtained ($E = P, As$). A main aspect is the application of β -diiminato ancillary ligands. Especially the influence of the ligand substituents will be emphasized, which are expected to direct the reactivity and to impact the reaction outcome.

Therefore, the following research objectives arise:

- Preparation of various β -diiminato based metal(I) complexes
- Variation of the complex centers by different late transition metals
- Implementation of β -diiminato ligands with systematically chosen substituents
- Investigation of their reactivity towards E_4 ($E = P, As$) under mild and comparable conditions
- Characterization and comparison of the E_n ligand complexes obtained
- Elucidation of distinct directing properties, which affect the reaction outcome

Preface

The following chapter has already been published: The article is reprinted with permission of Wiley-VCH. License Number: 4081210369441.

English version: 'Fixation and Release of Intact E₄ Tetrahedra (E = P, As)'

Angew. Chem. Int. Ed. **2015**, *54*, 4392-4396.

German version: 'Fixierung und Freisetzung von intakten E₄-Tetraedern (E = P, As)'

Angew. Chem. **2015**, *127*, 4467-4472.

Authors

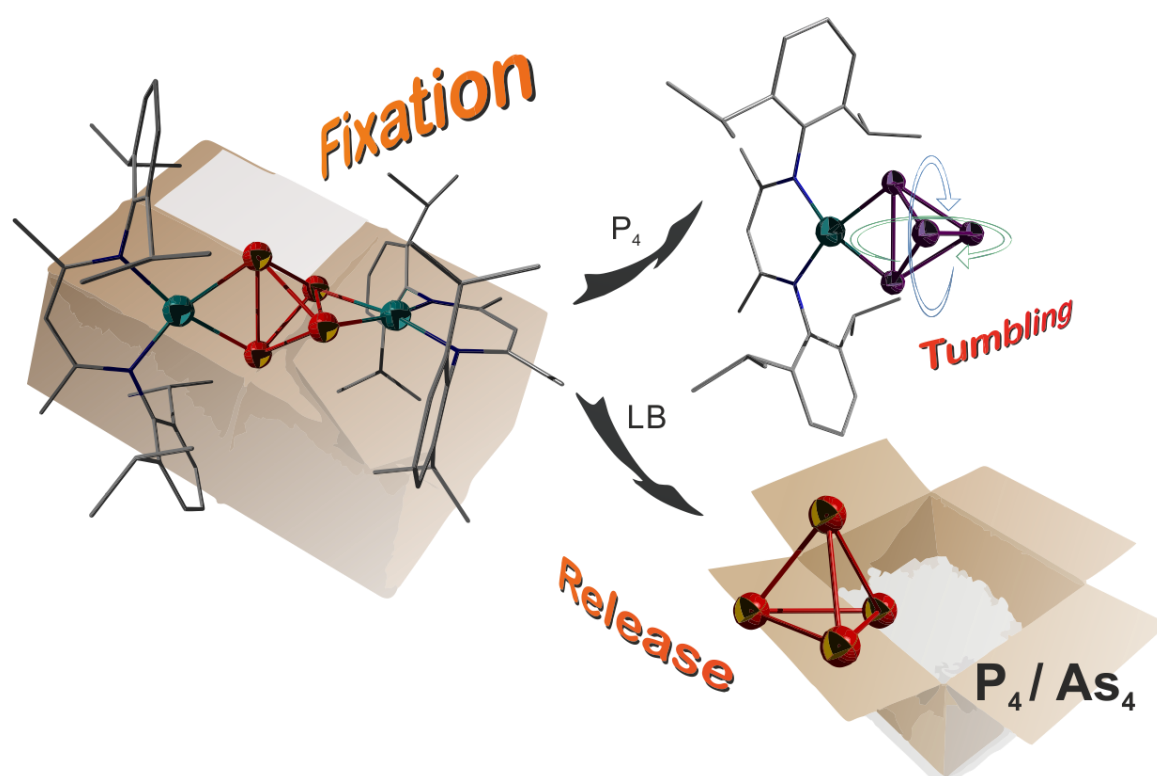
Fabian Spitzer, Marek Sierka, Mario Latronico, Piero Mastrorilli, Alexander V. Virovets, Manfred Scheer*

Author contributions

The preparation of the manuscript was done by the first author (F. Spitzer). M. Scheer supervised the research and revised the manuscript. Preparation and characterization (NMR, MS, EA, X-ray) of compound **1a** and **1b** have been part of the first author's master thesis as well as primarily investigations on compound **2** (NMR, MS), the first evaluation of its fluxional behavior by VT ³¹P{¹H} NMR and its equilibrium with **1a**. The proof was given by P. Mastrorilli and M. Latronico by ³¹P{¹H} EXSY NMR experiments, for which the first author prepared the samples. DFT calculations and the evaluation of the E₄ (E = P, As) ligand integrity were performed by M. Sierka. The release of the E₄ tetrahedra from **1a** and **1b** was performed by the first author. The first of both already in his master thesis. The synthesis of compound **2** and its work-up at low temperatures as well as its crystallization was performed by the first author. A. V. Virovets supported the single crystal X-ray diffraction measurement of compound **2**, conducted the twin refinement and provided the corresponding section in the Supporting Information. Sample preparation and interpretation of the Raman spectra of compounds **1a**, **1b** and **2** were done by the first author. An additional solvomorph, **1b** · 0.25 *n*-hexane, was characterized by the first author.

Acknowledgements

The authors thank the Deutsche Forschungsgemeinschaft and the Fonds der Chemischen Industrie for the financial support at the beginning of this project. The authors are grateful to Dr. C. Koch and Prof. Dr. R. M. Gschwind for the ⁷⁵As NMR measurements and Dr. W. Patterson for the measurements of Raman spectra.



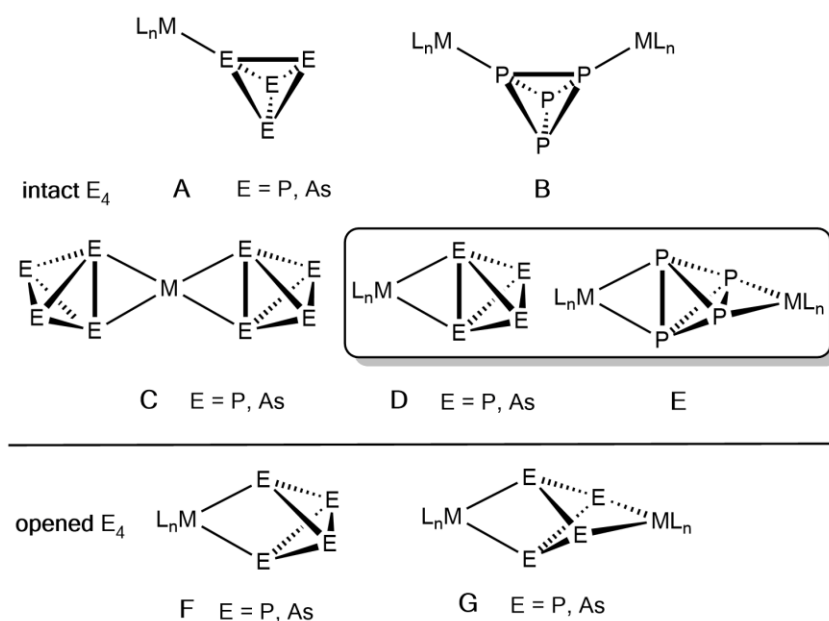
3. Fixation and Release of Intact E₄ Tetrahedra (E = P, As)

Abstract: By the reaction of [NacnacCu(NCMe)] with white phosphorus (P₄) and yellow arsenic (As₄) the stabilization and enclosure of the intact E₄ tetrahedra are realized and the disubstituted complexes [(NacnacCu)₂(μ-η²:η²-E₄)] (E = P (**1a**), As (**1b**)) are formed. The mono-substituted complex [NacnacCu(η²-P₄)] (**2**) was detected by the exchange reaction of **1a** with P₄ and was only isolated using low temperature work-up. All products were comprehensively spectroscopically and crystallographically characterized. The bonding situation in the products as intact E₄ units (E = P, As) was confirmed by theory and was experimentally proven by the pyridine promoted release of the bridging E₄ tetrahedra in **1a,b**.

3.1 Introduction

Since the first complex [(np₃)Ni(η¹-P₄)] (np₃ = tris(2-diphenyl-phosphinoethyl)amine) with an intact P₄ tetrahedron as ligand was discovered by Sacconi *et al.* in 1979,^[1] considerable progress has been made in the synthesis and characterization of complexes containing intact, that is, unopened, E₄ tetrahedra (E = P, As) as ligands. Such complexes reveal the first step of the E₄ activation by main group and transition metal complexes, respectively.^[2] For the P₄ tetrahedron, single^[1,3] (η¹, type **A**) and bridging^[3c,f,4] (μ-η¹:η¹, type **B**) end-on coordination modes are known in ionic and neutral complexes as well (Scheme 1). However, to date complexes containing intact single coordinated^[5] η²-, or bridging^[5c] μ-η²:η²-P₄ ligands in a side-on coordination mode have been exclusively obtained for cationic coinage metal complexes (types **C**, **D**) or as part of ion-contacted coordination polymers (type **E**).

In contrast to the rich chemistry of P₄ containing complexes, As₄ derivatives have been only sparingly studied because of the extreme light sensitivity and handling problems with yellow arsenic (As₄). Recently, we reported the synthesis of cationic complexes of Ru, Ag and Au containing intact As₄ as a ligand either in η¹- or η²-bonding mode (types **A**, **C**, **D**).^[6] The absence of neutral As₄ complexes of type **E** gave rise to the question as to whether a positively charged metal fragment is necessary for the η²-coordination of an intact As₄ tetrahedron.



Scheme 1. Comparison of coordination modes in complexes with intact (top) or opened (bottom) E₄ ligands (E = P, As).

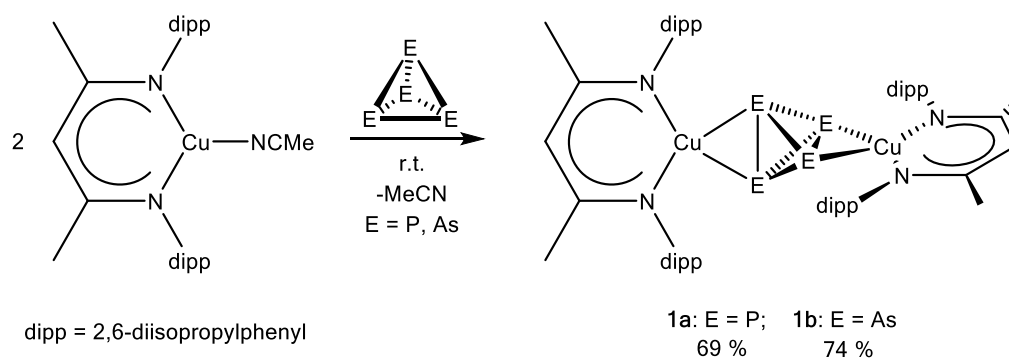
Few examples for neutral η^2 -P₄ ligand complexes are known: Ginsberg *et al.* reported the complex [RhCl(η^2 -P₄)(PPh₃)₂],^[7] for which finally the bonding situation was later corrected to be a [P₄]²⁻ ligand with an opened P–P edge (2.462(2) Å, type **F**).^[5a] Something similar occurs with the Co complexes [Cp*Co(L')(η^1 : η^1 -P₄)] and [(Cp*Co(L'))₂(μ - η^1 : η^1 : η^1 : η^1 -P₄)] (Cp* = C₅Me₅; L' = CO, *i*PrIm (1,3-di-isopropylimidazolin-2-ylidene)) of Scherer *et al.*^[8] and Radius^[9] *et al.* These compounds contain coordinated P₄ tetrahedra, also with elongated P–P edges (2.606(1) and 2.560(2)/2.597(2) Å and 2.6398(11) and 2.6161(16)/2.6282(18) Å), and calculations showed that the bonds are opened.^[9b] Also, there are several neutral compounds known containing an E₄ unit with open E–E edge(s) (type **F** and **G**),^[10] but no intact E₄ tetrahedra in η^2 - or μ - η^2 : η^2 -coordination mode have been described in neutral molecules to date (types **D** and **E**). Moreover, if the tetrahedron is intact, the release should be possible. Furthermore, Scherer and Akbayeva reported the complex [(Cp^{4Pr})Cu(η^2 -P₄)] (Cp^{4Pr} = C₅*i*Pr₄H),^[11] which recently could be reviewed to be a doubly organo-substituted P₄ butterfly compound (Cp^{4Pr})₂P₄.^[12] Thus, the quest for E₄ containing Cu complexes is still open.

To address these open topics, we searched for a combination of ligands and metals that could serve as a starting material for the synthesis of neutral E₄-containing complexes of types **D** and **E**. We chose the sterically demanding, β -diketiminato ligand [(N(C₆H₃*i*Pr₂-2,6)C(Me))₂CH]⁻. When it coordinates to a metal center, the aromatic dipp groups (dipp = 2,6-diisopropylphenyl) form a pocket, the size and shape of which is adequate to accommodate small molecules like E₄. Furthermore, we speculated that electron-rich

metals would better serve as neutral metal centers to coordinate intact E₄ moieties accordingly. Thus, we chose copper(I) also to address the missing P₄ coordination compound.

3.2 Results and Discussion

Herein we report the synthesis and characterization of [(LCu)₂(μ-η²:η²-E₄)] (L = [(N(C₆H₃Pr₂-2,6)C(Me))₂CH]⁻; E = P (**1a**), As (**1b**)), the first neutral complex containing intact E₄ tetrahedra as bridging ligands in a μ-η²:η²-coordination mode (type **E**) and the release of the E₄ tetrahedra by substitution with a stronger Lewis base. Furthermore, we report the formation of the mononuclear complex [LCu(η²-P₄)] (**2**) (type **D**) by the reaction of **1a** with P₄. Its dynamic behavior in solution was investigated by VT ³¹P{¹H} and ³¹P{¹H} EXSY NMR spectroscopy.



Scheme 2. Reaction of [LCu(NCMe)] with white phosphorus and yellow arsenic.

Compound **1a** is formed by the reaction of [LCu(NCMe)]^[13] with P₄ in a stoichiometric ratio of 2:1 in CH₃CN or *n*-hexane (Scheme 2). Density functional theory (DFT) calculations reveal that this reaction is exergonic with free energy change of 115 kJ·mol⁻¹. Despite higher free reaction energy of 126 kJ·mol⁻¹, the synthesis of the arsenic analogue **1b** is more difficult. Yellow arsenic (As₄) is a not storable compound, owing to its sensibility to light, air and moisture. It needs to be prepared freshly in solution and therefore stoichiometric reactions are difficult to carry out. However, by adding [LCu(NCMe)] to a freshly prepared As₄ solution in toluene (large excess of As₄), **1b** is formed in good yields (Scheme 2). The remaining yellow arsenic is rapidly converted into insoluble grey arsenic and can be removed by filtration. Both compounds **1a** and **1b** are soluble in dichloromethane and even in less-polar solvents such as *n*-hexane or toluene. Solutions of **1a** and **1b** slowly decompose within several days indicated by a color change and precipitation of black solid. However, as a solid, they are stable under ambient conditions and can be stored under argon for months. Complex **1a** should be stored in the dark because of its light sensitivity. Surprisingly, the arsenic compound **1b** is less sensitive to

light. They are unprecedented neutral molecular complexes with an intact (vide infra) $\mu\text{-}\eta^2\text{:}\eta^2\text{-}$ coordinated E₄ tetrahedron as a bridging ligand (type **E**).

The ¹H NMR spectra of **1a** and **1b** show the expected sets of signals for the β -diketiminato ligands L. In ³¹P{¹H} NMR spectrum of **1a** in CD₂Cl₂, a singlet at -426.9 ppm is observed. In contrast, **1b** does not show a signal in the ⁷⁵As{¹H} NMR spectrum owing to low symmetry of the molecule, as expected for the large quadrupole moment of the nucleus ⁷⁵As (*I* = 3/2). The Raman spectra of **1a** and **1b** are similar. Significant differences only can be obtained in the region between 500 and 150 cm⁻¹. For comparison, free white phosphorus and yellow arsenic show Raman modes at similar values.^[14]

The molecular structures of **1a** and **1b** show the side-on coordination of the E₄ tetrahedra by two opposite LCu fragments (Figures 1 and 2).^[15]

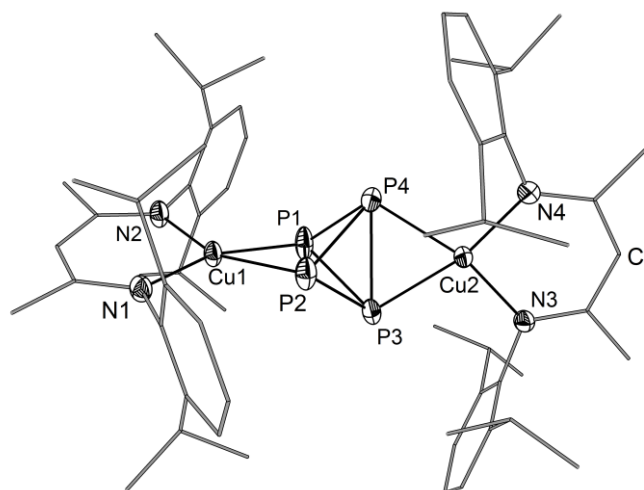


Figure 1. Molecular structure of **1a** in the crystal. Hydrogen atoms are omitted for clarity. Thermal ellipsoids are drawn at 50% probability level.

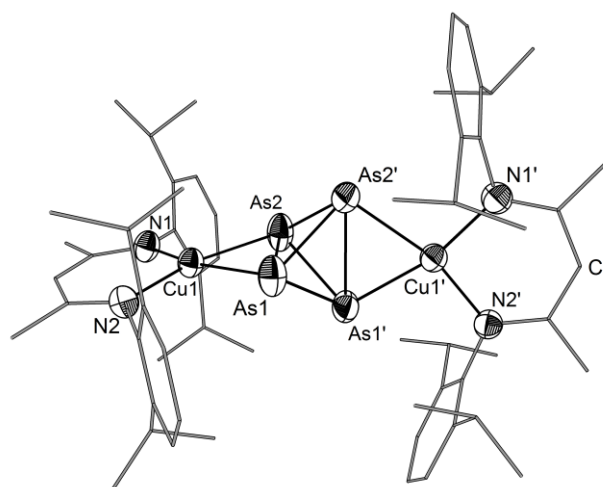


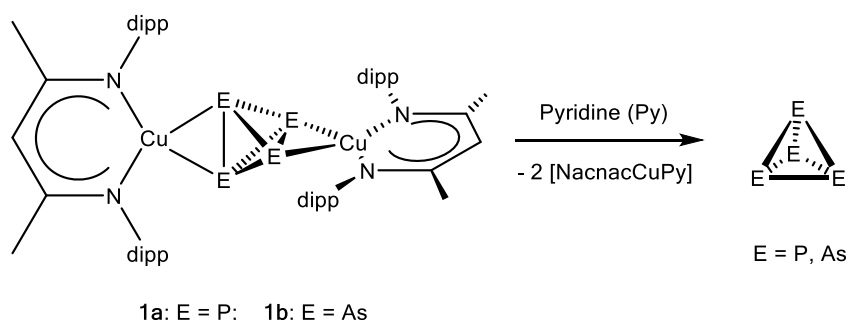
Figure 2. Molecular structure of **1b** · 2 C₆H₁₄ in the crystal. Hydrogen atoms and solvent molecules (*n*-hexane) are omitted for clarity. Thermal ellipsoids are drawn at 50% probability level.

The coordination geometry at Cu is almost square-planar. The maximum deviation from the coplanarity is less than 0.5° and 0.1° in **1a** and **1b**, respectively. The Cu–P distances in **1a** vary from 2.2592(6) Å to 2.2707(6) Å. They are slightly shorter than the Cu–P distances found in [Cu(η²-P₄)₂][pftb] (pftb = [Al{OC(CF₃)₃}₄])^[5b] (2.336(2)–2.345(2) Å), the latter being a complex that also has a planar arrangement around Cu. The distances between the coordinating P atoms P1–P2 and P3–P4 in **1a** (2.4285(8) Å and 2.4122(8) Å, respectively) are elongated compared to the P–P bond lengths in white phosphorus (determined by electron diffraction:^[16] 2.1994(3) Å, Raman spectroscopy:^[17] 2.2228(5) Å, DFT calculations:^[16] 2.1994(3) Å).

Compound **1b** has similar features. The As1–As2 distance (2.6491(8) Å) is elongated compared to the As–As bond length in yellow arsenic (determined by electron diffraction: 2.435(4)^[18] and 2.44(3)^[19] Å, by DFT calculations:^[20] 2.437 Å). The distances between non-coordinating As–As edges (2.4353(11)–2.4443(9) Å) are in the range of As–As single bonds. As no arsenic containing copper complex is so far reported, the closest known relative of **1b** is [Ag(η²-As₄)₂][pftb],^[6b] revealing coordinating As–As bonds of 2.585(2) and 2.569(2) Å, respectively.

In this context, the question arises as to whether the coordinating E–E edges should be considered as elongated but intact E–E bonds (ratio of E–E distance: **1a**/P_{4,free} = 1.1005; **1b**/As_{4,free} = 1.0879) or as cleaved ones. To gain deeper insight in the bonding situation of **1a** and **1b**, density functional theory (DFT) calculations were carried out. The calculation of the bond critical points (BCP), ring critical points (RCP), and the cage critical points (CCP) in **1a** and **1b** in comparison with that of the free E₄ tetrahedra confirm that the E₄ units (E = P, As) in these compounds can be considered as being intact and only a small depletion of the electron density of the coordinating E–E bond upon coordination to Cu occurred.^[14]

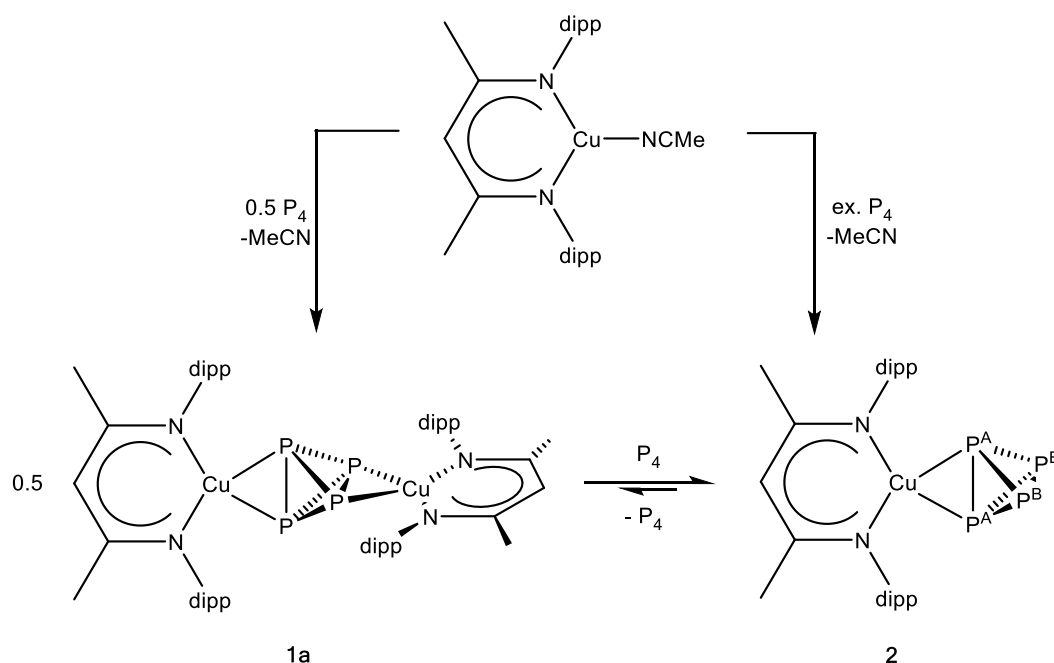
To confirm the theoretical prediction experimentally, a displacement of the bridging μ-η²:η²-E₄ tetrahedra in **1a** and **1b** by a much stronger Lewis base, such as pyridine (Py), was performed and monitored by ³¹P{¹H} and ⁷⁵As{¹H} NMR spectroscopy (Scheme 3).



Scheme 3. Release of intact E₄ tetrahedra from [(LCu)₂(μ-η²:η²-E₄)] (E = P (**1a**), As (**1b**)).

Compound **1a** shows a sharp singlet at -426.9 ppm in the $^{31}\text{P}\{^1\text{H}\}$ NMR spectrum in CD_2Cl_2 . After dissolving **1a** in pyridine, a singlet at -518 ppm was exclusively detected, which reveals free white phosphorus.^[21] Complex **1b** in contrast does not show a signal in $^{75}\text{As}\{^1\text{H}\}$ NMR spectrum, owing to low molecule symmetry and to the quadrupole moment of the ^{75}As nucleus. However, by adding an excess of pyridine to a solution of **1b** in CD_2Cl_2 a broad singlet at -912 ppm ($\omega_{1/2} = 5100$ Hz) was detected in the $^{75}\text{As}\{^1\text{H}\}$ NMR spectrum, which is characteristic for free yellow arsenic.^[14,22]

Furthermore, the question arises for the existence of mononuclear copper complexes of the type $[\text{LCu}(\eta^2\text{-E}_4)]$ (E = P, As). First evidence for the P derivative was obtained by monitoring a reaction between $[\text{LCu}(\text{NCMe})]$ and P_4 in a 1:1 stoichiometry by ^{31}P NMR spectroscopy. Here, besides traces of P_4 and the dinuclear complex **1a**, the desired complex $[\text{LCu}(\eta^2\text{-P}_4)]$ (**2**) was also detected as a broad signal at -475 ppm. However, all attempts to isolate compound **2** failed (Scheme 4), instead **1a** could be isolated in yields much higher than initially indicated by the ^{31}P NMR spectrum. The calculated free energy for the reaction of **1a** to **2** indicates that it is slightly endergonic. Therefore, shifting equilibrium towards **2** requires considerable excess of P_4 .



Scheme 4. Equilibrium between $[\text{LCu}(\text{NCMe})]$, P_4 , **1a** and **2** in solution. Labeling of the P atoms of **2** corresponds to the ^{31}P NMR data (see text for details).

Indeed, by adding a solution of $[\text{LCu}(\text{NCMe})]$ to an excess of P_4 (3.5 equivalents) in *n*-pentane, **2** was generated quantitatively at room temperature. The reaction mixture was cooled to 77 K to precipitate the supernatant P_4 . Filtration and evaporation of *n*-pentane were conducted at low temperatures of about 195 K. Light yellow crystals of

[LCu(η^2 -P₄)] (**2**) suitable for X-ray diffraction could be grown from concentrated *n*-pentane solution at that temperature. The molecular structure of **2** shows a P₄ tetrahedron coordinated to one LCu fragment (Figure 3). Despite the slightly exergonic reaction, all attempts to isolate the arsenic analogue complex of **2** using a similar procedure failed. Instead of the mononuclear complex, compound **1b** was crystallized accompanied by the formation of black solid of grey arsenic. Although working at 195 K, the dinuclear compound **1b** seems to be more stable.

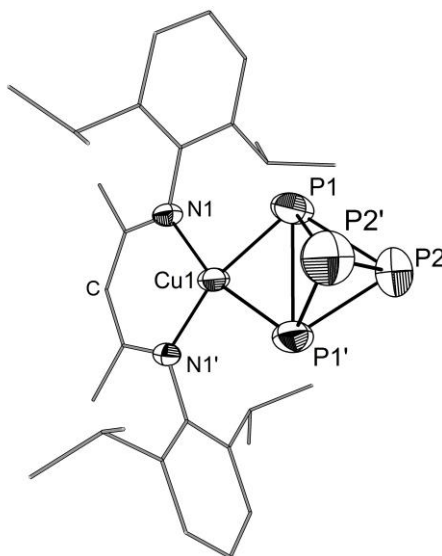


Figure 3. Molecular structure of **2** in the crystal. Hydrogen atoms are omitted for clarity. Thermal ellipsoids are drawn at 50% probability level.

Complex **2** reveals a square-planar coordination geometry at the Cu atom ($\Sigma_{\text{angles}} = 360.0(5)^\circ$). The Cu–P distances are with 2.280(3) Å slightly longer than the Cu–P distances in **1a** (2.2592(6)–2.2707(6) Å). The distance between the coordinating P atoms P1 and P1' of **2** (2.386(4) Å) are elongated compared to such P–P bond length in [Cu(η^2 -P₄)₂][pftb]^[5b] (average P–P_{coordinated}: 2.342(2) Å) and for free P₄ (2.1994(3)–2.2228(5) Å),^[16,17] but shorter than the coordinated P–P bonds in **1a** (2.4122(8) and 2.4285(8) Å). The distances P1–P2, P1–P2', P1'–P2, and P1'–P2' in **2** are between 2.180(4) and 2.192(4) Å, and thus longer than in [Cu(η^2 -P₄)₂][pftb]^[5b] (average P–P_{non-coordinated}: 2.173(3) Å), but shorter than comparable bonds in **1a** (2.2010(9)–2.2114(8) Å). The P2–P2' distance in **2** (2.141(6) Å) is smaller than the comparable distance in [Cu(η^2 -P₄)₂][pftb]^[5b] (2.197(3) Å).

The bonding situation of **2** was investigated by DFT calculations. The P₄ unit in compound **2** shows a pattern of critical points very similar to **1a** and can therefore be considered as being intact. Crystals of **2** can be stored at 195 K. Slow decomposition occurs at higher temperatures indicated by the color change to black. Moreover, compound **2** easily can be prepared in solution by adding an excess of P₄ to **1a** or

[LCu(NCMe)]. Such prepared solutions of **2** are stable even at room temperature and can be stored over months without decomposition if exclusion of light is ensured. Spectroscopic investigations of **2** prepared in situ could be conducted. Raman spectra of **2** in solution reveal one additional mode compared to **1a**.^[14] Moreover, a freshly prepared solution of **2** in CD_2Cl_2 was investigated in detail by variable-temperature $^{31}P\{^1H\}$ NMR spectroscopy.^[14] At 300 K a broad singlet at δ -475 ($\omega_{1/2} = 412$ Hz) for **2** is detected. Cooling the solution down to 273 K leads to breakdown of coalescence of the signal. At temperatures lower than 263 K two broad signals appear, which progressively transform into two mutually coupled triplets. At 193 K, the triplets centered at δ -450.5 (P^A) and δ -490.7 (P^B) reveal a coupling constant of $^1J_{PP} = 178$ Hz. This behavior is indicative of a dynamic process involving the coordinated P_4 molecule. It should be noted that η^1 -bonded P_4 complexes of type **A** are fluxional. For such Ru, Os^[23] or Mn^[3a] complexes, the main dynamic process (apart from the rotation about the metal-phosphorus axis) is a tumbling movement of the P_4 cage while remaining chemically coordinated to the metal. For $[Cp^*Fe(dppe)(\eta^1-P_4)]^+$, the main dynamic process is the dissociation of the complex and temporary release of free P_4 . To elucidate the dynamic process of **2**, which is responsible for the experimental ^{31}P NMR behavior, ^{31}P EXSY spectra of **2** (from **1a** and excess of P_4) in CD_2Cl_2 at various temperatures were recorded. The ^{31}P EXSY spectrum of **2** at 213 K (Figure 4) showed exchange cross-peaks between the triplets ascribed to the atoms P^A and P^B (for assignment, see Scheme 4) indicating that at low temperature the main dynamic process is the tumbling of coordinated P_4 .

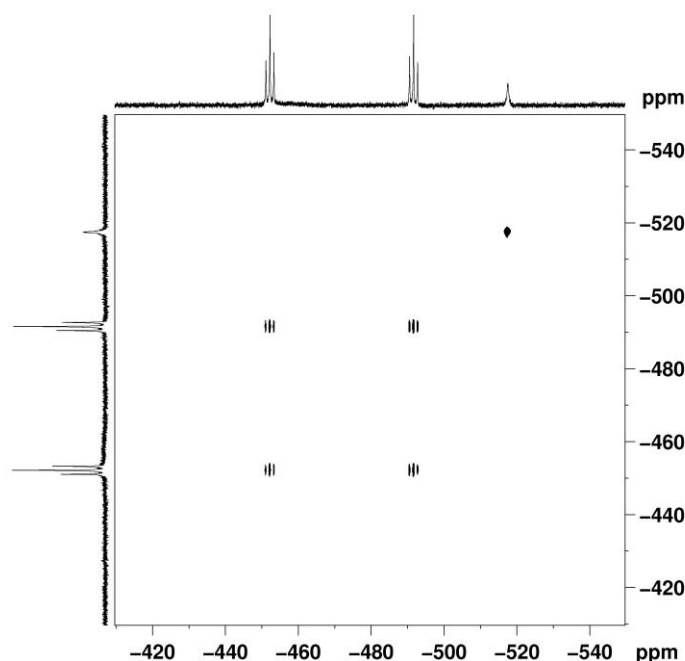


Figure 4. ^{31}P EXSY spectrum of **2** in CD_2Cl_2 at 213 K ($\tau_m = 0.200$ s).

However, on increasing the temperature, the dissociative process begins to occur. In fact, at 243 K, apart from the clear P^A/P^B exchange, a very weak cross-peak between $P^{A/B}$ and free P_4 becomes visible and, at 300 K, the exchange between $P^{A/B}$ (now consisting of a single broad signal), **1a** and free P_4 becomes predominant. It is interesting to note that dissociation of P_4 from **2** results in an equilibrium between **1a**, **2** and free P_4 , as indicated by the exchange cross-peaks between **1a**, **2** and free P_4 (δ -518) in the ^{31}P EXSY spectrum of **2** at 300 K (Figure 5).

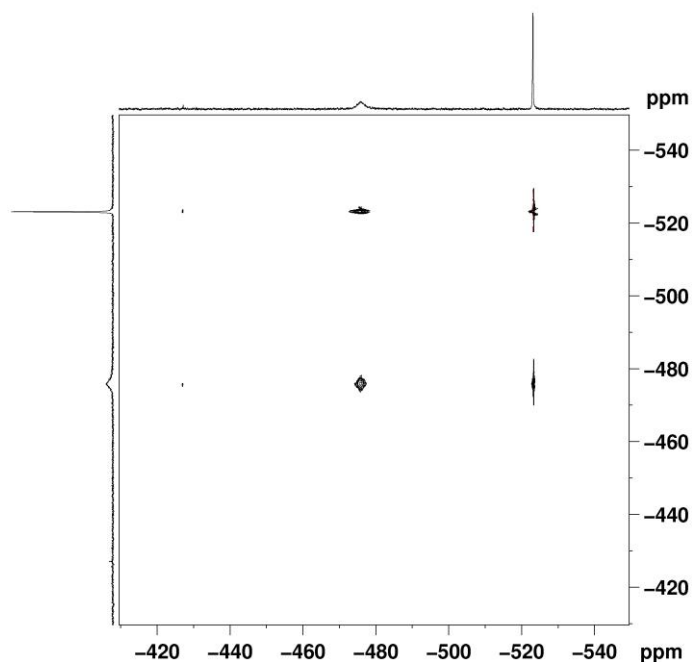


Figure 5. ^{31}P EXSY spectrum of **2** in CD_2Cl_2 at 300 K ($\tau_m = 0.200$ s).

Given that pure tumbling ($\eta^1 \rightarrow \eta^2 \rightarrow \eta^1$ walk down an edge of P_4)^[23] occurs only at low temperatures, we have carried out a line shape analysis of the $^{31}\text{P}\{^1\text{H}\}$ NMR spectra in the interval between 213 and 253 K, obtaining the following activation parameters: $\Delta H^\ddagger = 44.8 \text{ kJ}\cdot\text{mol}^{-1}$; $\Delta S^\ddagger = -41 \text{ kJ}\cdot\text{mol}^{-1}\cdot\text{K}^{-1}$; $\Delta G^\ddagger = 56.9 \text{ kJ}\cdot\text{mol}^{-1}$. The value of the free activation energy is comparable to those obtained for the neutral Mn complex $[\text{Cp}^{\text{BIG}}\text{Mn}(\text{CO})_2(\eta^1\text{-P}_4)]$ ^[3a] and for the cationic complexes $[\text{Ru}(\text{H})(\text{dppm})_2(\eta^1\text{-P}_4)]^+$ and $[\text{Ru}(\text{H})(\text{dppe})_2(\eta^1\text{-P}_4)]^+$ ^[24] (dppm = bis(diphenylphosphinomethane), dppe = 1,2-bis(diphenylphosphinoethane)).

3.3 Conclusion

In conclusion, we reported the synthesis of [(LCu)₂(μ-η²:η²-P₄)] (**1a**), the first neutral molecular complex containing an intact P₄ tetrahedron as a bridging side-on coordinated ligand. Additionally, the arsenic analogue [(LCu)₂(μ-η²:η²-As₄)] (**1b**) was synthesized as an unprecedented example of an intact As₄ tetrahedron as ligand fixed by two neutral complex fragments. Furthermore, [LCu(η²-P₄)] (**2**) was isolated, the first neutral molecular complex containing an intact P₄ tetrahedron in side-on coordination mode. The main dynamic behavior of **2** in solution was examined by VT ³¹P{¹H} and ³¹P{¹H} EXSY NMR spectroscopy. At low temperatures (up to 213 K) tumbling of the P₄ ligand takes place. By raising the temperature, dissociation of the P₄ ligand occurs. The existence of intact E₄ ligands (E = P, As) in **1a**, **1b** and **2** was confirmed by DFT calculations, as well as experimentally by the liberation of the E₄ (E = P, As) molecules by substitution with pyridine.

3.4 References

- [1] P. Dapporto, S. Midollini, L. Sacconi, *Angew. Chem. Int. Ed. Engl.* **1979**, *18*, 469-469; *Angew. Chem.* **1979**, *91*, 510-510.
- [2] a) B. M. Cossairt, N. A. Piro, C. C. Cummins, *Chem. Rev.* **2010**, *110*, 4164-4177; b) M. Caporali, L. Gonsalvi, A. Rossin, M. Peruzzini, *Chem. Rev.* **2010**, *110*, 4178-4235; c) M. Scheer, G. Balázs, A. Seitz, *Chem. Rev.* **2010**, *110*, 4236-4256; d) S. Khan, S. S. Sen, H. W. Roesky, *Chem. Commun.* **2012**, *48*, 2169-2179; e) N. A. Giffin, J. D. Masuda, *Coord. Chem. Rev.* **2011**, *255*, 1342-1359.
- [3] a) S. Heintl, E. V. Peresypkina, A. Y. Timoshkin, P. Mastroilli, V. Gallo, M. Scheer, *Angew. Chem. Int. Ed.* **2013**, *52*, 10887-10891; *Angew. Chem.* **2013**, *125*, 11087-11091; b) T. Gröer, G. Baum, M. Scheer, *Organometallics* **1998**, *17*, 5916-5919; c) M. Peruzzini, L. Marvelli, A. Romerosa, R. Rossi, F. Vizza, F. Zanobini, *Eur. J. Inorg. Chem.* **1999**, 931-933; d) I. de los Rios, J.-R. Hamon, P. Hamon, C. Lapinte, L. Toupet, A. Romerosa, M. Peruzzini, *Angew. Chem. Int. Ed.* **2001**, *40*, 3910-3912; *Angew. Chem.* **2001**, *113*, 4028-4030; e) M. Di Vaira, P. Frediani, S. S. Costantini, M. Peruzzini, P. Stoppioni, *Dalton Trans.* **2005**, 2234-2236; f) M. Caporali, M. Di Vaira, M. Peruzzini, S. Seniori Costantini, P. Stoppioni, F. Zanobini, *Eur. J. Inorg. Chem.* **2010**, 152-158.
- [4] P. Barbaro, M. Di Vaira, M. Peruzzini, S. Seniori Costantini, P. Stoppioni, *Chem. Eur. J.* **2007**, *13*, 6682-6690.
- [5] a) I. Krossing, L. van Wüllen, *Chem. Eur. J.* **2002**, *8*, 700-711; b) G. Santiso-Quinones, A. Reisinger, J. Slattery, I. Krossing, *Chem. Commun.* **2007**, 5046-5048; c) L. C. Forfar, T. J. Clark, M. Green, S. M. Mansell, C. A. Russell, R. A. Sanguramath, J. M. Slattery, *Chem. Commun.* **2012**, *48*, 1970-1972.
- [6] a) C. Schwarzmaier, A. Y. Timoshkin, M. Scheer, *Angew. Chem. Int. Ed.* **2013**, *52*, 7600-7603; *Angew. Chem.* **2013**, *125*, 7751-7755; b) C. Schwarzmaier, M. Sierka, M. Scheer, *Angew. Chem. Int. Ed.* **2013**, *52*, 858-861; *Angew. Chem.* **2013**, *125*, 891-894.
- [7] a) A. P. Ginsberg, W. E. Lindsell, *J. Am. Chem. Soc.* **1971**, *93*, 2082-2084; b) A. P. Ginsberg, W. E. Lindsell, K. J. McCullough, C. R. Sprinkle, A. J. Welch, *J. Am. Chem. Soc.* **1986**, *108*, 403-416.
- [8] a) O. J. Scherer, K. Pfeiffer, G. Wolmershäuser, *Chem. Ber.* **1992**, *125*, 2367-2372; b) O. J. Scherer, M. Swarowsky, G. Wolmershäuser, *Organometallics* **1989**, *8*, 841-842.
- [9] a) S. Dürr, D. Ertler, U. Radius, *Inorg. Chem.* **2012**, *51*, 3904-3909; b) B. Zarzycki, F. M. Bickelhaupt, U. Radius, *Dalton Trans.* **2013**, *42*, 7468-7481.
- [10] a) G. Prabusankar, A. Doddi, C. Gemel, M. Winter, R. A. Fischer, *Inorg. Chem.* **2010**, *49*, 7976-7980; b) Y. Xiong, S. Yao, M. Brym, M. Driess, *Angew. Chem. Int. Ed.* **2007**, *46*, 4511-4513; *Angew. Chem.* **2007**,

- 119, 4595-4597; c) Y. Peng, H. Fan, H. Zhu, H. W. Roesky, J. Magull, C. E. Hughes, *Angew. Chem. Int. Ed.* **2004**, *43*, 3443-3445; *Angew. Chem.* **2004**, *116*, 3525-3527; d) J. W. Dube, C. M. E. Graham, C. L. B. Macdonald, Z. D. Brown, P. P. Power, P. J. Ragona, *Chem. Eur. J.* **2014**, *20*, 6739 – 6744.
- [11] D. N. Akbayeva, O. J. Scherer, *Z. Anorg. Allg. Chem.* **2001**, *627*, 1429-1430.
- [12] S. Heinl, S. Reisinger, C. Schwarzmaier, M. Bodensteiner, M. Scheer, *Angew. Chem. Int. Ed.* **2014**, *53*, 7639-7642; *Angew. Chem.* **2014**, *126*, 7769-7773.
- [13] D. J. E. Spencer, N. W. Aboeella, A. M. Reynolds, P. L. Holland, W. B. Tolman, *J. Am. Chem. Soc.* **2002**, *124*, 2108-2109.
- [14] See the Supporting Information.
- [15] CCDC 1035004 (**1a**), CCDC 1035006 (**1b**·2 C₆H₁₄), and CCDC 1035007 (**2**) contain the supplementary crystallographic data for this paper. These data can be obtained free of charge from The Cambridge Crystallographic Data Centre via www.ccdc.cam.ac.uk/data_request/cif.
- [16] B. M. Cossairt, C. C. Cummins, A. R. Head, D. L. Lichtenberger, R. J. F. Berger, S. A. Hayes, N. W. Mitzel, G. Wu, *J. Am. Chem. Soc.* **2010**, *132*, 8459-8465.
- [17] N. J. Brassington, H. G. M. Edwards, D. A. Long, *J. Raman Spectrosc.* **1981**, *11*, 346-348.
- [18] Y. Morino, T. Ukaji, T. Ito, *Bull. Chem. Soc. Jpn.* **1966**, *39*, 64-71.
- [19] L. R. Maxwell, S. B. Hendricks, V. M. Mosley, *J. Chem. Phys.* **1935**, *3*, 699-709.
- [20] H. A. Spinney, N. A. Piro, C. C. Cummins, *J. Am. Chem. Soc.* **2009**, *131*, 16233-16243.
- [21] Control experiment: P₄ dissolved in pyridine; see the Supporting Information.
- [22] C. Schwarzmaier, A. Schindler, C. Heindl, S. Scheuermayer, E. V. Peresyphkina, A. V. Virovets, M. Neumeier, R. Gschwind, M. Scheer, *Angew. Chem. Int. Ed.* **2013**, *52*, 10896–10899; *Angew. Chem.* **2013**, *125*, 11097–11100.
- [23] V. Mirabello, M. Caporali, V. Gallo, L. Gonsalvi, D. Gudat, W. Frey, A. Ienco, M. Latronico, P. Mastrorilli, M. Peruzzini, *Chem. Eur. J.* **2012**, *18*, 11238-11250.
- [24] V. Mirabello, M. Caporali, V. Gallo, L. Gonsalvi, A. Ienco, M. Latronico, P. Mastrorilli, M. Peruzzini, *Dalton Trans.* **2011**, *40*, 9668-9671.

3.5 Supporting Information

General Remarks

All manipulations were performed with rigorous exclusion of oxygen and moisture using Schlenk-type glassware on a dual manifold Schlenk line with Argon inert gas or glove box filled with N₂ containing a high-capacity recirculator (<0.1 ppm O₂). Toluene, *n*-hexane and acetonitrile were dried using conventional techniques, degassed and saturated with Argon. CD₂Cl₂ was obtained from Deutero GmbH and degassed, dried and distilled from CaH₂ prior to use. ¹H, ¹³C, ³¹P NMR spectra were recorded on a Bruker Avance 400 (¹H: 400.130 MHz, ¹³C: 100.613 MHz, ³¹P: 161.976 MHz) spectrometer. The chemical shifts are reported in ppm relative to external TMS (¹H, ¹³C) and H₃PO₄ (³¹P). Mass spectrometry was performed using a Finnigan MAT95 LIFDI-MS spectrometer. Elemental analysis (CHN) was determined using a Vario micro cube and Vario EL III instrument.

Synthesis of [(LCu)₂(μ-η²:η²-P₄)] (1a)^[1]

Under stirring at room temperature a solution of 150 mg (0.288 mmol) [LCu(NCMe)] in 5 mL MeCN was added to a suspension of 17.8 mg (0.144 mmol) white phosphorus in 5 mL MeCN. A yellow precipitate was formed within minutes. The reaction mixture was stirred at room temperature until white phosphorus has disappeared. Supernatant solution was decanted and the remaining solid was dried in vacuum to yield **1a** (108 mg, 0.0994 mmol, 69%). Yellow crystals could be obtained from concentrated solution of **1a** in *n*-hexane at room temperature.

Analytical data:^[1]

¹ H NMR (400 MHz, CD ₂ Cl ₂ , 25 °C)	δ [ppm] = 7.08 (m, 12H, <u>H_{aryl}</u>), 4.76 (s, 2H, <u>H_β</u>), 2.83 (sept, ³ J _{HH} = 6.95 Hz, 8H, <u>CHMe₂</u>), 1.71 (s, 12H, <u>α-Me</u>), 1.09 (d, ³ J _{HH} = 6.95 Hz, 24H, <u>CHMeMe'</u>), 0.90 (d, ³ J _{HH} = 6.95 Hz, 24H, <u>CHMeMe'</u>). ^[1]
³¹ P{ ¹ H} NMR (162 MHz, CD ₂ Cl ₂ , 25 °C)	δ [ppm] = -426.85 (s, <u>P</u>). ^[1]
¹³ C{ ¹ H} NMR (101 MHz, CD ₂ Cl ₂ , 25 °C)	δ [ppm] = 163.21 (s, (H ₃ C) <u>CCHC</u> (CH ₃)), 146.18 (s, <u>C_{ipso}</u>), 141.84 (s, <u>C_{ortho}</u>), 124.63 (s, <u>C_{para}</u>), 123.70 (s, <u>C_{meta}</u>), 93.99 (s, (H ₃ C) <u>CCHC</u> (CH ₃)), 28.26 (s, <u>CH</u> (CH ₃) ₂), 24.86 (s, CH(<u>CH</u> ₃) ₂), 24.26 (s, CH(<u>CH</u> ₃) ₂), 24.11 (s, (H ₃ <u>C</u>)CCHC(<u>CH</u> ₃)). ^[1]
¹³ C{ ¹ H}-DEPT90 NMR (101 MHz, CD ₂ Cl ₂ , 25 °C)	δ [ppm] = 124.63 (s, <u>C_{para}</u>), 123.70 (s, <u>C_{meta}</u>), 93.99 (s, (H ₃ C) <u>CCHC</u> (CH ₃)), 28.26 (s, <u>CH</u> (CH ₃) ₂). ^[1]
¹³ C{ ¹ H}-DEPT135 NMR (101 MHz, CD ₂ Cl ₂ , 25 °C)	δ [ppm] = 124.63 (s, <u>C_{para}</u>), 123.70 (s, <u>C_{meta}</u>), 93.99 (s, (H ₃ C) <u>CCHC</u> (CH ₃)), 28.26 (s, <u>CH</u> (CH ₃) ₂), 24.86 (s, CH(<u>CH</u> ₃) ₂), 24.26 (s, CH(<u>CH</u> ₃) ₂), 24.11 (s, (H ₃ <u>C</u>)CCHC(<u>CH</u> ₃)). ^[1]
Elemental analysis (C ₅₈ H ₈₂ Cu ₂ N ₄ P ₄)	Calculated: C 64.13, H 7.61, N 5.16. Found: C 63.83, H 7.57, N 5.06. ^[1]
Mass spectrometry (LIFDI, toluene)	m/z: 1086.5 (100%) [M] ⁺ . ^[1]
Raman	vide infra, Figures S8 and S9.

Synthesis of [(LCu)₂(μ-η²:η²-As₄)] (1b)^[1]

Under stirring a solution of 200 mg (0.384 mmol) [LCu(NCMe)] in 10 mL MeCN was added to a freshly prepared, saturated solution of yellow arsenic in 250 mL toluene. The yellow reaction solution was stirred at room temperature for 10 minutes and dried in vacuum to transfer the excessive yellow arsenic into insoluble grey arsenic. The olive colored solid was dissolved in 70 mL *n*-hexane and filtered over celite to give an orange solution. Removing solvent to 10 mL and storing at -3 °C resulted in the formation of orange crystals. By concentrating the solution, another crop of crystals can be obtained.

Crystalline yield: 175 mg (0.1387 mmol, 72%).^[1]

Analytical data:

¹ H NMR (400 MHz, CD ₂ Cl ₂ , 25 °C)	δ [ppm] = 7.16 (m, 12H, <u>H_{aryl}</u>), 4.83 (s, 2H, <u>H_β</u>), 2.92 (sept, ³ J _{HH} = 6.85 Hz, 8H, <u>C<u>H</u>Me₂</u>), 1.77 (s, 12H, <u>α-Me</u>), 1.15 (d, ³ J _{HH} = 6.92 Hz, 24H, <u>CHMeMe'</u>), 0.99 (d, ³ J _{HH} = 6.84 Hz, 24H, <u>CHMeMe'</u>). ^[1]
⁷⁵ As{ ¹ H}	no signal
¹³ C{ ¹ H} NMR (101 MHz, CD ₂ Cl ₂ , 25 °C)	δ [ppm] = 162.90 (s, (H ₃ C) <u>C</u> CH <u>C</u> (CH ₃)), 146.87 (s, <u>C_{ipso}</u>), 142.05 (s, <u>C_{ortho}</u>), 124.70 (s, <u>C_{para}</u>), 123.93 (s, <u>C_{meta}</u>), 93.95 (s, (H ₃ C) <u>C</u> CHC(CH ₃)), 28.36 (s, <u>CH</u> (CH ₃) ₂), 24.97 (s, CH(<u>CH</u>) ₂), 24.51 (s, CH(<u>CH</u>) ₂), 24.18 (s, (H ₃ <u>C</u>)CCHC(<u>CH</u>)). ^[1]
¹³ C{ ¹ H}-DEPT90 NMR (101 MHz, CD ₂ Cl ₂ , 25 °C)	δ [ppm] = 124.70 (s, <u>C_{para}</u>), 123.93 (s, <u>C_{meta}</u>), 93.95 (s, (H ₃ C) <u>C</u> CHC(CH ₃)), 28.36 (s, <u>CH</u> (CH ₃) ₂). ^[1]
Elemental analysis (C ₅₈ H ₈₂ Cu ₂ N ₄ As ₄)	Calculated: C 55.20, H 6.55, N 4.44. Found: C 55.03, H 6.42, N 4.43. ^[1]
Mass spectrometry (LIFDI, toluene)	m/z: 1260.3 (100%) [M] ⁺ , 780.3 (5%) [NacnacCuAs ₄] ⁺ . ^[1]
Raman	vide infra, Figures S8 and S9.

Synthesis of [LCu(η²-P₄)] (2)

A solution of 200 mg (0.384 mmol) [LCu(NCMe)] in 15 mL *n*-pentane was added to a suspension of 170 mg P₄ (1.372 mmol) in 15 mL *n*-pentane. After filtration of black precipitate through celite the bright yellow solution was concentrated to 20 mL. The solution was chilled to 77 K in order to precipitate the excessive P₄. At 195 K, the precipitated, solid P₄ was removed by filtration and some solvent was removed in vacuum. Crystals of **2** could be grown from saturated *n*-pentane solution at -80 °C. Bright yellow crystals of **2** can be stored at -80°C and decompose at temperatures above, indicated by a color change to black.

Crystalline yield: 180 mg (0.298 mmol, 78%).

Compound **2** also can be generated and stored at room temperature in solution:^[1] 12.5 mg (0.10 mmol) white phosphorus was dissolved in 1.2 mL CD₂Cl₂. A solution of 30 mg (0.03 mmol) **1a** in 0.4 mL CD₂Cl₂ was added under stirring at room temperature and it was rewashed with 0.1 mL CD₂Cl₂.

Yield: According to the ³¹P{¹H} NMR spectroscopy, the used stoichiometry (P₄:**1a** = 3:1) already results in a quantitative conversation of **1a** into **2**.

Analytical data:^[1]

¹ H NMR (400 MHz, CD ₂ Cl ₂ , -80 °C)	δ [ppm] = 7.17 (m, 6H, <u>H_{aryl}</u>), 4.88 (s, 1H, <u>H_β</u>), 2.85 (sept, ³ J _{HH} = 6.5 Hz, 4H, <u>C<u>H</u>Me₂</u>), 1.73 (s, 6H, <u>α-Me</u>), 1.11 (d, ³ J _{HH} = 6.8 Hz, 12H, <u>CHMeMe'</u>), 1.03 (d, ³ J _{HH} = 6.7 Hz, 12H, <u>CHMeMe'</u>). ^[1]
³¹ P{ ¹ H} NMR (162 MHz, CD ₂ Cl ₂ , -80 °C)	δ [ppm] = -450.50 (t, 2P, ¹ J _{PP} = 178 Hz, η ² - <u>P₂</u>), -490.74 (t, 2P, ¹ J _{PP} = 178 Hz, <u>P₂</u>). ^[1]
¹³ C{ ¹ H} NMR (101 MHz, CD ₂ Cl ₂ , -80 °C)	δ [ppm] = 162.48 (s, (H ₃ C) <u>C<u>C</u>HC(CH₃)</u>), 144.86 (s, <u>C_{ipso}</u>), 141.02 (s, <u>C_{ortho}</u>), 123.88 (s, <u>C_{para}</u>), 123.09 (s, <u>C_{meta}</u>), 93.35 (s, (H ₃ C) <u>C<u>C</u>HC(CH₃)</u>), 27.26 (s, <u>CH(CH₃)₂</u>), 25.00 (s, <u>CH(CH₃)₂</u>), 23.74 (s, <u>CH(CH₃)₂</u>), 23.36 (s, (H ₃ C) <u>C<u>C</u>HC(CH₃)</u>). ^[1]
¹³ C{ ¹ H}-DEPT90 NMR (101 MHz, CD ₂ Cl ₂ , -80 °C)	δ [ppm] = 123.88 (s, <u>C_{para}</u>), 123.09 (s, <u>C_{meta}</u>), 93.35 (s, (H ₃ C) <u>C<u>C</u>HC(CH₃)</u>), 27.26 (s, <u>CH(CH₃)₂</u>). ^[1]
¹³ C{ ¹ H}-DEPT135 NMR (101 MHz, CD ₂ Cl ₂ , -80 °C)	δ [ppm] = 123.88 (s, <u>C_{para}</u>), 123.09 (s, <u>C_{meta}</u>), 93.34 (s, (H ₃ C) <u>C<u>C</u>HC(CH₃)</u>), 27.26 (s, <u>CH(CH₃)₂</u>), 25.01 (s, <u>CH(CH₃)₂</u>), 23.74 (s, <u>CH(CH₃)₂</u>), 23.36 (s, (H ₃ C) <u>C<u>C</u>HC(CH₃)</u>). ^[1]
Mass spectrometry (LIFDI, CH ₂ Cl ₂)	m/z: 1086.2 (100) [(NacnacCu) ₂ P ₄] ⁺ , 604.6 (11.4) [M] ⁺ . ^[1]
Raman	vide infra, Figure S10.

Crystallographic Details

Single crystal structure analyses were performed using Agilent Technologies diffractometer (Gemini R Ultra, Ruby detector (**1b** · 2 C₆H₁₄), SuperNova, Atlas (**1a**) or Titan^{S2} (**1b** · 0.25 C₆H₁₄, **2**) detector with Cu_{Kα} radiation. Special strategy of diffraction experiment was implemented for **2** (see below). Data reduction was performed with the CrysAlisPro ver. 171.37.34^[2] software package. Using the software Olex2^[3] the structure solution was carried out using the programs SUPERFLIP^[4] (**1a**, **1b** · 0.25 C₆H₁₄), SIR-97^[5] (**1b** · 2 C₆H₁₄) and SHELXS-2014 (**2**). Least squares refinements on F_o² were performed using SHELXL-2014.^[6] Further details are given in Table S1.

1b co-crystallized with *n*-hexane which could not be included to the model of **1b** · 2 C₆H₁₄ properly. Hence, the structure was treated with the SQUEEZE function of PLATON software^[7] resulting in a void of about 987 Å³ containing 120 electrons. This agrees well with two *n*-hexane molecules per formula unit. Additionally, in **1b** · 2 C₆H₁₄ one disordered diisopropylphenyl group was refined to a chemical occupancy 65:35. In case of **1b** · 0.25 C₆H₁₄ the solvent could be located and refined applying geometrical restraints (DFIX, SIMU). Molecular structures of compounds **1a**, **1b** · 0.25 C₆H₁₄, **1b** · 2 C₆H₁₄ and **2** are shown on Figure S1-S4.

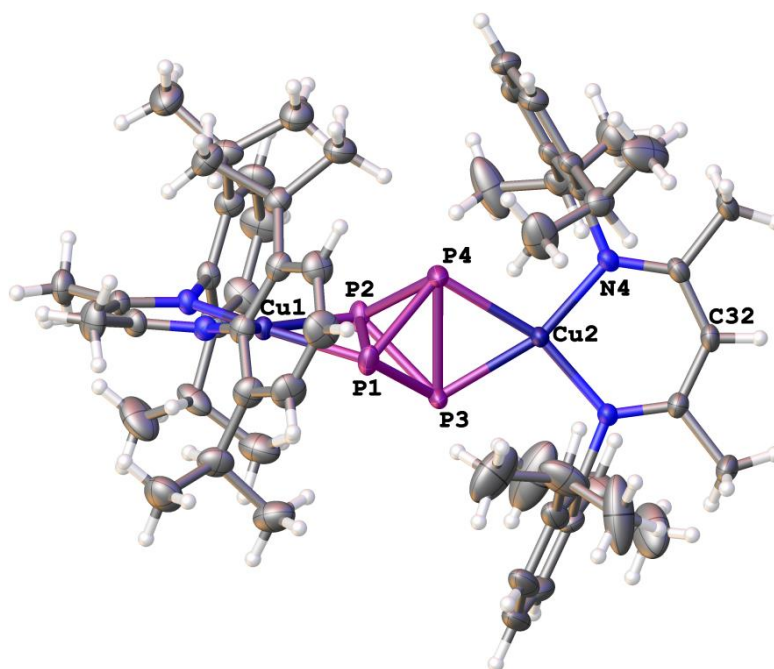


Figure S1. Molecular structure of compound **1a** in the crystal. Thermal ellipsoids are drawn at the 50% probability level. Selected bond lengths [Å] and angles [°]: Cu1–P1 2.2592(6), Cu1–P2 2.2707(6), Cu2–P4 2.2663(6), Cu2–P3 2.2627(6), P1–P2 2.4285(8), P3–P4 2.4122(8), P1–P3 2.2010(9), P2–P3 2.2114(8), P1–P4 2.2061(8), P2–P4 2.2043(8), P2–P1–P3 56.81(3), P2–P1–P4 56.55(3), P3–P1–P4 66.37(3), P1–P2–P3 56.40(3), P1–P2–P4 56.63(3), P3–P2–P4 66.22(3), P1–P3–P2 66.79(3), P1–P3–P4 56.92(3), P2–P3–P4 56.75(3), P1–P4–P2 66.82(3), P1–P4–P3 56.71(3), P2–P4–P3 57.03(3), P1–Cu1–P2 64.84(2), N1–Cu1–N2 96.90(8), P3–Cu2–P4 64.36(2), N3–Cu2–N4 97.04(8).

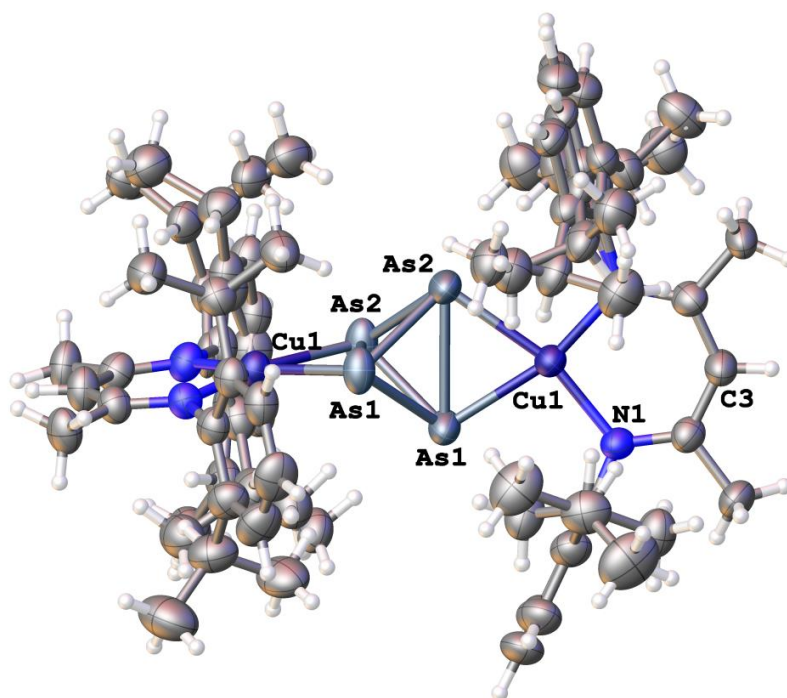


Figure S2. Molecular structure of compound **1b** · 2 C₆H₁₄ in the crystal. Solvent molecule (*n*-hexane) is omitted for clarity. Thermal ellipsoids are drawn at 50% probability level. Selected bond lengths [Å] and angles [°]: As1–Cu1 2.3761(9), As2–Cu1 2.3877(9), As1–As2 2.6491(8), As1–As1' 2.4353(11), As1–As2' 2.4443(9), As2–As1' 2.4443(9), As2–As2' 2.4375(12), As1'–As1–As2 57.28(2), As2–As1–As2' 57.01(3), As1'–As1–As2' 65.76(2), As1–As2–As1' 56.96(3), As1–As2–As2' 57.26(2), As1'–As2–As2' 65.73(2), As1–Cu1–As2 67.57(3), N1–Cu1–N2 97.35(18).

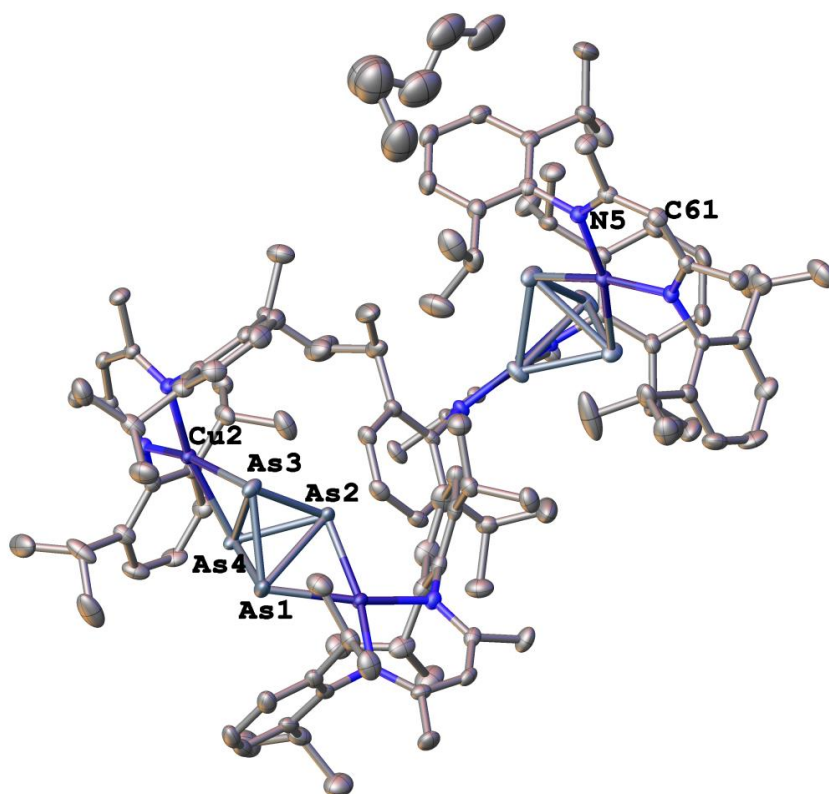


Figure S3. Molecular structure of compound **1b** · 0.25 C₆H₁₄ in the crystal. Hydrogen atoms are omitted for clarity. Thermal ellipsoids are drawn at 50% probability level.

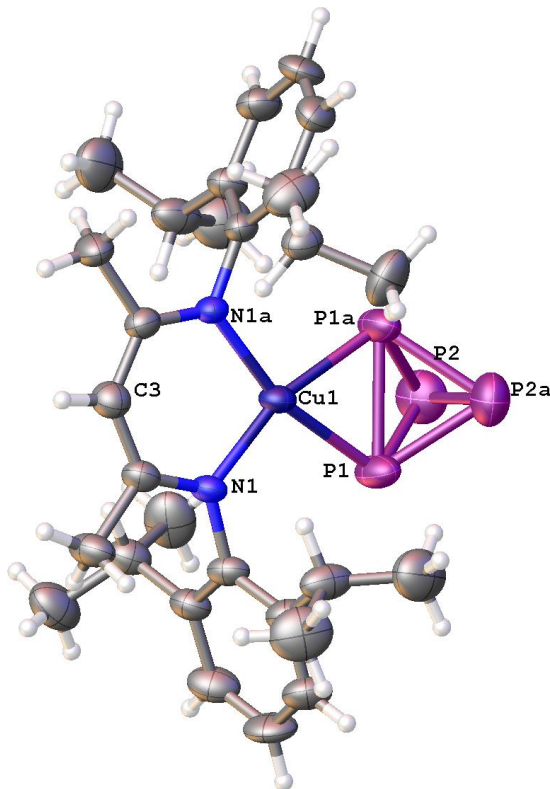
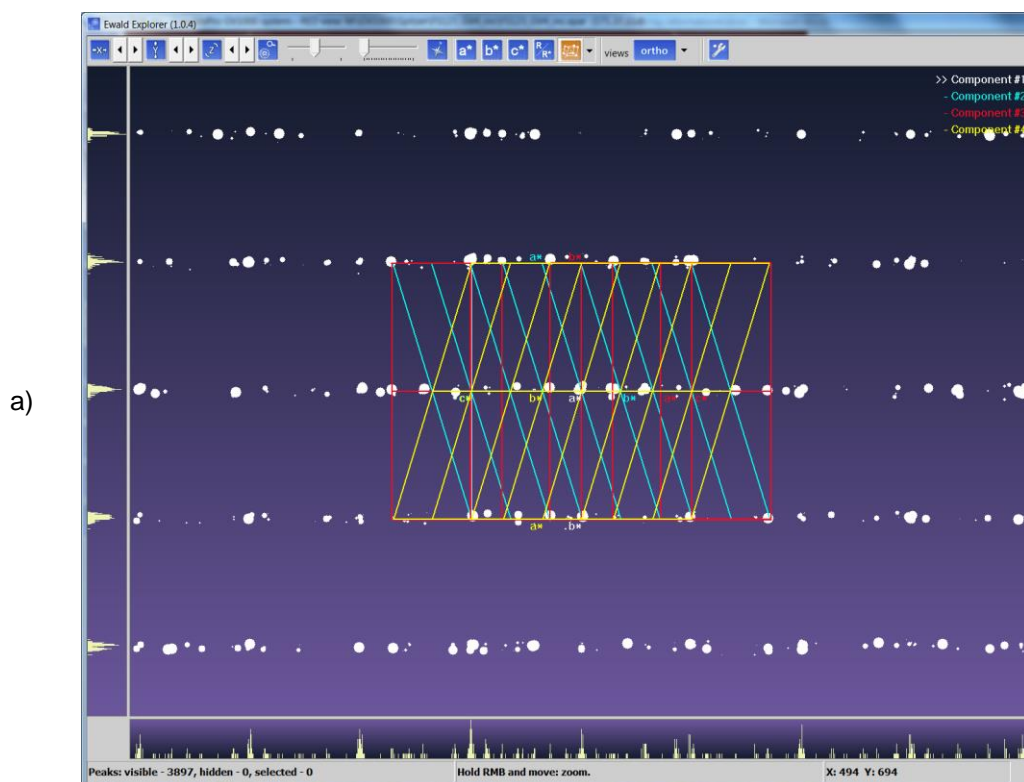


Figure S4. Molecular structure of compound **2** in the crystal. Thermal ellipsoids are drawn at 50% probability level. Selected bond lengths [Å] and angles [°]: P1–Cu1 2.280(3), P1–P1' 2.386(4), P1–P2 2.192(4), P1–P2' 2.180(4), P2–P2' 2.141(6), P1'–P1–P2 56.67(11), P1'–P1–P2' 57.16(12), P2'–P1–P2 58.65(18), P1–P2–P1' 66.17(13), P1–P2–P2' 60.39(14), P2'–P2–P1' 60.95(14), P1–Cu1–P1' 63.10(12), N1–Cu1–N1' 97.2(4).

Crystals of **2** demonstrate strong systematic tendency to multi-component twinning. Analysis of the diffraction pattern obtained from three different crystals shows similar orientation of twin components. After several measurements we have selected the crystal with diffraction pattern that can be successfully described as overlap of four twin components. In all other cases the tentative number of components was even larger, and various attempts to find single crystal failed. After 'peak hunting' procedure and twin indexing only 2 of 3897 reflections left unindexed (Table S2). The C-centered Bravais unit cell of the 2nd component is rotated by 90.0° around \mathbf{a}_1^* (a -reciprocal axis of the 1st component). Analogously, the Bravais unit cell of the 3rd component is rotated by 179.9° around \mathbf{a}_1 (a -direct of the 1st component). And finally, the Bravais unit cell for the 4th component is rotated by 90.0° around $-\mathbf{a}_1^*$. As the result, \mathbf{c}^* axes coincide for all four components (Figure S5) resulting in severe systematic overlap of the reflections (Table S2). The most probable reason for the systematic twinning in **2** is the closeness (within 0.14%) of \mathbf{a} and \mathbf{b} parameters of C-centered cell.

To obtain complete data, the reflection intensities in one half of the sphere in the reciprocal space were measured. To provide better resolution of overlapping reflections and better data for 3D-profile analysis, the special strategy was applied. It includes narrow 0.33° ω -scans, 2x2 detector binning mode, and the detector-crystal distance increased from usual 60 to 100 mm.

3D-profile analysis and simultaneous integration of the diffraction pattern were done using up-to-date version 171.37.34^[2] of CrysAlisPro program. Total 10081 reflections belonging to all 4 components were measured, of which 5904 are unique ($R_{int}=0.0725$). Merging of equivalent reflections was done by CrysAlisPro program and the resulted unique data were written to HKLF 5 type file. 5862 reflections left after rejection of systematic absences (space group $C2/c$) were used to refine the structure. The refined weights of components are in very good agreement with predicted from 3D-profile analysis (Table S2). Satisfactory final R_1 , wR_2 , low residual density and good, $1 < K < 1.84$, values of K ($K = \text{mean}[F_o^2]/\text{mean}[F_c^2]$),^[8] proves that even 4 component twin can be successfully used in X-ray structural analysis if weight of all components is similar.



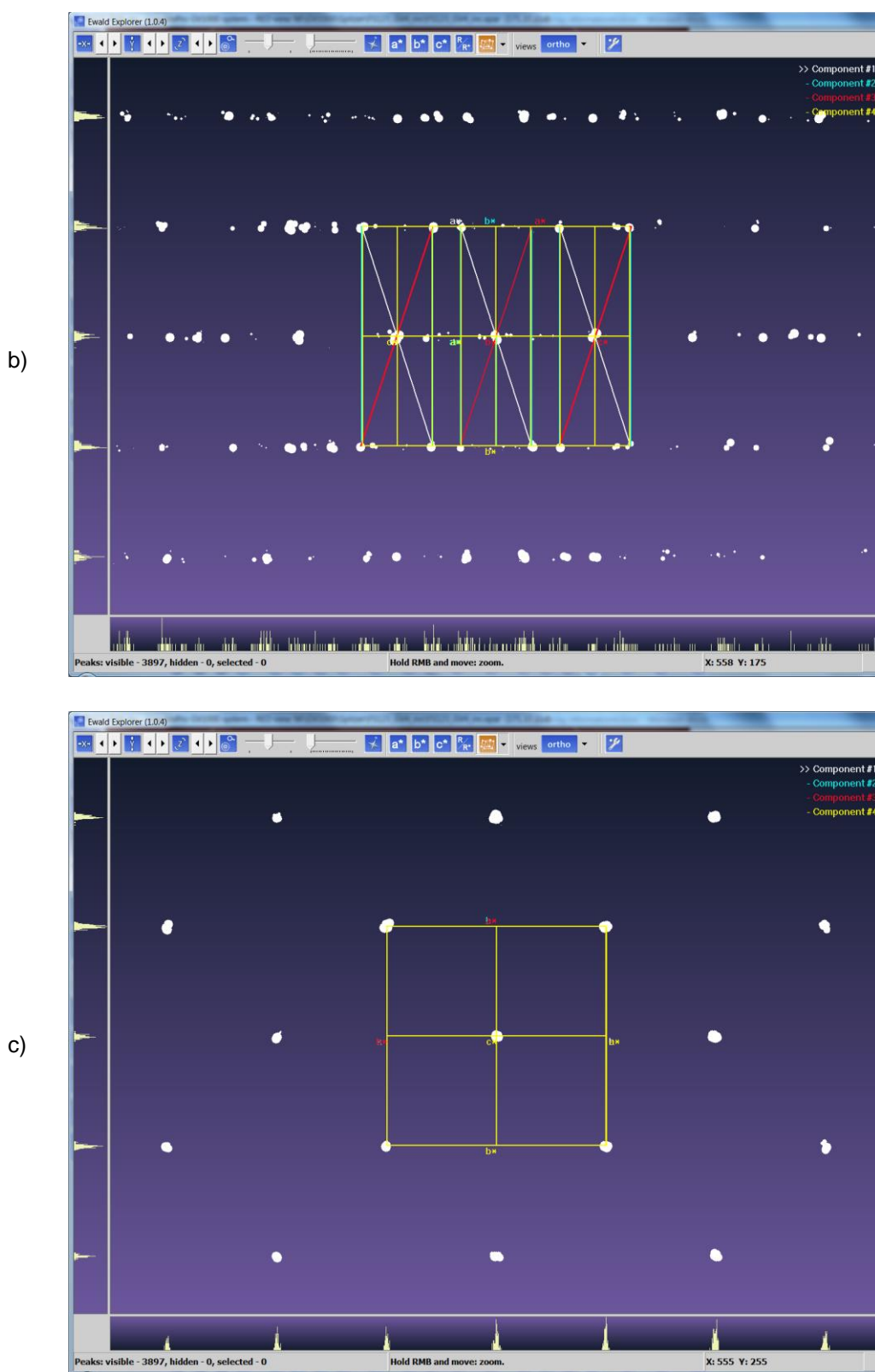


Figure S5. The mutual orientation of four twin components in the crystal of **2**, view along a^* (a), b^* (b) and c^* axis (c) of the 1st component. White spots depict observed reflections (after 'peak hunting' procedure) with radii proportional to the intensity.

Table S1. Crystallographic data and details of diffraction experiments for **1a**,^[1] **1b** · 0.25 C₆H₁₄, **1b** · 2 C₆H₁₄^[1] and **2**.

Compound	1a ^[1]	1b · 0.25 C ₆ H ₁₄	1b · 2 C ₆ H ₁₄ ^[1]	2
CCDC	1035004	1035005	1035006	1035007
Formula	C ₅₈ H ₈₂ Cu ₂ N ₄ P ₄	C ₁₁₉ H ₁₇₁ As ₈ Cu ₄ N ₈	C ₅₈ H ₈₂ As ₄ Cu ₂ N ₄	C ₂₉ H ₄₁ CuN ₂ P ₄
$\rho_{calc.}/\text{g cm}^{-3}$	1.216	1.373	1.213	1.296
μ/mm^{-1}	2.185	3.490	3.129	3.093
Formula Weight	1086.23	2567.15	1262.03	605.06
Color	yellow	yellow	orange	light yellow
Shape	block	block	block	prism
Max Size/mm	0.43	0.29	0.29	0.13
Mid Size/mm	0.29	0.25	0.12	0.11
Min Size/mm	0.16	0.13	0.10	0.11
<i>T</i> /K	123(1)	123(1)	123(1)	203(1)
Crystal System	orthorhombic	triclinic	trigonal	monoclinic
Space Group	<i>P</i> 2 ₁ 2 ₁ 2 ₁	<i>P</i> 1	<i>P</i> 3 ₁ 21	<i>C</i> 2/ <i>c</i>
<i>a</i> /Å	11.61930(8)	14.7906(3)	19.9408(2)	14.1096(15)
<i>b</i> /Å	19.82994(13)	20.2568(3)	19.9408(2)	14.0901(10)
<i>c</i> /Å	25.75580(18)	21.2884(3)	15.0522(3)	16.3789(14)
α°	90	89.8155(12)	90	90
β°	90	78.2653(13)	90	107.811(10)
γ°	90	84.1089(13)	120	90
<i>V</i> /Å ³	5934.40(7)	6210.93(17)	5183.41(15)	3100.1(5)
<i>Z</i>	4	2	3	4
<i>Z'</i>	1	1	0.5	0.5
Θ_{min}°	4.410	3.023	3.896	4.548
Θ_{max}°	73.603	74.022	66.408	72.725
Measured Refl.	39402	65820	11557	10081
Independent Refl.	11807	24202	5798	5862
Reflections Used	11546	22054	5470	5862
<i>R</i> _{int}	0.0284	0.0379	0.0336	0.0725 ^{b)}
Parameters	633	1320	429	171
Restraints	0	35	306	0
Largest Peak	0.327	1.466	0.638	0.850
Deepest Hole	-0.366	-0.674	-0.300	-0.408
GooF	1.029	1.032	1.017	1.105
<i>wR</i> ₂ (all data)	0.0647	0.1101	0.0986	0.2134
<i>wR</i> ₂	0.0641	0.1066	0.0964	0.2102
<i>R</i> ₁ (all data)	0.0249	0.0407	0.0387	0.0700
<i>R</i> ₁	0.0242	0.0372	0.0365	0.0674
Flack Parameter	-0.011(5) ^{a)}	-	-0.065(19) ^{a)}	-

a) Parsons, Flack and Wagner, Acta Cryst. B69 (2013) 249-259.

b) Merging was done by CrysAlisPro program during data reduction, using the same scaling for all four twin components. Only merged data were used for the structure refinement by SHELX.

Table S2. Analysis of the diffraction pattern from crystal of **2** after 'peak hunting' procedure.

No. comp.	Total (%)	Separate (%)	Overlapped (%)	Weight from profile analysis	Refined weight
1	2102 (53.9)	708 (18.2)	1394 (35.8)	0.358	0.374(3)
2	1664 (42.7)	413 (10.6)	1251 (32.1)	0.245	0.228(3)
3	1380 (35.4)	294 (7.5)	1251 (32.1)	0.192	0.186(3)
4	1438 (36.9)	302 (7.7)	1136 (29.2)	0.205	0.212(3)

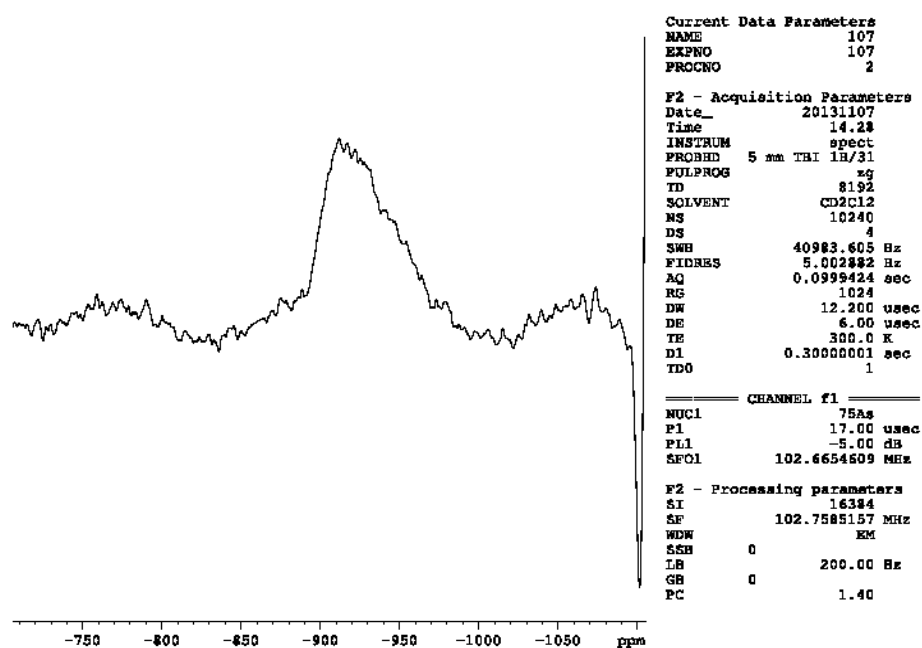
NMR Investigations

³¹P{¹H} NMR spectra were carried using a Bruker Avance 400 (³¹P: 161.976 MHz) spectrometer. The chemical shift is reported in ppm relative to external H₃PO₄ (³¹P). ⁷⁵As{¹H} NMR spectra were carried in cooperation with Dr. C. Koch using a Bruker Avance 600 NMR (⁷⁵As: 102.665 MHz) spectrometer. The chemical shift is reported in ppm relative to external KAsF₆ (⁷⁵As).

Liberation of the E₄ Tetrahedra (E = P,^[1] As):

[(LCu)₂(μ-η²:η²-P₄)] (**1a**) (9 mg) was dissolved in 1 mL pyridine and transferred into a NMR tube. The ³¹P{¹H} NMR experiment shows a singlet at -519 ppm, which can be assigned to free P₄ in pyridine with good agreement. For reference P₄ was dissolved in 0.8 mL Pyridine and ³¹P NMR experiment was conducted revealing a singlet at -518 ppm.^[1]

[(LCu)₂(μ-η²:η²-As₄)] (**1b**) (64 mg, 0.05 mmol, 1 equivalent) was dissolved in 1 mL CD₂Cl₂. Under stirring and exclusion of light [D₅]pyridine (50 μL, 12 equivalents) was added and stirred for 5 minutes. The intense orange solution was transferred into a NMR tube. The ⁷⁵As{¹H} NMR experiments reveal a broad signal at -911.8 ppm (ω_{1/2} = 5100 Hz) which can be assigned to free yellow arsenic in solution in good agreement to former ⁷⁵As{¹H} NMR measurements^[9] (Figure S6).

**Figure S6.** ⁷⁵As{¹H} NMR spectrum after liberation of As₄ from complex **1b** in CD₂Cl₂ at room temperature.

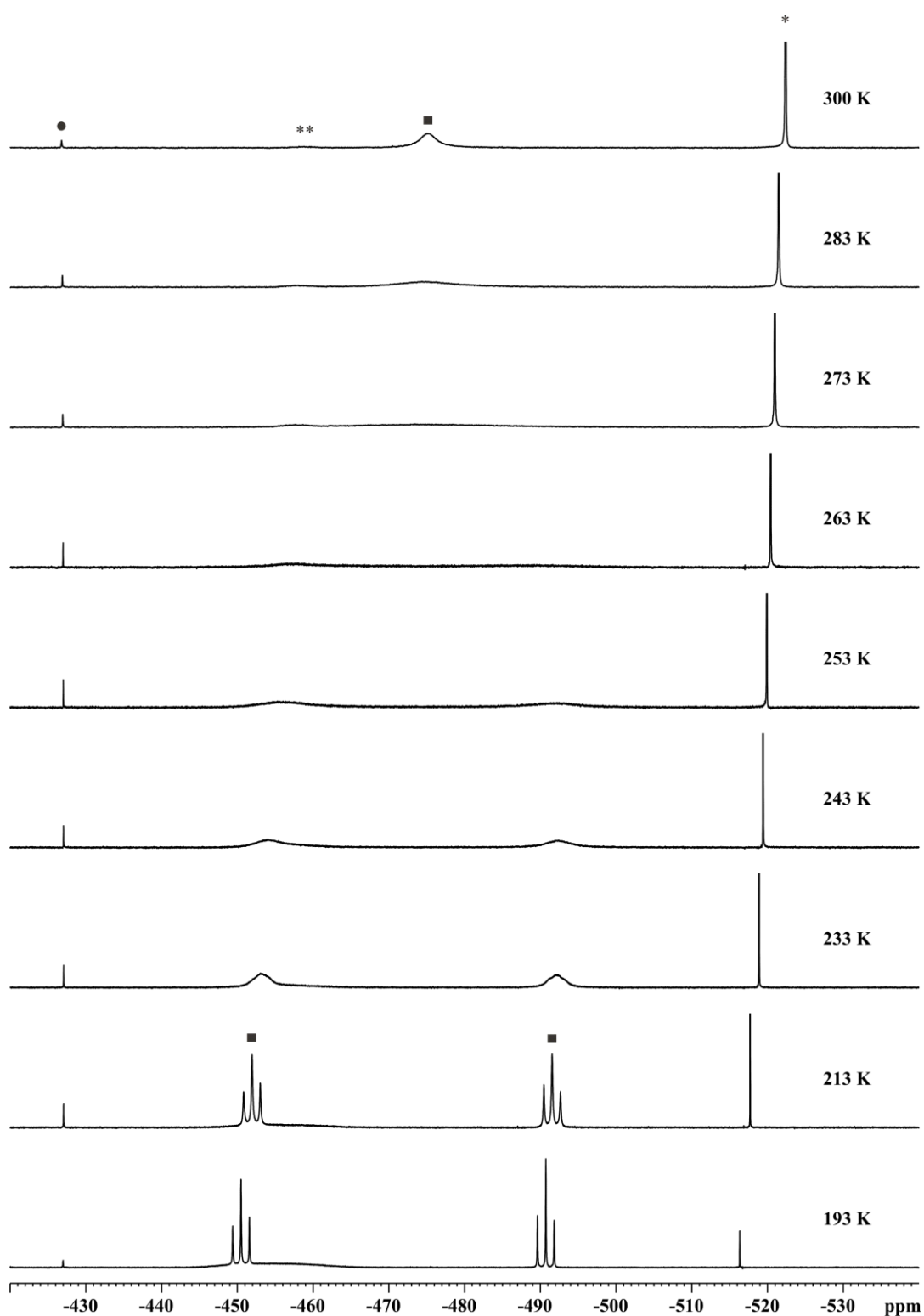
Variable-temperature ³¹P{¹H} NMR Spectra of **2** in the Temperature Range of 300 K – 193 K:^[1]

Figure S7.^[1] ³¹P{¹H} NMR spectra of a freshly prepared solution of complex **2** in CD₂Cl₂ in the temperature range of 300 K to 193 K. The signal set at $\delta = -427$ ppm and -516 ppm are assigned to **1a** (●) and P_{4,solv} (*), respectively. At $\delta = -455$ ppm P_{4,solid} (**) is detected. At 300 K compound **2** (■) is assigned to the signal at $\delta = -475.1$ ppm. Successive decrease of temperature results in splitting of the coalescence to signal sets at $\delta = -450.5$ ppm and -490.7 ppm (193 K).

Raman Spectroscopy

Raman spectra were measured using a DXR Raman Microscope (Thermo Scientific™) in cooperation with Dr. Wendy Patterson at Institute of Analytical Chemistry (University of Regensburg).

Excitation source: $\lambda_{\text{exc}} = 532 \text{ nm}$.

Laserpower: 8 mV.

Exposure time: **1a**: 30 seconds, **1b**: 20 sec. Crystals of complex **1a** did exhibit some fluorescence over time. For greater exposure times, the fluorescence in the $\sim 1600\text{--}1000 \text{ cm}^{-1}$ range was even more pronounced. The 30 seconds exposure time was found to be a good compromise, providing a strong Raman signal, and not too much fluorescence.

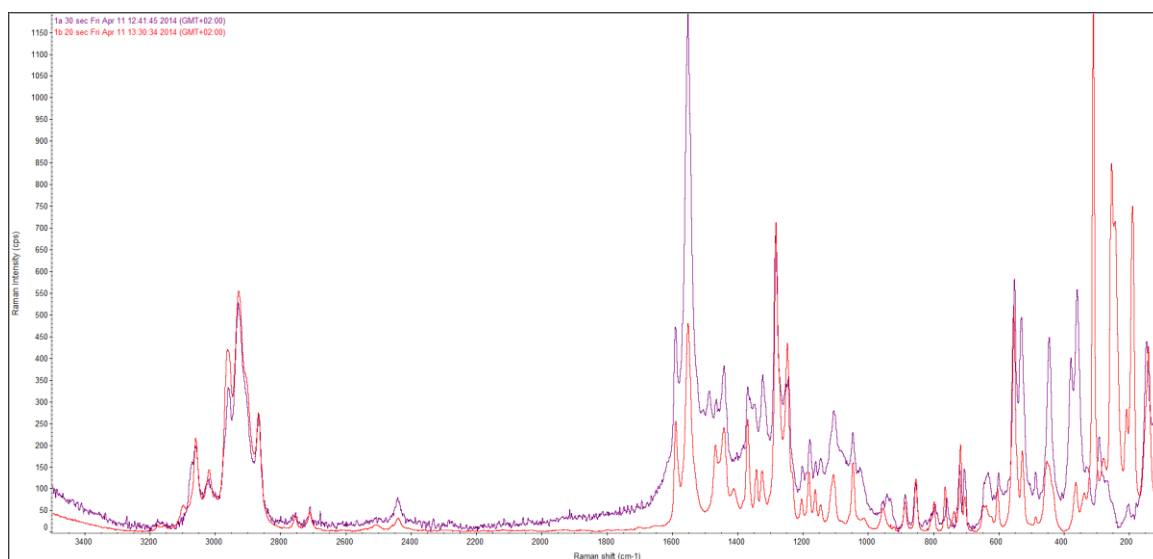


Figure S8. Full Raman spectrum comparing crystalline samples of **1a** (blue) and **1b** (red).

As seen in Figure S8, the Raman spectra of compound **1a** and **1b** are basically the same. They only differ in the 'region of interest' ($500\text{--}150 \text{ cm}^{-1}$), which is exhibited in Figure S9.

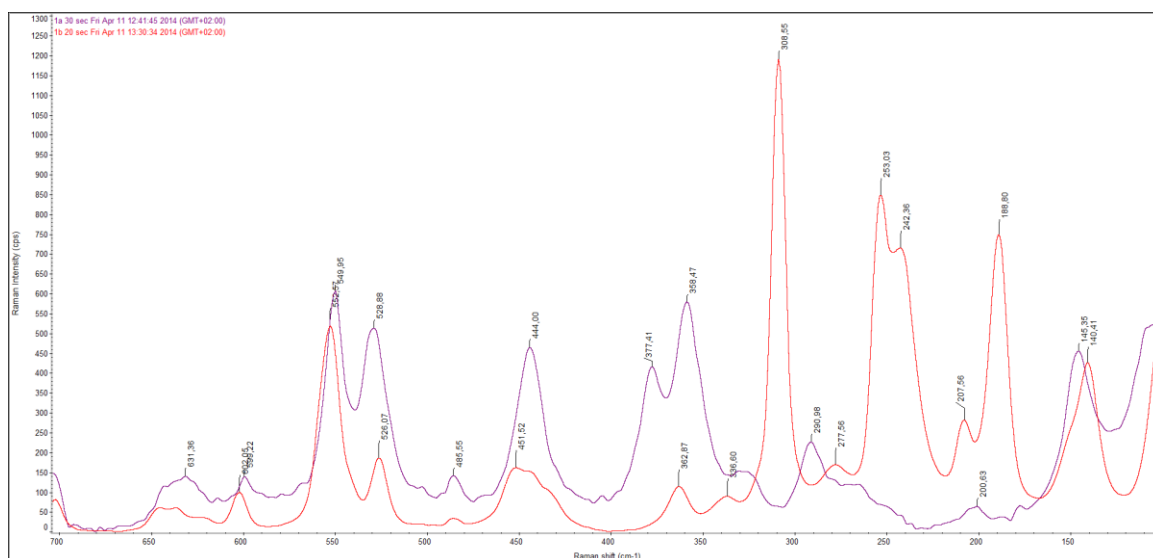


Figure S9. Raman spectrum comparing crystals of **1a** (blue) and **1b** (red) in the region $700\text{--}100 \text{ cm}^{-1}$.

In the region of interest some differences can be observed (Table S3): **1a** and **1b**, respectively, exhibit Raman modes at different values. As compound **1a** and **1b** only differ in the E₄ unit (E = P (**1a**), As (**1b**)), these Raman modes could be most likely assigned to ligand coupled E-E vibration modes.

Table S3. Comparison of observed Raman modes in 'region of interest' (500–150 cm⁻¹).

Compound	[(LCu) ₂ (μ-η ² :η ² -P ₄)] (1a)	[(LCu) ₂ (μ-η ² :η ² -As ₄)] (1b)
Raman modes in 'region of interest' (500–150 cm ⁻¹)	444.00 cm ⁻¹ 377.41 cm ⁻¹ 358.47 cm ⁻¹ 290.98 cm ⁻¹	308.55 cm ⁻¹ 253.03 cm ⁻¹ 242.36 cm ⁻¹ 188.80 cm ⁻¹

Due to vibration coupling with the connected LCu fragment and due to deficient agreement of theoretically predicted modes and experiment, the assignment of E-E stretching modes cannot be done with absolute certainty. Comparison of **1a** and **1b** with P₄, As₄, [Cu(η²-P₄)₂]⁺ and [Ag(η²-As₄)₂]⁺ show similarities between the observed Raman modes (Table S4).

Table S4. Comparison of Raman modes observed in P₄, As₄, [Cu(η²-P₄)₂]⁺ and [Ag(η²-As₄)₂]⁺.

Reference ^[10]	P ₄ in CS ₂ (300 K) ^[10]	As ₄ in vapor (950 K) ^[10]
$\tilde{\nu}_1(a_1)$	606.4 cm ⁻¹	342.0 cm ⁻¹
$\tilde{\nu}_3$	461.0 cm ⁻¹	251.0 cm ⁻¹
$\tilde{\nu}_2(e)$	364.7 cm ⁻¹	200.8 cm ⁻¹

Reference	[Cu(η ² -P ₄) ₂][pftb] ^[11]	[Ag(η ² -As ₄) ₂][pftb] ^[12]
	599(100) cm ⁻¹	343 cm ⁻¹
	468(19) cm ⁻¹	265 cm ⁻¹
	459(37) cm ⁻¹	210 cm ⁻¹
	409(20) cm ⁻¹	
	373(6) cm ⁻¹	
	361(7) cm ⁻¹	

Raman spectra of a freshly prepared solution of **2** in C₆D₆ were measured (pink) at 300 K (Figure S10). After the measurement of the Raman spectra the solution was investigated by NMR spectroscopy, revealing the following compounds to be in molar ratio **1a** : P₄ : **2** = 0.03 : 1.2 : 1. The Raman spectrum of **1a** (red) in C₆D₆ and the Raman spectrum of pure C₆D₆ (green) were measured and are depicted in Figure S10. The reference spectrum of P₄ (light blue) in C₆D₆ is shown in Figure S11.

Excitation source: $\lambda_{\text{exc}} = 532 \text{ nm}$.

Laserpower: 8 mV.

Exposure time: freshly prepared solution of **2** (pink): 20 seconds,

1a (red) in C₆D₆: 20 seconds,

C₆D₆: 1 sec (green).

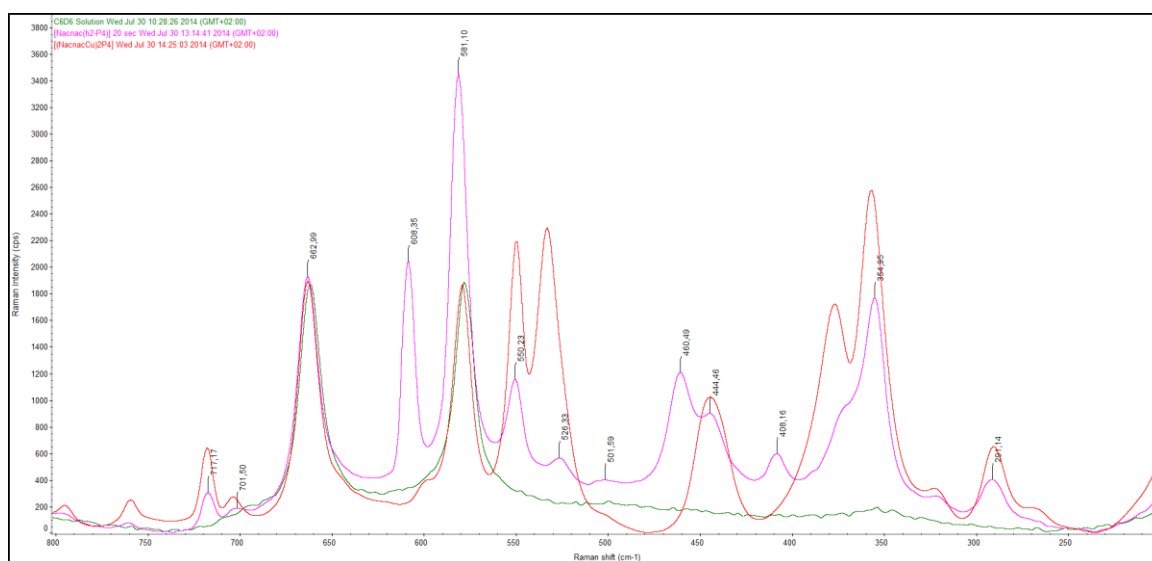


Figure S10. Raman spectrum in the region 800–200 cm⁻¹ containing the signal of **2**, **1a** and P₄ in a freshly prepared solution (pink) in C₆D₆. For reference the Raman spectrum of C₆D₆ (green) and a Raman spectrum of **1a** (red) in C₆D₆ are depicted.

For reference Raman spectrum of P₄ in C₆D₆ was measured.

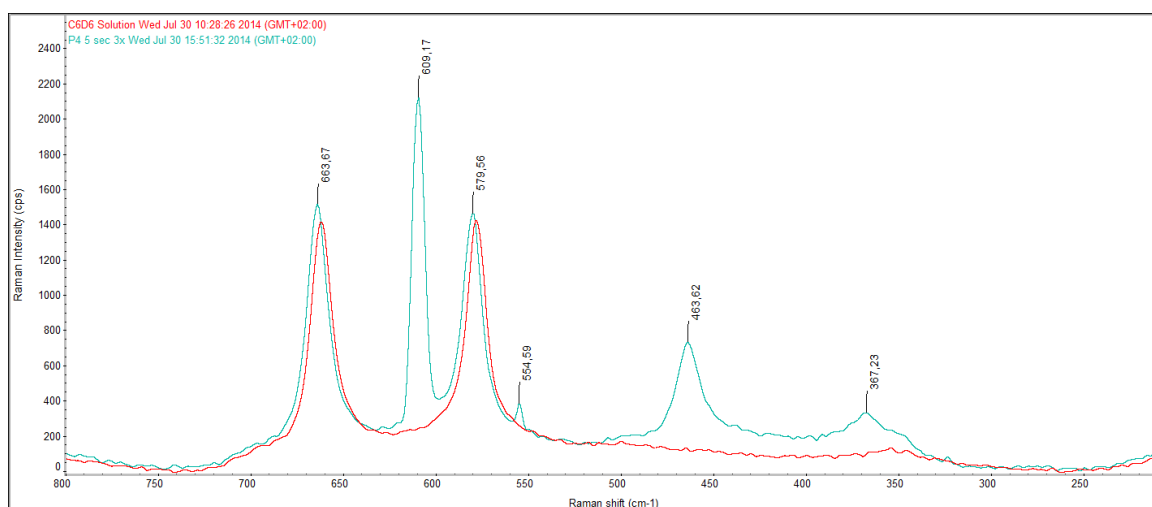


Figure S11. Raman spectrum of P₄ (light blue) in C₆D₆ in the region 800–200 cm⁻¹. For reference the Raman spectrum of C₆D₆ (red) is depicted.

Table S5. Assignment of Raman modes of compound **2** in C₆D₆ (left), compound **1a** in C₆D₆ solution and **1a** in solid state (right).

Compound	Pink spectrum containing 1a , P ₄ , C ₆ D ₆ and 2	Compound	[(LCu) ₂ (μ-η ² :η ² -P ₄)] (1a) in C ₆ D ₆	[(LCu) ₂ (μ-η ² :η ² -P ₄)] (1a) in solid state (see Figure S8)
C ₆ D ₆	717.17 cm ⁻¹	C ₆ D ₆	717.56 cm ⁻¹	-
C ₆ D ₆	662.99 cm ⁻¹	C ₆ D ₆	662.88 cm ⁻¹	-
P ₄	608.35 cm ⁻¹	P ₄	-	-
C ₆ D ₆	581.10 cm ⁻¹	C ₆ D ₆	578.99 cm ⁻¹	-
2	550.23 cm ⁻¹	1a	549.59 cm ⁻¹	549.95 cm ⁻¹
2	526.33 cm ⁻¹	1a	532.89 cm ⁻¹	528.88 cm ⁻¹
P ₄	460,49 cm ⁻¹	P ₄	-	-
2	444.46 cm ⁻¹	1a	444.25 cm ⁻¹	444.00 cm ⁻¹
2	408.16 cm ⁻¹			
2	371.50 cm ⁻¹	1a	376.69 cm ⁻¹	377.41 cm ⁻¹
2	354.95 cm ⁻¹	1a	356.69 cm ⁻¹	358.47 cm ⁻¹
2	291.14 cm ⁻¹	1a	290.14 cm ⁻¹	290.98 cm ⁻¹

In Table S5 the Raman modes of a freshly prepared solution of compound **2** in C₆D₆ are listed and a comparison with compound **1a** in C₆D₆ solution and **1a** in solid state is given. The modes (444.46, 371.50, 354.95 and 291.14 cm⁻¹) of compound **2** differ slightly from the modes obtained in complex **1a**, but most significantly one additional Raman mode at 408.16 cm⁻¹ is obtained in compound **2**.

Computational Details

Methods: Density functional theory (DFT) calculations were performed using the TURBOMOLE program package^[13] employing the BP86 exchange-correlation functional.^[14] To account for long-range van der Waals forces missing at this level of theory the dispersion correction by Grimme *et al.*^[15] (DFT-D3) has been added. All calculations use triple zeta valence plus a double set of polarization functions (TZVPP) basis sets.^[16] To speed up the calculations, the Coulomb part was evaluated by using the MARI-J^[17] method along with optimized auxiliary basis sets on all atoms.^[18] The minima on potential energy surfaces were characterized by calculations of vibrational frequencies based on analytical second derivatives of the energy with respect to the nuclear coordinates.^[19] The vibrational contributions to the Gibbs free energies at 293.15 K were calculated within harmonic approximation using DFT calculated frequencies. Solvation contributions to free energies were calculated using the conductor-like screening model (COSMO) approach.^[20] The topological analysis of the electron density obtained at the DFT has been performed using the DGrid program.^[21]

Topological analysis of the electron density: Table S6 summarizes properties of critical points (CPs) in the electron density within the E₄ units (E = P, As) of **1a**, **2** and **1b**: bond critical points (BCP), ring critical points (RCP) and the cage critical points (CCP). For comparison, the corresponding critical points in free E₄ species are given. The locations and labeling of the CPs is shown in Figure S12. Free P₄ and As₄ molecules show similar properties of all critical points. In particular the relatively large values of the electron density, ρ_{CP} , and the negative values of the total electronic energy density, H_{CP} , at the BCPs confirm the covalent character of the E–E bonds in free P₄ and As₄. In addition, small values of the bond ellipticity, ε_{CP} , indicate cylindrical symmetry of the E–E bonds.

In comparison to free E₄ molecules the P₄ units in **1a** and **2** as well as As₄ units in **1b** show appreciable changes only in properties of BCPs for the bonds between two E atoms directly involved in the coordination of Cu⁺ (P1–P2, P3–P4, As1–As2, As1'–As2' and P1–P1' in Figures 1, 2 and 3). The decrease of ρ_{CP} along with increase of $\nabla^2\rho_{\text{CP}}$ for these BCPs confirms the expected depletion of the electron density upon coordination to Cu⁺. The formation of the three-membered Cu–E rings results in increased bond ellipticity ε_{CP} compared to free E₄ molecules. In contrast, the properties (ρ_{b} , $\nabla^2\rho_{\text{b}}$ and H_{b}) of remaining BCPs as well as ring and cage critical points (RCP and CCP, respectively, Table S6) show only small differences. This demonstrates only a moderate change in the electronic structure of P₄ units in **1a** and **2** as well as As₄ units in **1b**, compared to free E₄ species. Therefore, we can conclude that the E₄ units in all three compounds can be considered as being intact.

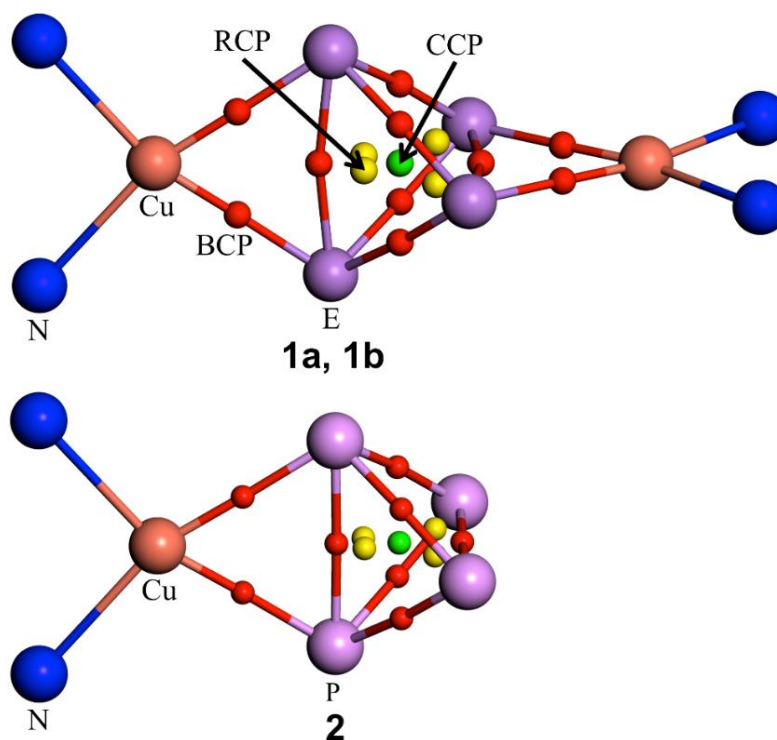


Figure S12. Location of critical points in the electron density within E₄ units of **1a** (E = P), **1b** (E = As) and **2**: bond critical points (BCP, red), ring critical points (RCP, yellow), and the cage critical point (CCP, green).

Table S6. Comparison of critical points (see Figure S12) in the electron density within P₄ and As₄ units of free P₄, **1a**, **2**, free As₄ and **1b**: values of electron density, ρ_{CP} , Laplacian of electron density, $\nabla^2\rho_{CP}$, bond ellipticity, ε_{CP} , and total electronic energy density, H_{CP} .

Compound	Critical point	ρ_{CP}	$\nabla^2\rho_{CP}$	ε_{CP}	H_{CP}
P ₄	P-P (BCP)	0.105	-0.060	0.10	-0.053
	P (RCP)	0.083	0.088	-	-0.026
	P (CCP)	0.078	0.125	-	-0.020
1a	P1-P3 (BCP)	0.103	-0.072	0.10	-0.050
	P1-P2 (BCP)	0.068	0.053	2.06	-0.021
	P1-Cu1 (BCP)	0.075	0.083	0.18	-0.024
	P (RCP)	0.067	0.081	-	-0.017
	P (CCP)	0.066	0.101	-	-0.014
	2	P1-P1' (BCP)	0.107	-0.066	0.05
P1-P2' (BCP)		0.103	-0.066	0.18	-0.051
P2-P2' (BCP)		0.054	0.060	2.00	-0.018
P1-Cu1 (BCP)		0.075	0.081	0.17	-0.025
P (RCP)		0.083	0.080	-	-0.025
P (CCP)		0.070	0.100	-	-0.018
As ₄	As-As (BCP)	0.078	-0.003	0.05	-0.031
	As (RCP)	0.058	0.071	-	-0.013
	As (CCP)	0.053	0.091	-	-0.009
1b	As1-As2' (BCP)	0.076	-0.009	0.07	-0.029
	As1-As2 (BCP)	0.050	0.043	2.04	-0.011
	As1-Cu1 (BCP)	0.065	0.067	0.11	-0.019
	As (RCP)	0.047	0.063	-	-0.008
	As (CCP)	0.045	0.072	-	-0.006

Reaction energies: Table S7 shows calculated energies and free energies of reactions R1–R6 in gas phase and in CH₂Cl₂ solution. For comparison gas-phase reaction energies calculated at the DFT level without the dispersion correction are shown. With exception of R3 all reactions are exergonic. Comparison of DFT and DFT-D3 calculated reaction energies demonstrates that due to the presence of bulky L ligand the main contribution is due to dispersion interaction between units of L. In most of the cases the pure DFT contribution accounts for less than 10% of total reaction energies.

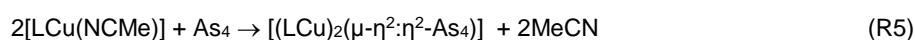
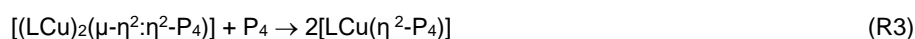
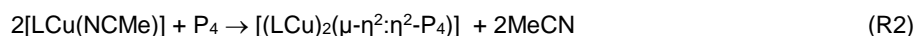


Table S7. Calculated gas-phase energies ($\Delta E_{\text{DFT-D3}}$), gas-phase free energies ($\Delta G_{\text{DFT-D3}}$) and free energies in CH₂Cl₂ solution ($\Delta G(f)_{\text{DFT-D3}}$) for reactions R1–R6. For comparison gas-phase reaction energies calculated at the DFT level (ΔE_{DFT}) are shown. All values in kJ/mol.

Reaction	$\Delta E_{\text{DFT-D3}}$	$\Delta G_{\text{DFT-D3}}$	$\Delta G(f)_{\text{DFT-D3}}$	ΔE_{DFT}
R1	-51.3	-39.0	-55.1	-5.5
R2	-117.9	-89.7	-114.7	-1.7
R3	15.5	11.7	4.6	-9.2
R4	-66.3	-52.0	-67.5	-9.8
R5	-144.4	-101.8	-126.0	-12.9
R6	11.8	-2.3	-9.0	-6.8

Reference

- [1] F. Spitzer, *Master Thesis, Universität Regensburg* **2013**.
- [2] CrysAlisPro Software System, Agilent Technologies UK Ltd, Yarnton, Oxford, UK (2014).
- [3] O.V. Dolomanov and L.J. Bourhis and R.J. Gildea and J.A.K. Howard and H. Puschmann, Olex2: A complete structure solution, refinement and analysis program, *J. Appl. Cryst.*, (2009), **42**, 339-341.
- [4] L. Palatinus and G. Chapuis, Superflip - a computer program for the solution of crystal structures by charge flipping in arbitrary dimensions, *J. Appl. Cryst.*, (2007), **40**, 786-790.
- [5] A. Altomare and M.C. Burla and M. Camalli and G.L. Casciarano and C. Giacovazzo and A. Guagliardi and A.G.G. Moliterni and G. Polidori and R. Spagna, SIR97: a new tool for crystal structure determination and refinement, *J. Appl. Cryst.*, (1999), **32**, 115-119.
- [6] Sheldrick, G.M., A short history of ShelX, *Acta Cryst.*, (2008), **A64**, 339-341.
- [7] P. van der Sluis & A.L. Spek (1990). *Acta Cryst.*, **A46**, 194-201.
- [8] R. Herbst-Irmer, G. M. Sheldrick, *Acta Cryst. B* (1998), **54**, 443-449
- [9] C. Schwarzmaier, A. Schindler, C. Heindl, S. Scheuermayer, E. V. Peresypkina, A. V. Virovets, M. Neumeier, R. Gschwind, M. Scheer, *Angew. Chem. Int. Ed.* **2013**, **52**, 10896-10899.
- [10] Y. M. Bosworth, R. J. H. Clark, D. M. Rippon, *J. Mol. Spectrosc.* **1973**, **46**, 240-255.
- [11] G. Santiso-Quinones, A. Reisinger, J. Slattey, I. Krossing, *Chem. Commun.* **2007**, 5046-5048.
- [12] C. Schwarzmaier, A. Y. Timoshkin, M. Scheer, *Angew. Chem. Int. Ed.* **2013**, **52**, 7600-7603.
- [13] TURBOMOLE V6.4 2013, a development of University of Karlsruhe and Forschungszentrum Karlsruhe GmbH, 1989-2007, TURBOMOLE GmbH, since 2007; available from <http://www.turbomole.com>.

- [14] a) A. D. Becke, *Phys. Rev. A* **1988**, 38, 3098-3100; b) J. P. Perdew, *Phys. Rev. B* **1986**, 33, 8822-8824; c) J. P. Perdew, *Phys. Rev. B* **1986**, 34, 7406-7406; d) S. H. Vosko, L. Wilk, M. Nusair, *Can. J. Phys.* **1980**, 58, 1200-1211.
- [15] S. Grimme, J. Antony, S. Ehrlich, H. Krieg, *J. Chem. Phys.* 2010, 132, 154104.
- [16] F. Weigend, R. Ahlrichs, *Phys. Chem. Chem. Phys.* **2005**, 7, 3297-3305.
- [17] a) K. Eichkorn, O. Treutler, H. Ohm, M. Haser, R. Ahlrichs, *Chem. Phys. Lett.* **1995**, 242, 652-660; b) M. Sierka, A. Hogekamp, R. Ahlrichs, *J. Chem. Phys.* **2003**, 118, 9136-9148.
- [18] F. Weigend, *Phys. Chem. Chem. Phys.* **2006**, 8, 1057-1065.
- [19] P. Deglmann, F. Furche, R. Ahlrichs, *Chem. Phys. Lett.* **2002**, 362, 511-518.
- [20] A. Klamt, G. Schürmann, *J. Chem. Soc., Perkin Trans.* **1993**, 2, 799-805.
- [21] M. Kohout, DGrid, version 4.6, Radebeul, 2011.

Preface

The following chapter has already been published as an open access article under the terms of the Creative Commons Attribution Non-Commercial NoDerivs (CC BY-NC-ND) License. The article is reprinted with permission of Wiley-VCH.

English version: 'Influence of the nacnac Ligand in Iron(I)-Mediated P₄ Transformations' *Angew. Chem. Int. Ed.* **2016**, *55*, 4340-4344. Copyright Wiley-VCH Verlag GmbH & Co. KGaA. Reproduced with permission.

German version: 'Der Einfluss des nacnac-Liganden in der Eisen(I)-vermittelten P₄-Umwandlung' *Angew. Chem.* **2016**, *128*, 4412-4416.

Authors

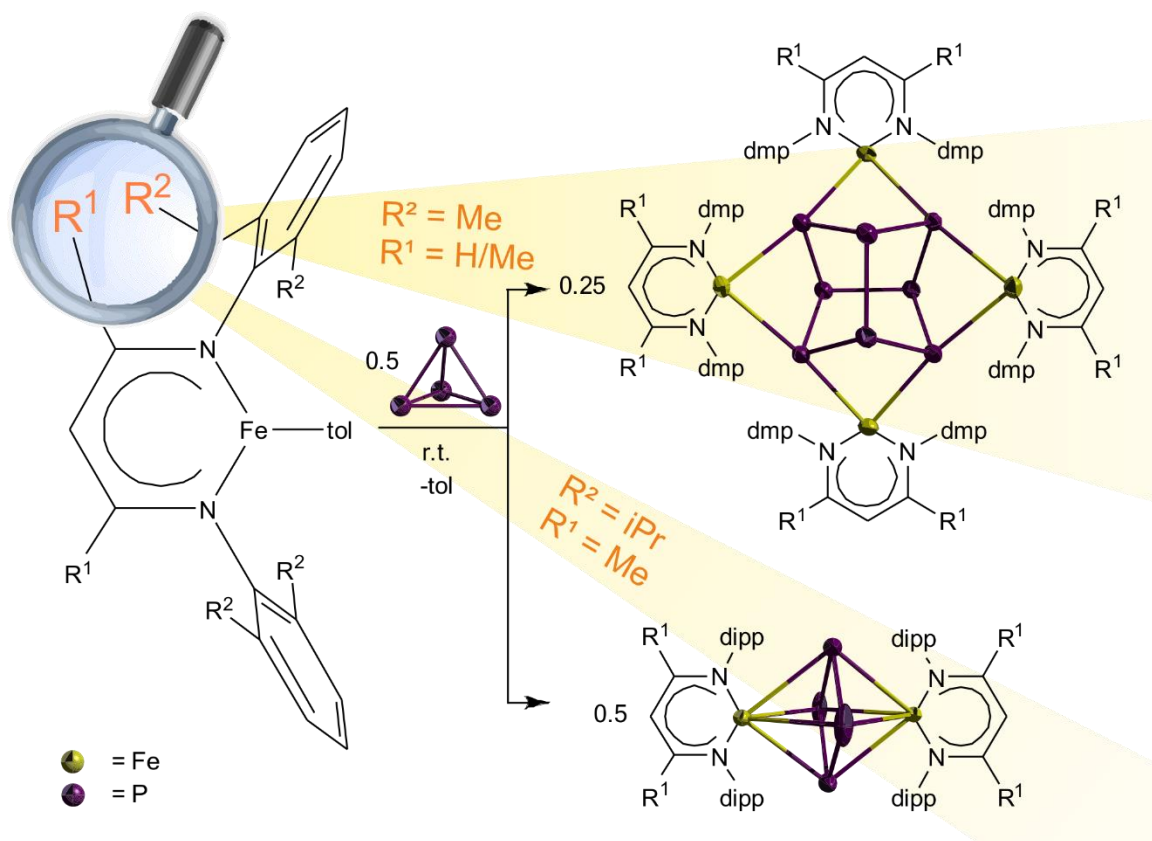
Fabian Spitzer, Christian Graßl, Gábor Balázs, Eva M. Zolnhofer, Karsten Meyer, Manfred Scheer*

Author contributions

The preparation of the manuscript was done by the first author (F. Spitzer). M. Scheer supervised the research and revised the manuscript. G. Balázs performed all DFT calculations and contributed the corresponding parts in the manuscript and the Supporting Information. C. Graßl described the synthesis and characterization of compounds **1a** and **2a** in his PhD thesis and contributed a sample of **2a** for the SQUID measurement. The first author recognized the dependencies of ligand design on the product formation and initiated their systematic investigations. The preparation of compounds L²H, **1b**, **1c**, **2b** and **2c** and their characterization was done by the first author. This includes the selective formation of **2b,c** irrespective of stoichiometry. The interpretation of all NMR spectra and the determination of the magnetic moment in solution (Evans method) of **1b,c** and **2a-c** was performed by the first author. The EPR samples of **1b,c** were prepared by the first author. Samples for SQUID, Mössbauer and EPR measurements of **2b** and **2c** were provided by the first author. The measurement and interpretation of SQUID and Mössbauer spectra of **2a-c** as well as the EPR spectra at 10 K were performed by E. M. Zolnhofer. The corresponding part in the Supporting Information was written by E. M. Zolnhofer and K. Meyer. The investigations presented in '4.6 Addendum' were performed by the first author.

Acknowledgements

This work was supported by the Deutsche Forschungsgemeinschaft. The European Research Council (ERC) is acknowledged for the support in the SELFPHOS AdG-339072 project. M. Modl is acknowledged for measurement of EPR spectra of **1b,c**.



4. Influence of the nacnac Ligand in Iron(I)-Mediated P₄ Transformations

Abstract: A study of P₄ transformations at low-valent iron is presented using β -diketiminato (L) Fe^I complexes [LFe(tol)] (tol = toluene; L = L¹ (**1a**), L² (**1b**), L³ (**1c**)) with different combinations of aromatic and backbone substituents at the ligand. The products [(LFe)₄(μ_4 - η^1 : η^1 : η^1 : η^1 : η^1 : η^1 : η^1 : η^1 -P₈)] (L = L¹ (**2a**), L² (**2b**)) containing a P₈ core were obtained by the reaction of **1a,b** with P₄ in toluene at room temperature. Using a slightly more sterically encumbered ligand in **1c** results in the formation of [(L³Fe)₂(μ - η^4 : η^4 -P₄)] (**2c**), possessing a cyclo-P₄ moiety. Compounds **2a-c** were comprehensively characterized and their electronic structures investigated by SQUID magnetization and ⁵⁷Fe Mössbauer spectroscopy as well as by DFT methods.

4.1 Introduction

The activation of white phosphorus (P₄) with main group^[1] and transition metal^[2] compounds is an ongoing area of research. The latter topic is dominated by Cp^R containing transition metal complexes.^[2] More recently, complexes of the β -diketiminato (nacnac = L) ligand have been employed for P₄ activation as well. For early transition metal compounds, exclusively Group 5 complexes were used,^[3] whereas for electron-rich metals Group 8–10 complexes have been applied so far.^[4] Selected examples of P_n complexes **A–D** with β -diketiminato ligands of late transition metals are shown in Figure 1. Recently, we reported on the Cu^I compounds [(LCu)₂(μ - η^2 : η^2 -E₄)] (E = P (**D**), As) and [LCu(η^2 -P₄)], respectively, containing intact E₄ moieties,^[5] while all other examples (**A–C**) contain transformed P₄ units. Also, we investigated the reaction of Fe^I complexes [LFe(tol)] with P₄. When the Driess group recently reported on the formation of the Fe^{III} complex [(L⁰Fe)₂(μ - η^2 : η^2 -P₂)₂] (**A**), containing two dianionic P₂ ligands,^[4a] we were surprised as our investigations showed quite different results. Since the reaction conditions were identical, we supposed that the reason for the different P₄ activation pathways (and products) was due to the slightly different aromatic flanking groups and α -backbone substituents of our [LFe(tol)] precursors. Therefore, we systematically studied the driving forces for the different outcome of P₄ activation by Fe^I centers.

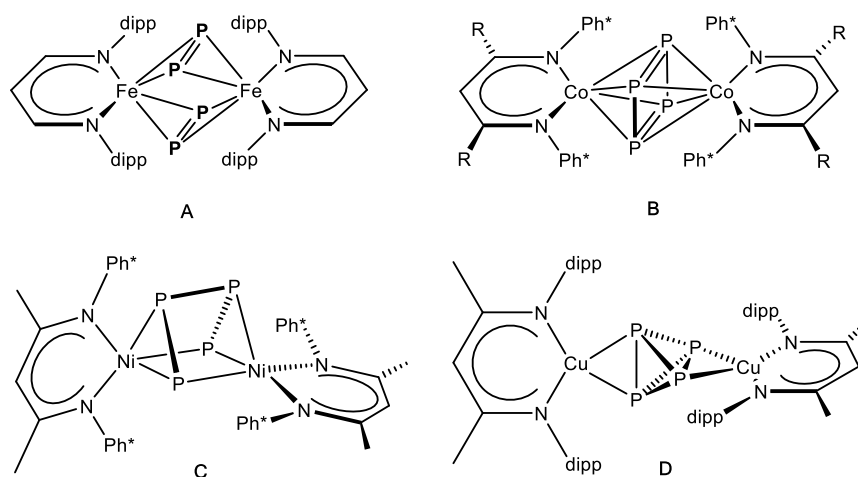
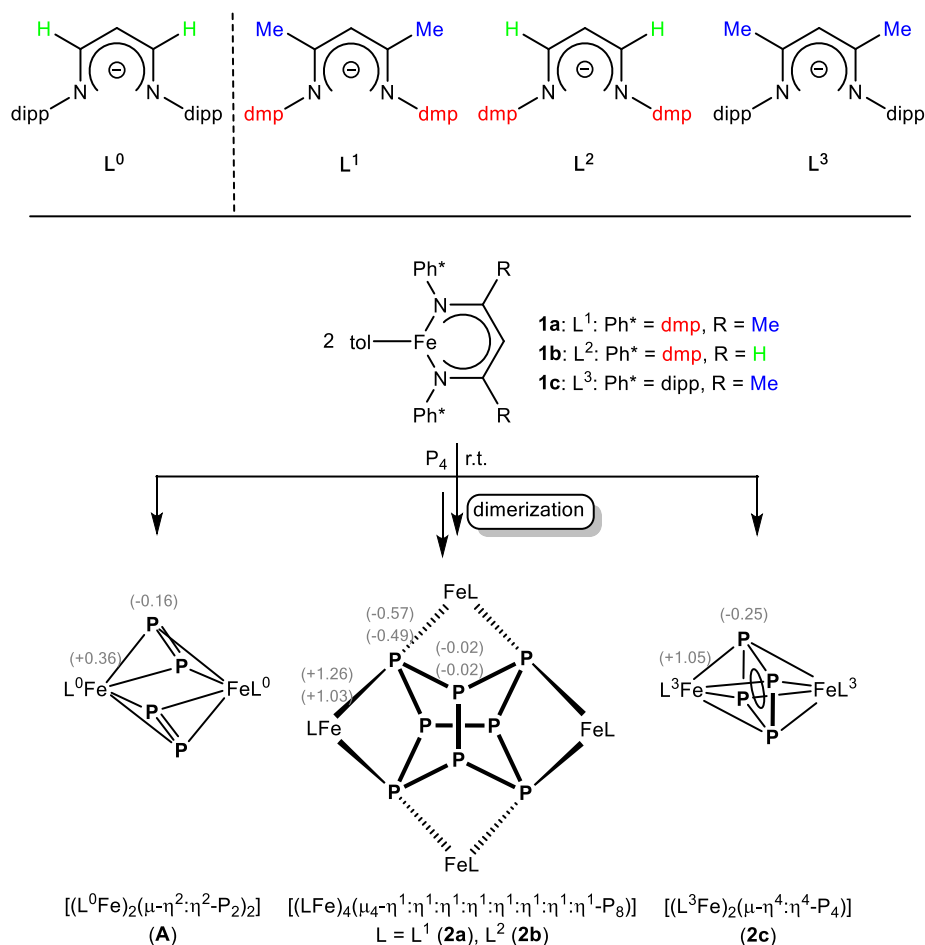


Figure 1. Selected examples of P_n ligand complexes with late transition metals Fe, Co, Ni, and Cu supported by the β -diiminato ligand.^[4,5]

4.2 Results and Discussion

Herein, we present a comparative study of P₄ activation by Fe^I β -diiminato (L) complexes [LFe(tol)] (L = L¹ (**1a**), L² (**1b**), L³ (**1c**)) with toluene (tol) as a labile leaving group. The starting materials [LFe(tol)] (L = L¹ (**1a**), L² (**1b**), L³ (**1c**)) were synthesized in a one-pot synthesis (see the Supporting Information) and characterized by single-crystal X-ray crystallography (**1b** and **1c**, see the Supporting Information).

The reaction of [L¹Fe(tol)] (**1a**) with 0.5 equivalent of P₄ in toluene at room temperature leads to the formation of a tetranuclear complex, namely [(L¹Fe)₄(μ_4 - η^1 : η^1 : η^1 : η^1 : η^1 : η^1 : η^1 : η^1 -P₈)] (**2a**), which displays a realgar-type^[6] P₈ moiety. Changing the stoichiometry of the reaction does not affect the product formation (ratio [L¹Fe(tol)]/P₄ = 2:1 and 1:2). The formation of a P₈ moiety in **2a** is in contrast to the recently reported product, [(L⁰Fe)₂(μ - η^2 : η^2 -P₂)₂] (**A**), published by the Driess group,^[4a] which contains two [P₂]²⁻ ligands (Scheme 1). A comparison of ligand L⁰ with L¹, however, displays only small differences in the aromatic (Ph* = dipp (= 2,6-diisopropylphenyl) or dmp (= 2,6-dimethylphenyl)) and in the backbone (R) substituents. In both cases the reaction conditions were identical. Therefore, we were interested to understand whether the steric demand or the electronic properties of the aromatic flanking groups Ph* and backbone α -substituents R cause the different reactivity of the Fe^I precursors towards P₄. According to DFT calculations at the BP86//def2-SVP/def2-TZVP (N, Fe, P) level, the dimerization of the hypothetical complex [(L¹Fe)₂(μ - η^4 : η^4 -P₄)] (quintet spin state) to **2a** (nonet spin state) is endothermic (91.5 kJ·mol⁻¹). This seems to be in contrast with the experimental results. However, considering that the unrestricted singlet spin state of **2a** is more stable than the nonet spin state (102.1 kJ·mol⁻¹), the reaction becomes exothermic. Furthermore, the natural population analyses (NPA) clearly indicates the presence of Fe^{II} centers and [P₈]⁴⁻ ligand in **2a**.



Scheme 1. Top: Comparison of L⁰ with ligands L¹, L², and L³, containing a variety of different substituents. Bottom: Coordinated P_n moieties obtained by P₄ transformation with different Fe^I precursors. The gray numbers in brackets represent the NPA charges at the corresponding atoms.^[7] For **2a,b** the upper value corresponds to **2a**.

Accordingly, we decided to additionally synthesize ligand L² (see Scheme 1, top), representing the missing combination between ligands L⁰ and L¹, to investigate the steric and electronic effects induced by the different substitution of the chelating N atoms and the ligand backbone. Conducting the reaction of [L²Fe(tol)] (**1b**) and P₄ under identical conditions (r.t., toluene) and same stoichiometries (2:1 and 1:2) facilitates the clean and selective formation of the P₈ moiety containing complex [(L²Fe)₄(μ₄-η¹:η¹:η¹:η¹:η¹:η¹:η¹:η¹-P₈)] (**2b**) (Scheme 1 and Figure 2). Even if a higher local concentration of P₄ was used by the dropwise addition of 1 equivalent of **1b** to a solution of 2 equivalents of P₄ in toluene, **2b** is the only product of the reaction. Comparing **2a** and **2b**, we assume that the methyl flanking groups in dmp are not able to prevent the dimerization reaction to the P₈ moiety, as the dipp substituents did in [(L⁰Fe)₂(μ-η²:η²-P₂)₂] (**A**). Along with **A**,^[4a] possessing two separate P₂ units, compounds **2a,b** are different activation steps of P₄ (Scheme 1).

A single crystal X-ray structural analysis reveals that compounds **2a** · 2 toluene and **2b** · toluene are isostructural (Figure 2 for **2b**). Both compounds contain a realgar-type P₈ ligand coordinating to four [LFe] (L = L¹ (**2a**), L² (**2b**)) fragments. All P–P distances are in the range of 2.1991(8) to 2.2813(7) Å in **2a** and 2.2111(6) to 2.2792(6) Å in **2b**; and therefore, are in line with P–P single bonds (for comparison: P–P single bond in white phosphorus determined by electron diffraction: 2.1994(3) Å,^[8] Raman spectroscopy: 2.2228(5) Å,^[9] and DFT calculations: 2.1994(3) Å^[8]). The coordination geometry of the Fe metal centers in **2a** and **2b**, respectively, is best described as distorted tetrahedral. The torsion angles between the Fe–P–P and Fe–N–N planes are between 74.66(6)° and 84.74(5)° in **2a** and 83.45(4)° and 84.91(6)° in **2b**. There are no significant differences in the P–P bond distances in **2a,b** and those of previously reported related P₈ ligands in [(NN^{fc}Sc)₄P₈], [(Cp*Sm)₄P₈] (Cp* = C₅Me₅), [Cp^{Me}₄Fe₄(CO)₆P₈] (Cp^{Me} = C₅H₄Me), [(Cp^{Me}₄Fe₆(CO)₁₃P₈], and [Cp*₂Ir₂Cr₃(CO)₁₇P₈].^[10]

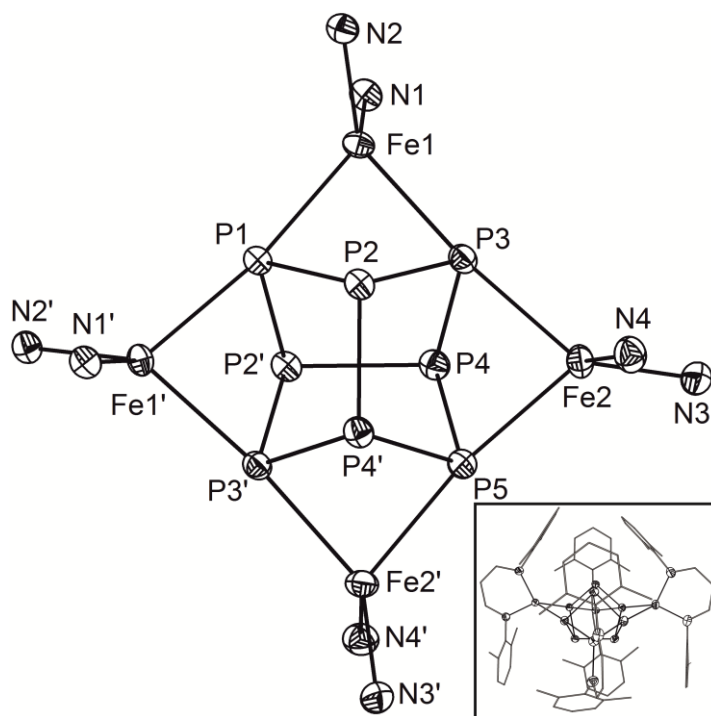


Figure 2. Core structure of **2b** in crystals of **2b** · toluene. Hydrogen and carbon atoms are omitted for clarity. Thermal ellipsoids are drawn at 50% probability level.^[15] A representation of **2b** with its complete ligands is shown in the inset.

The Fe–N distances lie between 1.983(2) and 2.006(2) Å in **2a** and between 1.982(2) and 1.990(2) Å in **2b**. The distances of Fe and the coordinating phosphorus atoms are in the range of 2.4559(6) and 2.5006(6) Å in **2a** and 2.4583(3) and 2.4807(5) Å in **2b**, respectively.

No signals were detected in the ³¹P{¹H} NMR spectra of **2a,b**. These solutions (**2a** in C₆D₆ and **2b** in [D₈]toluene) are also EPR-silent at room temperature as well as at 10 K,

suggesting a higher spin multiplicity or antiferromagnetically coupled iron centers that result in a non-magnetic (EPR-silent) ground state at low temperature. However, the ¹H NMR spectra of **2a** and **2b** reveal signals in the range from 273 ppm to -29 ppm; thus, indicating a paramagnetic spin state for **2a,b**. The careful analysis of the spectra enabled us to assign all resonances (see the Supporting Information). The effective magnetic moment (μ_{eff}) at room temperature was determined to be 6.79 μ_{B} for **2a** in C₆D₆ and 6.71 μ_{B} for **2b** in [D₈]THF solution (Evans method). These values are well-confirmed by temperature-dependent SQUID measurements in the solid state. Both complexes exhibit a similar magnetic behavior with a strong temperature dependency of their effective magnetic moments over a temperature range between 2 and 300 K. At 2 K, the effective magnetic moments amount to 1.14 μ_{B} (**2a**) and 0.54 μ_{B} (**2b**). With increasing temperature, the magnetic moments gradually increase until effective magnetic moments of 7.04 μ_{B} (**2a**) and 6.92 μ_{B} (**2b**) are reached at 300 K (see the Supporting Information). This magnetic behavior is likely caused by an antiferromagnetic coupling. The zero-field ⁵⁷Fe Mössbauer spectrum of **2b** at 77 K shows a doublet with an isomer shift δ of 0.73(1) mm·s⁻¹ and a quadrupole splitting ΔE_{Q} of 1.93(1) mm·s⁻¹, which is in agreement with a high-spin iron(II) complex. Similar Mössbauer parameters have been observed in the four-coordinate iron(II) complex [PhB(MesIm)₃Fe(N=PPh₃)].^[11] The presence of iron(II) centers in **2b** is also indicated by NPA analysis.

So far, we assume that the aromatic dmp substituents at the coordinating N atoms of the ligand play a crucial role for the formation of the P₈ ligand moieties in **2a** and **2b**, and the α -substituent of the ligand backbone does not have much influence on the outcome of P₄ activation. Regardless, to conclusively address this point, the ligand L³H was synthesized (Scheme 1). While L³ features aromatic dmp groups at the coordinating N atoms (like L⁰), its ligand backbone is substituted with two Me α -substituents (like L¹); and hence, represents the missing hybrid ligand between L⁰ and L¹. Owing to steric reasons, the Me substituents at the ligand backbone are restricting the rotational flexibility of the *i*Pr groups in dmp, thus increasing their steric pressure.^[12]

The reaction of **1c** with 0.5 equivalent of P₄ in toluene at room temperature leads to the formation of [(L³Fe)₂(μ - η^4 : η^4 -P₄)] (**2c**), containing a *cyclo*-P₄ moiety. Again, changing the stoichiometry of the reaction does not have an effect on the product formation ([L³Fe(tol)]/P₄ = 2:1 and 1:2). Different from our experience with the complexes of the dmp containing ligands L¹ and L², we now obtain a *cyclo*-P₄ unit in the product **2c**, which is also in contrast to Driess' product **A**, featuring two separated P₂ units (Scheme 1).

Single crystals of **2c** suitable for X-ray diffraction were grown from a saturated toluene solution (Figure 3).

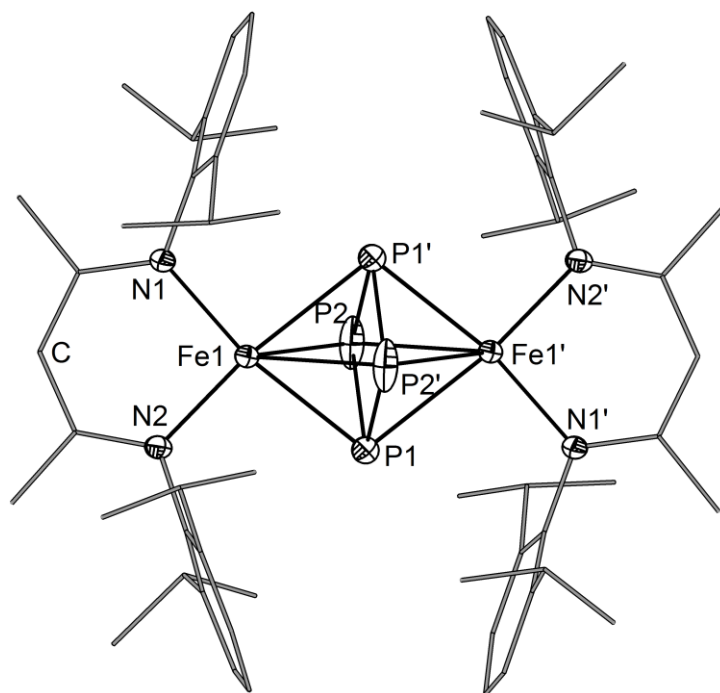


Figure 3. Molecular structure of **2c** in the crystal. Hydrogen atoms are omitted for clarity. Thermal ellipsoids are drawn at 50% probability level.^[15] Selected bond lengths [Å] and angles [°]: P1–P2 2.178(1), P1–P2' 2.207(1), Fe1–P1 2.4376(6), Fe1–P2 2.5064(6), Fe1–P1' 2.5163(6), Fe1–P2' 2.5064(6), Fe1–N1 2.018(2), Fe1–N2 2.025(2), Fe1–Fe1' 3.902, P2'–P1–P2 91.73(3), P1–P2–P1' 88.27(3).

Compound **2c** is a centrosymmetric dinuclear iron complex that consists of two [L³Fe] fragments bridged by a planar *cyclo*-P₄ ligand. The middle deck displays weak disorder (occupancy 97:3; see the Supporting Information). In the following, only the major component of the middle deck is discussed. The P–P distances within the central P₄ moiety (P1–P2 and P1–P2') in **2c** amount to 2.178(1) and 2.207(1) Å, respectively. These distances are longer than those reported for *cyclo*-[P₄]²⁻ ligands (2.146(1)–2.1484(9) Å)^[13] and shorter than those reported for *cyclo*-[P₄]⁴⁻ moieties (2.230(2)–2.259(2) Å).^[14] The angles of P2'–P1–P2 and P1–P2–P1' are 91.73(3)° and 88.27(3)°, respectively, indicating a slightly distorted ring conformation. The Fe–P distances are between 2.4376(6) and 2.5163(6) Å, comparable to those observed in **2a** and **2b**. Similarly, the Fe–N distances in **2c** (2.018(2) and 2.025(2) Å) are comparable to **A** (2.023(3) and 2.025(3) Å),^[4a] but slightly elongated compared to **2a** (1.983(2) and 2.006(2) Å) and **2b** (1.982(2) and 1.990(2) Å). The Fe1–Fe1' distance in **2c** is 3.902 Å, being significantly elongated compared to compound **A** (2.777 Å). One of the most remarkable differences between **2c** and **A** is the angle Θ between the Fe–Fe axis and the plane formed by the nitrogen atoms and the methine carbon atom in the ligand backbone, which is considerably smaller in **2c** (15°) compared to **A** (33°; Figure 4).

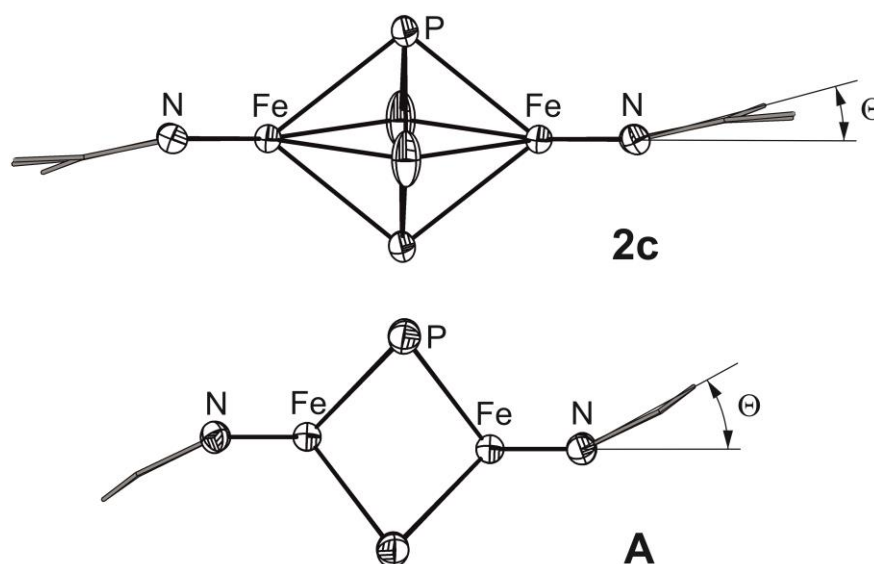


Figure 4. Comparison of the coordination geometry in **2c** and **A**^[4a].

Like in the tetranuclear complexes **2a,b**, no resonances were detected in the ³¹P{¹H} NMR spectra of **2c** and solutions of **2c** are EPR-silent at room temperature and at 10 K. However, the ¹H NMR spectra of **2c** in [D₈]THF reveals signals in the range from 7 ppm to -2 ppm. The magnetic moment of **2c** in [D₈]THF at room temperature was determined to be 3.09 μ_B (Evans method). Temperature-dependent SQUID measurements in the solid state are in agreement with this result with an effective magnetic moment of 3.46 μ_B at 300 K. The magnetism of complex **2c** is strongly temperature-dependent. At 2 K, the effective magnetic moment was determined to be 0.54 μ_B, and is rising to 1.00 μ_B at 20 K. Between 20 and 80 K, it remains roughly constant. Increasing the temperature to 300 K leads to a gradual increase of the effective magnetic moment up to a value of 3.46 μ_B at 300 K (see the Supporting Information). This magnetic behavior is explained by a S_{tot} = 0 ground state between 0 and 80 K and antiferromagnetic coupling of the two iron nuclei at higher temperatures. The zero-field ⁵⁷Fe Mössbauer spectrum of **2c** at 77 K features a doublet with an isomer shift δ of 0.74(1) mm·s⁻¹ and a quadrupole splitting ΔE_Q of 1.74(1) mm·s⁻¹, which is very similar to the Mössbauer parameters of **2b** and is in accordance with a high-spin iron(II) complex.

The optimized geometry of **2c** in the quintet spin state obtained from DFT calculations (BPW91/def2-SVP) is in good agreement with the experimentally found geometric parameters, with a slightly shorter Fe–Fe distance (3.827 Å) and slightly longer P–P distances (2.203–2.250 Å).^[15] Notably, the geometry optimization in the unrestricted singlet spin state instead leads to further shortening of the Fe–Fe distance (3.712 Å) and to a planar P₄ ring with two shorter and two longer P–P distances (2.181 Å and 2.325 Å, respectively). Since the Fe–Fe distance in **A** (2.777 Å) is significantly shorter than in **2c**,

the geometry of **2c** (quintet spin state) was optimized with a fixed Fe–Fe distance of 2.777 Å. In the optimized geometry, the *cyclo*-P₄ unit is cleaved into two P₂ units and the nacnac ligand shows the same type of folding like the one reported for **A**. The energy difference between both isomers is 29.19 kJ·mol⁻¹, favoring the relaxed geometry of **2c**. This points towards a flat energy surface and suggests that the outcome of the P₄ transformation is mostly determined by the Fe–Fe distance. Broken symmetry calculations (BPW91//def2-SVP/aug-cc-pVTZ (Fe, P)) indicate an antiferromagnetic coupling between the two Fe centers, which increases with the decrease of the Fe–Fe distance.^[15] The Mulliken population analysis for the quintet spin state of **2c** shows that the spin density is localized on iron atoms, but no considerable spin density was found on the P₄ or nacnac ligands. The Mayer bond order for the P–P bonds vary from 0.81 to 0.87; thus, indicating P–P single bonds.

4.3 Conclusion

In conclusion, we have shown that the different reactivity of β -diiminato Fe^I complexes [LFe(tol)] (L = L¹ (**1a**), L² (**1b**), L³ (**1c**)) towards P₄ is sensitive to minimal changes in the ligand: its flanking groups (Ph*), and its backbone α -substituents (R). By conducting the reactions under similar conditions (r.t.) in the same solvent (toluene), and irrespective of using exact stoichiometric amounts of P₄ ([LFe(tol)]/P₄ = 2:1) or even larger amounts of P₄ ([LFe(tol)]/P₄ = 1:2), a different outcome of P₄ activation is realized. By employing the aromatic dmp flanking groups as substituents of the coordinating N atoms, the formation of a [P₈]⁴⁻ structural motif in the iron(II) compounds [(LFe)₄(μ_4 - η^1 : η^1 : η^1 : η^1 : η^1 : η^1 : η^1 : η^1 -P₈)] (L = L¹ (**2a**), L² (**2b**)) is observed.^[7b] Employing the sterically more demanding dipp substituents leads to the formation of an iron(II) compound [(L³Fe)₂(μ - η^4 : η^4 -P₄)] (**2c**), containing a *cyclo*-[P₄]²⁻ moiety. This finding is in contrast to the formation of two separate [P₂]²⁻ units observed in the iron(III) complex **A**, with two H α -substituents being located in the ligand backbone instead of Me atoms in **2c**. This demonstrates the additional steric influence of the Me groups as α -substituents to push the dipp substituents closer together, thereby preventing the opening of the *cyclo*-P₄ ring by relaxing the Fe...Fe distance in **2c** in comparison with the rather short distance in **A**. The discussed ligand dependencies in the β -diiminato ligand complexes may foster the systematic study of such dependencies in other metal systems for the activation of small molecules in general and in particular for the controlled P_n ligand formation from white phosphorus.

4.4 References

- [1] a) M. Scheer, G. Balázs, A. Seitz, *Chem. Rev.* **2010**, *110*, 4236-4256; b) S. Khan, S. S. Sen, H. W. Roesky, *Chem. Commun.* **2012**, *48*, 2169-2179; c) N. A. Giffin, J. D. Masuda, *Coord. Chem. Rev.* **2011**, *255*, 1342-1359.
- [2] a) B. M. Cossairt, N. A. Piro, C. C. Cummins, *Chem. Rev.* **2010**, *110*, 4164-4177; b) M. Caporali, L. Gonsalvi, A. Rossin, M. Peruzzini, *Chem. Rev.* **2010**, *110*, 4178-4235.
- [3] a) B. L. Tran, M. Singhal, H. Park, O. P. Lam, M. Pink, J. Krzystek, A. Ozarowski, J. Telser, K. Meyer, D. J. Mindiola, *Angew. Chem. Int. Ed.* **2010**, *49*, 9871-9875; *Angew. Chem.* **2010**, *122*, 10067-10071; b) C. Camp, L. Maron, R. G. Bergman, J. Arnold, *J. Am. Chem. Soc.* **2014**, *136*, 17652-17661; c) B. Pintér, K. T. Smith, M. Kamitani, E. M. Zolnhofer, B. L. Tran, S. Fortier, M. Pink, G. Wu, B. C. Manor, K. Meyer, M.-H. Baik, D. J. Mindiola, *J. Am. Chem. Soc.*, **2015**, *137*, 15247-15261.
- [4] a) S. Yao, T. Szilvasi, N. Lindenmaier, Y. Xiong, S. Inoue, M. Adelhardt, J. Sutter, K. Meyer, M. Driess, *Chem. Commun.* **2015**, *51*, 6153-6156; b) S. Yao, N. Lindenmaier, Y. Xiong, S. Inoue, T. Szilvási, M. Adelhardt, J. Sutter, K. Meyer, M. Driess, *Angew. Chem.* **2015**, *127*, 1266-1270; c) S. Yao, Y. Xiong, C. Milsmann, E. Bill, S. Pfirrmann, C. Limberg, M. Driess, *Chem. Eur. J.* **2010**, *16*, 436-439.
- [5] F. Spitzer, M. Sierka, M. Latronico, P. Mastroilli, A. V. Virovets, M. Scheer, *Angew. Chem. Int. Ed.* **2015**, *54*, 4392-4396; *Angew. Chem.* **2015**, *127*, 4467-4472.
- [6] The term "realgar-type" P₈ moiety for the tricyclo[3.3.0.0^{3,7}]octaphosphane ligand comes from its analogy to the isostructural realgar (As₄S₄) molecule.
- [7] a) For **2a,b,c** calculated at the BP86/def2-SVP level. The NPA charges for **A** were taken from Ref. [4a]. It should be noted that different basis sets were used. b) For the relationship of the formal oxidation states and the spectroscopic and structural parameters (see the Supporting Information, Table S3).
- [8] B. M. Cossairt, C. C. Cummins, A. R. Head, D. L. Lichtenberger, R. J. F. Berger, S. A. Hayes, N. W. Mitzel, G. Wu, *J. Am. Chem. Soc.* **2010**, *132*, 8459-8465.
- [9] N. J. Brassington, H. G. M. Edwards, D. A. Long, *J. Raman Spectrosc.* **1981**, *11*, 346-348.
- [10] a) S. N. Konchenko, N. A. Pushkarevsky, M. T. Gamer, R. Köppe, H. Schnöckel, P. W. Roesky, *J. Am. Chem. Soc.* **2009**, *131*, 5740-5741; b) W. Huang, P. L. Diaconescu, *Chem. Commun.* **2012**, *48*, 2216-2218; c) M. E. Barr, B. R. Adams, R. R. Weller, L. F. Dahl, *J. Am. Chem. Soc.* **1991**, *113*, 3052-3060; d) M. Scheer, U. Becker, E. Matern, *Chem. Ber.* **1996**, *129*, 721-724; for structurally similar As₈ complexes, see: C. Schwarzmaier, A. Y. Timoshkin, G. Balázs, M. Scheer, *Angew. Chem. Int. Ed.* **2014**, *53*, 9077-9081; *Angew. Chem.* **2014**, *126*, 9223-9227.
- [11] J. J. Scepaniak, T. D. Harris, C. S. Vogel, J. Sutter, K. Meyer, J. M. Smith, *J. Am. Chem. Soc.* **2011**, *133*, 3824-3827.
- [12] D. J. E. Spencer, A. M. Reynolds, P. L. Holland, B. A. Jazdzewski, C. Duboc-Toia, L. Le Pape, S. Yokota, Y. Tachi, S. Itoh, W. B. Tolman, *Inorg. Chem.* **2002**, *41*, 6307-6321.
- [13] F. Kraus, J. C. Aschenbrenner, N. Korber, *Angew. Chem. Int. Ed.* **2003**, *42*, 4030-4033; *Angew. Chem.* **2003**, *115*, 4162-4165.
- [14] A. Velian, C. C. Cummins, *Chem. Sci.* **2012**, *3*, 1003-1006.
- [15] See the Supporting Information.

4.5 Supporting Information

General Remarks

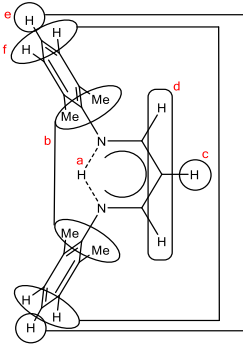
All manipulations were performed with rigorous exclusion of oxygen and moisture using Schlenk-type glassware on a dual manifold Schlenk line with Argon inert gas or glove box filled with N₂ containing a high-capacity recirculator (<0.1 ppm O₂). Solvents were dried using a MB SPS-800 device of company MBRAUN, degassed and saturated with argon to prevent N₂ activation while reduction reactions. Mass spectrometry was performed using an Agilent Q-TOF 6540 UHD (ESI-MS), Finnigan MAT 95 (LIFDI) and JEOL AccuTOF GCX (LIFDI) mass spectrometer, respectively. Elemental analysis (CHN) was determined using a Vario micro cube and Vario EL III instrument.

Fe(II) chloride, anhydrous; 98% was purchased by ABCR and used without further purification. Ligands **L¹H**^[1] and **L³H**^[2] were synthesized following the literature-known routes.

Synthesis of **L²H**

L²H was prepared using the standard β-diimine ligand preparation except that 1,1,3,3-tetramethoxypropane was used instead of 2,4-pentandione as starting material.^[2b] **L²H** was crystallized from THF.

Analytical data:

<p>NMR of L²H (C₆D₆, 300 K)</p> 	<p>¹H: δ [ppm] = 11.42 (1H, broad s, a), 7.05 (2H, d, ³J_{HH} = 6 Hz, d), 6.97 (4H, d, ³J_{HH} = 7 Hz, f), 6.91 (2H, dd, ³J_{HH} = 6 Hz, ³J_{HH} = 9 Hz, e), 4.79 (1H, t, ³J_{HH} = 6 Hz, c), 2.17 (12H, s, b).</p> <p>¹³C: δ [ppm] = 154.0 (C_α), 146.4 (C_{ipso}), 130.2 (C_o), 128.7 (C_m), 124.4 (C_p), 92.4 (C_β), 18.8 (2,6-Me-Ar).</p>
<p>Mass spectrometry (ESI-MS)</p>	<p>m/z: 279.19 (100%) [M+H]⁺.</p>

Synthesis of [**L¹Fe(tol)**] (**1a**)

Compound **1a** was prepared analogously to the literature method,^[3] beside that [**L¹FeBr**]₂ was used instead of [**L¹Co**](2,4-lutidine).

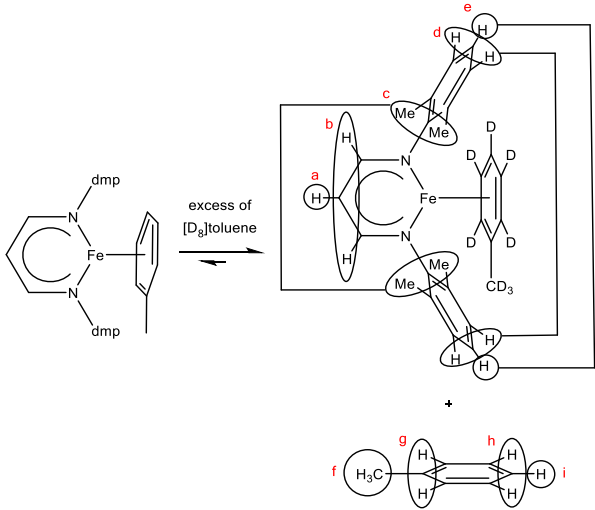
Synthesis of [**L²Fe(tol)**] (**1b**)

A yellow slurry of 6.68 g (24.0 mmol) **L²H** in 100 mL THF was treated with a solution of 15 mL (24.0 mmol) *n*-BuLi (1.6 M) in *n*-hexane. The formed clear red solution was stirred at r.t. for 1 hour. Within 1.5 hours the solution was slowly transferred into a slurry of 3.04 g (24.0 mmol) anhydrous FeCl₂ in 5 mL THF, forming an intense dark yellow solution, which was stirred at r.t. for 12 hours. After removal of solvent, the brownish solid was dissolved in 50 mL of toluene. The intense dark yellow solution was transferred into a slurry of 1.05 equivalents of potassium graphite in 10 mL toluene. The mixture was stirred at r.t. for 98 hours and a color change to olive green was observed. Remaining graphite and salts were removed by filtration of the olive green solution over celite. The solvent was removed in vacuum and a dark green brown solid was obtained. The solid was

dissolved in 100 mL *n*-hexane and the solution was filtered over celite. After concentration of the solution to a volume of ca. 20 mL, the intense green solution was stored at 5 °C for several hours and then at –15 °C for one night to yield 2.36 g of dark green crystalline blocks.

Crystalline yield: 2.36 g (5.55 mmol, 23%).

Analytical data:

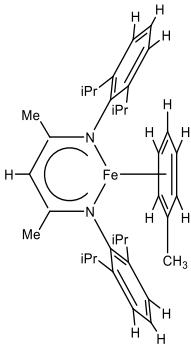
<p>NMR of 1b ([D₈]toluene, 298 K)</p> 	<p>¹H: δ [ppm] = 512.9 (2H, s, b), 487.6 (1H, s, a), 10.9 (4H, s, d), 9.8 (2H, s, e), 7.76 and 7.65 (ca. 5H, s, g/h/i), 2.78 (3H, s, f), 1.9 (12H, broad s, c).</p> <p>¹H NMR spectrum is shown in Figure S11 (vide infra).</p> <p>Note: An accurate signal integration is possible in the ¹H NMR spectra only with spectral width of 240 ppm or less. Therefore, we could not compare the integral ratio of the signals at δ = 512.9 and 487.6 ppm with the rest of the signals.</p>
<p>Evans-NMR ([D₈]toluene solution)</p>	<p>μ_{eff} = 2.01 μ_B (298 K)</p>
<p>Elemental analysis (C₂₆H₂₉FeN₂)</p>	<p>Calculated: C 73.41, H 6.87, N 6.59. Found: C 72.78, H 6.61, N 6.63.</p>
<p>Mass spectrometry (LIFDI, toluene)</p>	<p>m/z: 610.30 (24%) [(L²)₂Fe]⁺, 425.18 (100%) [M]⁺.</p>

Synthesis of [L³Fe(tol)] · 0.25 *n*-hexane (**1c**)

To a cooled (0 °C) solution of 6.03 g (14.4 mmol) **L³H** in 40 mL THF a solution of 9 mL (14.4 mmol) *n*-BuLi (1.6 M) in *n*-hexane was added. The solution was stirred for 3.5 hours and allowed to warm up to room temperature. Within 10 minutes the clear intense yellow solution was slowly added to a slurry of 1.83 g (14.5 mmol) anhydrous FeCl₂ in 20 mL THF. A color change to intense dark yellow occurred and the reaction mixture was stirred for 17.5 hours. After removal of the solvent, the dark yellow solid was dissolved in 45 mL toluene. The intense dark yellow solution was added to a slurry of 1.05 equivalents potassium graphite in 10 mL toluene. The mixture was stirred at r.t. for 48 hours. Remaining graphite and salts were removed by filtration over celite. The solvent was removed in vacuum and the resulting dark brown solid was dissolved in 65 mL *n*-hexane, filtered over celite and stored at 5 °C for 3 days to yield 3.01 g of black crystals. The supernatant solution was concentrated and 1.20 g of a second crystalline crop was obtained.

Crystalline yield: 4.21 g (7.45 mmol, 52%).

Analytical data:

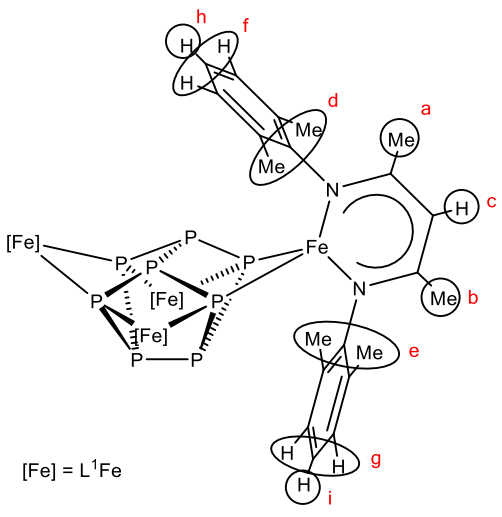
<p>NMR of 1c ([D₈]toluene, 300 K)</p> 	<p>Despite ¹H spectra were measured from 1100 ppm to -1100 ppm, only three very broad signals could be detected. This might be due to line broadening caused by the paramagnetic nature of 1c.</p> <p>¹H NMR spectrum is shown in Figure S12 (vide infra).</p>
<p>Evans-NMR ([D₈]toluene solution)</p>	<p>$\mu_{\text{eff}} = 1.89 \mu_{\text{B}}$ (300 K)</p>
<p>Elemental analysis (C₃₆H₄₉FeN₂)</p>	<p>Calculated: C 76.44, H 8.73, N 4.95. Found: C 76.24, H 8.79, N 4.83.</p>
<p>Mass spectrometry (LIFDI, toluene)</p>	<p>m/z: 565.34 (100%) [M]⁺.</p>

Synthesis of [(L¹Fe)₄(μ₄-η¹:η¹:η¹:η¹:η¹:η¹:η¹-P₈)] (**2a**)^[4]

506 mg (4.0 mmol, 2 equivalents) of P₄ were dissolved in 20 mL toluene. The solution was added to an intense reddish brown solution of 943 mg (2.0 mmol, 1 equivalent) of **1a** in 50 mL toluene. Within 1 hour, a color change to red was observed. After 16 hours, the solvent was concentrated and the solution was filtered over celite. Within 1 day red crystals were obtained by storing saturated solutions at 8 °C.

Crystalline yield: 50 mg (0.03 mmol, 6%).^[4]

Analytical data:^[4]

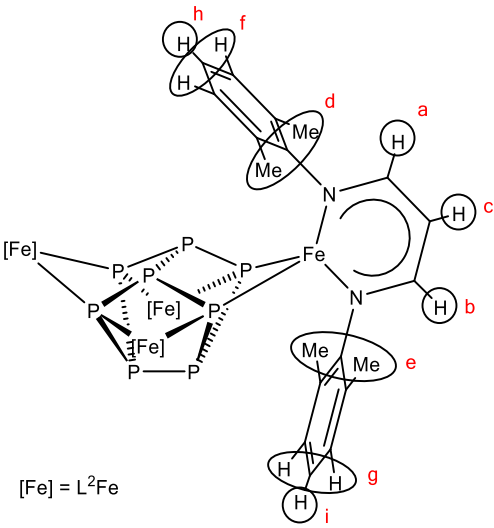
<p>NMR of 2a ([D₈]THF, 300 K)</p>  <p>[Fe] = L¹Fe</p>	<p>¹H: δ [ppm] = 11.4 (8H, s, f/g), 3.9 (8H, s, f/g), -4.4 (4H, s, c/h/i), -5.0 (24H, s, d/e), -20.9 (12H, s, a/b), -21.6 (4H, s, c/h/i), -23.1 (24H, s, d/e), -26.1 (4H, s, c/h/i), -28.7 (12H, s, a/b).^[5]</p> <p>³¹P{¹H}: No signal could be detected between 1200 to -1200 ppm.</p> <p>¹H NMR spectrum is shown in Figure S13 (vide infra).</p>
<p>Evans-NMR (C₆D₆ solution)</p>	<p>$\mu_{\text{eff}} = 6.79 \mu_{\text{B}}$ (300 K)^[5]</p>
<p>VT SQUID</p>	<p>$\chi_{\text{dia}} = 11.11 \cdot 10^{-4} \text{ cm}^3 \cdot \text{mol}^{-1}$ $\mu_{\text{eff}} = 7.04 \mu_{\text{B}}$ (300 K)</p>
<p>Elemental analysis (C₉₁H₁₀₈Fe₄N₈P₈)</p>	<p>Calculated: C 61.23, H 6.10, N 6.28. Found: C 61.42, H 6.28, N 6.59.^[4]</p>
<p>Mass spectrometry (LIFDI, toluene)</p>	<p>m/z: 1692.7 (100%) [M]⁺.^[4]</p>

Synthesis of [(L²Fe)₄(μ₄-η¹:η¹:η¹:η¹-P₈)] (2b)

44 mg (0.35 mmol, 0.5 equivalents) of P₄ were dissolved in 12 mL toluene. Within 15 minutes at r.t., the solution was added to an intense dark green solution of 300 mg (0.71 mmol, 1 equivalent) **1b** in 15 mL toluene. After 30 minutes the solution has changes color from olive green to dark brown. After stirring at r.t. for 20 hours, the brown reaction solution was filtered over celite and the solvent was concentrated to a volume of 5 mL. Several crops of crystalline brown blocks were obtained by cooling the concentrated solution to 5 °C.

Crystalline yield: 185.8 mg (0.12 mmol, 67%).

Analytical data:

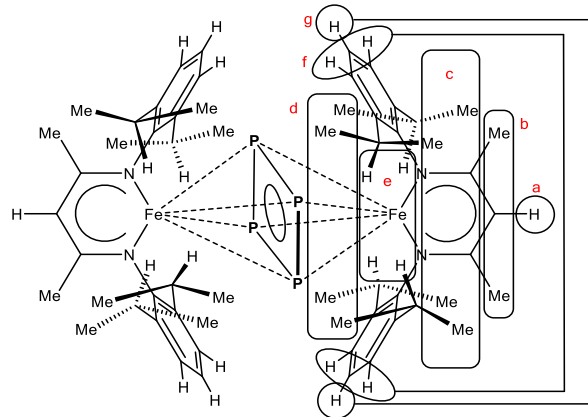
<p>NMR of 2b ([D₈]toluene, 300 K)</p>  <p>[Fe] = L²Fe</p>	<p>¹H: δ [ppm] = 273.1 (4H, s, a/b), 251.5 (4H, s, a/b), 12.3 (8H, broad s, f/g), 5.6 (8H, broad s, f/g), -5.0 (24H, s, d/e), -12.9 (4H, s, c/h/i), -14.8 (4H, s, c/h/i), -19.2 (4H, s, c/h/i), -19.3 (24H, s, d/e).</p> <p>³¹P{¹H}: No signal could be detected between 1200 to -1200 ppm.</p> <p>¹H NMR spectrum is shown in Figure S14 (vide infra).</p> <p>Note: An accurate signal integration is possible in ¹H NMR spectra only with spectral width of 240 ppm or less. Therefore, we could not compare the integral ratio of the signals at δ = 273.1 and 251.5 ppm with the rest of the signals.</p>
<p>Evans-NMR ([D₈]THF solution)</p>	<p>μ_{eff} = 6.71 μ_B (300 K)</p>
<p>VT SQUID</p>	<p>χ_{dia} = 10.16 · 10⁻⁴ cm³ · mol⁻¹</p> <p>μ_{eff} = 6.92 μ_B (300 K)</p>
<p>Zero-field Mössbauer</p>	<p>δ = 0.73(1) mm · s⁻¹, ΔE_Q = 1.93(1) mm · s⁻¹</p>
<p>Elemental analysis (C₇₆H₈₄Fe₄N₈P₈)</p>	<p>Calculated: C 57.75, H 5.36, N 7.09.</p> <p>Found: C 57.85, H 5.22, N 6.53.</p>
<p>Mass spectrometry (LIFDI, toluene)</p>	<p>m/z: 1580.13 (100%) [M]⁺, 278.17 (24%) [L²H]⁺.</p>

Synthesis of [(L³Fe)₂(μ-η⁴:η⁴-P₄)] (2c)

33 mg (0.27 mmol, 0.5 equivalents) of P₄ were dissolved in 10 mL toluene. Within 8 minutes at r.t. this solution was added to an intense reddish brown solution of 300 mg (0.53 mmol, 1 equivalent) **1c** in 15 mL toluene. After stirring at r.t. for 18 hours, the brown reaction solution was filtered over celite and the solvent was removed in vacuum to obtain a brown microcrystalline product, which was washed with 10 mL *n*-hexane and dried.

Microcrystalline yield: 176.2 mg (0.17 mmol, 62%).

Analytical data:

<p>NMR of 2c ([D₈]THF, 300 K)</p> 	<p>¹H: δ [ppm] = 6.7 (8H, d, ³J_{HH} = 7 Hz, f), 6.5 (12H, s, b), 2.3 (4H, t, ³J_{HH} = 7 Hz, g), 2.1 (24H, s, c/d), 0.7 (2H, s, a), -0.6 (8H, broad s, e), -2.0 (24H, s, c/d).</p> <p>³¹P{¹H}: No signal could be detected between 1200 to -1200 ppm.</p> <p>¹H NMR spectrum is shown in Figure S15 (vide infra).</p>
<p>Evans-NMR ([D₈]THF solution) double determination: $\mu_{\text{eff},1} = 2.97 \mu_{\text{B}}$ $\mu_{\text{eff},2} = 3.20 \mu_{\text{B}}$</p>	<p>$\mu_{\text{eff}} = 3.09 \mu_{\text{B}}$ (300 K)</p>
<p>VT SQUID</p>	<p>$\chi_{\text{dia}} = 7.45 \cdot 10^{-4} \text{ cm}^3 \cdot \text{mol}^{-1}$ $\mu_{\text{eff}} = 3.46 \mu_{\text{B}}$ (300 K)</p>
<p>Zero-field Mössbauer</p>	<p>$\delta = 0.74(1) \text{ mm} \cdot \text{s}^{-1}$, $\Delta E_{\text{Q}} = 1.74(1) \text{ mm} \cdot \text{s}^{-1}$</p>
<p>Elemental analysis (C₅₈H₈₂Fe₂N₄P₄)</p>	<p>Calculated: C 65.05, H 7.72, N 5.23. Found: C 65.08, H 7.56, N 5.23.</p>
<p>Mass spectrometry (LIFDI, toluene)</p>	<p>m/z: 1070.49 (100%) [M]⁺, 1039.52 (22%) [M-P]⁺, 1008.54 (23%) [M-P₂]⁺, 566.22 (4%) [L³FeP₃]⁺, 535.26 (10%) [L³FeP₂]⁺, 473.29 (7%) [L³Fe]⁺, 418.37 (22%) [L³]⁺.</p>

Crystallographic Details

Single crystal structure analyses were performed using Agilent Technologies diffractometer (GV1000, Titan^{S2} diffractometer (**1b**), Xcalibur, Atlas^{S2}, Gemini Ultra diffractometer (**1c**, **2b**), SuperNova, Single source at offset, Atlas diffractometer (**2a**), SuperNova, Single source at offset, Eos diffractometer (**2c**). Data reduction was performed with the CrysAlisPro^[6] software package. Using the software Olex2^[7] the structure solution was carried out using the programs ShelXT^[8] (Sheldrick, 2015) (**1a**, **1b**, **2b**, **2c**) and SIR2004^[9] (**2a**). Least squares refinements on F_o² were performed using SHELXL-2014 (**1b**, **1c**, **2a**, **2b**, **2c**).^[10] Further details are given in Table S2.

X-ray Diffraction on Crystals of **2c**

In **2c** one disordered methyl group was refined to a chemical occupancy 68:32. Additionally the slightly disordered *cyclo*-P₄ middle deck was refined to a chemical occupancy of 97:3. Due to the low electron density of the minor component two geometrical restraints (DFIX, SIMU) were used in case of the minor component (3% occupation).

Table S1. Comparison of geometrical details of major and minor *cyclo*-P₄ component in **2c**.

	major component (97%)	minor component (3%)
$d(\text{P1-P2}), d(\text{P1-P2}') / [\text{\AA}]$	2.178(1), 2.207(1)	2.18(1) \AA (DFIX), 2.25(3)
$d(\text{Fe1-P1}), d(\text{Fe1-P2}),$ $d(\text{Fe1-P1}'), d(\text{Fe1-P2}') / [\text{\AA}]$	2.4376(6), 2.5064(6), 2.5064(6), 2.5163(6)	2.43(2), 2.50(2), 2.55(2), 2.52(2)
$\sphericalangle(\text{P2}'\text{-P1-P2}), \sphericalangle(\text{P1-P2-P1}') / [^\circ]$	88.27(3), 91.73(3)	87(1), 94(1)

Molecular structures of compounds **1b**, **1c** and **2a** are shown in Figures S1–S3. Molecular structures of compounds **2b** and **2c** are shown in main part of the publication.

Crystallographic data and details of the diffraction experiments are given in Table S2. CIF files with comprehensive information on the details of the diffraction experiments and full tables of bond lengths and angles for **1** and **2** are deposited in Cambridge Crystallographic Data Centre under the deposition codes CCDC-1435936–1435939 and CCDC-1436088.

Table S2. Crystallographic data and details of diffraction experiments for **1b**, **1c**, **2a**, **2b** and **2c**.

Compound	1b	1c · 0.25 <i>n</i> -hexane	2a · 2 toluene ^[4]	2b · 1 toluene	2c
CCDC	1436088	1435936	1435937	1435938	1435939
Formula	C ₂₆ H ₂₉ FeN ₂	C ₃₆ H ₄₉ FeN ₂	C ₉₈ H ₁₁₆ Fe ₄ N ₈ P ₈	C ₈₃ H ₉₁ Fe ₄ N ₈ P ₈	C ₅₈ H ₈₂ Fe ₂ N ₄ P ₄
$\rho_{calc.}$ / g cm ⁻³	1.297	1.140	1.298	1.352	1.249
μ /mm ⁻¹	5.637	3.837	6.385	7.400	0.661
Formula Weight	425.36	565.62	1877.14	1671.79	1070.85
Color	clear dark green	black	red	clear dark brown	clear dark black
Shape	block	block	block	block	block
Max Size/mm	0.26	0.42	0.32	0.23	0.18
Mid Size/mm	0.23	0.17	0.13	0.13	0.14
Min Size/mm	0.18	0.07	0.07	0.09	0.07
<i>T</i> /K	123(1)	123(1)	123(1)	125(4)	123(1)
Crystal System	orthorhombic	tetragonal	triclinic	monoclinic	monoclinic
Space Group	<i>Pha</i> 2 ₁	<i>I</i> 4 ₁ / <i>a</i>	<i>P</i> 1	<i>C</i> 2/ <i>c</i>	<i>P</i> 2 ₁ / <i>n</i>
<i>a</i> /Å	12.1516(2)	37.7067(4)	13.59902(16)	24.7045(2)	14.2409(3)
<i>b</i> /Å	25.9683(6)	37.7067(4)	14.59579(18)	13.14969(13)	13.5520(3)
<i>c</i> /Å	6.90447(16)	9.27235(14)	25.7434(4)	26.0368(3)	15.2276(3)
α /°	90	90	91.9532(11)	90	90
β /°	90	90	105.1756(12)	103.8325(9)	104.288(2)
γ /°	90	90	102.0298(10)	90	90
<i>V</i> /Å ³	2178.74(8)	13183.4(3)	4801.96(12)	8212.95(14)	2847.91(11)
<i>Z</i>	4	16	2	4	2
<i>Z'</i>	1	1	1	0.5	0.5
Θ_{min} /°	3.404	3.315	3.427	3.685	3.144
Θ_{max} /°	74.165	66.624	73.093	66.647	28.282
Measured Refl.	9794	27919	35623	35496	46308
Independent Refl.	3724	5726	18648	7235	7046
Reflections Used	3614	5491	16595	6664	6142
<i>R</i> _{int}	0.0427	0.0297	0.0304	0.0296	0.0408
Parameters	268	393	1119	479	345
Restraints	1	0	131	0	7
Largest Peak	0.385	0.236	0.733	0.398	0.562
Deepest Hole	-0.342	-0.217	-0.580	-0.249	-0.831
GooF	1.054	1.107	1.022	1.027	1.054
<i>wR</i> ₂ (all data)	0.1073	0.0848	0.1084	0.0625	0.1042
<i>wR</i> ₂	0.1062	0.0779	0.1037	0.0607	0.1001
<i>R</i> ₁ (all data)	0.0393	0.0301	0.0462	0.0298	0.0473
<i>R</i> ₁	0.0382	0.0280	0.0404	0.0260	0.0402
Flack Parameter	-0.003(8)				
Hooft Parameter	0.041(7)				

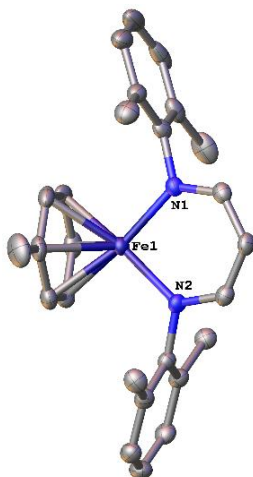


Figure S1. Molecular structure of compound **1b** in the crystal. Hydrogen atoms are omitted for clarity. Thermal ellipsoids are drawn at 50% probability level.

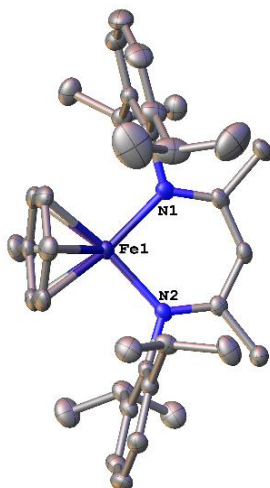


Figure S2. Molecular structure of compound **1b** in the crystal. Hydrogen atoms are omitted for clarity. Thermal ellipsoids are drawn at 50% probability level.

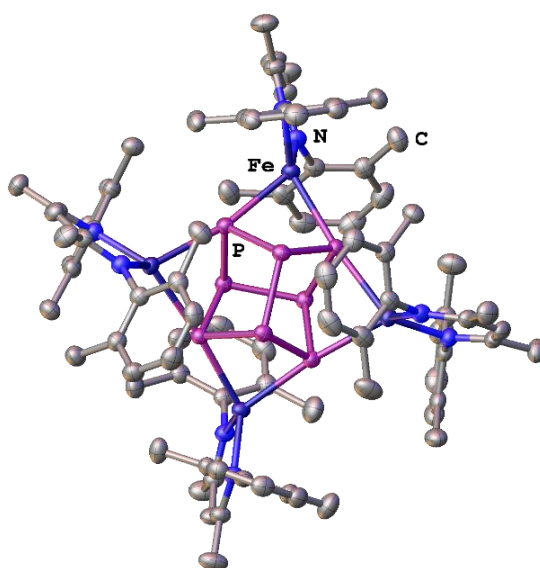


Figure S3.^[4] Molecular structure of compound **2a** in the crystal. Hydrogen atoms and solvent (toluene) molecules are omitted for clarity. Thermal ellipsoids are drawn at 50% probability level.

Magnetic Measurements in Solution (Evans Method)

Magnetic susceptibilities χ_M and effective magnetic moments μ_{eff} of paramagnetic compounds in solution were determined by ¹H NMR spectroscopy using the Evans method^[11] with pure solvent as internal reference and neglecting diamagnetic contributions according to equations^[12] (1) and (2). ¹H NMR spectra were recorded on a Bruker Avance III HD 400 (¹H: 400.130 MHz) spectrometer.

Equations:

$$\chi_M = \frac{3 \cdot \Delta f}{1000 \cdot f \cdot c} \quad (1)$$

$$\mu_{\text{eff}} = 798 \cdot \sqrt{T \cdot \chi_M} \quad (2)$$

Where

χ_M is the molar susceptibility of the sample in $\text{m}^3 \cdot \text{mol}^{-1}$,

Δf is the chemical shift difference between solvent in presence of paramagnetic solute and pure solvent in Hz,

f is the operating frequency of NMR spectrometer in Hz,

c is the concentration of paramagnetic sample in $\text{mol} \cdot \text{L}^{-1}$,

T is the absolute temperature in K, and

μ_{eff} is the effective magnetic moment in μ_B .

SQUID Magnetization Measurements and Mössbauer Spectra

General Remarks

Magnetic data were collected using a Quantum Design MPMS-XL SQUID magnetometer. Measurements were obtained for a finely ground microcrystalline powder (15–30 mg) restrained within a polycarbonate gel capsule. Samples used for magnetization measurement were checked for chemical composition and purity by ¹H NMR spectroscopy. Data reproducibility was checked on independently synthesized samples. Dc susceptibility data were collected in the temperature range 2–300 K under a dc field of 1 T. The data shown refer to the complete tetra- and dinuclear complexes, not mononuclear subunits. The data were corrected for core diamagnetism of the sample estimated using Pascal's constants^[13] ($\chi_{\text{dia}} = 11.11 \cdot 10^{-4} \text{ cm}^3 \cdot \text{mol}^{-1}$ for **2a**, $10.16 \cdot 10^{-4} \text{ cm}^3 \cdot \text{mol}^{-1}$ for **2b**, and $7.451 \cdot 10^{-4} \text{ cm}^3 \cdot \text{mol}^{-1}$ for **2c**). Magnetic susceptibility data was analyzed and simulated using the julX program written by E. Bill (MPI for Chemical Energy Conversion, Mülheim an der Ruhr).

⁵⁷Fe Mössbauer spectra were recorded on a WissEl Mössbauer spectrometer (MRG-500) at 77 K in constant acceleration mode. ⁵⁷Co/Rh was used as the radiation source. WinNormos for Igor Pro software has been used for the quantitative evaluation of the spectral parameters (least-squares fitting to Lorentzian peaks). The minimum experimental line widths were $0.20 \text{ mm} \cdot \text{s}^{-1}$. The temperature of the samples was controlled by an MBBC-HE0106 MÖSSBAUER He/N₂ cryostat within an accuracy of $\pm 0.3 \text{ K}$. Isomer shifts were determined relative to α -iron at 298 K.

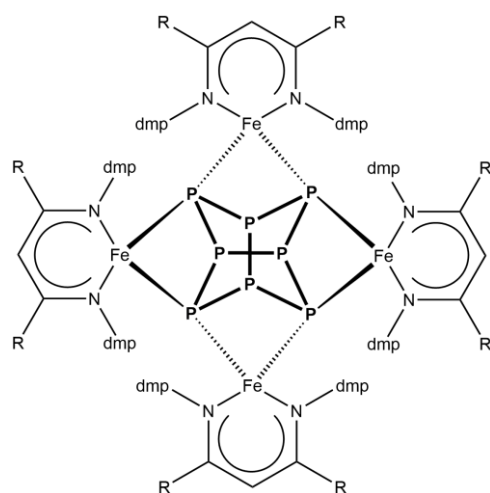


Figure S4. Molecular structure of **2a** (R = Me) and **2b** (R = H).

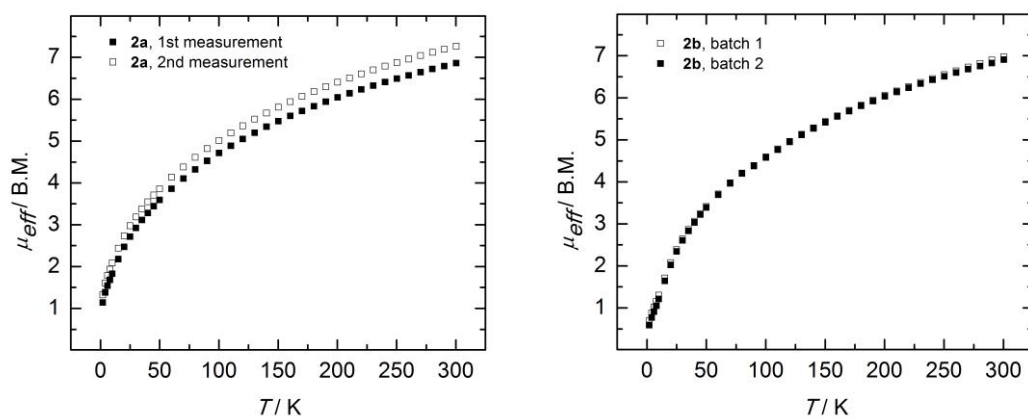


Figure S5. VT SQUID magnetization measurement of compounds **2a** (left) and **2b** (right).

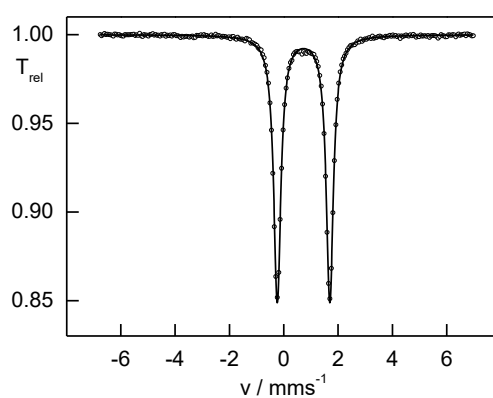
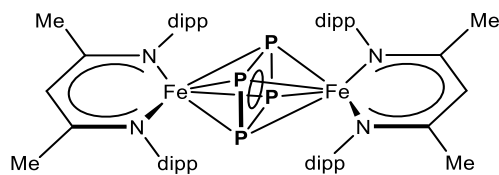
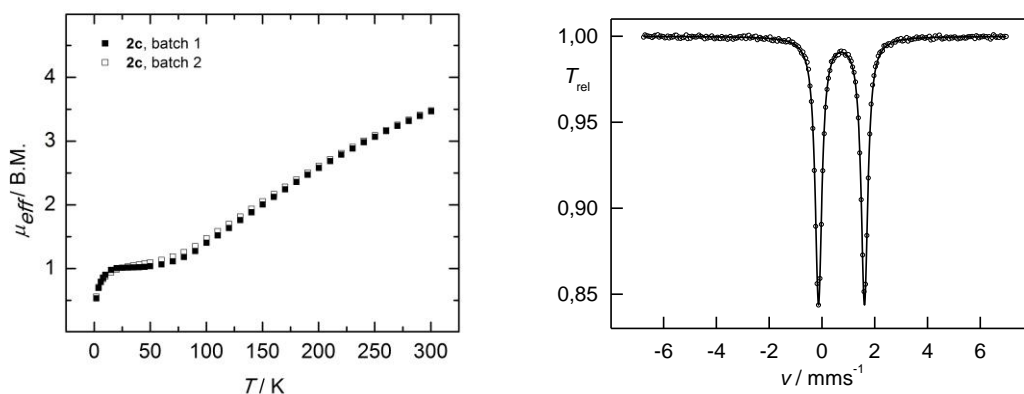


Figure S6. Zero-field ⁵⁷Fe Mössbauer spectrum of compound **2b**.

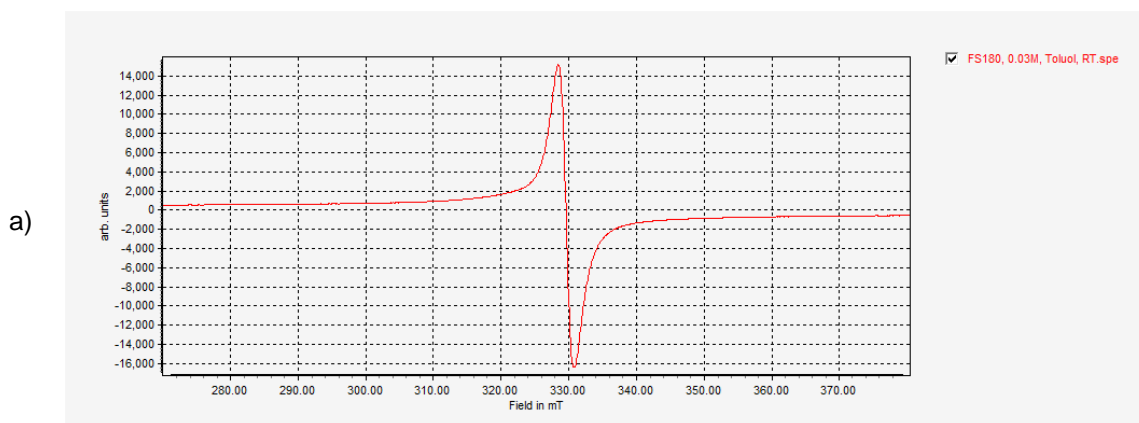
Figure S7. Molecular structure of **2c**.Figure S8. VT SQUID magnetization measurement (left) and zero-field ^{57}Fe Mössbauer spectrum (right) of compound **2c**.

^1H NMR and EPR Spectroscopy

General Remarks

^1H and ^{31}P NMR spectra were recorded on a Bruker Avance III HD 400 (^1H : 400.130 MHz, ^{31}P : 161.976 MHz). The chemical shifts are reported in ppm relative to external TMS (^1H) and H_3PO_4 (^{31}P). The X-band EPR measurements were carried out with a MiniScope MS400 device equipped with a Magnettech GmbH rectangular TE102 resonator at a frequency of 9.5 GHz. The compounds were dissolved in a glovebox under N_2 inert gas atmosphere, placed in tip-sealed pasteur pipettes, and were rubber plugged. The measurements were conducted at room temperature and 77 K, respectively.

EPR spectrum of [$\text{L}^2\text{Fe}(\text{tol})$] (**1b**):



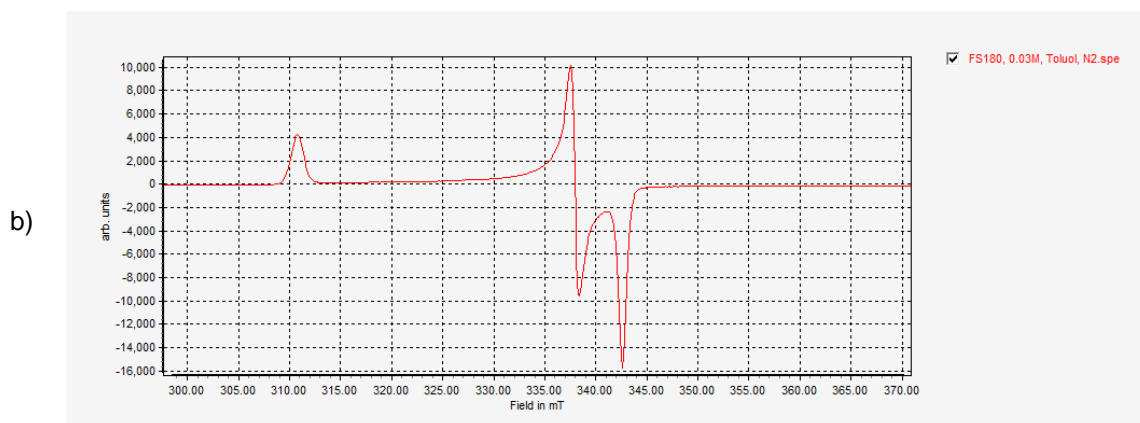


Figure S9. EPR spectrum of [L²Fe(tol)] (**1b**) in toluene (approx. 0.03 M) at r.t. (a): $g = 2.04$, and at 77 K (b): $g = 2.17, 2.00, 1.97$.

EPR spectrum of [L³Fe(tol)] · 0.25 *n*-hexane (**1c**):

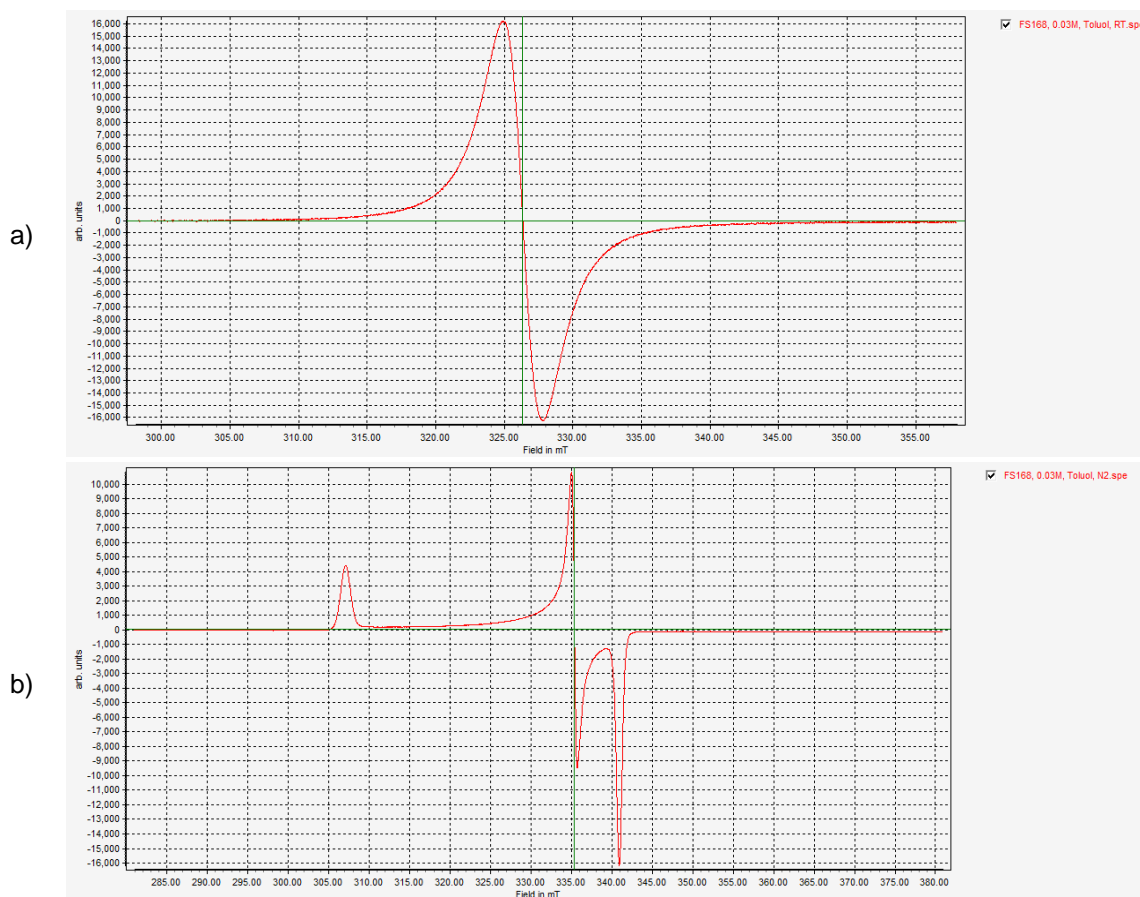


Figure S10. EPR spectrum of [L³Fe(tol)] · 0.25 *n*-hexane (**1c**) in toluene (approx. 0.03 M) at r.t. (a): $g = 2.06$, and at 77 K (b): $g = 2.20, 2.01, 1.98$.

Note: An EPR spectrum of [L³Fe(benzene)] in toluene at 77 K has already been published,^[14] containing identical signals like **1c** in toluene at 77 K.

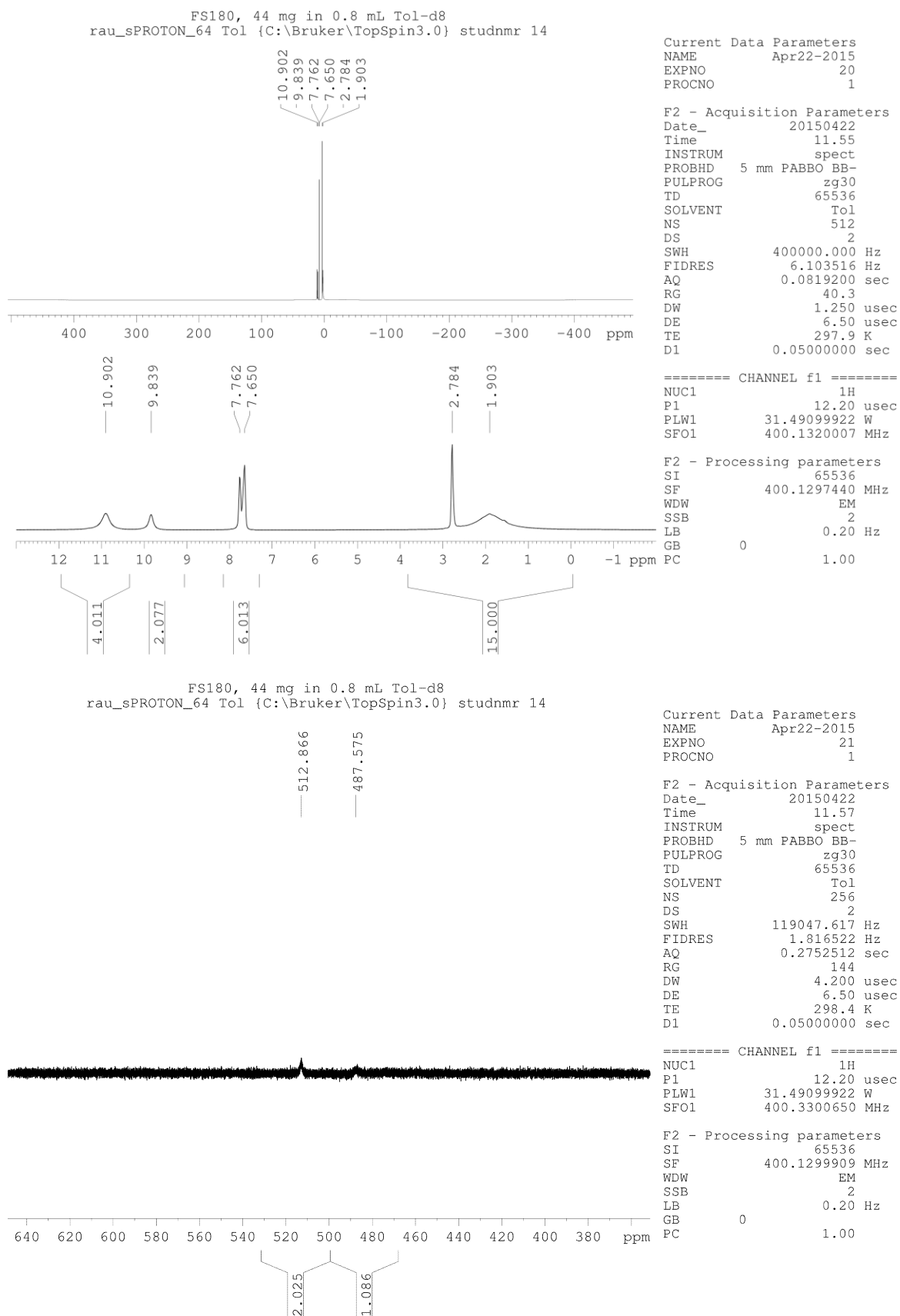
¹H NMR Spectra

Figure S11. ¹H NMR spectra of **1b** in [D₈]toluene. Depicted ranges: 500 to -500 ppm (top); 13 to -2 ppm (middle); 650 to 350 ppm (btom).

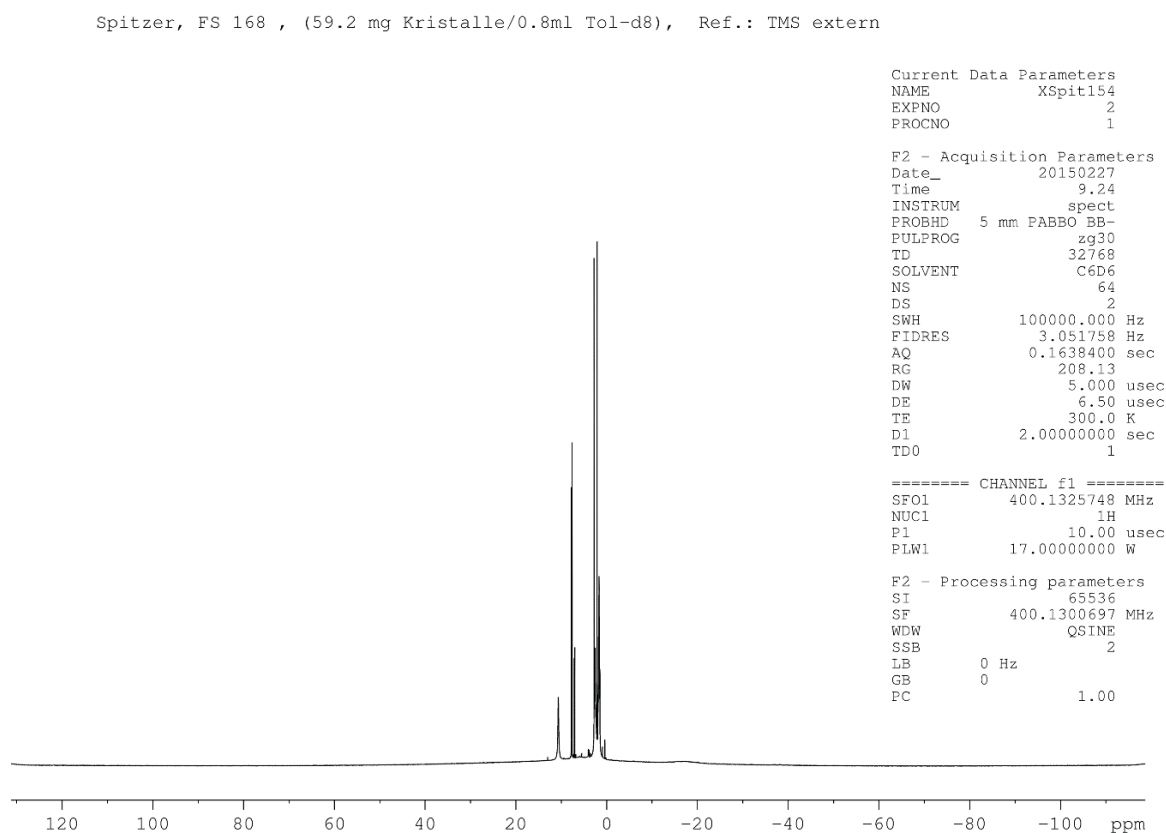
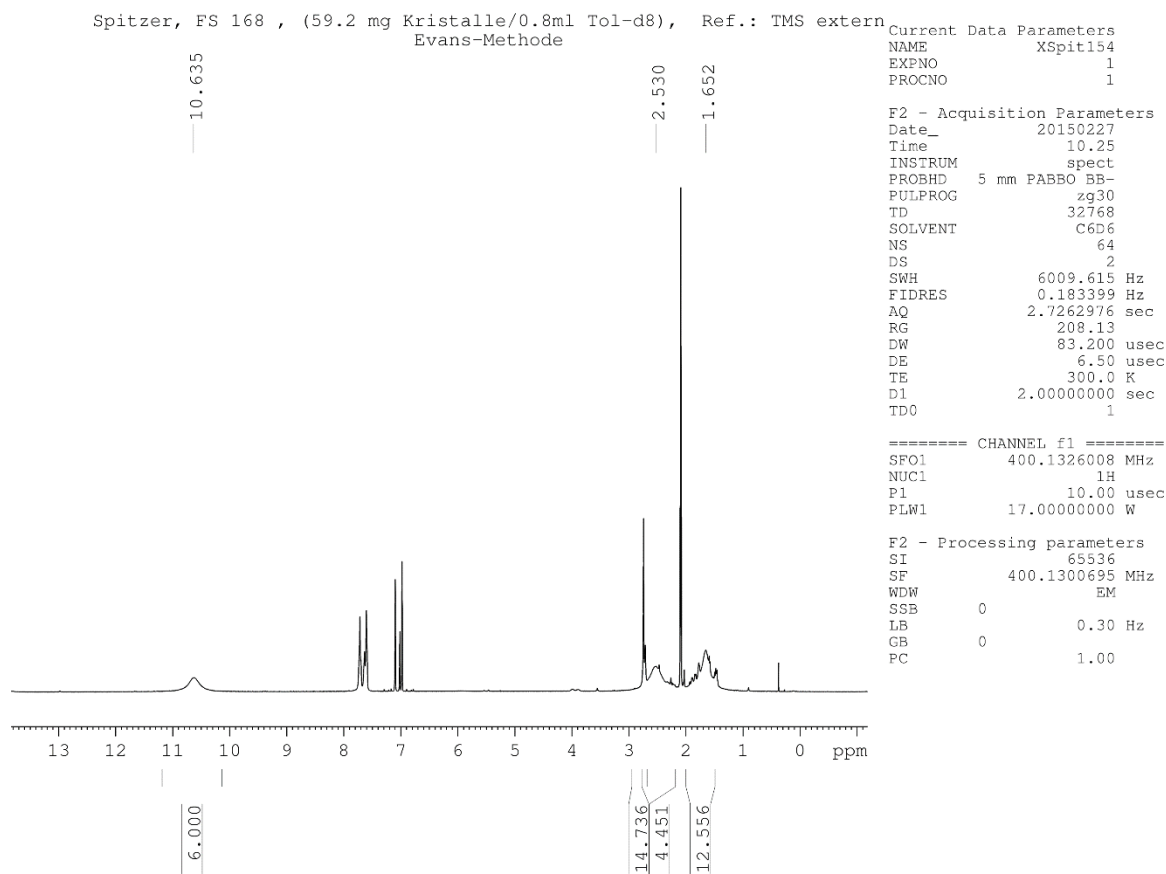


Figure S12. ¹H NMR spectra of **1c** in [D₈]toluene. Depicted ranges: 14 to -1 ppm (top); 140 to -140 ppm (bottom). Two individual sets of solvent signals are detected in the spectrum due to application of the Evans method.

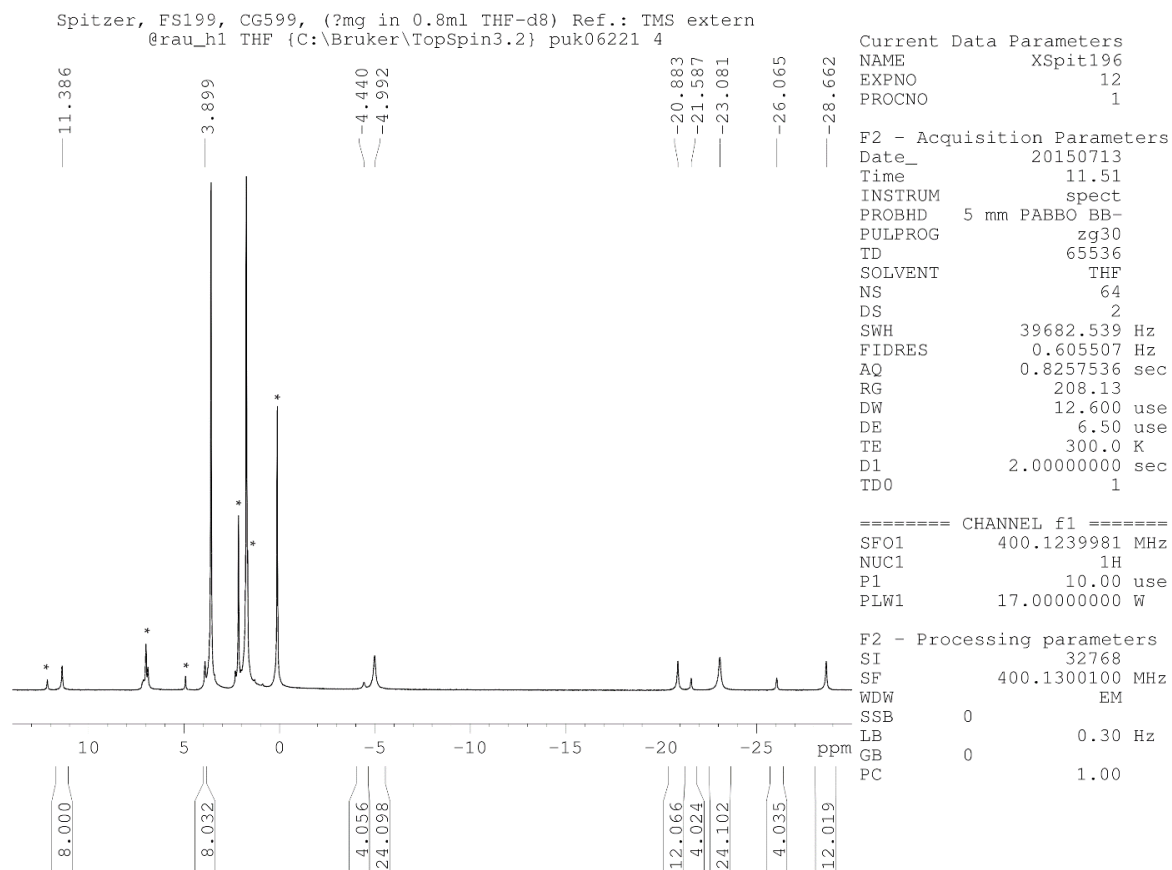
74 | SI: 4. Iron(I) Mediated P₄ Activation

Figure S13. ¹H NMR spectrum of **2a** in [D₈]THF. Impurities (* = toluene, **L¹H** and silicon grease) are marked.

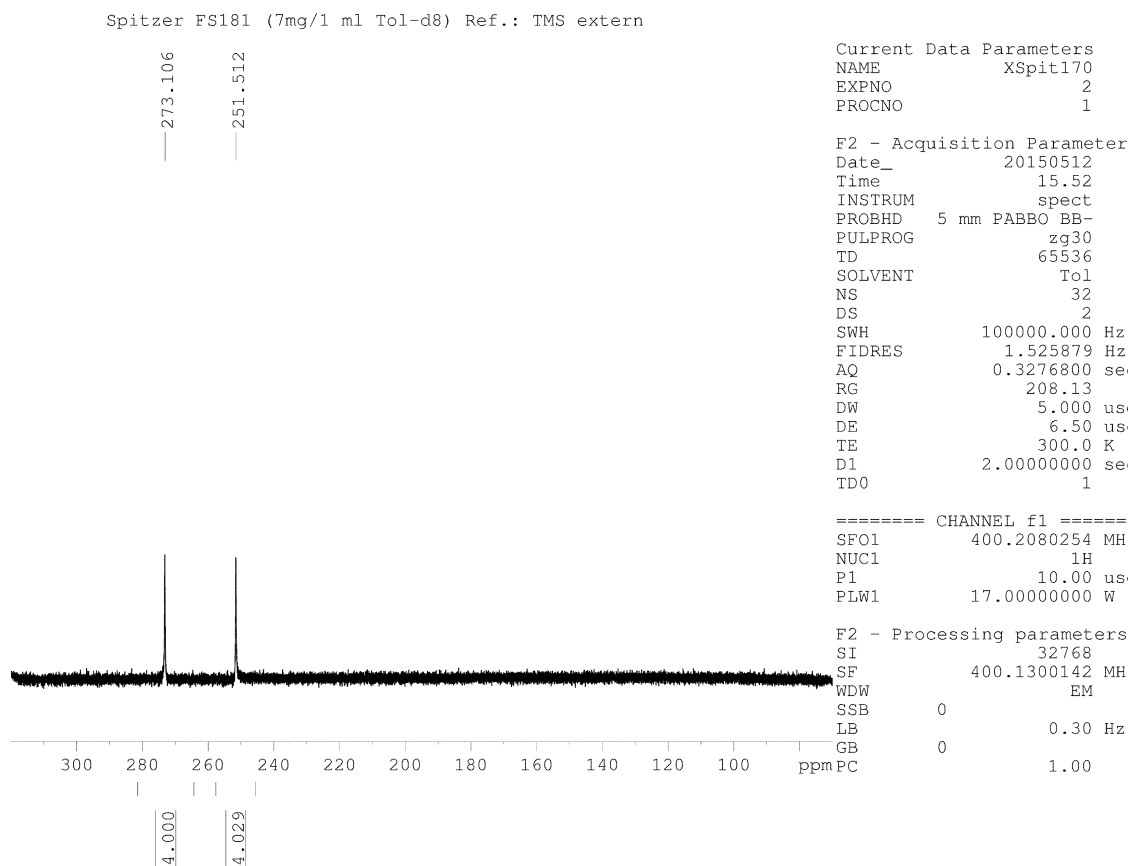
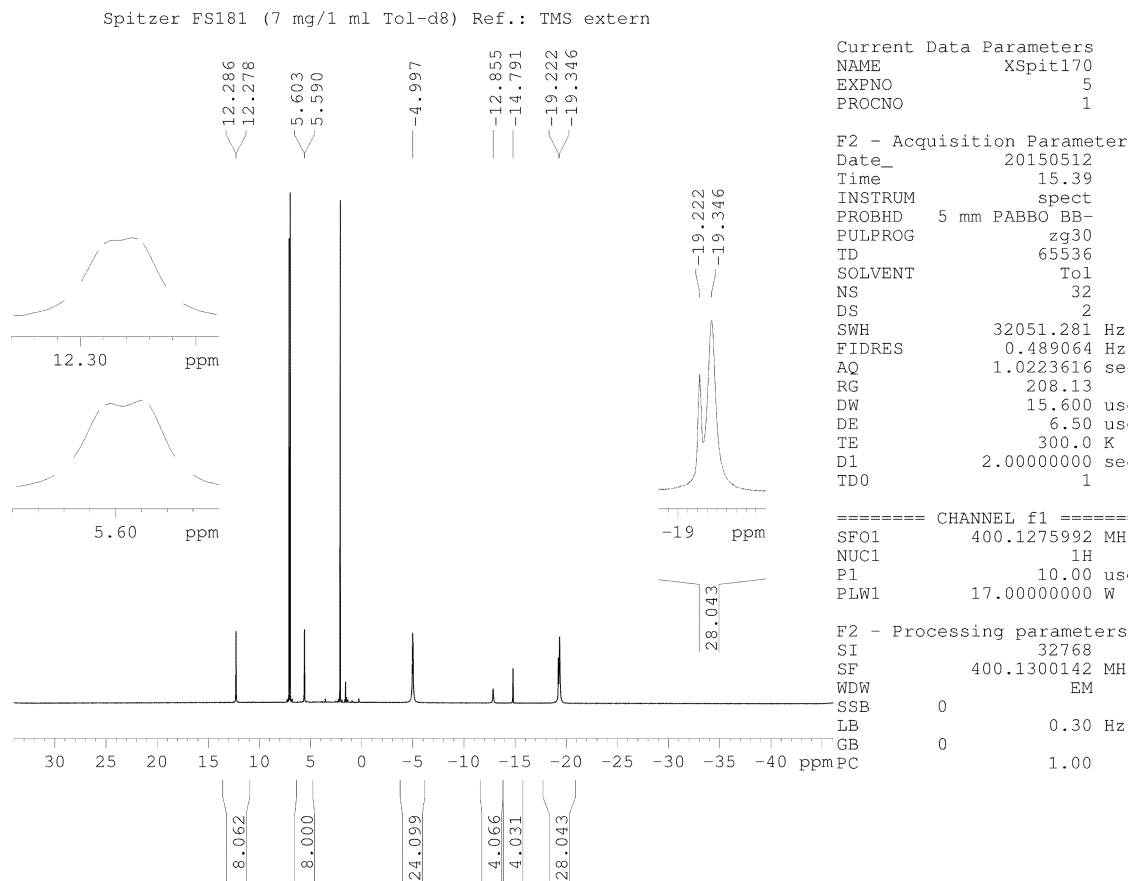
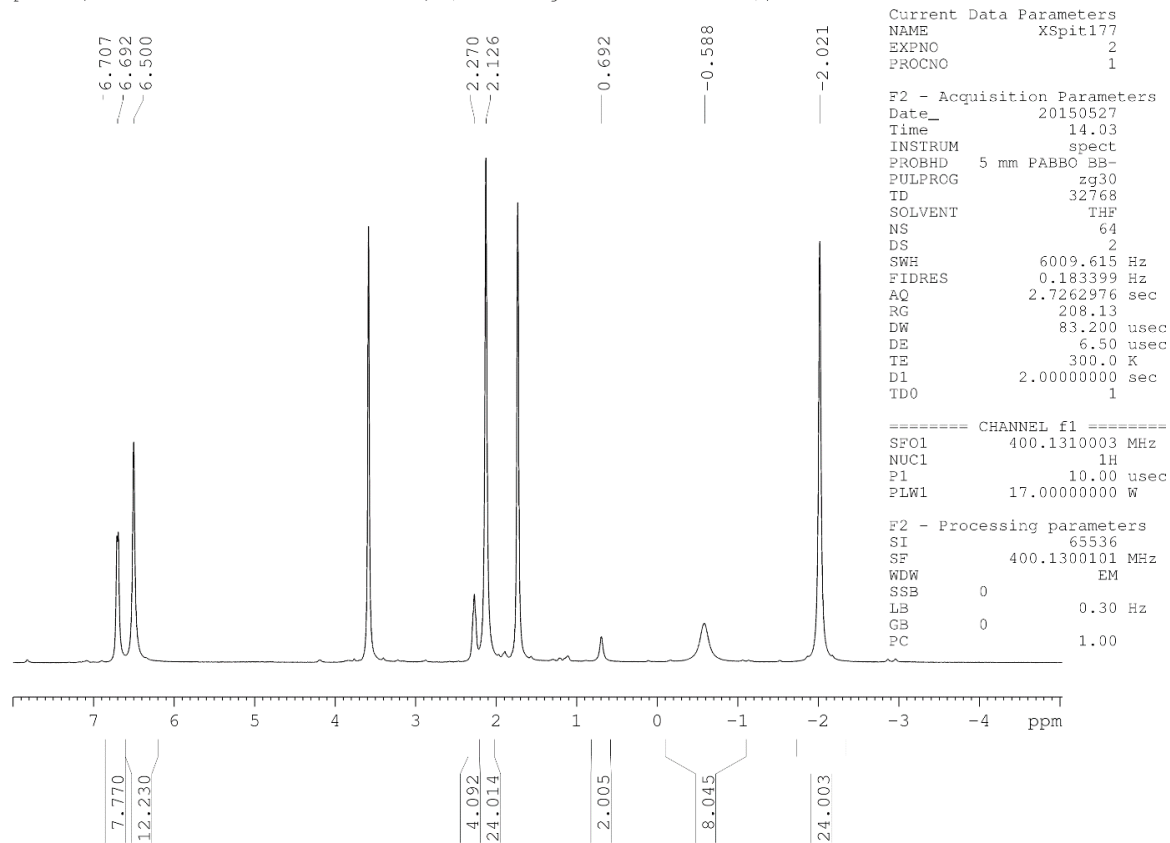


Figure S14. ¹H NMR spectra of **2b** in [D₈]toluene. Depicted ranges: 35 to -45 ppm (top); 320 to 70 ppm (bottom).

76 | SI: 4. Iron(I) Mediated P₄ Activation

Spitzer, FS189 Kristalle nach Waschen, (ca. 13 mg in 0.9 ml THF-d₈), Ref.: TMS extern



Spitzer, FS189 Kristalle nach Waschen, (ca. 13 mg in 0.9 ml THF-d₈), Ref.: TMS extern

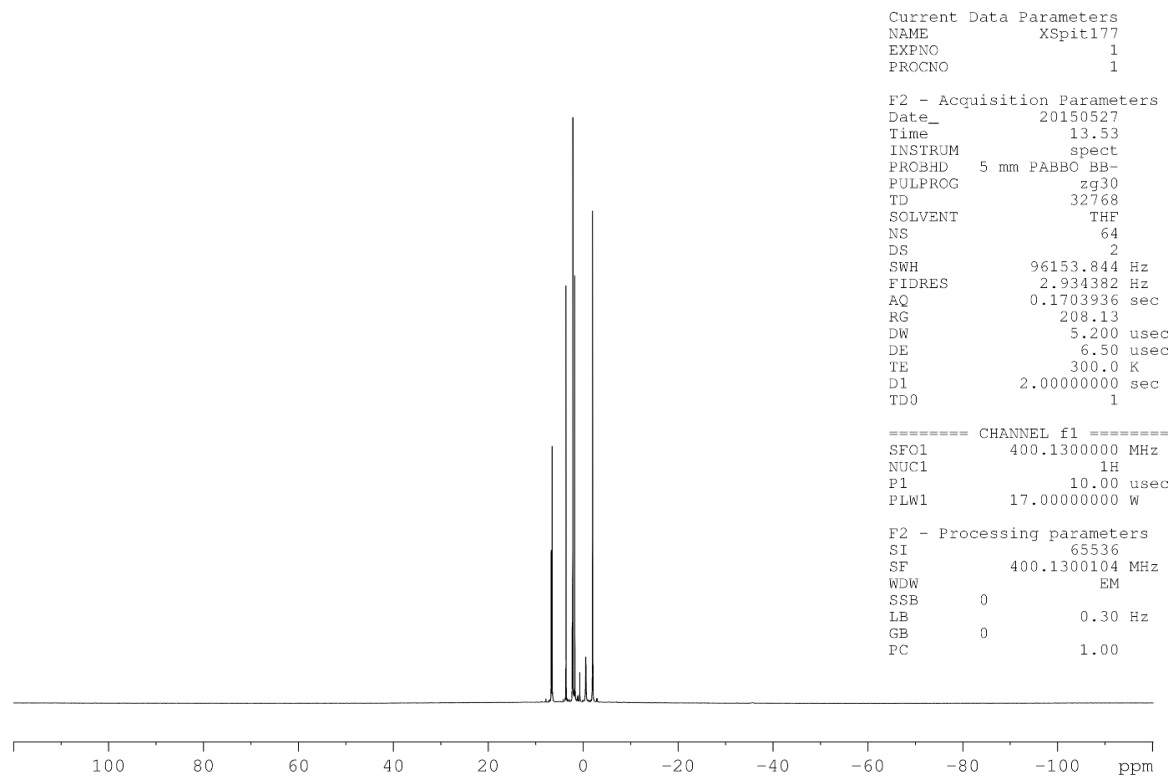


Figure S15. ¹H NMR spectra of **2c** in [D₈]THF. Depicted ranges: 8 to -5 ppm (top); 120 to -120 ppm (bottom).

Computational Details

Table S3. Oxidation states (obtained from NPA analysis for **2a,b,c** at the BP86/def2-SVP level of theory), selected geometric and Mössbauer parameter of **2a,b,c** and **A**.^[15]

Com- pound	oxidation state		atomic distances				Mössbauer	
	P _n ligand	metal center	d(N-Fe) / [Å]	d(Fe-P) / [Å]	d(P-P) / [Å]	d(Fe-Fe opposing) / [Å]	δ / [mm s ⁻¹]	ΔE _Q / [mm s ⁻¹]
2a	P ₈ ⁴⁻	Fe(+2)	1.983(2) 2.006(2)	2.4559(6) 2.5006(6)	2.1991(8) 2.2813(7)	6.740 6.756	n.a.	n.a.
2b	P ₈ ⁴⁻	Fe(+2)	1.982(2) 1.990(2)	2.4583(3) 2.4807(5)	2.2111(6) 2.2792(6)	6.765	0.73(1)	1.93(1)
2c	P ₄ ²⁻	Fe(+2)	2.018(2) 2.025(2)	2.4376(6) 2.5163(6)	2.178(1) 2.207(1)	3.902	0.74(1)	1.74(1)
A	2x P ₂ ²⁻	Fe(+3)	2.023(3) 2.025(3)	2.344(1) 2.377(1)	2.036(2)	2.777	0.42(1)	1.15(1)

DFT calculations on the complex [(L¹Fe)₄(μ₄-η¹:η¹:η¹:η¹:η¹:η¹:η¹:η¹-P₈)] (**2a**) and the hypothetical complex [(L¹Fe)₂(μ-η⁴:η⁴-P₄)] have been performed with the TURBOMOLE program package^[16] at the RI^[17]-BP86^[18]/def2-SVP^[19] level of theory, followed by single point calculations without the RI approximation and using the def2-TZVP basis set for N, P and Fe and the def2-SVP basis set for the C and H atoms. The Multipole Accelerated Resolution of Identity (MARI-J)^[20] approximation was used in the geometry optimization steps. The Natural Population Analysis (NPA) has been performed at the BP86/def2-SVP level of theory with the TURBOMOLE program. For **2c** the BPW91/def2-SVP optimized geometry was used. The DFT calculations for [(L³Fe)₂(μ-η⁴:η⁴-P₄)] (**2c**) have been performed with the ORCA program.^[21] The geometry optimization was performed at the BPW91^[22]/def2-SVP level followed by single point calculations in which for Fe and P the aug-cc-pVTZ^[23] basis set was used. Broken-symmetry (singlet spin-state) calculations for **2c** were done using the converged high-spin (quintet spin-state) as initial guess and flipping the spin on one iron. We found an antiferromagnetic coupling E(High-Spin)-E(BrokenSym) of 486 cm⁻¹. For the constrained geometry of [(L³Fe)₂(μ-η⁴:η⁴-P₄)] (Fe-Fe distance constrained to 2.777 Å) we obtained a E(High-Spin)-E(BrokenSym) coupling of 1360 cm⁻¹.

Table S4. Relative energies of [(L¹Fe)₄(μ₄-η¹:η¹:η¹:η¹:η¹:η¹:η¹:η¹-P₈)] (**2a**) in different spin-states at the BP86/def2-SVP level of theory.

Spin-state	Singlet (unrestricted)	Triplet	Quintet	Septet	Nonet
Rel. Energy (kJ·mol ⁻¹)	0	79.00	52.29	82.91	134.92

Table S5. Relative energies of [(L³Fe)₂(μ-η⁴:η⁴-P₄)] (**2c**) in different spin-states at the BPW91//def2-SVP/aug-cc-pVTZ (Fe, P) level of theory.

Spin-state	Singlet (unrestricted)	Triplet	Quintet
Rel. Energy (kJ·mol ⁻¹)	0	26.75	32.79

Table S6. Relative energies of the constrained geometry of [(L³Fe)₂(μ-η⁴:η⁴-P₄)] (geometry optimized with constrained Fe-Fe distance of 2.777 Å) in different spin-states at the BPW91//def2-SVP/aug-cc-pVTZ (Fe, P) level of theory.

Spin-state	Singlet (unrestricted)	Quintet
Rel. Energy (kJ·mol ⁻¹)	0	20.01

Table S7. Cartesian coordinates of the optimized geometry of $[(L^1Fe)_4(\mu_4-\eta^1:\eta^1:\eta^1:\eta^1-P_8)]$ (**2a**) (nonet spin-state) at the BP86/def2-SVP level of theory. Total Energy: -11168.28440919 a.u.

Atom	x	y	z	Atom	x	y	z
Fe	0.145172100	2.455462800	2.480034200	C	1.011576700	4.770971300	4.686155000
Fe	-1.046185100	-2.387140000	2.233742900	H	1.300565500	5.549019300	5.405555900
Fe	1.048027600	-2.341831100	-2.254303300	C	-1.587646700	5.879495500	1.404517800
Fe	-0.153392600	2.448535700	-2.461434700	H	-1.054941100	6.582761800	2.079126700
P	0.011266200	2.284478900	0.004470700	H	-2.038425100	6.473313500	0.586454800
P	1.328405700	-0.766884000	1.141096600	H	-0.810793800	5.215258300	0.971895900
P	-0.461136900	0.033041900	2.237509400	C	-4.009554900	5.288980500	1.902047100
P	-1.652542700	0.855898800	0.512751200	H	-4.312968800	6.056422200	1.172299300
P	0.029163600	-2.200299100	-0.004037000	C	-4.983933400	4.542380100	2.580321100
P	-1.302237100	-0.775355100	-1.113606600	H	-6.052224600	4.722614800	2.384982600
P	0.480433800	0.036606500	-2.219178400	C	-0.972758300	-5.120590600	3.277599500
P	1.677264700	0.857729600	-0.486464600	H	-0.421678800	-5.992447000	3.683845000
N	0.870962200	3.868333900	-3.389082100	C	-3.246681300	-4.273715900	2.678404500
N	-1.843957400	2.812858300	-3.422392300	H	-4.326247500	-4.526565700	2.679820800
N	0.249678900	-3.928600400	-3.137449700	C	-4.594223100	3.565196100	3.507920000
N	2.919092700	-2.962910400	-2.372780400	H	-5.357171300	2.978738600	4.043072000
N	-0.872995900	3.891109000	3.386643300	C	0.278749600	-2.748918800	5.667836700
N	1.841070400	2.845928700	3.425544700	H	-0.203451000	-1.930466800	5.091805600
N	-0.274773300	-3.982818300	3.136700300	H	0.672160600	-2.322629800	6.610472400
N	-2.925707800	-3.001527500	2.403917700	H	-0.528096800	-3.467121000	5.923300000
C	2.975957500	2.002117600	3.192393400	C	1.769733200	-5.301045300	1.520120600
C	-2.260669600	4.089858100	3.087070000	H	1.141769600	-6.209149100	1.638489400
C	-4.012263900	-2.070852000	2.306615100	H	2.693497000	-5.601494900	0.990414500
C	-2.636361500	5.077100300	2.136305600	H	1.200186800	-4.612096300	0.862284300
C	-3.234279100	3.323019400	3.780818400	C	-2.810085600	2.295318300	4.800060600
C	-0.323156100	4.761692600	4.249180200	H	-2.135926900	1.538877900	4.345335800
H	-0.997566500	5.539166800	4.660738500	H	-3.685659100	1.769174700	5.224353200
C	2.003424700	3.855211700	4.291016000	H	-2.244040500	2.756469400	5.636408500
H	3.010963900	3.967859500	4.739258100	C	2.190954700	0.535045500	5.117214600
C	1.078674600	-4.005656500	3.607858900	H	2.161192700	1.329823500	5.892112800
C	3.894140300	2.337805500	2.161918200	H	2.454442600	-0.419447600	5.609399800
C	3.168596900	0.860148000	4.015616600	H	1.157441100	0.447053600	4.719768800
C	-4.726450100	-1.930851600	1.087824200	C	5.010339200	1.500663800	1.966960600
C	1.372919900	-3.405424800	4.862239200	H	5.724607700	1.747043400	1.166192600
C	-4.373017100	-1.327273400	3.463817900	C	4.299590700	0.054126700	3.784440700
C	2.089340400	-4.653209300	2.845902500	H	4.452456200	-0.839728000	4.408657600
				C	-2.343633800	-5.297763700	3.017537300

Table S8. Cartesian coordinates of the optimized geometry of $[(L^1Fe)_4(\mu_4-\eta^1:\eta^1:\eta^1:\eta^1-P_8)]$ (**2a**) (unrestricted singlet spin-state) at the BP86/def2-SVP level of theory. Total Energy: -11482.579767331 a.u.

Atom	x	y	z	Atom	x	y	z
Fe	13.0002636	2.1986698	4.5072346	C	16.5743537	4.6729618	7.8121761
P	13.8180399	1.8383504	6.8320542	C	19.3896546	1.7199065	9.2779708
P	14.7707360	0.4318347	4.1241141	C	17.7272222	0.8928906	11.0107937
N	11.1777691	1.7243123	3.8850187	H	16.7765873	-5.6086909	1.4876177
N	12.9418417	4.0331098	3.7517639	H	18.1623524	-5.1258212	0.4498562
Fe	14.4499648	1.8131723	9.2442091	H	16.4857682	-4.6410626	0.0325374
P	15.7859588	1.5700712	5.7779494	H	19.4285516	-3.4815052	1.1077100
P	13.2487317	-0.2938826	7.2620403	C	12.9725771	-3.8091498	0.8507474
Fe	16.4533431	-1.3532248	3.4767794	C	14.6362672	-2.0063049	0.1861520
P	13.9408956	-1.3027625	5.2779752	C	13.3985263	-5.2951938	2.7193936
C	10.3404847	2.5484842	3.2211746	C	15.5391295	-5.1677504	4.0729455
C	10.7442056	0.3857614	4.1434737	H	20.3662155	-0.2687245	0.9915425
C	11.8897677	4.5647996	3.0878897	H	20.9902296	-1.9423014	1.1701931
C	14.0968718	4.8582562	3.9329368	H	21.0007919	-0.7997739	2.5591899
P	15.0710807	-0.5389178	8.5594425	C	18.7337063	2.8235421	2.0103913
N	13.1278199	2.3588000	10.6209954	C	17.4971462	1.0445235	0.6845473
N	15.9203673	2.9037620	10.0071777	C	19.7618033	2.3260456	4.1484455

P	16.6917725	-0.1558749	7.0577756	C	19.7439939	-0.0097689	5.1308208
P	16.0132203	-1.9204127	5.8587132	H	9.4377397	-3.2437874	4.7743148
N	16.3105030	-2.9696902	2.3087869	H	17.1582490	7.2649822	4.3000705
N	18.2198528	-0.7982742	2.7615011	C	13.9738191	-6.7782651	8.9760541
C	8.9600148	2.0528918	2.8287412	C	16.3671344	-6.0787143	8.7495615
C	10.6816546	3.8709968	2.8584871	C	12.8645845	-3.8116634	10.2242083
C	10.0734673	0.0886179	5.3604470	C	12.2671128	-4.1014106	7.8399514
C	10.9695271	-0.6189631	3.1626163	C	18.8398207	-5.9468763	9.0838246
C	11.9912943	5.9767978	2.5376468	C	18.9904261	-2.7012965	10.1498250
C	14.1574533	5.7472920	5.0414778	C	19.6267868	-3.0098135	7.7780143
C	15.1445473	4.8079213	2.9739512	C	9.2143956	0.7273707	10.5418820
Fe	15.8270883	-2.9211747	8.1284608	H	8.6806470	2.4614669	9.3444961
C	13.3701543	3.2395802	11.6190611	H	10.2111319	4.0940516	8.5293144
C	11.8189276	1.7844126	10.5487982	H	11.9495212	3.6370156	8.4411945
C	15.8099077	3.7239630	11.0728411	H	11.3536703	4.5833270	9.8202174
C	17.2016398	2.7751916	9.3838568	H	10.0384933	-0.8992051	11.7242400
C	17.3720437	-3.5075435	1.6677217	H	13.5094366	-0.3871154	11.2511654
C	15.0368892	-3.5982993	2.1260111	H	12.3158000	-1.1077843	12.3842252
C	19.0370473	-1.6204823	2.0690772	H	13.1032512	0.4607217	12.7594844
C	18.6182264	0.5683236	2.9191353	C	19.7529421	2.5770388	8.2284774
H	9.0198457	1.1657747	2.1656967	H	19.1079690	4.1832133	6.9100963
H	8.3907646	2.8430801	2.3058914	H	16.8897865	5.0872800	6.8373312
H	8.3801270	1.7313173	3.7179242	H	16.4718043	5.5179607	8.5282400
H	9.9089486	4.4292516	2.3135213	H	15.5608461	4.2401701	7.6914401
C	9.6146491	-1.2268679	5.5681959	H	20.0992428	0.9617733	9.6428693
C	9.8270156	1.1687682	6.3814081	H	18.5236453	0.1537669	11.2145856
C	10.4940141	-1.9199491	3.4132536	H	16.7922504	0.3421432	10.7735175
C	11.6864913	-0.2849700	1.8790096	H	17.5264541	1.4556601	11.9473252
H	12.1800255	6.7177251	3.3409774	C	12.5703443	-4.8758344	1.6685538
H	11.0624798	6.2615891	2.0105298	H	12.3297078	-3.4807655	0.0180960
H	12.8402894	6.0716531	1.8298863	H	13.8581016	-1.7490927	-0.5577694
C	15.2667402	6.6086548	5.1490287	H	15.5737743	-2.2368291	-0.3626043
C	13.0495824	5.7714705	6.0657324	H	14.8500254	-1.1026455	0.7951467
C	16.2397458	5.6793092	3.1292035	H	13.0873230	-6.1334100	3.3627158
C	15.0615011	3.8503289	1.8117822	H	16.4866810	-5.5957766	3.6818151
N	14.6047925	-4.4105703	8.6013931	H	15.0405990	-5.9491739	4.6768136
N	17.4866591	-3.9150985	8.6321184	H	15.8356436	-4.3409926	4.7516172
C	12.2687528	3.5613731	12.6141112	C	19.4661589	3.2423035	3.1318992
C	14.6136170	3.8811149	11.8084771	H	18.5039876	3.5387281	1.2043701
C	10.7879297	2.4715948	9.8509720	H	17.3005940	1.8877277	-0.0050508
C	11.5602529	0.5577972	11.2187364	H	16.5215603	0.6129640	0.9926051
C	17.0184947	4.5207396	11.5307448	H	18.0186681	0.2484094	0.1123034
C	17.5482040	3.6357856	8.3075600	H	20.3315023	2.6492669	5.0330340
C	18.1163392	1.8019412	9.8722291	H	20.7139387	-0.5007145	4.8914356
C	17.1974181	-4.7896171	0.8713149	H	18.9907144	-0.8136516	5.2277553
C	18.6545915	-2.9110726	1.6382434	H	19.8530595	0.4823629	6.1157082
C	14.1994257	-3.1516856	1.0663348	H	13.4318697	-6.6228724	9.9318863
C	14.6400323	-4.6753672	2.9665009	H	14.4499312	-7.7755251	9.0064807
C	20.4229176	-1.1399620	1.6765037	H	13.2015803	-6.7777625	8.1809959
C	18.2895730	1.4944287	1.8879010	H	16.5513266	-7.1563200	8.8525984
C	19.3534564	0.9790726	4.0622804	C	11.5115562	-3.5554647	10.5098803
C	9.8120497	-2.2228614	4.6011953	C	13.9074283	-3.8014018	11.3153365
H	9.0926215	-1.4626030	6.5085851	C	10.9255607	-3.8221012	8.1730497
H	9.5100871	0.7410680	7.3500585	C	12.6458915	-4.4544802	6.4242036
H	9.0424941	1.8817717	6.0448481	H	19.6111100	-5.7171453	8.3221278
H	10.7434155	1.7691357	6.5524065	H	18.7097524	-7.0433472	9.1345244
H	10.6734410	-2.7055505	2.6634034	H	19.2547699	-5.6013696	10.0536149
H	11.8511146	-1.1942197	1.2724347	C	20.2164547	-2.0441490	10.3711930
H	12.6735613	0.1795470	2.0872179	C	17.9982939	-2.8999434	11.2693285
H	11.1226670	0.4473388	1.2623788	C	20.8352983	-2.3352715	8.0443550
C	16.3000589	6.5826765	4.2004909	C	19.3359780	-3.5548010	6.4020279
H	15.3150753	7.3106690	5.9966985	H	8.1921169	0.3189292	10.5481422
H	13.3100108	6.4230496	6.9217459	H	20.7578293	2.5053328	7.7840851
H	12.8464362	4.7499956	6.4495205	H	11.6109131	-5.3833241	1.4844462
H	12.0908821	6.1375093	5.6396514	H	19.8020886	4.2872005	3.2138310

H	17.0531168	5.6494957	2.3877714	C	10.5433688	-3.5591312	9.4938553
H	15.9650488	3.9134626	1.1775674	H	11.2156599	-3.3543353	11.5518205
H	14.1751188	4.0470005	1.1721274	H	13.4630554	-3.5338484	12.2931749
H	14.9601431	2.8041351	2.1710027	H	14.7110916	-3.0701220	11.0868322
C	15.0080610	-5.6903419	8.7481813	H	14.4096773	-4.7856505	11.4255660
C	13.2350112	-4.0979573	8.8786232	H	10.1720052	-3.8210573	7.3707595
C	17.5189024	-5.2577970	8.7861661	H	11.9972784	-3.9370919	5.6919534
C	18.7047876	-3.1929915	8.8459056	H	12.5490296	-5.5484512	6.2424302
H	11.3754579	3.9870008	12.1135936	H	13.6955501	-4.1812114	6.2099506
H	12.6224604	4.2835421	13.3724176	C	21.1374546	-1.8608378	9.3287135
H	11.9188837	2.6472024	13.1362099	H	20.4521404	-1.6801927	11.3843645
H	14.6641912	4.5788337	12.6547057	H	18.3437430	-2.4201524	12.2051417
C	9.4888411	1.9271173	9.8689404	H	17.8176441	-3.9749611	11.4813270
C	11.0830892	3.7605599	9.1240332	H	17.0111843	-2.4689337	10.9989909
C	10.2483859	0.0466444	11.2013055	H	21.5555824	-2.1942821	7.2229537
C	12.6722609	-0.1579575	11.9440488	H	18.3504922	-3.2053605	6.0294397
H	17.8592358	3.8550535	11.8142299	H	19.2890504	-4.6647557	6.3941656
H	16.7665693	5.1554777	12.3999517	H	20.1109014	-3.2456579	5.6757225
H	17.4037447	5.1711230	10.7192796	H	9.4898245	-3.3502385	9.7340035
C	18.8336241	3.5180632	7.7434914	H	22.0936413	-1.3493585	9.5184661

Table S9. Cartesian coordinates of the optimized geometry of $[(L^3Fe)_2(\mu-\eta^4:\eta^4-P_4)]$ (**2c**) (quintet spin-state) at the BPW91/def2-SVP level of theory.

Atom	x	y	z	Atom	x	y	z
Fe	-0.518933221	0.969466542	-1.540574531	C	-4.065458149	-1.905444895	3.386985854
Fe	0.519666327	-1.011151160	1.565244811	C	-1.332912352	1.369675191	4.323792626
P	0.202792371	-1.365206524	-0.826384937	C	-3.638254344	0.314526023	4.245640073
P	-0.256163515	1.168230218	0.978855343	H	1.889842523	-2.802520957	5.293108916
P	-1.527516707	-0.530038572	0.252168806	H	-1.425505816	-2.723211598	5.515660187
P	1.510857519	0.321557633	-0.116334357	H	0.100347981	-2.520534963	6.433394201
N	0.421585619	1.286055617	-3.324356122	H	-0.952273860	-1.119125656	6.062953930
N	-2.192737187	2.049981058	-2.036171868	C	5.076744778	-1.959008901	-0.296974901
N	-0.369858247	-1.297407662	3.290086791	C	4.450465620	-0.315736949	1.532598190
N	2.101199711	-2.090384535	2.003772252	C	3.814240198	-3.963993592	-0.772715098
C	1.847572704	1.108509326	-3.426156974	C	1.754685295	-4.655912605	0.524971420
C	-0.203789551	1.836379651	-4.388565526	H	4.355258113	-3.411382561	2.726591187
C	-3.145138685	2.405480526	-1.015995895	H	4.062771812	-3.120024596	4.475347793
C	-2.426609539	2.479667446	-3.290788485	H	3.276000494	-4.484368978	3.659815409
C	2.111924671	3.428112675	-2.303914611	H	-3.309501986	-4.765401168	3.880081334
C	2.689626697	2.154840449	-2.930808496	H	-1.938056576	-5.532464447	3.030210898
C	2.417018242	-0.052129301	-4.032702568	H	-1.629661270	-4.421828302	4.389093895
C	-1.537958510	2.291815702	-4.375419006	H	-2.976260807	-2.988150680	0.480119097
C	0.549134874	2.048291705	-5.691792570	H	-2.601517775	-4.715093822	0.777829334
C	-4.243488072	1.532263606	-0.734137092	H	-4.089519117	-3.999836375	1.450896862
C	-2.998047807	3.640236614	-0.314011517	H	5.745316305	0.807109839	-3.765949534
C	-3.653516809	3.315487312	-3.631463485	H	2.915485101	-2.862951331	-4.007129329
C	2.118459904	4.608730598	-3.299259665	H	1.201434139	-3.334592426	-4.204433293
C	2.811521168	3.826722017	-0.991386656	H	1.718071253	-2.422409194	-2.754691216
C	-1.784994756	-1.043554392	3.446405322	H	1.621888278	-0.527723481	-6.707918455
C	0.219177675	-1.869209614	4.367239551	H	1.124258496	-2.228191242	-6.476921891
C	3.043516208	-2.431987421	0.958923124	H	2.839415885	-1.764584390	-6.312217243
C	2.375429091	-2.565632707	3.236888063	H	-5.762742248	3.405101715	1.727117906
C	-2.231775592	-3.424037420	2.503452217	H	-4.462367286	-1.006780097	0.326935536
C	4.083839793	2.022174343	-3.068062687	H	-5.010036695	-1.866470098	-1.147578418
C	1.581666435	-1.211096307	-4.589108921	H	-6.099061002	-0.715078171	-0.339582719
C	3.821700464	-0.131671155	-4.132424858	H	-6.376977756	0.796045564	-2.441725114
H	-1.898936308	2.688620544	-5.332256347	H	-5.546733232	-0.577189529	-3.231140248
H	1.502187682	2.584902699	-5.527756902	H	-4.954258397	1.083516248	-3.486770694
H	-0.059870475	2.623404120	-6.410841663	H	-1.558404072	5.386298825	1.424771233
H	0.816304079	1.083494480	-6.158651840	H	-0.172814471	5.631376227	0.327707139
C	-5.165029706	1.922144970	0.257679319	H	-0.524864829	3.996593884	0.980830347
C	-4.471934208	0.222440207	-1.499076196	H	-3.094349674	5.804246403	-2.066925177
C	-3.951004883	3.971541467	0.670444226	H	-1.621088020	6.644786462	-1.489888501

C	-1.881243271	4.643446494	-0.625478307	H	-3.049951485	6.503624863	-0.427058851
H	-1.174733181	-3.282633614	2.201762470	C	-4.537479354	-0.717686588	3.959680765
H	1.052212175	3.208935617	-2.059222232	H	-4.777971905	-2.708004386	3.145664478
H	-4.452735291	3.256343844	-2.875518144	H	-0.363701799	1.170091930	3.824927514
H	-4.061401699	3.013204427	-4.614020043	C	-1.888923757	2.692816170	3.757307290
H	-3.358019990	4.379722632	-3.725515435	C	-1.055461294	1.551980682	5.833026769
H	3.151325355	4.853717738	-3.619118122	H	-4.018249455	1.251606290	4.676321834
H	1.688159330	5.517303321	-2.833061133	H	5.942848960	-1.315033426	-0.500836911
H	1.527253962	4.390530839	-4.207614064	C	4.908278678	-3.134293638	-1.037874478
H	2.792707149	2.997777557	-0.258438392	H	3.485671724	-0.000758229	1.979980093
H	2.303257376	4.698615774	-0.535455214	C	4.970712664	0.851369063	0.672560925
H	3.869890243	4.114138859	-1.151752623	C	5.441602583	-0.569484858	2.690501388
C	-2.697447659	-2.096194681	3.116686469	H	3.693348203	-4.894687157	-1.344827365
C	-2.255096704	0.186153458	3.998047905	H	1.095232896	-4.203439173	1.291358599
C	1.527712855	-2.380289355	4.347903864	C	0.882961394	-4.977885840	-0.705305167
C	-0.549235380	-2.065455819	5.665128297	C	2.325825131	-5.969841996	1.107155193
C	4.167017137	-1.581153336	0.710819219	H	-5.608661689	-0.593901792	4.175428560
C	2.870581124	-3.645654553	0.225106445	H	-2.778710095	3.036660017	4.322283519
C	3.594474563	-3.431844795	3.522556038	H	-1.124829339	3.491626084	3.834378406
C	-2.278241658	-4.593660370	3.511034124	H	-2.179328243	2.598966940	2.695242035
C	-3.021438826	-3.796775051	1.233758660	H	-0.484966919	0.713490886	6.270965754
C	4.653261509	0.890981058	-3.665999285	H	-0.456997061	2.470340789	5.999763929
H	4.740316216	2.825304795	-2.702819553	H	-1.997822702	1.659593110	6.407213929
H	0.514993897	-0.958855902	-4.426858459	H	5.634044533	-3.403917868	-1.818816529
C	1.871540567	-2.529133338	-3.843642880	H	4.322583331	1.029927873	-0.204061472
C	1.802197416	-1.435764505	-6.102343966	H	5.007067201	1.781364498	1.273708441
H	4.272330463	-1.019402641	-4.599288314	H	6.000500129	0.667592010	0.306513476
H	-6.014234140	1.263994961	0.485270020	H	6.415043267	-0.934710783	2.306332085
C	-5.027963439	3.126773492	0.957685589	H	5.632169951	0.372544515	3.242509874
H	-3.478139819	-0.106766968	-1.866163124	H	5.068349607	-1.308713557	3.109732144
C	-5.039648397	-0.898657681	-0.608949842	H	1.473110432	-5.461126814	-1.509446430
C	-5.383432786	0.399726379	-2.734150981	H	0.071084562	-5.680099313	-0.429652304
H	-3.849455059	4.919816387	1.217221286	H	0.423020362	-4.063763003	-1.123369995
H	-1.241803774	4.191866514	-1.408917318	H	2.962289402	-5.796809642	1.993891936
C	-0.984340985	4.925954934	0.596041114	H	1.504410346	-6.653077314	1.402627790
C	-2.445107555	5.968026423	-1.186854013	H	2.945904219	-6.502763672	0.357684935

Table S10. Cartesian coordinates of the optimized geometry of $[(L^3Fe)_2(\mu-\eta^4:\eta^4-P_4)]$ (**2c**) (unrestricted singlet spin-state) at the BPW91/def2-SVP level of theory.

Atom	x	y	z	Atom	x	y	z
Fe	-0.495576822	0.947899852	-1.517143463	C	-4.125044158	-1.931955050	3.125442393
Fe	0.495465827	-0.947308914	1.517323742	C	-1.455175408	1.299822766	4.340500037
P	0.457646929	-1.221140580	-0.911563413	C	-3.754392384	0.284512761	4.016871206
P	-0.458099499	1.221764270	0.911079106	H	1.876798086	-2.659633685	5.273561569
P	-1.433714028	-0.702169113	0.041885729	H	-0.610957857	-3.170822818	5.810902276
P	1.433782633	0.701754232	-0.041228977	H	-0.003989059	-1.635880411	6.454826308
N	0.428410775	1.296933391	-3.223801953	H	-1.594916530	-1.691486452	5.624432263
N	-2.114082883	1.974158146	-1.979818675	C	5.116524960	-1.908417579	-0.287302399
N	-0.428706294	-1.296933108	3.223751335	C	4.471368080	-0.204325143	1.477642076
N	2.113505866	-1.974500241	1.979921682	C	3.845278835	-3.916232071	-0.730234976
C	1.852075405	1.068905308	-3.329400703	C	1.736150303	-4.530620309	0.529659424
C	-0.177175541	1.828646524	-4.305948361	H	4.394197249	-3.219192713	2.744944593
C	-3.059767548	2.329769709	-0.945955224	H	4.074368136	-2.906080323	4.485486994
C	-2.383394472	2.426513714	-3.222491589	H	3.339997819	-4.308794411	3.685912847
C	2.235701877	3.475111894	-2.435489265	H	-3.432467415	-4.756618670	3.770540219
C	2.740779122	2.123418022	-2.953055849	H	-1.955037265	-5.539070982	3.138155259
C	2.357230964	-0.153350572	-3.869758583	H	-1.838138880	-4.325176270	4.444294757
C	-1.514320338	2.263879768	-4.316191555	H	-2.831018475	-3.159256336	0.343926751
C	0.566806494	2.083621305	-5.611942328	H	-2.480386506	-4.866524824	0.765961215
C	-4.192378852	1.495088946	-0.690779167	H	-4.011016138	-4.118744463	1.288998415
C	-2.883465246	3.558235883	-0.237052173	H	5.717753455	0.611854640	-3.792970349
C	-3.628308776	3.247167689	-3.534410585	H	2.885425488	-2.978925405	-4.357988388
C	2.367782165	4.579078371	-3.507942374	H	1.192426008	-3.454522265	-4.082948911

C	2.932132143	3.922358254	-1.135608589	H	2.128596012	-2.682985586	-2.762437150
C	-1.852548529	-1.069784296	3.328915686	H	0.850515538	-0.425528112	-6.292187657
C	0.176810375	-1.828677734	4.305917081	H	0.657094405	-2.193973639	-6.176457901
C	3.059961354	-2.329069055	0.946407455	H	2.286419081	-1.481386128	-6.372296520
C	2.382910941	-2.426708906	3.222654709	H	-5.692071444	3.410146613	1.750803709
C	-2.235366618	-3.477140650	2.437311590	H	-4.314622794	-1.095034630	0.294495278
C	4.124881424	1.930458119	-3.126469662	H	-5.018612178	-1.884731467	-1.151262315
C	1.454015783	-1.300193207	-4.342221707	H	-6.000654388	-0.747222288	-0.198567720
C	3.753317957	-0.285202424	-4.019513290	H	-6.450886577	0.789161250	-2.243976193
H	-1.877304161	2.659533737	-5.273392948	H	-5.671631413	-0.541808860	-3.148187839
H	0.609630473	3.172342390	-5.810210583	H	-5.120085953	1.136386719	-3.384411060
H	0.005726868	1.636260959	-6.454627111	H	-1.493842921	5.406363752	1.479034206
H	1.595713024	1.694498534	-5.623109166	H	-0.043397672	5.521373272	0.448328127
C	-5.115941938	1.911655041	0.289171661	H	-0.493231405	3.952385884	1.192978627
C	-4.473198898	0.205886161	-1.475030757	H	-2.849750072	5.649388923	-2.084601052
C	-3.843267950	3.919190550	0.729387129	H	-1.395979310	6.489950624	-1.463315360
C	-1.733468771	4.530038052	-0.531398137	H	-2.881118618	6.409559545	-0.472336335
H	-1.157781942	-3.353149101	2.210720153	C	-4.634573915	-0.741026981	3.655057035
H	1.158447291	3.350643879	-2.207560146	H	-4.819327918	-2.739022545	2.848609433
H	-4.393887179	3.220370959	-2.743663235	H	-0.451724388	1.123359922	3.904061839
H	-4.078037823	2.899349238	-4.483507822	C	-1.948052130	2.675434002	3.849820618
H	-3.342379753	4.306084447	-3.692376470	C	-1.303380715	1.343463423	5.878147434
H	3.430420485	4.755178006	-3.770240554	H	-4.160876062	1.214563927	4.438088481
H	1.953948498	5.537250806	-3.135086064	H	5.991965359	-1.277827524	-0.494767494
H	1.834910179	4.323869056	-4.441449861	C	4.953291831	-3.104591129	-0.995138949
H	2.834598043	3.156313098	-0.343201179	H	3.508082804	0.118096135	1.922195094
H	2.481866286	4.863575656	-0.763571022	C	4.978332902	0.939990968	0.580014616
H	4.012420175	4.117558874	-1.289228888	C	5.473759246	-0.416737019	2.634461303
C	-2.740753934	-2.125056442	2.953589623	H	3.726072690	-4.860398827	-1.280382844
C	-2.358160207	0.152541374	3.868602511	H	1.064356043	-4.035263385	1.258141612
C	1.514221990	-2.263258344	4.316518402	C	0.897876404	-4.865364659	-0.720155324
C	-0.566625731	-2.082160708	5.612551262	C	2.249968014	-5.838629510	1.173549751
C	4.192256557	-1.493444888	0.692626551	H	-5.718588549	-0.612805103	3.789235261
C	2.885063953	-3.557142946	0.236523542	H	-2.886410659	2.978736656	4.355840760
C	3.626721524	-3.249220451	3.533726656	H	-1.193645812	3.453848042	4.079172571
C	-2.369376723	-4.580711036	3.509961033	H	-2.130942852	2.681329223	2.759986319
C	-2.930328431	-3.924659808	1.136727435	H	-0.849136687	0.427273502	6.290647786
C	4.633880434	0.739917518	-3.657486382	H	-0.659271037	2.195921657	6.173948316
H	4.819526404	2.736968091	-2.848918336	H	-2.287180484	1.480307541	6.370949405
H	0.450557522	-1.123803703	-3.905771286	H	5.693880613	-3.404704883	-1.750733156
C	1.946630536	-2.676250588	-3.852421422	H	4.319709635	1.096178835	-0.292801542
C	1.302616201	-1.342872151	-5.879916806	H	5.019004547	1.885954754	1.155198220
H	4.159364780	-1.215082962	-4.441564943	H	6.003792756	0.747644071	0.206278056
H	-5.991929803	1.282072874	0.497359070	H	6.445844293	-0.789357144	2.253766177
C	-4.951917064	3.108698297	0.995315065	H	5.665052462	0.543328499	3.154073201
H	-3.511178461	-0.115895807	-1.922766258	H	5.110722137	-1.133881405	3.390076350
C	-4.976417151	-0.938924117	-0.575935480	H	1.497076718	-5.402239639	-1.482633882
C	-5.479684662	0.418006507	-2.628347845	H	0.047374643	-5.522978811	-0.451420489
H	-3.723310384	4.863875665	1.278475484	H	0.493521293	-3.951202965	-1.192527479
H	-1.061669204	4.032365712	-1.258334945	H	2.855208918	-5.651975253	2.079435501
C	-0.895465241	4.866243059	0.718193655	H	1.401260523	-6.492516082	1.458304015
C	-2.245498217	5.837220007	-1.178320783	H	2.885218756	-6.409324546	0.465893947

Table S11. Cartesian coordinates of the optimized geometry (restricted) of $[(L^3Fe)_2(\mu-\eta^4-\eta^4-P_4)]$ (**2c**) (quintet spin-state) with the Fe–Fe distance fixed to 2.777 Å, at the BPW91/def2-SVP level of theory.

Atom	x	y	z	Atom	x	y	z
Fe	-0.320976920	0.801339516	-1.086904970	C	-4.234884571	-2.408997846	3.077318348
Fe	0.327411613	-0.805320190	1.083340565	C	-1.965517424	1.140376464	4.188137534
P	0.244856151	-1.455966223	-1.137514807	C	-4.098828877	-0.190378562	4.011686429
P	-0.335708298	1.425016694	1.141046645	H	1.877866194	-2.037747087	4.941474850
P	-1.578063430	-0.950675964	-0.220623556	H	-0.653831978	-3.053733161	5.381677218
P	1.536699199	1.009902786	0.279740318	H	0.051211701	-1.600792161	6.122034668
N	0.667135667	1.239083926	-2.865650445	H	-1.603747981	-1.551889794	5.421413574

N	-2.036212477	1.894569320	-1.590586524	C	5.142862579	-2.497994595	-0.476886645
N	-0.662388388	-1.251159048	2.873508428	C	4.649929017	-0.480611712	0.947072303
N	2.034936386	-1.889884087	1.578375075	C	3.663200403	-4.387517417	-0.708038118
C	2.101528005	1.228554952	-3.067967545	C	1.409731905	-4.526551915	0.429384563
C	-0.053739497	1.576892041	-3.953683545	H	4.304965211	-3.039578640	2.527346932
C	-2.976514586	2.467930281	-0.651126828	H	4.075078728	-2.258413887	4.129878802
C	-2.310216250	2.115164581	-2.889518755	H	3.301089142	-3.815684172	3.779390905
C	2.225973208	3.660796487	-2.156615204	H	-3.160071427	-5.096165754	3.511214321
C	2.855963230	2.403528403	-2.762475738	H	-1.684761684	-5.689271780	2.697546369
C	2.738248809	0.111788879	-3.698397873	H	-1.555789352	-4.518838844	4.041361422
C	-1.446152537	1.799042122	-3.960270839	H	-3.055684491	-3.308209173	0.111346557
C	0.600132830	1.902054569	-5.293428452	H	-2.489085369	-4.980227425	0.412697399
C	-4.227636485	1.830935137	-0.374309256	H	-4.037911918	-4.431012161	1.103550993
C	-2.690252823	3.753260744	-0.093936078	H	5.926431598	1.399724170	-3.960203553
C	-3.561234011	2.858774849	-3.352454544	H	3.637239297	-2.607620742	-3.904179132
C	2.130672592	4.802474704	-3.192083931	H	2.003934349	-3.310014973	-3.771741148
C	2.973168235	4.147520737	-0.898625586	H	2.675174134	-2.351290860	-2.418847414
C	-2.095363976	-1.228192585	3.079747553	H	1.456133772	-0.475622795	-6.187285521
C	0.060844886	-1.600843664	3.954250922	H	1.380492886	-2.239853655	-5.938203150
C	2.972145994	-2.466851550	0.637009356	H	2.962295652	-1.429774518	-6.102688830
C	2.317111928	-2.112929879	2.876953855	H	-5.620157542	4.254464292	1.646783832
C	-2.246261579	-3.643508857	2.130122707	H	-4.211878030	-0.659233370	0.838583464
C	4.225275320	2.436808060	-3.093775273	H	-5.223408101	-1.525393849	-0.354082628
C	1.995313804	-1.155537850	-4.140107974	H	-5.939082350	-0.243911625	0.657933687
C	4.114579879	0.201587148	-3.991073876	H	-6.768230612	1.010646819	-1.417785135
H	-1.862957034	2.016283359	-4.952255335	H	-6.131769595	-0.353294378	-2.373645549
H	0.678115549	3.002604180	-5.401511228	H	-5.672448109	1.319841470	-2.790159569
H	-0.041780710	1.545754344	-6.120344589	H	-1.337164095	5.899485932	1.307279596
H	1.611920826	1.491152771	-5.417888689	H	0.246736919	5.559769404	0.566480535
C	-5.145256449	2.494046146	0.467049020	H	-0.538160558	4.321575367	1.594210609
C	-4.668251931	0.493972060	-0.984907344	H	-2.088413820	5.229027593	-2.394977244
C	-3.655310378	4.371453885	0.725092888	H	-0.727099415	6.162248807	-1.710951879
C	-1.406321380	4.519047543	-0.418430145	H	-2.382041960	6.383488643	-1.065603416
H	-1.216950405	-3.379070736	1.822305224	C	-4.856386926	-1.324401918	3.703311167
H	1.197123403	3.392365062	-1.850704080	H	-4.827148637	-3.305143494	2.841502055
H	-4.281948528	3.077929456	-2.551003094	H	-0.929301235	1.064983090	3.803624874
H	-4.066865760	2.273945462	-4.144387701	C	-2.586398786	2.425641518	3.609404185
H	-3.265405576	3.821057283	-3.814208315	C	-1.893685299	1.269864407	5.726751693
H	3.135705363	5.107486419	-3.547074559	H	-4.584769342	0.659098687	4.512709324
H	1.651570045	5.696302280	-2.746670782	H	6.104708225	-2.014467855	-0.699553932
H	1.538968605	4.512160492	-4.079853446	C	4.883122511	-3.768595659	-0.997834088
H	3.022904050	3.353442385	-0.128572106	H	3.798104182	-0.083284325	1.534212527
H	2.455108583	5.020397220	-0.455506754	C	4.972346819	0.543815424	-0.155948140
H	4.009467223	4.465457368	-1.129264615	C	5.865999912	-0.597245538	1.894241743
C	-2.863934200	-2.388161211	2.752420252	H	3.459429709	-5.390253785	-1.108616845
C	-2.720311699	-0.112911641	3.725510992	H	0.704470124	-3.792473693	0.865222594
C	1.455442196	-1.814280054	3.953287170	C	0.736651098	-5.131708257	-0.818297098
C	-0.587820693	-1.950842310	5.290216395	C	1.666774280	-5.623829890	1.485344477
C	4.220071712	-1.827747464	0.352899222	H	-5.926204559	-1.363573953	3.953136252
C	2.692455862	-3.761294952	0.098228818	H	-3.592094647	2.621358094	4.032228932
C	3.580196428	-2.842316848	3.330553937	H	-1.954007288	3.301018147	3.857084111
C	-2.154410911	-4.795888553	3.153923309	H	-2.685085956	2.377606011	2.510767503
C	-3.002277328	-4.112271890	0.870762468	H	-1.389070694	0.415662951	6.209567811
C	4.858350986	1.350472100	-3.704878693	H	-1.334367998	2.185996017	6.003742113
H	4.806556724	3.344403054	-2.874999836	H	-2.905779494	1.355417850	6.170923408
H	0.954080014	-1.076593602	-3.770363493	H	5.630138497	-4.275465920	-1.627540672
C	2.614849475	-2.420916439	-3.519278440	H	4.138972538	0.651672672	-0.871823229
C	1.944899316	-1.322626295	-5.675792210	H	5.170540883	1.539057510	0.287944188
H	4.609129175	-0.649832020	-4.480233140	H	5.874690599	0.255449361	-0.730830782
H	-6.109534256	2.012829049	0.683809670	H	6.764858919	-0.958767573	1.354981912
C	-4.877688984	3.754452868	1.008106856	H	6.116416519	0.397906532	2.312800455
H	-3.813598197	0.089241662	-1.563016028	H	5.691457967	-1.281159868	2.742148564
C	-5.025480285	-0.536025747	0.102963047	H	1.351813900	-5.932484087	-1.276052704
C	-5.869389906	0.635718567	-1.947807904	H	-0.236220537	-5.585674828	-0.547883195
H	-3.446148659	5.367458115	1.139391906	H	0.550753900	-4.360165793	-1.589524242

H	-0.704473605	3.790397233	-0.868334841	H	2.075872642	-5.206089034	2.422415171
C	-0.726026991	5.104363450	0.834711256	H	0.728222213	-6.156756761	1.736703547
C	-1.666433770	5.631934865	-1.457127799	H	2.391163349	-6.375534110	1.111030255

References

- [1] P. H. M. Budzelaar, R. de Gelder, A. W. Gal, *Organometallics* **1998**, *17*, 4121-4123.
- [2] a) M. Stender, R. J. Wright, B. E. Eichler, J. Prust, M. M. Olmstead, H. W. Roesky, P. P. Power, *J. Chem. Soc., Dalton Trans.* **2001**, 3465-3469; b) J. Feldman, S. J. McLain, A. Parthasarathy, W. J. Marshall, J. C. Calabrese, S. D. Arthur, *Organometallics* **1997**, *16*, 1514-1516.
- [3] X. Dai, P. Kapoor, T. H. Warren, *J. Am. Chem. Soc.* **2004**, *126*, 4798-4799.
- [4] C. Graßl, *Dissertation, Universität Regensburg* **2013**.
- [5] Primal measurement (Evans method) reported in reference [4]. The magnetic moment in solution was re-calculation herein. The NMR measurement and interpretation of ¹H NMR signals was performed herein.
- [6] CrysAlisPro Software System, Agilent Technologies UK Ltd, Yarnton, Oxford, UK (2014).
- [7] O.V. Dolomanov and L.J. Bourhis and R.J. Gildea and J.A.K. Howard and H. Puschmann, Olex2: A complete structure solution, refinement and analysis program, *J. Appl. Cryst.*, **2009**, *42*, 339-341.
- [8] Sheldrick, G.M., *ShelXT, Acta Cryst.*, **2014**, *A71*, 3-8.
- [9] M. C. Burla and R. Caliendo and M. Camalli and B. Carrozzini and G. L. Cascarano and L. De Caro and C. Giacovazzo and G. Polidori and R. Spagna, SIR2004: an improved tool for crystal structure determination and refinement, *J. Appl. Cryst.*, **2005**, *38*, 381-388.
- [10] Sheldrick, G.M., A short history of ShelX, *Acta Cryst.*, **2008**, *A64*, 339-341.
- [11] D. F. Evans, *J. Chem. Soc. (Resumed)* **1959**, 2003-2005.
- [12] G. J. P. Britovsek, V. C. Gibson, S. K. Spitzmesser, K. P. Tellmann, A. J. P. White, D. J. Williams, *J. Chem. Soc., Dalton Trans.* **2002**, 1159-1171.
- [13] G. A. Bain, J. F. Berry, *J. Chem. Educ.* **2008**, *85*, 532
- [14] J. M. Smith, A. R. Sadique, T. R. Cundari, K. R. Rodgers, G. Lukat-Rodgers, R. J. Lachicotte, C. J. Flaschenriem, J. Vela, P. L. Holland, *J. Am. Chem. Soc.* **2006**, *128*, 756-769.
- [15] S. Yao, T. Szilvasi, N. Lindenmaier, Y. Xiong, S. Inoue, M. Adelhardt, J. Sutter, K. Meyer, M. Driess, *Chem. Commun.* **2015**, *51*, 6153-6156.
- [16] a) F. Furche, R. Ahlrichs, C. Hättig, W. Klopper, M. Sierka, F. Weigend, *WIREs Comput. Mol. Sci.* **2014**, *4*, 91-100. b) R. Ahlrichs, M. Bär, M. Häser, H. Horn, C. Kölmel, *Chem. Phys. Lett.* **1989**, *162*, 165-169; c) O. Treutler, R. Ahlrichs, *J. Chem. Phys.* **1995**, *102*, 346-354.
- [17] a) K. Eichkorn, O. Treutler, H. Oehm, M. Häser, R. Ahlrichs, *Chem. Phys. Lett.* **1995**, *242*, 652-660; b) K. Eichkorn, F. Weigend, O. Treutler, R. Ahlrichs, *Theor. Chem. Acc.* **1997**, *97*, 119.
- [18] a) P. A. M. Dirac, *Proc. Royal Soc. A*, 1929, **123**, 714-733. b) J. C. Slater, *Phys. Rev.* **1951**, *81*, 385-390. c) S. H. Vosko, L. Wilk, M. Nusair, *Can. J. Phys.* **1980**, *58*, 1200-1211. d) A. D. Becke, *Phys. Rev. A*, **1988**, *38*, 3098. e) J. P. Perdew, *Phys. Rev. B* **1986**, *33*, 8822-8824.
- [19] a) H. Horn, R. Ahlrichs, *J. Chem. Phys.* **1992**, *97*, 2571. b) F. Weigend, R. Ahlrichs, *Phys. Chem. Chem. Phys.* **2005**, *7*, 3297.
- [20] M. Sierka, A. Hogekamp, R. Ahlrichs, *J. Chem. Phys.* **2003**, *118*, 9136.
- [21] F. Neese, *WIREs Comput. Mol. Sci.*, **2012**, *2*, 73.
- [22] a) A. D. Becke, *Phys Rev A* **1988**, *38*, 3098. b) J. P. Perdew, Y. Wang, *Phys Rev B* **1992**, *45*, 13244.
- [23] a) D. E. Woon, T. H. Dunning, Jr., *J. Chem. Phys.* **1993**, *98*, 1358. b) N.B. Balabanov, K. A. Peterson, *J. Chem. Phys.* **2005**, *123*, 064107.

4.6 Addendum

The preparation of **2a,b,c** is presented in chapter '4.5 Supporting Information' and in the corresponding publication. Their synthesis was performed by the reaction of P₄ with **1a,b,c**, respectively, and a reaction time of 16, 20 or 18 hours.

For better comparability with other [LCo(tol)] systems of upcoming chapters, the reactions were additionally performed under same conditions, however with limited reaction time of 2 hours. The reaction outcome was found not to be altered by the shorter reaction time, which was proven by ¹H NMR spectroscopy in case of **2b** and **2c**. Moreover, we tested the reaction conditions of **A** and similarly did not observe a changed outcome, when reacted within 3 or 18 hours, respectively. This was proven by ¹H NMR spectroscopy.

In addition, the thermolytic treatment of **2c** was investigated. However, refluxing complex **2c** for 2.25 hours in toluene (approx. 100 °C) did not lead to a degradation of **2** or further reactivity. This was monitored by ¹H NMR spectroscopy.

Preface

The following chapter has already been published as an open access article under the terms of the Creative Commons Attribution Non-Commercial NoDerivs (CC BY-NC-ND) License. The article is reprinted with permission of Wiley-VCH.

'Nacnac-Cobalt-Mediated P₄ Transformations'

Chem. Eur. J. **2017**, *23*, 2716-2721. Copyright Wiley-VCH Verlag GmbH & Co. KGaA. Reproduced with permission.

Authors

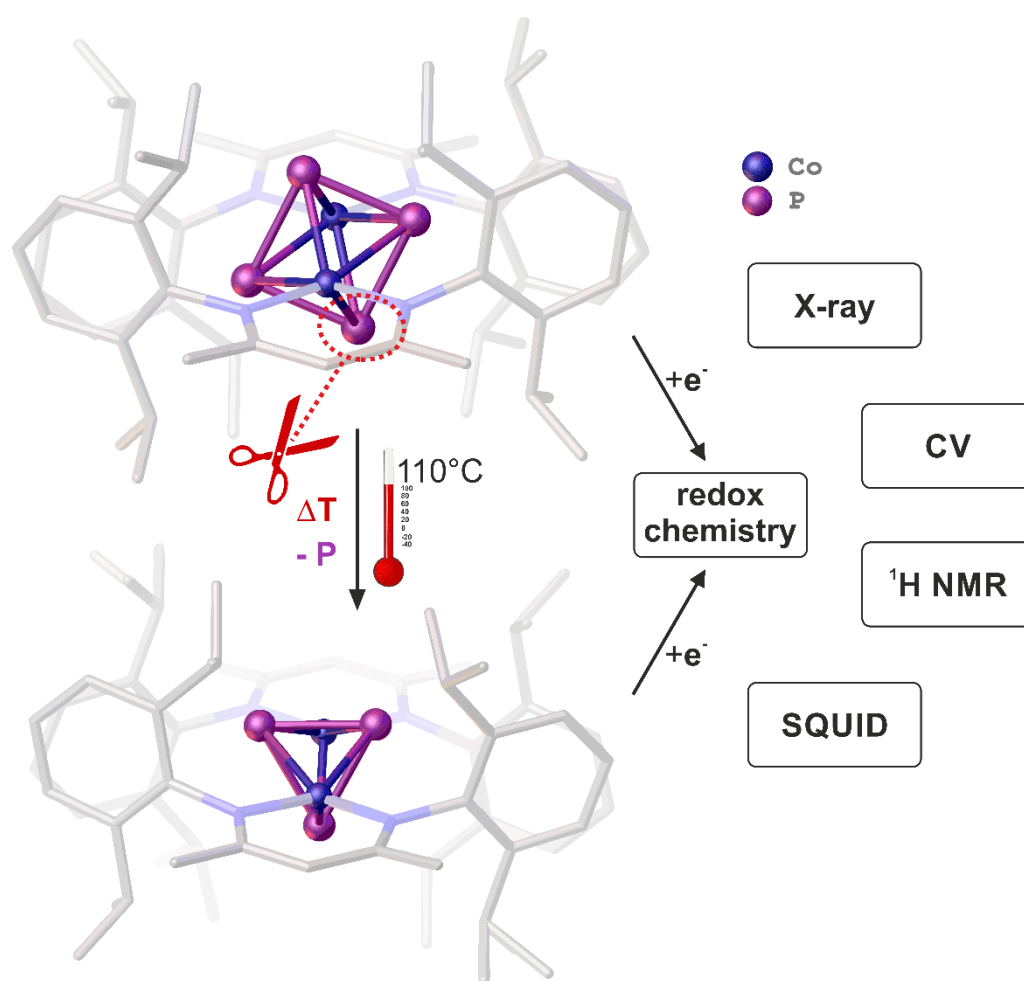
Fabian Spitzer, Christian Graßl, Gábor Balázs, Eric Mädl, Martin Keilwerth, Eva M. Zolnhofer, Karsten Meyer, Manfred Scheer*

Author contributions

The preparation of the manuscript was done by the first author (F. Spitzer). M. Scheer supervised the research and revised the manuscript. Preparation and characterization (X-ray, NMR, Evans method) of compound **1** · *n*-hexane and **2** were part of the first author's master thesis. Among them, the first author provides additional or improved analytical data for **1** · OEt₂ (single crystal X-ray diffraction), for **1** · *n*-hexane and **2** (EA, MS) and re-evaluated the selectivity of the P₄ reaction with compound **1**. A selective synthetic approach to **2** and **3a,b** as well as the complete characterization of **3a**, **3b**, **5b** and **5c** is provided by the first author. C. Graßl described the synthesis and characterization of compounds **4a**, **5a** and **6** in his PhD thesis, however additional or improved analytic data for **4a** and **5a** (EA, ¹H NMR), for **5a** (Evans method) and for **4a** (advanced synthesis) were provided by the first author. The molecular structures of **5a** and **6** were re-measured by the first author. Additionally, the calculation of all X-ray structures herein are performed by the first author as well as the interpretation of ¹H NMR spectra of paramagnetic compounds and the determination of the magnetic moment in solution (Evans method). The samples for the SQUID magnetization measurements were provided by the first author (**2**, **3a**, **5a**, **5b**) or C. Graßl (**6**), and their measurements were performed by E. M. Zolnhofer and M. Keilwerth. Their interpretation and the preparation of the corresponding part in the manuscript and the Supporting Information was performed by them and K. Meyer. E. Mädl performed the cyclic voltammetry measurements of **2**, **3**, **5a** and **6**, their interpretation and wrote the corresponding part in the manuscript and the Supporting Information. G. Balázs performed the DFT calculations and contributed the corresponding parts in the Supporting Information.

Acknowledgements

This work was supported by the Deutsche Forschungsgemeinschaft. The European Research Council (ERC) is acknowledged for the support in the SELFPHOS AdG-339072 project. We are thankful to Dr. M. Bodensteiner for his valuable support regarding the solution of X-ray structures. We extend our thanks to Dr. F. Dielmann for the initial X-ray measurement of **5a** and to Dr. W. Patterson for the Raman measurement of **1** · *n*-hexane.

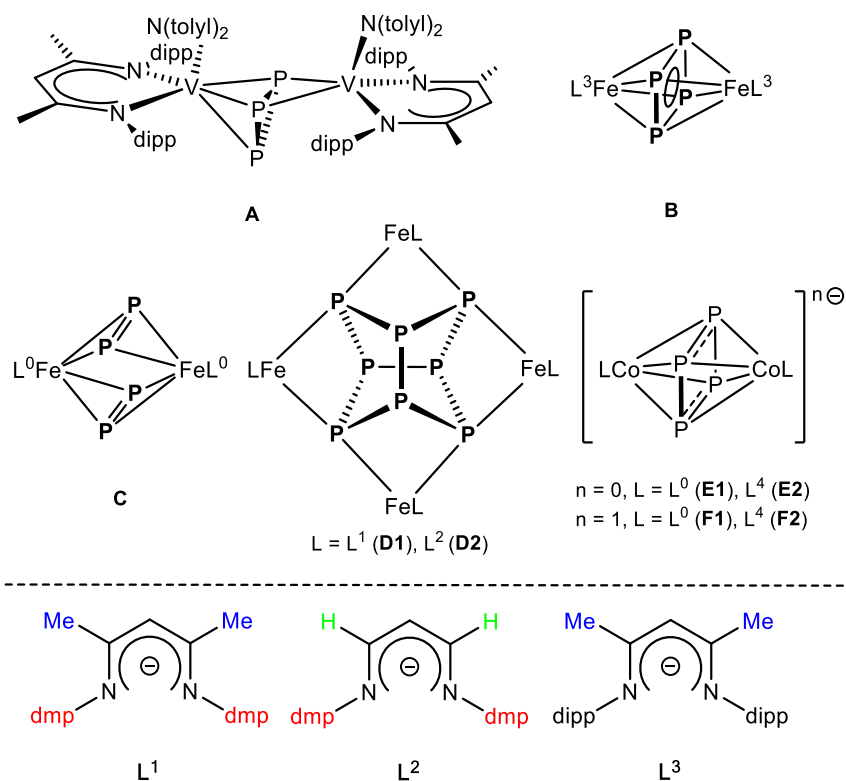


5. Nacnac-Cobalt-Mediated P₄ Transformations

Abstract: A comparison of P₄ activations mediated by low-valent β -diiminato (L) cobalt complexes is presented. The formal Co⁰ source [K₂(L³Co)₂(μ - η^1 : η^1 -N₂)] (**1**) reacts with P₄ to form a mixture of the monoanionic complexes [K(thf)₆][(L³Co)₂(μ - η^4 : η^4 -P₄)] (**2**) and [K(thf)₆][(L³Co)₂(μ - η^3 : η^3 -P₃)] (**3**). The analogue Co^I precursor [L³Co(tol)] (**4a**), however, selectively yields the corresponding neutral derivative [(L³Co)₂(μ - η^4 : η^4 -P₄)] (**5a**). Compound **5a** undergoes thermal P atom loss to form the unprecedented complex [(L³Co)₂(μ - η^3 : η^3 -P₃)] (**6**). The products **2** and **3** can be obtained selectively by an one-electron reduction of their neutral precursors **5a** and **6**, respectively. The electrochemical behavior of **2**, **3**, **5a** and **6** is monitored by cyclic voltammetry and their magnetism is examined by SQUID measurements and the Evans method. The initial Co^I-mediated P₄ activation is not influenced by applying the structurally different ligands L¹ and L², which is proven by the formation of the isostructural products [(LCo)₂(μ - η^4 : η^4 -P₄)] (L = L³ (**5a**), L¹ (**5b**), L² (**5c**)).

5.1 Introduction

The activation of white phosphorus (P₄) with transition metal (TM) complexes with the objective of generating organophosphorus compounds has been an ongoing research topic.^[1] For this purpose, an understanding of the P₄ transformation pathway in the coordination sphere of transition metals is necessary. Thus, a variety of P_n ligand moieties were stabilized to give insight into the stepwise P₄ degradation and aggregation processes using well-established ligand systems such as the Cp^R family (Cp = cyclopentadienyl).^[1] However, over the last years, β -diketiminato (nacnac = L) ligand systems have gained increasing attention in mild P₄ activations using M^I precursors: The initial P₄ fixation step of an intact P₄ tetrahedron at a metal center was achieved at an electron-rich Cu^I nacnac compound.^[2] In reactions with transition metal complexes of Groups 5^[3] and 8–10,^[4] products with modified [P₂]²⁻, [P₄]⁰, [P₄]²⁻ and [P₈]⁴⁻ ligands, respectively, were obtained. So far, for nacnac systems, a [P₃]³⁻ ligand was found solely in compound [(L³VR)₂(cyclo-P₃)]ⁿ⁻ (R = N(tolyl)₂, n = 0,1; R = O(dipp), n = 0) and [(L³V(N(tolyl)₂)₂)₂(μ - η^3 : η^2 -cyclo-P₃)] (**A**, Scheme 1).^[3c]



Scheme 1. Selected examples of P_n-TM complexes containing ligands L⁰–L⁴ (L⁰ = CH[CHN(2,6-*i*-Pr₂C₆H₃)₂]₂, L¹ = CH[C(Me)N(2,6-Me₂C₆H₃)₂]₂, L² = CH[CHN(2,6-Me₂C₆H₃)₂]₂, L³ = CH[C(Me)N(2,6-*i*-Pr₂C₆H₃)₂]₂, L⁴ = CH[C(Me)N(2,6-Et₂C₆H₃)₂]₂). Bottom: Comparison of the supporting ligands used in this study: L¹, L² and L³.^[5]

However, *cyclo*-P₃ complexes of the type [LM(μ-η³:η³-P₃)M'L']^{n±} have been structurally characterized using neutral, tridentate triphos (1,1,1-tris(diphenylphosphino)methyl)ethane) and etriphos (1,1,1-tris(diethylphosphinomethyl)ethane) ligands in different combinations with 3d metals (Fe, Co, Ni) and 4d metals (Rh, Pd).^[6] The influence of the ligand substituents in Fe^I-mediated P₄ transformation has recently been illustrated by a comparative study using a set of ligands L¹–L³ (Scheme 1).^[7] Despite the application of the same reaction conditions, different products were obtained, which are sensitively dependent on small changes of the ligand substituents. 2,6-diisopropylphenyl (dipp) substituents as the aromatic flanking groups of the ligand support the formation of the dinuclear complexes [(L³Fe)₂(μ-η⁴:η⁴-P₄)] (**B**)^[7] and [(L⁰Fe)₂(μ-η²:η²-P₂)₂] (**C**).^[4c] The latter was synthesized by the Driess group.^[4c] The ligands L⁰ and L³ only differ in their backbone substituents. However, for sterically less demanding 2,6-dimethylphenyl (dmp) substituents, the formation of the tetranuclear complexes [(LFe)₄(μ₄-η¹:η¹:η¹:η¹:η¹:η¹:η¹:η¹-P₈)] (L = L¹ (**D1**), L² (**D2**)) with dimerized P₄ units was observed.^[7] These results demonstrate that the product formation is affected by both the aromatic flanking groups and the ligand backbone substituents. Simultaneously, we investigated the [L³Co]-mediated transformations of white phosphorus, which resulted in novel P₄- and P₃-

containing complexes (vide infra). In the meantime, Driess and co-workers reported P₄ activation by [LCo] fragments leading to the neutral complexes [(LCo)₂(μ-η⁴:η⁴-P₄)] (L = L⁰ (**E1**), L⁴ (**E2**)) (Scheme 1).^[4b] One-electron reduction led to the monoanionic products [K(dme)₄][(LCo)₂(μ-η⁴:η⁴-P₄)] (L = L⁰ (**F1**), L⁴ (**F2**)) and transformed the [P₄]⁰ middle deck into a [P₄]²⁻ ligand. Recently, Wolf and co-workers have reported on [(BIAN)Co]⁻-mediated P₄ activations with a nacnac-related bidentate redox non-innocent BIAN (1,2-bis(2,6-diisopropylphenylimino)acenaphthene) ligand system yielding compounds containing [P₄]⁴⁻ moieties.^[8]

Motivated by our first results with [L³Co] compounds, we speculated that the P₄ activation outcome should be sensitive to the oxidation state of the precursor (Co⁰ versus Co^I). Additionally, we wanted to address the question of the ligand influence (L¹–L³) in Co^I-mediated P₄ activations and we were intrigued by the observed P-atom extrusion from the initially obtained P₄ middle deck to form P₃ compounds. The latter ones are still quite rare in comparison to P₄ ligand complexes.

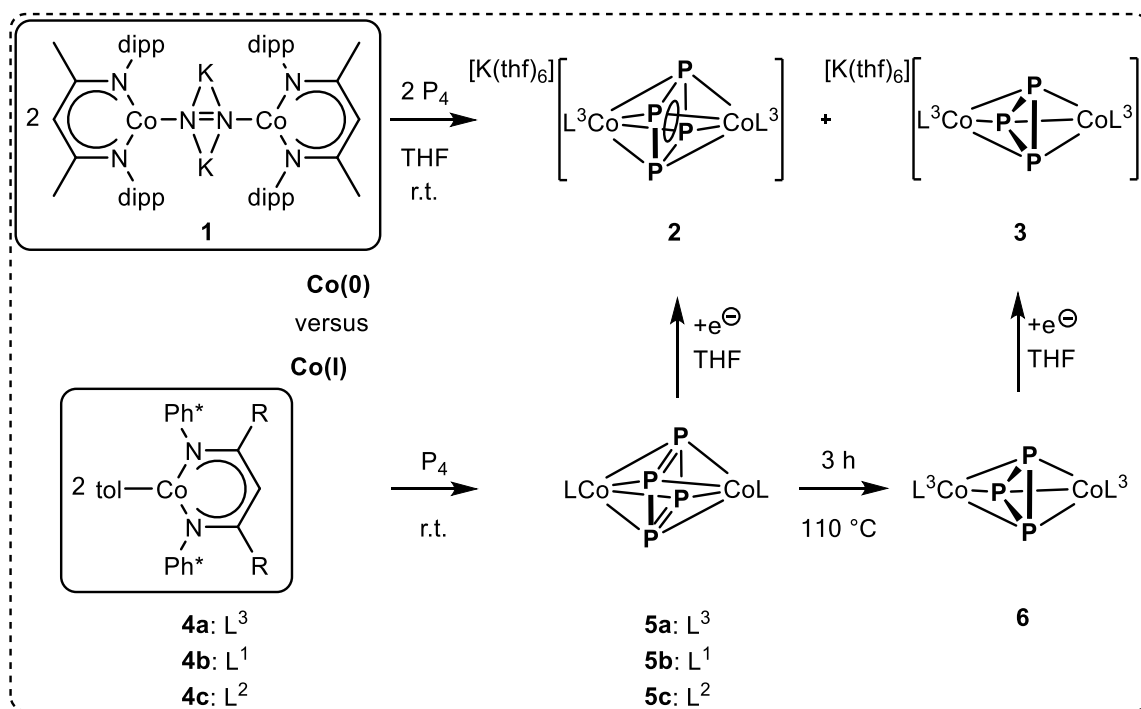
Here, we report on the P₄ activation by a formal Co⁰ precursor yielding the monoanionic [K(thf)₆][(L³Co)₂(μ-η⁴:η⁴-P₄)] (**2**) and [K(thf)₆][(L³Co)₂(μ-η³:η³-P₃)] (**3**). Through a Co^I-mediated P₄ transformation at room temperature or under thermolytic conditions, the corresponding neutral relatives are obtained, which generate **2** and **3** selectively after subsequent one-electron reduction. The redox chemistry of the products was investigated by cyclic voltammetry (CV), and their magnetic behavior was examined both in solution (Evans method) and in the solid state (SQUID).

5.2 Results and Discussion

The formal Co⁰ precursor [K₂(L³Co)₂(μ-η¹:η¹-N₂)] (**1**) was synthesized by a one-pot reaction and was isolated as two different solvomorphs, **1** · solv (solv = *n*-hexane^[9] or OEt₂).^[10] The X-ray structures of **1** · solv consist of two [L³Co] fragments bridged by a N₂ unit. Two potassium atoms cover the N₂ moiety and are coordinated in the phenyl pockets of the dipp substituents.^[11] The N–N distance in **1** · *n*-hexane /OEt₂ is 1.215(3) and 1.220(4) Å, respectively, which is in line with that (1.220(2) Å) of the previously reported [K₂(L⁵Co)₂(μ-η¹:η¹-N₂)] (L⁵ = CH[C(*t*Bu)N(2,6-*i*Pr₂C₆H₃)₂]).^[12] The presence of a [N₂]²⁻ moiety in **1** · *n*-hexane is supported by Raman spectroscopy ($\tilde{\nu}_{\text{NN}} = 1568 \text{ cm}^{-1}$).^[9] The reaction of **1** with P₄ proceeds by N₂ evolution, showing that the formal [N₂]²⁻ species is re-oxidized and revealing **1** as a formal dicobalt(0) starting material.

Conducting the reaction in 1:1 stoichiometry leads to the complete consumption of P₄ and the formation of a mixture of the monoanionic complexes [K(thf)₆][(L³Co)₂(μ-η⁴:η⁴-P₄)] (**2**) and [K(thf)₆][(L³Co)₂(μ-η³:η³-P₃)] (**3**), which were detected by ¹H NMR

spectroscopy.^[13] The appearance of a *cyclo*-P₃ moiety in product **3** indicates that an extrusion of one P atom from the *cyclo*-P₄ moiety in **2** is possible (Scheme 2). However, if the reaction is conducted with two equivalents of P₄, compound **2** is the only product found in the ¹H NMR spectrum.



Scheme 2. Performed Co⁰- and Co^I-mediated P₄ transformations.

The solid state structure of **2** · 2 thf reveals a salt consisting of two [K(thf)₆]⁺ cations and two crystallographically distinguishable [(L³Co)₂(μ-η⁴:η⁴-P₄)]⁻ monoanions (Figure 1).^[9] Each anion is a centrosymmetric dicobalt complex that consists of two [L³Co] fragments bridged by a planar *cyclo*-P₄ ligand.

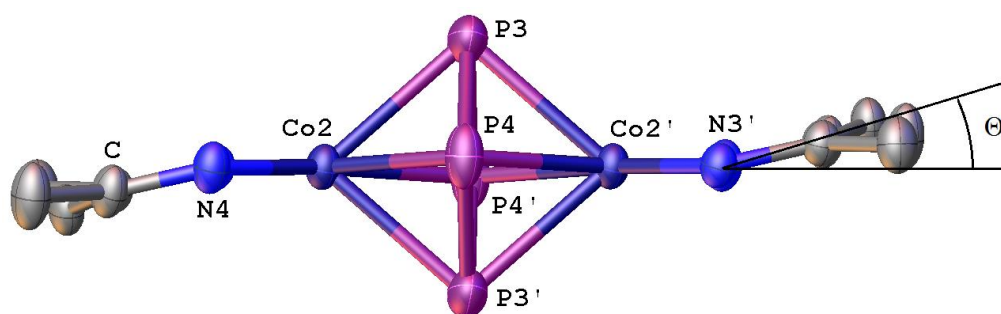


Figure 1. Anionic part of the molecular structure of **2** in the crystal. Hydrogen atoms and aromatic flanking groups are omitted for clarity. Thermal ellipsoids are drawn at 50% probability level. The angle Θ is depicted spanning between the Co...Co' axis and the plane formed by the nitrogen atoms and the methine carbon in the ligand backbone.

The P–P distances amount to 2.1913(10)–2.1951(10) Å in anion 1 and 2.1897(10)–2.2004(10) Å in anion 2, respectively. These values correspond well with the *cyclo*-[P₄]²⁻ moiety (2.178(1) and 2.207(1) Å) of the reported compound [(L³Fe)₂(μ-η⁴:η⁴-P₄)] (**B**).^[7] The central P₄ ligands in **2** are almost square planar with interior angles of 86.07(3) and 93.92(3)° in anion 1 and 86.38(3) and 93.62(3)° in anion 2. The Co–P distances range from 2.3362(7)–2.4149(7) Å in anion 1 and 2.3441(7)–2.4190(7) Å in anion 2. Selected atomic distances of compound **2** are summarized in Table 1. Minor deviations within the atomic parameters of compound **2** · 2 thf and the related compounds [K(dme)₄][(LCo)₂(μ-η⁴:η⁴-P₄)] (L = L⁰ (**F1**), L⁴ (**F2**)) can be explained by small changes in the organic environment of the counter ion and the nacnac ligands of the complex monoanions. They may affect the Co···Co' distances and their coordination geometry (angle Θ between the Co···Co' axis and the plane formed by the nitrogen atoms and the methine carbon in the ligand backbone; Figure 1 for graphical presentation of Θ).^[14]

Table 1. Comparison of P–P and Co···Co' atomic distances and angles Θ in anions of [K(solv)_x][(LCo)₂(μ-η⁴:η⁴-P₄)] (L = L³ (**2**)^[9], L⁰ (**F1**)^[4b], L⁴ (**F2**)^[4b]).

Complex	2: anion 1	2: anion 2	F1 ^[4b]	F2 ^[4b]
<i>d</i> (P–P) / [Å]				2.154(1) ^[a]
	2.1913(10)	2.1897(10)	2.1739(7)	2.163(1) ^[a]
	2.1951(10)	2.2004(10)	2.1976(7)	2.225(1) ^[a]
				2.230(1) ^[a]
<i>d</i> (Co···Co') / [Å]	3.603	3.625	3.626	3.603
Θ / [°]	13.87(6)	15.87(6)	15.33(4)	6.60(8) ^[a]
				14.97(7) ^[a]

[a]: Anion of **F2** is not centrosymmetric. Therefore, four individual *d*(P–P) and two Θ values are given.

The monoanionic [(L³Co)₂(μ-η³:η³-P₃)]⁻ was obtained in two different solvomorphs [K(dme)₄][(L³Co)₂(μ-η³:η³-P₃)] · dme (**3a**) and [K(thf)₆][(L³Co)₂(μ-η³:η³-P₃)] · 2 thf (**3b**). Both compounds are ionic and consist of solvent (DME or THF) molecules, one solvent-saturated potassium counter ion, and the [(L³Co)₂(μ-η³:η³-P₃)]⁻ monoanion (Figures 2 and 3). In both X-ray structures, the complex anions are built from two [L³Co] fragments bridged by a P₃ triangle. In **3a**, the L³ ligand planes are almost parallel to each other with a dihedral angle of 2.00(7)° (N1–N2 versus N3–N4). However, in **3b**, the ligand planes are in a twisted conformation with a dihedral angle of 74.2(4)° (N1–N2 versus N3–N4, Figure 2).

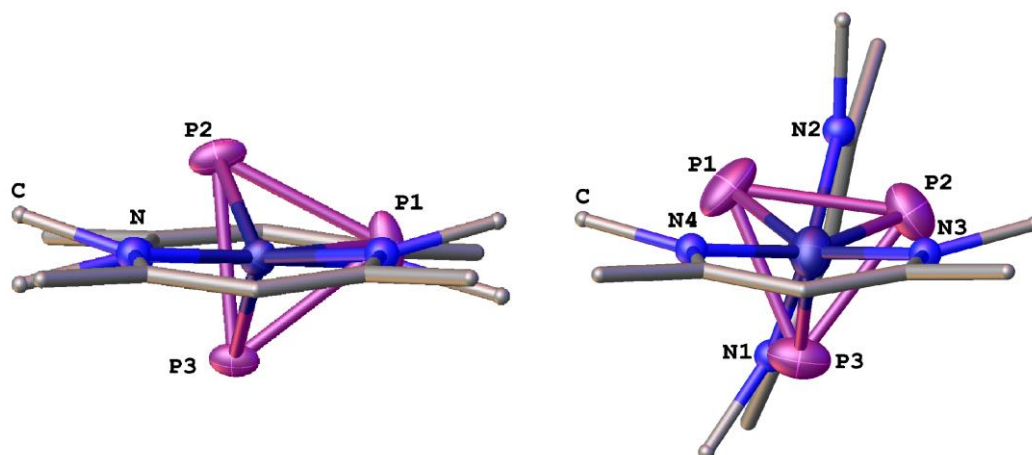


Figure 2. Comparison of the anions in the molecular structures of **3a** (left) and **3b** (right) in the crystal. Hydrogen atoms and aromatic flanking groups are omitted for clarity. Thermal ellipsoids of Co and P atoms are drawn at 50% probability level. Major component of disordered *cyclo*-P₃ ligand is drawn in **3a**.

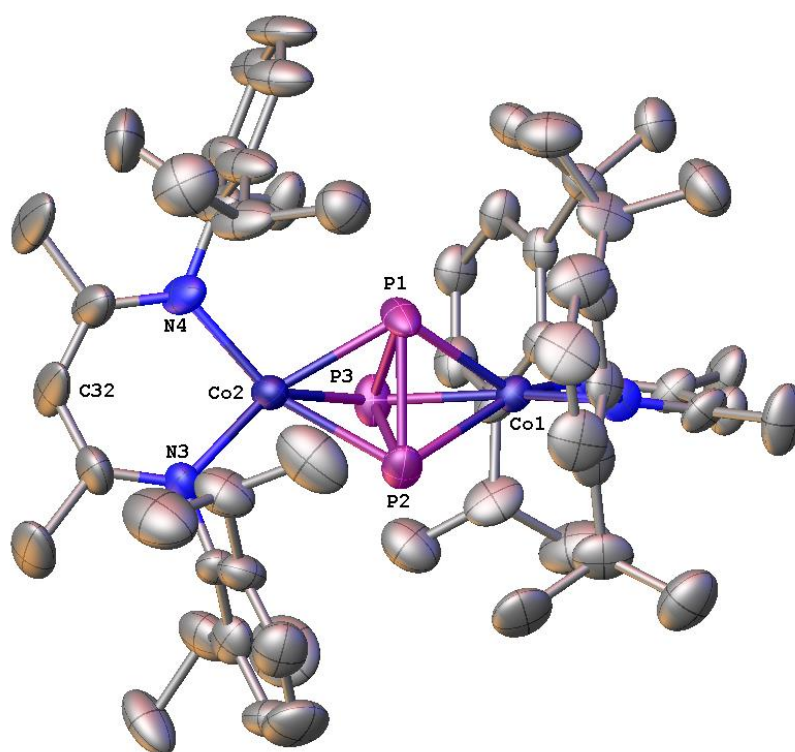


Figure 3. Anionic part of the molecular structure of **3b** in the crystal. Hydrogen atoms are omitted for clarity. Thermal ellipsoids are drawn at 50% probability level.

The different complex anion conformations may originate from packing effects probably directed by the unequally shaped counter cations. This is also confirmed by DFT calculations since the experimental geometry of **3a** relaxes during the geometry optimisation to a geometry in which the *nacnac* ligands are oriented almost perpendicular to each other, resembling to the experimental geometry of **3b**. In the solid state the *cyclo*-P₃ middle deck is disordered over two positions in **3a** (occupancy 81:19).^[15] The middle deck in **3b**, however, is localized at one distinct position.

Table 2. Comparison of selected atomic distances and angles in the [(L³Co)₂(μ-η³:η³-P₃)]⁻ anion in **3a** (major component) and **3b**, [(L³V(N(tolyl)₂)₂)₂(μ-η³:η²-cyclo-P₃)] (**A**),^[3c] and the dication in [(triphos)Co(μ-η³:η³-cyclo-P₃)Fe(etriphos)](PF₆)₂ (**G**).^[6b]

Complex	3a	3b	A ^[3c]	G ^[6b]
<i>d</i> (P–P) / [Å]	2.1674(13)	2.217(4)	2.1658(10)	2.226(8)
	2.1790(16)	2.224(4)	2.1804(9)	2.229(8)
	2.3303(17)	2.237(4)	2.2155(9)	2.234(8)
∠ (P–P–P) / [°]	57.34(5)	59.59(13)	59.03(3)	-
	57.82(5)	59.93(14)	59.68(3)	-
	64.84(5)	60.48(13)	61.29(3)	-
<i>d</i> (M···M') / [Å]	3.7359(5)	3.724(2)	4.460	3.80
∠ / [°]	9.43(7)	8.7(3)	-	-
	12.22(7)	13.5(6)	-	-

As can be seen in Table 2, the P–P distances in **3a** are similar to the ones in the nacnac containing compound [(L³V(N(tolyl)₂)₂)₂(μ-η³:η²-cyclo-P₃)] (**A**),^[3c] displaying a *cyclo*-[P₃]³⁻ moiety. In **3b**, they compare better with the ones in [(triphos)Co(μ-η³:η³-cyclo-P₃)Fe(etriphos)](PF₆)₂ (**G**).^[6b]

Overall, they are in line with P–P single bonds (for comparison: P–P single bond in white phosphorus determined by X-ray diffraction: 2.209(5) Å,^[16] electron diffraction: 2.1994(3) Å,^[17] Raman spectroscopy: 2.2228(5) Å,^[18] and DFT calculations: 2.1994(3) Å^[17]). The Co–P distances in **3a** are between 2.2046(17) and 2.3684(8) Å and for **3b** in the range of 2.248(3) and 2.277(3) Å. The Co···Co' distance in **3a** is 3.7359(5) Å and amounts to 3.724(2) Å in **3b**, which is slightly elongated compared to **2** (3.603 and 3.625 Å, Table 1).

The ¹H NMR spectra in [D₈]THF display signals between 11.42 and –35.29 ppm for **2**^[9] and 8.15 and –12.85 ppm for **3**, respectively. Except for the THF and DME signals, respectively, the ¹H NMR spectra of **3a,b** do not deviate from each other. No signals are detected in the ³¹P{¹H} NMR spectra for **2** and **3** due to their paramagnetic nature. Their magnetic moment (μ_{eff}) in [D₈]THF solution (r.t.) was determined by the Evans method: 3.90 μ_{B} (**2**) and 3.51 μ_{B} (**3**). In the solid state, these values are well confirmed by SQUID measurements displaying a gradual decrease of the magnetic moment in the temperature range from 300 to 2 K of 3.80 to 3.30 μ_{B} in **2** and 3.58 to 1.70 μ_{B} in **3a**. Therefore, the electronic structure of **2** is best described as containing a [P₄]²⁻ moiety bridging mixed valence Co^I and Co^{II} centers. This is in agreement with the previously reported compounds

F1 and **F2**.^[4b] Compound **3**, however, contains a [P₃]³⁻ ligand, which is bridged by two Co^{II} metal centers.

As mentioned above, starting from the formal Co⁰ precursor **1**, we obtained the compounds **2** and **3** as a mixture of products, the ratio of which is sensitively dependent on stoichiometry and reaction conditions. To discover an alternative approach, we targeted the use of the Co^I starting material [L³Co(tol)] (**4a**), which was speculated to yield the neutral analogues of **2** and **3**. After their one-electron reduction, the compounds **2** and **3** should be accessible.

Therefore, the Co^I compound [L³Co(tol)] (**4a**) was reacted with P₄, and [(L³Co)₂(μ-η⁴:η⁴-P₄)] (**5a**) was selectively formed (Scheme 2). Structural parameters and the characterization of compound **5a** are discussed in detail below.

Refluxing **5a** for three hours (110 °C, toluene) gives rise to the loss of one phosphorus atom and the formation of [(L³Co)₂(μ-η³:η³-P₃)] (**6**, Scheme 2),^[19] which was clearly characterized by mass spectrometry^[20] and ¹H NMR spectroscopy.^[21] The dinuclear compound contains two [L³Co] fragments and the bridging middle deck exhibits a savage disorder within its *cyclo*-P₃ moiety. We emphasize that the P–P distances cannot be precisely described. However, the initially localized electron density unambiguously displays triangle-shaped *cyclo*-P₃ constitution and enables an estimation of the P–P distances in **6** (approx. *d*(P–P): 2.147(3), 2.223(2), 2.235(2) Å). These values are comparable with the ones found in **3a** (2.1674(13), 2.1790(16), 2.3303(17) Å) and **3b** (2.217(4), 2.224(4) and 2.237(4) Å) and are elongated compared to the ones in **A** (2.1658(10), 2.1804(9) and 2.2155(9) Å).^[3c] The Co···Co' distance in **6** is 3.747 Å and therefore comparable to the ones in **3a** (3.7359(5) Å) and **3b** (3.724(2) Å), but elongated compared to its precursor complex **5a** (3.610 Å, *vide infra*).

The ¹H NMR spectrum of **6** reveals signals between 20.06 and –12.68 ppm. No signal is detected in the ³¹P{¹H} NMR spectrum. The magnetic moment (*μ*_{eff}) of **6** in C₆D₆ solution is 2.97 μ_B at room temperature (Evans method).^[22] This value is well confirmed in the solid state by a SQUID measurement. A successive decrease from 2.7 to 2.0 μ_B was measured in the temperature range from 300 to 2 K (see the Supporting Information). The values are in agreement with antiferromagnetically coupled Co^{II} and Co^{III} metal centers.

Electrochemistry

The electrochemical properties of the complexes **5a** and **6** were probed by cyclic voltammetry (CV) in THF solution containing Bu₄NPF₆ electrolyte (0.1 mol·L⁻¹, 295 K, see Supporting Information for further details).^[20] An irreversible oxidation was detected at *E*_{1/2} = –0.34 V for **5a** and *E*_{1/2} = –0.11 V for **6** (vs. Cp₂Fe/Cp₂Fe⁺). The compounds **5a** and

6 each reveal one reversible reduction at $E_{1/2} = -1.62$ V (vs. Cp₂Fe/Cp₂Fe⁺). The complexes **2**^[9] and **3** confirm these values by the corresponding electrochemical behavior. For **3**, an additional reduction event was monitored at -2.52 V (vs. Cp₂Fe/Cp₂Fe⁺).

We experimentally performed the reduction of **5a** and **6**, respectively, with one equivalent of potassium graphite in THF at room temperature. The corresponding anionic compounds [K(thf)₆][(L³Co)₂(μ-η⁴:η⁴-P₄)] (**2**) and [K(thf)₆][(L³Co)₂(μ-η³:η³-P₃)] (**3**), respectively, are selectively and quantitatively formed, which was proven by ¹H NMR spectroscopy of the crude reaction solution. On a preparative scale, the isolated yields obtained as single crystals are 41% for **2** and 62% for **3**. Consequently, regarding selectivity, this synthetic route is superior to the Co⁰-mediated P₄ activation, which, in contrast, yielded a mixture of products.

Impact of Ligand Design

Three β-diimines (L¹H, L²H, L³H) were synthesized to provide a comparable hybrid ligand set L¹–L³ with backbone (R = H, Me) and aromatic (Ph* = dmp or dipp) substituents (Scheme 1 and 2), and to investigate the influence of the ligand design on the Co^I-mediated P₄ transformation. The [LCo(tol)] (L = L³ (**4a**), L¹ (**4b**), L² (**4c**)) starting materials were prepared in one-pot reactions (see the Supporting Information). All conducted P₄ activation reactions were performed under the same conditions ([LCo(tol)]:P₄ = 2:1, toluene, 2–3 hours, r.t.) and yielded similar isolated products [(LCo)₂(μ-η⁴:η⁴-P₄)] (L = L³ (**5a**), L¹ (**5b**), L² (**5c**)). The crystals of all the new compounds **5a–c** were grown from saturated toluene solutions and single crystal X-ray diffraction was performed. The molecular structures of **5a–c** are shown in Figure S5 in the Supporting Information. As a representative, compound **5a** is presented in Figure 4. Its P₄ moiety is rectangularly shaped, consequently spanned by two shorter and two longer P–P atom distances. Together with two coordinating Co atoms, the [P₄Co₂] complex core builds a distorted octahedron. In **5a–c**, the shorter P–P atom distances are between 2.1256(6) and 2.1301(7) Å and the longer P–P atom distances are between 2.2513(10) and 2.2980(7) Å. Compared with a phosphorus single bond in the tetrahedral P₄, the planar rectangular-shaped P₄ moieties in **5a–c** contain a pair of shorter and a pair of elongated P–P bonds. The Co⋯Co' distances in **5a–c** are between 3.502 and 3.610 Å and therefore any bonding interaction can be ruled out. Due to the centrosymmetric molecular structure (*P2*₁/*n* in **5a–c**), the ligands are parallel to each other. In **5a–c**, the angles Θ (between the Co⋯Co' axis and the plane formed by the nitrogen atoms and the methine carbon in the ligand backbone) are between 3.40(6) and 12.32(6)°. In **5b,c** (and **E1,2**^[4b]), the P–P edges of the *cyclo*-P₄ unit are nearly parallel or rectangular, respectively, compared to the N–N axis of

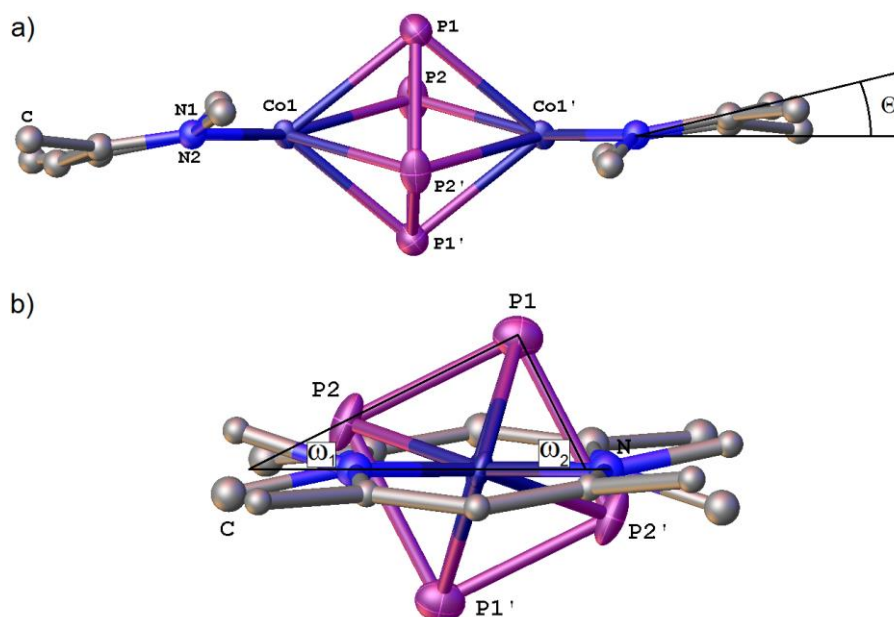


Figure 4. a) Molecular structure of **5a** in the crystal. Hydrogen atoms and aromatic flanking groups are omitted for clarity. Thermal ellipsoids are drawn at 50% probability level. The angle Θ is depicted, which spans between the Co \cdots Co' axis and the plane formed by the nitrogen atoms and the methine carbon in the ligand backbone; b) view along Co1 \cdots Co1' axis, revealing the angles ω_1 and ω_2 , which span between the N–N axis of coordinating nitrogen atoms and the edges of the *cyclo*-P₄ unit.

coordinating nitrogen atoms (compare $\sphericalangle(\text{NN-PP}_{\text{short}}) = \omega_1$ and $\sphericalangle(\text{NN-PP}_{\text{long}}) = \omega_2$, see Figure 4b). The structural parameters of **5a–c** and **E1,2** are summarized in Table 3.

Table 3. Comparison of P–P and Co \cdots Co' atomic distances in neutral [(LCo)₂(μ - η^4 : η^4 -P₄)] (L = L³ (**5a**), L¹ (**5b**), L² (**5c**), L⁰ (**E1**), L⁴ (**E2**)).

Complex	5a	5b	5c	E1 ^[4b]	E2 ^[4b]
$d(\text{P-P})$ short / [Å]	2.1295(10)	2.1256(6)	2.1301(7)	2.1237(13)	2.1298(14)
$d(\text{P-P})$ long / [Å]	2.2513(10)	2.2972(6)	2.2980(7)	2.2984(13)	2.2889(15)
$d(\text{Co}\cdots\text{Co}') / [\text{Å}]$	3.610	3.502	3.503	3.491	3.533
$\Theta / [^\circ]$	12.22(8)	12.32(6)	3.40(6)	14.88(9)	7.0(1)
$\omega_1 / [^\circ]$	26.34(6)	2.18(4)	1.97(4)	1.96(7)	2.58(8)
$\omega_2 / [^\circ]$	62.36(6)	87.87(4)	87.95(4)	88.02(7)	87.43(8)

The ¹H NMR spectra of the compounds **5a–c** display signals between 11.99 and –28.61 ppm and reveal their paramagnetic nature in solution. Therefore, no signals are detected in their ³¹P{¹H} NMR spectra. Their magnetic moment (μ_{eff}) in solution (r.t.) was determined by the Evans method: 3.02 μ_{B} (**5a**^[22] in C₆D₆), 2.42 μ_{B} (**5b** in C₆D₆), 1.84 μ_{B} (**5c** in [D₈]THF). In the solid state, however, the SQUID measurements of **5a** and **5b** display diamagnetic behavior in the temperature range of 2–300 K. Their electronic structure in

the solid state is best described as two antiferromagnetically coupled Co^I centers bridged by a [P₄]⁰ ligand similar to the previously reported compounds **E1,2**.^[4b] In solution, exclusively one signal set for the ligand is observed in the ¹H NMR spectrum of **5a-c**, respectively, suggesting the integrity of each dinuclear compound in solution on the NMR time scale (Figure S15 in the Supporting Information).

5.3 Conclusion

We reported different [LCo^I]-mediated P₄ activations yielding neutral complexes [(LCo)₂(μ-η⁴:η⁴-P₄)] (L = L¹, L², L³), each containing a similar, rectangular-shaped [P₄]⁰ moiety. In contrast to the P₄ activation by LFe^I compounds, for the Co system, the ligand substituents (L¹-L³) do not alter the reaction outcome. For the ligand system L³, we demonstrate that one P atom can be extruded thermolytically to generate an unprecedented neutral compound [(L³Co)₂(μ-η³:η³-P₃)] containing a *cyclo*-[P₃]³⁻ ligand. As a novel approach, we present the P₄ transformation with a formal [L³Co⁰] precursor, which generates corresponding monoanions with *cyclo*-[P₄]²⁻ and *cyclo*-[P₃]³⁻ ligands as a mixture of products. Each product was selectively accessed through the one-electron reduction of its neutral precursor.

5.4 References

- [1] a) D. Tofan, B. M. Cossairt, C. C. Cummins, *Inorg. Chem.* **2011**, *50*, 12349-12358; b) M. Caporali, L. Gonsalvi, A. Rossin, M. Peruzzini, *Chem. Rev.* **2010**, *110*, 4178-4235; c) M. Scheer, G. Balázs, A. Seitz, *Chem. Rev.* **2010**, *110*, 4236-4256; d) S. Khan, S. S. Sen, H. W. Roesky, *Chem. Commun.* **2012**, *48*, 2169-2179; e) N. A. Giffin, J. D. Masuda, *Coord. Chem. Rev.* **2011**, *255*, 1342-1359.
- [2] F. Spitzer, M. Sierka, M. Latronico, P. Mastrorilli, A. V. Virovets, M. Scheer, *Angew. Chem. Int. Ed.* **2015**, *54*, 4392-4396; *Angew. Chem.* **2015**, *127*, 4467-4472.
- [3] a) B. L. Tran, M. Singhal, H. Park, O. P. Lam, M. Pink, J. Krzystek, A. Ozarowski, J. Telsler, K. Meyer, D. J. Mindiola, *Angew. Chem. Int. Ed.* **2010**, *49*, 9871-9875; *Angew. Chem.* **2010**, *122*, 10067-10071; b) C. Camp, L. Maron, R. G. Bergman, J. Arnold, *J. Am. Chem. Soc.* **2014**, *136*, 17652-17661; c) B. Pinter, K. T. Smith, M. Kamitani, E. M. Zolnhofer, B. L. Tran, S. Fortier, M. Pink, G. Wu, B. C. Manor, K. Meyer, M.-H. Baik, D. J. Mindiola, *J. Am. Chem. Soc.* **2015**, *137*, 15247-15261.
- [4] a) S. Yao, Y. Xiong, C. Milsmann, E. Bill, S. Pfirrmann, C. Limberg, M. Driess, *Chem. Eur. J.* **2010**, *16*, 436-439; b) S. Yao, N. Lindenmaier, Y. Xiong, S. Inoue, T. Szilvási, M. Adelhardt, J. Sutter, K. Meyer, M. Driess, *Angew. Chem.* **2015**, *127*, 1266-1270; c) S. Yao, T. Szilvasi, N. Lindenmaier, Y. Xiong, S. Inoue, M. Adelhardt, J. Sutter, K. Meyer, M. Driess, *Chem. Commun.* **2015**, *51*, 6153-6156.
- [5] The ligands L⁰-L⁴ are called „nacnac“ in this report due to their structural similarities. More precisely, L⁰ and L² can be regarded as vinylogous amidines and therefore are part of the „vinamidine“ ligand family. See: D. Lloyd, H. McNab, *Angew. Chem. Int. Ed. Engl.* **1976**, *15*, 459-468.
- [6] a) for (triphos)Co,Ni(triphos) and (triphos)Ni,Ni(triphos), see: M. Di Vaira, S. Midollini, L. Sacconi, *J. Am. Chem. Soc.* **1979**, *101*, 1757-1763; b) for (triphos)Fe,Co(etriphos) and (triphos)Co,Co(triphos) (in footnote): C. Bianchini, M. D. Vaira, A. Meli, L. Sacconi, *Inorg. Chem.* **1981**, *20*, 1169-1173; c) for (triphos)Co,Rh(triphos) and (triphos)Ni,Rh(triphos): C. Bianchini, M. Di Vaira, A. Meli, L. Sacconi, *J. Am. Chem. Soc.* **1981**, *103*, 1448-1452; d) for (triphos)Pd,Pd(triphos): P. Dapporto, L. Sacconi, P. Stoppioni, F. Zanobini, *Inorg. Chem.* **1981**, *20*, 3834-3839; e) for a review, see: M. D. Vaira, L. Sacconi, *Angew. Chem. Int. Ed. Engl.* **1982**, *21*, 330-342; *Angew. Chem.* **1982**, *94*, 338-351; for additional examples: f) O.

- J. Scherer, B. Werner, G. Heckmann, G. Wolmershäuser, *Angew. Chem. Int. Ed. Engl.* **1991**, *30*, 553-555; *Angew. Chem.* **1991**, *103*, 562-563; g) E. Mädl, G. Balázs, E. V. Peresykina, M. Scheer, *Angew. Chem. Int. Ed.* **2016**, *55*, 7702-7707; *Angew. Chem.* **2016**, *128*, 7833-7838; h) Y. Nakanishi, Y. Ishida, H. Kawaguchi, *Inorg. Chem.* **2016**, *55*, 3967-3973.
- [7] F. Spitzer, C. Graßl, G. Balázs, E. M. Zolnhofer, K. Meyer, M. Scheer, *Angew. Chem. Int. Ed.* **2016**, *55*, 4340-4344; *Angew. Chem.* **2016**, *128*, 4412-4416.
- [8] S. Pelties, T. Maier, D. Herrmann, B. de Bruin, C. Rebreyend, S. Gärtner, I. G. Shenderovich, R. Wolf, *Chem. Eur. J.* **2017**, *23*, 6094-6102.
- [9] F. Spitzer, Master thesis, *University of Regensburg*, **2013**.
- [10] After lithiation of L³H and subsequent transmetalation with CoBr₂, its reduction was performed with an excess of potassium graphite under N₂ atmosphere.
- [11] In **1** · *n*-hexane the NCCCN ligand planes are orientated parallel to each other. However, in **1** · OEt₂, they are twisted (dihedral angle of coordinating N atoms: 32.38(9)°). Further analytical data (X-ray, ¹H NMR, Evans method, EA, Raman spectrum) and pictures of **1** · solv are presented in the Supporting Information.
- [12] K. Ding, A. W. Pierpont, W. W. Brennessel, G. Lukat-Rodgers, K. R. Rodgers, T. R. Cundari, E. Bill, P. L. Holland, *J. Am. Chem. Soc.* **2009**, *131*, 9471-9472.
- [13] For initial investigations see reference [9]. The identification of products **2** and **3** in ¹H NMR spectra was enabled after their selective preparation.
- [14] The dependency of angle Θ and Fe···Fe' distance was already recognized in citation [7].
- [15] Due to the disorder of the *cyclo*-P₃ moiety, only the geometric parameters of the major component are discussed. Furthermore, it has to be noted that the positions of the disordered P3 and P3A atoms are close to each other and hence, the involved bond lengths might not be determined with high accuracy.
- [16] In β -P₄: A. Simon, H. Borrmann, H. Craubner, *Phosphorus Sulfur Silicon Relat. Elem.* **1987**, *30*, 507-510.
- [17] B. M. Cossairt, C. C. Cummins, A. R. Head, D. L. Lichtenberger, R. J. F. Berger, S. A. Hayes, N. W. Mitzel, G. Wu, *J. Am. Chem. Soc.* **2010**, *132*, 8459-8465.
- [18] N. J. Brassington, H. G. M. Edwards, D. A. Long, *J. Raman Spectrosc.* **1981**, *11*, 346-348.
- [19] The crystal structures of **6** and **5a** were initially reported in reference [20]. However, to present improved structural values, crystals of **6** and **5a** were re-measured.
- [20] C. Graßl, PhD thesis, *University of Regensburg*, **2013**.
- [21] During the thermolysis, a black, pyrophoric precipitate is formed. The CHN analysis of the washed and dried precipitate suggests only some organic content (C%: ≈35, H%: ≈5, N%: ≈3). Exclusively, compound **6** and L³H were detected in the ¹H NMR spectrum (reaction control) as the only soluble products formed during the thermolysis reaction.
- [22] For initial investigations see reference [20]. For further information see the Supporting Information.

5.5 Supporting Information

General Remarks

All manipulations were performed with rigorous exclusion of oxygen and moisture using Schlenk-type glassware on a dual manifold Schlenk line with Argon (generally) or N₂ (only for synthesis of **1**) inert gas or glove box filled with N₂ containing a high-capacity recirculator (<0.1 ppm O₂). Solvents were dried using a MB SPS-800 device of company MBRAUN, degassed and saturated with argon to prevent N₂ activation while reduction reactions (for **4a-c**). Mass spectrometry was performed using a ThermoQuest Finnigan TSQ 7000 (ESI-MS), Finnigan MAT 95 (LIFDI) and JEOL AccuTOF GCX (LIFDI) mass spectrometer, respectively. Elemental analysis (CHN) was determined using a Vario micro cube and Vario EL III instrument. ¹H NMR spectra were recorded on a Bruker Avance III HD 400 (¹H: 400.130 MHz) spectrometer. The chemical shifts are reported in ppm relative to external TMS.

The used potassium graphite exhibits an elemental distribution of KC₁₀, which was examined by titration.

Ligands L¹H^[1], L²H^[2] and L³H^[3] were synthesized according to literature methods.

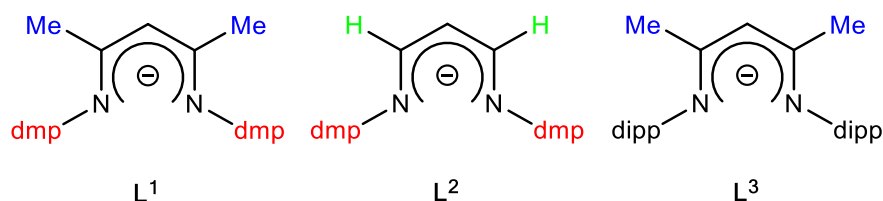


Figure S1. Used ligand systems L¹, L² and L³, each containing an individual combination of backbone and aromatic substituents (dmp = 2,6-dimethylphenyl; dipp = 2,6-diisopropylphenyl).

Synthesis of [L¹Co(tol)] (**4b**) is published.^[4] Related compounds [L⁰Co(tol)] and [L⁴Co]₂ are reported using a different synthetic protocol.^[5] Compound [L³Co(tol)] (**4a**) was synthesized by a related protocol, which is presented below. Compound [L¹Co(tol)] (**4b**) and [L²Co(tol)] (**4c**) can be synthesized according to this protocol.

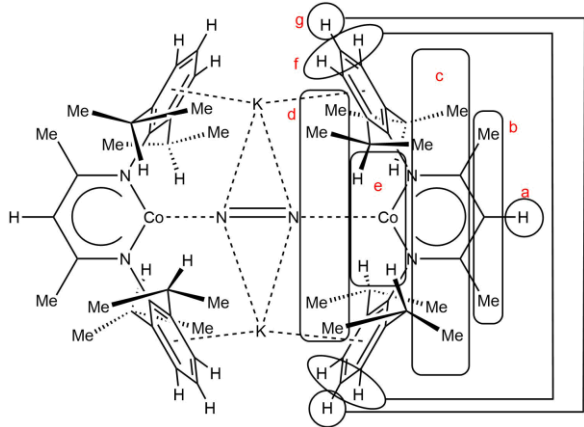
Synthesis of [K₂(L³Co)₂(μ-η¹:η¹-N₂)] (1)^[6]

8.0 g (19.1 mmol) L³H in 50 mL THF were cooled to 0 °C and 12 mL (19.1 mmol) *n*-BuLi (1.6 M in *n*-hexane) were added. The color turned yellow and the solution was stirred at r.t. for 16 hours. A deep blue slurry of 4.2 g (19.1 mmol) CoBr₂ anhydrous in 50 mL THF was cooled to -75 °C and the yellow solution was added within 10 minutes. After stirring for 1 hour at -75 °C the solution was allowed to reach r.t. within 16 hours. Meanwhile, the color changed from green to brown. The solvent was removed in vacuum.

The following steps are conducted under N₂ gas atmosphere:^[6] 2.8 g (3.1 mmol) of the remained brown powder [Li(thf)₄][L³CoBr₂]^[7] were dissolved in 60 mL Et₂O and transferred into a slurry of 1.9 g (13.7 mmol, 4.5 equivalents) potassium graphite in 15 mL Et₂O. At r.t. gaseous N₂ was bubbled through the reaction mixture for 20 minutes. The color changed to deep purple and the reaction mixture was stirred at r.t. for further 16 hours. After filtration over celite the solvent was removed in vacuum. The residue was extracted with 50 mL *n*-hexane or Et₂O, filtered over celite and several crops of dark purple crystals of 1 · solv (solv = *n*-hexane or Et₂O) were obtained by storing this saturated solution at -8 °C for several days.

Crystalline yield: 1.0 g (0.88 mmol, 58%).^[6]

Analytical data:

<p>NMR of 1</p> 	<p>¹H (C₆D₆, 300 K): δ [ppm] = 23.34 (8H, s, f), 17.48 (8H, s, e), 8.72 (24H, s, c/d), 3.40 (24H, s, c/d), -21.66 (4H, s, g), -68.09 (2H, s, a), -103.96 (12H, s, b).^[6]</p> <p>¹H NMR spectrum is shown in Figure S7 (vide infra).</p> <p>¹H ([D₈]THF, 300 K): δ [ppm] = 23.53 (8H, s, f), 17.21 (8H, s, e), 8.72 (24H, s, c/d), 3.32 (24H, s, c/d), -21.36 (4H, s, g), -68.85 (2H, s, a), -104.74 (12H, s, b).</p>
<p>Evans-NMR (C₆D₆ solution)</p>	<p>μ_{eff} = 4.47 μ_B (300 K)^[6]</p>
<p>Elemental analysis (C₅₈H₈₂Co₂K₂N₆)</p>	<p>Calculated: C 65.76, H 7.80, N 7.93. Found: C 64.82, H 8.15, N 5.94.^[6] The deviation of calculated and experimental data is due to high sensitivity to air and moisture of compound 1.</p>
<p>Raman</p>	<p>ν_{NN} = 1568 cm⁻¹.^[6] Raman spectrum is shown in Figure S24 (vide infra).</p>

Synthesis of [K(thf)₆][(L³Co)₂(μ-η⁴:η⁴-P₄)] (2)

Method 1:^[6] P₄ Activation with the Formal Co⁰ Precursor 1

200 mg (0.176 mmol, 1 equivalent) **1** were dissolved in 5 mL THF to form an intense purple solution. 22 mg (0.176 mmol, 1 equivalent) P₄ were dissolved in 10 mL THF and added to the purple solution within 5 minutes at room temperature. The color changed to red and gas formation was recognized. The solution was stirred at r.t. for 24 hours and filtered over celite. The solvent was reduced to 5 mL and crystals were obtained after storing the solution for 3 hours at -8 °C.

Crystalline yield: 101 mg (0.08 mmol, 34%).^[6]

The ¹H NMR spectrum of the crystals identifies compound **2** (~91%) and **3** (~7%) as the major and minor product of the reaction, respectively. Additionally, traces (~2%) of an unknown product are formed. When conducting the reaction with two equivalents P₄, however, exclusively compound **2** is detected in the ¹H NMR spectrum.

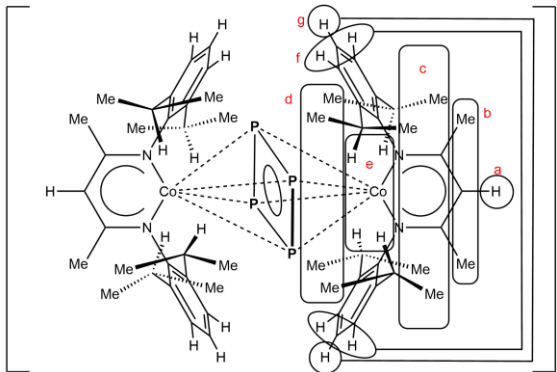
Method 2: Chemical Reduction of 5a with Potassium Graphite

200 mg (0.19 mmol, 1 equivalent) **5a** and 32.5 mg potassium graphite (0.20 mmol, 1.1 equivalents) were placed in a schlenk tube and 30 mL THF were added. The red slurry was stirred at r.t. for 1 hour and filtered over celite. The solvent was reduced to 2 mL and crystals were obtained after storing at -8 °C after 2 hours.

Crystalline yield: 118.8 mg (0.08 mmol, 41%).

According to the ¹H NMR spectrum, the conversion is > 99%.

Analytical data:

<p>NMR of 2 ([D₈]THF, 300 K)</p> 	<p>¹H: δ [ppm] = 11.42 (8H, d, ³J_{HH} = 5 Hz, f), 6.51 (8H, s, e), 2.01 (24H, s, c/d), 1.94 (24H, s, c/d), -0.46 (4H, broad t, g), -23.63 (12H, s, b), -35.29 (2H, s, a).^[6]</p> <p>³¹P{¹H}:^[6] no signal (1200 to -1200 ppm).</p> <p>¹H NMR spectrum is shown in Figure S8 (vide infra).</p>				
<p>Evans-NMR ([D₈]THF solution)</p> <p>double determination:</p> <p>$\mu_{\text{eff},1} = 3.91 \mu_{\text{B}}$ (300 K)</p> <p>$\mu_{\text{eff},2} = 3.89 \mu_{\text{B}}$ (300 K)^[6]</p>	<p>$\mu_{\text{eff}} = 3.90 \mu_{\text{B}}$ (300 K)</p>				
<p>Elemental analysis (C₈₂H₁₃₀Co₂KN₄O₆P₄)</p>	<p>Calculated: C 63.59, H 8.46, N 3.62.</p> <p>Found: C 62.70, H 7.45, N 4.32.</p>				
<p>Mass spectrometry (ESI-MS, DME)</p>	<table border="1"> <tbody> <tr> <td data-bbox="884 1794 1066 1877">cation: m/z:</td> <td data-bbox="1066 1794 1401 1877">308.9 (15%) [K(dme)₃]⁺, 218.8 (100%) [K(dme)₂]⁺.</td> </tr> <tr> <td data-bbox="884 1877 1066 2051">anion: m/z:</td> <td data-bbox="1066 1877 1401 2051">1107.7 (3%) [M+P]⁻, 1076.7 (100%) [M]⁻, 1045.7 (3%) [M-P]⁻, 1014.7 (3%) [M-2P]⁻.</td> </tr> </tbody> </table>	cation: m/z:	308.9 (15%) [K(dme) ₃] ⁺ , 218.8 (100%) [K(dme) ₂] ⁺ .	anion: m/z:	1107.7 (3%) [M+P] ⁻ , 1076.7 (100%) [M] ⁻ , 1045.7 (3%) [M-P] ⁻ , 1014.7 (3%) [M-2P] ⁻ .
cation: m/z:	308.9 (15%) [K(dme) ₃] ⁺ , 218.8 (100%) [K(dme) ₂] ⁺ .				
anion: m/z:	1107.7 (3%) [M+P] ⁻ , 1076.7 (100%) [M] ⁻ , 1045.7 (3%) [M-P] ⁻ , 1014.7 (3%) [M-2P] ⁻ .				

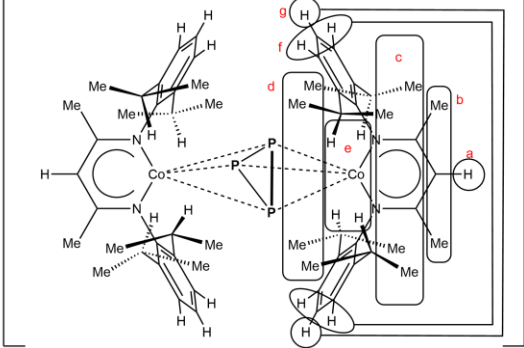
Synthesis of [K(dme)₄][(L³Co)₂(μ-η³:η³-P₃)] (3a)

200 mg (0.19 mmol, 1 equivalent) **6** and 33.5 mg (0.21 mmol, 1.1 equivalents) potassium graphite were placed in a schlenk tube and 20 mL THF were added. The color changes from brown to red. After 1.5 hours stirring at r.t. all volatiles were removed. The residue was extracted in 20 mL DME (or **3b** with THF) and filtrated over celite. After reducing the volume to 8 mL crystals were obtained by storing the saturated solution at 8 °C overnight.

Crystalline yield: 171 mg (0.12 mmol, 62%).

According to the ¹H NMR spectrum, the conversion is > 99%.

Analytical data:

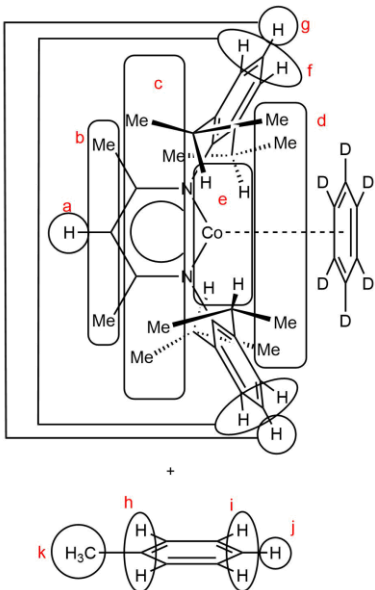
<p>NMR of 3a ([D₈]THF, 300 K)</p> 	<p>¹H: δ [ppm] = 8.14 (8H, d, ³J_{HH} = 8 Hz, f), 3.43 (11H, s, dme), 3.26 (17H, s, dme), 2.37 (8H, s, e), 1.22 (24H, s, c/d), -0.06 (4H, t, ³J_{HH} = 8 Hz, g), -2.80 (24H, s, c/d), -12.67 (12H, s, b), -12.85 (2H, s, a).</p> <p>³¹P{¹H}: no signal (1200 to -1200 ppm).</p> <p>¹H NMR spectrum is shown in Figure S9 (vide infra).</p>				
<p>Evans-NMR ([D₈]THF solution)</p>	<p>μ_{eff} = 3.51 μ_B (300 K)</p>				
<p>Elemental analysis (C₇₄H₁₂₂Co₂KN₄O₈P₃)</p>	<p>Calculated: C 61.48, H 8.51, N 3.88. Found: C 61.68, H 8.22, N 4.09.</p>				
<p>Mass spectrometry (ESI-MS, DME)</p>	<table border="1"> <tbody> <tr> <td data-bbox="823 1202 986 1361"> <p>cation: m/z:</p> </td> <td data-bbox="991 1202 1350 1361"> <p>219.1 (60%) [K(dme)₂]⁺, 129.0 (<5%) [K(dme)]⁺. Peaks at m/z 406.9 (30%) and 303.0 (100%) were not assigned.</p> </td> </tr> <tr> <td data-bbox="823 1368 986 1606"> <p>anion: m/z:</p> </td> <td data-bbox="991 1368 1350 1606"> <p>1076.6 (<5%) [M+P]⁻, 1045.6 (100%) [M]⁻, 1014.6 (5%) [M-P]⁻. Peaks at m/z 714.4 (15%) and 640.4 (12%) were not assigned.</p> </td> </tr> </tbody> </table>	<p>cation: m/z:</p>	<p>219.1 (60%) [K(dme)₂]⁺, 129.0 (<5%) [K(dme)]⁺. Peaks at m/z 406.9 (30%) and 303.0 (100%) were not assigned.</p>	<p>anion: m/z:</p>	<p>1076.6 (<5%) [M+P]⁻, 1045.6 (100%) [M]⁻, 1014.6 (5%) [M-P]⁻. Peaks at m/z 714.4 (15%) and 640.4 (12%) were not assigned.</p>
<p>cation: m/z:</p>	<p>219.1 (60%) [K(dme)₂]⁺, 129.0 (<5%) [K(dme)]⁺. Peaks at m/z 406.9 (30%) and 303.0 (100%) were not assigned.</p>				
<p>anion: m/z:</p>	<p>1076.6 (<5%) [M+P]⁻, 1045.6 (100%) [M]⁻, 1014.6 (5%) [M-P]⁻. Peaks at m/z 714.4 (15%) and 640.4 (12%) were not assigned.</p>				

Synthesis of [(L³Co)(tol)] (4a)^[7]

8.0 g (19.1 mmol) L³H in 50 mL THF were cooled to 0 °C and 12 mL (19.1 mmol) *n*-BuLi (1.6 M in *n*-hexane) were added. The color turned yellow and the solution was stirred at r.t. for 16 hours. A deep blue slurry of 4.2 g (19.1 mmol) CoBr₂ anhydrous in 50 mL THF was cooled to -75 °C and the yellow solution was added within 10 minutes. After stirring for 1 hour at -75 °C the solution was allowed to reach r.t. within 16 hours. Meanwhile, the color changed from green to brown. The solvent was removed in vacuum. The remaining brown solid was dissolved in 60 mL toluene and the brown solution was transferred to 3.36 g (21.0 mmol, 1.1 equivalents) potassium graphite. The reaction mixture was stirred at r.t. for 16 hours. After filtration over celite, the solvent was removed in vacuum. The brown solid was dissolved in 80 mL Et₂O and again filtered over celite. The volume was reduced to 30 mL and different crops of crystals were obtained at r.t. and -28 °C.

Crystalline yield: 6.13 g (10.8 mmol, 56%).

Analytical data:

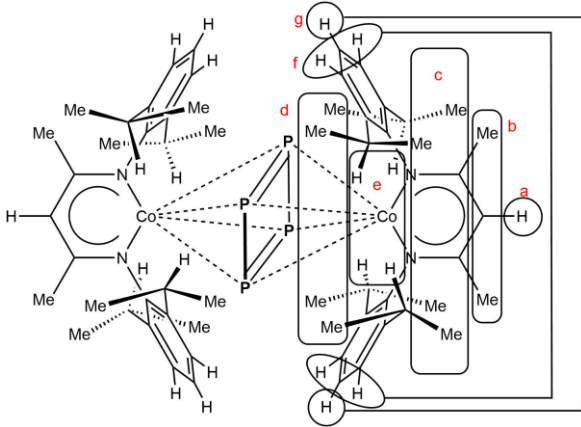
<p>NMR of 4a (C₆D₆, 300 K)</p>  <p>L³Co(tol) (4a) $\xrightarrow{\text{excess C}_6\text{D}_6}$</p>	<p>¹H: δ [ppm] = 20.69 (4H, s, f), 18.69 (4H, s, e), 7.03 (ca. 5H, m, h/i/j), 4.44 (12H, s, c/d), 2.11 (3H, s, k), 2.06 (12H, s, c/d), -1.92 (2H, s, g), -40.22 (6H, s, b), -78.84 (1H, s, a).</p> <p>¹H NMR spectrum is shown in Figure S10 (vide infra).</p>
<p>Evans-NMR (C₆D₆ solution)</p>	<p>$\mu_{\text{eff}} = 2.91 \mu_{\text{B}}$ (300 K)^[8]</p>
<p>Elemental analysis (C₃₆H₄₉CoN₂)</p>	<p>Calculated: C 76.03, H 8.68, N 4.93. Found: C 70.76, H 8.02, N 4.92. The deviation of calculated and experimental data is due to high sensitivity to air and moisture of compound 4a.</p>
<p>Mass spectrometry (LIFDI, toluene)</p>	<p>m/z: 568.5 (100%) [M]⁺, 557.7 (50%) [L³CoBr]⁺.^[7]</p>

Synthesis of [(L³Co)₂(μ-η⁴:η⁴-P₄)] (5a)^[7]

230 mg (0.2 mmol, 1 equivalent) **4a** were dissolved in 5 mL toluene and a solution of 25 mg P₄ (0.2 mmol, 0.5 equivalent) in 5 mL toluene was added at room temperature. The color changed from red to reddish-brown. After stirring for 2 hours at r.t. the solvent was removed in vacuum and the purple residue was dissolved in 10 mL THF. Crystals of **4a** were obtained after storing at -28 °C.

Crystalline yield: 150 mg (0.14 mmol, 70%).^[7]

Analytical data:

<p>NMR of 5a (C₆D₆, 300 K)</p> 	<p>¹H: δ [ppm] = 11.99 (8H, d, ³J_{HH} = 7 Hz, f), 3.90 (8H, s, e), 1.81 (24H, s, c/d), 0.76 (24H, s, c/d), -1.58 (4H, t, ³J_{HH} = 7 Hz, g), -15.36 (12H, s, b), -28.61 (2H, s, a).</p> <p>³¹P{¹H}:^[7] no signal (1200 to -600 ppm).</p> <p>¹H NMR spectrum is shown in Figure S11 (vide infra).</p>
<p>Evans-NMR: in [D₈]THF: μ_{eff} = 3.48 μ_B (300 K) double determination in C₆D₆: μ_{eff,1} = 2.95 μ_B (300 K) μ_{eff,2} = 3.09 μ_B (300 K)^[8]</p>	<p>μ_{eff 1,2} = 3.02 μ_B (300 K, C₆D₆)</p>
<p>Elemental analysis (C₅₈H₈₂N₄Co₂P₄)</p>	<p>Calculated: C 64.68, H 7.67, N 5.20. Found: C 64.47, H 7.39, N 5.18.</p>
<p>Mass spectrometry (LIFDI, toluene)</p>	<p>m/z: 1077 (100%) [M]⁺, 1045 (10%) [M-P]⁺, 419 (20%) [L³H]⁺.^[7]</p>

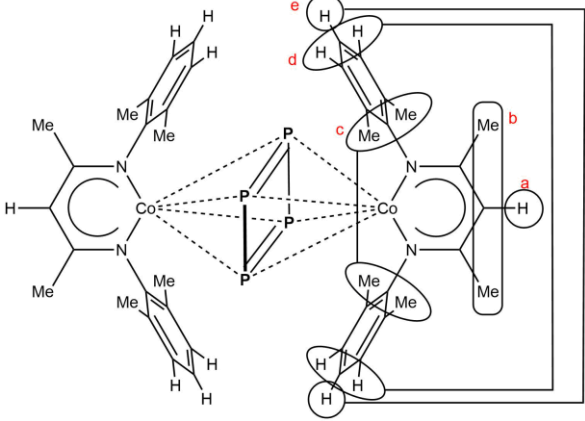
Synthesis of [(L¹Co)₂(μ-η⁴:η⁴-P₄)] (5b)

200 mg (0.44 mmol, 1 equivalent) **4b** were dissolved in 5 mL toluene and a solution of 27.5 mg (0.22 mmol, 0.5 equivalent) in 10 mL toluene was added at r.t. within 20 minutes. The color changed from brown to wine red. After stirring for 2 hours, the reaction mixture was filtered over celite. The solution was reduced to a volume of 8 mL and after 2 hours storing at 8 °C crystals were obtained.

Crystalline yield: 82.4 mg (0.10 mmol, 44%).

Analytical data:

<p>NMR of 5b (C₆D₆, 300 K)</p>	<p>¹H: δ [ppm] = 8.91 (8H, d, ³J_{HH} = 7 Hz, d), 4.70 (4H, t, ³J_{HH} = 7 Hz, e), 3.48 (24H, s, c), -5.78 (12H, s, b), -11.84 (2H, s, a).</p> <p>³¹P{¹H}: no signal (1200 to -1200 ppm).</p>
---	--

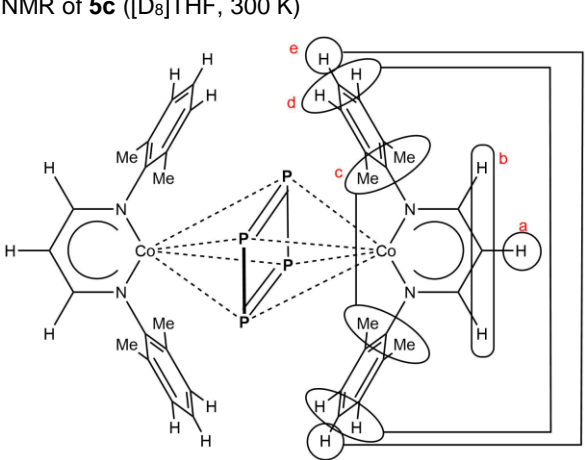
	¹ H NMR spectrum is shown in Figure S12 (vide infra).
Evans-NMR (C ₆ D ₆ solution)	$\mu_{\text{eff}} = 2.42 \mu_B$ (300 K)
Elemental analysis (C ₄₂ H ₅₀ N ₄ Co ₂ P ₄)	Calculated: C 59.16, H 5.91, N 6.57. Found: C 59.08, H 5.84, N 6.55.
Mass spectrometry (LIFDI, toluene)	m/z: 852.1990 (100%) [M] ⁺ , 821.2196 (3%) [M-P] ⁺ .

Synthesis of [(L²Co)₂(μ-η⁴:η⁴-P₄)] (5c)

200 mg (0.47 mmol, 1 equivalent) **4c** were dissolved in 7 mL toluene and a solution of 29 mg P₄ (0.23 mmol, 0.5 equivalent) in 7 mL toluene was added at r.t. within 1 minute. The color changed from brown to wine red. After stirring for 3 hours, the reaction mixture was filtered over celite and washed with 3 ml toluene. The volume was reduced to 6 mL and crystals were obtained after storing saturated solutions of **5c** at -30 °C after some days.

Crystalline yield: 32.2 mg (0.04 mmol, 17%).

Analytical data:

<p>NMR of 5c ([D₈]THF, 300 K)</p> 	¹ H: δ [ppm] = 11.15 (4H, s, b), 8.00 (8H, d, ³ J _{HH} = 8 Hz, d), 6.15 (4H, t, ³ J _{HH} = 8 Hz, e), 2.57 (24H, s, c), -6.58 (2H, s, a). ³¹ P{ ¹ H}: no signal (1200 to -1200 ppm). ¹ H NMR spectrum is shown in Figure S13 (vide infra).
Evans-NMR ([D ₈]THF solution)	$\mu_{\text{eff}} = 1.84 \mu_B$ (300 K) Chemical shift difference Δf measured in Evans method was obtained from comparison of silicon grease signals, which were sharper than THF signals.

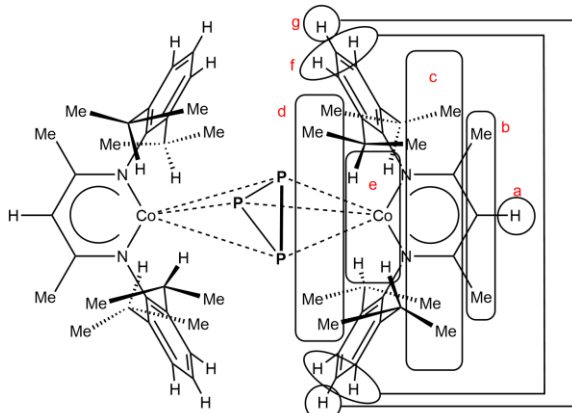
Elemental analysis (C ₃₈ H ₄₂ Co ₂ N ₄ P ₄)	Calculated: C 57.30, H 5.31, N 7.03. Found: C 57.64, H 5.45, N 7.20.
Mass spectrometry (LIFDI, toluene)	m/z: 1592.2300 (10%) [M ₂] ⁺ , 796.1055 (100%) [M] ⁺ , 765.1359 (5%) [M-P] ⁺ .

Synthesis of [(L³Co)₂(μ-η³:η³-P₃)] (6)^[7]

600 mg (1.0 mmol, 1 equivalent) **5a** and 65 mg (0.5 mmol, 0.5 equivalent) P₄ were dissolved in 20 mL toluene and refluxed for 3 hours. The solvent was removed in vacuum and the brown residue was extracted with 10 mL THF and filtered over celite. After reducing the volume to 5 mL and layering with 5 mL acetonitrile, crystals were obtained.

Crystalline yield: 200 mg (0.19 mmol, 40%).^[7] It has to be noted that the yield can strongly vary.

Analytical data:

<p>NMR of 6 (C₆D₆, 300 K)</p> 	<p>¹H:^[8] δ [ppm] = 20.06 (2H, s, a), 9.22 (12H, s, b), 3.36 (8H, d, ³J_{HH} = 8 Hz, f), 1.42 (24H, s, c/d), -1.82 (4H, t, ³J_{HH} = 8 Hz, g), -9.57 (24H, s, c/d), -12.68 (8H, s, e).</p> <p>³¹P{¹H}: no signal (0 to -600 ppm).</p> <p>¹H NMR spectrum is shown in Figure S14 (vide infra).</p>
Evans-NMR (C ₆ D ₆ solution)	μ _{eff} = 2.97 μ _B (300 K) ^[8]
Elemental analysis (C ₅₈ H ₈₂ N ₄ Co ₂ P ₃)	Calculated: C 66.59, H 7.90, N 5.36. Found: C 65.59, H 7.59, N 5.21. ^[7]
Mass spectrometry (LIFDI, toluene)	m/z: 1045.8 (100%) [M] ⁺ . ^[7]

Crystallographic Details

Single crystal structure analyses were performed using Rigaku Oxford Diffraction (formerly Agilent Technologies) CCD diffractometer GV-50, Titan^{S2} CCD (**1** · Et₂O, **5a**, **5b**, **6**), Gemini Ultra Atlas^{S2} CCD (**5c**), SuperNova Atlas CCD (**2**, **1** · *n*-hexane, **4a**) and SuperNova Eos CCD (**3a**, **3b**). Data reduction was performed with the CrysAlisPro^[9] software package. Using the software Olex2^[10] the structure solution was carried out using the programs ShelXT^[11] (Sheldrick, 2015) (**1** · Et₂O, **1** · *n*-hexane, **2**, **3a**, **3b**, **4a**, **5a**, **5b**, **5c**, **6**). Least squares refinements on F_o² were performed using SHELXL-2014 (**1** · Et₂O, **1** · *n*-hexane, **2**, **3a**, **3b**, **4a**, **5a**, **5b**, **5c**, **6**).^[12]

Crystallographic data and details of the diffraction experiments are given in Tables S3 and S4. CIF files with comprehensive information on the details of the diffraction experiments and full tables of bond lengths and angles for **1** · Et₂O, **1** · *n*-hexane, **2**, **3a**, **3b**, **4a**, **5a-c**, **6** are deposited in Cambridge Crystallographic Data Centre under the deposition codes CCDC-1517559-1517568.

Molecular structures of compounds **2**, **3a**, **3b** and **5a** are shown in main part of the publication. Molecular structures of compounds **1** · *n*-hexane, **1** · Et₂O, **3a**, **3b**, **4a**, **5a-c** and **6** are shown in Figures S2–S6.

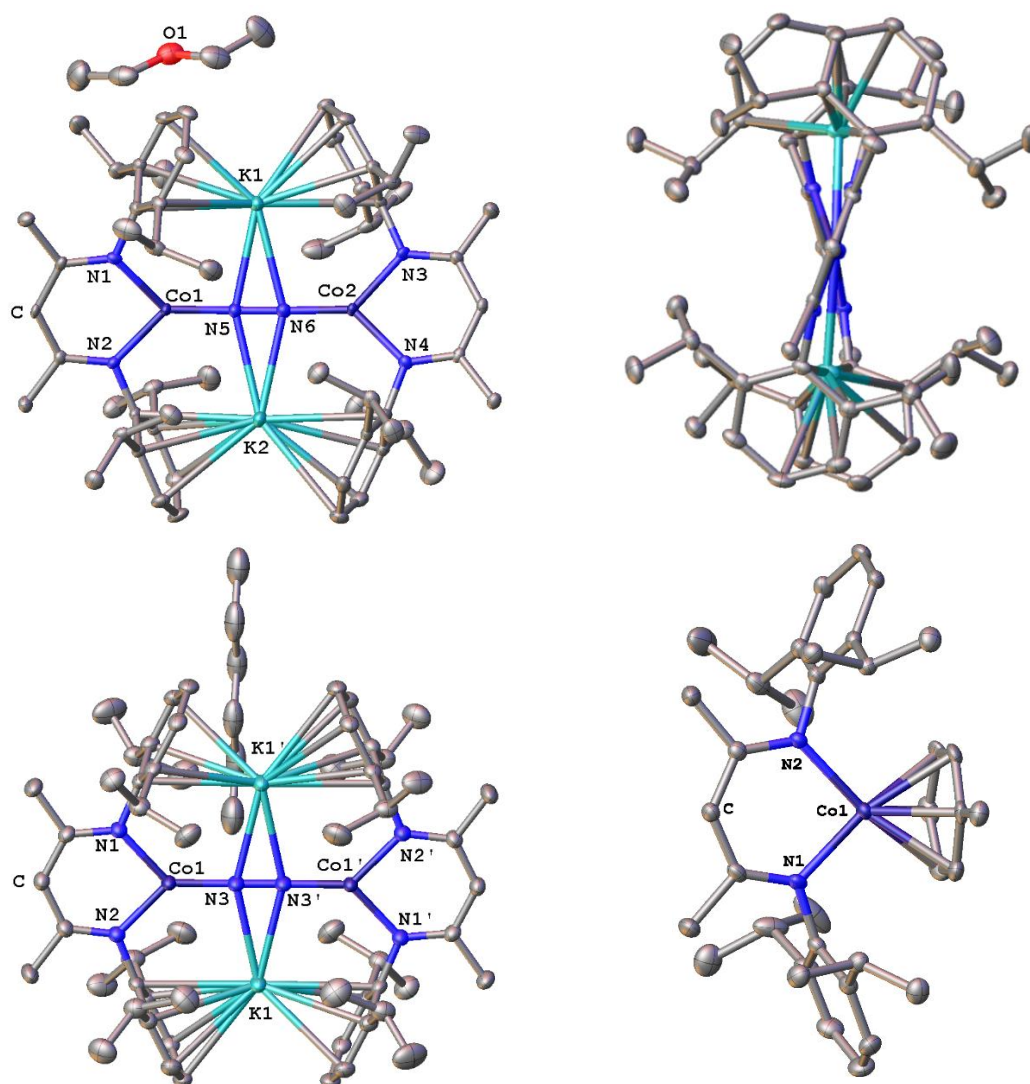


Figure S2. Molecular structure of compound **1** · Et₂O (upper part, left) in the crystal and its end-on view, which visualizes the twist of ligand planes (upper part, right). Molecular structure of **1** · *n*-hexane (bottom, left) and **4a** (bottom, right) in the crystal. Hydrogen atoms are omitted for clarity. Thermal ellipsoids are drawn at 50% probability level.

X-ray Diffraction on Crystals of 3a

The crystal structure of $[\text{K}(\text{dme})_4][(\text{L}^3\text{Co})_2(\mu\text{-}\eta^3\text{:}\eta^3\text{-P}_3)] \cdot \text{dme}$ (**3a**) was refined as 2-component twin. The molecular structure can be solved in space group $P1$, in spite of metric parameter ($\alpha = 90.000(1)^\circ$, $\beta = 90.160(1)^\circ$, $\gamma = 108.218(2)^\circ$, $a = 14.2642(2) \text{ \AA}$, $b = 16.6236(3) \text{ \AA}$, $c = 18.4993(3) \text{ \AA}$) suggesting monoclinic crystal system. However, monoclinic space groups did not result in appropriate structure solutions. One disordered methyl group was refined to a chemical occupancy of 60:40. The central *cyclo*-P₃ moiety is located between two $[\text{L}^3\text{Co}]$ fragments and was refined to a chemical occupancy of 81:19 (Figure S3). Within both disordered *cyclo*-P₃ moieties there are two almost overlapping atoms (P3 and P3A). Due to the low occupancy of the minor component (19%), only the major component is discussed. The precise localization of the P3 atom might be affected by the electron density of adjacent P3A atom, which results in some uncertainty concerning precise determination of P–P distances. However, even neglecting the SIMU restraints, there is no significant variation of the position of P3 (major component) and corresponding bond lengths.

Table S1. Comparison of geometrical details of *cyclo*-P₃ moiety (major and minor component) in **3a**.

	3a major component (81%)		3a minor component (19%)
$d(\text{P1-P2}) / [\text{Å}]$	2.1674(13)	$d(\text{P1A-P2A}) / [\text{Å}]$	2.122(8) (SIMU)
$d(\text{P1-P3}) / [\text{Å}]$	2.1790(16)	$d(\text{P1A-P3A}) / [\text{Å}]$	2.249(10) (SIMU)
$d(\text{P2-P3}) / [\text{Å}]$	2.3303(17)	$d(\text{P2A-P3A}) / [\text{Å}]$	2.312(11) (SIMU)
$\angle (\text{P-P-P}) / [^\circ]$	57.34(5), 57.82(5), 64.84(5)	$\angle (\text{P-P-P}) / [^\circ]$	55.4(3), 60.8(3), 63.8(3)

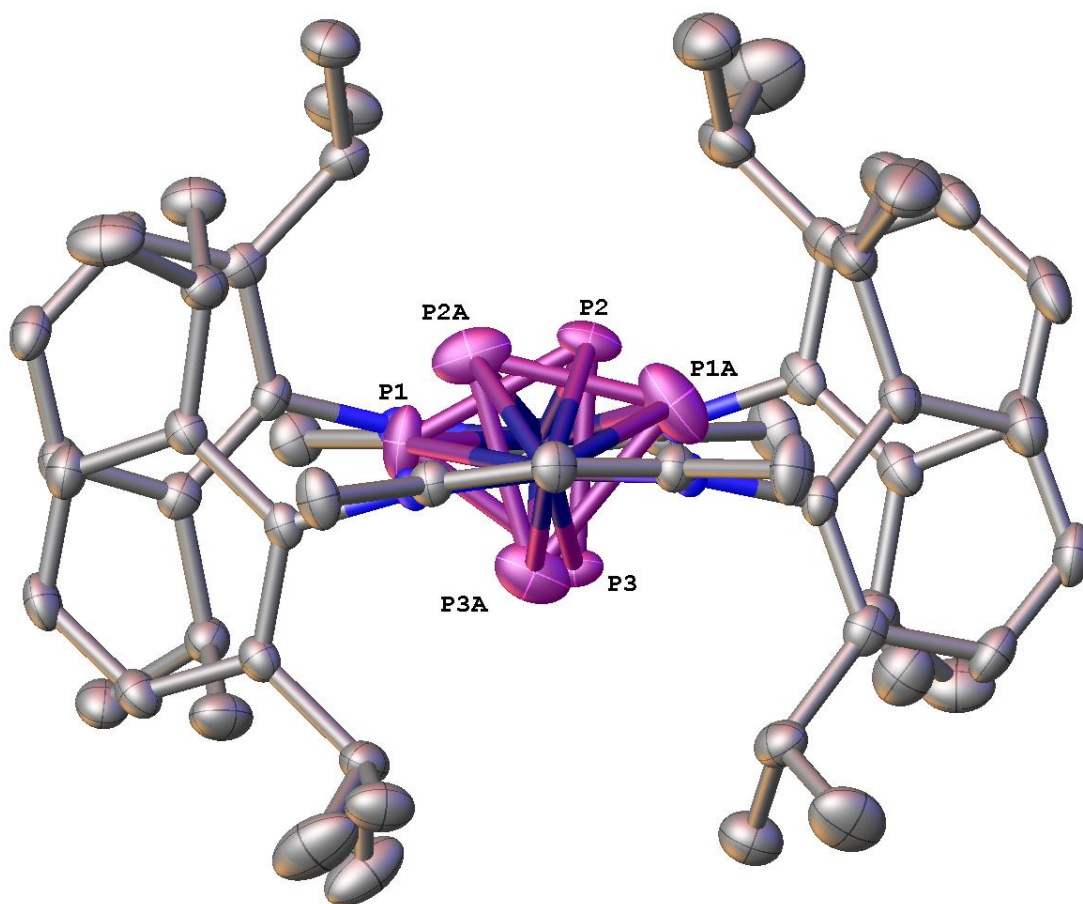


Figure S3. Anionic part of the compound **3a** in the crystal displaying the disordered *cyclo*-P₃ middle deck. The $[\text{K}(\text{dme})_4]^+$ counter ion, hydrogen atoms and the DME solvent molecule are omitted for clarity. Thermal ellipsoids are drawn at 50% probability level.

X-ray Diffraction on Crystals of **3b**

The X-ray diffraction experiment of $[\text{K}(\text{thf})_6][(\text{L}^3\text{Co})_2(\mu\text{-}\eta^3\text{:}\eta^3\text{-P}_3)] \cdot 2 \text{ thf}$ (**3b**) suffers from low intensity data and a very minor twin component that cannot be separated properly. Therefore, only elevated R_1 and wR_2 values are achieved. We present the best structure solution in space group $Pna2_1$ revealing a $[\text{K}(\text{thf})_6]^+$ cation, two THF solvent molecules and one $[(\text{L}^3\text{Co})_2(\mu\text{-}\eta^3\text{:}\eta^3\text{-P}_3)]^-$ monoanion. Models in monoclinic space groups do not improve the structure model and the experimental data are not complete for those. Therefore, the solution in $Pna2_1$ provides the most satisfying model. The anionic part of **3b** is already proven by the structure of compound **3a** and its precursor **6**. The benefit of structure **3b** is the absence of disorder within the *cyclo*-P₃ unit (Figure S4) in comparison to the disordered *cyclo*-P₃ fragment in **3a** (Figure S3). SIMU and one ISOR restraints were used in structure refinement of *l*Pr groups and THF molecules.

Table S2. Selected geometrical details of *cyclo*-P₃ moiety in **3b**.

3b	
$d(\text{P1-P2}) / [\text{\AA}]$	2.224(4)
$d(\text{P1-P3}) / [\text{\AA}]$	2.237(4)
$d(\text{P2-P3}) / [\text{\AA}]$	2.217(4)
$\sphericalangle (\text{P-P-P}) / [^\circ]$	59.59(13), 59.93(14), 60.48(13)

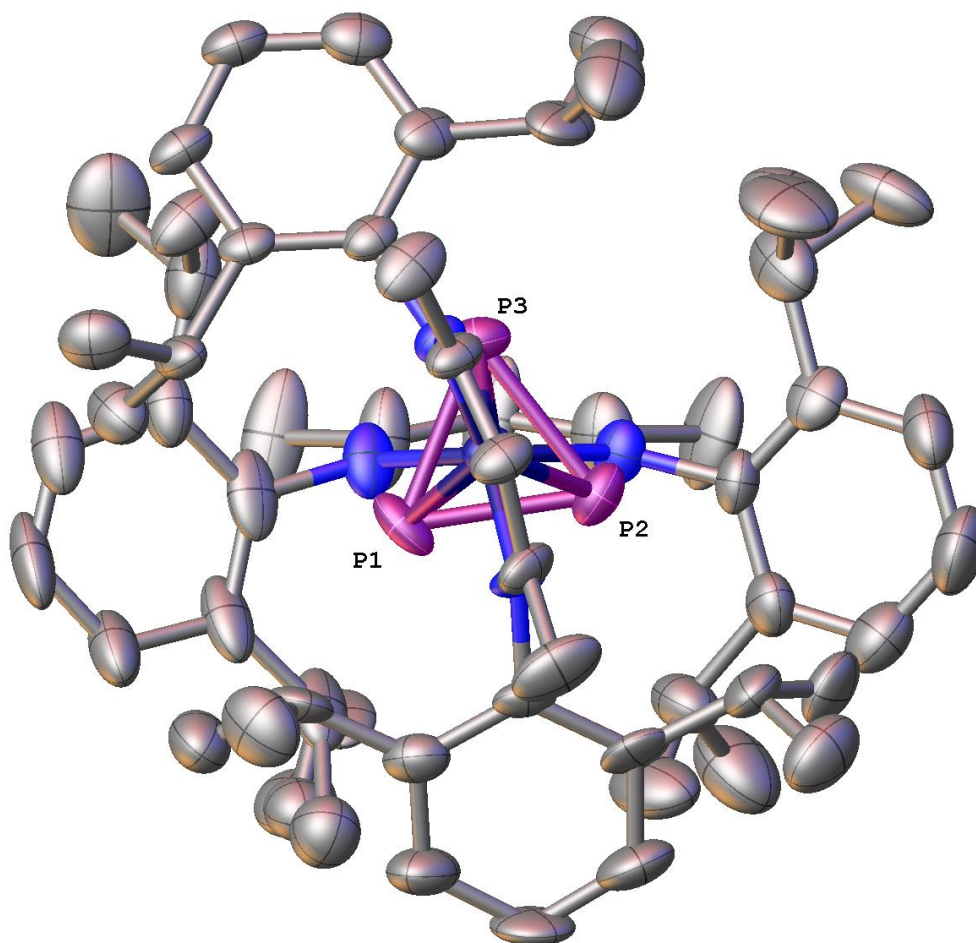


Figure S4. Anionic part of the compound **3b** in the crystal displaying the localized *cyclo*-P₃ deck. The $[\text{K}(\text{thf})_6]^+$ counter ion, hydrogen atoms and two THF molecules are omitted for clarity. Thermal ellipsoids are drawn at 50% probability level.

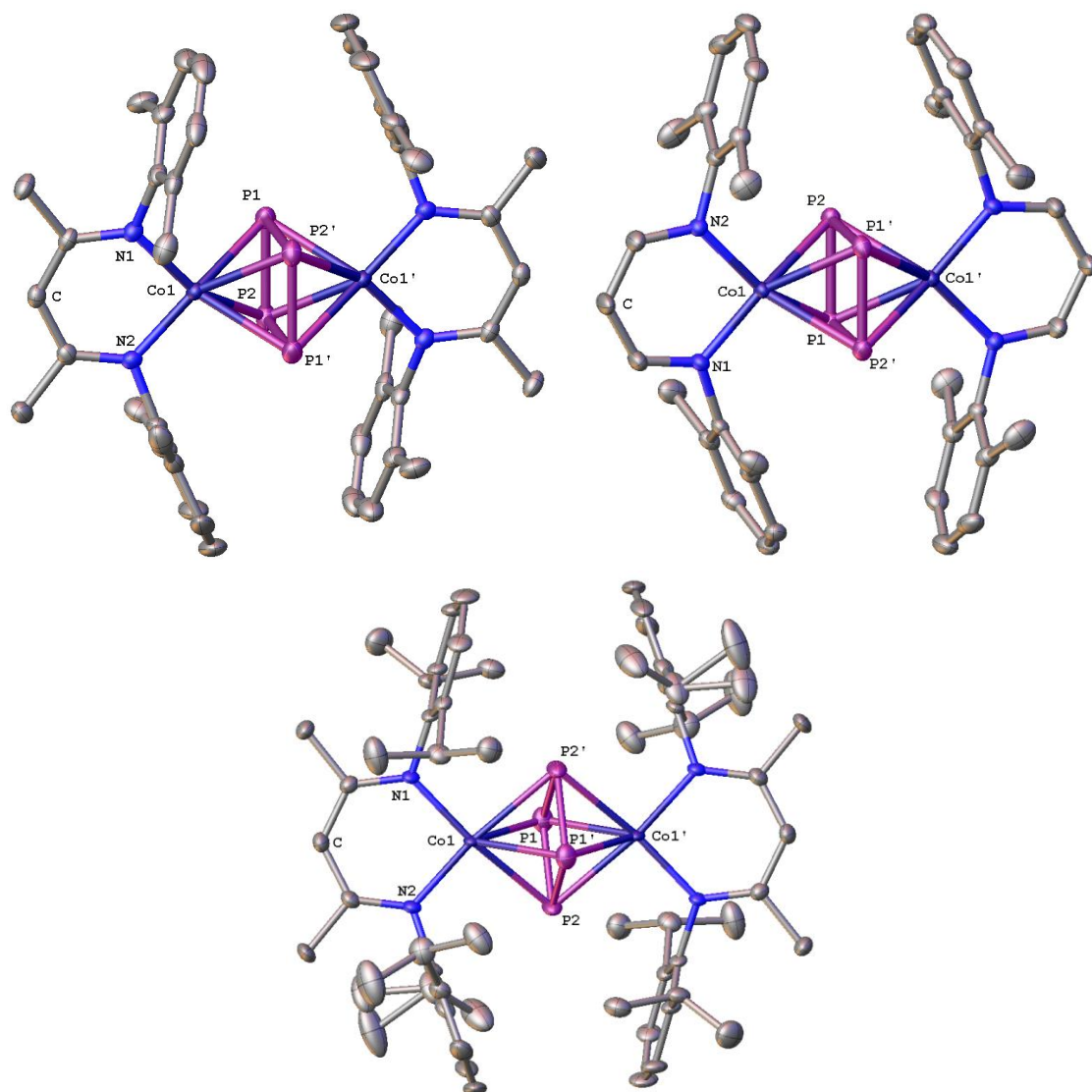


Figure S5. Molecular structure of compounds **5b** (upper part, left), **5c** (upper part, right) and **5a** (bottom) in the crystal. Hydrogen atoms are omitted for clarity. Thermal ellipsoids are drawn at 50% probability level.

X-ray Diffraction on Crystals of **6**^[13]

[(L³Co)₂(μ-η³:η³-P₃)] (**6**) exhibits severe disorder within its middle deck, which is not resolved even in space group *P*1. Crystals of **6** undergo phase transition at approximately 110 K, which limits the accurate localization of phosphorus atoms within the electron density donut (Figure S6). Therefore, the P–P atom distances cannot be determined reliably. However, the localization of electron density unambiguously confirms the *cyclo*-P₃ constitution and allows an estimation of approx. *d*(P–P) 2.147(3), 2.223(2) and 2.235(2) Å.

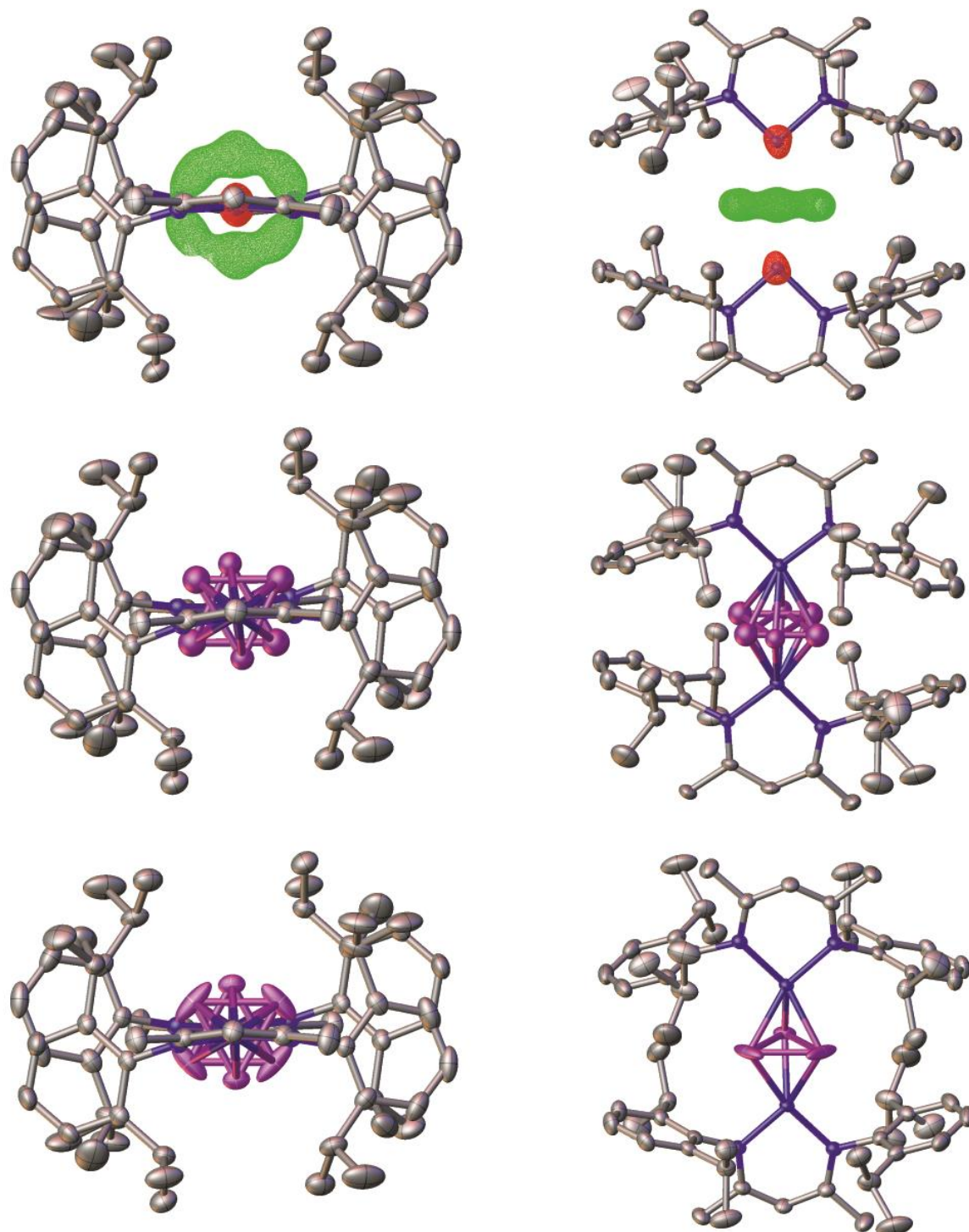


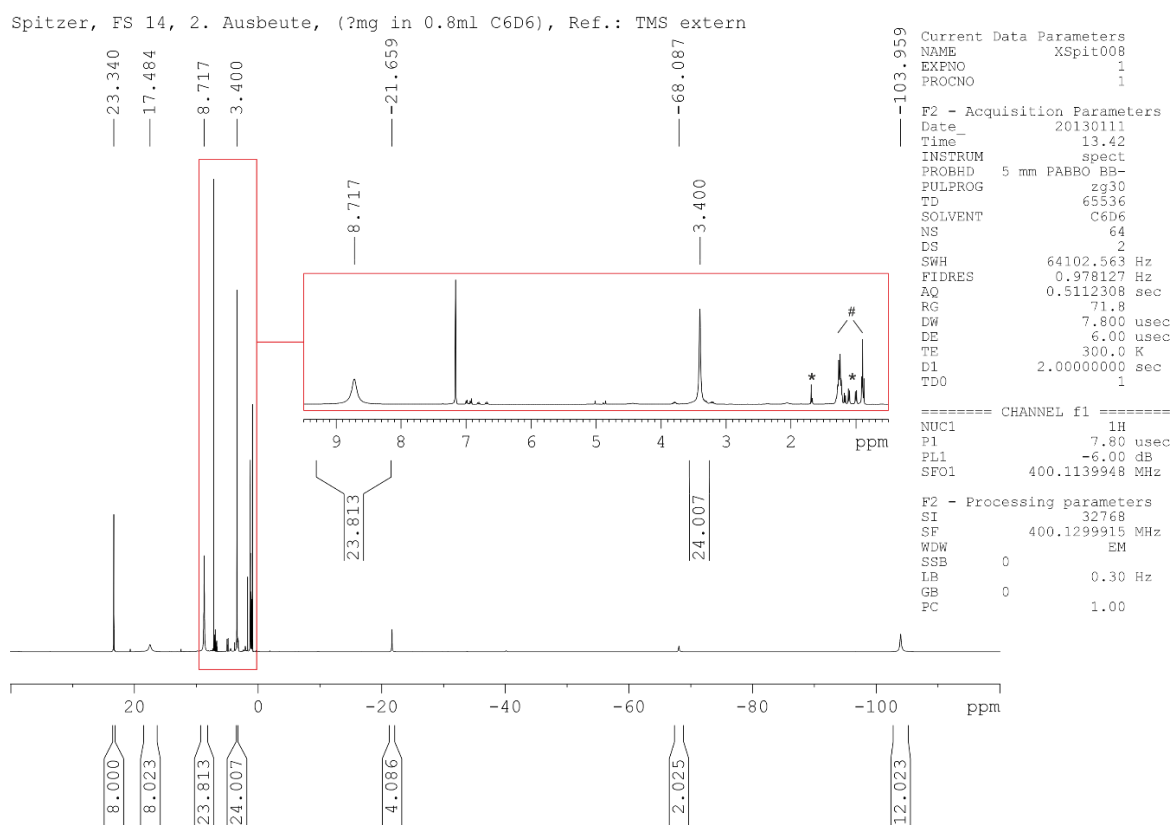
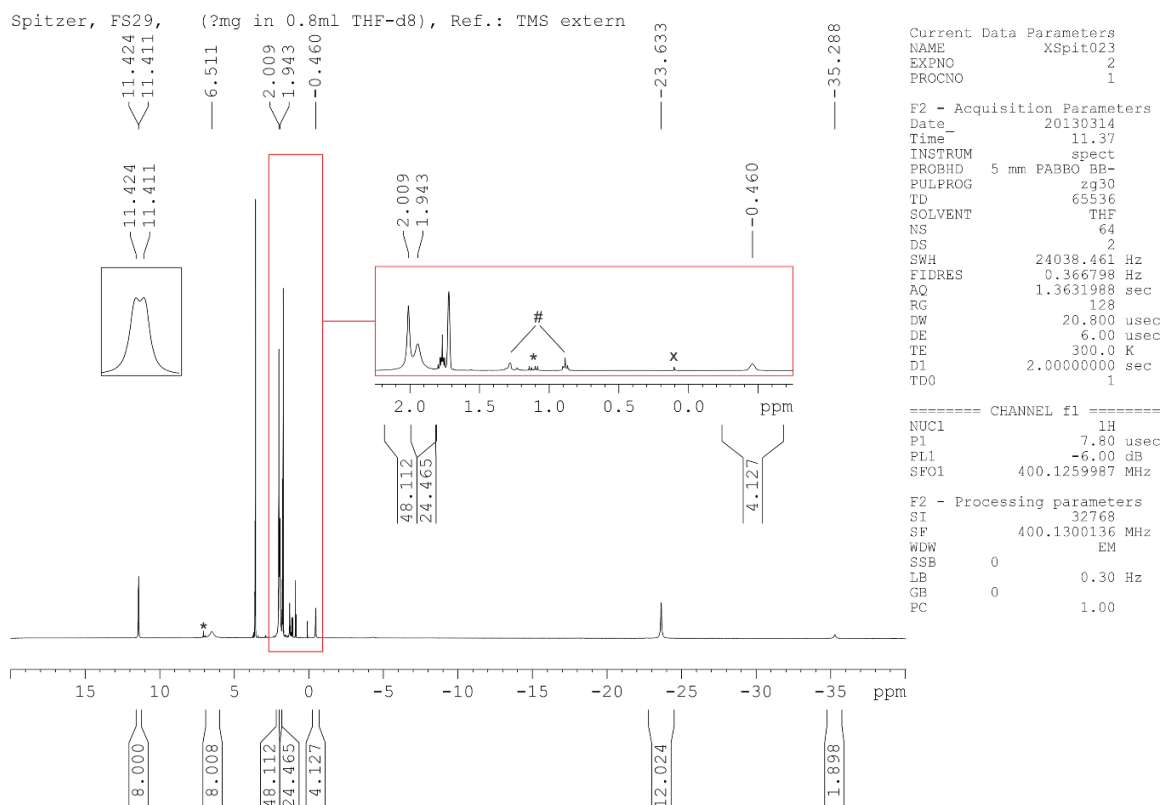
Figure S6. Electron density map (top) and molecular structure (bottom) of complex **6** in the crystal at 123 K. Hydrogen atoms are omitted for clarity. Phosphorus atoms are drawn with isotropic (middle) and anisotropic (bottom) ellipsoids at 50% probability level.

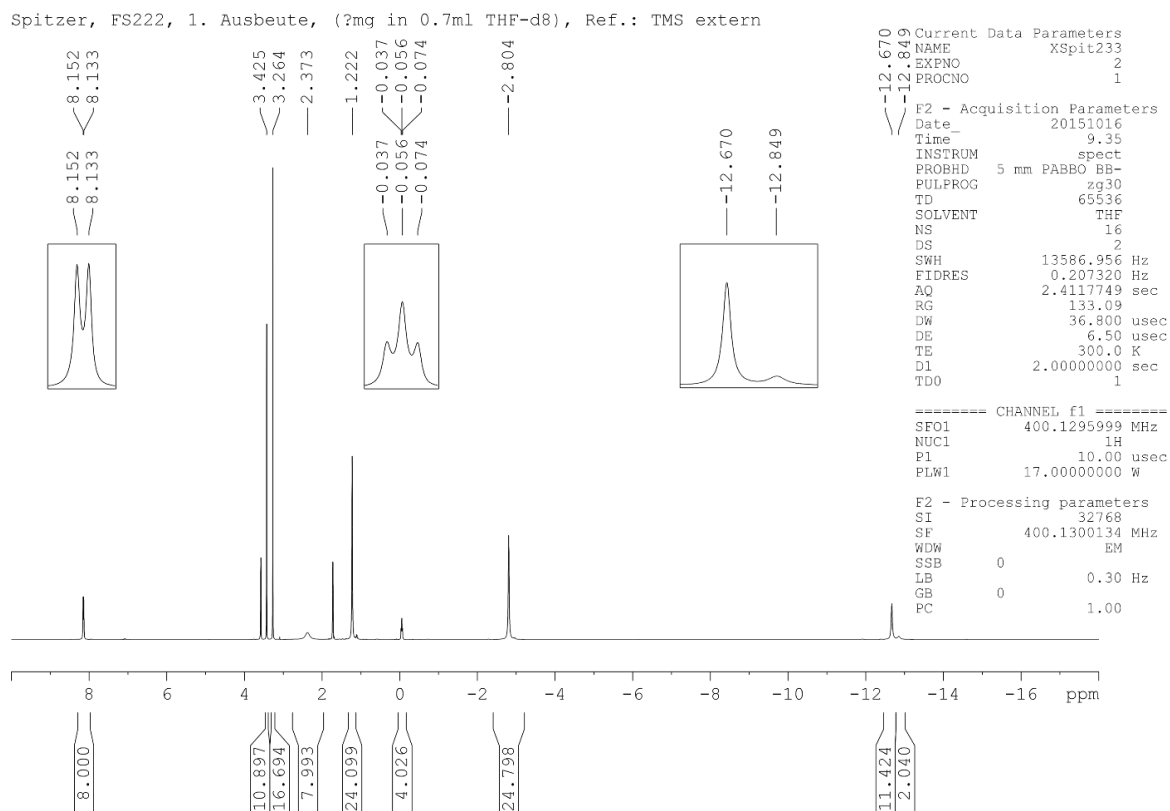
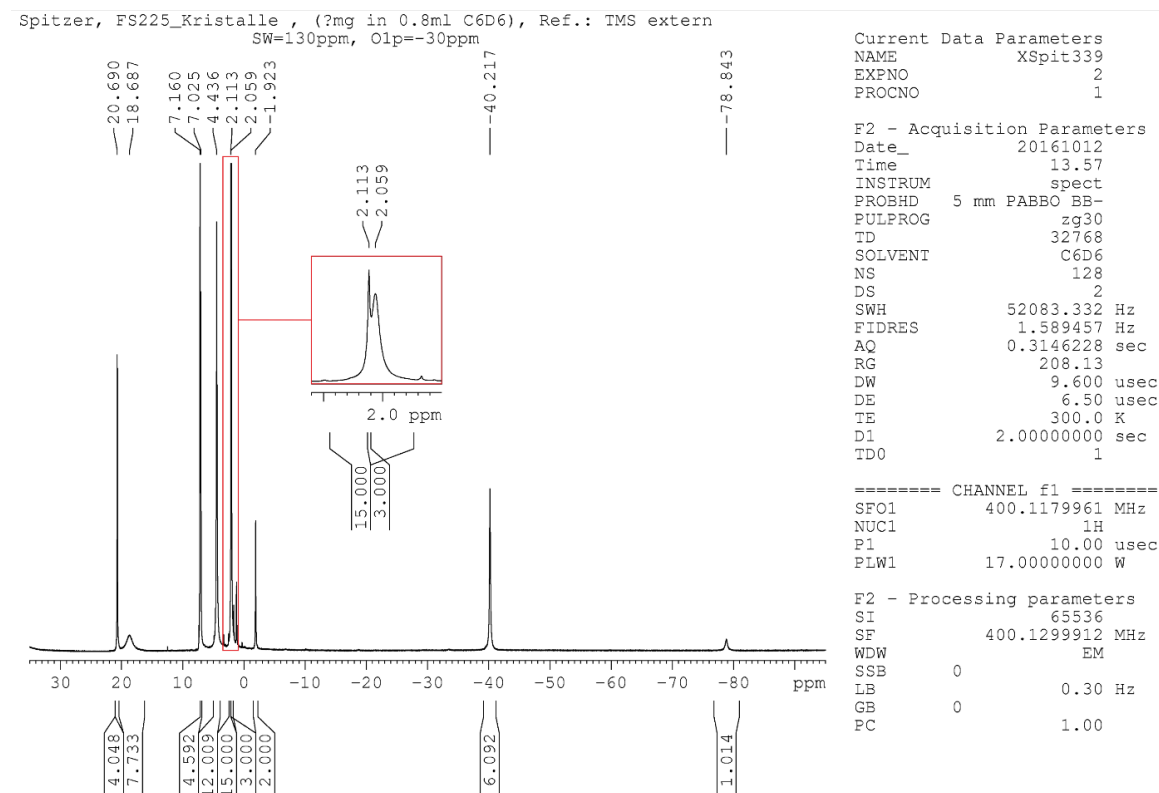
Table S3. Crystallographic data and details of diffraction experiments for **1** · *n*-hexane, **1** · Et₂O, **2**, **3a** and **3b**.

Compound	1 · <i>n</i> -hexane ^[6]	1 · Et ₂ O	2 ^[6]	3a	3b
Formula	C ₆₄ H ₉₆ Co ₂ K ₂ N ₆	C ₆₂ H ₉₂ Co ₂ K ₂ N ₆ O	C ₉₀ H ₁₄₆ Co ₂ KN ₄ O ₈ P ₄	C ₇₈ H ₁₃₂ Co ₂ KN ₄	C ₉₀ H ₁₄₆ Co ₂ KN ₄ O ₈
CCDC No.	1517560	1517559	1517561	O ₁₀ P ₃ 1517562	P ₃ 1517563
$\rho_{calc.}/\text{g cm}^{-3}$	1.192	1.218	1.215	1.224	1.203
μ/mm^{-1}	5.543	5.733	4.281	0.561	0.513
Formula Weight	1145.52	1133.47	1692.94	1535.74	1661.97
Color	clear dark violet	clear dark violet	clear dark red	clear dark red	clear dark red
Shape	block	block	block	block	block
Size/mm ³	0.47×0.14×0.09	0.36×0.15×0.11	0.40×0.17×0.15	0.37×0.19×0.12	0.20×0.16×0.11
<i>T</i> /K	123(2)	123(1)	123(1)	123(1)	123(1)
Crystal System	monoclinic	orthorhombic	triclinic	triclinic	orthorhombic
Space Group	<i>P</i> 2 ₁ / <i>n</i>	<i>P</i> 2 ₁ 2 ₁ 2 ₁	<i>P</i> 1	<i>P</i> 1	<i>P</i> na2 ₁
<i>a</i> /Å	12.5021(2)	15.8819(3)	13.1606(4)	14.2642(2)	27.6261(17)
<i>b</i> /Å	19.4917(3)	18.5203(4)	18.5422(5)	16.6236(3)	17.7957(8)
<i>c</i> /Å	13.5640(2)	21.0098(5)	19.0015(5)	18.4993(3)	18.6663(8)
α°	90	90	89.692(2)	90.0000(10)	90
β°	105.0699(15)	90	88.371(2)	90.1600(10)	90
γ°	90	90	86.559(2)	108.218(2)	90
<i>V</i> /Å ³	3191.70(9)	6179.8(2)	4626.6(2)	4166.70(13)	9176.8(8)
<i>Z</i>	2	4	2	2	4
<i>Z'</i>	0.5	1	1	1	1
Wavelength/Å	1.54184	1.54184	1.54184	0.71073	0.71073
Radiation type	CuK α	CuK α	CuK α	MoK α	MoK α
Θ_{min}°	4.066	3.181	3.340	2.877	3.145
Θ_{max}°	73.691	74.386	73.731	28.267	28.270
Measured Refl.	18068	29863	42012	17818	28730
Independent Refl.	6197	11493	17873	17818	16861
Reflections Used	5417	10939	15434	16719	11749
<i>R</i> _{int}	0.0347	0.0491	0.0363	.	0.0507
Parameters	345	680	1070	951	1023
Restraints	0	0	0	18	235
Largest Peak	0.851	0.377	0.600	0.649	0.757
Deepest Hole	-0.364	-0.543	-0.387	-0.493	-0.461
GooF	1.025	1.042	1.025	1.044	1.076
<i>wR</i> ₂ (all data)	0.1132	0.0957	0.1312	0.1074	0.2314
<i>wR</i> ₂	0.1072	0.0941	0.1239	0.1042	0.2082
<i>R</i> ₁ (all data)	0.0468	0.0384	0.0561	0.0440	0.1302
<i>R</i> ₁	0.0405	0.0360	0.0478	0.0401	0.0908
Flack Parameter		-0.026(2)			0.447(12)
Hooft Parameter		-0.0358(16)			0.462(11)

Table S4. Crystallographic data and details of diffraction experiments for **4a**, **5a–c** and **6**.

Compound	4a ^[7]	5a ^[13]	5b	5c	6 ^[13]
Formula	C ₃₆ H ₄₉ CoN ₂	C ₅₈ H ₈₂ Co ₂ N ₄ P ₄	C ₄₂ H ₅₀ Co ₂ N ₄ P ₄	C ₃₈ H ₄₂ Co ₂ N ₄ P ₄	C ₅₈ H ₈₂ Co ₂ N ₄ P ₃
CCDC No.	1517564	1517565	1517566	1517567	1517568
$\rho_{calc.}$ / g cm ⁻³	1.212	1.293	1.408	1.406	1.256
μ /mm ⁻¹	4.495	6.092	8.236	1.084	5.814
Formula Weight	568.70	1077.01	852.60	796.49	1046.04
Color	dark red	dark brown	clear dark brown	dark brown	dark brown
Shape	plate	block	prism	block	block
Size/mm ³	0.14×0.07×0.02	0.22×0.20×0.10	0.22×0.17×0.15	0.28×0.24×0.11	0.17×0.12×0.09
<i>T</i> /K	123(1)	123(1)	123(2)	123(1)	123(1)
Crystal System	triclinic	monoclinic	monoclinic	monoclinic	monoclinic
Space Group	<i>P</i> 1	<i>P</i> 2 ₁ / <i>n</i>	<i>P</i> 2 ₁ / <i>n</i>	<i>P</i> 2 ₁ / <i>n</i>	<i>P</i> 2 ₁ / <i>n</i>
<i>a</i> /Å	9.5644(7)	14.2363(5)	13.34736(12)	8.3461(3)	14.3827(2)
<i>b</i> /Å	12.3418(11)	13.4580(3)	8.77564(8)	18.9201(6)	13.36836(13)
<i>c</i> /Å	13.7429(11)	14.9786(4)	17.6300(2)	11.9598(3)	14.95129(17)
α /°	76.108(7)	90	90	90	90
β /°	81.609(6)	105.386(3)	103.1225(11)	94.857(3)	105.8346(13)
γ /°	87.614(7)	90	90	90	90
<i>V</i> /Å ³	1557.9(2)	2766.93(14)	2011.11(4)	1881.78(10)	2765.64(6)
<i>Z</i>	2	2	2	2	2
<i>Z'</i>	1	0.5	0.5	0.5	0.5
Wavelength/Å	1.54184	1.54184	1.54184	0.71073	1.54184
Radiation type	CuK α	CuK α	CuK α	MoK α	CuK α
θ_{min} /°	3.689	3.809	3.770	3.285	3.780
θ_{max} /°	73.246	74.503	74.308	32.848	74.316
Measured Refl.	9815	13413	20827	42136	32005
Independent Refl.	5887	5474	4003	6578	5508
Reflections Used	5325	5100	3938	5367	4933
<i>R</i> _{int}	0.0477	0.0538	0.0554	0.0409	0.0415
Parameters	363	327	241	221	335
Restraints	0	6	0	0	0
Largest Peak	0.535	0.953	0.441	0.892	0.641
Deepest Hole	-0.468	-0.785	-0.587	-0.318	-0.633
GooF	1.057	1.017	1.049	1.070	1.027
<i>wR</i> ₂ (all data)	0.1415	0.1437	0.0869	0.0953	0.0995
<i>wR</i> ₂	0.1348	0.1388	0.0864	0.0881	0.0955
<i>R</i> ₁ (all data)	0.0609	0.0557	0.0326	0.0562	0.0460
<i>R</i> ₁	0.0544	0.0523	0.0322	0.0400	0.0399

¹H NMR Spectra**Figure S7.** ¹H NMR spectrum of **1** in C₆D₆. Impurities of L³H (*) and H grease (#) are marked.^[6]**Figure S8.** ¹H NMR spectrum of **2** in [D₈]THF. Impurities of L³H (*), H grease (#) and silicon grease (x) are marked.

Figure S9. ¹H NMR spectrum of **3** in [D₈]THF.Figure S10. ¹H NMR spectrum of **4a** in C₆D₆.

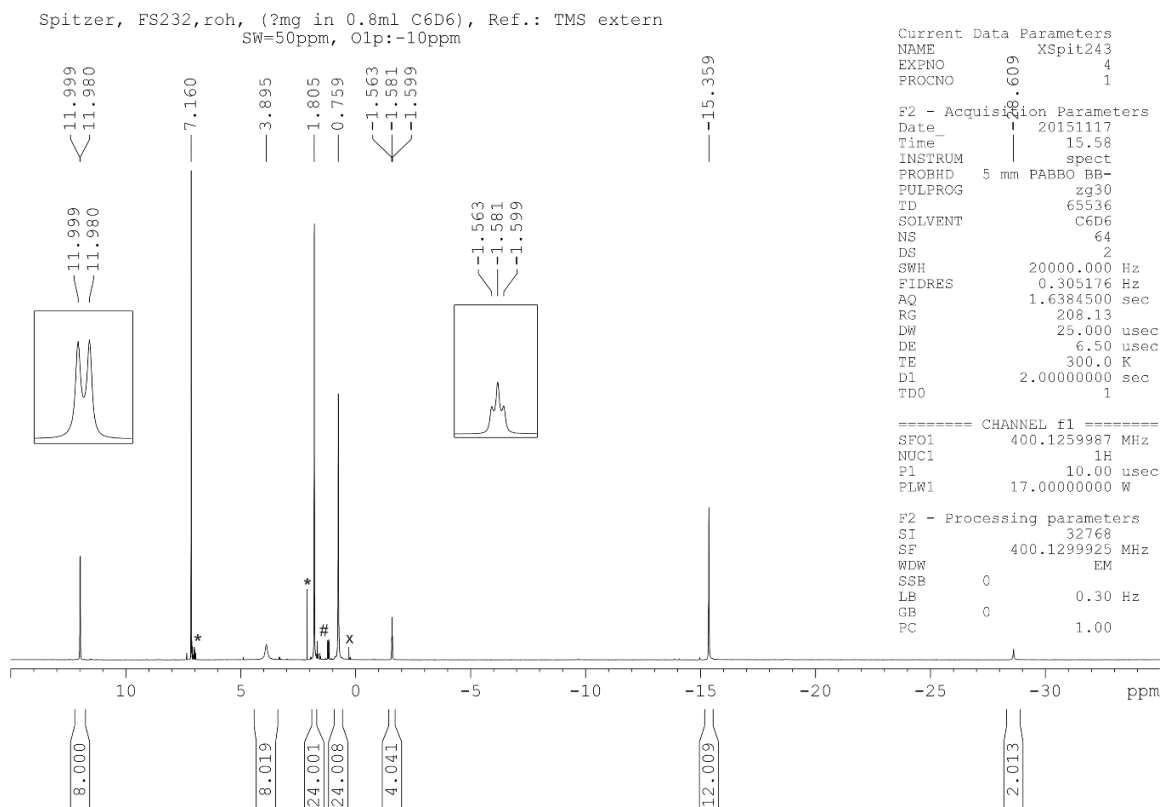


Figure S11. ¹H NMR spectrum of **5a** in C₆D₆. Impurities of toluene (*) , L³H (#) and silicon grease (x) are marked.

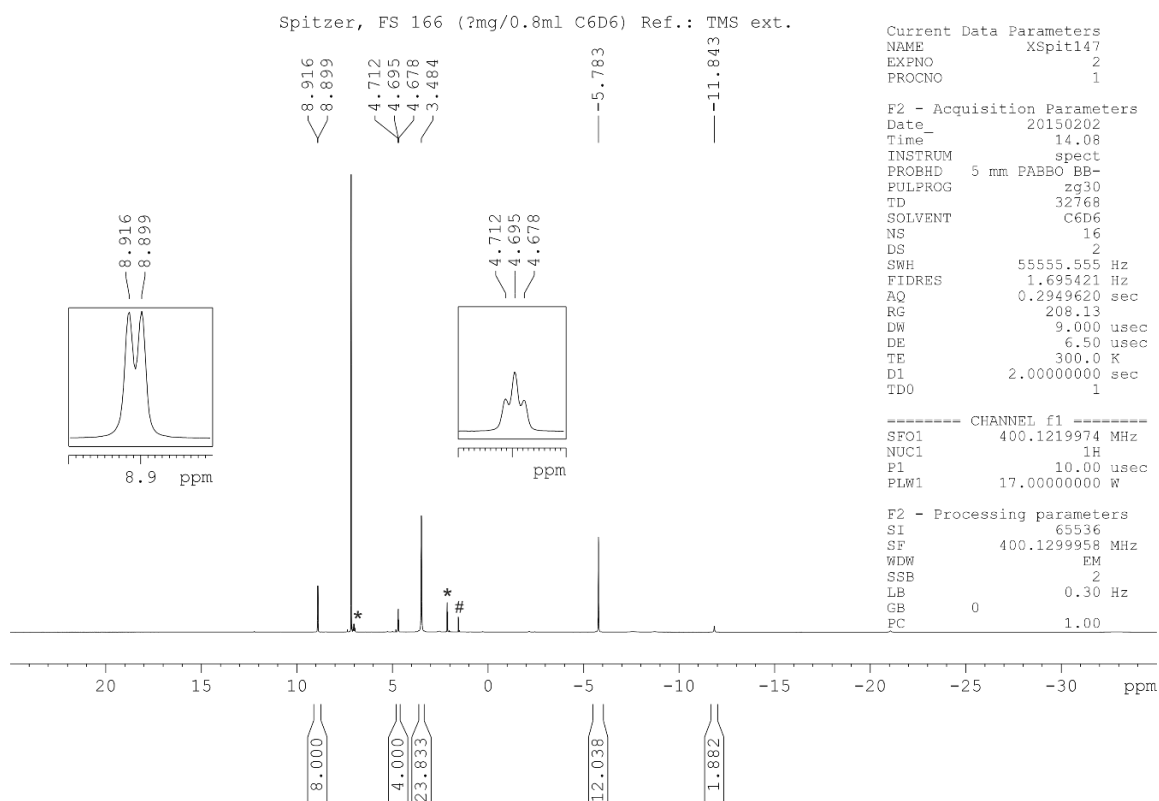


Figure S12. ¹H NMR spectrum of **5b** in C₆D₆. Impurities of toluene (*) and acetone (#) are marked.

SI: 5. Cobalt Mediated P₄ Activation | 119

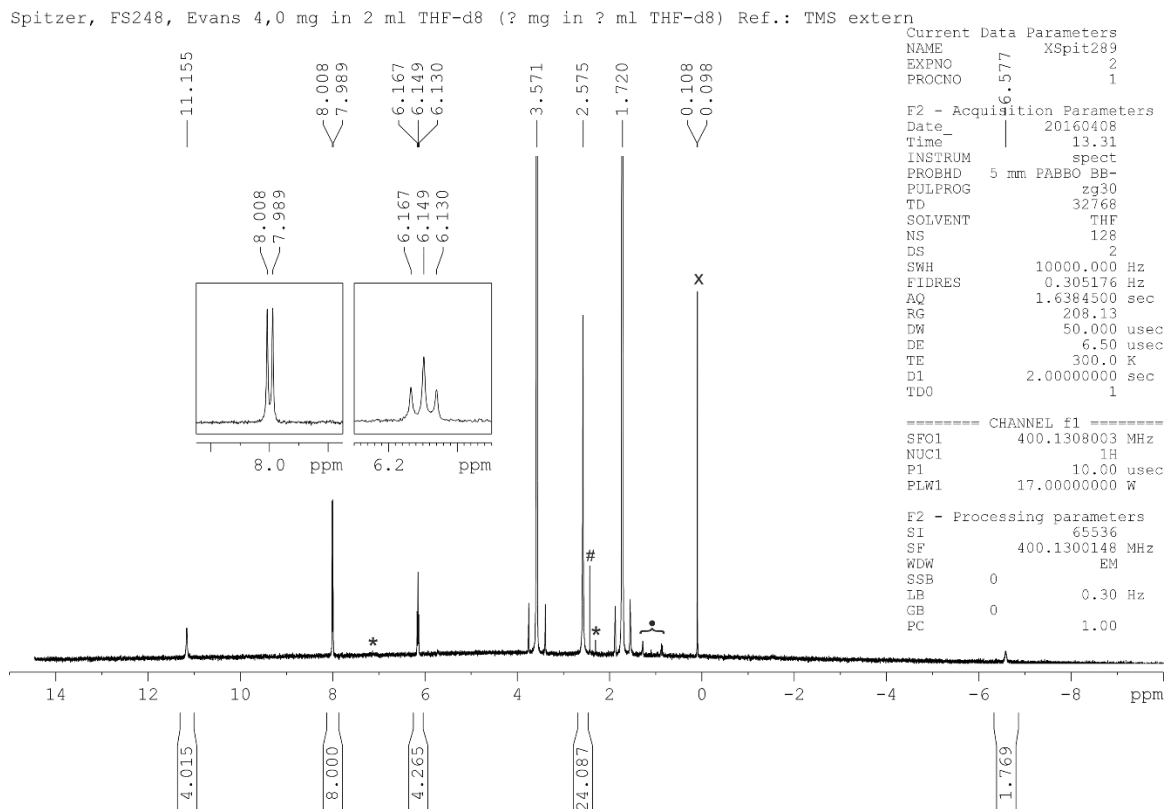


Figure S13. ¹H NMR spectrum of **5c** in [D₈]THF. Impurities of toluene (*), water (#), *n*-hexane (•) and silicon grease (x) are marked.

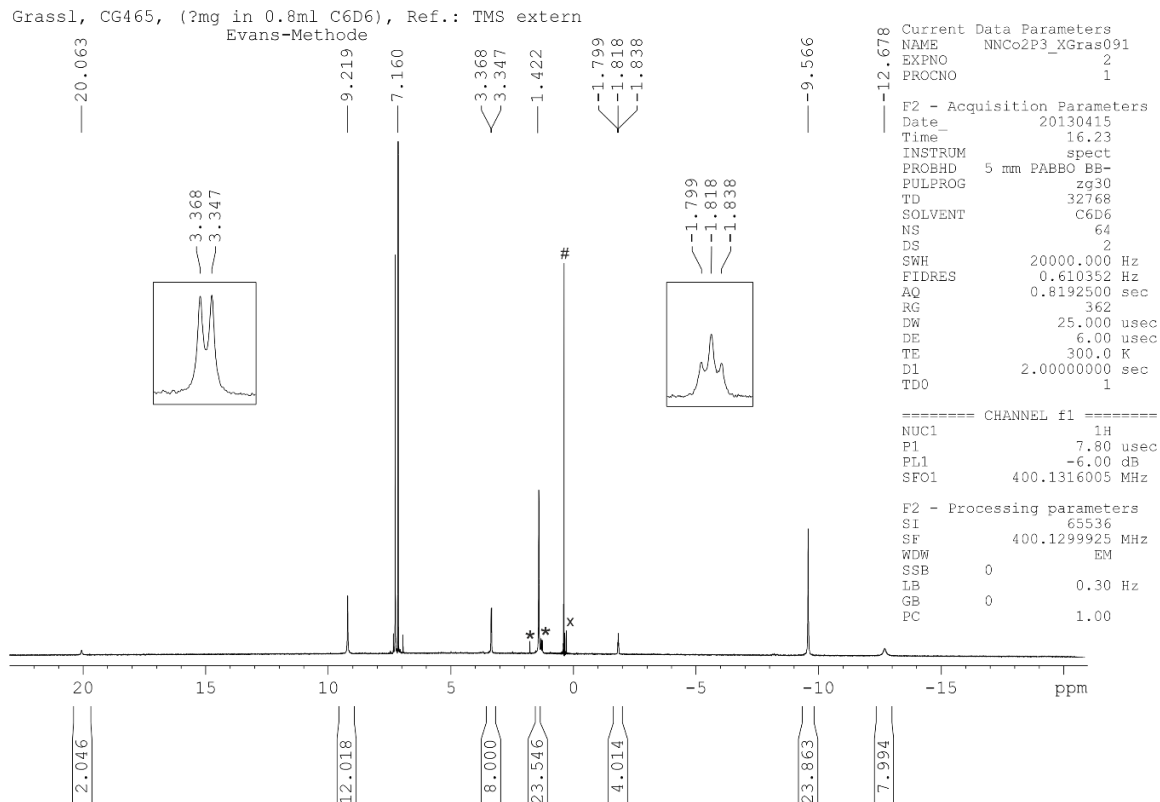


Figure S14. ¹H NMR spectrum of **6** in C₆D₆. Impurities of L³H (*), water (#) and silicon grease (x) are marked.

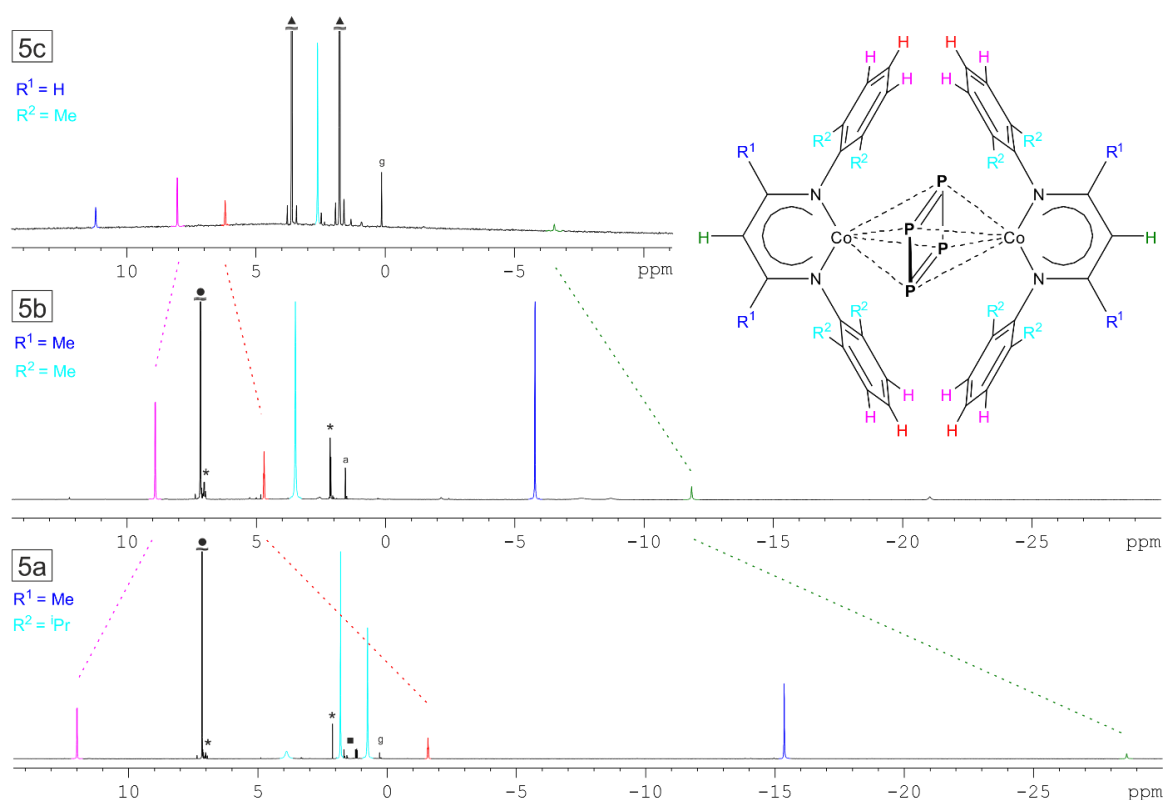
¹H NMR Spectra of Compounds 5a–c in Comparison

Figure S15. Comparison of ¹H NMR spectra of compounds **5c** (top), **5b** (middle) and **5a** (bottom). Dotted lines in spectra highlight the trends in chemical shifts of H_{meta} (purple), H_{para} (red) and H_{backbone} (green) protons, which are present in ligands L^{1–3} of compounds **5a–c**. Each ligand displays a unique combination of α -backbone substituents (R¹, dark blue) and substituents in 2,6-position (R², turquoise) of aromatic flanking group. Solvent (\blacktriangle : thf, \bullet : benzene) and very minor impurities are marked (g: grease, a: acetone, *: toluene, \blacksquare : L³H).

Figure S15 displays ¹H NMR signals of H_{meta}, H_{para} and H_{backbone} substituents, which are present in each ligands L¹, L² or L³ of compounds **5a–c**. Comparing these signals of compound **5c**, **5b** and **5a**, a trend in chemical shifts is recognized, which can be rationalized with the increasing steric strain of their ligands L² (in **5c**), L¹ (in **5b**) to L³ (in **5a**). Additionally, the steric strain of the ligands should sensitively impact the Co \cdots Co' distances in solution, which again influences the conformation of its Co₂P₄ core in solution. We recognize that this trend correlates with the increasing magnetic moment from **5c**, **5b** to **5a** in solution measured with the Evans method, respectively.

Magnetic Measurements in Solution (Evans Method)

Effective magnetic moments μ_{eff} of paramagnetic compounds in solution were determined by ¹H NMR spectroscopy using the Evans method^[14] with pure solvent as internal reference. ¹H NMR spectra were recorded on a Bruker Avance III HD 400 (¹H: 400.130 MHz) spectrometer. The molar paramagnetic susceptibility χ_P was obtained from molar (overall, measured) magnetic susceptibility χ_M after the correction of diamagnetic contributions χ_D according to equation (1).^[15] The molar magnetic susceptibility χ_M can be derived from equation (2).^[16] The effective magnetic moment μ_{eff} of paramagnetic compound was derived from equation (3).^[15]

Equations:

$$\chi_P = \chi_M - \chi_D \quad (1)$$

$$\chi_M = \frac{3000 \cdot \Delta f}{4\pi \cdot f \cdot c} \quad (2)$$

$$\mu_{\text{eff}} = \sqrt{8 \cdot T \cdot \chi_P} \quad (3)$$

Where

χ_P is the molar paramagnetic susceptibility of the sample in $\text{emu} \cdot \text{mol}^{-1}$,

χ_D is the molar diamagnetic susceptibility of the sample in $\text{emu} \cdot \text{mol}^{-1}$,

χ_M is the molar (overall, measured) magnetic susceptibility of the sample in $\text{emu} \cdot \text{mol}^{-1}$,

Δf is the chemical shift difference between solvent in presence of paramagnetic solute and pure solvent in Hz,

f is the operating frequency of NMR spectrometer in Hz,

c is the concentration of paramagnetic sample in $\text{mol} \cdot \text{L}^{-1}$,

μ_{eff} is the effective magnetic moment in μ_B , and

T is the absolute temperature in K.

SQUID Magnetization Measurements

General Remarks

Magnetic data were collected using a Quantum Design MPMS-XL SQUID magnetometer. Measurements were obtained for a finely ground microcrystalline powder (15–30 mg) restrained within a polycarbonate gel capsule. Samples used for magnetization measurement were checked for chemical composition and purity by ¹H NMR spectroscopy. Data reproducibility was checked on independently synthesized samples. Dc susceptibility data were collected in the temperature range of 2–300 K under a dc field of 1 T. The data shown refer to the complete dinuclear complexes, not mononuclear subunits. The data were corrected for core diamagnetism of the sample estimated using Pascal's constants^[15] ($\chi_{\text{dia}} = 10.74 \cdot 10^{-4} \text{ cm}^3 \cdot \text{mol}^{-1}$ for **2**, $7.168 \cdot 10^{-4} \text{ cm}^3 \cdot \text{mol}^{-1}$ for **6**, and $9.853 \cdot 10^{-4} \text{ cm}^3 \cdot \text{mol}^{-1}$ for **3**). Magnetic susceptibility data was analyzed using the julX program written by E. Bill (MPI for Chemical Energy Conversion, Mülheim an der Ruhr).

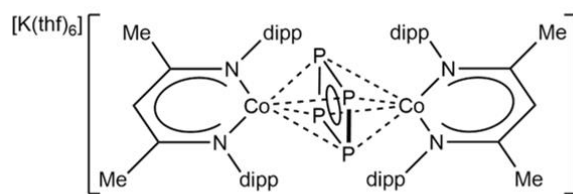


Figure S16. Molecular Structure of compound 2.

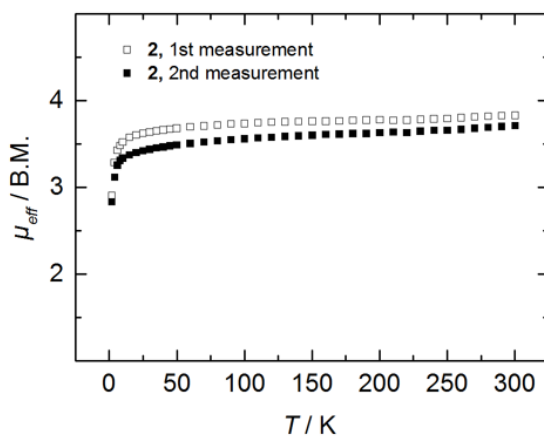


Figure S17. VT SQUID magnetization measurement of compound 2.

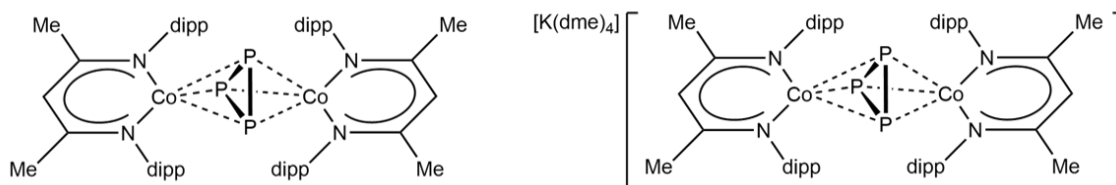


Figure S18. Molecular Structure of compound 6 (left) and compound 3a (right).

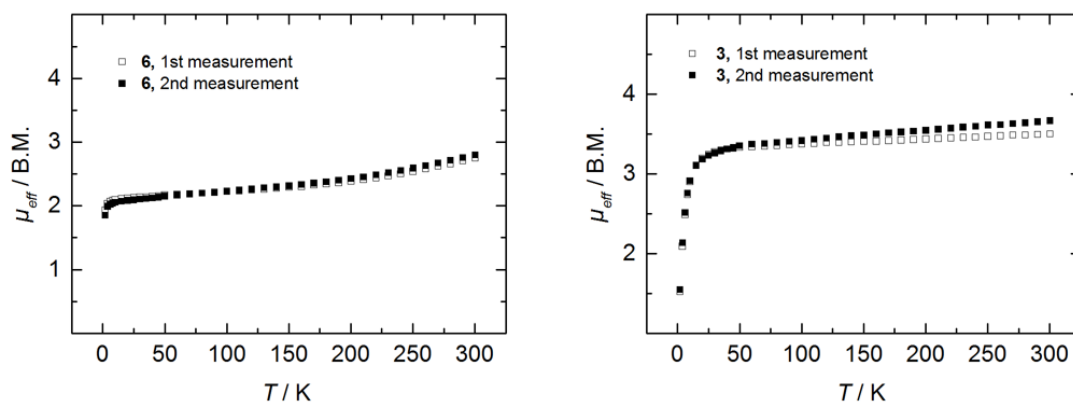


Figure S19. VT SQUID magnetization measurement of compound 6 (left) and compound 3a (right).

Cyclic Voltammetry (CV)

All cyclic voltammetry measurements were performed in THF at 295 K in a three electrode setup, with a platinum disc electrode (working electrode, 3 mm diameter), an Ag-wire (pseudo-reference electrode) and a Pt-wire (auxiliary electrode), in combination with a *Methrom Autolab PGSTAT101* potentiostat. Bu₄NPF₆ (0.1 mol/L) was used as supporting electrolyte and all cyclic voltammograms are referenced against the Cp₂Fe/Cp₂Fe⁺ redox couple.

Table S5. Data of the cyclic voltammetry measurements of **2**^[6], **3**, **5a**^[7] and **6**^[7] at 100 mV/s.

	E _{pc} / [V]	E _{pa} / [V]	E _{1/2} / [V]	i _{pf} / [μA]	i _{pr} / [μA]	i _{pr} /i _{pf}
5a ^[7]	-1.66	-1.57	-1.62	2.27	2.18	0.96
6 ^[7]	-1.67	-1.56	-1.62	2.96	2.96	1.00
2 ^[6]	-1.65	-1.53	-1.59	1.89	1.80	0.95
3	-1.72	-1.59	-1.66	2.60	2.51	0.97

Note: We extensively investigated the electrochemical behavior of **5a** at negative potentials in order to detect a second redox couple (in analogy to compound **E1**^[5]) or at least an irreversible reduction. However, no additional redox event was detected.

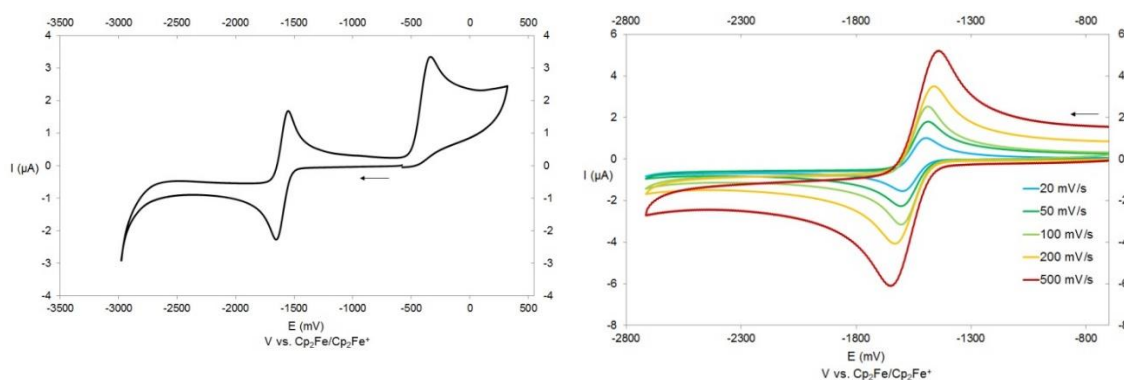


Figure S20. Cyclic voltammogram of **5a** at 100 mV/s scan rate (left) and the redox event at E_{1/2} = -1.62 V at different scan rates (right).^[7]

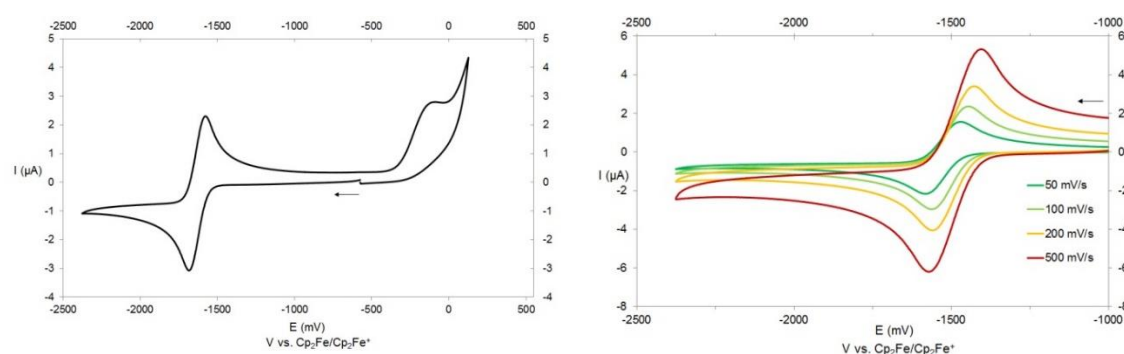


Figure S21. Cyclic voltammogram of **6** at 100 mV/s scan rate (left) and the redox event at E_{1/2} = -1.62 V at different scan rates (right).^[7]

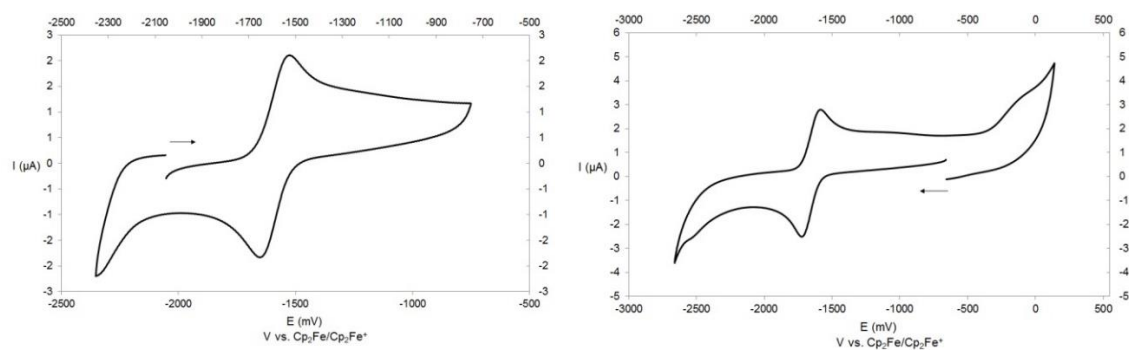


Figure S22. Cyclic voltammogram of **2**^[6] (left) and **3** (right) at 100 mV/s scan rate.

Note: By increasing the concentration of **3** an irreversible reduction at -2.52 V is monitored (Figure S23).

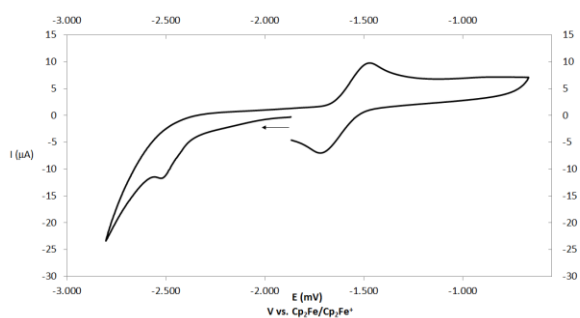


Figure S23. Cyclic voltammogram of **3** (increased concentration) at 100 mV/s scan rate.

Raman Spectrum of Complex 1 · *n*-hexane^[6]

Raman spectrum of complex 1 · *n*-hexane in solid state was measured using a DXR Raman Microscope (Thermo Scientific™) in cooperation with Dr. Wendy Patterson at the Institute of Analytical Chemistry (University of Regensburg).^[6]

Excitation source: $\lambda_{\text{exc}} = 532 \text{ nm}$.

Laserpower: 8 mV.

Exposure time: 20 sec.

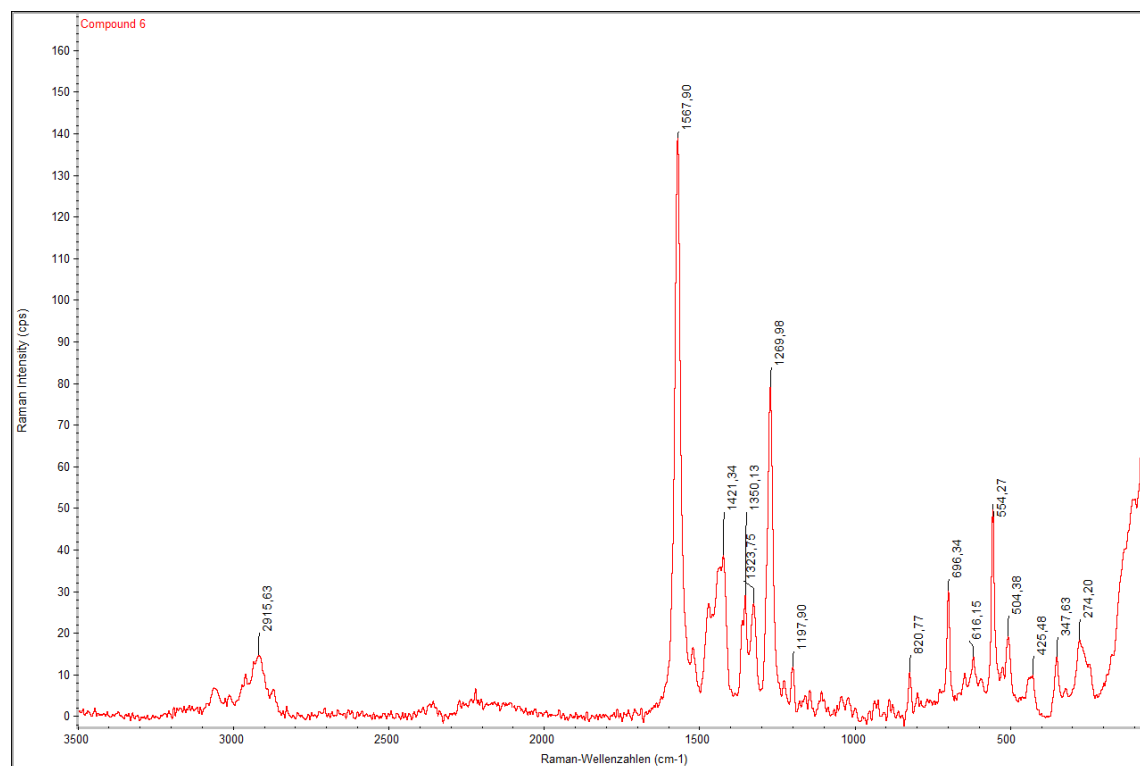


Figure S24. Raman spectrum of compound 1 · *n*-hexane in solid state.^[6]

DFT Calculations

All calculations have been performed with the TURBOMOLE program package^[17] at the RI^[18]-BP86^[19]/def2-TZVP^[20] level of theory. To speed up the geometry optimization the Multipole Accelerated Resolution-of-the-Identity (MARI-J)^[21] approximation has been used. The final energy of the molecules was determined by single point calculations without using the RI formalism. The experimental geometry of **3a** relaxes during the geometry optimisation steps to a geometry in which the nancac ligands are oriented almost perpendicular to each other (torsion angle N-Co-Co-N 50.65°), resmbing to the experimantal geometry of **3b**.

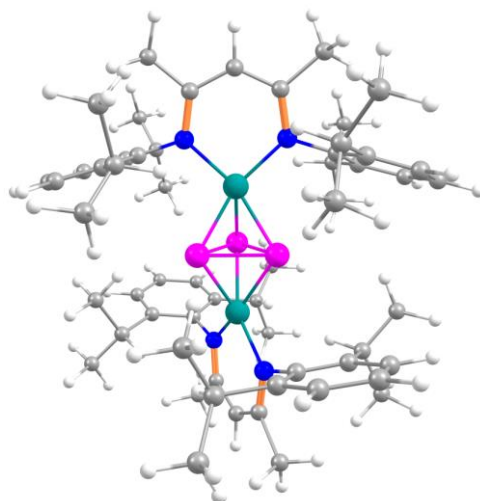


Figure S25. Optimised geometry of **3** in the gas phase, in the triplet spin state.

Table S6. Selected distances in the optimised geometry of **3b** in different spin states.

	Unrestricted Singlet	Triplet	Quintet
$d(\text{Co}\cdots\text{Co}) / [\text{\AA}]$	3.778	3.794	3.947
$d(\text{P}-\text{P}) / [\text{\AA}]$	2.213	2.263	2.238
$d(\text{P}-\text{P}) / [\text{\AA}]$	2.262	2.274	2.275
$d(\text{P}-\text{P}) / [\text{\AA}]$	2.382	2.287	2.345

Table S7. Selected distances in the optimised geometry of **3a** (triplet spin state) with fixed N-Co-Co-N torsion angle to 3.07° as found in the experimental geometry.

	Triplet
$d(\text{Co}\cdots\text{Co}) / [\text{\AA}]$	3.807
$d(\text{P}-\text{P}) / [\text{\AA}]$	2.216
$d(\text{P}-\text{P}) / [\text{\AA}]$	2.223
$d(\text{P}-\text{P}) / [\text{\AA}]$	2.276

Table S8. Relative energy (kJ·mol⁻¹) of **3b** in different spin states.

	Unrestricted Singlet	Triplet	Quintet
Relative Energy (kJ·mol ⁻¹)	6.95	0.00	70.92

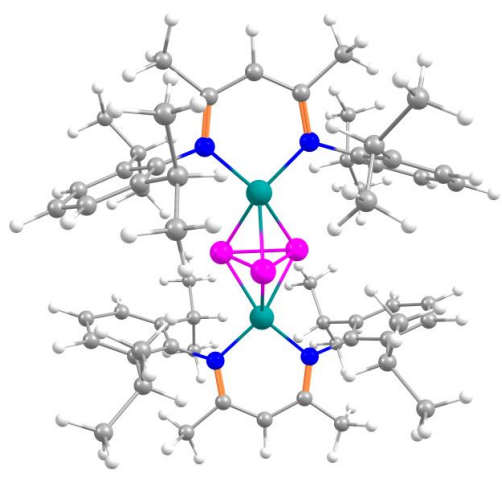
Table S9. Cartesian coordinates of the optimized geometry of **3b** (triplet spin state) at the RI-BP86/def2-TZVP level of theory.

Atom	x	y	z
Co	0.2266493	-0.0158067	1.8756788
Co	-0.2051416	-0.0398556	-1.8743333
P	0.4937679	1.1576227	-0.0495345
P	-1.2792218	-0.2197321	0.1512498
P	0.7938215	-1.0558880	-0.0968816
N	1.6106428	0.7594378	3.0523362
N	-0.8310869	-0.8069948	3.3485472
N	0.9987755	-0.5170914	-3.3655005
N	-1.7128153	0.5116765	-3.0333586
C	2.6996333	1.5007351	2.4827602
C	2.5416318	2.8929421	2.2381184
C	3.4141995	-0.0488864	-3.0902143
C	-2.0819006	-1.4500342	3.0666311
C	2.3330513	-0.9687651	-3.0918619
C	1.6406115	0.6059641	4.3880095
C	-0.4870214	-0.7439572	4.6466802
C	2.7856121	1.1656716	5.2182562
H	3.6452945	0.4789014	5.2078922
H	2.4698991	1.2835177	6.2629175
H	3.1475439	2.1303497	4.8440777
C	-3.2978480	-0.7245048	3.1834255
C	-2.9611025	0.8998693	-2.4412284
C	3.6332764	3.6164904	1.7420034
H	3.5233270	4.6857346	1.5539515
C	3.2169405	1.4484817	-3.3098928
H	2.1525667	1.6125554	-3.5306880
C	0.6660724	-0.0958726	5.1145530
H	0.8241811	-0.1377937	6.1916158
C	3.9333858	0.8608408	2.1939993
C	-3.3298680	0.7600177	3.5383342
H	-2.2998534	1.0641357	3.7725080
C	4.9901864	1.6325624	1.6913569
H	5.9414875	1.1453741	1.4652133
C	0.6748547	-0.3987980	-4.6654353
C	1.2215949	3.6017441	2.5273880
H	0.4338432	2.8370835	2.4322620
C	-3.2440572	2.2619646	-2.1700809
C	-4.5057975	-1.3937171	2.9493322
H	-5.4442107	-0.8402803	3.0305711
C	4.7111759	-0.5346895	-2.8746966
H	5.5468963	0.1688427	-2.8693471
C	2.5693583	-2.3502611	-2.8516041
C	-1.6779784	0.4970669	-4.3769905
C	-0.5701442	0.0625188	-5.1209332
H	-0.6865757	0.1034727	-6.2033909
C	-2.2337883	3.3719684	-2.4381642
H	-1.3440686	2.9045848	-2.8842201
C	-1.3662104	-1.3666738	5.7191485
H	-2.2312689	-0.7247533	5.9432718
H	-0.7950041	-1.4937606	6.6476177
H	-1.7722859	-2.3388970	5.4135578
C	4.9571580	-1.8892328	-2.6692426
H	5.9757400	-2.2475550	-2.5078457
C	-1.7950817	4.0524923	-1.1303772
H	-2.6466513	4.5429459	-0.6332279
H	-1.0336545	4.8215131	-1.3318817
H	-1.3644402	3.3224742	-0.4321206
C	3.5587510	2.2491896	-2.0415639
H	2.9490896	1.9270748	-1.1872721
H	3.3751576	3.3228651	-2.2030431
H	4.6176029	2.1261941	-1.7674527

Atom	x	y	z
C	-2.7679681	4.4304101	-3.4221326
H	-3.0941952	3.9845269	-4.3721508
H	-1.9871237	5.1736720	-3.6457144
H	-3.6283675	4.9710243	-2.9977893
C	-4.4946150	2.5968462	-1.6318503
H	-4.7182450	3.6450438	-1.4193550
C	-3.9248083	-0.1033252	-2.1448546
C	-3.8041170	1.6097297	2.3458346
H	-3.1730662	1.4429109	1.4631280
H	-3.7703088	2.6808136	2.5993682
H	-4.8394135	1.3598186	2.0679676
C	-2.8530480	1.0068503	-5.1970325
H	-3.8229425	0.7233486	-4.7716720
H	-2.7899676	0.6294644	-6.2256709
H	-2.8393356	2.1066890	-5.2444744
C	0.9100898	4.7196874	1.5216252
H	1.5813792	5.5846869	1.6438805
H	-0.1173233	5.0829380	1.6714979
H	0.9956556	4.3578924	0.4883643
C	-3.3385628	-3.4432126	2.4837224
H	-3.3620371	-4.4988719	2.2054177
C	4.3772255	-1.3643165	1.0725170
H	3.5309447	-1.2187799	0.3884764
H	4.4945178	-2.4462220	1.2405573
H	5.2861771	-1.0016300	0.5687875
C	5.3347776	-0.9277307	3.3543155
H	6.2903209	-0.6118162	2.9075471
H	5.4042864	-2.0085858	3.5513141
H	5.2363264	-0.4126545	4.3201411
C	-5.1608775	0.2866570	-1.6162609
H	-5.9060571	-0.4770809	-1.3860698
C	1.1641526	-3.9812821	-4.2178512
H	0.8789028	-3.2260208	-4.9607059
H	0.3454752	-4.7153393	-4.1573942
H	2.0611650	-4.5047432	-4.5862647
C	-4.2074863	1.0567966	4.7693014
H	-5.2676835	0.8387898	4.5674082
H	-4.1356416	2.1214394	5.0400175
H	-3.9091382	0.4640258	5.6457941
C	-5.4561603	1.6260355	-1.3654762
H	-6.4255551	1.9086292	-0.9502179
C	-3.6396229	-1.5799793	-2.4044035
H	-2.5449881	-1.6791555	-2.4687068
C	-4.1206714	-2.4863280	-1.2616973
H	-3.7345976	-2.1477655	-0.2915047

C	-4.5376992	-2.7458644	2.6155918	H	-3.7711024	-3.5166152	-1.4279764
H	-5.4906987	-3.2497549	2.4433097	H	-5.2198050	-2.5227124	-1.1989616
C	3.8864213	-2.7818516	-2.6506460	C	-0.5656277	-4.5468852	3.7505312
H	4.0789578	-3.8405892	-2.4695435	H	-0.4842079	-3.9801738	4.6878146
C	4.8555875	3.0010392	1.4760812	H	0.3714234	-5.1095847	3.6164737
H	5.6928807	3.5841965	1.0877200	H	-1.3838198	-5.2759865	3.8653753
C	-0.8151241	-3.6235781	2.5421541	C	1.6235958	-4.4695596	-1.7922037
H	0.0098603	-2.8969072	2.4959777	H	2.4408627	-5.1537496	-2.0706899
C	1.4231671	-3.3573435	-2.8321385	H	0.7085236	-5.0741958	-1.7091946
H	0.5210566	-2.7921204	-2.5478934	H	1.8451962	-4.0489392	-0.8021179
C	-2.1018134	-2.8193126	2.6934098	C	-0.7868624	-4.4376621	1.2396384
C	4.0426520	1.9854542	-4.4953886	H	-1.5553161	-5.2265351	1.2303386
H	5.1226930	1.9182258	-4.2919298	H	0.1904046	-4.9284305	1.1217632
H	3.8063855	3.0457384	-4.6740032	H	-0.9479140	-3.7894890	0.3678845
H	3.8469537	1.4331234	-5.4253008	C	1.1556590	4.1605846	3.9626431
C	1.6813134	-0.7248132	-5.7584372	H	1.2337773	3.3666888	4.7157907
H	2.3496920	0.1307166	-5.9387552	H	0.1984296	4.6805769	4.1242911
H	1.1580857	-0.9388313	-6.6993829	H	1.9676183	4.8843910	4.1395392
H	2.3220873	-1.5771275	-5.5044198	C	-4.2343066	-2.0621347	-3.7424754
C	4.1537364	-0.6342361	2.4081131	H	-5.3285041	-1.9318496	-3.7544421
H	3.2391353	-1.0413059	2.8625408	H	-4.0205555	-3.1322551	-3.8907036
				H	-3.8169747	-1.5173030	-4.5989924

Table S10. Cartesian coordinates of the optimized geometry of **3a** (triplet spin state) at the RI-BP86/def2-TZVP level of theory. The N-Co-Co-N torsion angle has been restrained to 3.07°.

Atom	x	y	z				
Co	0.1971083	-0.2853246	1.8544186				
Co	-0.1930747	0.2933533	-1.8880031				
P	0.0514471	1.2780064	0.1728054				
P	-1.1507123	-0.5841295	0.0089625				
P	1.1117157	-0.6247223	-0.2359898				
N	1.7983823	-0.4300272	3.0410590				
N	-1.0992286	-0.5648279	3.3461752				
N	1.1120090	0.4832359	-3.3775778				
N	-1.7711802	0.5510351	-3.0649195				
C	3.0726660	-0.0210670	2.5248430				
C	3.3894208	1.3665216	2.5212417				
C	3.4657204	1.0879522	-2.8721887				
C	-2.4891992	-0.2913877	3.1286198				
C	2.4804899	0.1111926	-3.1631408				
C	1.7580804	-0.8124977	4.3282334				
C	-0.7556341	-0.9059916	4.5996946				
C	3.0280738	-0.9809384	5.1493208				
H	3.3945204	-2.0162550	5.0758020				
H	2.8239619	-0.7821889	6.2096601				
H	3.8391403	-0.3246323	4.8138806				
C	-3.0176796	0.9829338	3.4642209				
C	-3.0773003	0.2062084	-2.5805935				
C	4.6281514	1.7736763	2.0125387				
H	4.8794032	2.8358386	2.0079869				
C	3.1291962	2.5721818	-2.7714219				
H	2.1007823	2.7025808	-3.1378992				
C	0.5696023	-1.0882452	5.0222153				
H	0.6929251	-1.3943021	6.0609794				
C	4.0139605	-0.9673837	2.0414177				
C	-2.1574252	2.0800852	4.0884779				
H	-1.1933152	1.6281160	4.3607646				
C	5.2317072	-0.5019657	1.5264878				
H	5.9527915	-1.2237798	1.1365637				
C	0.7998566	0.9005469	-4.6172070				
C	2.4355196	2.3945299	3.1247467				
H	1.4271188	1.9549249	3.0740794				
C	-3.8873005	1.1710826	-1.9292382				
				Atom	x	y	z
				H	-4.4015512	3.4139631	-3.5482994
				H	-3.9523129	4.6424232	-2.3448559
				H	-5.3622645	3.5969196	-2.0665017
				C	-5.1502870	0.7859567	-1.4604228
				H	-5.7724655	1.5217630	-0.9461383
				C	-3.5620612	-1.1155020	-2.7751316
				C	-1.8609198	3.2169676	3.0958919
				H	-1.3268527	2.8434933	2.2117022
				H	-1.2367273	3.9897816	3.5718253
				H	-2.7912978	3.6962812	2.7547466
				C	-2.9842718	1.1621139	-5.1504035
				H	-3.5188477	0.2139547	-5.3075941
				H	-2.7477972	1.5897280	-6.1325460
				H	-3.6893430	1.8282343	-4.6362830
				C	2.3952416	3.7272921	2.3644450
				H	3.3518715	4.2698472	2.4255786
				H	1.6236817	4.3801949	2.7995134
				H	2.1509276	3.5770615	1.3055197
				C	-4.6882725	-1.0032885	2.3943310

C	-4.3770103	1.2307146	3.2312877	H	-5.3458231	-1.7655770	1.9748055
H	-4.7895366	2.2123610	3.4757361	C	3.6913551	-3.1063750	0.7018725
C	4.7876748	0.6704108	-2.6662708	H	2.9111644	-2.6223820	0.1008345
H	5.5490499	1.4152148	-2.4251282	H	3.4639218	-4.1814132	0.7777425
C	2.8400925	-1.2616661	-3.2600190	H	4.6447197	-2.9987872	0.1621980
C	-1.7124906	0.9542730	-4.3467421	C	4.8581816	-3.1983625	2.9219738
C	-0.5116990	1.1712233	-5.0387952	H	5.8316060	-3.1566162	2.4093020
H	-0.6143054	1.5217963	-6.0648379	H	4.5972363	-4.2607386	3.0477925
C	-3.4305909	2.6129656	-1.7349929	H	4.9923392	-2.7576205	3.9190253
H	-2.4172893	2.6928202	-2.1544287	C	-4.8315870	-1.4482086	-2.2872100
C	-1.8029873	-1.0427282	5.6951131	H	-5.2056949	-2.4654978	-2.4260329
H	-1.9910185	-0.0663583	6.1686321	C	1.7159503	-2.5651574	-5.1264214
H	-1.4403116	-1.7217762	6.4783628	H	1.4345696	-1.6542269	-5.6700751
H	-2.7667112	-1.4074431	5.3232652	H	0.9618368	-3.3355414	-5.3516048
C	5.1516544	-0.6694358	-2.7648928	H	2.6842413	-2.9141004	-5.5199254
H	6.1877546	-0.9726401	-2.6025236	C	-2.7861129	2.6559201	5.3719704
C	-3.3493832	2.9817058	-0.2460775	H	-3.7077875	3.2169806	5.1535893
H	-4.3425213	2.9551076	0.2284912	H	-2.0862821	3.3517783	5.8597595
H	-2.9411134	3.9965378	-0.1218958	H	-3.0426867	1.8670576	6.0936663
H	-2.7003554	2.2828154	0.2956418	C	-5.6275617	-0.5109523	-1.6311119
C	3.1567510	3.0499428	-1.3113950	H	-6.6125683	-0.7910294	-1.2530706
H	2.4558003	2.4678680	-0.6985166	C	-2.7453959	-2.1762626	-3.5094453
H	2.8746387	4.1126243	-1.2456285	H	-1.8263134	-1.6914305	-3.8667427
H	4.1599265	2.9326191	-0.8748355	C	-2.3256716	-3.3241777	-2.5756410
C	-5.2129167	0.2510027	2.7022946	H	-1.7485635	-2.9448580	-1.7214931
H	-6.2690736	0.4633959	2.5254953	H	-1.7030766	-4.0531148	-3.1177164
C	4.1778960	-1.6221952	-3.0623009	H	-3.2040055	-3.8587738	-2.1824722
H	4.4637155	-2.6731285	-3.1334242	C	-2.8257766	-3.6415462	3.4903981
C	5.5461658	0.8534273	1.5083124	H	-2.1816786	-3.2877162	4.3042740
H	6.5014455	1.1927366	1.1031919	H	-2.4704444	-4.6417683	3.1965470
C	-2.7986082	-2.6948753	2.2732145	H	-3.8501945	-3.7493232	3.8819803
H	-1.7438046	-2.5586794	1.9854339	C	2.0157531	-3.6565402	-2.8772388
C	1.7996722	-2.3229213	-3.6061696	H	2.9269123	-4.1733251	-3.2176306
H	0.8274303	-1.9208894	-3.2780404	H	1.1681344	-4.3301491	-3.0733488
C	-3.3352324	-1.3027134	2.5968233	H	2.0894217	-3.5117322	-1.7918676
C	4.0586111	3.4521462	-3.6287661	C	-3.5239591	-3.3598791	1.0953820
H	5.0888496	3.4452082	-3.2411151	H	-4.5470519	-3.6685800	1.3644140
H	3.7109766	4.4966270	-3.6159369	H	-2.9823747	-4.2671142	0.7885138
H	4.0977433	3.1181662	-4.6757659	H	-3.5830692	-2.6866858	0.2303848
C	1.8799861	1.1132376	-5.6659657	C	2.7608130	2.6518905	4.6100799
H	2.4297504	2.0480228	-5.4798917	H	2.6965461	1.7335502	5.2075680
H	1.4306584	1.1822752	-6.6646333	H	2.0549610	3.3813011	5.0374177
H	2.6242349	0.3068992	-5.6664420	H	3.7784977	3.0597993	4.7208613
C	3.7718490	-2.4739650	2.1005653	C	-3.4902592	-2.7372672	-4.7358813
H	2.8010421	-2.6316489	2.5924602	H	-4.4024164	-3.2781237	-4.4394419
C	-4.3380158	3.6187345	-2.4702775	H	-2.8480583	-3.4443422	-5.2832296
				H	-3.7877945	-1.9417731	-5.4339374

Literatur

- [1] P. H. M. Budzelaar, R. de Gelder, A. W. Gal, *Organometallics* **1998**, *17*, 4121-4123.
- [2] F. Spitzer, C. Graßl, G. Balázs, E. M. Zolnhofer, K. Meyer, M. Scheer, *Angew. Chem. Int. Ed.* **2016**, *55*, 4340-4344.
- [3] a) M. Stender, R. J. Wright, B. E. Eichler, J. Prust, M. M. Olmstead, H. W. Roesky, P. P. Power, *J. Chem. Soc., Dalton Trans.* **2001**, 3465-3469; b) J. Feldman, S. J. McLain, A. Parthasarathy, W. J. Marshall, J. C. Calabrese, S. D. Arthur, *Organometallics* **1997**, *16*, 1514-1516.
- [4] X. Dai, P. Kapoor, T. H. Warren, *J. Am. Chem. Soc.* **2004**, *126*, 4798-4799.
- [5] S. Yao, N. Lindenmaier, Y. Xiong, S. Inoue, T. Szilvási, M. Adelhardt, J. Sutter, K. Meyer, M. Driess, *Angew. Chem.* **2015**, *127*, 1266-1270
- [6] F. Spitzer, Master thesis, *Universität Regensburg* **2013**.
- [7] C. Graßl, PhD thesis, *Universität Regensburg* **2013**.

- [8] Primal measurement (Evans method) reported in reference [7]. The magnetic moment in solution was re-calculation herein. The interpretation of ¹H NMR signals was performed herein.
- [9] CrysAlisPro Software System, Agilent Technologies UK Ltd, Yarnton, Oxford, UK.
- [10] O.V. Dolomanov and L.J. Bourhis and R.J. Gildea and J.A.K. Howard and H. Puschmann, Olex2: A complete structure solution, refinement and analysis program, *J. Appl. Cryst.*, **2009**, *42*, 339-341.
- [11] Sheldrick, G.M., ShelXT, *Acta Cryst.*, **2014**, *A71*, 3-8.
- [12] Sheldrick, G.M., A short history of ShelX, *Acta Cryst.*, **2008**, *A64*, 339-341.
- [13] Crystal structure of compound **5a** and **6** was primary reported in citation [7]. However, we remeasured crystals of **5a** and **6** in order to present improved structural values.
- [14] D. F. Evans, *J. Chem. Soc. (Resumed)* **1959**, 2003-2005.
- [15] G. A. Bain, J. F. Berry, *J. Chem. Educ.* **2008**, *85*, 532.
- [16] S. K. Sur, *Journal of Magnetic Resonance (1969)*, **1989**, *82*, 169-173.
- [17] a) R. Ahlrichs, M. Bär, M. Häser, H. Horn, C. Kölmel, *Chem. Phys. Lett.* **1989**, *162*, 165–169; b) O. Treutler, R. Ahlrichs, *J. Chem. Phys.* **1995**, *102*, 346–354.
- [18] a) K. Eichkorn, O. Treutler, H. Oehm, M. Häser, R. Ahlrichs, *Chem. Phys. Lett.* **1995**, *242*, 652–660; b) K. Eichkorn, F. Weigend, O. Treutler, R. Ahlrichs, *Theor. Chem. Acc.* **1997**, *97*, 119.
- [19] a) P. A. M. Dirac, *Proc. Royal Soc. A* **1929**, *123*, 714-733; b) J. C. Slater, *Phys. Rev.* **1951**, *81*, 385-390; c) S. H. Vosko, L. Wilk, M. Nusair, *Can. J. Phys.* **1980**, *58*, 1200-1211; d) A. D. Becke, *Phys. Rev. A*, **1988**, *38*, 3098; e) J. P. Perdew, *Phys. Rev. B* **1986**, *33*, 8822-8824; Erratum: J. P. Perdew *Phys. Rev. B* **1986**, *34*, 7406.
- [20] a) A. Schäfer, C. Huber, R. Ahlrichs, *J. Chem. Phys.* **1994**, *100*, 5829; b) K. Eichkorn, F. Weigend, O. Treutler, R. Ahlrichs, *Theor. Chem. Acc.* **1997**, *97*, 119.
- [21] a) M. Sierka, A. Hogekamp, R. Ahlrichs, *J. Chem. Phys.* **2003**, *118*, 9136; b) K. Eichkorn, O. Treutler, H. Oehm, M. Häser, R. Ahlrichs, *Chem. Phys. Lett.* **1995**, *242*, 652–660; c) K. Eichkorn, F. Weigend, O. Treutler, R. Ahlrichs, *Theor. Chem. Acc.* **1997**, *97*, 119.

Preface

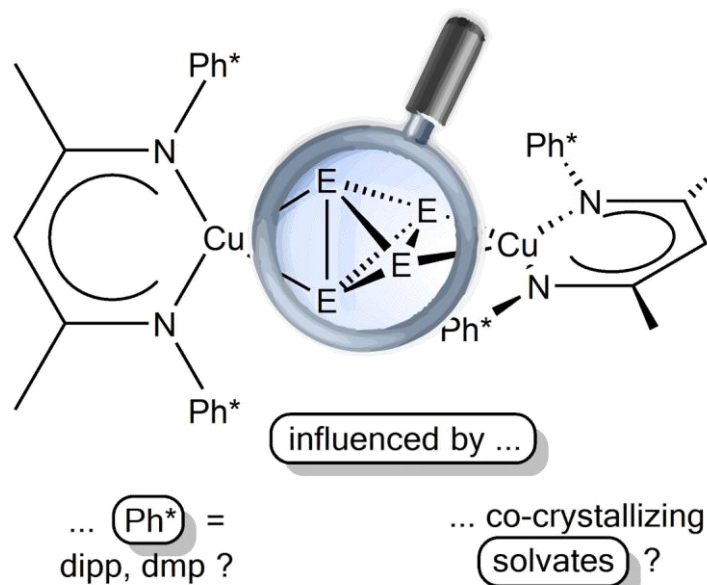
The following chapter has not been published until the submission of this thesis.

Authors

Fabian Spitzer, Manfred Scheer*

Author contributions

F. Spitzer prepared the manuscript and performed the synthesis and characterization of the herein presented compounds **1a'** and **2'**. The molecular structures of **1a** and both solvomorph crystal structures of **1b** were already reported in chapter 3 of this thesis. M. Scheer supervised the research and revised the manuscript.

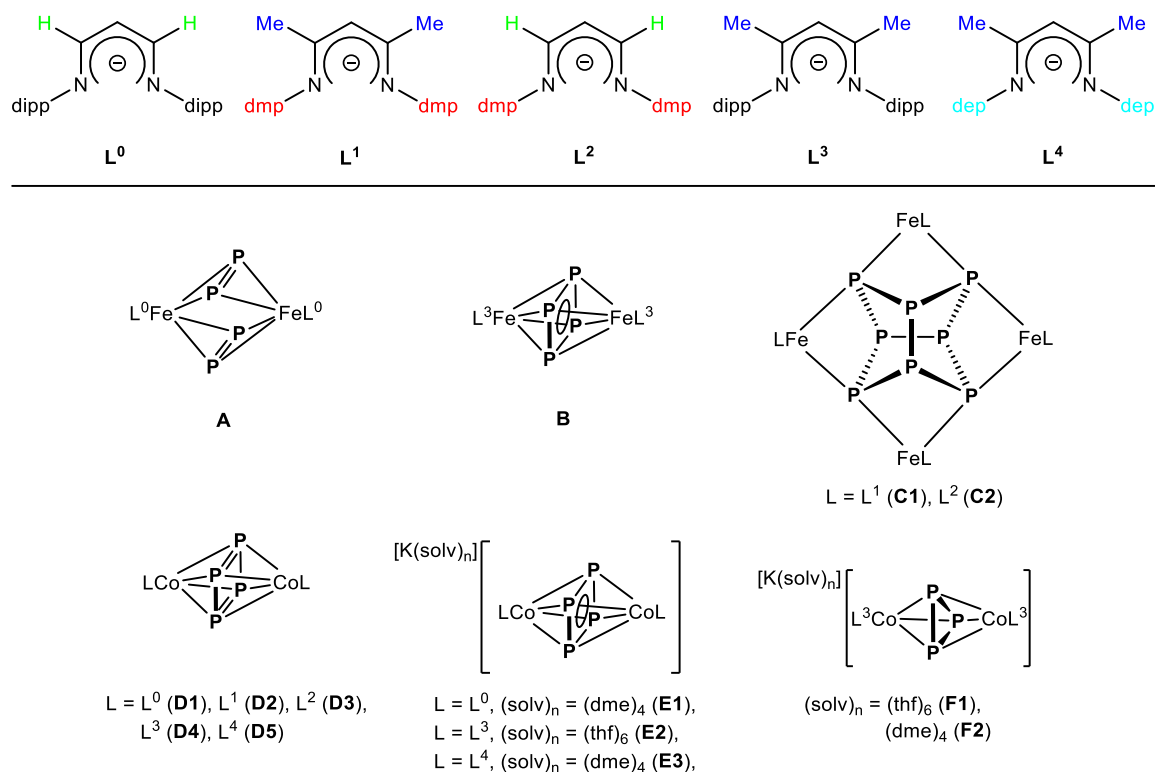


6. Influence of β -diketiminato Ligand Design and Solvates on the Solid State Structures of [(NacnacCu)₂(μ - η^2 : η^2 -E₄)] (E = P, As)

Abstract: The crystal structures of [(LCu)₂(μ - η^2 : η^2 -P₄)] (L = L³ (**1a**), L¹ (**1a'**)) are compared, highlighting the influence of the aromatic ligand substituents (dipp = 2,6-diisopropylphenyl (in L³) or dmp = 2,6-dimethylphenyl (in L¹)) on the molecular structure in the solid state. The reactivity of **1a'** was examined in solution and was found to be in equilibrium with the mononuclear complex [L¹Cu(η^2 -P₄)] (**2'**). The dynamic behavior was monitored by VT³¹P{¹H} NMR spectroscopy. Moreover, the influence of solvates on the molecular structure of [(L³Cu)₂(μ - η^2 : η^2 -As₄)] (**1b**) is discussed based on two solvomorph crystal structures.

6.1 Introduction

Understanding the influence of ligand substituents is a key step in tuning the properties of organometallic compounds, which paves the way for future applications. The β -diketiminato ligand was recently applied in catalysis^[1] and small molecule activation. For example, the β -diiminato copper(I) mediated O₂ reactions yield diverse structural peroxo- and/or bis(μ -oxo)dicopper motifs, which are significantly influenced by the chosen ligand substituents.^[2] Furthermore, the choice of alkali metal (A) combination was found to impact the geometric situation in the dinuclear β -diketiminato complexes [A₂(LM)₂(μ - η^1 : η^1 -N₂)] (L = L³, M = Fe, A₂ = Na₂, K₂, Rb₂, Cs₂; M = Ni, A₂ = Na₂, K/Na, K₂).^[3] Recently, a set of ligands (L⁰–L³, see Scheme 1) was introduced in transition metal mediated P₄ activation, which aims for the systematic investigation of the applied β -diiminato ligand design. The first reaction of a β -dialdiminato iron(I) precursor with P₄ was reported by Driess *et al.* and a dinuclear product [(L⁰Fe)₂(μ - η^2 : η^2 -P₂)₂] (**A**) with [P₂]²⁻ ligands was formed (Scheme 1).^[4] A subsequent comparative study by our group, using three further ligands L¹–L³, led to the discovery of a dinuclear product [(L³Fe)₂(μ - η^4 : η^4 -P₄)] (**B**), containing a [P₄]²⁻ ligand.^[5] The remaining ligands L¹ and L² lead to the formation of tetranuclear products [(LFe)₂(μ - η^1 : η^1 : η^1 : η^1 : η^1 : η^1 : η^1 : η^1 -P₈)] (L = L¹ (**C1**), L² (**C2**)) with realgar-type [P₈]⁴⁻ motifs. The analogous cobalt(I) reactions exclusively resulted in isostructural [(LCo)₂(μ - η^4 : η^4 -P₄)] (L = L⁰ (**D1**), L¹ (**D2**), L² (**D3**), L³ (**D4**), L⁴ (**D5**)) compounds stabilizing planar [P₄]⁰ ligands.^[6] They are not significantly altered by the ligand substituents of L⁰–L⁴ (Scheme 1). The one electron reduction leads to conversion of their [P₄]⁰ into [P₄]²⁻ ligands, which are stabilized in the isostructural complexes [K(solvent)_n][(LCo)₂(μ - η^4 : η^4 -P₄)] (L = L⁰ (**E1**), L³ (**E2**), L⁴ (**E3**)).



Scheme 1. Top: Set of β -diiminato ligands with systematic variation of backbone substituents and flanking groups. Bottom: Selected P_n ligand complexes obtained by iron(I) and cobalt(I) mediated reactions with P₄.

However, a changed complex geometry was observed for the *cyclo*-[P₃]³⁻ containing [K(solv)_n][(L³Co)₂(μ - η^3 : η^3 -P₃)] ((solv)_n = (thf)₆ (**F1**), (dme)₄ (**F2**)) in the solid state, which is affected by the differently shaped counterions ([K(thf)₆]⁺ versus [K(dme)₄]⁺) and co-crystallizing solvent.^[6b] While the molecular structure of **F1** · 2 thf reveals a twisted ligand conformation, the ligand planes are parallel in the crystals of **F2** · dme. It is emphasized that both anions cannot be distinguished in solution. Consequently, the crystal packing is affected by solvates.

Recently, we reported the complexes [(L³Cu)₂(μ - η^2 : η^2 -E₄)] (E = P (**1a**), As (**1b**)) containing tetrahedral shaped, intact E₄ moieties.^[7] Motivated by the previously recognized dependencies of ligand design on the reaction outcome as well as the influence of solvates on the crystal structure, the question arose if the reaction outcome in the copper(I) systems can be altered in a similar manner. Given that these copper(I) systems possess d¹⁰ electron configuration, their geometry should mainly be driven by steric effects and weak intermolecular interactions. This suggests [LCu] complexes to be adequate for the investigation of the ‘pure’ ligand influence.

For a quantitative description of the geometry of [(LCu)₂(μ - η^2 : η^2 -E₄)] (E = P, As), several parameters are introduced. Selected ones are depicted in Figure 1. This enables the quantitative comparison of their structures and includes

- the distance d between both copper centers
- the angle Θ spanning between the Cu...Cu' axis and the plane formed by the coordinating nitrogen atoms and the methine carbon in the ligand backbone (for terminal coordination modes, this value is close to zero)
- the orientation of both NCCCN ligand planes compared to each other, which is described by the twist angle Φ between both N–N lines
- Σ_{angles} surrounding the copper centers, which describes the deviation from ideal quadratic planar coordination geometry.

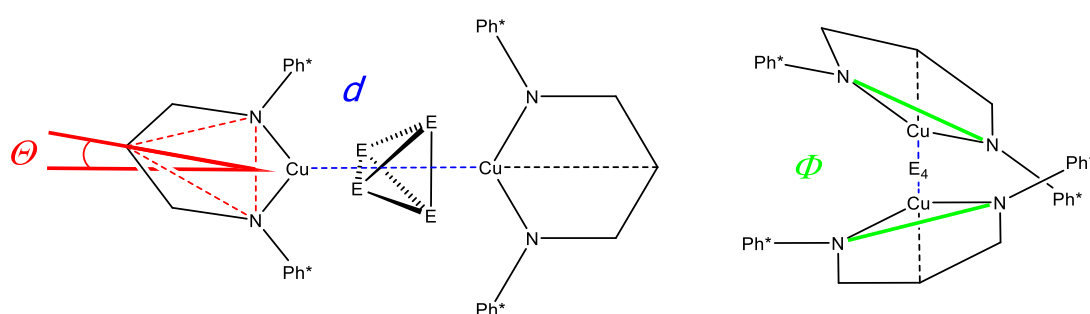


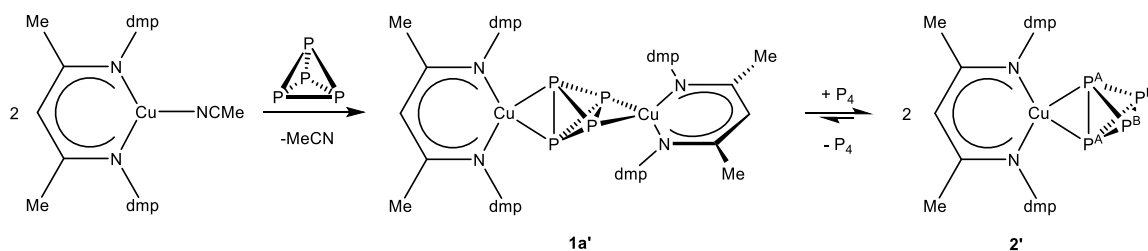
Figure 1. Definition of selected parameters describing the geometric situation in dinuclear β -diiminato complexes $[(\text{LCu})_2(\mu\text{-}\eta^2\text{:}\eta^2\text{-E}_4)]$ (E = P, As).

6.2 Results and Discussion

Herein, two findings are presented exemplifying the extent to which the coordination geometry of $[(\text{LCu})_2(\mu\text{-}\eta^2\text{:}\eta^2\text{-E}_4)]$ (L = 'NacNac', E = P, As) complexes are influenced: The variation of aromatic substituents is tested, which leads to different steric requirements of the ligand. The effect on the dynamic behavior in solution is tested and compared to related complexes. Then, the molecular structures of $[(\text{LCu})_2(\mu\text{-}\eta^2\text{:}\eta^2\text{-P}_4)]$ (L = L³ (**1a**), L¹ (**1a'**)) are compared. This is followed by the comparison of two solvomorph crystal structures of $[(\text{L}^3\text{Cu})_2(\mu\text{-}\eta^2\text{:}\eta^2\text{-As}_4)]$ (**1b**), which differ in the number of solvate molecules incorporated in the crystal.

Changing the Ligand Substituents in $[(\text{LCu})_2(\mu\text{-}\eta^2\text{:}\eta^2\text{-P}_4)]$ (L = L³ (**1a**), L¹ (**1a'**))

To address the first point, the aromatic dipp (= 2,6-diisopropylphenyl) substituents in L³ were changed to sterically less demanding dmp (= 2,6-dimethylphenyl) flanking groups in L¹. The reaction of $[\text{L}^1\text{Cu}(\text{NCMe})]$ with half an equivalent of P₄ was performed in toluene at room temperature. In the course of 20 minutes, the color changed from yellow to red and the dinuclear compound $[(\text{L}^1\text{Cu})_2(\mu\text{-}\eta^2\text{:}\eta^2\text{-P}_4)]$ (**1a'**) was obtained. Reacting **1a'** with 3.5 equivalents of P₄ leads to a mononuclear compound $[\text{L}^1\text{Cu}(\eta^2\text{-P}_4)]$ (**2'**). The reactivity is depicted in Scheme 2.



Scheme 2. Reaction of [L¹Cu(NCMe)] with P₄ to yield [(L¹Cu)₂(μ-η²:η²-P₄)] (**1a'**) and [L¹Cu(η²-P₄)] (**2'**). Labelling of the P atoms of **2'** corresponds to the text (vide infra).

The product **1a'** was characterized by LIFDI-MS, EA, single crystal X-ray diffraction and heteronuclear NMR spectroscopy. Compound **2'** was characterized by heteronuclear NMR spectroscopy at various temperatures. The VT ³¹P{¹H} NMR spectra are depicted in the Supporting Information (Figure S1). While the ³¹P{¹H} NMR spectra of complex **1a'** display a sharp singlet at δ = -430.3 ppm at 300 K, the mononuclear compound **2'** shows a broad singlet (ω_{1/2} = 2152 Hz) at δ = -479.2 ppm. This is indicative for a highly dynamic behavior. Between 273 and 253 K, compound **2'** undergoes a breakdown of coalescence and a successive signal splitting is monitored. At 193 K two mutually coupled triplets (¹J_{PP} = 178 Hz) are detected at δ = -449.6 ppm (P^A) and -499.6 ppm (P^B) for compound **2'**. An analogous behavior (signal splitting at 193 K: δ = -450.5 and -490.7 ppm, ¹J_{PP} = 178 Hz) was observed for the previously reported, related complex [L³Cu(η²-P₄)] (**2**), which is in equilibrium with P₄ and its dinuclear precursor [(L³Cu)₂(μ-η²:η²-P₄)] (**1a**) at room temperature (δ = -426.9 ppm).^[7] As those complexes exclusively differ in their aromatic flanking groups (dipp in L³ and dmp in L¹), the equal reactivity and analogous behavior of compounds **1a** and **1a'** as well as **2** and **2'** are expected in solution. The equilibrium between **1a'**, P₄ and **2'** is concluded by their sensitivity to the P₄ concentration, which was monitored by their ³¹P{¹H} NMR spectra at room temperature.

Single crystals of [(L¹Cu)₂(μ-η²:η²-P₄)] (**1a'**) were obtained by crystallization from saturated *n*-hexane solution. The molecular structure shows a side-on coordinated P₄ ligand, which bridges two opposing [L¹Cu] fragments (Figure 2, left). In Table 1, the structural parameters of product **1a'** are summarized and compared to the previously reported complex **1a**. No significant deviations are found within the Cu–P distances of **1a'** and **1a**. However, their Cu...Cu distances are affected only to a minor extent. The edges of the P₄ moiety are divided into metal coordinating and non-coordinating ones. The latter P–P distances are in the range of 2.1919(8) Å and 2.2091(9) Å in **1a'** and are in accordance with the ones in **1a**. They are assigned to P–P single bonds (e.g. in white phosphorus determined by electron diffraction: 2.1994(3) Å,^[8] Raman spectroscopy: 2.2228(5) Å,^[9] and DFT calculations: 2.1994(3) Å^[17]). However, the coordinating edges in **1a'** display unequal P–P distances of 2.3651(7) and 2.4567(8) Å. They are assigned to

elongated phosphorus single bonds. These values deviate from the ones determined in **1a** (2.4121(8) and 2.4286(9) Å), which is attributed to the differing coordination geometries of the copper centers: The copper centers in **1a'** – in contrast to **1a** – exhibit deviation from planar coordination geometry (Σ_{angles} up to 370.8°). As can be seen in Figure 2, this is the consequence of the [L¹Cu] fragment twisting around the Cu...Cu axis and also manifests in a twist angle Φ of 66.562(46)° between the (hypothetical) N–N lines of both terminal L¹ ligands. This ligand orientation deviates significantly from the one in **1a** ($\Phi = 82.367(76)^\circ$) and from the expected ideal orthogonal conformation.

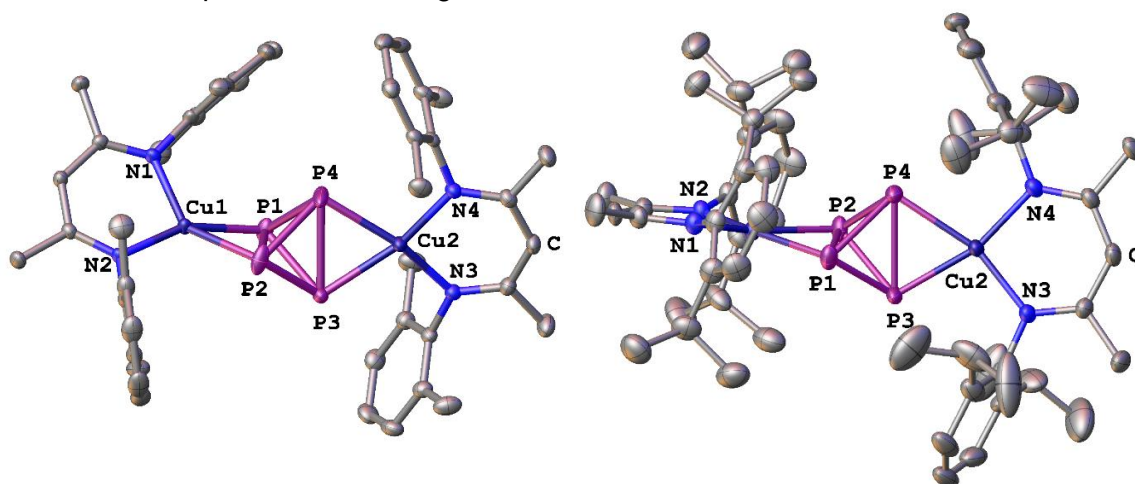


Figure 2. Molecular structures of **1a'** (left) and **1a** (right) in the crystal. Hydrogen atoms are omitted for clarity. Thermal ellipsoids are drawn at 50% probability level. Note the differing coordination geometry of the [LCu] fragments (L = L¹ (**1a'**), L³ (**1a**)) on the left-hand side of the complexes.

Table 1. Comparison of the structural parameters in [(LCu)₂(μ-η²:η²-P₄)] (L = L¹ (**1a'**), L³ (**1a**)^[7]).

Complex	1a'	1a ^[7]
$d(\text{Cu}\cdots\text{Cu}) / [\text{Å}]$	5.1646(4)	5.2066(6)
$d(\text{P}-\text{P}) / [\text{Å}]$	2.3651(7)	2.4121(8)
coord. edges	2.4567(8)	2.4286(9)
$d(\text{P}-\text{P}) / [\text{Å}]$	2.1919(8)	2.201(1)
non-coord edges	2.1992(6)	2.2044(9)
	2.2048(6)	2.2061(9)
	2.2091(9)	2.2115(7)
$d(\text{Cu}-\text{P}) / [\text{Å}]$	1.9277(12)	1.9396(19)
	1.9397(14)	1.9410(19)
	1.9452(13)	1.9416(18)
	1.9465(13)	1.9570(19)
$\Sigma_{\text{angles}} / [^\circ]$	370.8	360.4
	361.8	362.1
$\Theta / [^\circ]$	0.91(5)	1.78(6)
	8.00(4)	2.40(8)
$\Phi / [^\circ]$	66.562(46)	82.367(76)

Effect of Co-crystallizing Solvates on the Conformation of [(L³Cu)₂(μ-η²:η²-As₄)]

The effect of co-crystallizing solvates on the molecular geometry of a distinct compound in the solid state can be discussed by the comparison of its diverse solvomorph crystal structures. The crystal structures can be differentiated by the number or the nature of co-crystallizing solvent molecules. The previously reported compound [(L³Cu)₂(μ-η²:η²-As₄)] (**1b**) satisfies these requirement in its crystal structures **1b** · 2 *n*-hexane and **1b** · 0.25 *n*-hexane. These structures were previously reported, but no detailed discussion was provided so far.^[7] The first structure contains half an equivalent of **1b** in the asymmetric unit and will further be entitled as **1b-1**. The second one contains two distinguishable isomers of **1b**, which are named **1b-2** and **1b-3** and are depicted in Figure 3. The structural parameters of all isomers **1b-1**, **1b-2** and **1b-3** are presented in Table 2.

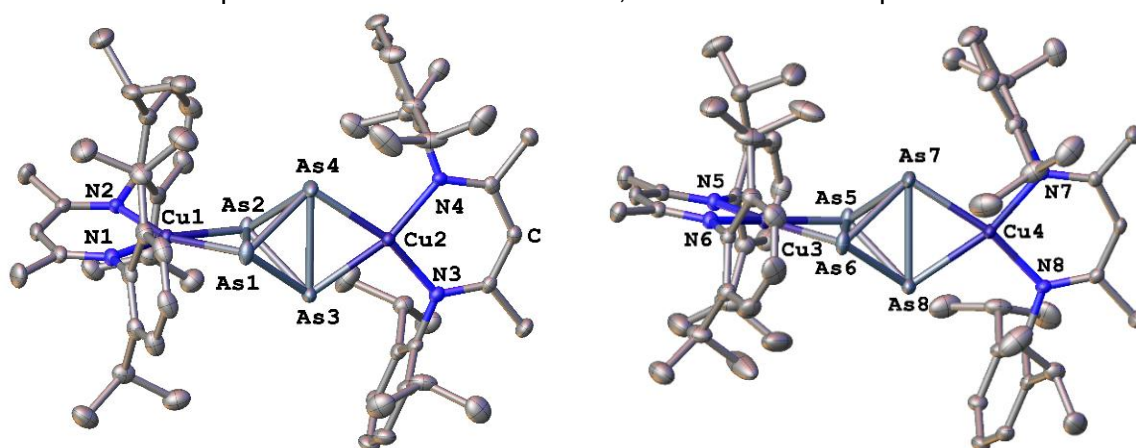


Figure 3. Molecular structure of **1b-2** (left) and **1b-3** (right) in crystal structure **1b** · 0.25 *n*-hexane. Hydrogen atoms are omitted for clarity. Thermal ellipsoids are drawn at 50% probability level.

Table 2. Comparison of the structural parameters in isomers **1b-1**, **1b-2** and **1b-3**, which origin from different solvomorphs **1b** · 2 *n*-hexane and **1b** · 0.25 *n*-hexane.^[7]

Complex	1b-1	1b-2	1b-3
$d(\text{Cu}\cdots\text{Cu}) / [\text{\AA}]$	5.5039(13)	5.4883(6)	5.5116(5)
$d(\text{As}-\text{As}) / [\text{\AA}]$ coord. edges	2.6491(9)	2.6563(6) 2.6616(5)	2.6568(6) 2.6594(5)
$d(\text{As}-\text{As}) / [\text{\AA}]$ non-coord. edges	2.4352(13) 2.4376(9) 2.4444(10) 2.4444(10)	2.4386(6) 2.4439(6) 2.4440(4) 2.4516(6)	2.4388(6) 2.4411(4) 2.4464(6) 2.4467(6)
$d(\text{Cu}-\text{As}) / [\text{\AA}]$	2.3877(13) 2.3762(10)	2.3673(5) 2.3821(6) 2.3853(5) 2.3979(6)	2.3741(5) 2.3811(6) 2.3932(4) 2.4022(6)
$\Sigma_{\text{angles}} / [^\circ]$	360	360.0 361.1	360.0 360.5
$\Theta / [^\circ]$	1.97(15)	3.59(6) 7.29(6)	6.32(7) 8.65(7)
$\Phi / [^\circ]$	84.46(17)	79.123(74)	78.214(70)

As can be seen by the comparison in Table 2, the coordination geometries in **1b-1**, **1b-2** and **1b-3** do not deviate significantly from each other. All copper centers display a planar coordination geometry and show similar Cu...Cu distances (5.4883(6)–5.5116(5) Å). However, some variation of the ligand plane twist angle ϕ is observed, which shifts within the range from 78.214(70)° in **1b-3** to 84.46(17)° in **1b-1**. There is also a very minor variation within their Θ angles, which are in the range of 1.97(15)° and 8.65(7)°. However, the coordinating As–As edges in **1b-1**, **1b-2** and **1b-3** display distances in the range of 2.6491(9) and 2.6616(5) Å and therefore, no significant deviations are found.

6.3 Conclusion

The synthesis and characterization of the dinuclear complex $[(L^1Cu)_2(\mu-\eta^2:\eta^2-P_4)]$ (**1a'**) and the mononuclear complex $[(L^1Cu)_2(\eta^2-P_4)]$ (**2'**) is presented. In solution, an equilibrium is found between **1a'**, P₄ and **2'**. This agrees with the previously reported compounds **1a** and **2**, which differ from **1a'** and **2'** exclusively in their β -diketiminato ancillary ligands (L¹ vs. L³). The crystal structures of **1a'** and **1a** are compared and reveal slightly modified geometries of their [Cu₂P₄] complex cores. The changed ligand plane twist of their [LCu] fragments (L = L¹ (**1a'**), L³ (**1a**)) is found to affect the coordinating P–P edges of the bridging P₄ units. Additionally, the influence of co-crystallizing solvent molecules is evaluated in two solvomorph crystal structures of $[(LCu)_2(\mu-\eta^2:\eta^2-As_4)]$ (**1b**). The coordination geometry of the [Cu₂As₄] complex core did not change significantly. However, the comparison of **1b** · 2 *n*-hexane with **1b** · 0.25 *n*-hexane reveals very minor variation of the twisted ligand orientations.

6.4 References

- [1] a) C. Chen, M. B. Hecht, A. Kavara, W. W. Brennessel, B. Q. Mercado, D. J. Weix, P. L. Holland, *J. Am. Chem. Soc.* **2015**, *137*, 13244-13247; b) R. L. Webster, *Dalton Trans.* **2017**, *46*, 4483-4498.
- [2] a) N. W. Aboeella, E. A. Lewis, A. M. Reynolds, W. W. Brennessel, C. J. Cramer, W. B. Tolman, *J. Am. Chem. Soc.* **2002**, *124*, 10660-10661; b) D. J. E. Spencer, N. W. Aboeella, A. M. Reynolds, P. L. Holland, W. B. Tolman, *J. Am. Chem. Soc.* **2002**, *124*, 2108-2109; c) L. M. R. Hill, B. F. Gherman, N. W. Aboeella, C. J. Cramer, W. B. Tolman, *Dalton Trans.* **2006**, 4944-4953.
- [3] a) S. F. McWilliams, K. R. Rodgers, G. Lukat-Rodgers, B. Q. Mercado, K. Grubel, P. L. Holland, *Inorg. Chem.* **2016**, *55*, 2960-2968; b) B. Horn, S. Pfirrmann, C. Limberg, C. Herwig, B. Braun, S. Mebs, R. Metzinger, *Z. Anorg. Allg. Chem.* **2011**, *637*, 1169-1174.
- [4] S. Yao, T. Szilvasi, N. Lindenmaier, Y. Xiong, S. Inoue, M. Adelhardt, J. Sutter, K. Meyer, M. Driess, *Chem. Commun.*, **2015**, *51*, 6153-6156.
- [5] F. Spitzer, C. Graßl, G. Balázs, E. M. Zolnhofer, K. Meyer, M. Scheer, *Angew. Chem. Int. Ed.* **2016**, *55*, 4340-4344.
- [6] a) S. Yao, N. Lindenmaier, Y. Xiong, S. Inoue, T. Szilvasi, M. Adelhardt, J. Sutter, K. Meyer, M. Driess, *Angew. Chem.* **2015**, *127*, 1266-1270; b) F. Spitzer, C. Graßl, G. Balázs, E. Mädl, M. Keilwerth, E. M. Zolnhofer, K. Meyer, M. Scheer, *Chem. Eur. J.* **2017**, *23*, 2716-2721.
- [7] F. Spitzer, M. Sierka, M. Latronico, P. Mastroianni, A. V. Virovets, M. Scheer, *Angew. Chem. Int. Ed.* **2015**, *54*, 4392-4396.
- [8] B. M. Cossairt, C. C. Cummins, A. R. Head, D. L. Lichtenberger, R. J. F. Berger, S. A. Hayes, N. W. Mitzel, G. Wu, *J. Am. Chem. Soc.* **2010**, *132*, 8459-8465.
- [9] N. J. Brassington, H. G. M. Edwards, D. A. Long, *J. Raman Spectrosc.* **1981**, *11*, 346-348.

6.5 Supporting Information

General Remarks

All manipulations were performed with rigorous exclusion of oxygen and moisture using Schlenk-type glassware on a dual manifold Schlenk line with Argon inert gas or glove box filled with N₂ containing a high-capacity recirculator (<0.1 ppm O₂). Toluene, *n*-hexane and acetonitrile were dried using conventional techniques, degassed and saturated with Argon. CD₂Cl₂ was obtained from Deutero GmbH and degassed, dried and distilled from CaH₂ prior to use. ¹H, ¹³C, ³¹P NMR spectra were recorded on a Bruker Avance 400 (¹H: 400.130 MHz, ¹³C: 100.613 MHz, ³¹P: 161.976 MHz). The chemical shifts are reported in ppm relative to external TMS (¹H, ¹³C) and H₃PO₄ (³¹P). Mass spectrometry was performed using a JEOL AccuTOF GCX (LIFDI) mass spectrometer. Elemental analysis (CHN) was determined using a Vario micro cube and Vario EL III instrument.

Synthesis of [(L¹Cu)₂(μ-η²:η²-P₄)] (1a')

30 mg (0.24 mmol, 0.5 equivalents) P₄ were dissolved in 10 mL toluene and were transferred into a yellow solution of 213 mg (0.52 mmol, 1 equivalent) [L¹Cu(NCMe)] in 10 mL toluene. All manipulations were performed at room temperature. Within 20 minutes a color change from yellow to red was observed. The reaction mixture was stirred for additional 15 minutes. The solvent was removed in vacuum. The orange solid was dissolved in 5 mL *n*-hexane and filtered over celite. The intense reddish-orange filtrate was stored at 8 °C for 48 hours to yield crystalline orange blocks.

Crystalline Yield: 125.0 mg (0.24 mmol, 60%).

Analytical data:

¹ H NMR (400 MHz, CD ₂ Cl ₂ , 300 K)	δ [ppm] = 7.10 (d, ³ J _{HH} = 7.44 Hz, 8H, <u>H_{meta}</u>), 6.96 (t, ³ J _{HH} = 7.46 Hz, 4H, <u>H_{para}</u>), 4.79 (s, 2H, <u>H_β</u>), 1.94 (s, 24H, ortho- <u>Me</u>), 1.60 (s, 12H, α- <u>Me</u>).
³¹ P{ ¹ H} NMR (162 MHz, CD ₂ Cl ₂ , 300 K)	δ [ppm] = -430.32 (s, <u>P</u>).
¹³ C{ ¹ H} NMR (101 MHz, CD ₂ Cl ₂ , 300 K)	δ [ppm] = 162.66 (s, (H ₃ C) <u>CCHC</u> (CH ₃)), 148.89 (s, <u>C_{ipso}</u>), 131.76 (s, <u>C_{ortho}</u>), 128.53 (s, <u>C_{meta}</u>), 123.76 (s, <u>C_{para}</u>) 94.41 (s, (H ₃ C) <u>CCHC</u> (CH ₃)), 23.86 (s, (H ₃ <u>C</u>)CCHC(<u>CH</u> ₃)), 18.98 (s, ortho- <u>CH</u> ₃). Signal assignment in accordance with HSQC and HMBC spectra.
¹ H NMR (400 MHz, CD ₂ Cl ₂ , 193 K)	δ [ppm] = 7.11 (d, ³ J _{HH} = 7.56 Hz, 8H, <u>H_{meta}</u>), 6.97 (t, ³ J _{HH} = 7.44 Hz, 4H, <u>H_{para}</u>), 4.79 (s, 2H, <u>H_β</u>), 1.83 (s, 24H, ortho- <u>Me</u>), 1.53 (s, 12H, α- <u>Me</u>).
³¹ P{ ¹ H} NMR (162 MHz, CD ₂ Cl ₂ , 193 K)	δ [ppm] = -431.37 (s, <u>P</u>). Measured range: 600 to -600 ppm.
¹³ C{ ¹ H} NMR (101 MHz, CD ₂ Cl ₂ , 193 K)	δ [ppm] = 161.58 (s, (H ₃ C) <u>CCHC</u> (CH ₃)), 147.14 (s, <u>C_{ipso}</u>), 131.02 (s, <u>C_{ortho}</u>), 127.68 (s, <u>C_{meta}</u>), 123.04 (s, <u>C_{para}</u>) 93.61 (s, (H ₃ C) <u>CCHC</u> (CH ₃)), 23.86 (s, (H ₃ <u>C</u>)CCHC(<u>CH</u> ₃)), 18.72 (s, ortho- <u>CH</u> ₃). Signal assignment in accordance with HSQC and HMBC spectra.
Elemental analysis (C ₄₂ H ₅₀ Cu ₂ N ₄ P ₄)	Calculated: C 58.53, H 5.85, N 6.50. Found: C 58.81, H 6.02, N 6.39.
Mass spectrometry (LIFDI, toluene)	m/z: 860.2 (78%) [M] ⁺ , 770.3 (5%) [(L ² Cu) ₂ (OH) ₂] ⁺ , 736.3 (100%) [M-P ₄] ⁺ , 492.0 (9%) [(L ² Cu)P ₄] ⁺ .

Synthesis of [L¹Cu(η²-P₄)] (2')

18 mg (0.021 mmol, 1 equivalent) [(L¹Cu)₂(μ-η²:η²-P₄)] (**1a'**) and 9 mg (0.073 mmol, 3.5 equivalents) P₄ were stirred in 1 mL CD₂Cl₂ resulting in a bright yellow solution of **2'**.

Yield: In accordance with the ³¹P{¹H} NMR spectra at room temperature, the used stoichiometry (P₄:**1a'** = 3.5:1) results in a quantitative conversion of **1a'** into **2'**.

Analytical data:

¹ H-NMR (400 MHz, CD ₂ Cl ₂ , 300 K)	δ [ppm] = 7.15 (d, ³ J _{HH} = 7.48 Hz, 4H, <u>H_{meta}</u>), 6.96 (t, ³ J _{HH} = 7.48 Hz, 2H, <u>H_{para}</u>), 4.89 (s, 1H, <u>H_β</u>), 2.07 (s, 12H, ortho- <u>Me</u>), 1.69 (s, 6H, <u>α-Me</u>).
³¹ P{ ¹ H} NMR (162 MHz, CD ₂ Cl ₂ , 300 K)	δ [ppm] = -479.19 (s, ω _{1/2} = 2152 Hz, <u>P</u>).
³¹ P NMR (162 MHz, CD ₂ Cl ₂ , 300 K)	δ [ppm] = -478.97 (s, ω _{1/2} = 2153 Hz, <u>P</u>).
¹³ C{ ¹ H} NMR (101 MHz, CD ₂ Cl ₂ , 300 K)	δ [ppm] = 162.74 (s, (H ₃ C) <u>C</u> CHC(CH ₃)), 148.66 (s, <u>C_{ipso}</u>), 132.16 (s, <u>C_{ortho}</u>), 128.53 (s, <u>C_{meta}</u>), 123.91 (s, <u>C_{para}</u>), 94.64 (s, (H ₃ C) <u>C</u> CHC(CH ₃)), 24.20 (s, (H ₃ <u>C</u>)CCHC(<u>C</u> H ₃)), 19.14 (s, ortho- <u>C</u> H ₃). Signal assignment in accordance with HSQC and HMBC spectra.
¹ H NMR (400 MHz, CD ₂ Cl ₂ , 193 K)	δ [ppm] = 7.13 (d, ³ J _{HH} = 7.4 Hz, 4H, <u>H_{meta}</u>), 6.94 (t, ³ J _{HH} = 7.4 Hz, 2H, <u>H_{para}</u>), 4.88 (s, 1H, <u>H_β</u>), 1.95 (s, 12H, ortho- <u>Me</u>), 1.61 (s, 6H, <u>α-Me</u>). Contamination with compound 1a' (vide Figure S1).
³¹ P{ ¹ H} NMR (162 MHz, CD ₂ Cl ₂ , 193 K)	δ [ppm] = -449.63 (t, 2P, ¹ J _{PP} = 178 Hz, η ² - <u>P₂</u>), -499.62 (t, 2P, ¹ J _{PP} = 178 Hz, <u>P₂</u>). Contamination with P _{4,solv} and precipitation of P _{4,solid} (vide Figure S1).

³¹P{¹H} NMR Spectra of 2' and 1a' in the Temperature Range of 300 K – 193 K:

Spitzer, FS 173, (18+9mg/0.8 ml CD₂Cl₂), Ref.: 85%ige H₃PO₄ extern
 P31{H1} bei 193K bis 300K

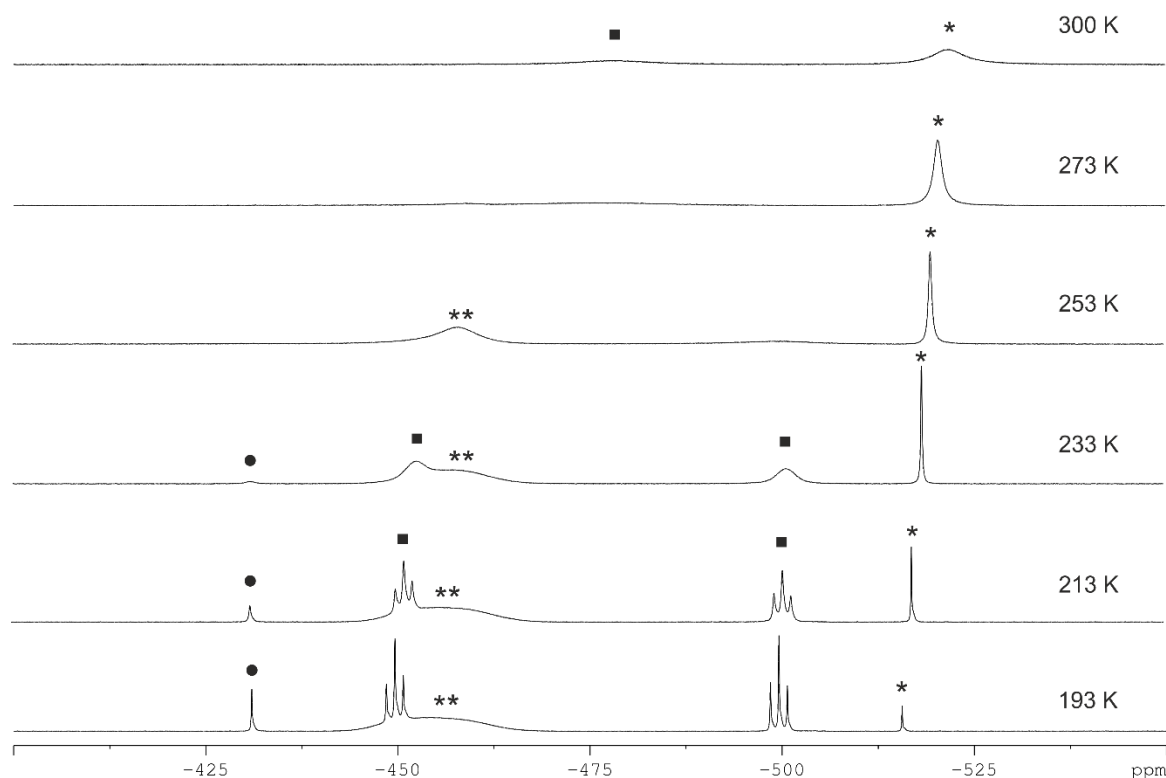


Figure S1. ³¹P{¹H} NMR spectra of a freshly prepared solution of complex **2'** in CD₂Cl₂ in the temperature range of 300 K to 193 K. The signal at $\delta = -522$ ppm is assigned to P_{4,solv} (*) and the one at $\delta = -431$ ppm is assigned to **1a'** (●). At $\delta = -455$ ppm P_{4,solid} (**) is detected, which precipitates from solution with successively decreasing the temperature. At 300 K compound **2'** (■) is assigned to the broad signal at $\delta = -479.2$ ppm. Successive decrease of the temperature leads to the breakdown of the coalescence signal and a final signal splitting at $\delta = -449.6$ ppm (P^A) and -499.6 ppm (P^B) at 193 K.

Crystallographic Details

Single crystal structure analysis of crystalline **1a'** was performed using a Rigaku Oxford Diffraction (formerly Agilent Technologies) CCD diffractometer GV-50, Titan^{S2} CCD. Data reduction was performed with the CrysAlisPro^[1] software package. Using the software Olex2^[2] the structure solution was carried out using the program ShelXT^[3] (Sheldrick, 2015). Least squares refinement on F_o² was performed using SHELXL-2014 (Version 2016/6).^[4]

Crystallographic data and details of the diffraction experiment of **1a**, **1b** · 0.25 *n*-hexane, **1b** · 2 *n*-hexane, see 'Chapter 3'.

Table S1. Crystallographic data and details of diffraction experiment for **1a'**.

Compound	1a'
Data set	FS165_abs_rint025
(internal naming)	
Formula	C ₄₂ H ₅₀ Cu ₂ N ₄ P ₄
$\rho_{calc.}/\text{g cm}^{-3}$	1.373
μ/mm^{-1}	2.971
Formula Weight	861.82
Color	clear orange
Shape	block
Size/mm ³	0.40x0.22x0.09
T/K	122.97(11)
Crystal System	monoclinic
Space Group	<i>P</i> 2 ₁ / <i>n</i>
<i>a</i> /Å	13.50049(6)
<i>b</i> /Å	14.42791(5)
<i>c</i> /Å	21.44106(10)
α°	90
β°	93.6512(4)
γ°	90
<i>V</i> /Å ³	4167.90(3)
<i>Z</i>	4
<i>Z'</i>	1
Wavelength/Å	1.54184
Radiation type	CuK α
Θ_{min}°	3.695
Θ_{max}°	74.441
Measured Refl.	132557
Independent Refl.	8426
Reflections Used	8169
<i>R</i> _{int}	0.0849
Parameters	481
Restraints	0
Largest Peak	0.437
Deepest Hole	-0.580
GooF	1.031
<i>wR</i> ₂ (all data)	0.0905
<i>wR</i> ₂	0.0896
<i>R</i> ₁ (all data)	0.0333
<i>R</i> ₁	0.0326

References

- [1] CrysAlisPro Software System, Agilent Technologies UK Ltd, Yarnton, Oxford, UK.
- [2] O.V. Dolomanov and L.J. Bourhis and R.J. Gildea and J.A.K. Howard and H. Puschmann, Olex2: A complete structure solution, refinement and analysis program, *J. Appl. Cryst.*, **2009**, *42*, 339-341.
- [3] Sheldrick, G.M., ShelXT, *Acta Cryst.*, **2014**, *A71*, 3-8.
- [4] Sheldrick, G.M., A short history of ShelX, *Acta Cryst.*, **2008**, *A64*, 339-341.

Preface

The following chapter has not been published until the submission of this thesis.

Authors

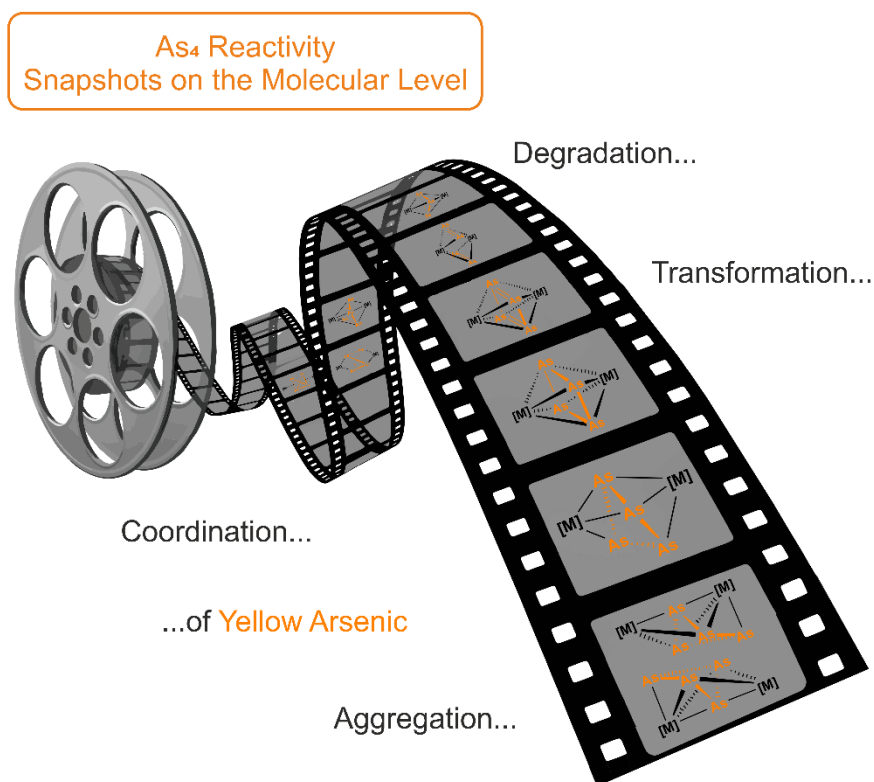
Fabian Spitzer, Christian Graßl, Gábor Balázs, Manfred Scheer*

Author contributions

F. Spitzer prepared the manuscript and performed the synthesis, characterization and description of herein presented compounds **1a**, **1b**, **3**, **4a**, **4b**, **5**, **6**, **7a**, **7b**, **7c** and **8**. Compound **2** was synthesized and characterized by C. Graßl in his PhD thesis. The X-ray measurement of **2** was performed by C. Graßl in his PhD thesis. The presented structural parameters of **2** were re-calculated by the first author. M. Scheer supervised the research and revised the manuscript. All DFT calculations were performed by G. Balázs.

Acknowledgements

We are grateful to Dr. M. Bodensteiner for his valuable advice and support of solution and refinement of the X-ray structures.



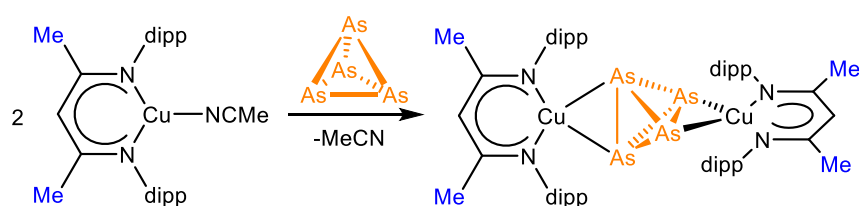
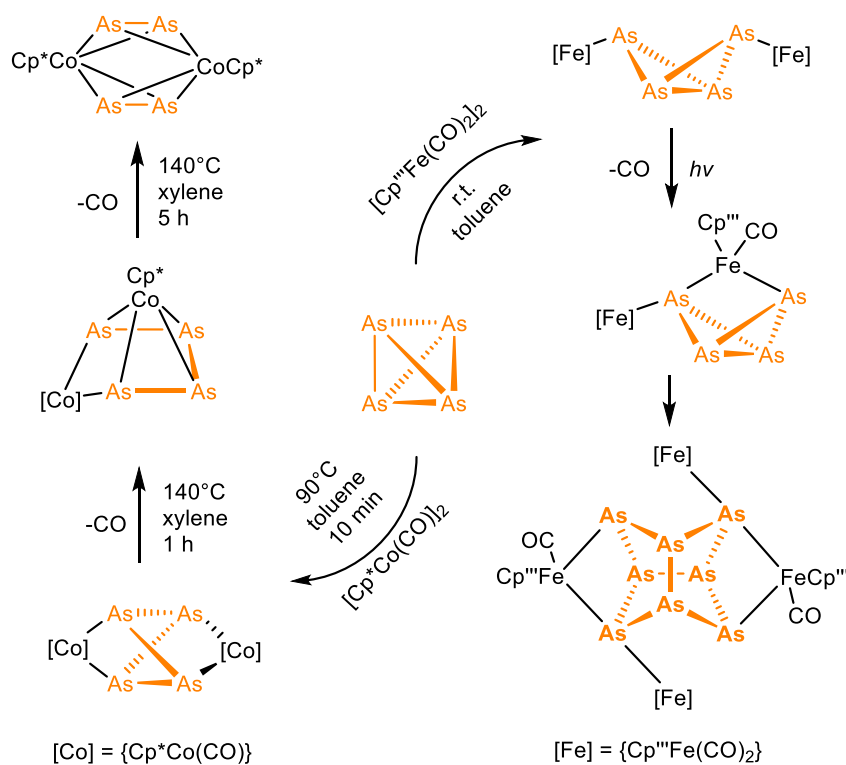
7. Snapshots of As₄ Transformation - Degradation and Aggregation Induced by β -diiminato-M (M = Co, Fe) Fragments

Abstract: A systematic activation study of tetrahedral As₄ (yellow arsenic) is presented. The use of versatile low-valent β -diiminato (L) cobalt(I) and iron(I) precursors highlight the role of the corresponding metal centers and the influence of the supporting ligands: Four different hybrid ligands with *dipp* (2,6-diisopropylphenyl) and *dmp* (2,6-dimethylphenyl) flanking groups were applied, two of those with H substituents in the backbone (β -dialdiminates L⁰ and L²) and two with Me substituents (β -diketimines L¹ and L³). Various dinuclear products [(LM)₂As₄] (LM = L⁰Fe (**1a**), L³Fe (**4a**), L⁰Co (**5**), L¹Co (**6**), L²Co (**7a**), L³Co (**8**)) were isolated, each containing an individually shaped As₄ ligand in the solid state. Furthermore, tetranuclear complexes [(LM)₄As₈] (LM = L¹Fe (**2**), L²Fe (**3**), L²Co (**7b**)) were obtained, which possess isostructural realgar-type As₈ central cores. Additionally, two products [(LM)₂As₃] (LM = L³Fe (**4b**), L²Co (**7c**)) with an As₃ middle deck were obtained and one complex [(L⁰Fe)₂(As₂)₂] (**1b**) with As₂ ligands. All products were comprehensively characterized by single crystal X-ray diffraction, LIFDI-MS and ¹H NMR spectroscopy. A rational explanation for the diverse reactivity is given and DFT calculations shed light into the nature of the highly flexible [M₂As₄] cores.

7.1 Introduction

Yellow arsenic (As₄) is known as the isostructural heavier congener of white phosphorus (P₄), both representing metastable but (the only) soluble group 15 allotropes. Despite their analogous appearance, there are differences in the E–E bond dissociation energy: 197 (P–P) or 151 (As–As) kJ·mol⁻¹.^[1] While P₄ is stable at ambient conditions, yellow arsenic tends to polymerize (particularly in the solid state), which prevents its storage.^[2] The reactivity of P₄ towards main group and transition metal compounds has been extensively investigated.^[3] In contrast, the reactivity of As₄ is less explored and only few publications have been reported on this topic in the last years.^[4] This can be rationalized by the challenging synthesis, the difficult handling and toxicity, the lack of storage possibilities, the thermal sensitivity and extremely high photosensitivity of yellow arsenic.^[5] Different synthetic approaches to As_n ligand complexes have been established using yellow arsenic or [As₇]³⁻ Zintl ion precursors. Several complexes containing

unsubstituted As_n ligands have been obtained by using these routes. The formed ligands can be categorized into cyclic and acyclic As_n units (n = 1 – 8).^[6] Most of those compounds are supported by Cp^R (cyclopentadienyl) and strongly donating carbonyl ligands. The ways for As₄ transformation can be exemplified by the reactions of [Cp^{*}Co(CO)]₂ (Cp^{*} = C₅Me₅) or [Cp^{'''}Fe(CO)]₂ (Cp^{'''} = C₅H₂tBu₃) with As₄ (Scheme 1, top).^[7] A mixture of different products is obtained, each originating from a successive carbonyl loss at the metal center leading to a further transformation of the As₄ ligand.

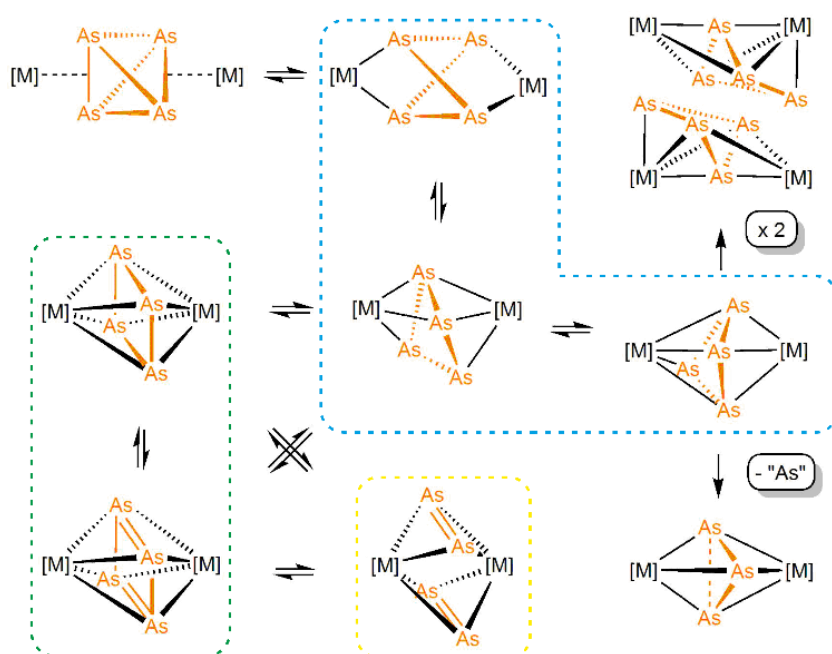


Scheme 1. Selected examples of metal(I) mediated As₄ transformations involving Cp^R(CO)_n or β-diketiminato ligands, respectively.

Recently, β-diiminato (L) compounds gained increased attention in the exceptionally mild and selective reactivity towards small molecules (e.g. O₂, N₂, P₄) and the influence of ligand design was probed.^[8] These [LM(solv)] precursors are known to stabilize metal(I) centers (of first row group 5–12),^[9] which gain protection by the aromatic flanking groups of the ligand and by one weakly donating solvent ligand like toluene or acetonitrile. The latter is detached in solution leaving a sterically highly exposed metal center ready for subsequent reductive activation reactions. This stands in stark contrast to the previously

mentioned cyclopentadienyl-carbonyl precursors, which need abstraction of one or more carbonyl ligand(s) under relatively harsh, thermolytic or photolytic conditions prior to accessing the naked metal center. In these cases, the formation of thermodynamically stable products is favored. In contrast, the β -diiminato containing [LM(solv)] precursors dissociate in solution - even at low temperatures. For this reason, metastable products should be isolable in the reactions with E₄ (E = P, As).

In catalysis, a known concept is the iterative bond cleavage, conformation change, reorganization and (new) bond formation of the substrate within the coordination sphere of transition metals. It is expected that the hypothetical dinuclear β -diiminato transition metal compounds of the type [(LM)₂As₄] should undergo similar fluctuation processes. Accordingly, a continuum of interchanging conformers and different isomers are expected in solution (Scheme 2). However, an experimental proof for this reactivity is pending.



Scheme 2. Hypothetical transformation and degradation of yellow arsenic between two metal centers [M]. Dashed boxes are due to the classification into non-planar (blue), planar (green) As₄ and As₂ (yellow) ligands (vide infra).

So far, the only example for a reaction of As₄ with a β -diketiminato transition metal complex is reported to yield [(L³Cu)₂(μ - η^2 : η^2 -As₄)], which contains an intact As₄ tetrahedron stabilized between two [L³Cu] fragments (Scheme 1, bottom).^[10]

The question arises if more electron deficient metal systems would be promising candidates for As₄ reaction studies by opening As-As bonds and give insight into subsequent transformation, degradation or aggregation reactions. Furthermore, the question arises if those reactions can be influenced by different ligand substituents.

To address these questions, a systematic reactivity study of yellow arsenic was performed using iron(I) and cobalt(I) complexes in combination with four different β -diiminato ligands. Each ligand L⁰–L³ provides individual steric and electronic properties (see Scheme 3, central box). Herein we report a variety of reactions of As₄ with different [LM(tol)] (L = L⁰–L³, M = Fe, Co) precursors under comparable conditions and the characterization of the products by ¹H NMR spectroscopy, LIFDI mass spectrometry and single crystal X-ray diffraction.

7.2 Results

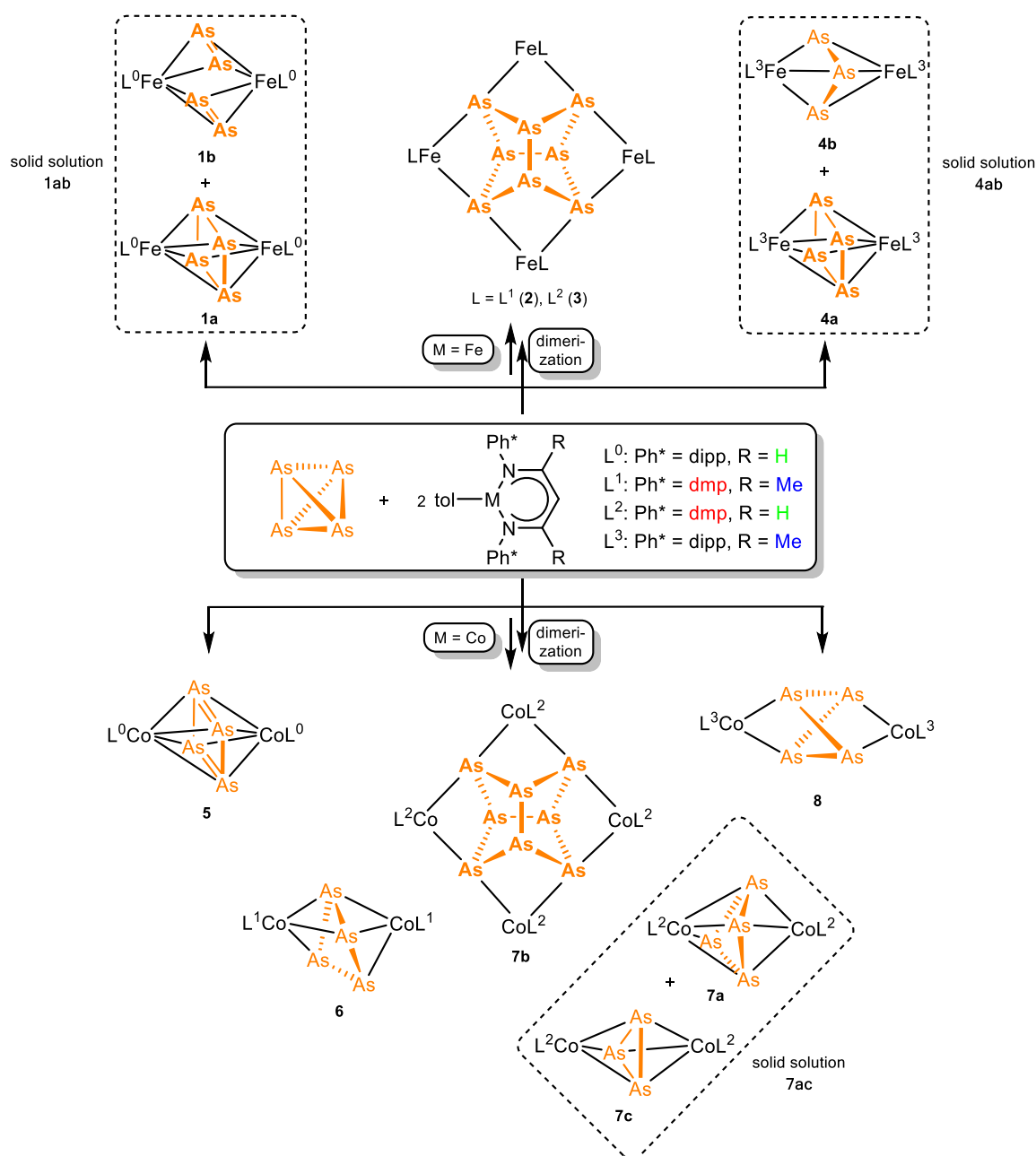
7.2.1 Synthesis

All reactions demand special set up and requirements. Owing to the extraordinary high photosensitivity of yellow arsenic in solution and solid state, all manipulations were conducted under rigorous exclusion of light. Prior to its reaction, it is mandatory to precipitate the yellow arsenic from the freshly prepared solution and to remove impurities by evacuation. This purification process is necessary due to the remarkable sensitivity of the metal(I) precursors [LM(tol)] (L = L⁰–L³, M = Fe, Co) towards moisture and oxygen.^[11] To prevent thermally induced degradation of the initially forming As₄ containing compounds, the reaction time was limited to 15 minutes (or 1 hour in two cases, see the Supporting Information) and the temperature was not allowed to exceed room temperature.^[12] In order to ensure comparability, all reactions were executed according to the same synthetic protocol, which is given in the Supporting Information. This also includes reaction control by ¹H NMR spectroscopy for the evaluation of the selectivity and LIFDI mass spectrometry for evaluation of the (di- or tetra) nuclearity of the formed compounds.

All obtained products can be classified into di- and tetranuclear iron or cobalt complexes, respectively. A graphical representation of obtained products is given in Scheme 3. The tetranuclear compounds **2**, **3** and **7b** contain an As₈ ligand, each. The dinuclear products **1a**, **1b**, **4a**, **4b**, **5**, **6**, **7a**, **7c** and **8** contain bridging As_n moieties, which can be further classified into As₄, As₃ and As₂ ligands. The differently shaped As₄ units realize various bridging coordination modes ranging from $\eta^4:\eta^4$ over $\eta^4:\eta^3$ and $\eta^3:\eta^3$ to $\eta^1:\eta^1:\eta^1:\eta^1$ in the solid state. For As₃ and As₂ units, exclusively bridging $\eta^3:\eta^3$ or $\eta^2:\eta^2$ coordination patterns are observed.

Selected products could not be crystallized as pure compounds, but were exclusively obtained as mixtures in their crystalline solid solutions. This is indicated by dashed boxes

in Scheme 3. Correspondingly, the solid solutions **1ab**, **4ab** and **7ac** represent mixtures of products **1a** and **1b**, **4a** and **4b**, or **7a** and **7c**, respectively. Each dinuclear complex reveals an individual organic ligand environment and a distinct [M₂As_n] central core. In their solid solutions, each As₄ ligand of the first component (**1a**, **4a**, **7a**) is superposed by an additional As_n (n = 2, 3) ligand of the second component (**1b**, **4b**, **7c**), which is localized at the same crystallographic position.



Scheme 3. Overview of the reactions of [LM(tol)] (L = L⁰–L³, M = Fe, Co) with yellow arsenic. Top: Synthesized complexes based on iron. Bottom: Synthesized complexes based on cobalt. Products in dashed boxes were exclusively obtained as part of solid solutions (vide infra).

7.2.2 LIFDI-MS and ¹H NMR Spectroscopy

All complexes **1–8** were comprehensively characterized by single crystal X-ray diffraction, ¹H NMR spectroscopy and LIFDI mass spectrometry.

Mass spectrometry enables differentiation between di- and tetranuclearity of obtained products. For both ligands L⁰ and L³ with the sterically encumbered dipp (2,6-diisopropylphenyl) flanking groups, molecular ion peaks are detected corresponding to dinuclear products [(LM)₂As₄] and no peaks for tetranuclear [(LM)₄As₈].^[13] This indicates the hindrance of the reaction of [(LM)₂As₄] towards their hypothetical tetranuclear dimers [(LM)₄As₈]. In contrast, this dimerization is enabled for dmp (2,6-dimethylphenyl) containing compounds, which is confirmed by their molecular ion peaks [(LM)₄As₈]⁺.

Those findings are supported by ¹H NMR spectroscopy. All compounds are paramagnetic in solution and display signals in a broad spectral range from approx. 300 to –50 ppm. Symmetry considerations allow the signal assignment and enable the differentiation between di- and tetranuclear complexes. For tetranuclear [(LM)₄As₈] compounds (e.g. **3** and **7b**) a signal pattern for half a ligand is detected in solution (*D*_{2d} symmetry).^[14] This is due to the σ_d dihedral plane, which contains the ligand backbone and cuts both dmp groups. In contrast, all dinuclear products display a signal pattern of a quartered ligand (two perpendicular mirror planes; relaxed *D*_{2h} or *D*_{2d} symmetry).^[15] Details on ¹H NMR spectra and signal assignment are given in the Supporting Information.

X-ray diffraction studies were performed for all products **1–8**, revealing their structure in the solid state. Due to their structural similarities, the tetranuclear compounds **2**, **3** and **7b** are discussed at first, followed by a detailed comparison of various dinuclear complexes.

7.2.3 Structural Characterization

The molecular structures of all obtained complexes **1–8** can be grouped in di- and tetranuclear products. The tetranuclear complexes are exclusively isolated with dmp containing ligands L¹ and L². In contrast, dinuclear compounds are obtained with dipp containing ligands L⁰ and L³. In some case for L¹ and L² also dinuclear complexes could be identified. All dinuclear compounds divide into complexes with non-planar or planar As₄ ligands as well as As₃ and As₂ bridged products. See colored boxes in Scheme 2 for the As_n ligand classification.

In the following, the exceptional tetranuclear complexes are described, followed by the discussion of the dinuclear complexes in the order of their successively decreasing M...M distance. This formally imitates a hypothetical activation process of intact As₄ by two [LM] fragments (Scheme 2). The reported compound [(L³Cu)₂(μ-η²:η²-As₄)] can serve as a

starting point for this thought experiment, as it stabilizes an intact yellow arsenic ligand. Its Cu...Cu distance is reported to range between 5.488 and 5.512 Å.^[10]

Tetranuclear Products

Single crystal X-ray diffraction was performed on crystals of **2** · 2.5 toluene, **3** · toluene and **7b** · Et₂O. The molecular structures reveal [(LM)₄(μ₄-η¹:η¹:η¹:η¹:η¹:η¹:η¹:η¹-As₈)] (LM = L¹Fe (**2**), L²Fe (**3**), L²Co (**7b**)) as tetranuclear complexes, each containing a realgar-type As₈ unit. As a representative, the molecular structure of **3** is depicted in Figure 1.

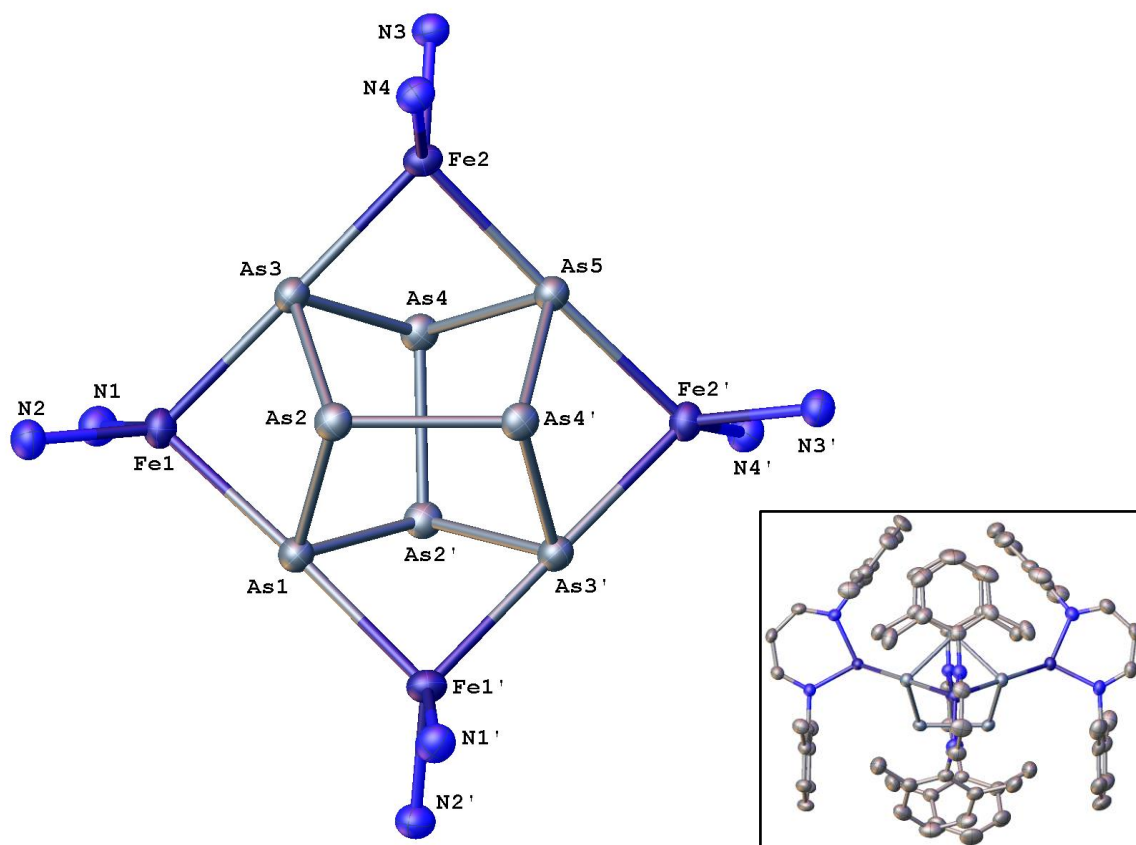


Figure 1. Core structure of **3** in **3** · toluene. Hydrogen and carbon atoms are omitted for clarity. A representation of **3** with its complete ligands is shown in the right box.^[16] Thermal ellipsoids are drawn at 50% probability level.

In compounds **2**, **3** and **7b** the As–As distances, which involve the metal coordinating As atoms, are between 2.4250(3)–2.4430(5) Å. This is in line with an As–As single bond (determined in yellow arsenic by electron diffraction: 2.435(4)^[17] and 2.44(3)^[18] Å, by DFT calculations:^[19] 2.437 Å). The distance between the bridgehead arsenic atoms are between 2.4788(5) and 2.4973(3) Å, which corresponds to a moderately elongated As–As single bond. Those findings are in agreement with previously reported As–As bond lengths in [{Cp^{'''}Fe(CO)₂}]₂{Cp^{'''}Fe(CO)}₂(μ₄-η¹:η¹:η²:η²-As₈) (**A**) and [{Cp^{*}Cr(CO)₃}]₄(μ₄-η¹:η¹:η¹:η¹-As₈) (**B**), which are the only examples for realgar-type As₈ ligand complexes so far.

However, their coordination mode differs from that in **2**, **3** and **7b**. The As–As distances within the As₈ ligands of **A**, **B**, **2**, **3** and **7b** are not significantly changed by the different nature of the metal centers (Fe, Co, Cr), their coordination modes (η^1 vs. $\eta^1:\eta^1$) or the supporting ligand systems (Cp^R vs. L¹, L²). A detailed comparison is given in Table 1.

Table 1. Comparison of the structural parameters in [(LM)₄(μ_4 - $\eta^1:\eta^1:\eta^1:\eta^1$ -As₈)] (LM = L¹Fe (**2**), L²Fe (**3**), L²Co (**7b**)) with [(Cp^{'''}Fe(CO)₂)₂{Cp^{'''}Fe(CO)}₂(μ_4 - $\eta^1:\eta^1:\eta^2:\eta^2$ -As₈)] (**A**)^[7] and [(Cp^{*}Cr(CO)₃)₄(μ_4 - $\eta^1:\eta^1:\eta^1:\eta^1$ -As₈)] (**B**)^[7].

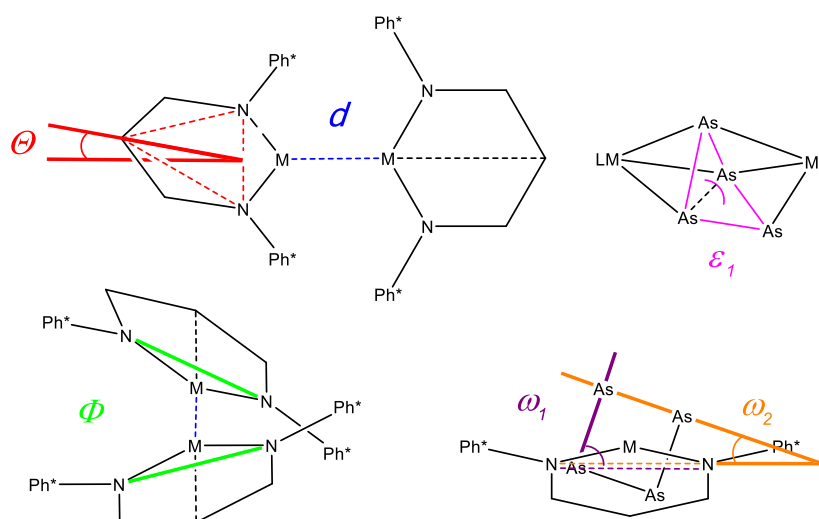
Complex	2	3	7b	A ^[7]	B ^[7]
$d(\text{M}\cdots\text{M}) / [\text{\AA}]$ (opposing)	6.973	7.016	6.866	7.212	– [a]
	5.091	5.083	4.980		
$d(\text{M}\cdots\text{M}) / [\text{\AA}]$ (adjacent)	5.136	5.084	5.002	– [a]	– [a]
	5.138	5.113	5.035		
	5.139	5.113	5.035		
	2.4250(3)			2.4317(5)	2.4229(8)
	2.4261(3)			2.4323(4)	2.4246(8)
$d(\text{As}-\text{As}) / [\text{\AA}]$ (metal coordinating)	2.4348(3)	2.4379(5)	2.4360(4)	2.4356(4)	2.4266(8)
	2.4361(3)	2.4384(5)	2.4367(5)	2.4423(4)	2.4267(8)
	2.4405(3)	2.4397(5)	2.4393(4)	2.4499(4)	2.4356(8)
	2.4415(3)	2.4430(5)	2.4413(5)	2.4557(4)	2.4412(8)
	2.4421(3)			2.4562(4)	2.4423(8)
	2.4423(3)			2.4607(4)	2.4470(8)
$d(\text{As}-\text{As}) / [\text{\AA}]$ (bridgehead)	2.4947(3)	2.4929(5)	2.4788(5)	2.4299(4)	2.4543(8)
	2.4973(3)			2.4348(5)	2.4600(8)
	2.5443(4)				
	2.5534(4)			2.4067(6)	
$d(\text{M}-\text{As}) / [\text{\AA}]$	2.5588(4)	2.5421(5)	2.4903(5)	2.4205(5)	2.608(1) ^[b]
	2.5641(4)	2.5427(5)	2.5012(5)	2.4213(6)	2.626(1) ^[b]
	2.5681(4)	2.5544(7)	2.5147(6)	2.4253(5)	2.628(1) ^[b]
	2.5715(4)	2.5585(7)	2.5207(6)	2.4675(6) ^[b]	2.635(1) ^[b]
	2.5743(4)			2.4692(6) ^[b]	
	2.5806(4)				

[a] position of η^1 -coordinated [LM] fragments mainly influenced by packing. Therefore, these values are not given; [b] η^1 -coordination.

Parameters for the Description of the Coordination Geometry

Several parameters can be considered for the description of the individual molecular geometry in a distinct dinuclear β -diiminato complex $[(LM)_2As_4]$ in the solid state (see Scheme 4 for graphical description) and understanding the formation of differently structured As_n moieties. These parameters are:

- 1) The distance d between both metal centers.
- 2) The angle Θ spanning between the $M \cdots M'$ axis and the plane formed by the coordinating nitrogen atoms and the methine carbon in the ligand backbone.
- 3) The orientation of both NCCCN ligand planes compared to each other, which is described by the twist angle Φ between both N–N lines.
- 4) In the case of non-planar As₄ ligands: The torsion angle ε_1 and ε_2 within the As₄ ligand, which describes the extent of tetrahedron opening. For planar As₄ ligands: The angles ω_1 and ω_2 , which are spanned between the N–N lines and the edges of the As₄ moiety.



Scheme 4. Definition of several parameters describing the geometry in dinuclear complexes $[(LM)_2As_4]$.

Dinuclear Products with Non-planar *cyclo*-As₄ Ligands

Compound $[(L^3Co)_2(\mu-\eta^1:\eta^1:\eta^1:\eta^1-As_4)]$ (**8**) is a dinuclear cobalt complex. The two metal centers are bridged by a twofold edge-opened As₄ tetrahedron (Figure 2). The As \cdots As distances along the cleaved edges are 3.057(1) and 3.070(1) Å and therefore exclude any bonding interaction. The remaining As–As distances are between 2.4466(12) and 2.4616(12) Å and therefore they are in the range of an As–As single bond (determined in yellow arsenic by electron diffraction: 2.435(4)^[17] and 2.44(3)^[18] Å, by DFT calculations: 2.437 Å^[19]). The ligand planes of both $[L^3Co]$ units are in an almost rectangular conformation ($\Phi = 80.8(2)^\circ$). The structural parameters of **8** are comparable to the ones

reported for $[\{\text{Cp}^*\text{Co}(\text{CO})\}_2(\mu\text{-}\eta^1\text{:}\eta^1\text{:}\eta^1\text{:}\eta^1\text{-As}_4)]$ (**C**), which contains an analogous, doubly edge-opened As₄ tetrahedron.^[20] A detailed summary of the geometric parameters of **8** and a comparison with **C** is given in Table 2.

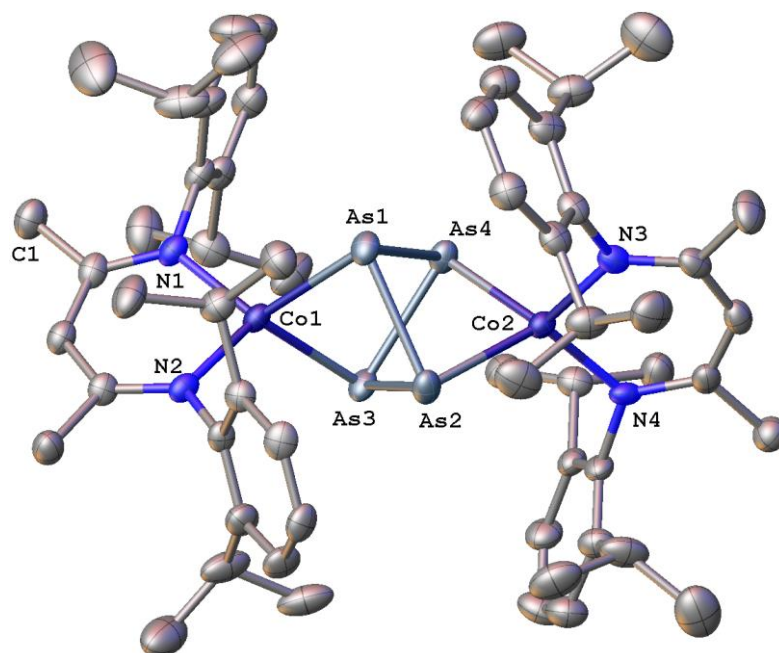


Figure 2. Molecular structure of **8** in the crystal. Hydrogen atoms are omitted for clarity. Thermal ellipsoids are drawn at 50% probability level.

Table 2. Comparison of the structural parameters in $[(\text{L}^3\text{Co})_2(\mu\text{-}\eta^1\text{:}\eta^1\text{:}\eta^1\text{:}\eta^1\text{-As}_4)]$ (**8**) with $[\{\text{Cp}^*\text{Co}(\text{CO})\}_2(\mu\text{-}\eta^1\text{:}\eta^1\text{:}\eta^1\text{:}\eta^1\text{-As}_4)]$ (**C**).^[20]

Complex	8	C ^[20]
$d(\text{Co}\cdots\text{Co}) / [\text{\AA}]$	4.615	5.227
$d(\text{As}\text{--}\text{As}) / [\text{\AA}]$	2.4466(12)	2.462(2)
	2.4530(13)	2.479(2)
	2.4561(13)	2.480(2)
	2.4616(12)	2.487(2)
$d(\text{As}\cdots\text{As}) / [\text{\AA}]$ (opened edge)	3.057(1)	2.838(2)
	3.070(1)	2.881(2)
$d(\text{Co}\text{--}\text{As}) / [\text{\AA}]$	2.3077(14)	2.373(2)
	2.3139(14)	2.374(2)
	2.3143(14)	2.377(2)
	2.3217(15)	2.383(2)
$\varepsilon_1, \varepsilon_2 / [^\circ]$	105.90(5)	89.49(9)
	106.13(5)	90.36(9)
$\Theta / [^\circ]$	8.3(2)	-
	6.0(2)	-
$\Phi / [^\circ]$	80.8(2)	-

A shorter Co...Co distance is observed in the solid state structure of compound $[(L^1Co)_2(\mu-\eta^3:\eta^3-As_4)]$ (**6** and **6'**). The asymmetric unit contains two individual isomers **6** and **6'** displaying marginal differences within their structural parameters of their $[L^1Co]$ fragments and the bridging As_4 units. In comparison to complex **8**, each metal center is coordinated by an additional arsenic atom of the As_4 unit, resulting in an unprecedented $\eta^3:\eta^3$ -coordination mode and a decreased Co...Co distance (av.: 3.95 Å). The central $[Co_2As_4]$ core can be described as a distorted polyhedron adopting a distinct constitution between a trigonal prismatic and a trigonal anti-prismatic geometry (Figure 3). All As–As distances of **6** and **6'**, respectively, are between 2.3890(15) and 2.5357(10) Å and therefore are in the range of an As–As single bond. A detailed comparison of **6** and **6'** and their geometric parameters are summarized in Table 3.

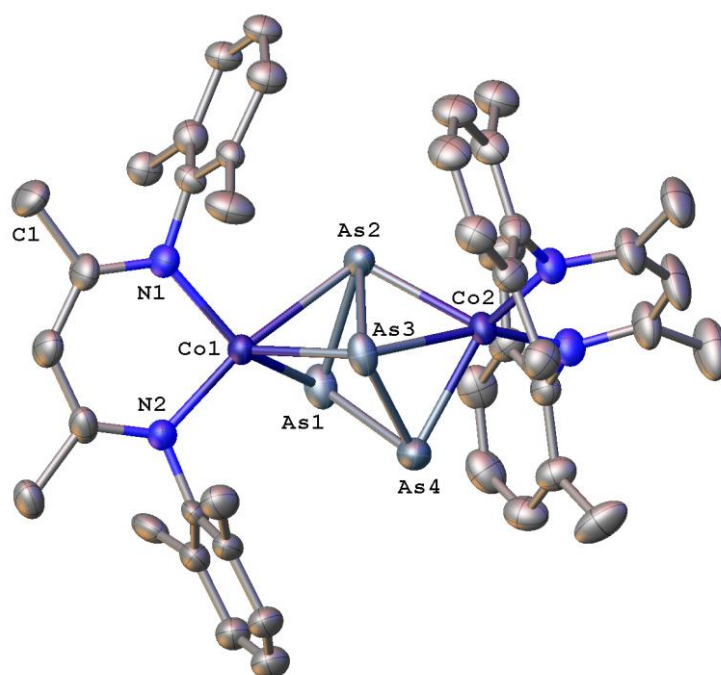


Figure 3. Molecular structure of **6** in the crystal. The second isomer **6'** is not depicted. The central $[Co_2As_4]$ constitution is between a trigonal prismatic and trigonal anti-prismatic geometry. Hydrogen atoms are omitted for clarity. From the disordered dmp groups only one position is depicted. Thermal ellipsoids are drawn at 50% probability level.

The shortening of the Co...Co distance and the As_4 planarization process is even more pronounced in $[(L^2Co)_2(\mu-\eta^4:\eta^3-As_4)]$ (**7a**), which reveals an unprecedented $\eta^4:\eta^3$ -coordination mode of the As_4 unit (Figure 4, top).^[21] Compared to **6**, the As_4 middle deck in **7a** is more planar and shows an additional bond to one cobalt center (Table 3). Furthermore, all transformations are accompanied by a decrease of the Co...Co distance (approx. 3.75 Å) in **7a** and a successive opening of the As_4 ligand ($\epsilon_1 = 137.9(5)^\circ$, $\epsilon_2 = 145.5(4)^\circ$). Due to the reorganized bonding situation within the As_4 unit, there are minor changes of the As–As distances in **6** and **7a**. However, in **7a** all As–As distances are

between 2.397(8) and 2.557(9) Å and therefore in the range of an As–As single bond. Figure 4 displays **7a** from two different perspectives. The second representation (bottom) gives rise to two different hypotheses: The [Co₂As₄] core resembles half the geometry of previously discussed tetranuclear products, e.g. complex **7b**. It can be proposed that the dimerization of **7a** proceeds by this pre-orientation and the attack of a second equivalent **7a** to yield the tetranuclear complex **7b** (vide supra, top right corner in Scheme 2). An alternative hypothesis describes **7a** as a precursor for the As₃ containing product **7c**, which will be discussed below. In an extreme view, the As₄ ligand in **7a** can be considered as a $\mu\text{-}\eta^3\text{:}\eta^3\text{-As}_3$ ligand and an attached As₁ atom which is pre-organized to be split off.

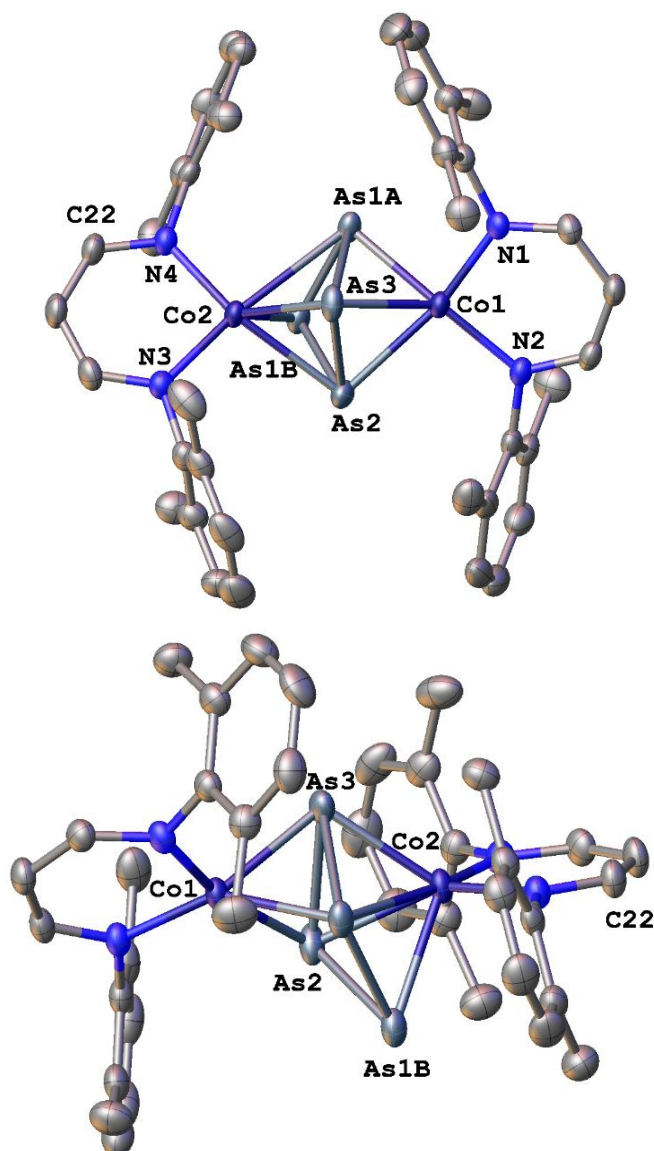


Figure 4. Top: Molecular structure of complex **7a** in the crystalline solid solution **7ac** highlighting the relation of complex **7a** and **6** (cf. Figure 3). Bottom: View of complex **7a** from a different perspective highlighting its pre-orientation prior to the hypothetical dimerization process (cf. top right corner in Scheme 2). Solvent molecules and hydrogen atoms are omitted for clarity. Thermal ellipsoids are drawn at 50% probability level.

Both hypotheses are supported by the fact that complex **7a** was only obtained as minor component (5% occupation) in its crystalline solid solution **7ac**. This may be assigned to the favored As atom abstraction of compound [(L²Co)₂(μ-η⁴:η³-As₄)] (**7a**) towards the As₃ containing complex **7c** or its aggregation towards the tetranuclear complex **7b**.

Table 3. Comparison of the structural parameters in both isomers [(L¹Co)₂(μ-η³:η³-As₄)] (**6** and **6'**) and [(L²Co)₂(μ-η⁴:η³-As₄)] (**7a**).

Complex	6	6'	7a	
$d(\text{Co}\cdots\text{Co}) / [\text{\AA}]$	3.966	3.944	3.750	
$d(\text{As1}-\text{As2}) / [\text{\AA}]$	2.4152(10)	2.4021(14)	2.408(15)	$d(\text{As1B}-\text{As1A}) / [\text{\AA}]$
$d(\text{As2}-\text{As3}) / [\text{\AA}]$	2.5266(10)	2.5357(10)	2.557(9)	$d(\text{As1A}-\text{As3}) / [\text{\AA}]$
$d(\text{As3}-\text{As4}) / [\text{\AA}]$	2.4064(11)	2.3890(15)	2.4663(7)	$d(\text{As3}-\text{As2}) / [\text{\AA}]$
$d(\text{As1}-\text{As4}) / [\text{\AA}]$	2.4501(11)	2.4239(18)	2.397(8)	$d(\text{As1B}-\text{As2}) / [\text{\AA}]$
$d(\text{Co}-\text{As}) / [\text{\AA}]$	2.3403(11)	2.3280(13)	2.2814(7)	
	2.3411(12)	2.3326(12)	2.3243(7)	
	2.3582(11)	2.3430(11)	2.359(9)	
	2.3601(11)	2.3445(11)	2.4565(7)	
	2.5011(11)	2.4872(11)	2.460(9)	
	2.5155(11)	2.5214(11)	2.4783(7)	
			2.683(9)	
$\varepsilon_1, \varepsilon_2 / [^\circ]$	127.84(5)	127.80(6)	137.9(5)	
	128.55(5)	127.85(6)	145.5(4)	
$\Theta / [^\circ]$	4.6(3)	6.5(2)	6.1(1)	
	10.8(2)	10.0(2)	6.5(2)	
$\Phi / [^\circ]$	60.4(2)	71.9(2)	46.8(1)	

Dinuclear Products with Planar *cyclo*-As₄ Ligands

Three different dinuclear products [(LM)₂(μ-η⁴:η⁴-As₄)] (LM = L⁰Co (**5**), L³Fe (**4a**), L⁰Fe (**1a**)) were isolated, which contain planar *cyclo*-As₄ ligands. As a representative, complex **5** is shown in Figure 5. Without exception, they are centrosymmetric in the solid state and therefore their β-diiminato ligands are parallel to each other. Different values for $d(M\cdots M)$, Θ and ω_1/ω_2 are found, which depend on the metal center and the β-diiminato supporting ligands involved. Their middle decks are composed of *cyclo*-As₄ ligands, either with equidistant or with alternating bond lengths, respectively, which will be discussed below.

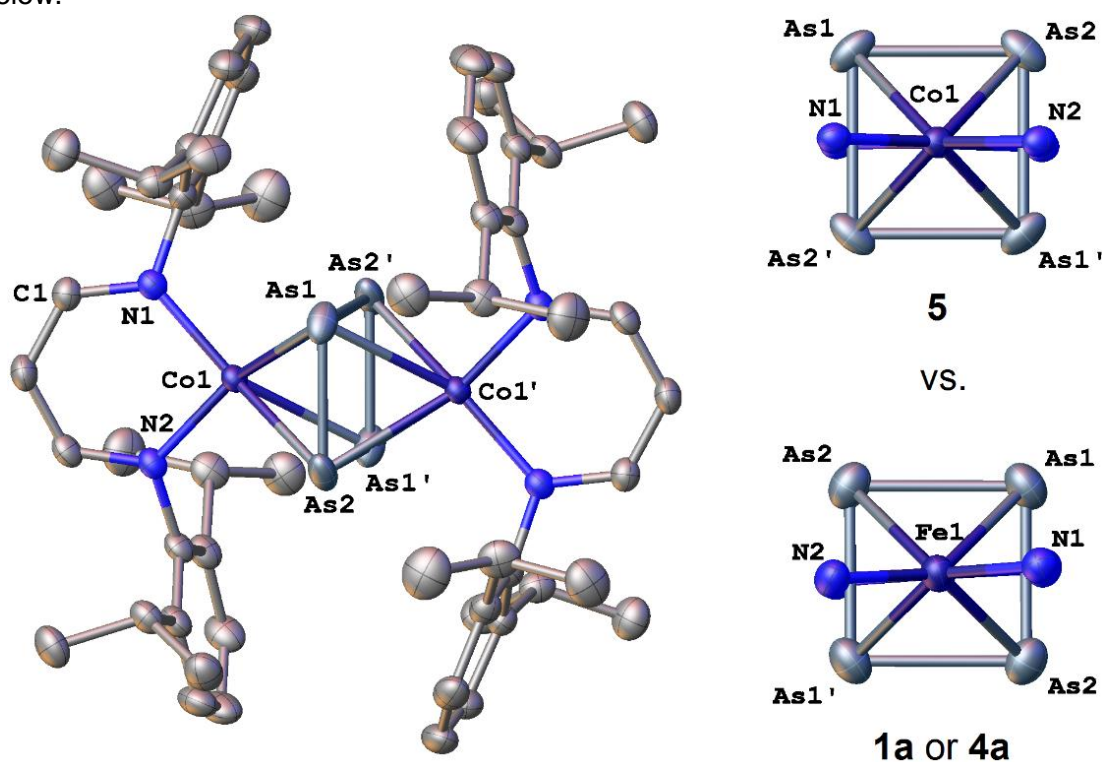


Figure 5. Left: Molecular structure of **5** in the crystal. Right: Comparison of *cyclo*-As₄ ligands: Rectangular in **5** (top) and almost equidistant in **1a/4a** (bottom), respectively. Hydrogen and selected carbon atoms are omitted for clarity. Thermal ellipsoids are drawn at 50% probability level.

At first, the cobalt complex [(L⁰Co)₂(μ-η⁴:η⁴-As₄)] (**5**) is discussed due to following reason: Envisioning the previously discussed compounds **8**, **6** and **7a**, the product **5** finishes the hypothetical, incremental planarization sequence of their As₄ moieties. This is accompanied by the shrinking of the Co⋯Co' distance in **8** (4.615 Å), **6** (av.: 3.95 Å), **7a** (3.750 Å) to a value of 3.587 Å in complex **5**. As can be seen in Figure 5, complex **5** consists of two [L⁰Co] fragments which are bridged by a rectangular shaped *cyclo*-As₄ unit^[22] with As-As-As angles of 89.86(2) and 90.14(2)°. Two pairs of longer (2.4884(5) Å) and shorter (2.3299(5) Å) arsenic distances are present in complex **5** (Table 4). The first ones are longer than As-As single bonds in yellow arsenic (2.44(3) Å^[17,18,19]), whereas the

latter are significantly shorter. However, they are right between the values of an arsenic single and double bond (As=As double bond determined in diarsene (R¹As=AsR²) by single crystal X-ray diffraction: 2.224(2)–2.2634(3) Å^[23]). The bonding situation in **5** resembles that of the phosphorus analogous complex [(L⁰Co)₂(μ-η⁴:η⁴-P₄)], which contains a neutral tetraphosphacyclobutadiene ligand.^[24]

Table 4. Comparison of the structural parameters in [(LM)₂(μ-η⁴:η⁴-As₄)] (LM = L⁰Co (**5**), L³Fe (**4a**), L⁰Fe (**1a**)) and [(Cp^{BiG}Fe)₂(μ-η⁴:η⁴-As₄)] (**D**).^[25]

Complex	5	4a	1a	D ^[25]
$d(M\cdots M') / [\text{Å}]$	3.587	3.982	3.787	3.5431(10)
				2.3905(8)
$d(\text{As}-\text{As}) / [\text{Å}]$	2.3299(5)	2.3898(8)	2.4276(7)	2.4217(8)
	2.4884(5)	2.4200(10)	2.4423(6)	2.4335(7)
				2.4562(7)
				2.4156(8)
				2.4399(8)
$d(M-\text{As}) / [\text{Å}]$	2.4638(5)	2.5707(5)	2.5516(7)	2.4438(8)
	2.4748(5)	2.6301(7)	2.5579(7)	2.4635(8)
	2.4762(5)	2.6347(6)	2.5588(7)	2.4637(8)
	2.4816(5)	2.6374(5)	2.5681(7)	2.4911(8)
				2.5015(8)
				2.5132(8)
$\omega_1, \omega_2 / [^\circ]$	1.13(5)	41.26(5)	3.69(6)	-
	89.11(5)	50.21(5)	86.69(6)	
$\Theta / [^\circ]$	15.03(7)	15.19(8)	17.5(1)	-
$\Phi / [^\circ]$	0	0	0	-

Due to their similarities, the structural parameters of the iron complexes [(L³Fe)₂(μ-η⁴:η⁴-As₄)] (**4a**) and [(L⁰Fe)₂(μ-η⁴:η⁴-As₄)] (**1a**) are discussed together (see also Table 4). Their structural parameters originate from X-ray diffraction experiments on solid solutions of **4ab** and **1ab**, respectively, in which both complexes are the major components.^[26] It is noted, that another co-crystallizing and crystallographically distinguishable isomer **1a'** is obtained in the solid solution **1ab**. The structural parameters of **1a'** are very similar to **1a**. However, they are not discussed herein, but are given in the Supporting Information.

Each dinuclear complex **4a** and **1a** is centrosymmetric and displays a planar *cyclo*-As₄ ligand with As-As-As angles of 88.54(3)/91.46(3)° in **4a** and 89.62(2)/90.38(2)° in **1a**. The As-As bonds are almost equidistant (2.3898(8) and 2.4200(10) Å in **4a**, 2.4276(7) and 2.4423(6) Å in **1a**). The values in **4a** are comparable to the ones found in the Zintl phase [(K@18-crown-6)₂As₄] (2.3871(4) and 2.3898(4) Å) containing a *cyclo*-[As₄]²⁻ unit.^[27] The

As–As distances in **1a** are in the range of As–As single bonds (2.44(3) Å^[17,18,19]) and resemble the ones found in [(Cp^{BIG}Fe)₂(μ-η⁴:η⁴-As₄)] (**D**) (2.3905(8)–2.4562(7) Å, see Table 4) (Cp^{BIG} = C₅(4-*n*-BuC₆H₄)₅).^[25] The most remarkable differences between complexes **4a** and **1a** are the Fe···Fe' distances (3.982 Å in **4a** vs. 3.787 Å in **1a**) and the orientation of the As₄ ligand related to the [L^{3,0}Fe] planes (see ω₁/ω₂ and further details in Table 4).

Dinuclear Products with Parallel As₂ Ligands

The structure determination of compound [(L⁰Fe)₂(μ-η²:η²-As₂)₂] (**1b**) was performed on crystals of **1ab**, a solid solution of two co-crystallizing and crystallographically distinguishable isomers **1a**, **1a'** and a superposed component **1b**. The extent (**1b** versus **1a'**) to which complex **1b** is observed in the solid solution of **1ab** may be influenced by the crystallization temperature. Crystals grown at different temperatures display unequal **1b**:**1a'** ratios, e.g. at 8°C 77:23 and at –30°C 36:64, respectively. The herein presented structural parameters of complex **1b** originate from a single crystal X-ray diffraction experiment in which **1b** is the 77% component. A second kind of crystals display comparable structural values, but slightly different content of **1b**.^[28] However, they are not discussed herein, but are given in the Supporting Information.

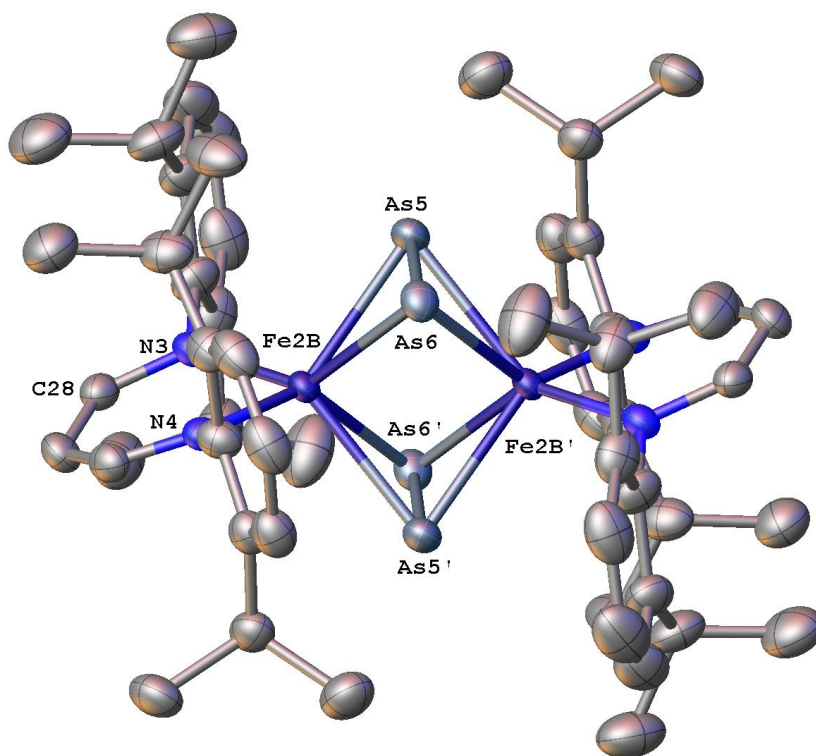


Figure 6. Molecular structure of **1b** in the crystalline solid solution **1ab**. Hydrogen atoms are omitted for clarity. Thermal ellipsoids are drawn at 50% probability level.

Product $[(L^0Fe)_2(\mu-\eta^2:\eta^2-As_2)_2]$ (**1b**) is centrosymmetric and consists of two $[L^0Fe]$ fragments bridged by a pair of As_2 ligands (Figure 6). In comparison to the previously discussed complexes **4a** (3.982 Å), **1a** (3.787 Å) and **5** (3.587 Å), the $Fe\cdots Fe'$ distance in complex **1b** is further decreased to a value of 2.940(5) Å.^[29] Doubtlessly, the shape of the arsenic ligands in product **1b** is significantly different. The distance between both As_2 units is 3.314(2) Å, which excludes any bonding interaction of the arsenic atoms. The $As-As$ distance within each As_2 ligand is 2.2414(13) Å and therefore is in the range of an $As=As$ double bond (e.g. in diarsene $R^1As=AsR^2$: 2.224(2)–2.2634(3) Å^[30]). Additionally, it is in accordance with the $As-As$ distances (2.272(2)–2.300(2) Å) of As_2 ligand containing complexes,^[31] especially with $[(Cp^RCo)(\mu-\eta^2:\eta^2-As_2)]_2$ ($R = tBu_3$ (**E**)^[31a], Me_4Et (**F** and **F'**, two isomers)^[31b]), which display isostructural $[M_2(\mu-\eta^2:\eta^2-As_2)_2]$ cores (Table 5).

Table 5. Comparison of the structural parameters in $[(L^0Fe)_2(\mu-\eta^2:\eta^2-As_2)_2]$ (**1b**) and $[(Cp^RCo)(\mu-\eta^2:\eta^2-As_2)]_2$ ($R = tBu_3$ (**E**)^[31a], Me_4Et (**F**)^[31b])

Complex	1b	E	F	F'
$d(M\cdots M') / [\text{Å}]$	2.940(5)	3.251	3.188	3.185
$d(As-As)_{intra} / [\text{Å}]$	2.2414(13)	2.2795(5)	2.272(1)	2.279
$d(As\cdots As)_{inter} / [\text{Å}]$	3.314(2)	2.8209(4)	2.844(1)	2.838
$d(M-As) / [\text{Å}]$	2.461(2)	2.4211(5)	2.414	2.416
	2.4673(17)	2.4355(5)	2.415	2.417
	2.499(2)	2.441	2.424	2.418
	2.5022(19)	2.443	2.424	2.421
$\omega_1, \omega_2 / [^\circ]$	0.4(2)	-	-	-
	90(2)	-	-	-
$\Theta / [^\circ]$	25.2(3)	-	-	-
$\Phi / [^\circ]$	0	-	-	-

Dinuclear Products with As₃ Ligands

Two different compounds $[(L^3Fe)_2(\mu-\eta^3:\eta^3-As_3)]$ (**4b**) and $[(L^2Co)_2(\mu-\eta^3:\eta^3-As_3)]$ (**7c** and **7c'**) containing As_3 ligands were identified by single crystal X-ray diffraction. Each complex is one component of the solid solution of **4ab** or **7ac**, respectively (vide supra). While complex **4b** is the minor component (22%) in the solid solution **4ab** and is disordered, the solid solution **7ac** consists of two distinguishable isomers **7c** and **7c'**, whereas only **7c'** (95%) is superposed by complex **7a** to a minor extent (5%, vide supra). The determined occupancies in the solid solutions **4ab** and **7ac** are confirmed by ¹H NMR spectroscopy on the dissolved crystals. All these dinuclear compounds **4b**, **7c** and **7c'**

consist of two [LM] fragments, which contain As₃ ligands with different geometric parameters. A summary is given in Table 6.

Table 6. Comparison of the structural parameters in [(L³Fe)₂(μ-η³:η³-As₃)] (**4b**), two isomers [(L²Co)₂(μ-η³:η³-As₃)] (**7c** and **7c'**) and [(triphos)Co]₂(μ-η³:η³-As₃)²⁺ (**G**).^[33]

Complex	4b	7c	7c'	G ^[33]
$d(\text{M}\cdots\text{M}') / [\text{\AA}]$	3.982	3.750	3.738	-
$d(\text{As}-\text{As}) / [\text{\AA}]$	2.527(6)	2.4145(6)	2.4166(7)	2.42(2)
	2.534(6)	2.4663(7)	2.4884(7)	2.45(1)
	2.875(7)	2.6149(6)	2.5861(7)	2.45(2)
$d(\text{M}-\text{As}) / [\text{\AA}]$	2.432(5)	2.2814(7)	2.2788(8)	2.40(2)
	2.499(3)	2.3243(7)	2.3083(7)	2.40(2)
	2.501(3)	2.3602(7)	2.3708(7)	2.40(2)
	2.502(3)	2.3620(7)	2.3744(7)	2.41(1)
	2.556(5)	2.4565(7)	2.4374(7)	2.42(2)
	2.604(5)	2.4783(7)	2.4389(7)	2.44(2)
$\Theta / [^\circ]$	15.19(8)	6.1(1)	2.6(1)	-
		6.5(2)	5.1(1)	
$\Phi / [^\circ]$	0	46.8(1)	41.0(1)	-

Product [(L³Fe)₂(μ-η³:η³-As₃)] (**4b**) is a centrosymmetric complex with an Fe⋯Fe' distance of 3.982 Å. Due to symmetry reasons its As₃ ligand is equally (50:50) disordered^[32] over two positions (Figure 7). Two As-As distances (2.527(6) and 2.534(6) Å) are in the range of elongated single bonds (in yellow arsenic: 2.44(3) Å^[17,18,19]). The third one (2.875(7) Å) is longer than the sum of arsenic covalent radii and therefore the two arsenic atoms can be considered as non-bonded or only weakly interacting. The As-As-As angles are 55.5(2), 55.3(2) and 69.2(2)° within the As₃ unit.

Complex [(L²Co)₂(μ-η³:η³-As₃)] (**7c** and **7c'**) was obtained as major component of the solid solution **7ac** and in form of two different isomers (Figure 8). Both **7c** and **7c'** display minor deviations within their structural parameters (Table 6). Therefore, they are distinguishable in the solid state. The As atom positions in isomer **7c'** (95%) were localized accurately despite superposition of the minor component **7a** (5%). The As-As distances within both As₃ units of **7c** and **7c'** are in the range of 2.4145(6) and 2.6149(6) Å, which relates to As-As single bonds (in yellow arsenic: 2.44(3) Å).^[17,18,19] Comparable values were obtained in the reported dicationic *cyclo*-As₃ complex [(triphos)Co]₂(μ-η³:η³-As₃)²⁺ (**G**, see Table 6; triphos = 1,1,1-tris(diphenylphosphinomethyl)ethane).^[33] The As-As-As angles are 56.65(2), 58.57(2), 64.78(2)° in isomer **7c** and 56.84(2), 59.55(2), 63.62(2)° in isomer **7c'**.

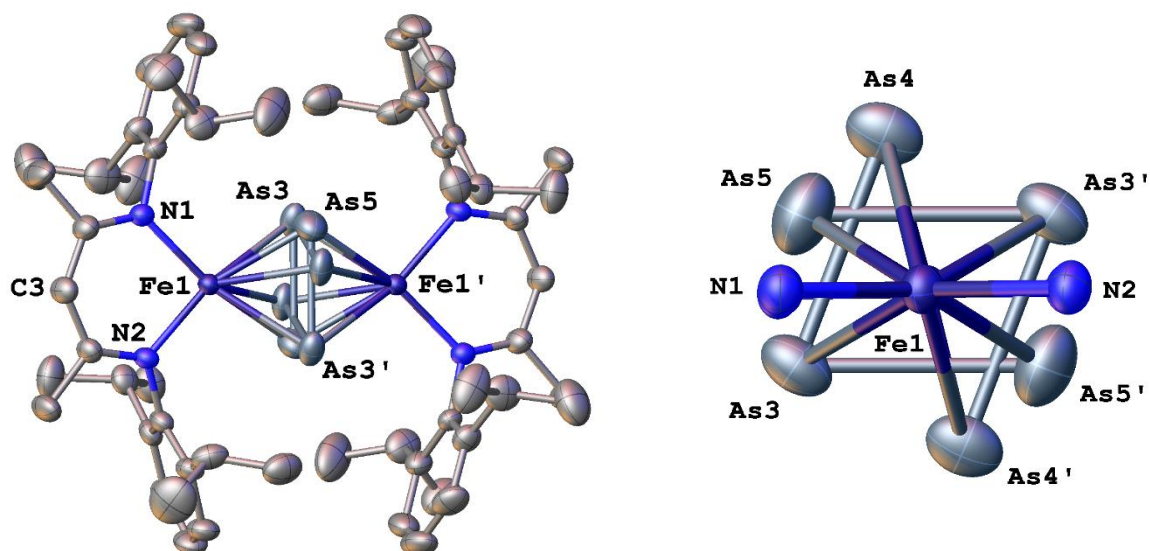


Figure 7. Left: Molecular structure of **4b** in the crystalline solid solution **4ab**. Right: Top view presentation of its disordered [Fe₂As₃] central core. The major *cyclo*-As₄ middle deck of **4a**, the hydrogen atoms and selected carbon atoms are omitted for clarity. Thermal ellipsoids are drawn at 50% probability level.

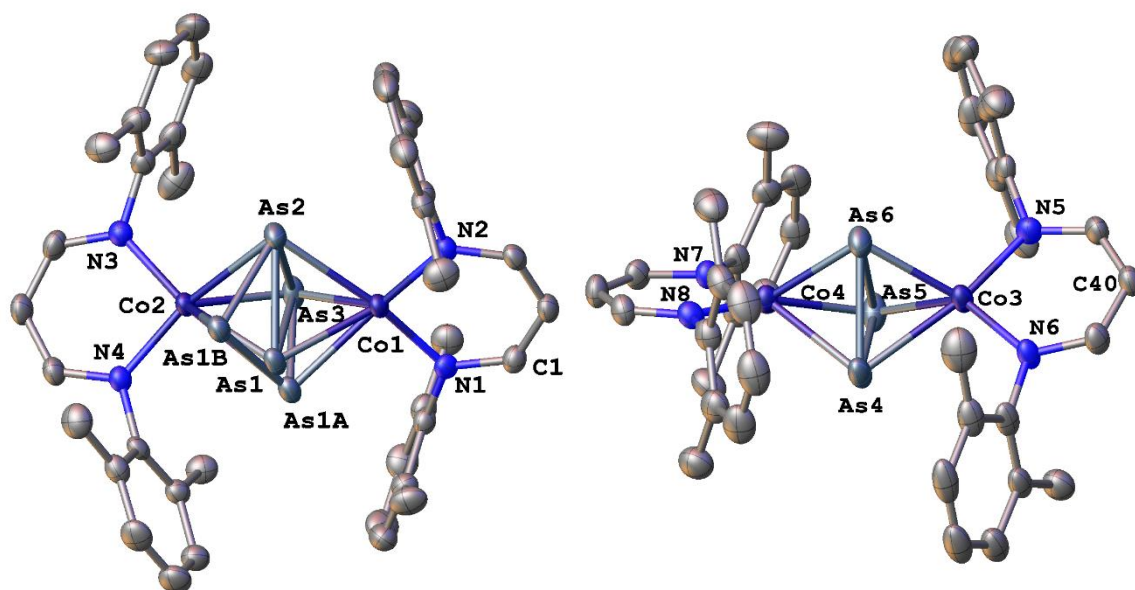


Figure 8. Molecular structures of **7a**, **7c** and **7c'** in the crystalline solid solution **7ac**. Left: Superposition of the As₄ ligand of **7a** and the As₃ ligand in **7c'**. Right: Second isomer **7c**. Hydrogen atoms and Et₂O molecules are omitted for clarity. Thermal ellipsoids are drawn at 50% probability level.

7.3 Discussion

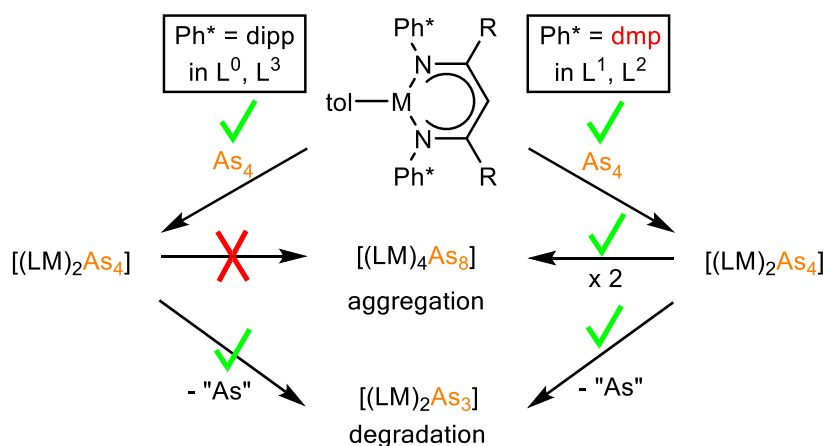
The mild reactions of yellow arsenic with a set of [LM(tol)] (L = L⁰–L³, M = Fe, Co) precursors are presented. The [LM(tol)] dissociation in solution enables the smooth reaction of metastable As₄ with two highly exposed metal centers at ambient conditions. A variety of di- and tetranuclear products **1–8** (vide supra) were isolated and characterized. An influence of the ligand design on the reaction outcome was recognized:

Ligand systems (L¹, L²) with dmp (2,6-dimethylphenyl) as an aromatic Ph* flanking group yielded tetranuclear products [(LM)₄As₈] (LM = L¹Fe (**2**), L²Fe (**3**), L²Co (**7b**)). In addition to this, in case of the L¹ and L² cobalt system, the dinuclear complexes [(LM)₂As₄] (LM = L¹Co (**6**), L²Co (**7a**)) were isolated. Both are assigned to their intermediary precursors in the proposed dimerization reaction towards the tetranuclear products. Di- and tetranuclear products are distinguishable by ¹H NMR spectroscopy due to different signal patterns in solution. In the mass spectra, molecular ion peaks for the tetranuclear complexes were detected in both cases – for the isolated dinuclear dmp intermediates and tetranuclear dmp products, as well.

For dipp (2,6-diisopropylphenyl) substituted ligand systems (L⁰, L³), the formation of exclusively dinuclear products was observed. This is confirmed by single crystal X-ray diffraction and the interpretation of ¹H NMR spectra, as well. The most significant hint, however, is the absence of the molecular ion peak [(LM)₄As₈]⁺ of the hypothetical tetranuclear dimerized complex. Within the conditions of LIFDI mass spectrometry, such signals were not detected for the dipp substituted compounds - even at elevated temperatures.

All dinuclear products do not only display peaks for their molecular ion peak [(LM)₂As₄]⁺ in the LIFDI mass spectra, but contain additional peaks assignable to [(LM)₂As₃]⁺. The formation of [(LM)₂As₃]⁺ is attributed either to the fragmentation of [(LM)₂As₄]⁺ in the conditions of mass spectrometry or to an As atom abstraction from [(LM)₂As₄] complexes during their synthesis and work-up. Due to the fact that the As₃ ligand containing compounds **4b** and **7c** were isolated, it can be assumed that for the other systems comparable As₃ ligand complexes ligands might be isolable.

Our assumptions are summarized in Scheme 5 and described below:



Scheme 5. Possible reaction pathways of the As₄ reaction with [LM(tol)] (L = L⁰–L³, M = Fe, Co) in dependency of incorporated Ph* flanking groups.

- 1) Irrespective of ligands used, the first traceable step of a [LM] mediated As₄ activation is the generation of the dinuclear products [(LM)₂As₄].
- 2) In **dipp** containing systems (L⁰ and L³), the dinuclear [(LM)₂As₄] product is preserved and the **aggregation** reaction towards its hypothetical [(LM)₄As₈] dimer is **hindered** due to steric reasons.^[34] In the **dmp** supported systems (L¹ and L²), this **aggregation** is **enabled** and results in the formation of the [(LM)₄As₈] dimerization products.
- 3) Simultaneously, the competitive **degradation** reaction of [(LM)₂As₄] towards [(LM)₂As₃] can occur in **dipp and dmp** containing systems, which proceeds very likely by extrusion of one arsenic atom.
- 4) In solid state each dinuclear [(LM)₂As₄] product displays an individual β-diiminato ligand constitution, which directs its θ and ϕ angles and its $M \cdots M'$ distance. The latter **fine-tunes** the As₄ ligand geometry and therefore a variety of different As₄ **transformations** were observed in the different solid state structures.
- 5) Each observed structure represents a possible step in the hypothetical (see Scheme 2) transformation, degradation and aggregation reaction of yellow arsenic in the coordination sphere of two [LM] fragments:

A snapshot on the molecular level.

7.4 DFT Calculations

DFT calculations were performed to support our assumptions. Therefore, the hypothetical molecule $[(L^0Co)_2(\mu-\eta^2:\eta^2-As_2)_2]$ (**CALC**) was chosen as a model system. Starting with the structural parameters of the experimentally obtained iron complex $[(L^0Fe)_2(\mu-\eta^2:\eta^2-As_2)_2]$ (**1b**), displaying the shortest M...M' distance in all dinuclear products **1–8**, a potential energy surface (PES) scan was performed along the Co...Co reaction coordinate at the BP86/def2-SVP level of theory. The relative energy of the relaxed geometries, with constrained Co...Co distances in different spin states was computed. The results of the PES scan are summarized in Figure 9 and are discussed in the following:

A general feature is the flat PES surface, especially between 3.6 to 4.6 Å. The relative energy of the unrestricted singlet and triplet spin states are very close to each other, while the quintet spin state is higher in energy all the way through. Furthermore, several spin crossover points might be expected between the unrestricted singlet and triplet spin states.

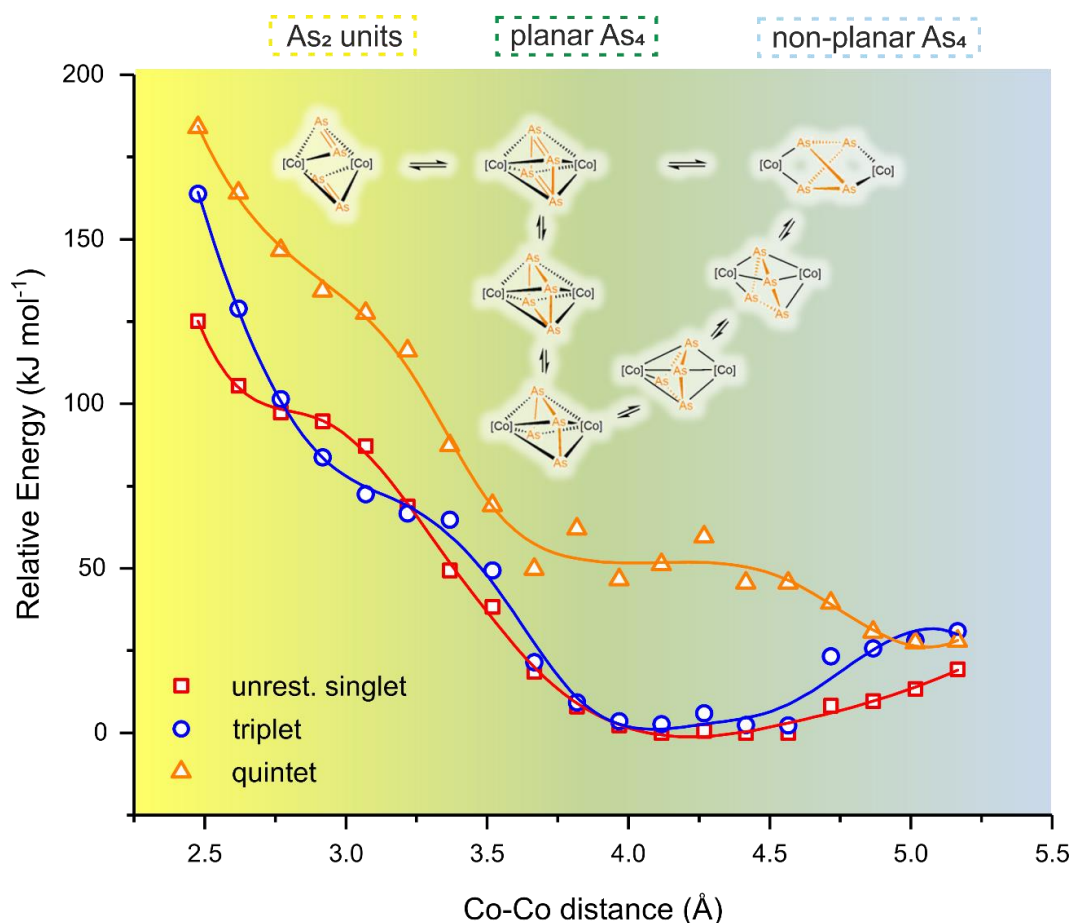


Figure 9. Potential energy surface scan in $[(L^0Co)_2(As_4)]$ along the Co...Co reaction coordinate, calculated at the BP86/def2-SVP level of theory. The found $[Co_2As_4]$ core geometries at corresponding Co...Co distances are depicted. Due to the possible antiferromagnetic couplings and limited accuracy of DFT calculations for open shell systems, the PES scan represents only an approximate qualitative description.

The nature of the [Co₂As₄] core geometry is also very strongly influenced by the Co...Co distance. The resulting geometries are depicted in Figure 9, in which the position of the depicted molecules correspond to the restrained Co...Co distance. Formally, the graph can be divided into three sections corresponding to their Co...Co distance. In the yellow one (up to roughly 3 Å), exclusively ligands with As₂ ligands are predicted (see also Scheme 2). On the right-hand side (blue area, at distances longer than 4.6 Å) complexes with non-planar, folded *cyclo*-As₄ ligands are predicted. At last, in the central green area, progressively butadiene like As₄ ligands are formed, followed by planar *cyclo*-As₄ units. Generally, the optimized geometries in different spin states and with fixed Co...Co distances reproduce the experimental results observed in the crystal structures of **5**, **6**, **7a** and **8**. The slope of function in this area is emphasized to be very low regardless of the spin state. This suggests that the difference in relative energy ΔE within all observed isomers is low, especially in comparison to different energy contributions from packing effects, dispersion interactions, thermal energy, etc. Therefore, the observed geometry in the solid state is suggested to be mainly driven by a combination of these factors. This explains the variety of different [Co₂As₄] cores experimentally found in the solid state of dinuclear cobalt compounds **5**, **6**, **7a** and **8**.

Table 7. Relative energy (kJ·mol⁻¹) of [(L⁰Co)₂(As₄)] in different spin states calculated using different DFT functionals.

Functional	unrestricted singlet	triplet	quintet
BP86	32.31	0.00	60.89
B3LYP	27.96	0.00	-0.55
PBE0	-4.25	0.00	-39.40

In this type of complexes, the nature of the functional used in the calculations plays an important role. To investigate the effect of the functional on the relative energy of different spin states in [(L⁰Co)₂(As₄)] (**CALC**), single point calculations on the BP86/def2-TZVP optimized geometries have been performed. The functional BP86 predicts the triplet spin state as being the energy minimum, while the hybrid functionals PBE0 and B3LYP predict the quintet spin state as energy minima (Table 7). Since the geometry of complex [(L⁰Co)₂(As₄)] (**5**) in the solid state is close to the optimized geometry in the singlet spin state, we calculated the energy of the triplet spin state by single point calculations on the geometry optimized in the unrestricted singlet spin state. The triplet spin state is with 29.47 kJ·mol⁻¹ higher in energy. This indicates that the singlet-triplet excitation energy (by preserving the geometry) is small and hence, the spin state of the complex is strongly

influenced by different energy contributions. Once again, this indicates the flat PES surface and the high flexibility of the As₄ middle deck.

7.5 Conclusion

In summary, we performed the reductive activation of yellow arsenic with eight different iron(I) or cobalt(I) starting materials [LM(tol)] (L = L⁰–L³, M = Fe, Co). The formation of various dinuclear [(LM)₂As_n] (n = 4: LM = L⁰Fe (**1a**), L³Fe (**4a**), L⁰Co (**5**), L¹Co (**6**), L²Co (**7a**), L³Co (**8**); n = 3: LM = L³Fe (**4b**), L²Co (**7c**); n = 2: LM = L⁰Fe (**1b**)) and tetranuclear [(LM)₄As₈] (LM = L¹Fe (**2**), L²Fe (**3**), L²Co (**7b**)) products was observed. The products are supported by four different β-diiminato ligands. The aromatic flanking groups Ph* of the ligands were found either to enable (Ph* = dmp, in L¹ and L²) or to prohibit (Ph* = dipp, in L⁰ and L³) the reaction of the initially forming dinuclear [(LM)₂As₄] intermediates towards a further dimerized [(LM)₄As₈]. In the solid state, each dinuclear [(LM)₂As₄] complex displays an individual ligand environment with a distinct M···M' distance, which leads to a planar or non-planar As₄ or As₂ ligand constitution. DFT calculations support the dependency of the [Co₂As₄] core structure on the Co···Co' distance. All experimentally observed solid state structures are understood as a snapshot of the As₄ transformation, aggregation or degradation reaction in the coordination sphere of two metal centers.

7.6 References

- [1] Determination by heats of atomization of E₄ (E = P, As): B. M. Cossairt, C. C. Cummins, *J. Am. Chem. Soc.* **2009**, *131*, 15501-15511.
- [2] A. Rodionov, R. Kalendarev, J. Eiduss, Y. Zhukovskii, *J. Mol. Struct.* **1996**, *380*, 257-266.
- [3] a) D. Tofan, B. M. Cossairt, C. C. Cummins, *Inorg. Chem.* **2011**, *50*, 12349-12358; b) M. Caporali, L. Gonsalvi, A. Rossin, M. Peruzzini, *Chem. Rev.* **2010**, *110*, 4178-4235; c) M. Scheer, G. Balázs, A. Seitz, *Chem. Rev.* **2010**, *110*, 4236-4256; d) S. Khan, S. S. Sen, H. W. Roesky, *Chem. Commun.* **2012**, *48*, 2169-2179; e) N. A. Giffin, J. D. Masuda, *Coord. Chem. Rev.* **2011**, *255*, 1342-1359.
- [4] Main group compounds: a) S. Heintl, G. Balázs, A. Stauber, M. Scheer, *Angew. Chem. Int. Ed.* **2016**, *55*, 15524-15527; b) A. D. Fanta, R. P. Tan, N. M. Comerlato, M. Driess, D. R. Powell, R. West, *Inorg. Chim. Acta* **1992**, *198-200*, 733-739; transition metal complexes: c) Graßl, M. Bodensteiner, M. Zabel, M. Scheer, *Chem. Sci.* **2015**, *6*, 1379-1382; d) S. Heintl, M. Scheer, *Chem. Sci.* **2014**, *5*, 3221-3225; e) C. Schwarzmaier, M. Bodensteiner, A. Y. Timoshkin, M. Scheer, *Angew. Chem. Int. Ed.* **2014**, *53*, 290-293; f) C. Schwarzmaier, A. Y. Timoshkin, G. Balázs, M. Scheer, *Angew. Chem. Int. Ed.* **2014**, *53*, 9077-9081; g) C. Schwarzmaier, M. Sierka, M. Scheer, *Angew. Chem., Int. Ed.* **2013**, *52*, 858-861; h) C. Schwarzmaier, A. Y. Timoshkin, M. Scheer, *Angew. Chem. Int. Ed.* **2013**, *52*, 7600-7603; i) C. Schwarzmaier, A. Noor, G. Glatz, M. Zabel, A. Y. Timoshkin, B. M. Cossairt, C. C. Cummins, R. Kempe, M. Scheer, *Angew. Chem.* **2011**, *123*, 7421-7424; j) J. J. Curley, N. A. Piro, C. C. Cummins, *Inorg. Chem.* **2009**, *48*, 9599-9601; k) H. A. Spinney, N. A. Piro, C. C. Cummins, *J. Am. Chem. Soc.* **2009**, *131*, 16233-16243.
- [5] a) H. Erdmann, M. V. Unruh, *Z. anorg. Chem.* **1902**, *32*, 437-452; b) O. J. Scherer, H. Sitzmann, G. Wolmershäuser, *J. Organomet. Chem.* **1986**, *309*, 77-86; c) J. J. Curley, N. A. Piro, C. C. Cummins, *Inorg. Chem.* **2009**, *48*, 9599-9601; d) H. A. Spinney, N. A. Piro, C. C. Cummins, *J. Am. Chem. Soc.* **2009**, *131*, 16233-16243.
- [6] Selected review articles: a) O. J. Scherer, *Angew. Chem.* **1990**, *102*, 1137-1155; b) O. J. Scherer, *Acc. Chem. Res.* **1999**, *32*, 751-762; c) B. Rink, O. J. Scherer, G. Heckmann, G. Wolmershäuser, *Chem. Ber.* **1992**, *125*, 1011-1016; d) O. J. Scherer, *Angew. Chem. Int. Ed. Engl.* **1985**, *24*, 924-943.

- [7] a) O. J. Scherer, K. Pfeiffer, G. Wolmershäuser, *Chem. Ber.* **1992**, *125*, 2367-2372; b) C. Schwarzmaier, A. Y. Timoshkin, G. Balázs, M. Scheer, *Angew. Chem. Int. Ed.* **2014**, *53*, 9077-9081.
- [8] Selected examples: a) D. J. E. Spencer, N. W. Aboeella, A. M. Reynolds, P. L. Holland, W. B. Tolman, *J. Am. Chem. Soc.* **2002**, *124*, 2108-2109; b) J. M. Smith, R. J. Lachicotte, K. A. Pittard, T. R. Cundari, G. Lukat-Rodgers, K. R. Rodgers, P. L. Holland, *J. Am. Chem. Soc.* **2001**, *123*, 9222-9223; c) K. Ding, A. W. Pierpont, W. W. Brennessel, G. Lukat-Rodgers, K. R. Rodgers, T. R. Cundari, E. Bill, P. L. Holland, *J. Am. Chem. Soc.* **2009**, *131*, 9471-9472; d) F. Spitzer, C. Graßl, G. Balázs, E. M. Zolnhofer, K. Meyer, M. Scheer, *Angew. Chem. Int. Ed.* **2016**, *55*, 4340-4344.
- [9] Selected examples for **Vanadium**: a) Y.-C. Tsai, P.-Y. Wang, K.-M. Lin, S.-A. Chen, J.-M. Chen, *Chem. Commun.* **2008**, 205-207; b) K.-C. Chang, C.-F. Lu, P.-Y. Wang, D.-Y. Lu, H.-Z. Chen, T.-S. Kuo, Y.-C. Tsai, *Dalton Trans.* **2011**, *40*, 2324-2331; **Chromium**: c) W. H. Monillas, G. P. A. Yap, L. A. MacAdams, K. H. Theopold, *J. Am. Chem. Soc.* **2007**, *129*, 8090-8091; d) Y.-C. Tsai, P.-Y. Wang, S.-A. Chen, J.-M. Chen, *J. Am. Chem. Soc.* **2007**, *129*, 8066-8067; **Manganese**: d) J. Chai, H. Zhu, A. C. Stückl, H. W. Roesky, J. Magull, A. Bencini, A. Caneschi, D. Gatteschi, *J. Am. Chem. Soc.* **2005**, *127*, 9201-9206; **Iron**: e) J. M. Smith, R. J. Lachicotte, K. A. Pittard, T. R. Cundari, G. Lukat-Rodgers, K. R. Rodgers, P. L. Holland, *J. Am. Chem. Soc.* **2001**, *123*, 9222-9223; f) J. M. Smith, A. R. Sadique, T. R. Cundari, K. R. Rodgers, G. Lukat-Rodgers, R. J. Lachicotte, C. J. Flaschenriem, J. Vela, P. L. Holland, *J. Am. Chem. Soc.* **2006**, *128*, 756-769; **Cobalt**: g) X. Dai, P. Kapoor, T. H. Warren, *J. Am. Chem. Soc.* **2004**, *126*, 4798-4799; h) K. Ding, A. W. Pierpont, W. W. Brennessel, G. Lukat-Rodgers, K. R. Rodgers, T. R. Cundari, E. Bill, P. L. Holland, *J. Am. Chem. Soc.* **2009**, *131*, 9471-9472; **Nickel**: i) S. Yao, Y. Xiong, C. Milsman, E. Bill, S. Pfirrmann, C. Limberg, M. Driess, *Chem. Eur. J.* **2010**, *16*, 436-439; **Copper**: j) D. J. E. Spencer, A. M. Reynolds, P. L. Holland, B. A. Jazdzewski, C. Duboc-Toia, L. Le Pape, S. Yokota, Y. Tachi, S. Itoh, W. B. Tolman, *Inorg. Chem.* **2002**, *41*, 6307-6321; **Zinc**: k) Y. Wang, B. Quillian, P. Wei, H. Wang, X.-J. Yang, Y. Xie, R. B. King, P. v. R. Schleyer, H. F. Schaefer, G. H. Robinson, *J. Am. Chem. Soc.* **2005**, *127*, 11944-11945.
- [10] F. Spitzer, M. Sierka, M. Latronico, P. Mastroilli, A. V. Virovets, M. Scheer, *Angew. Chem. Int. Ed.* **2015**, *54*, 4392-4396.
- [11] Therefore, a freshly prepared solution of As₄ in toluene was filtered over celite and was cooled until a yellow solid formed. Supernatant solution was decanted off and several pump-flush cycles were performed.
- [12] See the Supporting Information for further details about each conducted reaction.
- [13] Though, measuring in m/z ranges of their hypothetical teranuclear aggregates. See Supporting Information.
- [14] Similar signal patterns were already observed in phosphorus analogous compounds [(LFe)₄(μ₄-η¹:η¹:η¹:η¹:η¹:η¹:η¹:η¹-P₈)] (L = L¹, L²). See ref.: F. Spitzer, C. Graßl, G. Balázs, E. M. Zolnhofer, K. Meyer, M. Scheer, *Angew. Chem. Int. Ed.* **2016**, *55*, 4340-4344.
- [15] Note: Also detected for intermediates **6** and **7a**, which are expected to adopt a relaxed molecular geometry in solution. See Supporting Information.
- [16] Molecular structures were drawn with Olex² software package (latest version 1.2.8): O.V. Dolomanov and L.J. Bourhis and R.J. Gildea and J.A.K. Howard and H. Puschmann, Olex2: A complete structure solution, refinement and analysis program, *J. Appl. Cryst.*, (2009), **42**, 339-341.
- [17] Y. Morino, T. Ukaji, T. Ito, *Bull. Chem. Soc. Jpn.* 1966, *39*, 64-71.
- [18] L. R. Maxwell, S. B. Hendricks, V. M. Mosley, *J. Chem. Phys.* 1935, *3*, 699-709.
- [19] H. A. Spinney, N. A. Piro, C. C. Cummins, *J. Am. Chem. Soc.* **2009**, *131*, 16233-16243.
- [20] O. J. Scherer, K. Pfeiffer, G. Wolmershäuser, *Chem. Ber.* **1992**, *125*, 2367-2372.
- [21] Complex **7a** was obtained as a minor component in the solid solution **7ac**. The major component of **7ac** is [(L²Co)₂(μ-η³:η³-As₃)] (**7c**). It will be discussed below.
- [22] The major component (94% occupation) of the middle deck is assigned to the *cyclo*-As₄ ligand. Remaining electron density was not interpreted due to lacking chemical reliability. See the Supporting Information for more details.
- [23] for R¹As=AsR², e.g.: a) 2.2634(3) Å (R¹, R² = Mes*): M. Bouslikhane, H. Gornitzka, J. Escudié, H. Ranaivonjatovo, *J. Organomet. Chem.* **2001**, *619*, 275-279, b) 2.243(1) and 2.245(1) Å (R¹, R² = C(SiMe₃)₃): A. H. Cowley, N. C. Norman, M. Pakulski, *Journal of the Chemical Society, Dalton Transactions* **1985**, 383-386, c) 2.224(2) Å (R¹ = Mes*, R² = CH(SiMe₃)₂): A. H. Cowley, J. G. Lasch, N. C. Norman, M. Pakulski, *J. Am. Chem. Soc.* **1983**, *105*, 5506-5507.

- [24] S. Yao, N. Lindenmaier, Y. Xiong, S. Inoue, T. Szilvási, M. Adelhardt, J. Sutter, K. Meyer, M. Driess, *Angew. Chem. Int. Ed.* **2015**, *54*, 1250-1254.
- [25] S. Heini, *Dissertation, Universität Regensburg* **2014**.
- [26] For structure **4ab**: Solely structural parameters of As₄ containing (major) component **4a** are discussed. Minor components (As₃ ligand complex **4b**) are discussed below. For solid solution **1ab**: Two different compounds **1a** (major component) and **1b** (minor component) were obtained in the structure. The first one crystallizes at two different crystallographic positions, giving rise to a pair of distinguishable isomers **1a** and **1a'**. At the second crystallographic position, compound **1a'** and **1b** are superposed. The **1a':1b** distribution (occupation 23:77 vs. 64:36) seems to be influenced by crystallization temperature, which is indicated by the single crystal X-ray diffraction experiment of another batch of crystals **1ab**. Herein, only the structural parameters of isomer **1a** are discussed, as those of **1a'** vary with the extent of its occupancy. See the Supporting Information for further information on solid solutions **4ab** and **1ab**.
- [27] F. Kraus, T. Hanauer, N. Korber, *Inorg. Chem.* **2005**, *45*, 1117-1123.
- [28] The structural values in the second kind of crystals may be attached with uncertainties due to the overlapping As₄ middle deck of superposing **1a'** and the As₂ ligands of **1b**. The decreased deviation of its **1b:1a'** occupancy ratio complicates the accurate localization of the overlapping As atoms in the second experiment. These details are described in the Supporting Information.
- [29] Any bonding interaction between both iron atoms are ruled out, due to its reported covalent radius of 1.16 Å. See: P. Pyykkö, M. Atsumi, *Chem. Eur. J.* **2009**, *15*, 186-197.
- [30] for R¹As=AsR², e.g.: a) 2.2634(3) Å (R¹, R² = Mes*): M. Bouslikhane, H. Gornitzka, J. Escudié, H. Ranaivonjatovo, *J. Organomet. Chem.* **2001**, *619*, 275-279, b) 2.243(1) and 2.245(1) Å (R¹, R² = C(SiMe₃)₃): A. H. Cowley, N. C. Norman, M. Pakulski, *Journal of the Chemical Society, Dalton Transactions* **1985**, 383-386, c) 2.224(2) Å (R¹ = Mes*, R² = CH(SiMe₃)₂): A. H. Cowley, J. G. Lasch, N. C. Norman, M. Pakulski, *J. Am. Chem. Soc.* **1983**, *105*, 5506-5507.
- [31] a) [((Cp^o)Co)(μ-η²:η²-As₂)]₂ (2.2795(5) vs. 2.8209(4) Å): C. Graßl, M. Bodensteiner, M. Zabel, M. Scheer, *Chemical Science* **2015**, *6*, 1379-1382; b) [((Cp^{Me4Et})Co)(μ-η²:η²-As₂)]₂ (2.272(1) vs. 2.844(1) Å): O. J. Scherer, K. Pfeiffer, G. Heckmann, G. Wolmershäuser, *J. Organomet. Chem.* **1992**, *425*, 141-149; c) [CpMo(CO)(μ-η²:η²-As₂)]₂ (2.272(2) and 2.281(2) Å): A.-J. DiMaio, C. J. Baldacchini, A. L. Rheingold, *Acta Cryst. Section C* **1990**, *46*, 492-494; d) [Cp^{Me}Mo(CO)(μ-η²:η²-As₂)]₂ (2.279(2) and 2.300(2) Å): A.-J. DiMaio, A. L. Rheingold, *J. Chem. Soc., Chem. Commun.* **1987**, 404-405.
- [32] The overlapping *cyclo*-As₄ unit of complex **4a** and the disordered As₃ ligand in **4b** may influence the accurate localization of its As atom positions.
- [33] M. Di Vaira, S. Midollini, L. Sacconi, *J. Am. Chem. Soc.* **1979**, *101*, 1757-1763.
- [34] In all herein discussed solid state structures, the aromatic Ph* (dmp or dipp) planes are approximately orthogonal to the backbone plane of the ligands. Therefore, the electronic effect of their 2,6 substituents should be considered as being only marginal.

7.7 Supporting Information

General Remarks

All manipulations were performed with rigorous exclusion of oxygen and moisture using Schlenk-type glassware on a dual manifold Schlenk line with Argon inert gas or glove box filled with N₂ containing a high-capacity recirculator (<0.1 ppm O₂). Solvents were dried using a MB SPS-800 device of company MBRAUN. Mass spectra were measured using a JEOL AccuTOF GCX (LIFDI) or Finnigan MAT95 LIFDI-MS (for **2**) mass spectrometer. Elemental analysis (CHN) was determined using a Vario micro cube instrument. ¹H NMR spectra were recorded on a Bruker Avance III HD 400 (¹H: 400.130 MHz) spectrometer. The chemical shifts are reported in ppm relative to external TMS.

Preparation of Ligands LH (L = L⁰, L¹, L², L³)

Ligands L¹H^[1], L²H^[2] and L³H^[3] were synthesized according to literature methods. L⁰H was prepared according to synthesis of L²H^[2] except that 2,6-diisopropylaniline was used instead of 2,6-dimethylaniline. All herein used ligands LH (L = L⁰, L¹, L², L³) are depicted in Figure S1.

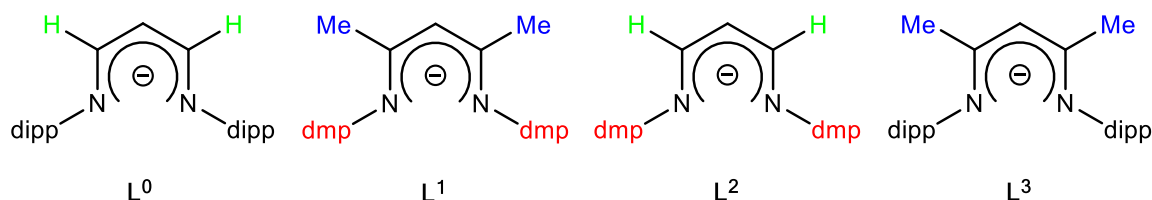


Figure S1. Used ligand systems L⁰, L¹, L² and L³, each containing an individual combination of backbone (H, Me) and aromatic substituents (dmp = 2,6-dimethylphenyl; dipp = 2,6-diisopropylphenyl).

Preparation of Precursor Complexes [LM(tol)] (L = L⁰, L¹, L², L³; M = Fe, Co)

Synthesis of [L¹Co(tol)] is published.^[4] Preparation of the related compound [L⁰Co(tol)] is reported using a different synthetic protocol.^[5] We synthesized the cobalt precursors [LCo(tol)] (L = L⁰, L¹, L², L³) according to related protocol previously published.^[6]

The iron precursors [LFe(tol)] (L = L¹, L², L³) were prepared according to previously published protocols.^[2] Compound [L⁰Fe(tol)] was analogously synthesized. Another related synthetic approach is published in the original literature.^[7]

Reactions of As₄ with the [LM(tol)] (L = L⁰, L¹, L², L³; M = Fe, Co) Precursors

All As₄ activations were **performed under rigorous exclusion of light** and following the two-step protocol presented hereafter:

1. Synthesis of yellow arsenic and its purification.
2. Addition of the [LM(tol)] precursor (L = L⁰, L¹, L², L³; M = Fe, Co).

A saturated solution of As₄ in toluene is generated according to modified literature procedure:^[8] Chunks of arsenic (3.4 – 8.0 g, vendor: abcr; 99.99%) were heated in a tubular furnace until complete sublimation. The yellow arsenic vapor, which formed inside the glass pipe, was continuously introduced (constant argon flow) into a flask filled with 250 mL toluene. The black precipitate, which formed during this procedure, was removed by filtration. The obtained filtrate was divided into a pair of equivalent portions and each was processed, successively, as follows: Each batch was cooled to approx. -95 °C to precipitate the yellow arsenic. Supernatant solution was decanted and the remaining yellow solid was degassed using several pump-flush cycles.

A solution of approx. 200 mg [LM(tol)] (L = L⁰, L¹, L², L³; M = Fe, Co) in approx. 10 mL toluene was added to the chilled yellow solid. The reaction mixture was stirred approx. 15–60 minutes at room temperature. Subsequently, the solvent was removed in vacuum and the dried solid was stored at

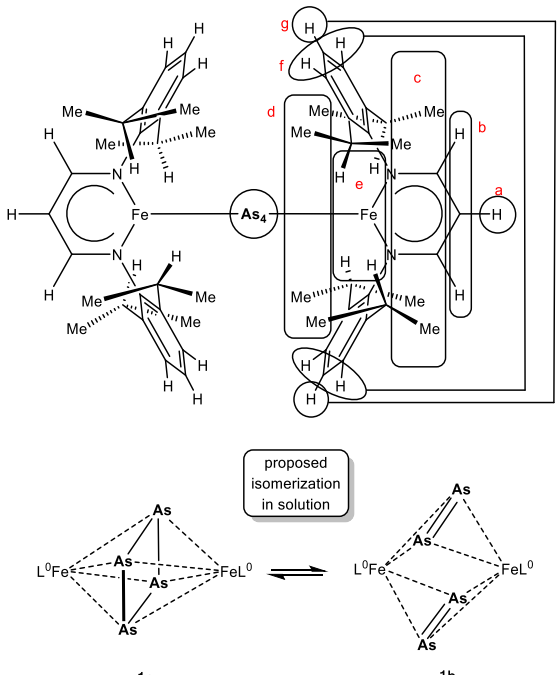
room temperature at least over night to forward the desired degradation of excessive, unreacted As₄ into As_{grey}. After dissolving the remaining solid in Et₂O or toluene, the insoluble grey arsenic was removed by filtration over celite. Samples of this crude solution were taken to perform the reaction control based on crude ¹H NMR spectroscopy and LIFDI mass spectrometry. The volume of the remaining solution was reduced and the solution was stored at 8 °C or -30 °C, respectively.

Synthesis of [(L⁰Fe)₂(μ-η⁴:η⁴-As₄)] (1a) and [(L⁰Fe)₂(μ-η²:η²-As₂)₂] (1b)

200 mg (0.372 mmol) [L⁰Fe(tol)] were dissolved in 8 mL toluene. The intense green solution was transferred into a freshly prepared load of As₄ (vide supra). The mixture was stirred at r.t. for 15 minutes. The solvent was removed in vacuum and the brownish black residue was stored at r.t. for approx. 8 weeks. After addition of 10 mL Et₂O, the solution was filtered over celite. Storing the solution at -30 °C yielded crystals of **1ab**.

Crystalline yield: 23.0 mg (0.019 mmol, 10%).

Analytical data:

<p>NMR of 1ab (C₆D₆, 300 K)</p>  <p>proposed isomerization in solution</p> <p>1a</p> <p>1b</p>	<p>¹H: δ [ppm] = 109.08 (4H, s, b), 8.14 (8H, d, ³J_{HH} = 8 Hz, f), 3.75 (24H, s, c/d), 1.11 (4H, t, ³J_{HH} = 7 Hz, g), -1.87 (24H, s, c/d), -2.02 (8H, s, e), -15.00 (2H, s, a).</p> <p>Measured range: 900 ppm to -900 ppm.</p> <p>¹H NMR spectrum is shown in Figure S15 (vide infra).</p>
<p>Mass spectrometry (LIFDI, toluene)</p> <p>prior to filtration (m/z: 200–2500)</p> <p>after filtration (m/z: 250–2500)</p>	<p>m/z: 1265.0 (46%) [M+As]⁺, 1190.1 (40%) [M]⁺, 1115.2 (100%) [M-As]⁺, 850.5 (25%) [(L⁰Fe)₂Fe(O)]⁺. A peak at m/z 1162.6 (20%) was not assigned.</p> <p>No observation of [M₂]⁺.</p> <p>m/z: 1265.1 (12%) [M+As]⁺, 1190.2 (46%) [M]⁺, 1115.2 (100%) [M-As]⁺, 924.5 (37%) [(L⁰Fe)₂(OH)₂]⁺, 906.5 (34%) [(L⁰Fe)₂(O)]⁺, 850.5 (8%) [(L⁰)₂Fe(O)]⁺, 834.5 (9%) [(L⁰)₂Fe]⁺, 390.3 (55%) [L⁰H]⁺.</p> <p>No observation of [M₂]⁺.</p>

Synthesis of [(L¹Fe)₄(μ₄-η¹:η¹:η¹:η¹:η¹:η¹-As₈)] (2)^[9]

This protocol was previously reported:^[9] 190 mg (0.419 mmol) [L¹Fe(tol)] were dissolved in 50 mL toluene and transferred into a freshly prepared As₄ solution in 250 mL toluene at r.t. (without further purification). The mixture was stirred at r.t. for 1 hour. The solvent was removed in vacuum. Toluene was added to the red-brown residue. After filtration over celite the volume was reduced. Storing the solution at 8 °C yielded crystals of **2** · 2.5 toluene.

Crystalline Yield: 20 mg (0.010 mmol, 9%).^[9]

Analytical data:

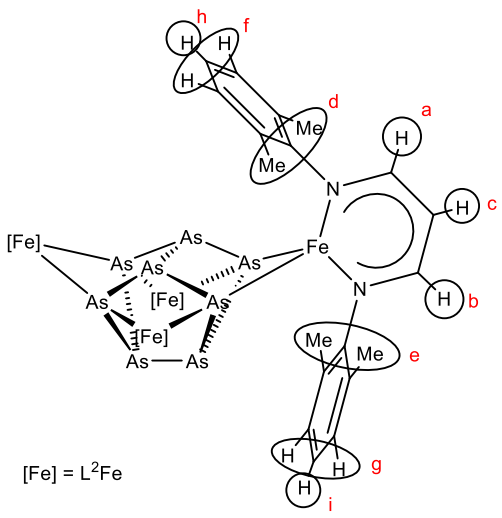
Elemental analysis (C ₈₄ H ₁₀₀ As ₈ Fe ₄ N ₈)	Calculated: C 52.18, H 5.25, N 5.03. ^[9] Found: C 52.40, H 5.58, N 4.99. ^[9]
Mass spectrometry (LIFDI, toluene)	m/z: 2043.7 (100%) [M] ⁺ . ^[9]

Synthesis of [(L²Fe)₄(μ₄-η¹:η¹:η¹:η¹:η¹:η¹-As₈)] (3)

200 mg (0.470 mmol) [L²Fe(tol)] were dissolved in 6 mL toluene. The intense green solution was transferred into a freshly prepared load of As₄ (vide supra). The mixture was stirred at r.t. for 15 minutes. The solvent was removed in vacuum and the brown residue was stored at r.t. for 24 hours upon addition of 25 mL Et₂O and 25 mL toluene. After filtration over celite the volume was reduced to a volume of 4 mL. Storing the solution at 8 °C yielded crystals of **3** · toluene.

Crystalline yield: 16.5 mg (0.008 mmol, 3%).

Analytical data:

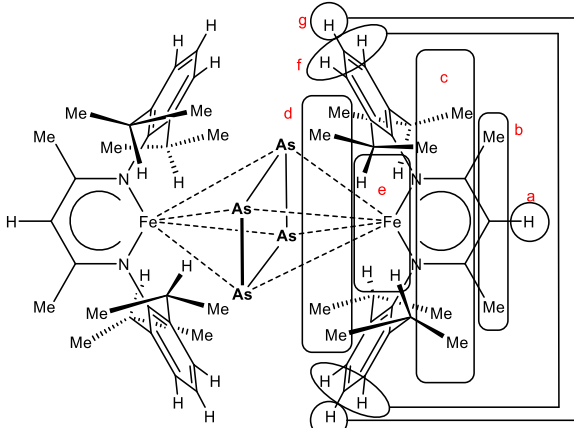
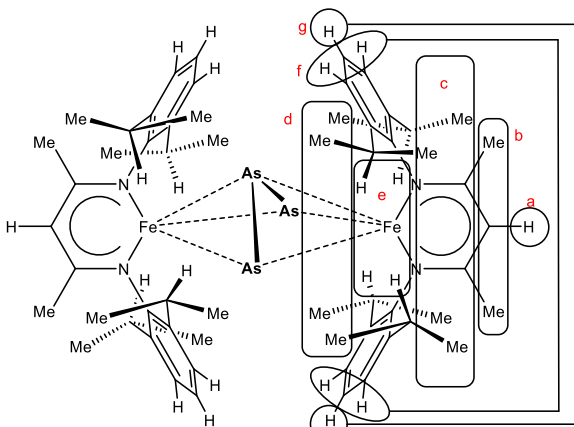
<p>NMR of 3 (C₆D₆, 300 K)</p>  <p>[Fe] = L²Fe</p>	<p>¹H: δ [ppm] = 311.15 (4H, s, <i>a/b</i>), 297.85 (4H, s, <i>a/b</i>), 14.44 (8H, s, <i>f/g</i>), 7.85 (8H, s, <i>f/g</i>), -3.55 (24H, s, <i>d/e</i>), -14.69 (24H, s, <i>d/e</i>), -17.38 (4H, s, <i>h/i</i>), -21.43 (4H, s, <i>c</i>), -22.82 (4H, s, <i>h/i</i>).</p> <p>Measured range: 720 ppm to -720 ppm. Signal assignment due to comparison of signal intensities in different ¹H NMR spectra. Due to low solubility of 3 in C₆D₆ the signal assignment of "<i>c</i>" is not assured.</p>
<p>Mass spectrometry (LIFDI, toluene) mother liquor (m/z: 250–2000)</p>	<p>m/z: 1931.8 (22%) [M]⁺, 610.3 (100%) [(L²)₂Fe]⁺, 278.2 (14%) [L²H]⁺. Also detected: m/z: 700.2 [(L²FeOH)₂]⁺, 1040.9 [(L²Fe)₂As₅]⁺. A signal at m/z 958.4 (7%) was not assigned. No observation of [₂^M]⁺.</p>

Synthesis of [(L³Fe)₂(μ-η⁴:η⁴-As₄)] (4a) and [(L³Fe)₂(μ-η³:η³-As₃)] (4b)

200 mg (0.354 mmol) [L³Fe(tol)] was dissolved in 8 mL toluene. The brown solution was transferred into a freshly prepared load of As₄ (vide supra). The mixture was stirred at r.t. for 15 minutes. The solvent was removed in vacuum and the brown black residue was stored at r.t. for approx. 2 days upon addition of 30 mL Et₂O. After filtration over celite the volume was reduced to a volume of 12 mL. Storing the solution at -30 °C yielded crystals of **4ab**.

Crystalline yield: 5.4 mg (approx. 0.004 mmol, approx. 2%).

Analytical data:

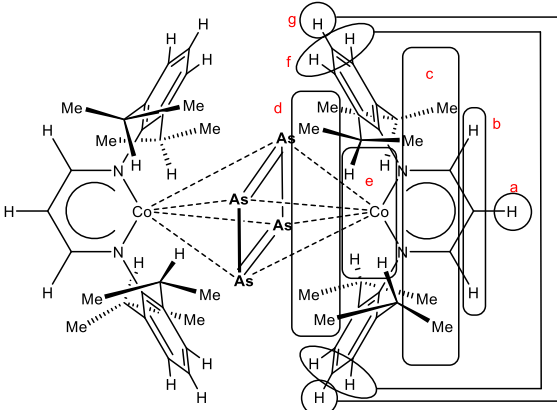
<p>NMR of 4a (C₆D₆, 300 K)</p> 	<p>¹H: δ [ppm] = 9.41 (12H, s, b), 7.81 (8H, s, f), 2.75 (24H, s, c/d), 0.98 (4H, s, g), approx. -2.49 (24H+8H, two overlapping s, c/d+e), -5.71 (2H, s, a).</p> <p>Measured range: 120 ppm to -120 ppm.</p> <p>¹H NMR spectrum is shown in Figure S16 (vide infra).</p>
<p>NMR of 4b (C₆D₆, 300 K)</p> 	<p>¹H: δ [ppm] = 7.95 (8H, d, ³J_{HH} = 6 Hz, f), 4.38 (2H, s, a), 3.87 (12H, s, b), 2.31 (24H, s, c/d), 0.57 (4H, t, ³J_{HH} = 7 Hz, g), -3.38 (24H, s, c/d), -4.97 (8H, s, e).</p> <p>Measured range: 120 ppm to -120 ppm.</p> <p>¹H NMR spectrum is shown in Figure S17 (vide infra).</p>
<p>Mass spectrometry (LIFDI, toluene)</p> <p>prior to filtration (m/z: 250–2500)</p> <p>crystals of 4b (m/z: 350–1500)</p>	<p>m/z: 1246.2 (27%) [M (4a)]⁺, 1171.3 (100%) [M-As (4b)]⁺, 980.5 (13%) [(L³FeOH)₂]⁺, 962.5 (17%) [(L³Fe)₂O]⁺, 418.3 (22%) [L³H]⁺.</p> <p>No observation of [M₂]⁺.</p> <p>m/z: 1171.2 (100%) [M (4b)]⁺, 1096.3 (3%) [M-As]⁺.</p>

Synthesis of [(L⁰Co)₂(μ-η⁴:η⁴-As₄)] (5)

Approx. 200 mg (0.37 mmol) [L⁰Co(tol)] were dissolved in 8 mL toluene. The intense reddish brown solution was transferred into a freshly prepared load of As₄ (vide supra). The mixture was stirred at r.t. for 15 minutes. The solvent was removed in vacuum and the brown residue was stored at r.t. for 2 days upon addition of 8 mL Et₂O. After filtration over celite the volume was reduced to a volume of 4 mL. Storing the solution at 8 °C yielded crystals of **5**.

Crystalline yield: 9.1 mg (0.04 mmol, 4%).

Analytical data:

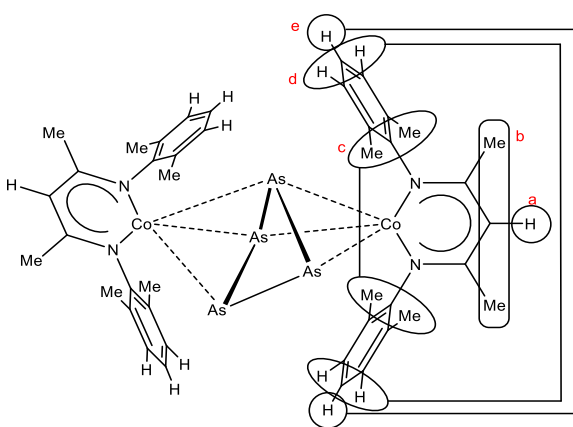
<p>NMR of 5 (C₆D₆, 300 K)</p> 	<p>¹H: δ [ppm] = 60.99 (4H, s, b), 13.97 (~8H, d, ³J_{HH} = 6 Hz, f), 4.24 (8H, s, e), 2.15 (~4H, t, ³J_{HH} = 6 Hz, g), 1.40 (24H, s, c/d), 1.03 (24H, s, c/d), -49.00 (2H, s, a).</p> <p>Measured range: 520 ppm to -120 ppm.</p> <p>¹H NMR spectrum is shown in Figure S18 (vide infra). Signal assignment due to comparison of signal intensities in different ¹H NMR spectra.</p>
<p>Mass spectrometry (LIFDI, toluene) microcrystalline solid (m/z: 200–2750)</p> <p>after filtration (m/z: 250–2550)</p>	<p>m/z: 1196.1 (100%) [M]⁺, 1121.2 (21%) [M-As]⁺. No observation of [M₂]⁺.</p> <p>m/z: 1196.1 (100%) [M]⁺, 1121.2 (21%) [M-As]⁺, 853.5 (<5%) [(L⁰)₂Co+O]⁺. No observation of [M₂]⁺.</p>

Synthesis of [(L¹Co)₂(μ-η³:η³-As₄)] (6)

278 mg (0.609 mmol) [L¹Co(tol)] was dissolved in 8 mL toluene. The intense reddish brown solution was transferred into a freshly prepared load of As₄ (vide supra). The mixture was stirred at r.t. for 15 minutes. The solvent was removed in vacuum and the brownish black residue was stored at r.t. for 1 month upon addition of 25 mL Et₂O. After filtration over celite the volume was reduced to a volume of 16 mL. Storing the solution at -30 °C yielded crystals of **6**.

Crystalline yield: 14.1 mg (0.014 mmol, 5%).

Analytical data:

<p>NMR of 6 (C₆D₆, 300 K)</p> 	<p>¹H: δ [ppm] = 14.68 (24H, s, c), 13.64 (8H, d, d), ³J_{HH} = 7 Hz, d), -6.75 (4H, t, ³J_{HH} = 7 Hz, e), -13.58 (12H, s, b), -14.88 (2H, s, a).</p> <p>Measured range: 520 ppm to -520 ppm.</p> <p>¹H NMR spectrum is shown in Figure S19 (vide infra).</p> <p>Note: The detected signals suggest <i>D</i>_{2h} or <i>D</i>_{2d} symmetry in solution.</p>
<p>Mass spectrometry (LIFDI, toluene) reaction mixture (m/z: 150–2300)</p> <p>after filtration (m/z: 250–2550)</p>	<p>m/z: 1028.1 (15%) [M]⁺, 953.1 (44%) [M-As]⁺, 685.4 (18%) [(L¹)₂Co+O]⁺, 669.4 (100%) [(L¹)₂Co]⁺.</p> <p>at elevated temperatures: m/z: 2056.1 (75%) [M₂]⁺, 1332.3 (20%) [(L¹Co)₂As₈+4H]⁺.</p> <p>m/z: 1028.0 (16%) [M]⁺, 953.1 (39%) [M-As]⁺, 762.3 (37%) [(L¹Co)₂(OH)₂]⁺, 685.4 (20%) [(L¹)₂Co+O]⁺, 669.4 (100%) [(L¹)₂Co]⁺, 306.2 (8%) [L¹H]⁺.</p>

Synthesis of [(L²Co)₂(μ-η⁴:η³-As₄)] (**7a**) and [(L²Co)₂(μ-η³:η³-As₃)] (**7c**) and

Synthesis of [(L²Co)₄(μ₄-η¹:η¹:η¹:η¹:η¹:η¹:η¹:η¹-As₈)] (**7b**)

The reaction was conducted two times (**A** and **B**).

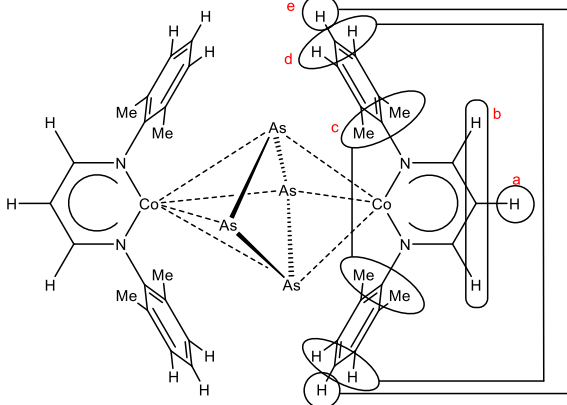
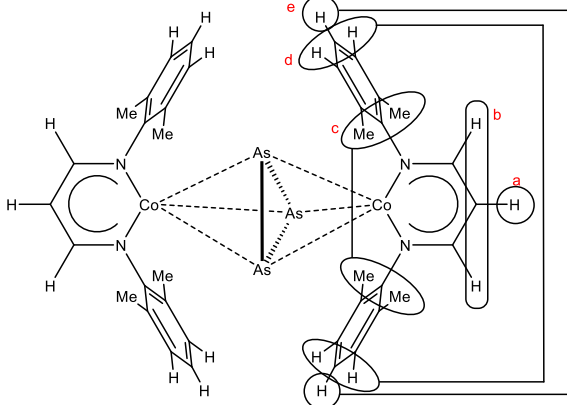
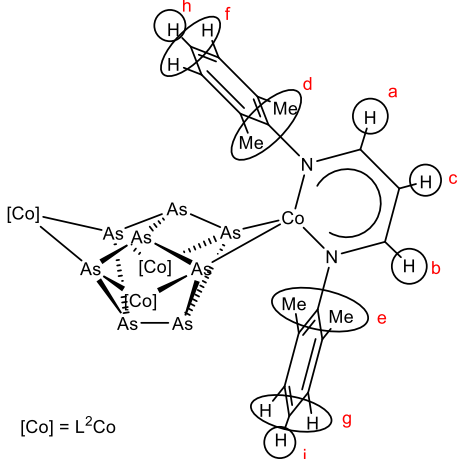
200 mg (0.467 mmol) [L²Co(tol)] was dissolved in toluene (**A**: 45 mL, **B**: 10 mL). The intense reddish brown solution was transferred into a freshly prepared load of As₄ (vide supra). The mixture was stirred at r.t. (**A**: 30 min; **B**: 13 min). The solvent was removed in vacuum and the brownish black residue was stored at r.t. (**A**: approx. 24 h; **B**: 4 weeks) upon addition of Et₂O (**A**: 15 mL; **B**: 8 mL). After filtration over celite the volume was reduced to a volume of 4 mL (**A**). Reaction control by ¹H NMR spectra display a mixture of different compounds (vide infra). Storing the solution (**A**: at 8 °C, **B**: at -30 °C) yielded crystals of **7ac** · Et₂O (**A**) and **7b** · Et₂O (**B**).

Crude ¹H NMR investigations:

Despite rigorous exclusion of light, air, water and elevated temperature, we failed to synthesize complexes **7a**, **7b** and **7c** in a selective manner. Separation by crystallization failed due to formation of the solid solution **7ac**. However, we put effort into suggesting a signal assignment for compounds **7a**, **7b** and **7c**: It is based on comparison of signal intensities in different crude ¹H NMR spectra. The ¹H NMR signal sets for **7a** and **7c** display relative signal intensities of 2/4/4/8/24 as expected for a relaxed dinuclear molecule conformation in solution (*D*_{2h} or *D*_{2d} symmetry). For **7b**, we suggest an assignment with intensity ratio of 4/4/4/4/8/8/24/24 as expected for *D*_{2d} symmetry in solution (vide similarity to signal set for previously reported [(L²Fe)₄P₈]^[2]). The ¹H NMR spectrum of handpicked **7b** crystals confirms the assignment of the high intensity signals (due to lacking solubility the low intensity signals were not detected).

Repeated measurements of the crude ¹H NMR sample after one day and their comparison reveals changed (increased and decreased) intensities of the signal sets, which the signal assignment of compounds **7a**, **7b**, **7c** are based on.

Analytical data:

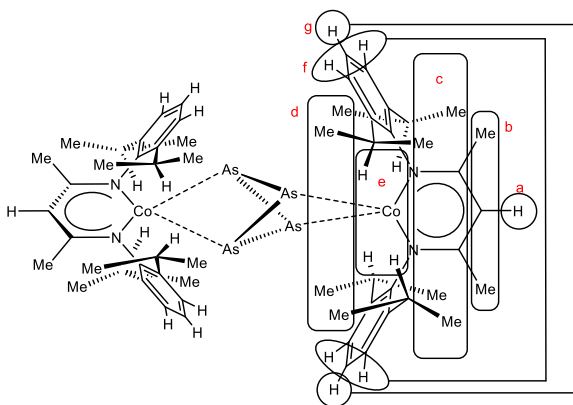
<p>NMR of 7a (C₆D₆, 300 K)</p> 	<p>¹H: δ [ppm] = 88.43 (4H, s, b), 12.64 (8H, d, ³J_{HH} = 7 Hz, d), 9.16 (24H, s, c), -1.03 (4H, t, ³J_{HH} = 7 Hz, e), -23.46 (2H, s, a).</p> <p>Assigned chemical shifts are based on crude ¹H NMR and are to understand as a suggestion.</p> <p>Note: The detected signals suggest <i>D</i>_{2h} or <i>D</i>_{2d} symmetry in solution.</p>
<p>NMR of 7c (C₆D₆, 300 K)</p> 	<p>¹H: δ [ppm] = 55.79 (4H, s, b), 6.37 (2H, s, a), 5.48 (8H, d, ³J_{HH} = 7 Hz, d), 2.66 (4H, t, ³J_{HH} = 7 Hz, e), -2.24 (24H, s, c).</p>
<p>NMR of 7b (C₆D₆, 300 K)</p>  <p>[Co] = L²Co</p>	<p>¹H: δ [ppm] = 192.09 (4H, s, a/b), 191.75 (4H, s, a/b), 12.47 (8H, d, ³J_{HH} = 7 Hz, f/g), 6.83 (8H, d, ³J_{HH} = 7 Hz, f/g), -3.40 (24H, s, d/e), -4.21 (4H, t, ³J_{HH} = 7 Hz, h/i), -7.52 (4H, t, ³J_{HH} = 7 Hz, h/i), -11.07 (4H, s, c), -11.80 (24H, s, d/e).</p>
<p>Mass spectrometry (LIFDI, toluene) after filtration (m/z: 500–2000)</p>	<p>m/z: 1944.0 (traces) [M₂ (7b)]⁺, 971.9 (3%) [M (7a)]⁺, 897.0 (100%) [M-As (7c)]⁺. A signal at m/z 944.5 (3%) was not assigned.</p>

Synthesis of [(L³Co)₂(μ-η¹:η¹:η¹-As₄)] (8)

200 mg (0.352 mmol) [L³Co(tol)] was dissolved in 8 mL toluene. The intense reddish brown solution was transferred into a freshly prepared load of As₄ (vide supra). The color of the reaction mixture changed to brown and the mixture was stirred at r.t. for 1 hour. The solvent was removed in vacuum and the brown residue was stored at r.t. for 1 week upon addition of 15 mL Et₂O. After filtration over celite the volume was reduced to a volume of 5 mL. Storing the solution at -30 °C yielded crystals of **8** · Et₂O. Additional crops of crystals were obtained from the mother liquor.

Crystalline yield: 78.9 mg (0.176 mmol, 36%).

Analytical data:

<p>NMR of 8 (C₆D₆, 300 K)</p> 	<p>¹H: δ [ppm] = 10.47 (8H, d, ³J_{HH} = 7 Hz, f), 3.30 (8H, s, e), 2.05 (24H, s, c/d), 0.59 (24H, s, c/d), 0.08 (2H, s, a), -4.64 (4H, t, ³J_{HH} = 7 Hz, g), -5.92 (12H, s, b).</p> <p>Measured range: 520 ppm to -520 ppm.</p> <p>¹H NMR spectrum is shown in Figure S20 (vide infra).</p>
<p>Evans-NMR (300 K, C₆D₆)</p>	<p>μ_{eff} = 2.68 μ_B</p>
<p>Elemental analysis (C₅₈H₈₂As₄Co₂N₄)</p>	<p>Calculated: C 55.60, H 6.60, N 4.47. Found: C 55.74, H 6.56, N 4.28.</p>
<p>Mass spectrometry (LIFDI, toluene)</p> <p>crude solution (m/z: 150–1750)</p> <p>crystals (m/z: 250–2750)</p>	<p>m/z: 1252.2 (100%) [M]⁺, 1177.3 (29%) [M-As]⁺, 986.5 (14%) [(L³Co)₂(OH)₂]⁺.</p> <p>m/z: 1252.3 (100%) [M]⁺, 1177.4 (47%) [M-As]⁺. No observation of [M₂]⁺.</p>

Crystallographic Details

Single crystal X-ray structure analyses were performed using Rigaku Oxford Diffraction (formerly Agilent Technologies) CCD diffractometers GV-50, Titan^{S2} CCD (**1ab**, **3** · toluene, **4ab**, **5**, **6**, **7ac** · Et₂O, **8** · Et₂O), Gemini Ultra Ruby CCD (**2** · 2.5 toluene) and SuperNova Atlas CCD (**7b** · Et₂O). Data reduction was performed with the CrysAlisPro^[10] software package. Using the software Olex2^[11] the structure solution was carried out using the programs ShelXT^[12] (Sheldrick, 2015) (**1ab**, **2** · 2.5 toluene, **3** · toluene, **4ab**, **5**, **7b** · Et₂O, **7ac** · Et₂O, **8** · Et₂O) or Superflip^[13] (**6**). Least squares refinements on F_o² were performed using SHELXL-2014^[14] (Version 2016/6) (**1ab**, **2** · 2.5 toluene, **3** · toluene, **4ab**, **5**, **6**, **7b** · Et₂O, **7ac** · Et₂O, **8** · Et₂O).

Crystallographic data and details of the diffraction experiments **1ab**, **2** · 2.5 toluene, **3** · toluene, **4ab**, **5**, **6**, **7ac** · Et₂O, **7b** · Et₂O and **8** · Et₂O are given in Table S3 and Table S4.

Selected molecular structures (**3**, **8**, **6**, **7a**, **5**, **1b**, **4b** and **7c**) are shown in main part of this work. Additionally, molecular structures of compounds **2** · 2.5 toluene, **3** · toluene, **7b** · Et₂O and **8** · Et₂O are depicted in Figures S2–S5. Special details for X-ray diffraction experiments on structures **1ab**, **4ab**, **5**, **6** and **7ac** · Et₂O are given below.

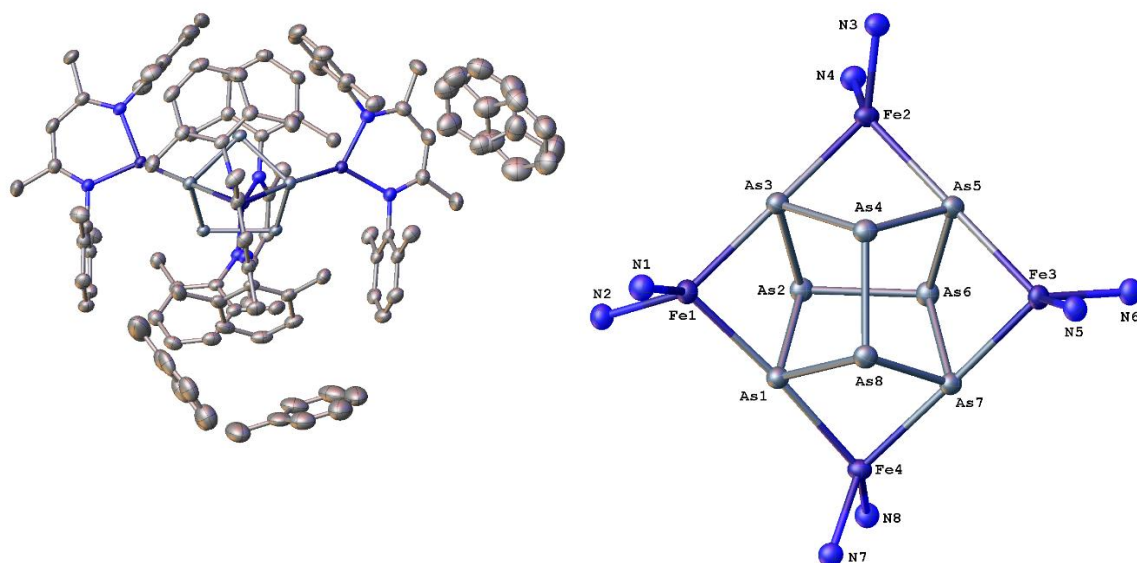


Figure S2. Molecular structure of compound **2** in crystals of **2** · 2.5 toluene (left) and a representation of its core structure (right). Hydrogen atoms are omitted for clarity. Thermal ellipsoids are drawn at 50% probability level.

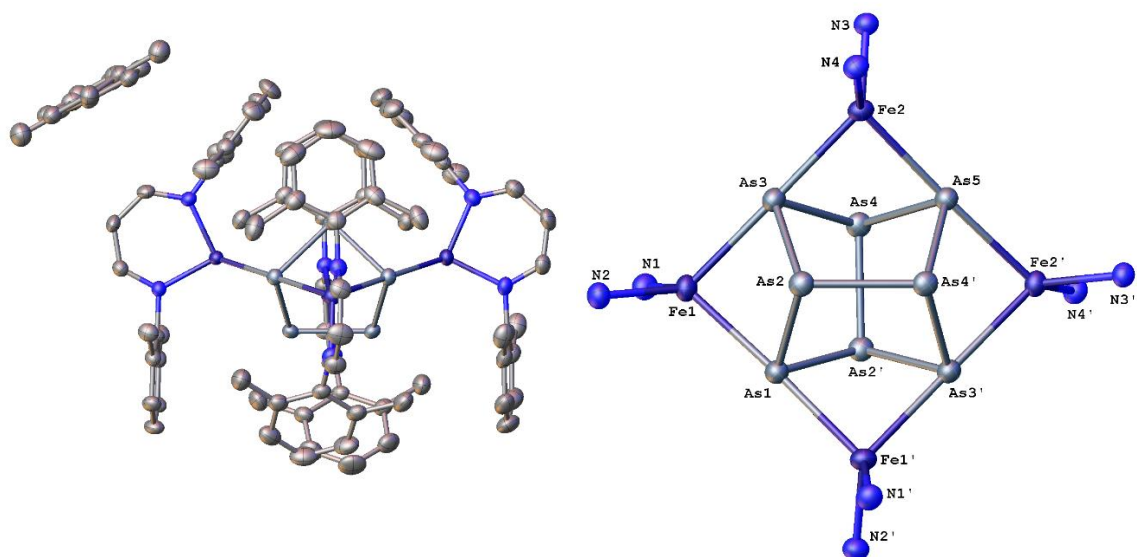


Figure S3. Molecular structure of compound **3** in crystals of **3** · toluene (left) and a representation of its core structure (right). Hydrogen atoms are omitted for clarity. Thermal ellipsoids are drawn at 50% probability level.

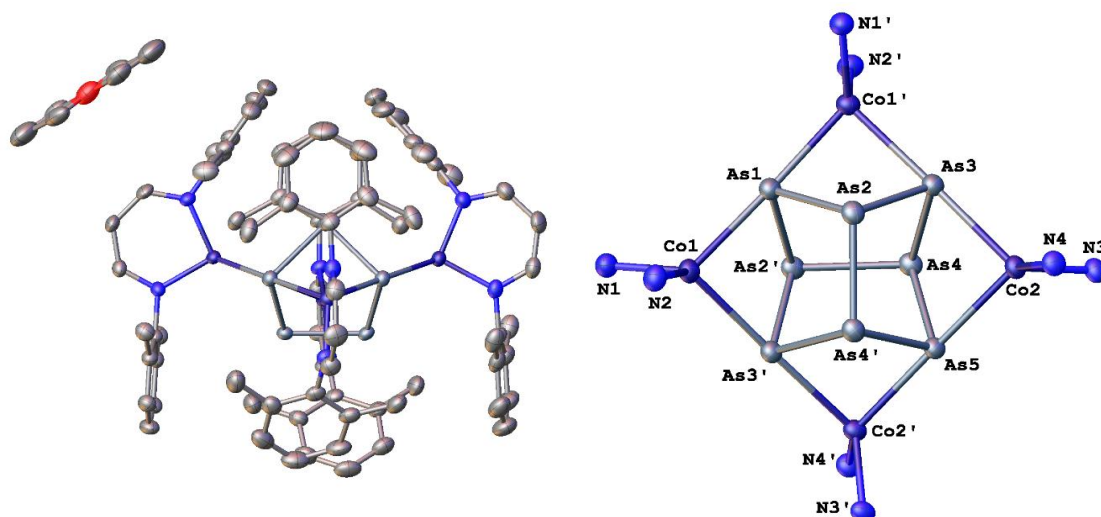


Figure S4. Molecular structure of compound **7b** in crystals of **7b** · Et₂O (left) and a representation of its core structure (right). Hydrogen atoms are omitted for clarity. Thermal ellipsoids are drawn at 50% probability level.

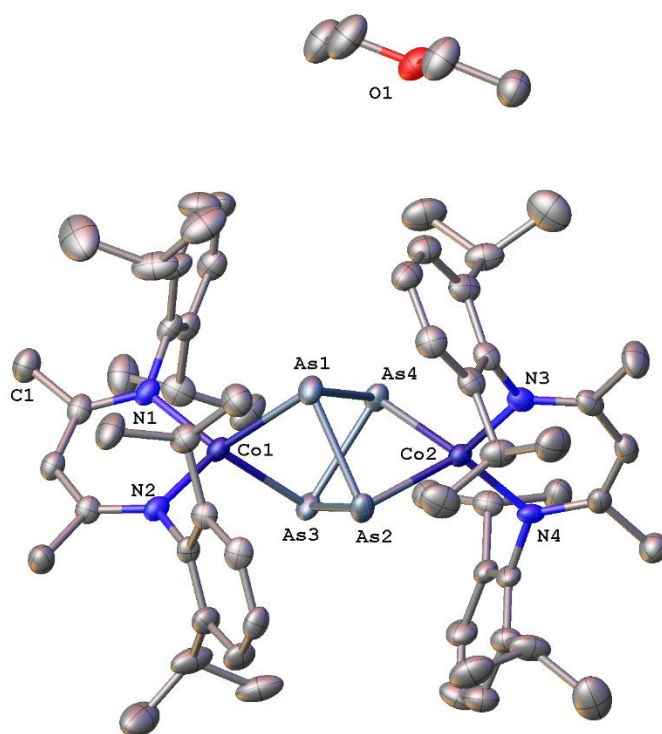


Figure S5. Molecular structure of compound **8** in crystals of **8** · Et₂O. Hydrogen atoms are omitted for clarity. Thermal ellipsoids are drawn at 50% probability level.

X-ray Diffraction on Crystals of **1ab**

The solid state structure **1ab** contains two crystallographic positions, each providing space for a [(L⁰Fe)₂As_n] molecule with its unique L⁰ ligand environment. Each molecule adopts an individual ligand conformation (Table S1) and therefore being crystallographically distinguishable. The centrosymmetric molecules consist of two [L⁰Fe] fragments, which are bridged by distinct As_n moieties. The first position in **1ab** is fully occupied by compound [(L⁰Fe)₂(μ-η⁴:η⁴-As₄)] (**1a**) containing a *cyclo*-As₄ moiety. The second position contains a mixture of two different complexes [(L⁰Fe)₂(μ-η²:η²-As₂)₂] (**1b**) and [(L⁰Fe)₂(μ-η⁴:η⁴-As₄)] (**1a'**). The latter **1a'** is comparable to **1a** concerning the structural parameters of the L⁰ ligand conformation, the Fe...Fe' distance and their *cyclo*-As₄ moieties (vide infra, Table S1). In contrast, complex **1b** contains a pair of bridging As₂ ligands and a significantly decreased Fe...Fe' distance compared to **1a** and **1a'**.

Interestingly, crystallization temperature influences the isomer distribution of **1a'** and **1b** determined in the solid state. Crystals obtained at 8°C (FS265) display a **1b**:**1a'** ratio of 77:23, whereas crystals obtained at -30°C (FS294) display a **1b**:**1a'** ratio of 36:64.

Table S1. Comparison of structural parameters obtained for compounds **1a**, **1a'** and **1b** in X-ray diffraction experiment 'FS265' and 'FS294' (internal naming).

Crystals of batch 'FS265'	1a (100%)	1a' (23%)	1b (77%)
$d(\text{As}-\text{As}) / [\text{\AA}]$	2.4276(7)	2.391(18)	2.2414(13)
$d(\text{As}-\text{As}') / [\text{\AA}]$	2.4423(6)	2.451(8)	3.314
$d(\text{Fe}\cdots\text{Fe}') / [\text{\AA}]$	3.787	3.834	2.940
$\Theta / [^\circ]$	17.5(1)	15.2(9)	25.2(2)
$\omega / [^\circ]$	3.69(6)	6.9(7)	0.4(2)
$\Phi / [^\circ]$	0	0	0

Crystals of batch 'FS294'	1a (100%)	1a' (64%)	1b (36%)
$d(\text{As}-\text{As}) / [\text{\AA}]$	2.4285(7)	2.475(3)	2.256(5)
$d(\text{As}-\text{As}') / [\text{\AA}]$	2.4329(7)	2.493(3)	2.861
$d(\text{Fe}\cdots\text{Fe}') / [\text{\AA}]$	3.788	3.924	3.120
$\Theta / [^\circ]$	18.4(1)	14.4(3)	21.8(8)
$\omega / [^\circ]$	4.66(6)	13.1(2)	7.2(4)
$\Phi / [^\circ]$	0	0	0

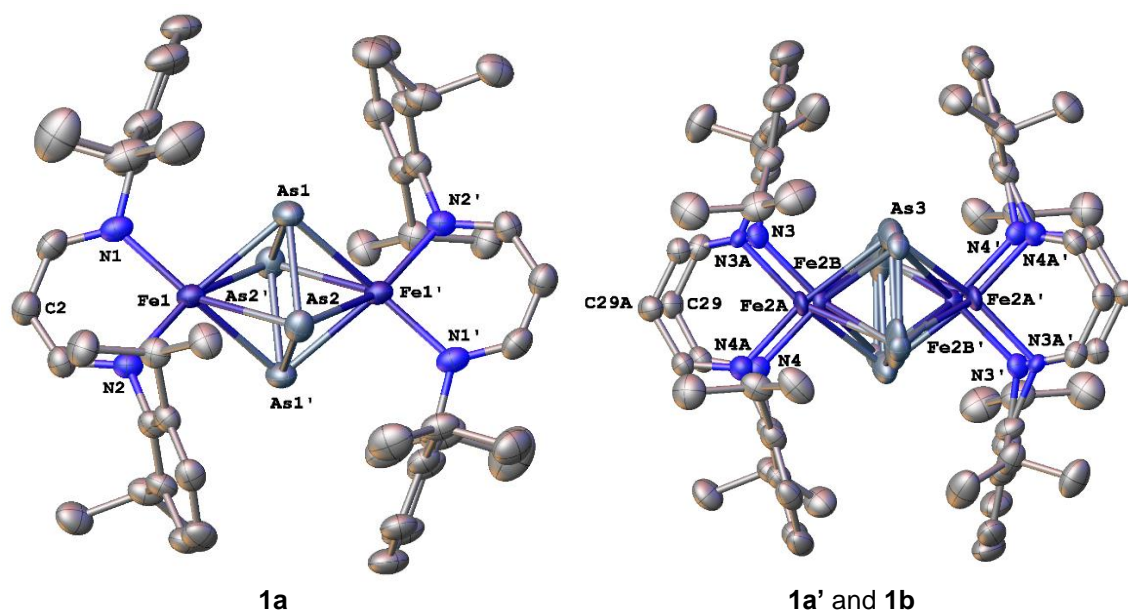


Figure S6. Overview of both distinguishable crystallographic positions in the solid solution **1ab** (in 'FS265'). Left: Ordered fully occupied position of complex **1a**. Right: Superposition of complex **1a'** (isomeric to **1a**) and **1b**. Hydrogen atoms are omitted for clarity. Thermal ellipsoids are drawn at 50% probability level.

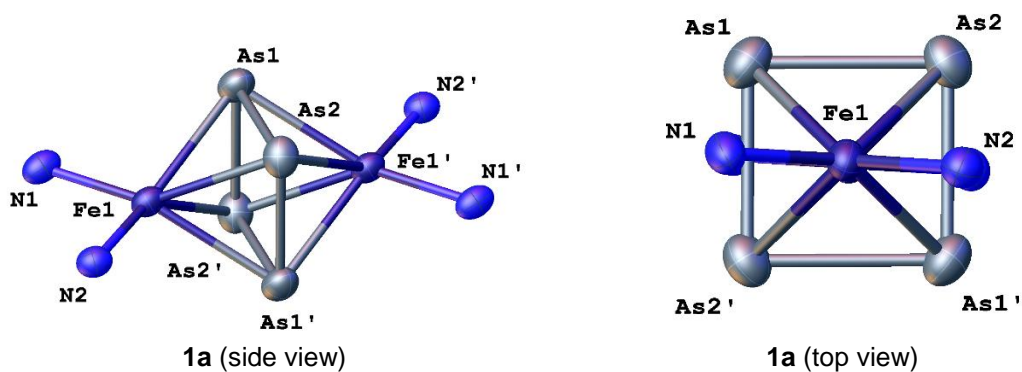


Figure S7. Central complex core in compound **1a** (fully occupied position). Data originate from diffraction experiment 'FS265'. Carbon and hydrogen atoms are omitted for clarity.

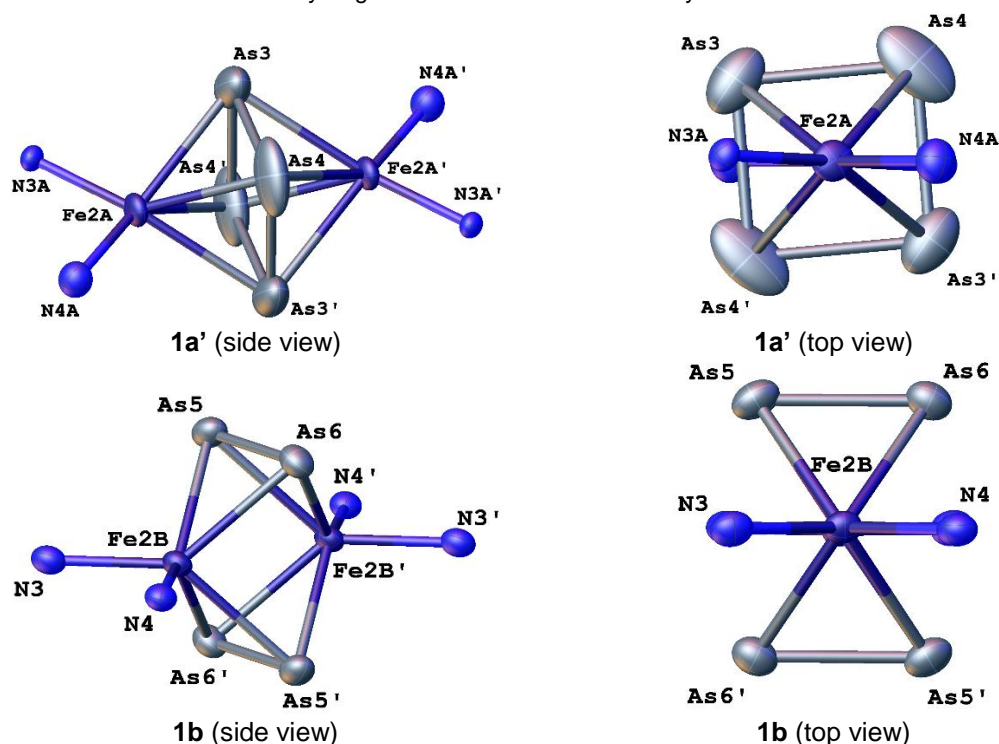


Figure S8. Central core representation of superposing compounds (**1a'**, 23%, upper part) and (**1b**, 77%, lower part). Data originate from diffraction experiment 'FS265'. Carbon and hydrogen atoms are omitted for clarity.

X-ray Diffraction on Crystals of **4ab**

The single crystal X-ray diffraction measurement was performed at 123 K. After this experiment the crystal was allowed to reach room temperature. This was followed by a slow cooling procedure (20K/hour) to a final temperature of 123 K at which the crystal spontaneously underwent a (kinetically hindered) phase transition.

X-ray diffraction of **4ab** at 123 K reveals a two component solid solution (Figure S9): The major component $[(L^3Fe)_2(\mu-\eta^4:\eta^4-As_4)]$ (**4a**) (78% occupation) contains a *cyclo*-As₄ middle deck (Figure S10, top). The minor component $[(L^3Fe)_2(\mu-\eta^3:\eta^3-As_3)]$ (**4b**) (2x 11% occupation) contains a *catena*-As₃ unit, which is disordered over two distinct positions (Figure S10, bottom). Compound **4b** represents a possible degradation product of **4a**, which is not separated by crystallization.

An ISOR restraint was used on the arsenic atoms for calculation of minor *catena*-As₃ unit (2x 11%) in compound **4b**. Additionally two ISOR restraints were used in two different disordered *iPr* groups (42:58, each) of the ligand L³.

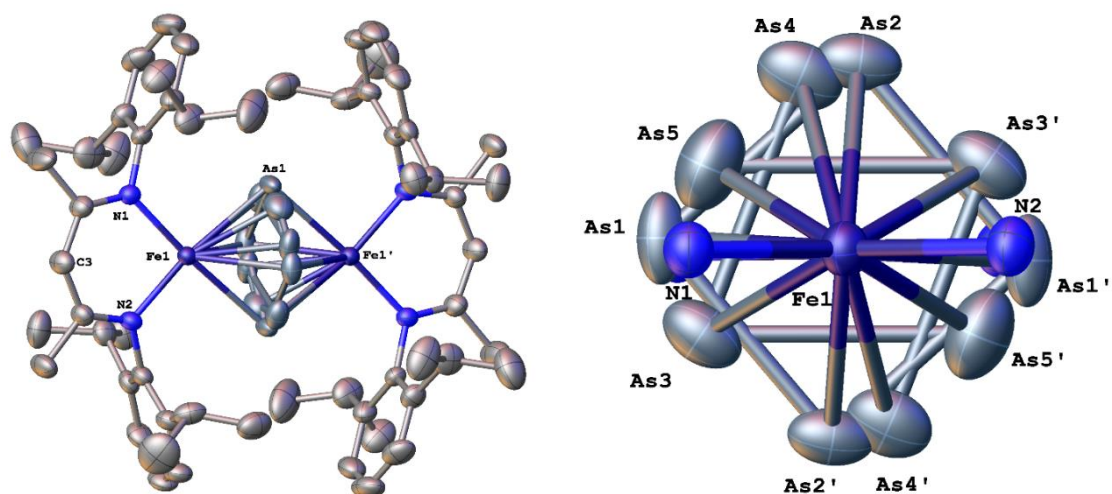


Figure S9. Solid solution of compounds **4a** (major) and **4b** (minor) in the solid solution **4ab**; Side view (left) and enlarged top view presentation (right) of their middle decks. Hydrogen atoms are omitted for clarity. Thermal ellipsoids are drawn at 50% probability level.

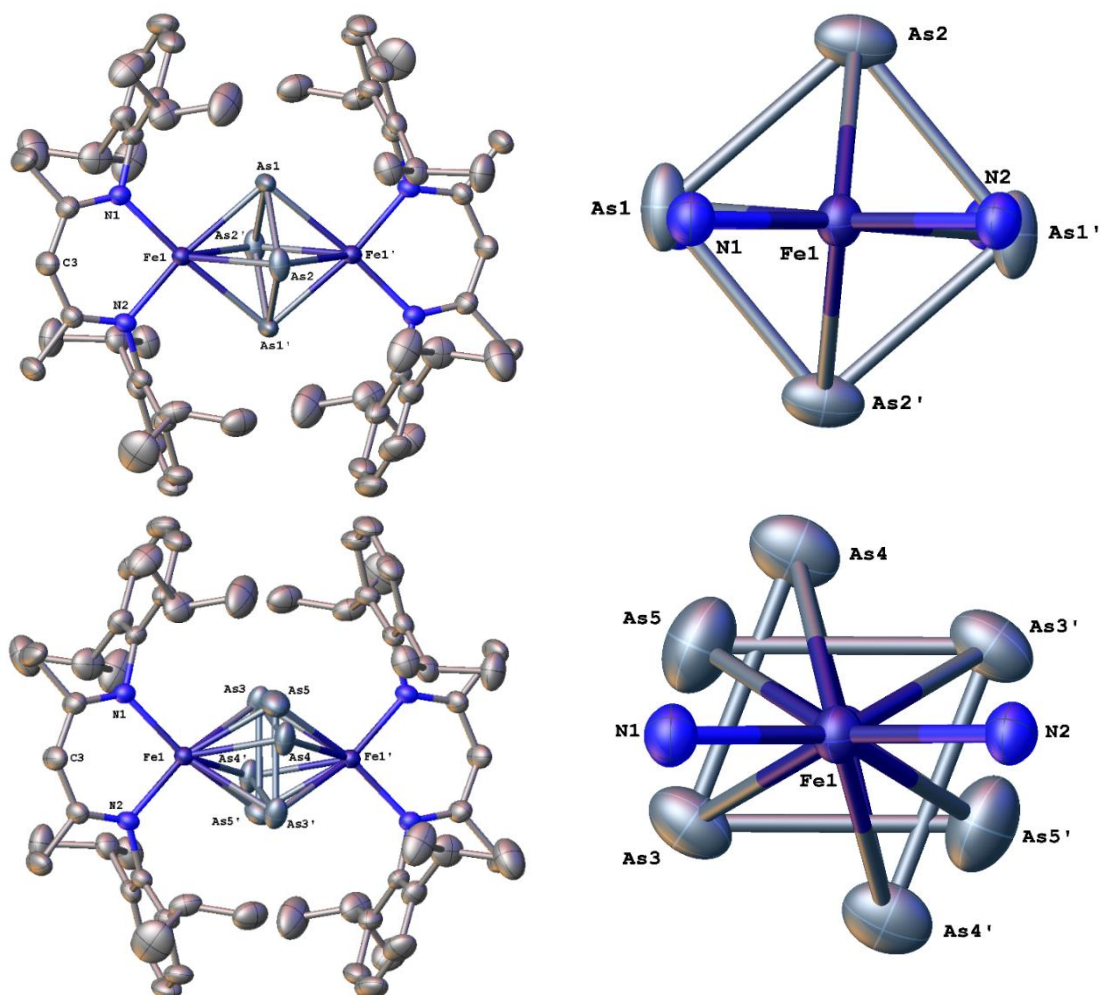


Figure S10. Top: Major component (78%, compound **4a**) in solid solution **4ab**. Bottom: Minor component (2x 11%, compound **4b**) in solid solution **4ab**. Side view presentation (left) and enlarged top view presentation (right) of their *cyclo*-As₄ or *catena*-As₃ middle decks, respectively. Hydrogen atoms are omitted for clarity. Thermal ellipsoids are drawn at 50% probability level.

X-ray Diffraction on Two Crystal Batches of 5

For characterization of compound **5**, crystals from two separately executed reactions were investigated by single crystal X-ray diffraction. The molecular structure consists of centrosymmetric, dinuclear [L⁰Co] complexes with a different distribution of bridging middle decks. In both crystal batches, the major component is [(L⁰Co)₂(μ-η⁴:η⁴-As₄)] (**5**). Complex **5** contains a *cyclo*-As₄ ligand, which was obtained in 94% and 79% refined occupancy in experiment 'FS258_As4' or 'FS253' (internal naming), respectively. There is no significant deviation within the geometric parameters of this bridging *cyclo*-As₄ units in both structures (Table S2). We tried to assign the residual electron density to a chemical reliable solution (see contour plane in Table S2). The LIFDI mass spectrum of microcrystalline **5** shows a peak for [M-As]⁺. Therefore, a superposed As₃ ligand complex should be considered as minor component in both crystal batches. However, all attempts failed to assign the remaining electron density to a As₃-, As₂- or oxygen containing middle deck.

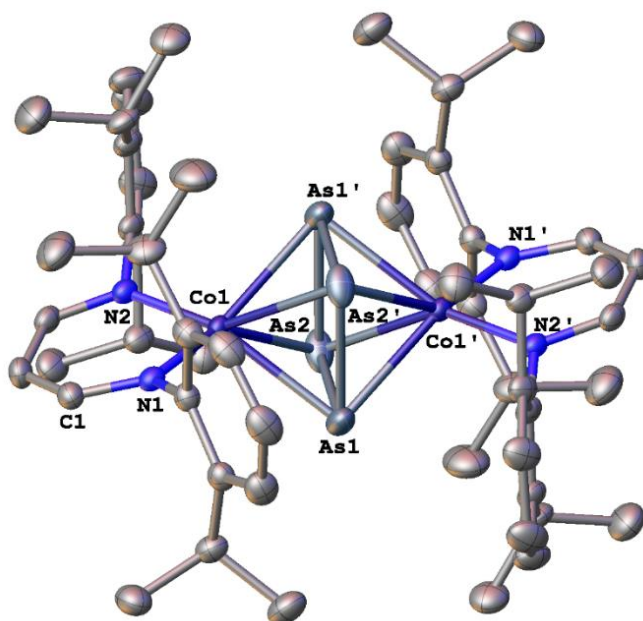


Figure S11. Molecular structure of compound **5** in the crystal. Hydrogen atoms are omitted for clarity. Thermal ellipsoids are drawn at 50% probability level.

Table S2. Contour plane of the residual electron distribution in the 'As₄ ligand'-plane of compound **5** obtained in two different X-ray diffraction experiments.

<p>Major <i>cyclo</i>-As₄ component: refined occupancy: 94% in data set 'FS258_As4' <i>d</i>(As-As) = 2.330, 2.489 Å</p>	<p>Major <i>cyclo</i>-As₄ component: refined occupancy: 79% in data set 'FS253' <i>d</i>(As-As) = 2.329, 2.487 Å</p>

X-ray Diffraction on Crystals of **6**

The crystal structure of compound $[(L^1Co)_2(\mu-\eta^3:\eta^3-As_4)]$ reveals an equivalent of two isomers **6** and **6'**, each displaying distinguishable ligand conformations (Figure S12). Each isomer consists of two $[L^1Co]$ fragments and a bridging As_4 moiety, which coordinates in a distinct $\eta^3:\eta^3$ -fashion. The disordered dmp groups of the L^1 ligands are refined using several SADI, FLAT, SIMU, RIGU and ISOR restraints.

The X-ray diffraction was conducted on crystals of **6**, which exclusively were obtained as two component twin. Two different measurements 'FS295' and 'FS295_2' (internal naming) were conducted, however exclusively 'FS295_2' is discussed herein. Analysis of the diffraction pattern shows similar orientation of the twin components (Cell constant c^* equals diagonal between cell constants a^* and b^*). The integration of the diffraction pattern (approx. 25% overlapping reflections) was conducted with the program CrysAlisPro (version 171.38.43).^[1] The resulting unique data were written to HKLF5, which was applied in the final structure refinement resulting in satisfying R_1 and wR_2 values. Remaining residual electron density within the complex core of both isomers has not been assigned to a chemical relevant interpretation. ¹H NMR spectra of crystalline **6** confirm its isomerization in solution and exclude chemical relevant quantities of L^1 containing impurities.

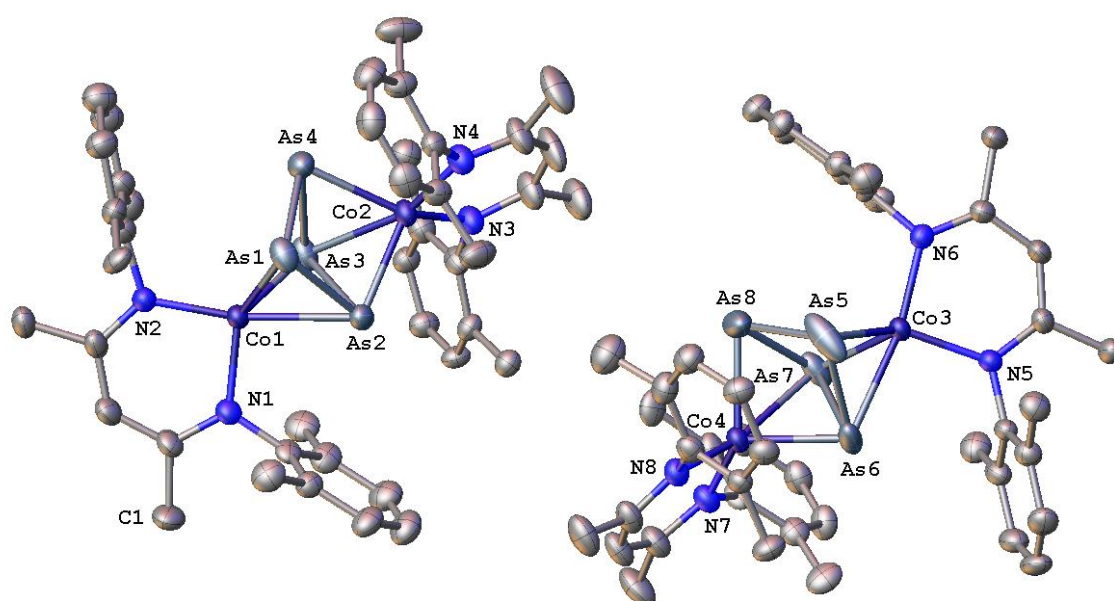


Figure S12. Molecular structure of compounds $[(L^1Co)_2(\mu-\eta^3:\eta^3-As_4)]$ (**6** and **6'**) in the crystal, each displaying a distinguishable conformation. Hydrogen atoms and the disordered dmp groups are omitted for clarity. Thermal ellipsoids are drawn at 50% probability level.

X-ray Diffraction on Crystals of **7ac** · Et₂O

The single crystal X-ray diffraction measurement of **7ac** · Et₂O at 123 K reveals one disordered Et₂O molecule and two individual isomers $[(L^2Fe)_2(\mu-\eta^3:\eta^3-As_3)]$ (**7c** and **7c'**) in two distinguishable conformations (Figure S13). Both isomers contain a *cyclo*-As₃ middle deck. The position of isomer **7c'** is superposed by a minor (5% occupation) component $[(L^2Fe)_2(\mu-\eta^4:\eta^3-As_4)]$ (**7a**), which is integrated in Figure S13 (right side). We interpret **7a** as precursor of compounds **7b** or **7c**, respectively. A representation of the minor component **7a** and selected bond lengths within the bridging As_4 ligand is depicted in Figure S14.

A SIMU restraint was used in refinement of the arsenic atoms in isomer **7c'** and compound **7a**. Isomer **7c** contains one disordered dmp group which was refined to a chemical occupancy of 19:81 using geometrical restraints (SADI-, FLAT-, SIMU-, RIGU- and ISOR). One Et₂O solvent molecule is disordered over two positions (33:67). Geometrical restraints (EADP and DFIX) were used for its modelling and refinement.

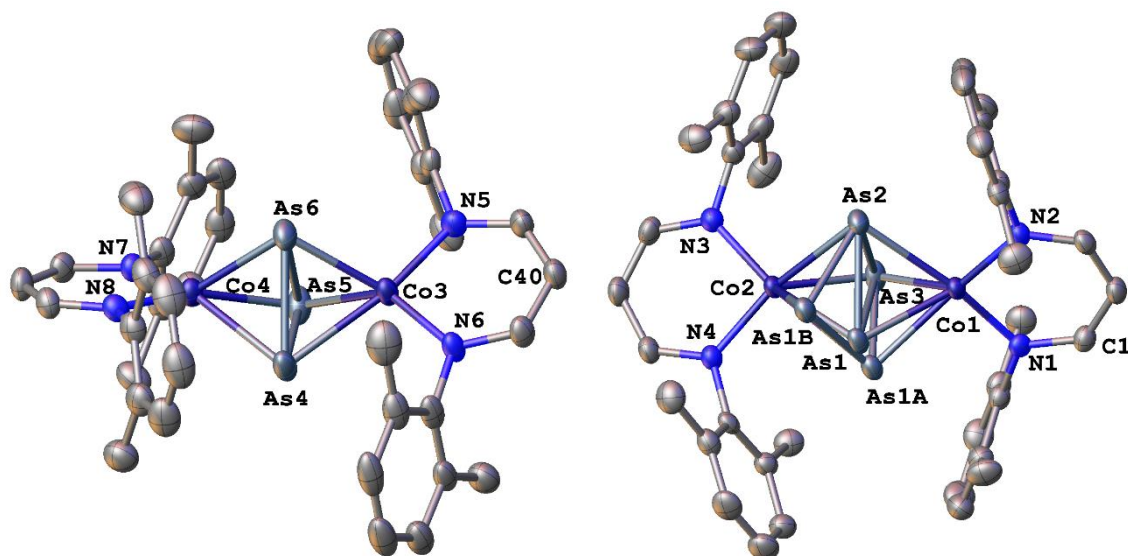


Figure S13. Left: Side view presentation of compound **7c** in the solid solution **7ac** · Et₂O. Right: Isomer **7c'** and superposing **7a** (minor component). Hydrogen atoms and Et₂O molecules are omitted for clarity. Thermal ellipsoids are drawn at 50% probability level.

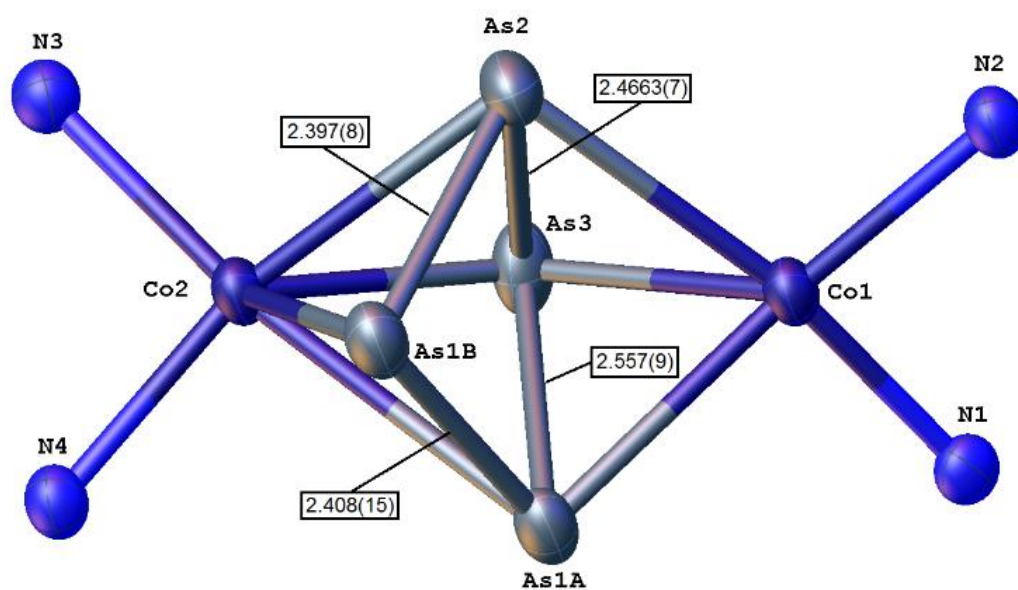


Figure S14. Core structure of compound **7a** (5% component) in the solid solution **7ac** · Et₂O. Hydrogen and carbon atoms are omitted for clarity. Thermal ellipsoids are drawn at 50% probability level. Bond lengths are given in Å.

Table S3. Crystallographic data and details of diffraction experiments for **1ab**, **2** · 2.5 toluene, **3** · toluene and **4ab**.

Compound	1ab	2 · 2.5 toluene ^[15]	3 · toluene	4ab
Data set (internal naming)	FS265_abs	cg357_calc_abs	FS283#1_calc_abs	FS284WH2_calc_mP_abs
Formula	C ₅₄ H ₇₄ As ₄ Fe ₂ N ₄	C _{101.5} H ₁₂₀ As ₈ Fe ₄ N ₈	C ₈₃ H ₉₂ As ₈ Fe ₄ N ₈	C ₅₈ H ₈₂ As _{3.775} Fe ₂ N ₄
$\rho_{calc.}/g\ cm^{-3}$	1.451	1.527	1.625	1.408
μ/mm^{-1}	7.246	7.957	9.439	6.698
Formula Weight	1190.55	2274.81	2024.40	1229.79
Color	dark brown	dark red	dark black	dark black
Shape	block	block	block	block
Size/mm ³	0.10×0.08×0.04	0.32×0.17×0.12	0.14×0.12×0.11	0.34×0.25×0.20
<i>T</i> /K	123(1)	123.00(14)	123(1)	123(1)
Crystal System	triclinic	triclinic	monoclinic	monoclinic
Space Group	<i>P</i> 1	<i>P</i> 1	<i>C</i> 2/ <i>c</i>	<i>P</i> 2 ₁ / <i>n</i>
<i>a</i> /Å	13.2431(6)	13.60288(12)	24.8828(7)	14.2884(2)
<i>b</i> /Å	13.9354(8)	14.75365(14)	12.9874(3)	13.60190(10)
<i>c</i> /Å	16.0383(7)	26.0325(2)	26.3513(7)	15.3559(2)
$\alpha/^\circ$	89.203(4)	82.1763(8)	90	90
$\beta/^\circ$	87.031(4)	76.4461(8)	103.716(3)	103.8790(10)
$\gamma/^\circ$	67.239(5)	78.1144(8)	90	90
<i>V</i> /Å ³	2725.6(2)	4948.88(8)	8272.9(4)	2897.28(6)
<i>Z</i>	2	2	4	2
<i>Z'</i>	1	1	0.5	0.5
Wavelength/Å	1.54184	1.54184	1.54184	1.54184
Radiation type	Cu K α	Cu K α	Cu K α	Cu K α
$\Theta_{min}/^\circ$	2.759	3.396	3.453	3.797
$\Theta_{max}/^\circ$	74.322	66.512	74.607	74.815
Measured Refl.	45715	32388	22193	53667
Independent Refl.	10933	16930	8197	5889
Reflections Used	9491	16065	6357	5807
<i>R</i> _{int}	0.0600	0.0245	0.0447	0.0319
Parameters	666	1215	571	365
Restraints	60	495	456	30
Largest Peak	1.448	0.920	0.577	0.796
Deepest Hole	-1.080	-0.593	-0.636	-0.922
GooF	1.056	1.034	1.014	1.043
<i>wR</i> ₂ (all data)	0.1461	0.0754	0.0732	0.0933
<i>wR</i> ₂	0.1385	0.0743	0.0667	0.0931
<i>R</i> ₁ (all data)	0.0568	0.0295	0.0541	0.0355
<i>R</i> ₁	0.0498	0.0279	0.0346	0.0352

Table S4. Crystallographic data and details of diffraction experiments for **5**, **6**, **7b** · Et₂O, **7ac** · Et₂O and **8** · Et₂O.

Compound	5	6	7b · Et ₂ O	7ac · Et ₂ O	8 · Et ₂ O
Data set (internal naming)	FS258_As4_abs	FS295_2_abs3_t win1_hklf4	FS286_exp_199_c alc_abs	FS254_As3_abs	FS230_abs
Formula	C ₅₄ H ₇₄ As _{3.765} Co ₂ N ₄	C ₄₂ H ₅₀ As ₄ Co ₂ N ₄	C ₈₀ H ₉₄ As ₈ Co ₄ N ₈ O	C ₄₀ H ₄₇ As _{3.025} Co ₂ N ₄ O _{0.5}	C ₆₂ H ₉₂ As ₄ Co ₂ N ₄ O
ρ_{calc} / g cm ⁻³	1.466	1.646	1.649	1.560	1.380
μ /mm ⁻¹	7.740	10.067	10.272	9.571	6.676
Formula Weight	1179.10	1028.40	2018.71	936.31	1326.93
Color	dark black	dark black	dark brown	dark black	dark brown
Shape	plate	block	plate	plate	block
Size/mm ³	0.25x0.13x0.07	0.15x0.10x0.07	0.19x0.13x0.04	0.24x0.15x0.04	0.50x0.25x0.16
<i>T</i> /K	123.00(10)	122.99(13)	123(1)	123(1)	123(1)
Crystal System	monoclinic	triclinic	monoclinic	triclinic	orthorhombic
Space Group	<i>C2/c</i>	<i>P1</i>	<i>C2/c</i>	<i>P1</i>	<i>P2₁2₁2₁</i>
<i>a</i> /Å	21.9496(3)	12.3273(5)	24.9097(9)	11.9394(2)	14.03210(10)
<i>b</i> /Å	15.5419(2)	18.4149(5)	12.7779(3)	18.2854(3)	14.25110(10)
<i>c</i> /Å	15.6672(2)	20.2510(4)	26.2880(9)	21.0048(4)	31.9359(4)
α /°	90	100.038(2)	90	64.956(2)	90
β /°	91.7360(10)	99.456(3)	103.589(4)	74.984(2)	90
γ /°	90	109.244(3)	90	77.839(2)	90
<i>V</i> /Å ³	5342.23(12)	4150.4(2)	8133.1(5)	3985.89(14)	6386.31(10)
<i>Z</i>	4	4	4	4	4
<i>Z'</i>	0.5	2	0.5	2	1
Wavelength/Å	1.54184	1.54184	1.54184	1.54184	1.54184
Radiation type	Cu K α	Cu K α	Cu K α	Cu K α	Cu K α
Θ_{min} /°	3.485	2.281	3.459	3.859	3.396
Θ_{max} /°	73.577	74.181	74.278	73.627	74.201
Measured Refl.	14921	27603	41274	75483	44802
Independent Refl.	5200	27603	8178	15806	12727
Reflections Used	4981	22643	7550	14191	12438
<i>R</i> _{int}	0.0291	.	0.0615	0.0446	0.0542
Parameters	299	1395	477	1000	680
Restraints	0	1233	0	236	0
Largest Peak	2.213	2.341	0.842	1.972	1.527
Deepest Hole	-0.604	-1.161	-1.016	-1.528	-1.089
GooF	1.032	1.076	1.080	1.030	1.078
<i>wR</i> ₂ (all data)	0.0964	0.2200	0.1086	0.1141	0.1478
<i>wR</i> ₂	0.0953	0.2029	0.1050	0.1104	0.1472
<i>R</i> ₁ (all data)	0.0375	0.0809	0.0407	0.0505	0.0531
<i>R</i> ₁	0.0361	0.0708	0.0377	0.0453	0.0524
Flack Parameter					-0.004(2)
Hooft Parameter					-0.0224(15)

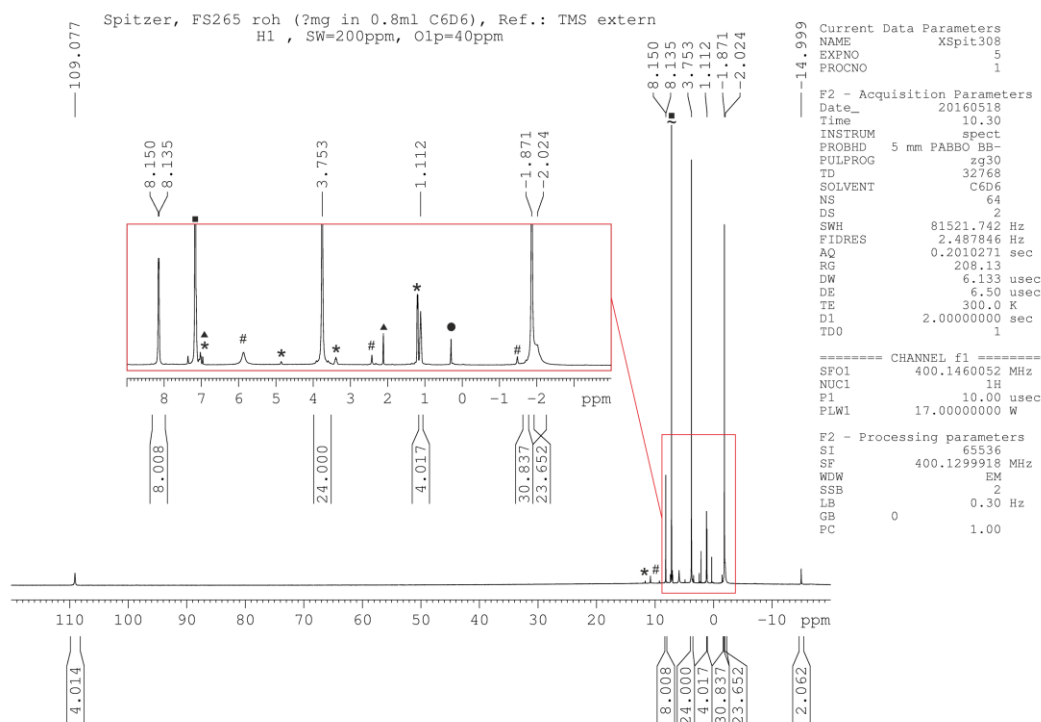
¹H NMR Spectra

Figure S15. ¹H NMR spectrum of **1ab** in C₆D₆. Signals for the solvent (■) and silicon grease (●) are marked. Additionally, signals of an unknown impurity (#), toluene (▲) and L⁰H (*) are highlighted.

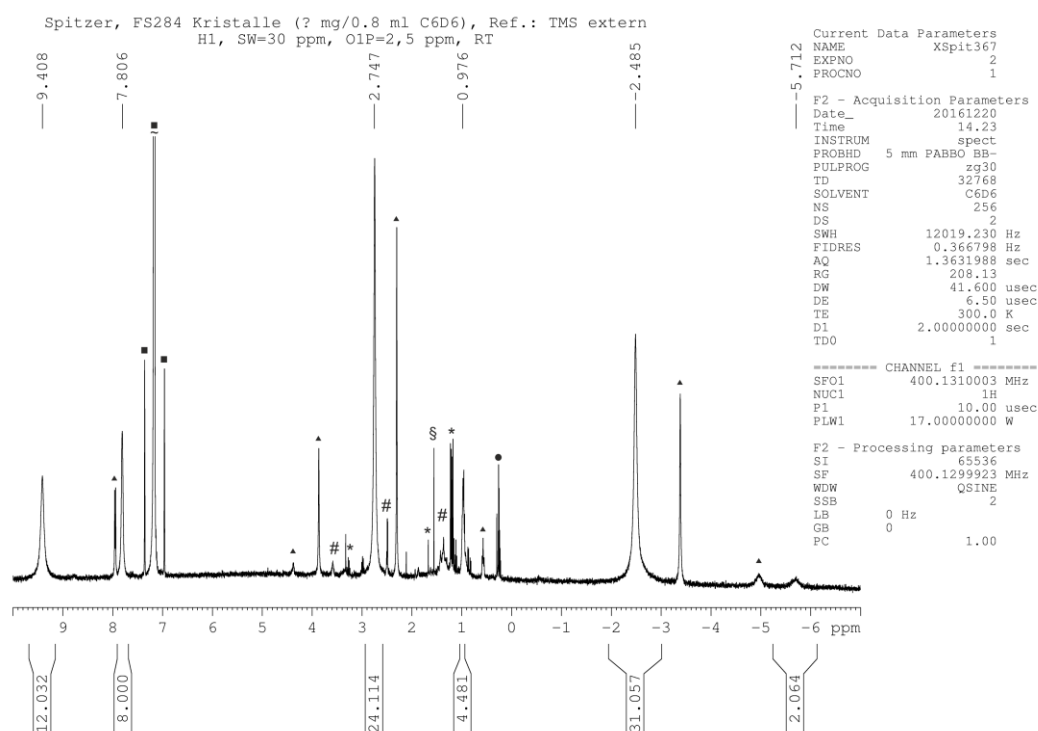


Figure S16. ¹H NMR spectrum of **4a** in C₆D₆. Signals for the solvent (■) and silicon grease (●) are marked. Additionally, signals of impurities are highlighted: **4b** (▲), H₂O (§), L³H (*) and an unknown product (#).

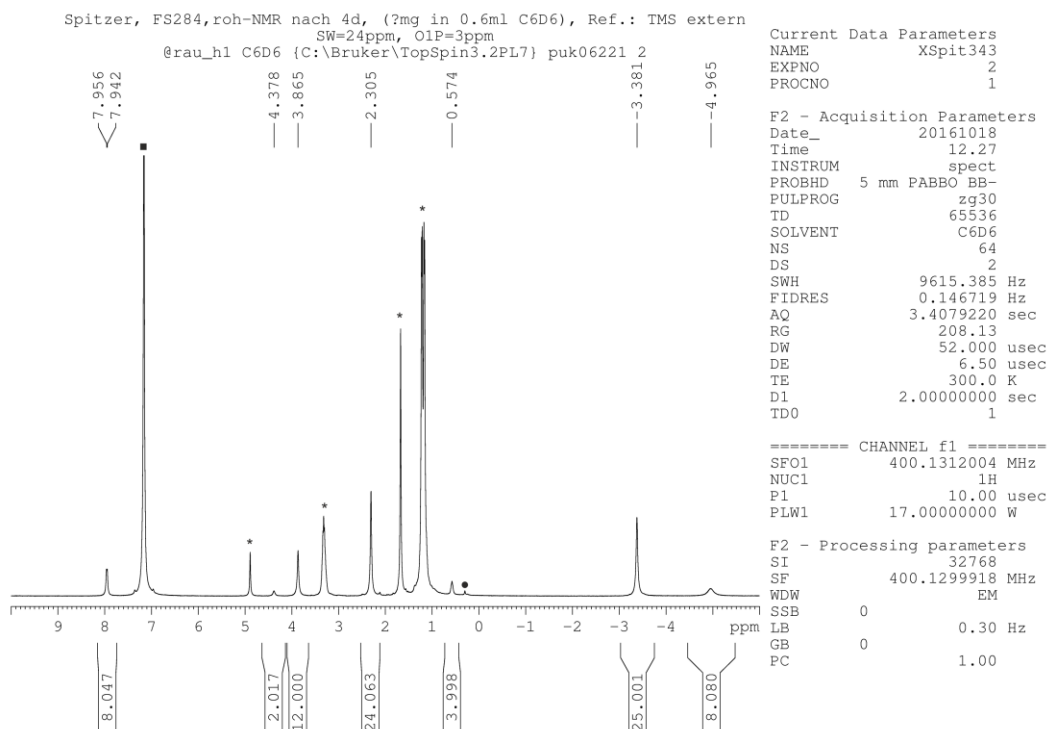


Figure S17. ¹H NMR spectrum of **4b** in C₆D₆. Signals for the solvent (■) and silicon grease (●) are marked. Additionally, signals of L³H (*) are highlighted.

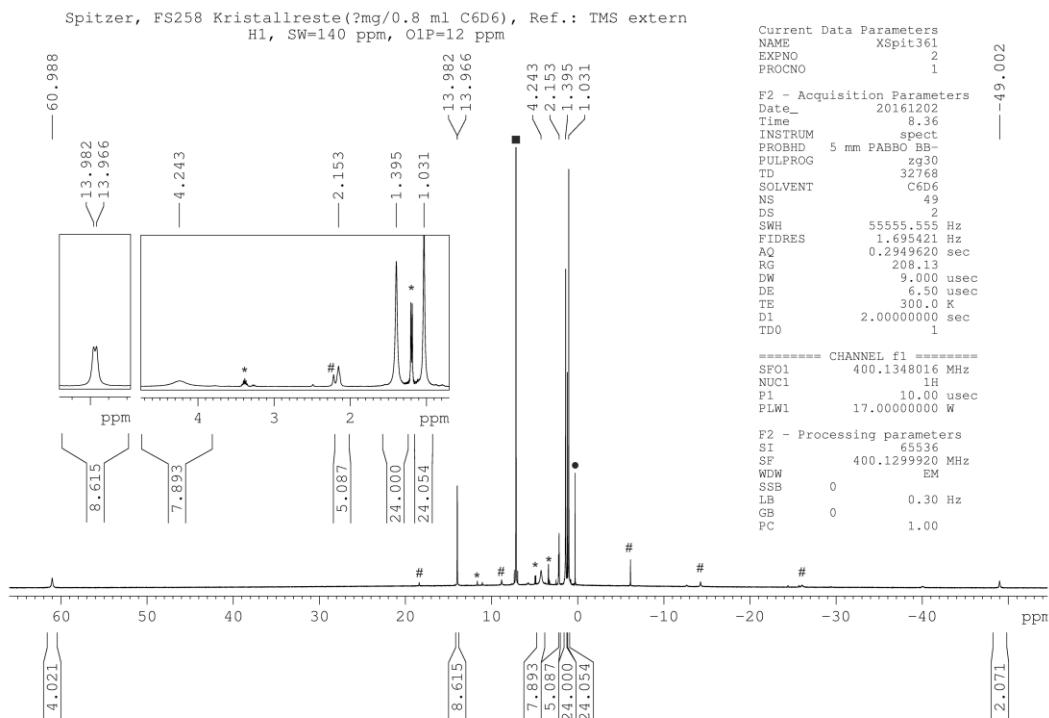


Figure S18. ¹H NMR spectrum of **5** in C₆D₆. Signals for the solvent (■) and silicone grease (●) are marked. Additionally, signals of an unknown impurity are highlighted (#).

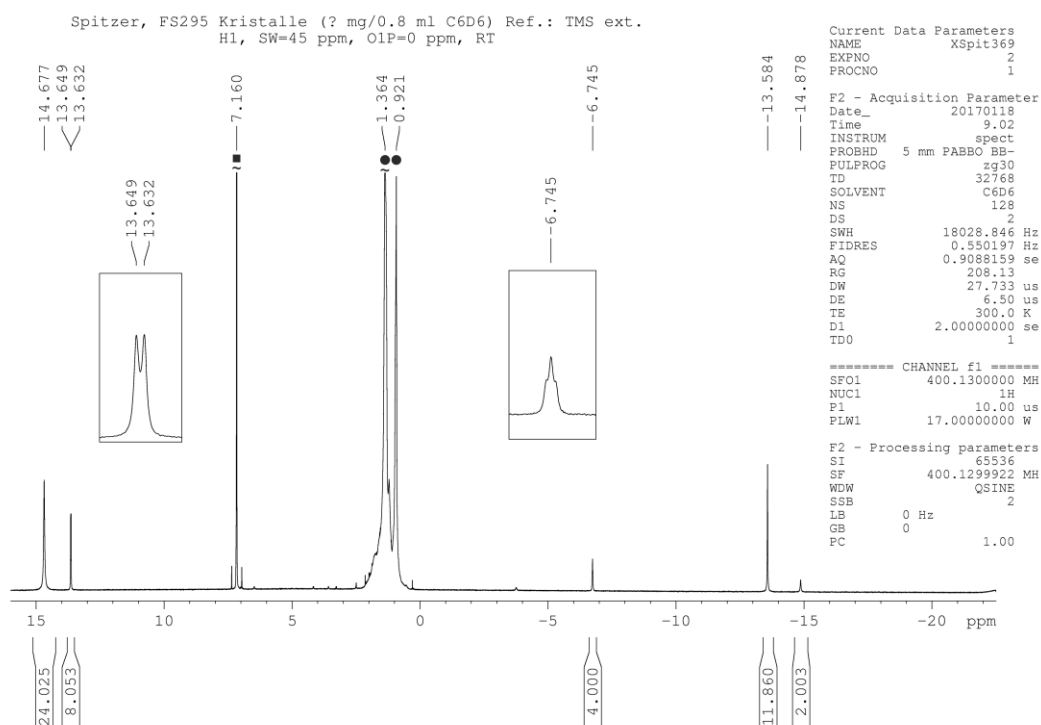


Figure S19. ¹H NMR spectrum of **6** in C₆D₆. The crystalline sample of **6** was stored under mineral oil and washed with *n*-hexane prior to dissolving in C₆D₆ for the NMR measurement. Signals for the solvent (■) and remaining mineral oil (●) are marked.

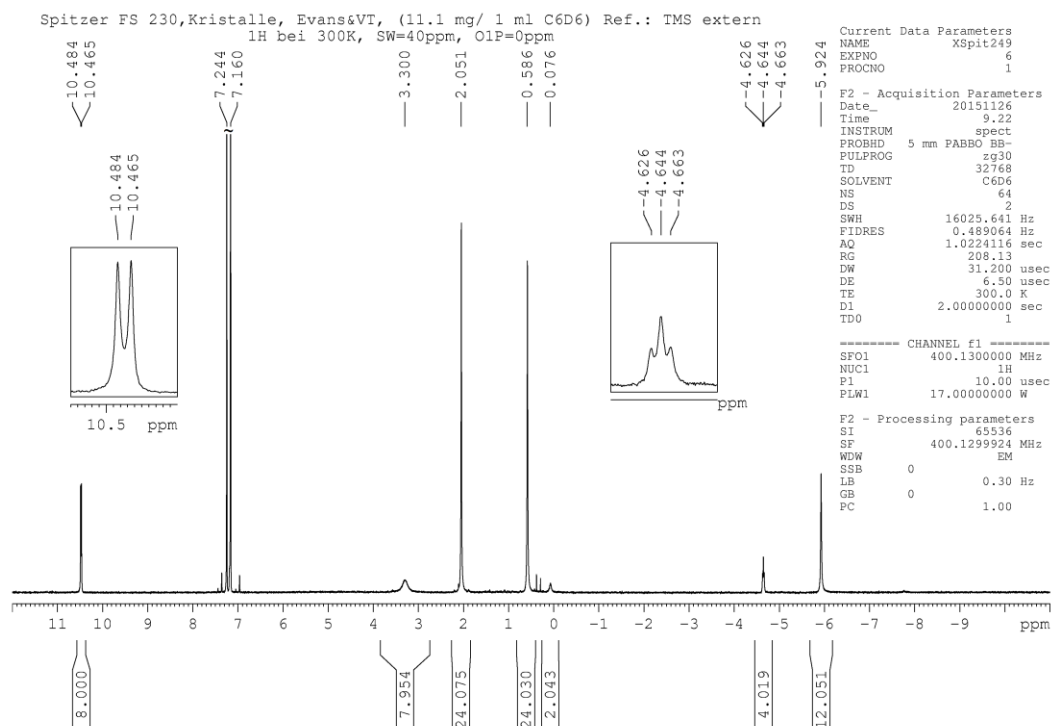


Figure S20. ¹H NMR spectrum of **8** in C₆D₆. Two solvent signals are detected due to performance of Evans method.

DFT Calculations

The geometry optimizations have been performed with the TURBOMOLE program package^[16] at the RI^[17]-BP86^[18]/def-SVP^[19] level of theory. To speed up the geometry optimization, the Multipole Accelerated Resolution-of-the-Identity (MARI-J)^[20] approximation has been used. For the calculation of relative energies, the SCF energies were used. For the Potential Energy Scan (PES) along the Co...Co coordinate, a restricted geometry optimization was performed in which only the Co...Co distance was fixed, and all other parameters were freely optimized.

To investigate the effect of the functionals on the energy difference between the unrestricted singlet and triplet spin states, single point calculations with the functionals BP86, B3LYP,^[18a-d,21] PBE0^[18a-b,22] and B97-D^[23] have been performed on the BP86/def2-TZVP optimized geometry in the above mentioned spin states. The results are summarized in Table S5.

Table S5. Relative energy of the constrained optimized geometries of [(L⁰Co)₂(As₄)] in different spin states at the RI-BP86/def-SVP level of theory. Only the Co...Co distances were fixed, all other parameters were freely optimized.

Co...Co distance (Å)	Unrestricted Singlet (kJ·mol ⁻¹)	Triplet (kJ·mol ⁻¹)	Quintet (kJ·mol ⁻¹)
2.4769	125.08	163.8	184.01
2.6203	105.51	129.0	164.06
2.7690	97.31	101.4	146.59
2.9175	94.67	83.8	134.30
3.0702	87.14	72.6	127.54
3.2190	68.82	66.7	116.15
3.3672	49.36	64.7	87.34
3.5189	29.01	49.4	69.09
3.6668	18.54	21.5	49.70
3.8176	7.99	9.3	61.93
3.9677	2.22	3.6	46.54
4.1170	0.00	2.6	51.10
4.2675	0.60	5.9	59.59
4.4165	0.02	2.4	45.54
4.5663	0.02	2.2	45.55
4.7163	8.28	23.3	39.49
4.8661	9.59	25.6	30.67
5.0161	13.36	28.1	27.32
5.1661	19.26	30.9	27.80

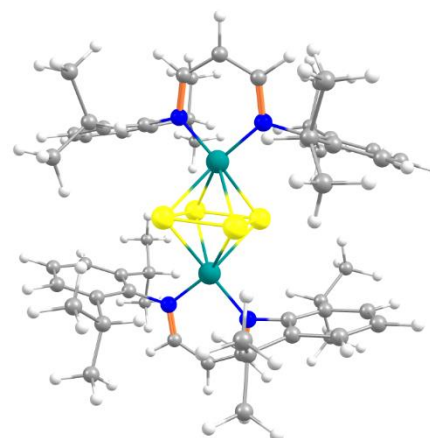
Table S6. Relative energy (kJ·mol⁻¹) of [(L⁰Co)₂(As₄)] in different spin states calculated using different DFT functionals. (nc = SCF did not converge)

Functional	unrestricted singlet	triplet	quintet
BP86	32.31	0.00	60.89
B3LYP	27.96	0.00	-0.55
PBE0	-4.25	0.00	-39.40
B97-D	64.67	0.00	nc

Table S7. Cartesian coordinates of the optimized geometry of $[(L^0Co)_2(As_4)]$ in unrestricted singlet spin state at the RI-BP86/def2-TZVP level of theory. Total energy = -14033.23410032 ha.

Atom	x	y	z
As	-1.1078740	1.3014393	0.2871521
As	0.0444235	-0.1813175	1.7231492
As	-0.0445196	0.1811903	-1.7231729
Co	1.3858717	1.1761849	0.1026499
Co	-1.3858777	-1.1761703	-0.1026693
As	1.1080234	-1.3013416	-0.2871466
N	3.0487279	1.1657885	1.0834079
N	1.6800075	2.9298823	-0.6488971
H	2.6986162	1.6727469	-2.4715141
N	-3.0487766	-1.1657052	-1.0833351
N	-1.6800048	-2.9299224	0.6487751
H	-2.6986446	-1.6730596	2.4715282
C	3.8333901	2.2334568	1.2449171
C	3.6038303	-0.0306168	1.6887078
C	0.8928199	3.4637711	-1.7446626
C	2.6460263	3.7637853	-0.2575473
C	2.4914841	2.2744431	-3.3703748
C	-3.8334684	-2.2333441	-1.2448923
C	-3.6038657	0.0307547	-1.6885251
C	-0.8927786	-3.4639189	1.7444610
C	-2.6460492	-3.7637911	0.2574078
C	-2.4914192	-2.2747872	3.3703454
H	4.7292437	2.0906964	1.8600892
C	3.6429972	3.4887693	0.6742021
C	3.4390601	-0.2687731	3.0755419
C	4.3784462	-0.9023239	0.8813987
C	1.2576547	3.1204939	-3.0715817
C	-0.1624036	4.3730876	-1.4864528
H	2.6698015	4.7447520	-0.7458268
C	2.3091177	1.3043500	-4.5471428
C	3.7151769	3.1802917	-3.6192002
H	-4.7293523	-2.0905224	-1.8600072
C	-3.6430723	-3.4886991	-0.6742650
C	-3.4392370	0.2689625	-3.0753683
C	-4.3783699	0.9024658	-0.8811055
C	-1.2575795	-3.1207825	3.0714237
C	0.1624573	-4.3731875	1.4861356
H	-2.6698082	-4.7447953	0.7456137
C	-2.3089894	-1.3047376	4.5471418
C	-3.7150640	-3.1806831	3.6192293
H	4.3644909	4.2709891	0.9008184
C	2.7227865	0.7128414	3.9990499
C	4.0142803	-1.4276568	3.6175035
C	4.9302867	-2.0435140	1.4783834
C	4.7024885	-0.5725141	-0.5724686
C	0.5077924	3.6586538	-4.1257126
C	-0.4988294	4.8642432	-0.0811433
C	-0.8785449	4.8786058	-2.5815567
H	1.4280372	0.6625379	-4.4090473
H	3.1920804	0.6550653	-4.6375263
H	2.1987351	1.8336013	-5.5052759
H	3.5493522	3.8227954	-4.4973763
H	4.6134188	2.5731325	-3.8068561
H	3.9214658	3.8319790	-2.7594603
H	-4.3645886	-4.2708934	-0.9008954
C	-2.7231044	-0.7126429	-3.9989954
C	-4.0144876	1.4278763	-3.6172339
_C	-4.9302351	2.0436912	-1.4779916
C	-4.7022495	0.5726324	0.5727931
C	-0.5076601	-3.6590080	4.1254802
C	0.4988460	-4.8642073	0.0807715
C	0.8786469	-4.8787902	2.5811648
H	-1.4279362	-0.6628973	4.4090017
H	-3.1919623	-0.6554799	4.6376228
H	-2.1985113	-1.8340207	5.5052459
H	-3.5491545	-3.8232162	4.4973675
H	-4.6133183	-2.5735678	3.8069684
H	-3.9213777	-3.8323433	2.7594764
H	2.0905236	1.3565427	3.3686141
C	3.7311160	1.6177304	4.7380442
C	1.8123989	0.0201763	5.0265660

Atom	x	y	z
H	-0.0702844	4.1426601	0.6312662
C	-2.0113593	4.9451815	0.1838570
C	0.1429857	6.2401706	0.1952539
H	-1.7027213	5.5704832	-2.4034972
H	-2.0908655	-1.3564564	-3.3686475
C	-3.7315619	-1.6173862	-4.7379998
C	-1.8127166	-0.0199748	-5.0265104
H	-3.8891268	1.6356211	-4.6805877
C	-4.7441028	2.3148696	-2.8313000
H	-5.5248426	2.7283201	-0.8718587
H	-3.9147560	-0.1065136	0.9353998
C	-6.0468348	-0.1782280	0.6650792
C	-4.7221314	1.7980681	1.4985583
H	-0.7706237	-3.4030703	5.1526270
C	0.5591769	-4.5221600	3.8879555
H	0.0703226	-4.1425369	-0.6315652
C	2.0113700	-4.9452055	-0.1842329
C	-0.1430340	-6.2400809	-0.1957521
H	1.7028165	-5.5706494	2.4030094
H	4.4038380	1.0149128	5.3667502
H	3.2015716	2.3272181	5.3916386
H	4.3531965	2.1991871	4.0448511
H	1.1281294	-0.6914069	4.5455846
H	1.2106892	0.7701511	5.5606534
H	2.3943525	-0.5263054	5.7835533
H	5.1786224	-3.2112609	3.2763554
H	6.0377262	1.1053527	-0.0755531
H	6.2708448	0.4432078	-1.7088919
H	6.8685582	-0.4511595	-0.2899251
H	5.5537871	-2.4792736	-1.2632428
H	4.8542429	-1.4769239	-2.5417066
H	3.7857187	-2.3685792	-1.4339061
H	-1.1335938	4.9263419	-4.7230615
H	-2.4836711	5.7540018	-0.3933616
H	-2.1951533	5.1570712	1.2473840
H	-2.5173594	4.0049179	-0.0725573
H	1.2363954	6.2152128	0.0984718
H	-0.0975463	6.5771709	1.2148075
H	-0.2386243	6.9941912	-0.5098041
H	-4.4042604	-1.0144583	-5.3666229
H	-3.2021352	-2.3268888	-5.3916733
H	-4.3536620	-2.1988134	-4.0448016
H	-1.1283516	0.6915040	-4.5455056
H	-1.2111076	-0.7699580	-5.5606974
H	-2.3946607	0.5266285	-5.7834168
H	-5.1787898	3.2114758	-3.2759159
H	-6.0375434	-1.1052355	0.0760235
H	-6.2704590	-0.4431121	1.7093992
H	-6.8683456	0.4512770	0.2905178
H	-5.5534846	2.4793625	1.2637362
H	-4.8537191	1.4770065	2.5420719



H	3.8887734	-1.6353960	4.6808420	H	-3.7853840	2.3687062	1.4341231
C	4.7439705	-2.3146742	2.8316667	H	1.1337767	-4.9267080	4.7226618
H	5.5249936	-2.7281385	0.8723430	H	2.4836418	-5.7541188	0.3928870
H	3.9150398	0.1066265	-0.9351805	H	2.1951493	-5.1569761	-1.2477851
C	6.0470919	0.1783380	-0.6645966	H	2.5174197	-4.0049999	0.0722964
C	4.7224871	-1.7979637	-1.4982083	H	-1.2364379	-6.2150770	-0.0989331
H	0.7707906	3.4026254	-5.1528283	H	0.0974500	-6.5770015	-1.2153434
C	-0.5590394	4.5218433	-3.8883003	H	0.2385525	-6.9941893	0.5092238

Table S8. Cartesian coordinates of the optimized geometry of $[(L^0Co)_2(As_4)]$ in triplet spin state at the RI-BP86/def2-TZVP level of theory. Total energy = -14033.24643079 ha.

Atom	x	y	z				
As	-1.0606597	0.7827201	0.5254124				
As	0.7539200	-0.1581894	1.8974104				
As	0.4142730	0.0593481	-1.3668250				
Co	1.5586125	1.2906058	0.2862440				
Co	-1.4392508	-1.4456001	-0.1444373				
As	0.8178105	-1.8848959	0.0876365				
N	3.4519120	1.2096224	0.5790898				
N	1.4874279	3.2089299	-0.0262352				
H	1.6063143	2.9784687	-2.4391970				
N	-2.7468648	-1.5788811	-1.5778975				
N	-2.2279629	-2.7934757	0.9682568				
H	-3.0193812	-0.8913151	2.2843267				
C	4.2633179	2.2684896	0.5484928				
C	4.0956668	-0.0454660	0.8859636				
C	0.2808612	3.9162211	-0.3733638				
C	2.5715439	3.9916723	0.0191353				
C	0.9152035	3.7234777	-2.8605818				
C	-3.7705096	-2.4399003	-1.5468712				
C	-2.7396199	-0.7347680	-2.7457275				
C	-1.6321040	-3.1414175	2.2361248				
C	-3.3178053	-3.4918700	0.6443405				
C	-2.9893275	-1.2518731	3.3244982				
H	5.3267784	2.0800826	0.7391466				
C	3.8767485	3.5836660	0.2904138				
C	4.3460487	-0.3988012	2.2367190				
C	4.4883114	-0.8946400	-0.1794098				
C	-0.0108442	4.1733052	-1.7354352				
C	-0.5610652	4.3952896	0.6619613				
H	2.4146671	5.0593002	-0.1800838				
C	0.1640836	3.0528035	-4.0213451				
C	1.7593492	4.9026667	-3.3845292				
H	-4.4507518	-2.4246426	-2.4077557				
C	-4.0583590	-3.3481602	-0.5290249				
C	-1.9677348	-1.1192424	-3.8711807				
C	-3.5485312	0.4277281	-2.7722356				
C	-1.9571356	-2.3717903	3.3817506				
C	-0.7542022	-4.2522217	2.3230941				
H	-3.6586286	-4.2387548	1.3715054				
C	-2.6470938	-0.0543561	4.2232710				
C	-4.3932842	-1.7894300	3.6700523				
H	4.6522701	4.3473582	0.2935822				
C	4.0275490	0.5393716	3.3975107				
C	4.9629367	-1.6313866	2.4923710				
C	5.1028990	-2.1138329	0.1373530				
C	4.3310668	-0.4734272	-1.6357147				
C	-1.1639280	4.9116227	-2.0361329				
C	-0.2113897	4.1884649	2.1311795				
C	-1.6977893	5.1307924	0.3032979				
H	-0.4563199	2.2151695	-3.6760233				
H	0.8813651	2.6629272	-4.7585122				
H	-0.4915068	3.7619759	-4.5484345				
H	1.1134162	5.6876648	-3.8064950				
H	2.4435233	4.5646970	-4.1772307				
H	2.3627374	5.3590995	-2.5879201				
H	-4.9310484	-3.9860912	-0.6560872				
C	-1.1568030	-2.4097985	-3.8757075				
C	-2.0218826	-0.3148865	-5.0165480				
C	-3.5613201	1.1970128	-3.9440898				
H	0.4714619	3.3257436	2.1815309				
C	-1.4322129	3.8695207	3.0075318				
C	0.5430737	5.4105470	2.6923688				
H	-2.3558274	5.5128752	1.0850100				
H	-0.9651058	-2.6736019	-2.8236409				
C	-1.9655927	-3.5630841	-4.5030481				
C	0.2026443	-2.2714302	-4.5777875				
H	-1.4395733	-0.5959571	-5.8951922				
C	-2.8101811	0.8336115	-5.0588738				
H	-4.1790916	2.0956620	-3.9843553				
H	-4.1016241	0.2440042	-0.7233564				
C	-5.9082695	0.4579284	-1.8678131				
C	-4.3175576	2.3129967	-1.2345195				
H	-1.5949701	-2.1337760	5.4939896				
C	-0.4758834	-3.7874124	4.7001979				
H	-0.7405201	-4.6052739	0.2204991				
C	1.0147621	-5.5539354	1.0078795				
C	-1.3402243	-6.4307621	1.1861040				
H	0.4956027	-5.3950503	3.6569457				
H	6.0603170	0.6106065	4.2050563				
H	5.0470548	2.0008321	4.6636026				
H	5.7251233	1.8928211	3.0235417				
H	2.5179977	-0.7628286	4.3174008				
H	3.0901028	0.5605346	5.3589791				
H	4.1163086	-0.8572240	5.0942232				
H	5.8108082	-3.4430825	1.6829394				
H	5.8583597	1.1068337	-1.5334464				
H	5.4848227	0.5555939	-3.1821527				
H	6.4690219	-0.4624895	-2.1018758				
H	4.7796861	-2.3547546	-2.6823527				
H	3.7335673	-1.2443126	-3.5773382				
H	3.0738573	-2.1748887	-2.2103640				
H	-2.8917170	5.9664695	-1.2887436				
H	-2.1129238	4.7294964	3.0935713				
H	-1.1080257	3.6099047	4.0257210				
H	-2.0056436	3.0226098	2.6049547				
H	1.4634515	5.6134825	2.1279937				
H	0.8202938	5.2444310	3.7442991				

C	-4.4351285	0.8242166	-1.5965118	H	-0.0869823	6.3118771	2.6446807
C	-1.3596639	-2.7156648	4.6020732	H	-2.2068155	-3.3417574	-5.5539184
C	-0.4668891	-5.1601509	1.1305414	H	-1.3883228	-4.4996273	-4.4763748
C	-0.1858096	-4.5475206	3.5700864	H	-2.9107270	-3.7330390	-3.9695570
H	-1.6316358	0.3187125	4.0289705	H	0.7814927	-1.4305055	-4.1706180
H	-3.3544686	0.7670846	4.0397016	H	0.7920005	-3.1898685	-4.4423180
H	-2.7172158	-0.3075472	5.2917293	H	0.0925729	-2.1142574	-5.6611859
H	-4.4151310	-2.1857548	4.6966631	H	-2.8383161	1.4452348	-5.9620224
H	-5.1422949	-0.9864789	3.5988558	H	-6.0333173	-0.6162113	-2.0616866
H	-4.6978914	-2.5972978	2.9910076	H	-6.5365295	0.7222396	-1.0039942
H	3.2971887	1.2775568	3.0333475	H	-6.2908257	1.0029403	-2.7442055
C	5.2887984	1.3075154	3.8440627	H	-4.7109993	2.9601921	-2.0325301
C	3.4020689	-0.1777217	4.6058335	H	-4.8992453	2.5264265	-0.3256325
H	5.1604782	-1.9235871	3.5247836	H	-3.2760860	2.6062471	-1.0472569
C	5.3342237	-2.4874730	1.4587614	H	-0.0187389	-4.0349988	5.6595300
H	5.4099326	-2.7816431	-0.6684045	H	1.3349693	-6.2072687	1.8330094
H	3.5139666	0.2638317	-1.6736820	H	1.1783390	-6.1091194	0.0726549
C	5.6104664	0.2252537	-2.1400294	H	1.6694396	-4.6717539	0.9979663
C	3.9577959	-1.6314467	-2.5729954	H	-2.4121663	-6.1920190	1.2009289
H	-1.4050840	5.1209637	-3.0796125	H	-1.1473901	-7.0689153	0.3106857
C	-2.0014101	5.3903199	-1.0318917	H	-1.1155317	-7.0170657	2.0899657

References

- [1] P. H. M. Budzelaar, R. de Gelder, A. W. Gal, *Organometallics* **1998**, *17*, 4121-4123.
- [2] F. Spitzer, C. Graßl, G. Balázs, E. M. Zolnhofer, K. Meyer, M. Scheer, *Angew. Chem. Int. Ed.* **2016**, *55*, 4340-4344.
- [3] a) M. Stender, R. J. Wright, B. E. Eichler, J. Prust, M. M. Olmstead, H. W. Roesky, P. P. Power, *J. Chem. Soc., Dalton Trans.* **2001**, 3465-3469; b) J. Feldman, S. J. McLain, A. Parthasarathy, W. J. Marshall, J. C. Calabrese, S. D. Arthur, *Organometallics* **1997**, *16*, 1514-1516.
- [4] X. Dai, P. Kapoor, T. H. Warren, *J. Am. Chem. Soc.* **2004**, *126*, 4798-4799.
- [5] S. Yao, N. Lindenmaier, Y. Xiong, S. Inoue, T. Szilvási, M. Adelhardt, J. Sutter, K. Meyer, M. Driess, *Angew. Chem. Int. Ed.* **2015**, *54*, 1250-1254.
- [6] F. Spitzer, C. Graßl, G. Balázs, E. Mädl, M. Keilwerth, E. M. Zolnhofer, K. Meyer, M. Scheer, *Chem. Eur. J.* **2017**, *23*, 2716-2721.
- [7] S. Yao, T. Szilvasi, N. Lindenmaier, Y. Xiong, S. Inoue, M. Adelhardt, J. Sutter, K. Meyer, M. Driess, *Chem. Commun.* **2015**, *51*, 6153-6156.
- [8] a) H. Erdmann, M. V. Unruh, *Zeitschrift für anorganische Chemie* **1902**, *32*, 437-452; b) O. J. Scherer, H. Sitzmann, G. Wolmershäuser, *J. Organomet. Chem.* **1986**, *309*, 77-86; c) J. J. Curley, N. A. Piro, C. C. Cummins, *Inorg. Chem.* **2009**, *48*, 9599-9601; d) H. A. Spinney, N. A. Piro, C. C. Cummins, *J. Am. Chem. Soc.* **2009**, *131*, 16233-16243.
- [9] C. Graßl, *Dissertation, Universität Regensburg* **2013**.
- [10] CrysAlisPro Software System, Agilent Technologies UK Ltd, Yarnton, Oxford, UK.
- [11] O.V. Dolomanov and L.J. Bourhis and R.J. Gildea and J.A.K. Howard and H. Puschmann, Olex2: A complete structure solution, refinement and analysis program, *J. Appl. Cryst.*, **2009**, *42*, 339-341.
- [12] Sheldrick, G.M., *ShelXT, Acta Cryst.*, **2014**, *A71*, 3-8.
- [13] L. Palatinus and G. Chapuis, Superflip - a computer program for the solution of crystal structures by charge flipping in arbitrary dimensions, *J. Appl. Cryst.*, (2007), **40**, 786-790.
- [14] Sheldrick, G.M., A short history of ShelX, *Acta Cryst.*, **2008**, *A64*, 339-341.
- [15] Single crystal X-ray determination of **2** was performed by Christian Graßl in [9]. The structural parameters were re-calculated herein.
- [16] a) F. Furche, R. Ahlrichs, C. Hättig, W. Klopper, M. Sierka, F. Weigend, *WIREs Comput. Mol. Sci.* **2014**, *4*, 91-100; b) R. Ahlrichs, M. Bär, M. Häser, H. Horn, C. Kölmel, *Chem. Phys. Lett.* **1989**, *162*, 165-169; c) O. Treutler, R. Ahlrichs, *J. Chem. Phys.* **1995**, *102*, 346-354; d) TURBOMOLE V6.4, a development of University of Karlsruhe and Forschungszentrum Karlsruhe GmbH, <http://www.turbomole.com>.
- [17] K. Eichkorn, O. Treutler, H. Oehm, M. Häser, R. Ahlrichs, *Chem. Phys. Lett.* **1995**, *242*, 652-660; b) K. Eichkorn, F. Weigend, O. Treutler, R. Ahlrichs, *Theor. Chem. Acc.* **1997**, *97*, 119-124.
- [18] a) P. A. M. Dirac, *Proc. Royal Soc. A* **1929**, *123*, 714-733; b) J. C. Slater, *Phys. Rev.* **1951**, *81*, 385-390; c) S. H. Vosko, L. Wilk, M. Nusair, *Can. J. Phys.* **1980**, *58*, 1200-1211; d) A. D. Becke, *Phys. Rev. A* **1988**, *38*, 3098-3100; e) J. P. Perdew, *Phys. Rev. B* **1986**, *33*, 8822-8824; Erratum: J. P. Perdew, *Phys. Rev. B* **1986**, *34*, 7406-7406.

- [19] A. Schäfer, H. Horn, R. Ahlrichs *J. Chem. Phys.* **1992**, *97*, 2571. b) K. Eichkorn, O. Treutler, H. Öhm, M. Häser, R. Ahlrichs *Chem. Phys. Letters* **1995**, *242*, 652.
- [20] M. Sierka, A. Hogekamp, R. Ahlrichs, *J. Chem. Phys.* **2003**, *118*, 9136-9148.
- [21] a) A. D. Becke, *J. Chem. Phys.* **1993**, *98*, 5648-5652; b) C. Lee, W. Yang, R. G. Parr, *Phys. Rev. B* **1988**, *37*, 785-789.
- [22] a) J. P. Perdew, Y. Wang, *Phys. Rev. B* **1992**, *45*, 13244; b) J. P. Perdew, K. Burke, M. Ernzerhof, *Phys. Rev. Lett.* **1996**, *77*, 3865; c) J. P. Perdew, M. Ernzerhof, K. Burke, *J. Chem. Phys.* **1996**, *105*, 9982.
- [23] S. Grimme, *J. Comput. Chem.* **2006**, *27*, 1787-1799.

Preface

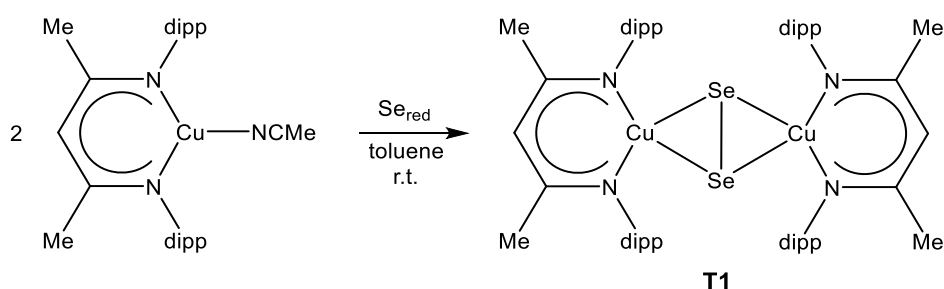
The following chapter includes preliminary, unpublished results, which will be included in future publications or provide a basis for future research efforts.

Some of the obtained compounds could not be fully characterized, however, all data and knowledge that was acquired about the described products and reactions will be presented.

Prior to their publication, further efforts need to be made to provide additional information or improve analytical data.

8. Thesis Treasury

8.1 Reactivity of $[L^3Cu(NCMe)]$ with Se_{red}



Scheme 1. Reaction of $[L^3Cu(NCMe)]$ with Se_{red} .

The reaction of $[L^3Cu(NCMe)]$ ($L^3 = \{[N(C_6H_3iPr_2-2,6)C(Me)]_2CH\}^-$) with Se_{red} was performed at room temperature and proceeds by fragmentation of the Se_8 rings into Se_2 units (Scheme 1). The product $[(L^3Cu)_2(\mu-\eta^2:\eta^2-Se_2)]$ (**T1**) was quantitatively formed, which was proven by 1H NMR spectroscopy. In the 1H and $^{13}C\{^1H\}$ NMR spectra, a characteristic signal set for the L^3 ligand is detected. In the $^{77}Se\{^1H\}$ NMR spectrum, a singlet is detected at $\delta = 1246$ ppm, which indicates chemical equivalence of the two Se atoms. Additionally, compound **T1** is characterized by elemental analysis and LIFDI-MS, which shows the molecular ion peak for **T1**. Single crystals suitable for X-ray diffraction were grown from a saturated toluene solution.

The molecular structure of $[(L^3Cu)_2(\mu-\eta^2:\eta^2-Se_2)]$ (**T1**) is a centrosymmetric and dinuclear complex (Figure 1). Both $[L^3Cu]$ fragments are parallel to each other and are bridged by a Se_2 unit. The L^3 supporting ligands coordinate the copper atoms in a terminal fashion ($\Theta = 10.89(5)^\circ$). The $[N_4Cu_2Se_2]$ core adopts a flat conformation and the copper centers have quadratic planar ($\Sigma_{Cu} = 360.0^\circ$) coordination geometry. The $Cu \cdots Cu$ distance is $3.9849(5)$ Å, which considerably exceeds the sum of atomic radii (Cu atomic radius: 1.35 Å)^[1]. Therefore, no bonding interaction is assigned between the copper atoms.

The Se–Se distance in complex **T1** is $2.4527(4)$ Å. This is longer than the values commonly assigned to a Se=Se double bond (2.166 Å in Se_2)^[2] or to a Se–Se single bond (e.g. 2.33 Å in $MeSe-SeMe$).^[3] The question arises whether the Se_2 ligand in **T1** should be regarded as a $[Se_2]^{2-}$ (diselenide), $[Se_2]^{3-}$ (subselenide) or a pair of split $[Se]^{2-}$ (selenide) ligands. In complex **T1**, the Se–Se distance ($2.4527(4)$ Å) is longer than the one found in the structurally related $[Se_2]^{2-}$ containing complex $[(L^3Ni)_2(\mu-\eta^2:\eta^2-Se_2)]$ (**T-A**, $2.3304(6)$ Å),^[4] however shorter than the distance found in $[Se_2]^{3-}$ containing complex $[(iPr_4C_5H)Ni)_2(\mu-Se_2)]$ ($2.915(2)$ Å).^[5] Notably, in selenide complexes such as $[(Cp)Ni(\mu-SePh)]_2$ a Se \cdots Se distance of $3.292(1)$ Å is found, which excludes any bonding interaction between the selenium atoms.^[6]

Moreover, a benchmark $[\text{Se}_2]^{2-}$ moiety in a bridging $\mu\text{-}\eta^2\text{:}\eta^2\text{-}$ coordination mode is reported in the crystal structure of $[\text{K}(\text{18-crown-6})]_2(\text{Se}_2) \cdot \text{en}$ (en = ethylenediamine).^[7] Its Se–Se distance (2.4063(4) Å) is comparable to the one in **T1** (2.4527(4) Å). Therefore, the selenium ligand in **T1** may be understood as a $[\text{Se}_2]^{2-}$ unit.

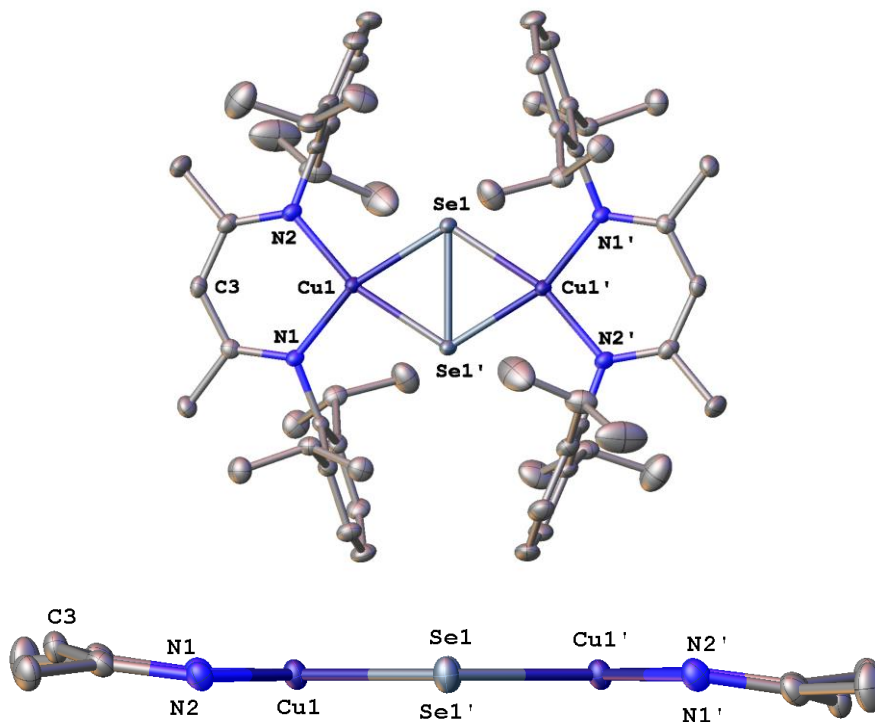
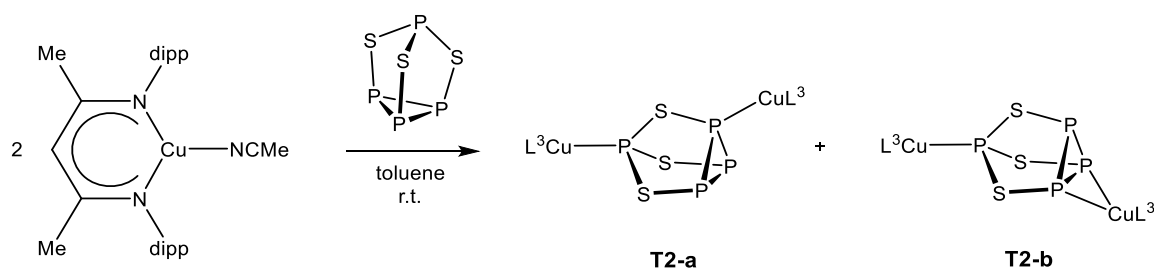


Figure 1. Molecular structure of **T1** (top) in the crystal and its side view presentation (bottom; the dipp flanking groups are omitted for clarity). Hydrogen atoms are omitted for clarity. Thermal ellipsoids are drawn at 50% probability level.

As mentioned above, the complexes $[(\text{L}^3\text{M})_2(\mu\text{-}\eta^2\text{:}\eta^2\text{-Se}_2)]$ ($\text{M} = \text{Cu}$ (**T1**), Ni (**T-A**)) are structurally related. However, in contrast to the planar coordination geometry in **T1**, the complex **T-A** adopts a $[\text{Ni}_2\text{Se}_2]$ butterfly-like structure with a fold of approx. 134° along the Se–Se edge.^[4] Moreover, the coordination spheres of each nickel center in **T-A** is tilted (N–N vs. Se–Se: approx. 22°). The deviation of their Se–Se distances (2.4527(4) Å in **T1** vs. 2.3304(6) Å in **T-A**) may be attributed to the differing coordination geometries.

Under the assumption of a $[\text{Se}_2]^{2-}$ moiety in **T1**, two copper(II) centers are expected (d^9 configuration). However, no signal was detected in the EPR spectra at room temperature and 77 K. Moreover, in the ^1H , $^{13}\text{C}\{^1\text{H}\}$ and $^{77}\text{Se}\{^1\text{H}\}$ NMR spectra signals were detected, which are characteristic for diamagnetic compounds, but would not be expected for paramagnetic complexes. This might be explained by two strongly antiferromagnetically coupled copper(II) centers leading to an overall singlet spin state. Further investigations need to be conducted for the characterization and unambiguous interpretation of complex **T1**. The possible description as $[\text{Se}_2]^0$ ligand has to be evaluated by DFT calculation.

8.2 Reactivity of $[L^3Cu(NCMe)]$ with P_4S_3



Scheme 2. Reaction of $[L^3Cu(NCMe)]$ with P_4S_3 .

The reaction of $[L^3Cu(NCMe)]$ with the cage compound P_4S_3 was performed at room temperature (Scheme 2). In the $^{31}P\{^1H\}$ NMR spectrum of the reaction solution in $[D_8]toluene$ at room temperature, a dynamic behavior is indicated by two broad singlets at $\delta = 71.0$ ppm ($\omega_{1/2} = 166.0$ Hz) and at $\delta = -124.9$ ppm ($\omega_{1/2} = 244.1$ Hz). Their intensity ratio is 1:3 and the signals are assigned to one apical and three basal phosphorus atoms of an intact P_4S_3 ligand. The chemical shifts of the detected signals are comparable to those found for P_4S_3 molecules in toluene ($\delta = 66.3$ ppm (q, $^2J_{PP} = 70$ Hz) and -124.9 ppm (d, $^2J_{PP} = 71$ Hz)). Single crystals were grown from saturated *n*-hexane solutions in 27% yield. The molecular structure of $[(L^3Cu)_2(P_4S_3)]$ (**T2**) contains two $[L^3Cu]$ fragments bridged by an intact P_4S_3 cage ligand in two superposed conformations (Figure 2).

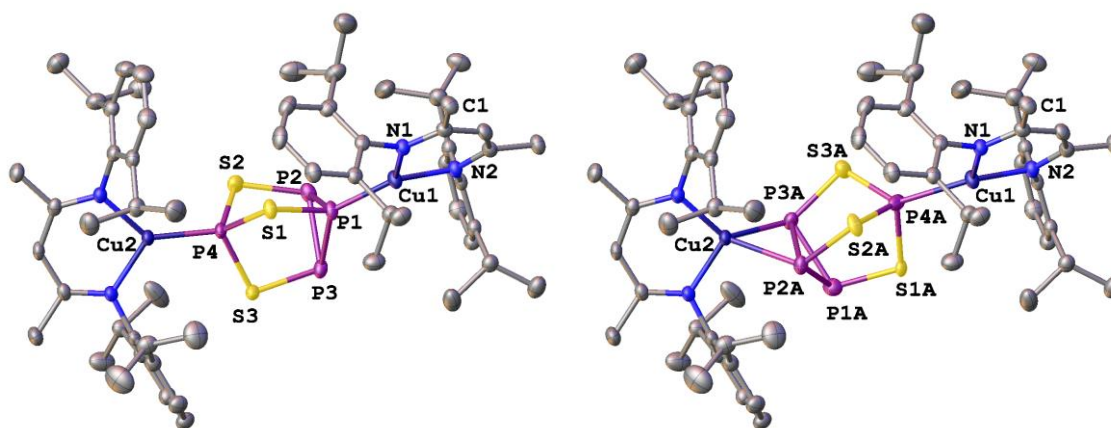


Figure 2. Molecular structure of $[(L^3Cu)_2(P_4S_3)]$ (**T2**) in the crystal with the P_4S_3 moiety in a $\mu\text{-}\eta^1:\eta^1$ -coordination mode in **T2-a** (left, 93% occupation) and in a $\mu\text{-}\eta^1:\eta^2$ -coordination mode in **T2-b** (right, 7% occupation). Hydrogen atoms are omitted for clarity. Thermal ellipsoids are drawn at 50% probability level.

In the crystal, both $[L^3Cu]$ fragments build a bonding pocket, which accommodates a P_4S_3 unit. The latter is disordered over two positions with 93% and 7% occupancy. The major component shows the η^1 -coordination of the apical and one basal P atom. In the following, this isomer is called **T2-a** (Figure 2, left). The minor component of the P_4S_3 unit shows a η^1 coordination of the apical P atom and a η^2 -coordination of the basal P_3 unit

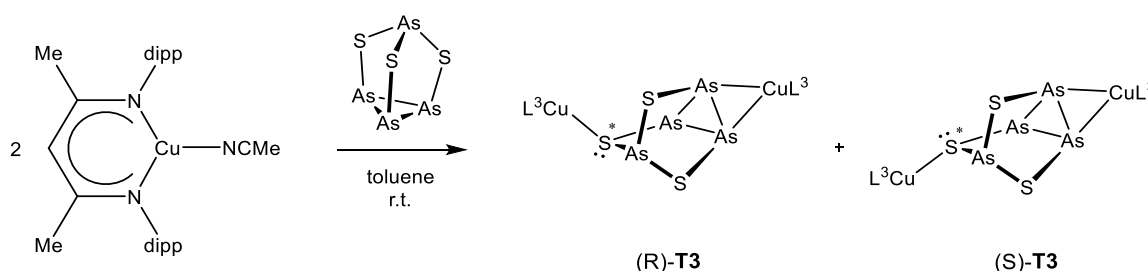
(Figure 2, right). This molecule will be referred as **T2-b**. The atomic distances of the bridging P₄S₃ ligands are summarized in Table 1 and are compared to α -P₄S₃.^[8]

Table 1. Comparison of structural parameters in **T2-a**, **T2-b** and α -P₄S₃.

Compound	T2-a	T2-b	α -P ₄ S ₃ ^[8]	
	(occupancy 93%)	(occupancy 7%)	(two molecules in asym. unit)	
$d(\text{P}_{\text{basal}}-\text{P}_{\text{basal}}) / [\text{\AA}]$	2.2297(16)	2.22(3)	2.240	2.223
	2.230(3)	2.26(3)	2.246	2.232
	2.255(2)	2.404(9)		
$d(\text{P}_{\text{apical}}-\text{S}) / [\text{\AA}]$	2.0951(9)	2.077(18)	2.091	2.070
	2.0964(7)	2.15(3)	2.096	2.087
	2.1020(17)	2.16(3)		
$d(\text{P}_{\text{basal}}-\text{S}) / [\text{\AA}]$	2.092(2)	2.02(3)	2.089	2.092
	2.0927(7)	2.090(9)	2.097	2.095
	2.0977(16)	2.105(11)		
$d(\text{Cu}-\text{P}_{\text{apical}}) / [\text{\AA}]$	2.1048(5)	2.35(2)	-	-
$d(\text{Cu}-\text{P}_{\text{basal}}) / [\text{\AA}]$		2.336(6)	-	-
	2.0973(17)	2.427(7)		

No significant changes are detected in the bond distances - except that of basal P2A–P3A (2.404(9) Å) in **T2-b**, which is significantly elongated compared to the corresponding ones in uncoordinated α -P₄S₃. Similar elongation was observed in [(L³Cu)₂(μ - η^2 : η^2 -P₄)] (Chapter 3), which displays an edge coordinated P₄ ligand. Accordingly, the P₄S₃ ligands in **T2-b** (and **T2-a**) are considered as being intact.

8.3 Reactivity of [L³Cu(NCMe)] with As₄S₃



Scheme 3. Reaction of $[\text{L}^3\text{Cu}(\text{NCMe})]$ with As_4S_3 yielding two different stereoisomers (R)-**T3** and (S)-**T3**.

The reaction of $[\text{L}^3\text{Cu}(\text{NCMe})]$ with the cage compound As_4S_3 was performed at room temperature (Scheme 3). Single crystals were obtained from saturated *n*-hexane solutions in 21% yield. The molecular structure is depicted in Figure 3.

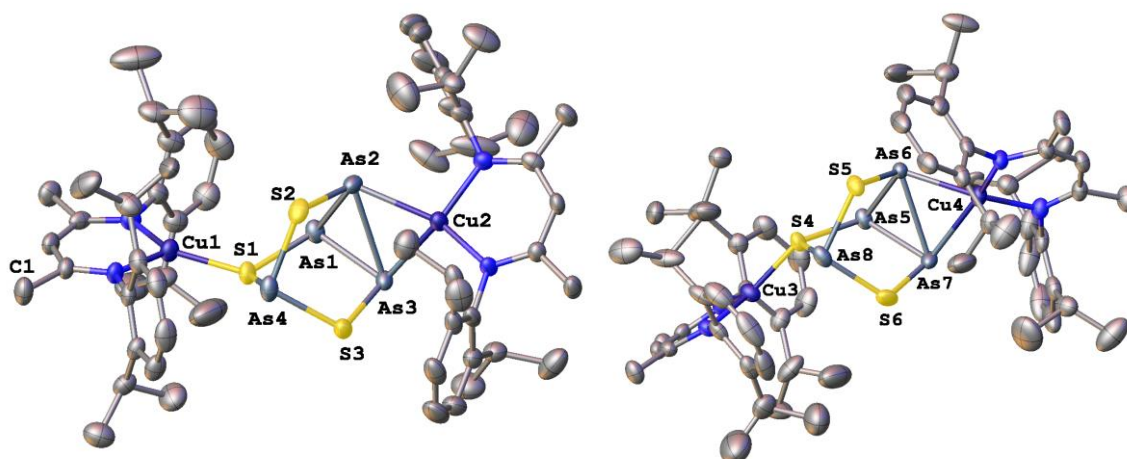


Figure 3. Molecular structure of $[(L^3Cu)_2(As_4S_3)]$ (**T3**) in the crystal with two co-crystallizing enantiomers (R)-**T3** (left) and (S)-**T3** (right). Exclusively, the major components of the disordered As_4S_3 ligands are depicted. Hydrogen atoms are omitted for clarity. Thermal ellipsoids are drawn at 50% probability level.

The crystal structure of $[(L^3Cu)_2(As_4S_3)]$ (**T3**) contains a racemic mixture of two co-crystallizing, enantiomeric molecules (R)-**T3** and (S)-**T3**. Each consists of a pair of $[L^3Cu]$ fragments and a bridging As_4S_3 ligand. For the basal As_3 unit, a η^2 -coordination is found. The chirality is introduced by η^1 -coordination of the opposing S1 or S4 atom, respectively (Figure 3). Additionally, the As_4S_3 unit in each enantiomer displays disorder with a ratio of 89:11 in (R)-**T3** and a ratio of 65:35 in (S)-**T3**. The interatomic distances of the bridging As_4S_3 ligands are summarized in Table 2 and are compared to β - As_4S_3 .^[9]

Table 2. Comparison of structural parameters in (R)-**T3**, (S)-**T3** and β - As_4S_3 .

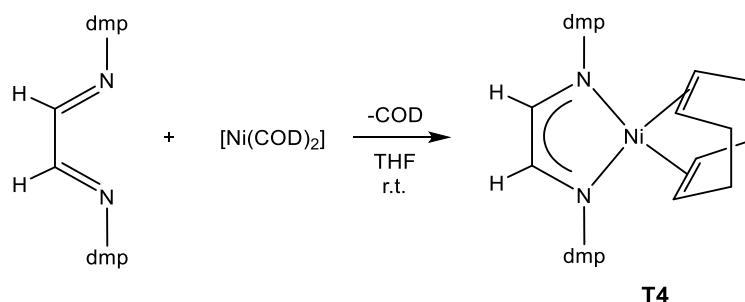
Compound	(R)- T3		(S)- T3		β - As_4S_3 ^[9]
	major 89%	minor 11% ^[a]	major 65%	minor 35%	
$d(As_{\text{basal}}-As_{\text{basal}}) / [\text{\AA}]$	2.4508(10)	2.442(12)	2.4587(13)	2.448(2)	2.460(7)
	2.4618(10)	2.470(12)	2.4651(14)	2.464(3)	2.480(7)
	2.7429(10)	2.762(11)	2.7273(13)	2.779(2)	
$d(As_{\text{apical}}-S) / [\text{\AA}]$	2.206(2)	1.849(18)	2.212(3)	2.222(6)	2.230(8)
	2.2215(19)	2.21(3)	2.235(2)	2.223(5)	2.234(16)
	2.2605(18)	2.25(2)	2.260(2)	2.258(5)	
$d(As_{\text{basal}}-S) / [\text{\AA}]$	2.2116(19)	2.157(18)	2.211(2)	2.208(5)	2.218(10)
	2.230(2)	2.21(3)	2.235(2)	2.223(5)	2.221(12)
	2.2334(18)	2.22(2)	2.235(3)	2.235(5)	
$d(Cu-S_{\text{coord}}) / [\text{\AA}]$	2.1154(18)	1.95(2)	2.083(2)	2.023(4)	-
$d(Cu-As_{\text{basal}}) / [\text{\AA}]$	2.3685(11)	2.459(7)	2.3698(12)	2.3922(19)	-
	2.4510(11)	2.627(8)	2.5207(13)	2.5829(19)	

[a]: The accurate localization of atom positions in the minor component of (R)-**T3** might be affected with uncertainties due to the disorder.

Most notably, the η^2 -coordinated basal As–As edges in (R)-**T3** and (S)-**T3** are elongated (2.7273(13)–2.779(2) Å) in comparison to uncoordinated β -As₄S₃ (2.460(7) or 2.480(7) Å)^[9]. A bond elongation to a comparable extent was observed in [(L³Cu)₂(μ - η^2 : η^2 -As₄)], which was previously discussed in chapter 3.^[10]

8.4 Synthesis of [(DAD)Ni(COD)]

On the quest for ligand variation, the α -diimine ligand class was expected to serve as a promising supporting ligand in the transition metal mediated E₄ activation (E = P, As). Formally, it differs from β -diiminato ligands by one lacking methine group in the ligand backbone. Additionally, α -diimine ligands are reported to be non-innocent and to serve as flexible electron reservoirs in their complexes. The reduction of the neutral α -diimine ligand to a radical monoanionic or dianionic ligand can be easily accomplished. The formal electronic structure of the ligand in the solid state can be elucidated by the C–C and C–N bond distances in the ligand backbone obtained by single crystal X-ray diffraction.^[11]



Scheme 4. Reaction of DAD with [Ni(COD)₂].

A neutral α -dialdimine ligand with dmp (= 2,6-dimethylphenyl) groups was chosen for initial investigations and will be named ‘DAD’ in the following. The neutral DAD ligand was reacted with the nickel(0) precursor [Ni(COD)₂] (COD = 1,5-cyclooctadiene) in a mild substitution reaction in THF at room temperature (Scheme 4). The mononuclear product [(DAD)Ni(COD)] (**T4**) was selectively and quantitatively obtained, which was proven by ¹H NMR spectroscopy. Similar reactions were reported previously.^[12] The product was characterized by ¹H and ¹³C{¹H} NMR spectroscopy, as well as by EA, LIFDI-MS and single crystal X-ray diffraction. Single crystals were grown from a saturated *n*-hexane solution in 64% yield. The molecular structure of **T4** is depicted in Figure 4.

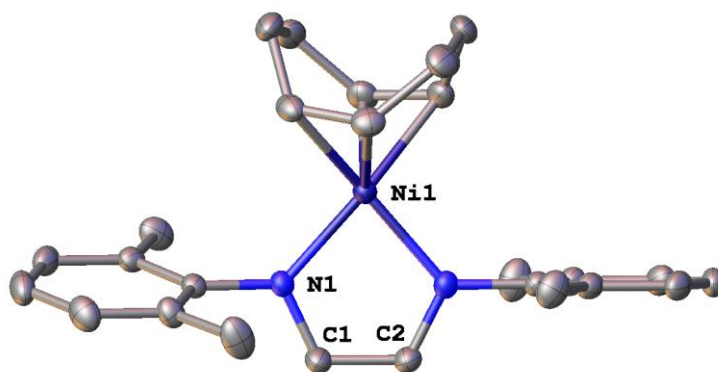
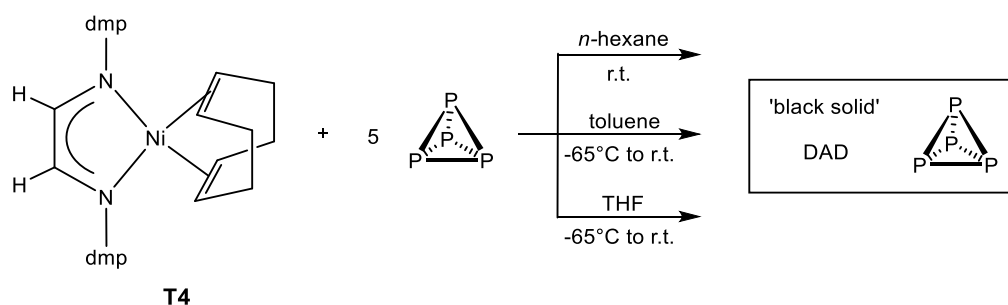


Figure 4. Molecular structure of **T4** in the crystal. Hydrogen atoms are omitted for clarity. Thermal ellipsoids are drawn at 50% probability level.

Compound **T4** is a mononuclear nickel complex containing one COD and one DAD supporting ligand. The olefinic parts of the COD ligand are tilted by approx. 31° compared to the DAD ligand backbone. The oxidation state of the nickel center can be evaluated by examination of the atomic distances in the DAD ligand backbone. The C1–C2 distance is $1.404(2)$ Å and both C–N distances are $1.333(2)$ Å. The geometric parameters in solid state correspond to the expected parameters of a monoanionic ligand.^[11] Therefore, complex **T4** can be described as a nickel(I) complex in the crystal.

8.5 Reactivity of [(DAD)Ni(COD)] with P_4

Recently, Wolf *et al.* reported the (BIAN)nickel(0) mediated P_4 reaction, which leads to interesting complexes with $[P_4]^{4-}$ ligands (BIAN = 1,2-bis(2,6-diisopropylphenyl-imino)acenaphthene).^[13] Moreover, nickel(I) sources should be suitable for reductive P_4 activation, too. Therefore, the [(DAD)Ni(COD)] (**T4**) is a promising candidate for reactions with P_4 .



Scheme 5. Reaction procedure of **T4** with 5 equivalents of P_4 under different conditions.

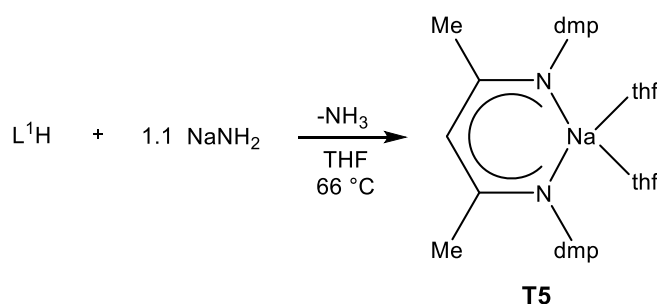
The reaction of **T4** with 5 equivalents of P_4 was performed in *n*-hexane at room temperature (Scheme 5). During the reaction, a black precipitate formed. After completed addition, the reaction suspension was stirred for approx. 18 hours. The supernatant orange

solution exclusively contains the DAD ligand and white phosphorus in solution. The black precipitate is not soluble in *n*-hexane and THF.

The experiment was repeated at $-65\text{ }^{\circ}\text{C}$ in toluene and THF. The dark brown reaction solution was allowed to reach room temperature within 15 hours. However, no change of reactivity is observed: In the supernatant orange solution, the DAD ligand and white phosphorus are observed in the ^1H and $^{31}\text{P}\{^1\text{H}\}$ NMR spectra. Additionally, the precipitation of an insoluble, black solid is observed.

8.6 Synthesis and Characterization of $[\text{L}^1\text{Na}(\text{thf})_2]$

The deprotonation of L^1H ($\text{L}^1 = \{[\text{N}(\text{C}_6\text{H}_3\text{Me-2,6})\text{C}(\text{Me})_2\text{CH}]^-\}$) with NaNH_2 under thermolytic conditions in THF leads to the formation of $[\text{L}^1\text{Na}(\text{thf})_2]$ (**T5**, Scheme 6). Compound **T5** is characterized by ^1H , $^{13}\text{C}\{^1\text{H}\}$, EA, LIFDI-MS and single crystal X-ray diffraction. The ^1H and $^{13}\text{C}\{^1\text{H}\}$ NMR spectra display signal sets which are assigned to the supporting ligand L^1 and to the coordinating THF molecules, respectively.



Scheme 6. Deprotonation of L^1H with NaNH_2 in THF under thermolytic conditions.

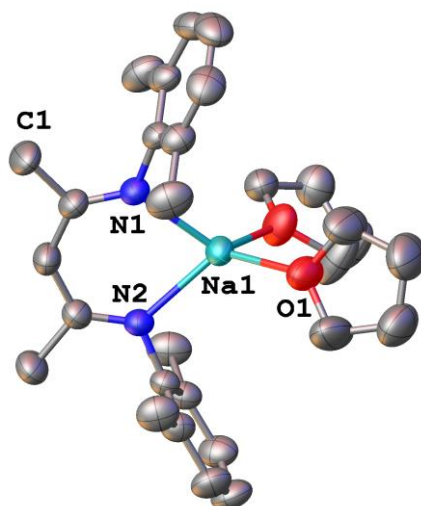


Figure 5. Molecular structure of **T5** in the crystal. The second $[\text{L}^1\text{Na}(\text{thf})_2]$ molecule as well as all hydrogen atoms are omitted for clarity. Thermal ellipsoids are drawn at 50% probability level.

The molecular structure contains two co-crystallizing and crystallographically independent $[L^1Na(thf)_2]$ (**T5**) molecules (Figure 5). The sodium atoms display tetrahedral coordination geometry by one bidentate L^1 ligand and two THF molecules, each. The single crystal X-ray diffraction experiment was performed at 203 K. At lower temperatures, the crystals lose their crystallinity probably due to a phase transition. In one $[L^1Na(thf)_2]$ molecule, both THF molecules are disordered over two positions.

8.7 References

- [1] J. C. Slater, *J. Chem. Phys.* **1964**, *41*, 3199-3204.
- [2] P. Pyykkö, M. Atsumi, *Chem. Eur. J.* **2009**, *15*, 12770-12779.
- [3] P. Pyykkö, M. Atsumi, *Chem. Eur. J.* **2009**, *15*, 186-197.
- [4] S. Yao, Y. Xiong, X. Zhang, M. Schlangen, H. Schwarz, C. Milsmann, M. Driess, *Angew. Chem. Int. Ed.* **2009**, *48*, 4551-4554.
- [5] S. A. Yao, K. M. Lancaster, A. W. Götz, S. DeBeer, J. F. Berry, *Chem. Eur. J.* **2012**, *18*, 9179-9183.
- [6] A. F. Bartlone, M. J. Chetcuti, P. E. Fanwick, K. J. Haller, *Inorg. Chem.* **1993**, *32*, 1435-1441.
- [7] G. Thiele, L. Vondung, C. Donsbach, S. Pulz, S. Dehnen, *Z. Anorg. Allg. Chem.* **2014**, *640*, 2684-2700.
- [8] Y. C. Leung, J. Waser, S. v. Houten, A. Vos, G. A. Wiegers, E. H. Wiebenga, *Acta Cryst.* **1957**, *10*, 574-582.
- [9] H. J. Whitfield, *Dalton Trans.* **1973**, 1737-1738.
- [10] F. Spitzer, M. Sierka, M. Latronico, P. Mastrorilli, A. V. Virovets, M. Scheer, *Angew. Chem. Int. Ed.* **2015**, *54*, 4392-4396.
- [11] N. Muresan, C. C. Lu, M. Ghosh, J. C. Peters, M. Abe, L. M. Henling, T. Weyhermöller, E. Bill, K. Wieghardt, *Inorg. Chem.* **2008**, *47*, 4579-4590.
- [12] T. Schaub, U. Radius, *Z. Anorg. Allg. Chem.* **2006**, *632*, 807-813.
- [13] S. Pelties, T. Maier, D. Herrmann, B. de Bruin, C. Rebreyend, S. Gärtner, I. G. Shenderovich, R. Wolf, *Chem. Eur. J.* **2017**, *23*, 6094-6102.

8.8 Supporting Information

General Remarks

All manipulations were performed with rigorous exclusion of oxygen and moisture using Schlenk-type glassware on a dual manifold Schlenk line with Argon inert gas or glove box filled with N₂ containing a high-capacity recirculator (<0.1 ppm O₂). Solvents were dried using a MB SPS-800 device of company MBRAUN. Mass spectrometry was performed using a Finnigan MAT95 LIFDI-MS (**T1–T4**) or JEOL AccuTOF GCX (**T5**) mass spectrometer. Elemental analysis (CHN) was determined using a Vario micro cube and Vario EL III instrument. The X-band EPR measurements were carried out with a MiniScope MS400 device equipped with a Magnettech GmbH rectangular TE102 resonator at a frequency of 9.5 GHz. ¹H NMR spectra were recorded on a Bruker Avance III HD 400 (¹H: 400.130 MHz, ³¹P: 161.976 MHz, ⁷⁷Se: 100.627 MHz) spectrometer. The chemical shifts are reported in ppm relative to external TMS (¹H, ¹³C), H₃PO₄ (³¹P) or SeMe₂ (⁷⁷Se).

The synthesis of L¹H,^[1] [L³Cu(NCMe)]^[2] and [Ni(COD)₂] are published.

Synthesis of T1

A solution of 100 mg (0.192 mmol) [L³Cu(NCMe)] in 5 mL toluene was added to a slurry of 76 mg (0.962 mmol, 5 equivalents) Se_{red} in 5 mL toluene. The reaction mixture was stirred for approx. 20 hours at room temperature and filtered over celite. Crystals were grown from saturated toluene solutions at –30 °C.

Crystalline yield: 38 mg (0.034 mmol, 35%).

Analytical data:

¹ H NMR (400 MHz, C ₆ D ₆ , 25 °C)	δ [ppm] = 7.13 (t, ³ J _{HH} = 7.6 Hz, 4H, <u>H</u> _{para}), 7.01 (d, ³ J _{HH} = 7.6 Hz, 8H, <u>H</u> _{meta}), 4.90 (s, 2H, <u>H</u> _β), 3.11 (sept, ³ J _{HH} = 6.8 Hz, 8H, <u>CH</u> Me ₂), 1.58 (s, 12H, <u>α</u> -Me), 1.23 (d, ³ J _{HH} = 6.7 Hz, 24H, <u>CH</u> MeMe'), 1.11 (d, ³ J _{HH} = 6.7 Hz, 24H, <u>CH</u> MeMe').
¹³ C{ ¹ H} NMR (101 MHz, C ₆ D ₆ , 25 °C)	δ [ppm] = 163.7 (s, (H ₃ C) <u>C</u> CH <u>C</u> (CH ₃)), 150.3 (s, <u>C</u> _{ipso}), 140.0 (s, <u>C</u> _{ortho}), 125.8 (s, <u>C</u> _{para}), 124.2 (s, <u>C</u> _{meta}), 94.8 (s, (H ₃ C) <u>C</u> CHC(CH ₃)), 28.5 (s, <u>CH</u> (CH ₃) ₂), 24.8 (s, CH(<u>CH</u> ₃) ₂), 24.3 (s, CH(<u>CH</u> ₃) ₂), 22.5 (s, (H ₃ C) <u>C</u> CHC(<u>CH</u> ₃)). Signal assignment by HSQC and HMBC.
⁷⁷ Se{ ¹ H} NMR (76 MHz, C ₆ D ₆ , 25 °C)	δ [ppm] = 1246 (s). Measured range: 3000 to –600 ppm.
EPR	silent at r.t. and 77 K.
Elemental analysis (C ₅₈ H ₈₂ Cu ₂ N ₄ Se ₂)	Calculated: C 62.18, H 7.38, N 5.00. Found: C 62.58, H 7.20, N 4.86.
Mass spectrometry (LIFDI, toluene)	m/z: 1120.6 (100%) [M] ⁺ , 992.2 (12%) [not assigned], 418.6 (13%) [L ³ H] ⁺ .

Synthesis of $[(L^3Cu)_2(P_4S_3)]$ (T2)

A solution of 150 mg (0.288 mmol) $[L^3Cu(NCMe)]$ in 5 mL toluene was added to a slurry of 33 mg (0.150 mmol) P_4S_3 in 4 mL toluene. The color changed from yellow to orange. The reaction solution was stirred at room temperature for approx. 16 hours. After filtration over celite, the solvent was removed and crystals were grown from *n*-hexane solution at room temperature.

Crystalline yield: 45 mg (0.038 mmol, 27%).

Analytical data:

$^{31}P\{^1H\}$ NMR (162 MHz, $[D_8]$ toluene, 25°C)	δ [ppm] = 71.0 (s, $\omega_{1/2}$ = 166.0 Hz, 1P, P_{apical}), -124.9 (s, $\omega_{1/2}$ = 244.1 Hz, 3P, P_{basal}).
Elemental analysis ($C_{58}H_{82}Cu_2N_4P_4S_3$)	Calculated: C 58.91, H 6.99, N 4.74, S 8.14. Found: C 58.71, H 7.00, N 4.55, S 7.97.
Mass spectrometry (LIFDI, toluene)	m/z: 1182.4 (100%) $[M]^+$, 700.2 (7%) $[(L^3Cu)P_4S_3]^+$, 480.4 (14%) $[L^3Cu]^+$, 418.6 (10%) $[L^3H]^+$.

Synthesis of $[(L^3Cu)_2(As_4S_3)]$ (T3)

Within 13 minutes, a solution of 150 mg (0.288 mmol) $[L^3Cu(NCMe)]$ in 8 mL toluene was transferred into a slurry of 56.5 mg (0.143 mmol) As_4S_3 in 8 mL toluene. The color changed from yellow to intense blood red. The reaction solution was stirred at room temperature for approx. 20 hours. The solvent was removed and the residue was dissolved in 25 mL *n*-hexane. After filtration over celite, the solvent was reduced to a volume of 4 mL and crystals were grown at room temperature.

Crystalline yield: 40.5 mg (0.029 mmol, 21%).

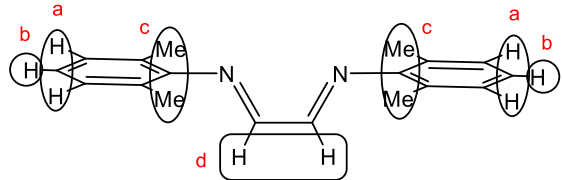
Analytical data:

Elemental analysis ($C_{58}H_{82}Cu_2N_4As_4S_3$)	Calculated: C 51.29, H 6.09, N 4.12, S 7.08. Found: C 49.99, H 5.81, N 3.90, S 7.09.
Mass spectrometry (LIFDI, toluene)	m/z: 1357.9 (100%) $[M]^+$, 960.8 (5%) $[(L^3Cu)_2]^+$, 876.0 (5%) $[L^3Cu(As_4S_3)]^+$, 480.4 (6%) $[L^3Cu]^+$, 418.6 (21%) $[L^3H]^+$.

Synthesis of the 'DAD' Ligand

The diazadiene (DAD) ligand with dmp (= 2,6-dimethylphenyl) groups was synthesized according to literature method.^[3]

Analytical data:

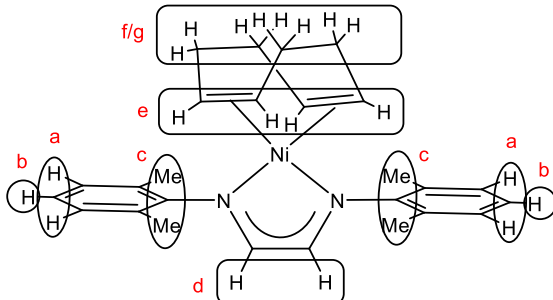
1H NMR of DAD (400 MHz, C_6D_6 , 25 °C)	δ [ppm] = 7.93 (s, 2H, d), 6.95 (m, 6H, a+b , overlapping), 2.07 (s, 12H, c).
	

Synthesis of [(DAD)Ni(COD)] (T4)

1413 mg (5.35 mmol) of the DAD ligand were dissolved in 30 mL THF. Within 40 minutes, the orange solution was transferred into a slurry of 1466 mg (5.35 mmol) $[\text{Ni}(\text{COD})_2]$ in 25 mL THF at room temperature. Within 1 minute, the color changed to dark brown. After stirring for 19 hours, the solvent was removed. The residue was dissolved in 90 mL *n*-hexane and filtered over celite. The solvent was reduced to a volume of 40 mL and crystals were obtained from saturated solution at 8 °C.

Crystalline yield: 1475 mg (3.43 mmol, 64%).

Analytical data:

^1H NMR of T4 (400 MHz, C_6D_6 , 25 °C) 	δ [ppm] = 7.71 (s, 2H, d), 7.16 (s, 6H, a+b , overlapping), 3.73 (s, 4H, e), 2.37 (m, 4H, f/g), 2.19 (s, 12H, c), 1.40 (m, 4H, f/g).
$^{13}\text{C}\{^1\text{H}\}$ NMR (101 MHz, C_6D_6 , 25 °C)	δ [ppm] = 156.7 (s, C_{ipso}), 140.7 (s, $\text{C}_{\text{backbone}}$), 128.4 (s, C_{ortho}), 128.1 (s, C_{meta}), 124.4 (s, C_{para}), 88.0 (s, COD-CH), 30.6 (s, COD- CH_2), 18.1 (s, <u>Me</u>). Signal assignment by HSQC and HMBC.
Elemental analysis ($\text{C}_{26}\text{H}_{32}\text{N}_2\text{Ni}$)	Calculated: C 72.41, H 7.48, N 6.50. Found: C 72.07, H 7.42, N 6.45.
Mass spectrometry (LIFDI, toluene)	m/z : 430.3 (100%) $[\text{M}]^+$.

Synthesis of [L¹Na(thf)₂] (T5)

A two-necked flask with reflux condenser was loaded with 2.00 g (0.051 mol) NaNH₂. A solution of 14.25 g (0.047 mol) L¹H dissolved in 50 mL THF was added under stirring. The reaction mixture was heated to reflux for approx. 18 hours. The solvent was removed and the brown powder was suspended in 200 mL *n*-hexane and filtered over celite. The solvent of the filtrate was reduced to a volume of 70 mL and single crystals were grown from the saturated solution at -30 °C.

Yield: 16.72 g (0.035 mol, 76%).

Analytical data:

¹ H NMR (400 MHz, C ₆ D ₆ , 25 °C)	δ [ppm] = 7.10 (d, ³ J _{HH} = 7.5 Hz, 4H, <u>H_{meta}</u>), 6.89 (t, ³ J _{HH} = 7.5 Hz, 2H, <u>H_{para}</u>), 4.79 (s, 1H, <u>H_β</u>), 3.16 (m, 7H, thf), 2.26 (s, 12H, ortho- <u>Me</u>), 1.84 (s, 6H, α- <u>Me</u>), 1.23 (m, 7H, thf).
¹³ C{ ¹ H} NMR (101 MHz, C ₆ D ₆ , 25 °C)	δ [ppm] = 162.4 (s, (H ₃ C) <u>C</u> CH <u>C</u> (CH ₃)), 154.6 (s, <u>C</u> _{ipso}), 129.8 (s, <u>C</u> _{ortho}), 128.0 (s, <u>C</u> _{meta}), 120.7 (s, <u>C</u> _{para}), 90.8 (s, (H ₃ C) <u>C</u> CHC(CH ₃)), 67.8 (s, thf), 25.4 (s, thf), 23.7 (s, (H ₃ <u>C</u>)CCHC(<u>C</u> H ₃)), 18.9 (s, ortho- <u>C</u> H ₃). Signal assignment in accordance with HSQC and HMBC spectra.
Elemental analysis (C ₂₉ H ₄₁ N ₂ NaO ₂)	Calculated: C 73.70, H 8.74, N 5.93. Found: C 73.59, H 8.48, N 6.30.
Mass spectrometry (LIFDI, toluene)	m/z: 351.1908 (100%) [L ¹ Na ₂] ⁺ , 328.2040 (48%) [L ¹ Na] ⁺ .

Crystallographic Details

Single crystal structure analyses were performed using Rigaku Oxford Diffraction (formerly Agilent Technologies) diffractometers GV-50, Titan^{S2} CCD (**T1**, **T4**), Gemini Ultra Ruby CCD (**T2**) or Gemini Ultra Atlas^{S2} CCD (**T3**, **T5**). Data reduction was performed with the CrysAlisPro^[4] software package. Using the software Olex2^[5] the structure solution was carried out using the program ShelXT^[6] (Sheldrick, 2015) (**T1**, **T2**, **T3**, **T4**, **T5**). Least squares refinements on F_o² were performed using SHELXL-2014 (Version 2016/6) (**T1**, **T2**, **T3**, **T4**, **T5**).^[7]

In the structure solution of [(L³Cu)₂(As₄S₃)] (**T3**), several ISOR restraints were used for the calculation of disordered *i*Pr groups of the supporting ligand L³. The As₄S₃ ligand is disordered in both dinuclear bonding pockets (65:35 and 89:11). For the description of the sulfur atoms in the minor (11%) As₄S₃ component of (R)-**T3**, additional ISOR restraints were applied. The assignment of the remaining electron density (approx. 3 e·Å⁻³) to another As₄S₃ component did not result in better structural values and therefore was not included in the atomic model.

The single crystal X-ray diffraction experiment of **T5** was performed at 203 K, due to phase transitions at lower temperatures. Several ISOR restraints were applied for the modelling of savagely disordered THF molecules.

Crystallographic data and details of the diffraction experiments are given in Table S1 and Table S2.

Table S1. Crystallographic data and details of diffraction experiments for **T1**, **T2** and **T3**.

Compound	T1	T2	T3
Data set	FS118_abs	FS78_2_abs	FS127_abs
(Internal naming)			
Formula	C ₅₈ H ₈₂ Cu ₂ N ₄ Se ₂	C ₅₈ H ₈₂ Cu ₂ N ₄ P ₄ S ₃	C ₅₈ H ₈₂ As ₄ Cu ₂ N ₄ S ₃
$\rho_{calc.}/\text{g cm}^{-3}$	1.357	1.281	1.458
μ/mm^{-1}	2.764	3.089	4.459
Formula Weight	1120.27	1182.41	1358.21
Color	brownish green	clear yellow	clear dark red
Shape	block	block	block
Size/mm ³	0.12×0.09×0.07	0.57×0.21×0.16	0.28×0.23×0.23
<i>T</i> /K	123.0(2)	123	123.3(8)
Crystal System	monoclinic	triclinic	triclinic
Space Group	<i>P</i> 2 ₁ / <i>n</i>	<i>P</i> 1	<i>P</i> 1
<i>a</i> /Å	9.07280(10)	12.3168(3)	16.91640(10)
<i>b</i> /Å	14.2744(2)	16.3685(4)	17.09880(10)
<i>c</i> /Å	21.1898(2)	16.9091(5)	22.02770(10)
α°	90	104.138(2)	97.7850(10)
β°	92.2040(10)	93.023(2)	101.3520(10)
γ°	90	110.306(2)	90.1230(10)
<i>V</i> /Å ³	2742.23(6)	3064.66(15)	6186.57(6)
<i>Z</i>	2	2	4
<i>Z'</i>	0.5	1	2
Wavelength/Å	1.54184	1.54184	1.54184
Radiation type	CuK α	CuK α	CuK α
Θ_{min}°	3.735	3.442	3.547
Θ_{max}°	74.256	66.707	66.821
Measured Refl.	23846	30599	369364
Independent Refl.	5499	10714	21878
Reflections Used	5123	10072	21003
<i>R</i> _{int}	0.0499	0.0285	0.0386
Parameters	308	724	1595
Restraints	0	12	96
Largest Peak	0.654	0.720	3.141
Deepest Hole	-0.511	-0.718	-0.989
GooF	1.047	1.037	1.137
<i>wR</i> ₂ (all data)	0.0855	0.0856	0.1685
<i>wR</i> ₂	0.0833	0.0838	0.1678
<i>R</i> ₁ (all data)	0.0338	0.0336	0.0612
<i>R</i> ₁	0.0317	0.0316	0.0596

Table S2. Crystallographic data and details of diffraction experiments for **T4** and **T5**.

Compound	T4	T5
Data set	FS105_abs	FS160_abs
(Internal naming)		
Formula	C ₂₆ H ₃₂ N ₂ Ni	C ₂₉ H ₄₁ N ₂ NaO ₂
$\rho_{calc.}/\text{g cm}^{-3}$	1.280	1.094
μ/mm^{-1}	1.335	0.659
Formula Weight	431.24	472.63
Color	dark brown	colorless
Shape	block	block
Size/ mm^3	0.22×0.19×0.09	0.53×0.34×0.30
<i>T</i> /K	123	203.00(14)
Crystal System	monoclinic	monoclinic
Space Group	<i>P</i> 2 ₁ / <i>n</i>	<i>P</i> 2 ₁ / <i>c</i>
<i>a</i> /Å	8.1661(3)	13.5030(2)
<i>b</i> /Å	15.4659(6)	27.1859(3)
<i>c</i> /Å	18.1208(7)	16.4144(2)
$\alpha/^\circ$	90	90
$\beta/^\circ$	102.191(4)	107.6970(10)
$\gamma/^\circ$	90	90
<i>V</i> /Å ³	2236.98(15)	5740.43(13)
<i>Z</i>	4	8
<i>Z'</i>	1	2
Wavelength/Å	1.54184	1.54184
Radiation type	CuK α	CuK α
$\Theta_{min}/^\circ$	3.794	3.436
$\Theta_{max}/^\circ$	74.344	66.716
Measured Refl.	7610	83300
Independent Refl.	4285	10145
Reflections Used	3685	8838
<i>R</i> _{int}	0.0306	0.0343
Parameters	266	715
Restraints	0	126
Largest Peak	0.560	0.401
Deepest Hole	-0.326	-0.278
GooF	1.031	1.028
<i>wR</i> ₂ (all data)	0.1182	0.1602
<i>wR</i> ₂	0.1101	0.1537
<i>R</i> ₁ (all data)	0.0480	0.0598
<i>R</i> ₁	0.0408	0.0538

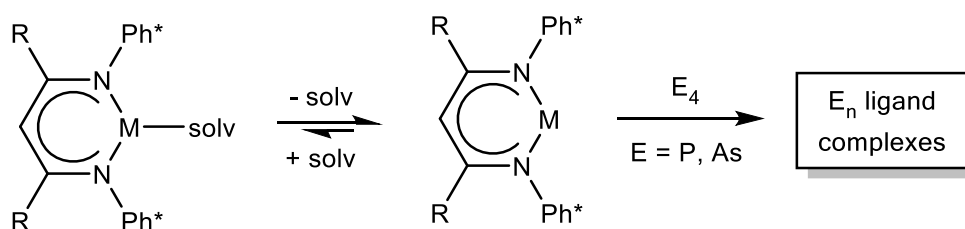
References

- [1] P. H. M. Budzelaar, R. de Gelder, A. W. Gal, *Organometallics* **1998**, *17*, 4121-4123.
- [2] D. J. E. Spencer, N. W. Aboeella, A. M. Reynolds, P. L. Holland, W. B. Tolman, *J. Am. Chem. Soc.* **2002**, *124*, 2108-2109.
- [3] E. Merino, E. Poli, U. Diaz, D. Brunel, *Dalton Trans.* **2012**, *41*, 10913-10918.
- [4] CrysAlisPro Software System, Agilent Technologies UK Ltd, Yarnton, Oxford, UK.
- [5] O.V. Dolomanov and L.J. Bourhis and R.J. Gildea and J.A.K. Howard and H. Puschmann, Olex2: A complete structure solution, refinement and analysis program, *J. Appl. Cryst.*, **2009**, *42*, 339-341.
- [6] Sheldrick, G.M., ShelXT, *Acta Cryst.*, **2014**, *A71*, 3-8.
- [7] Sheldrick, G.M., A short history of ShelX, *Acta Cryst.*, **2008**, *A64*, 339-341.

9. Conclusion

This work provides a detailed insight into the reactivity of late transition metal (Fe, Co, Cu) complexes towards white phosphorus (P_4) and yellow arsenic (As_4). Of particular interest is the application of differently substituted β -diiminato supporting ligands and their influence on the E_n ligand complex formation ($E = P, As$).

Therefore, a set of β -diiminato ligands L^0 – L^3 is herein introduced (depicted in Figure 1), exhibiting a systematic combination of backbone ($R = H$ or Me) and aromatic substituents ($Ph^* = 2,6$ -diisopropylphenyl (dipp), 2,6-dimethylphenyl (dmp)). The general synthetic procedure leading to E_n ligand complexes is illustrated in Scheme 1. The metal(I) precursors $[LM(solv)]$ ($L = L^0, L^1, L^2, L^3$; $M = Fe, Co, Cu$) are reacted with E_4 ($E = P, As$) in solution. Thereby, the weakly bound solvent ligand ($solv = MeCN$ or toluene) is readily substituted by E_4 under mild conditions, which allows the isolation of metastable E_n ligand complexes.



Scheme 1. General synthetic procedure: The dissociation of $[LM(solv)]$ ($L = L^0, L^1, L^2, L^3$; $M = Fe, Co, Cu$) in solution and the reaction with E_4 ($E = P, As$) leading to E_n ligand complexes.

The Systematic Approach

As a matter of principle, all herein presented reactions with white phosphorus or yellow arsenic, respectively, were conducted under basically comparable conditions. This includes conducting the reaction in the same solvent (toluene) and under ambient temperature and pressure. The reactions with P_4 were performed in a stoichiometric manner. However, for iron and cobalt (*vide infra*) the reaction outcome was found not to be influenced by the stoichiometry. The reaction time was 2–3 hours for phosphorus. It was limited to 15–60 minutes for the presented As_4 activations in order to prevent further degradation of the metastable products. Allover, three metal systems were part of the herein presented investigations: The late transition metals iron, cobalt and copper. Four different ancillary ligands L^0 – L^3 were applied, each providing different steric and electronic properties in the backbone substituents R and the aromatic flanking groups Ph^* (Figure 1).

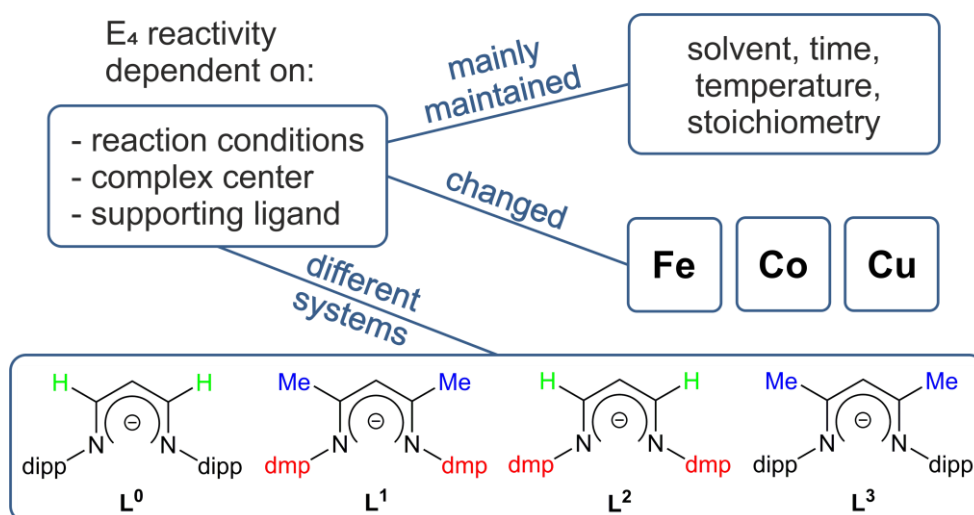


Figure 1. Dependencies in the reactions of $[LM(solv)]$ ($L = L^0, L^1, L^2, L^3$; $M = Fe, Co, Cu$) with E_4 ($E = P, As$). The herein applied supporting ligands (L^0 – L^3) are depicted. Aromatic Ph^* substituents: $dipp = 2,6$ -diisopropylphenyl, $dmp = 2,6$ -dimethylphenyl.

An overview of all prepared E_n ligand complexes is depicted in Scheme 2 (top: $E = P$; bottom: $E = As$). The complexes **A** and **B** were reported by Driess *et al.* during drafting of this thesis.^[1] Compounds **C5** and **C17** were part of preliminary investigations by C. Graßl in his PhD thesis.^[2] These four compounds represent valuable contributions for a comparative and complete overview, and therefore were integrated into Scheme 2. The complexes in dashed boxes were part of previous work of Scheer *et al.*^[2,3] They were re-investigated herein and significant contributions were provided for their complete characterization. The products in black boxes were prepared in the course of this work.

Parameters for the Description of the Coordination Geometry

Overall, the formation of mono-, di- or tetranuclear products was observed. It was recognized that the molecular structures of dinuclear compounds adopt a variety of different coordination geometries. Therefore, parameters were introduced for their description and detailed comparison. Most importantly the $M \cdots M'$ distance d , the angle Θ for the evaluation of the ligand coordination mode and the twist angle Φ of opposing β -diiminato ligands (Figure 2).

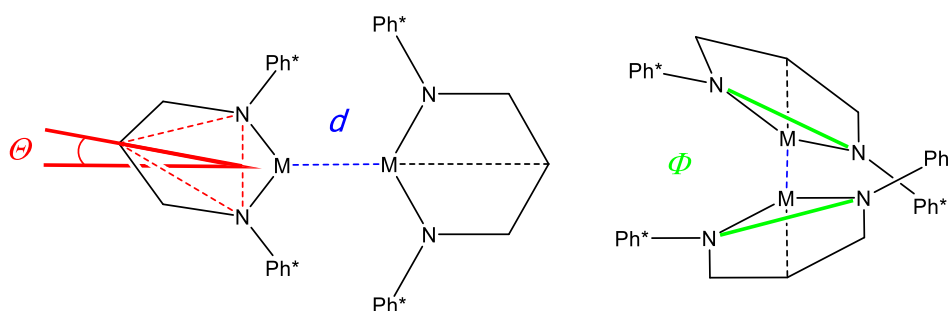
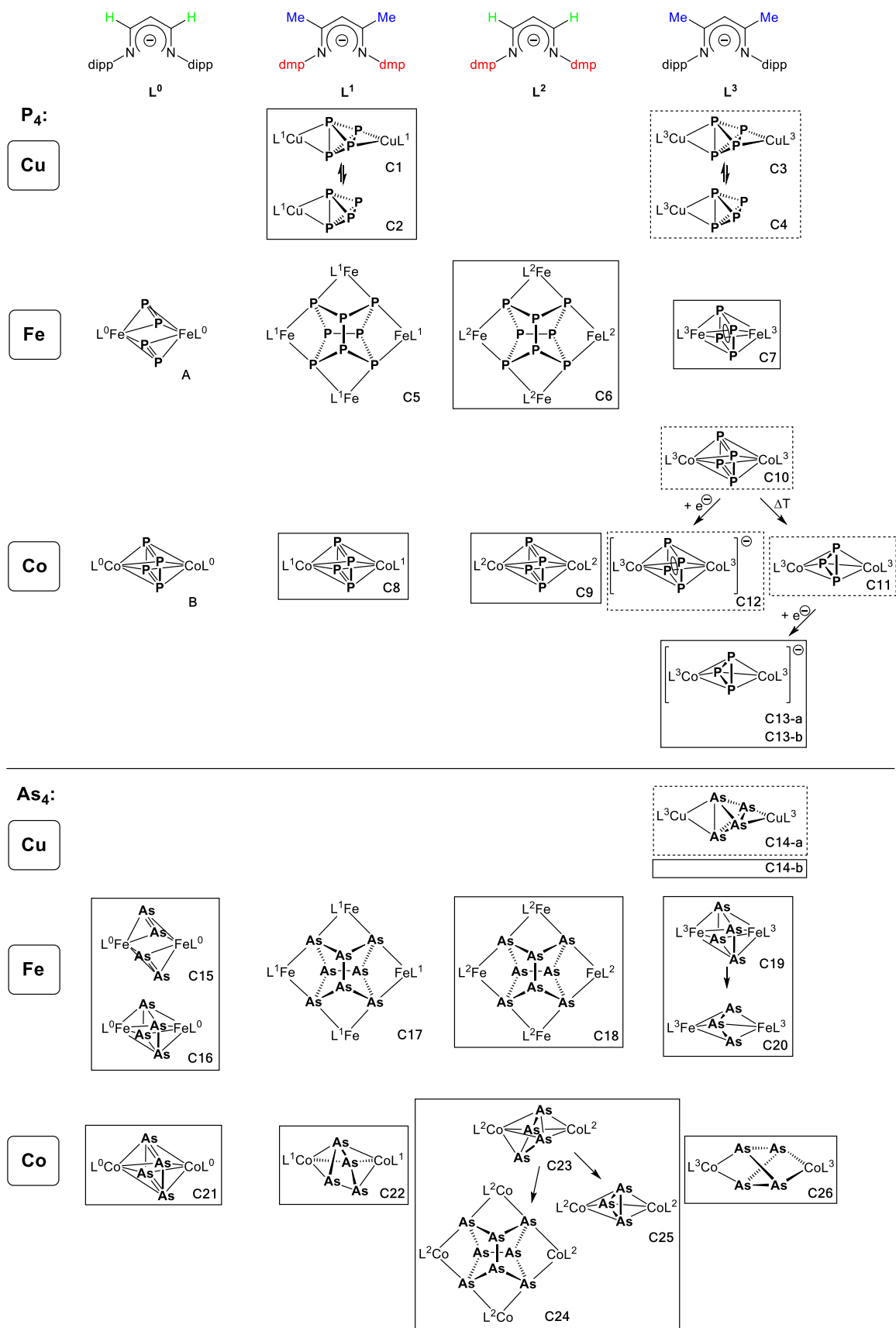
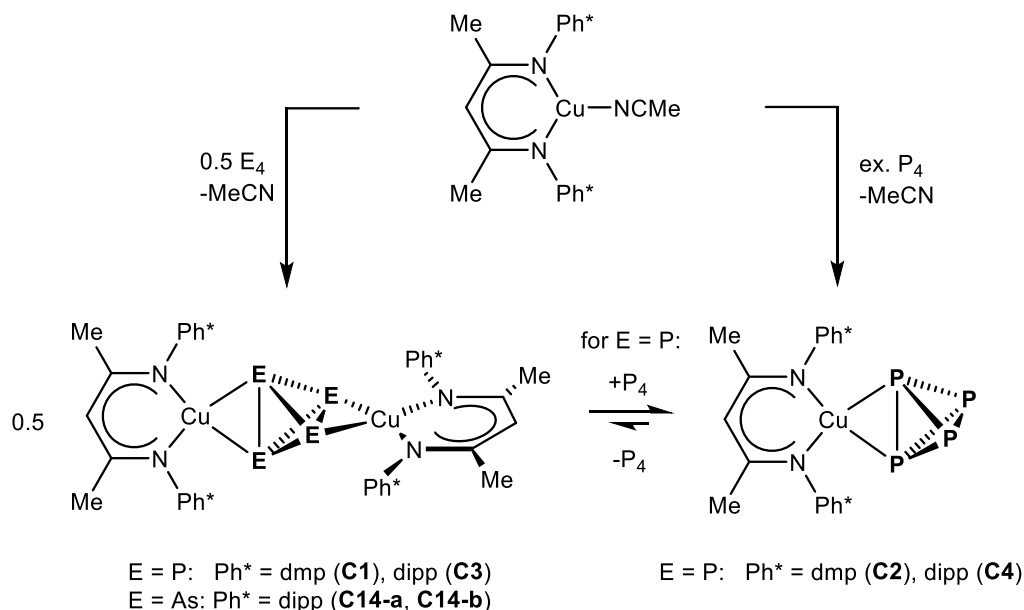


Figure 2. Parameters $d(M \cdots M)$, Θ and Φ for the description of the coordination geometry.



Coordination Chemistry of E₄ (E = P, As) in Copper(I) Complexes

The reaction of [L³Cu(NCMe)] with white phosphorus or yellow arsenic, respectively, leads to the dinuclear complexes [(L³Cu)₂(μ-η²:η²-E₄)] (E = P (**C3**), As (**C14-a**)). A mononuclear product [L³Cu(η²-P₄)] (**C4**) was synthesized by reaction of **C3** with additional equivalents of P₄ (Scheme 3). Preliminary studies on **C3**, **C14-a** and **C4** were already part of the author's master thesis.^[3] In this work, their characterization has been completed. An overview of performed reactions is given in Scheme 3.



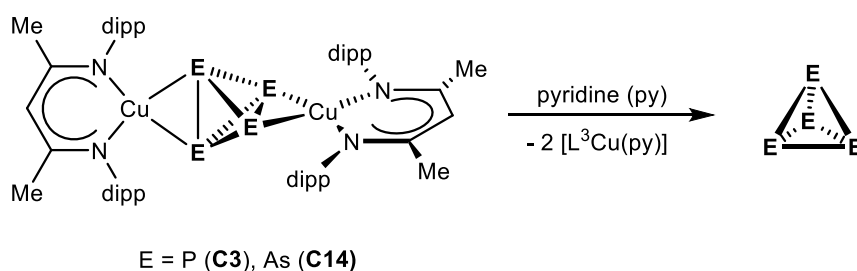
Scheme 3. Reactivity of different copper(I) precursors towards E₄ (E = P, As).

³¹P EXSY NMR spectroscopy at various temperatures was performed on solutions of **C3** with P₄ in excess. They provided an experimental proof for the equilibrium between the dinuclear complex **C3**, the mononuclear species **C4** and free P₄ at room temperature. This main dynamic dissociation process of **C3** and **C4** and the temporary release of free P₄ does not proceed at lower temperatures (below 243 K). For **C4**, it changes into a 'tumbling motion' with the P₄ ligand remaining chemically attached to the [L³Cu] fragment while undergoing changes in the coordination modes (η²→η¹→η²).

With these findings the isolation of the mononuclear complex **C4** was accomplished. An extensive low temperature work-up of **C4** was performed at 195 K in order to prevent its degradation towards **C3** (equilibrium shift) and enabling the crystallization of **C4**. The molecular structure of **C4** (as well as the ones of **C3** and **C14-a**)^[3] reveals bond elongation of the coordinating E–E edges (2.386(4) Å in **2**, 2.4122(8)/2.4285(8) Å in **C3**, 2.6491(8) Å in **C14-a**) in comparison with free white phosphorus and yellow arsenic. Raman spectra of **C3**, **C4** and **C14-a** display modes for the E₄ ligand comparable to the ones of free white

phosphorus or yellow arsenic, respectively. They support the integrity of the coordinated E_4 ligands.

DFT calculations suggest that the coordinating edges of the E_4 ligands in **C3**, **C4** and **C14** should be considered as elongated, but being intact. As an experimental proof the E_4 ($E = P,^{[3]}As$) ligands could be released from complex **C3** and **C14** by substitution with the stronger Lewis base pyridine (Scheme 4).



Scheme 4. Release of E_4 ($E = P,^{[3]}As$) from **C3** or **C14**, respectively, by substitution with pyridine.

A new solvomorph crystal structure **C14-b** was obtained by crystallization of $[(L^3Cu)_2(\mu-\eta^2:\eta^2-As_4)]$ from saturated *n*-hexane solutions. Interestingly, the structures differ in the number of co-crystallizing *n*-hexane molecules. The comparison of **C14-a** with **C14-b** shows no significant differences in the bonding parameters of their molecular structures.

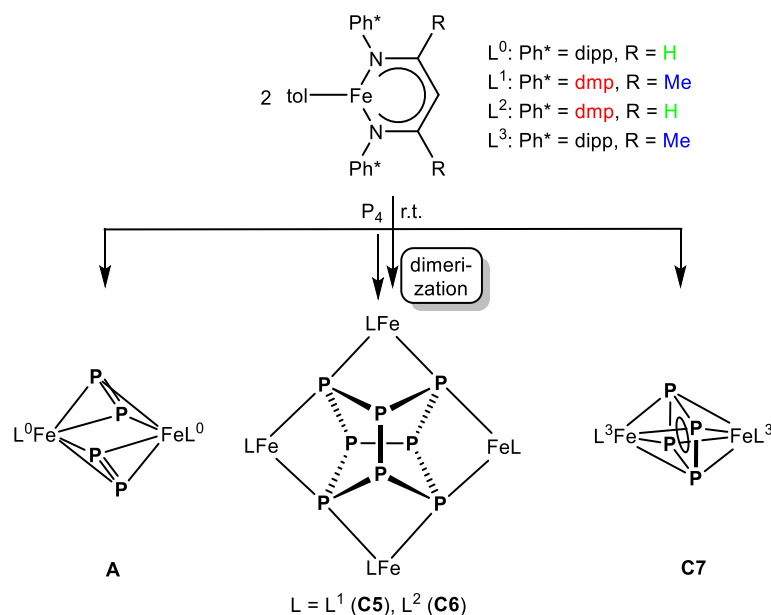
The variation of Ph^* substituents (dipp vs. dmp) was tested by introducing the ligand L^1 (with a dmp substituent) in the reaction of $[L^1Cu(NCMe)]$ with P_4 . No change in the reactivity was found in solution (Scheme 3). The dinuclear compound $[(L^1Cu)_2(\mu-\eta^2:\eta^2-P_4)]$ (**C1**) was formed and was found to be in equilibrium with the mononuclear complex $[L^1Cu(\eta^2-P_4)]$ (**C2**). The $^{31}P\{^1H\}$ NMR spectra of both compounds at various temperatures reveal analogous temperature-dependent fluxional behavior like **C3** and **C4**. However, in the solid state the different steric requirements of the ligands L^1 and L^3 affect the crystal packing and a different coordination geometry of $[(LCu)_2(\mu-\eta^2:\eta^2-P_4)]$ ($L = L^3$ (**C3**) vs. L^1 (**C1**)) was observed. The twisted orientation of one $[L^1Cu]$ fragment in **C1** results in an elongated P–P bond distance of the coordinating P_4 ligand edges (2.3651(7) and 2.4567(8) Å). This comparison emphasizes the influence of the crystal packing on bonding parameters of the P_4 ligand in the crystal.

In summary, the fixation of E_4 units between two $[LCu]$ ($L = L^1, L^3$) fragments does not lead to an oxidative addition of the E–E edges towards the copper centers. Moreover, these complexes represent the initial side-on coordination step of an E_4 tetrahedron towards a metal center with considerably elongated, but still intact E–E bonds.

Besides **C1** and **C2**, complexes **C3**, **C4** and **C14** represent the first neutral molecules with intact E_4 tetrahedra in a side-on coordination mode. More importantly, complex **C14** is the first reported As_n ligand complex with β -diiminato supporting ligands.

Transformation and Aggregation of P_4 by $[LFe(tol)]$ ($L = L^1, L^2, L^3$)

The question arose if more electron deficient metal centers would alter the P_n ligand formation. Therefore, reactions of P_4 with different iron(I) precursors $[LFe(tol)]$ ($L = L^1, L^2, L^3$) were performed (Scheme 5).



Scheme 5. Reactivity of different iron(I) precursors towards P_4 .

These reactions were conducted under identical reaction conditions: in toluene at room temperature with a reaction time of 16–20 hours. The reaction outcome was found not to be influenced by a shorter reaction time (2–3 hours) as well as by a different stoichiometry. However, it is sensitive to minor substituent changes of the ancillary ligand: Driess *et al.* reported the iron(III) complex $[(L^0\text{Fe})_2(\mu-\eta^2:\eta^2-P_2)_2]$ (**A**), which contains $[P_2]^{2-}$ ligands and which is realized in the presence of L^0 ligands.^[1a] With sterically less bulky ligands L^1 or L^2 , exclusively tetranuclear complexes $[(L\text{Fe})_4(\mu_4-\eta^1:\eta^1:\eta^1:\eta^1:\eta^1:\eta^1:\eta^1-P_8)]$ ($L = L^1$ (**C5**),^[2] L^2 (**C6**)) were obtained, each containing a realgar-type $[P_8]^{4-}$ moiety. The ancillary ligand L^3 containing the bulky dipp substituents and CH_3 groups in the ligand backbone directed the formation of the dinuclear complex $[(L^3\text{Fe})_2(\mu-\eta^4:\eta^4-P_4)]$ (**C7**), which contains a *cyclo*- $[P_4]^{2-}$ ligand. This emphasizes the influence of the aromatic flanking groups in the P_n ligand formation: For sterically more demanding dipp substituents, dinuclear products **A** and **C7** were observed. For less demanding dmp groups a dimerization to the tetranuclear complexes **C5** and **C6** with $[P_8]^{4-}$ motifs was observed.

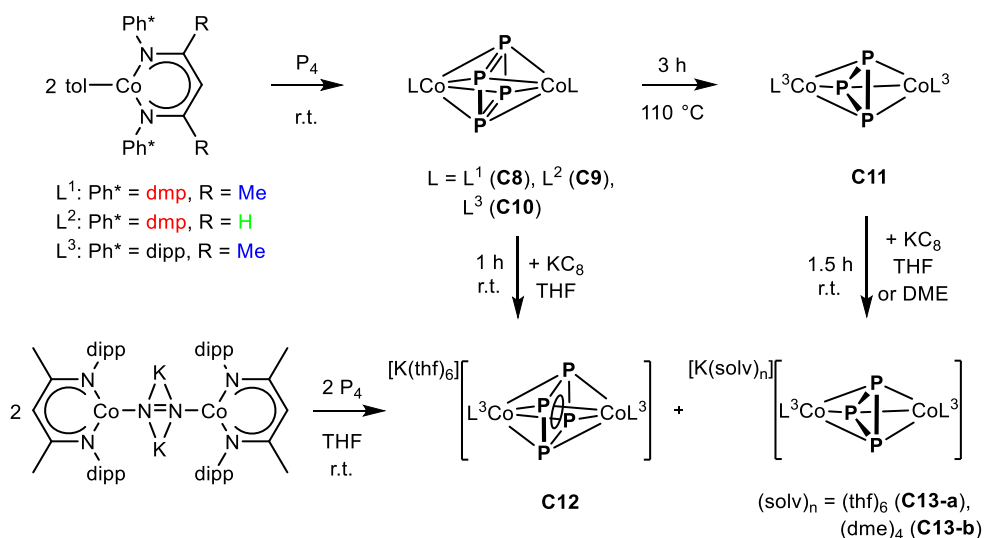
All compounds **C5**, **C6** and **C7** are paramagnetic, however, a complete assignment of the signals in the ^1H NMR spectra could be made. This enabled the evaluation of the selectivity of the reactions. Their magnetic moment was determined in solution by the Evans method and in the solid state by SQUID magnetization measurements. The iron(II) oxidation state of **C6** and **C7** was elucidated by Mössbauer spectroscopy and DFT calculations. Furthermore, the latter show that the dimerization of two hypothetical dinuclear $[(\text{L}^1\text{Fe})_2\text{P}_4]$ complexes into a tetranuclear complex $[(\text{L}^1\text{Fe})_4\text{P}_8]$ (**C5**) is exothermic. This dimerization reaction is experimentally observed for the L^1 and L^2 systems, which contain dmp flanking groups.

For the sterically more encumbered dipp containing ligands L^0 and L^3 this dimerization is not observed, probably due to the steric repulsion of the bulky dipp substituents. The reaction results in dinuclear complexes **C7** and **A**, which contain a *cyclo*- $[\text{P}_4]^{2-}$ or a pair of $[\text{P}_2]^{2-}$ ligand(s). Their molecular structures were compared and a significantly different $\text{Fe}\cdots\text{Fe}'$ distance (3.902 Å in **C7** vs. 2.777 Å in **A**) was found, as well as a differently *trans*-bent orientation ($\Theta = 15^\circ$ in **C7** vs. 33° in **A**) of the ligand backbone planes. DFT calculations on $[(\text{L}^3\text{Fe})_2(\mu\text{-}\eta^4\text{:}\eta^4\text{-P}_4)]$ (**C7**) with a restricted $\text{Fe}\cdots\text{Fe}'$ distance of 2.777 Å leads to the splitting of the *cyclo*- $[\text{P}_4]^{2-}$ unit into two $[\text{P}_2]^{2-}$ ligands in the optimized geometry. This confirms the direct dependency of the resulting P_n ligand nature on the $\text{Fe}\cdots\text{Fe}'$ distance and the accompanied *trans*-bent coordination mode of the L^3 supporting ligand. The energy difference between both $[\text{P}_4]^{2-}$ and $[\text{P}_2]^{2-}$ containing isomers was found to be low (29.19 $\text{kJ}\cdot\text{mol}^{-1}$).

In summary, these results represent unprecedented, comparative investigations of the β -diiminato ligand design in iron(I) mediated P_4 activations. By using sterically different aromatic flanking groups (dmp vs. dipp), the P_n ligand formation was significantly influenced ($[\text{P}_8]^{4-}$ vs. $[\text{P}_4]^{2-}$ vs. $[\text{P}_2]^{2-}$). In dinuclear complexes, the nature of the $[\text{Fe}_2\text{P}_n]$ core is sensitively dependent on the *trans*-bent orientation of the supporting ligands and the $\text{Fe}\cdots\text{Fe}'$ distance.

Transformation and Degradation of P_4 by $[\text{LCo}(\text{tol})]$ ($\text{L} = \text{L}^1, \text{L}^2, \text{L}^3$) and $[\text{K}_2(\text{L}^3\text{Co})_2(\mu\text{-}\eta^1\text{:}\eta^1\text{-N}_2)]$ Precursors

We were intrigued if the cobalt(I) reactions with P_4 can be influenced by the β -diiminato ligand substituents in an analogous way as observed for the iron case. In addition, a comparative reaction with an electron richer cobalt(0) precursor would be interesting. On the one side, due to the nature of the formed complexes, on the other side, to gain insight into the redox chemistry of P_n ligand complexes, since for cobalt a more pronounced redox behavior is expected.



Scheme 6. Reactivity of cobalt(I) (top) and cobalt(0) (bottom) complexes towards P₄.

Therefore, white phosphorus was reacted with various [LCo(tol)] (L = L¹, L², L³) precursors (Scheme 6, top). In order to allow a strict comparison, all reactions have been performed under the same conditions: in toluene at room temperature and with a reaction time of 2–3 hours. The isostructural dinuclear compounds [(LCo)₂(μ-η⁴:η⁴-P₄)] (L = L¹ (**C8**), L² (**C9**), L³ (**C10**)) were obtained, each containing a *cyclo*-[P₄]⁰ ligand in their molecular structures in the solid state. Therefore, the L¹–L³ ligands did not influence the reaction outcome, which was different in comparison with the iron reactions (vide supra). For the L³ containing **C10**, the thermolytically induced P atom extrusion was observed under formation of [(L³Co)₂(μ-η³:η³-P₃)] (**C11**), which contains a *cyclo*-[P₃]³⁻ ligand. By one-electron reduction of **C10** or **C11**, respectively, the corresponding monoanionic complexes [K(thf)₆][(L³Co)₂(μ-η⁴:η⁴-P₄)] (**C12**) and [K(solv)_n][(L³Co)₂(μ-η³:η³-P₃)] (**C13**) were selectively and quantitatively obtained (Scheme 6). The *cyclo*-[P₄]²⁻ unit in **C12** is the result of a two electron reduction of the *cyclo*-[P₄]⁰ unit of the **C10** precursor. The reduction of **C11** towards **C13** proceeds under retention of the *cyclo*-[P₃]³⁻ ligand, since no considerable change in the structural parameters of the *cyclo*-[P₃]³⁻ unit in **C11** and **C13** was observed. The electronic structures of the *cyclo*-[P₄]²⁻ and *cyclo*-[P₃]³⁻ ligands in **C11**, **C12** and **C13** were elucidated by SQUID magnetization measurements.

The corresponding redoxchemical behavior of **C10**, **C11**, **C12** and **C13** was monitored by cyclic voltammetry measurements. All complexes show very similar behavior.

All compounds **C8–C13** are paramagnetic in solution. Nevertheless, all signals in the ¹H NMR spectra could be assigned. Their magnetic moment in solution was determined by the Evans method.

The monoanionic **C13** was obtained in two solvomorph crystal structures differing in the incorporated solvate; THF (**C13-a**) or DME (**C13-b**). The orientation of the L^3 supporting ligands differs significantly in both cases ($\Phi = 74^\circ$ vs. 2°), which highlights the influence of the counterion shape and the co-crystallizing solvates on the molecular geometry.

As a novel approach, the reaction of P_4 with the formally cobalt(0) precursor $[K_2(L^3Co)_2(\mu-\eta^1:\eta^1-N_2)]$ was investigated. It yields a reaction mixture of **C12** and **C13**, hence lacking in selectivity (Scheme 6). Therefore, the previously mentioned, relective one-electron reduction of **C10** or **C11** was found to be the more suitable approach for the synthesis of **C12** or **C13**, respectively.

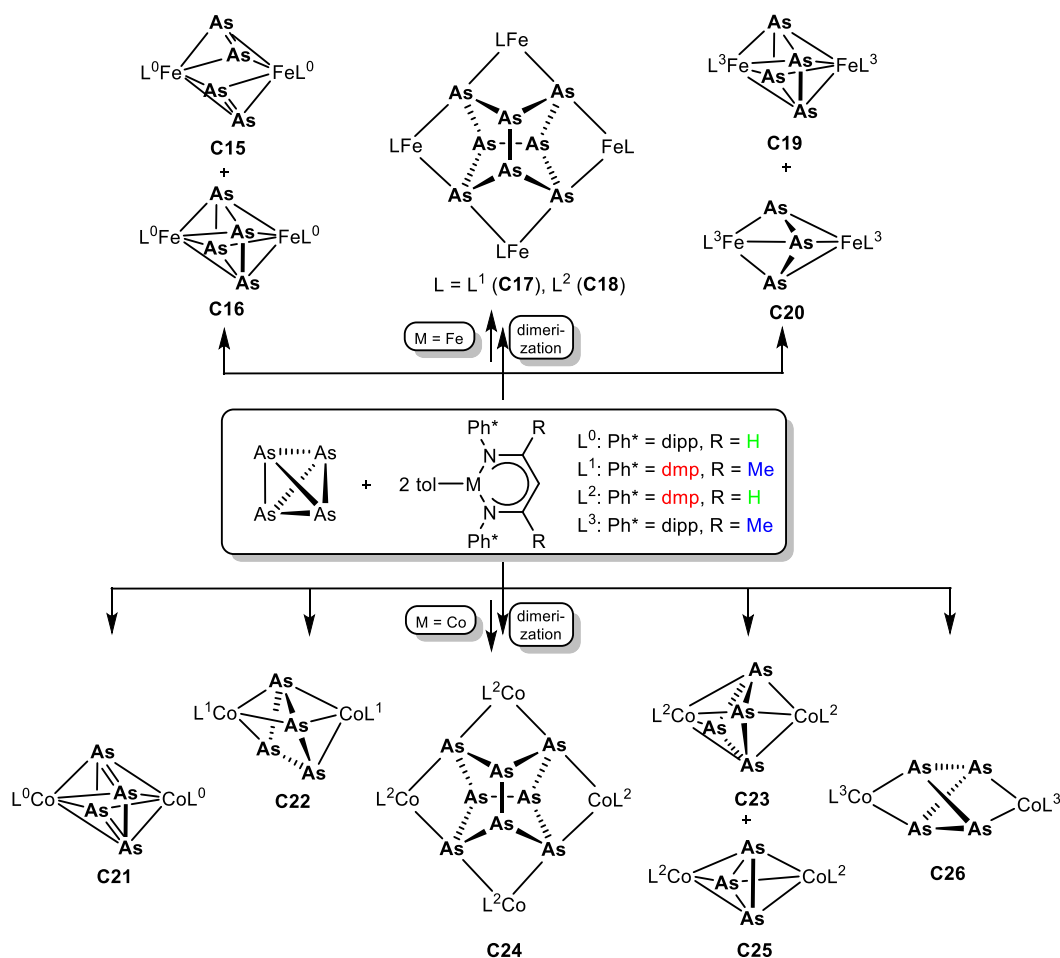
In conclusion, the results show that the reactions of $[LCo(tol)]$ ($L = L^1, L^2, L^3$) with P_4 yield only dinuclear products $[(LCo)_2(\mu-\eta^4:\eta^4-P_4)]$. This stands in contrast to the reactions of the iron derivatives (vide supra), which lead to di- or tetranuclear products under analogous conditions. The unprecedented extrusion of one phosphorus atom from the $cyclo-[P_4]^0$ unit into a $cyclo-[P_3]^{3-}$ ligand was observed by thermolytic treatment. This behavior was not observed in the case of the iron derivative. It was demonstrated that the molecular geometry of the monoanionic $[(L^3Co)_2(\mu-\eta^3:\eta^3-P_3)]^-$ (**C13**) can be affected by co-crystallizing solvates as well as the shape of its counter ion. Two synthetic procedures for the synthesis of monoanionic $[(L^3Co)_2(\mu-\eta^n:\eta^n-P_n)]^-$ ($n = 4$ (**C12**), 3 (**C13**)) were presented, which differ in their selectivity.

Snapshots of As_4 Transformation, Aggregation and Degradation Induced by $[LM(tol)]$ ($L = L^0, L^1, L^2, L^3$; $M = Fe, Co$) Precursors

In an earlier chapter, the synthesis and characterization of $[(L^3Cu)_2(\mu-\eta^2:\eta^2-As_4)]$ (**C14**) was presented, the first reported As_n ligand complex with β -diiminato supporting ligands. Complex **C14** contains an intact As_4 tetrahedron with considerably elongated As–As edges. More electron deficient metal systems were speculated to cleave these bonds and to induce the transformation of the As_4 ligand. We were intrigued if different β -diiminato ligand substituents in L^0, L^1, L^2 and L^3 would play a decisive role in the reactions of iron(I) and cobalt(I) precursors towards As_4 .

Yellow arsenic is a not storable compound and it needs to be freshly generated by an elaborated and complicated procedure prior to use. To avoid oxidation or hydrolysis of the sensitive $[LM(sol)]$ ($L = L^0, L^1, L^2, L^3$; $M = Fe, Co$) precursors, a purification process was introduced. It involves the precipitation of As_4 from a freshly prepared toluene solution in order to remove undesired impurities. However, this procedure prevented a stoichiometric reaction with the metal(I) sources and the reactions were performed with excess of As_4 .

All presented reactions were conducted in toluene and the reaction time was limited to 15 minutes in most cases. An overview of the obtained As_n ligand complexes is given in Scheme 7.



Scheme 7. Reactivity of different iron(I) and cobalt(I) precursors towards As_4 .

Various dinuclear complexes $[(LM)_2As_4]$ ($LM = L^0Fe$ (**C16**), L^3Fe (**C19**), L^0Co (**C21**), L^1Co (**C22**), L^2Co (**C23**), L^3Co (**C26**)) were isolated. Each product stabilizes an individually shaped As_4 ligand in the solid state and reveals a distinct coordination mode. Furthermore, tetranuclear complexes $[(LM)_4(\mu_4-\eta^1:\eta^1:\eta^1:\eta^1-As_8)]$ ($LM = L^1Fe$ (**C17**), L^2Fe (**C18**), L^2Co (**C24**)) were obtained, which possess realgar-type As_8 cores. Two products $[(LM)_2(\mu-\eta^3:\eta^3-As_3)]$ ($LM = L^3Fe$ (**C20**), L^2Co (**C25**)) with *catena-As₃* or *cyclo-As₃* units were found as well as one complex $[(L^0Fe)_2(\mu-\eta^2:\eta^2-As_2)_2]$ (**C15**) with two As_2 ligands. The products **C15/C16**, **C19/C20** and **C23/C25** were exclusively obtained as solid solutions, which prevents the purification of one selected product by crystallization. The selectivity of the performed reactions was evaluated by LIFDI mass spectrometry and by 1H NMR spectroscopy. The product ratio found in the crystalline solid solutions **C19/C20** and **C23/C25** corresponds to that found by 1H NMR spectroscopy. This again shows that

the signal assignment of paramagnetic compounds in ^1H NMR spectra can be used as a powerful tool in this kind of chemistry.

A rational explanation for the diverse reactivity was suggested: The first traceable reaction step is the formation of dinuclear compounds $[(\text{LM})_2\text{As}_4]$. The subsequent reaction is dependent on the applied ligand substituents. While the sterically less demanding dmp groups (in L^1 , L^2) enable the dimerization of two dinuclear intermediates $[(\text{LM})_2\text{As}_4]$ towards the tetranuclear products $[(\text{LM})_4\text{As}_8]$, the sterically more encumbered dipp substituents (in L^0 , L^3) do not allow the latter reaction pathway.

The coordination modes of the As_4 ligands in the molecular structures of the dinuclear $[(\text{LM})_2\text{As}_4]$ complexes was observed to be manifold (e.g. $\mu\text{-}\eta^1\text{:}\eta^1\text{:}\eta^1\text{:}\eta^1\text{-As}_4$ in **C26**, $\mu\text{-}\eta^3\text{:}\eta^3\text{-As}_4$ in **C22**, $\mu\text{-}\eta^3\text{:}\eta^4\text{-As}_4$ in **C23**, $\mu\text{-}\eta^4\text{:}\eta^4\text{-As}_4$ in **C16,19,21** and $\mu\text{-}\eta^2\text{:}\eta^2\text{-As}_2$ in **C15**). Therefore, the nature of the $[\text{Co}_2\text{As}_4]$ core structure was investigated by DFT calculations. An energy surface scan along the $\text{Co}\cdots\text{Co}'$ distance of the hypothetical $[(L^0\text{Co})_2(\text{As}_2)_2]$ reveals various core geometries, especially in the remarkable flat region from 3.6 Å to 4.6 Å. The found direct correlation of the $[\text{Co}_2\text{As}_4]$ core geometry and the $\text{Co}\cdots\text{Co}'$ distance is experimentally supported by the molecular structures of **C21**, **C22**, **C23** and **C26**. These complexes show increasing $\text{Co}\cdots\text{Co}'$ separation (respective order: 3.587 Å, 3.750 Å, 3.944/3.966 Å and 4.615 Å), different $L^0\text{--}L^3$ ligands and different geometries of the central As_4 unit. Furthermore, the molecular structures of **C15** and **C16** contain the same ligand L^0 , but crystallize with different $\text{Fe}\cdots\text{Fe}'$ distances (2.940(5) Å in **C15** vs. 3.787 Å in **C16**). As a direct result two structurally changed As_n ligand motifs were observed (As_2 in **C15** vs. As_4 in **C16**).

Each molecular structure of all the dinuclear products can be understood as a reaction step of the successive transformation of an intact As_4 tetrahedron into differently bound As_n ligands. The molecular structure of **C23** can be understood as a preorientation for the hypothetical, subsequent dimerization (aggregation) towards the As_8 ligand containing **C24**. It also could be understood as a preorientation for an As atom abstraction process (degradation) towards complex **C25**, which contains a As_3 ligand.

In conclusion, the compounds **C15–C26** are the first examples for As_n ligand complexes with iron or cobalt β -diiminato fragments. They contain rare and unprecedented As_n structural motifs. Irrespective of their interpretation, all obtained molecular structures with their individual structural parameters give insight into the transformation, degradation or aggregation reaction of yellow arsenic in the coordination sphere of iron and cobalt complexes. Therefore, they are snapshots on the molecular level.

References

- [1] a) S. Yao, T. Szilvasi, N. Lindenmaier, Y. Xiong, S. Inoue, M. Adelhardt, J. Sutter, K. Meyer, M. Driess, *Chem. Commun.*, **2015**, 51, 6153-6156; b) S. Yao, N. Lindenmaier, Y. Xiong, S. Inoue, T. Szilvási, M. Adelhardt, J. Sutter, K. Meyer, M. Driess, *Angew. Chem.* **2015**, 127, 1266-1270.
- [2] C. Graßl, *Dissertation, Universität Regensburg* **2013**.
- [3] F. Spitzer, *Master Thesis, Universität Regensburg* **2013**.

10. Appendix

10.1 Thematic List of Abbreviations

NMR Spectroscopy

NMR	Nuclear Magnetic Resonance
δ	chemical shift
ppm	part per million
Hz	Herz, s ⁻¹
<i>J</i>	coupling constant, Hz
s	singlet
d	doublet
t	triplet
sept	septet
<i>I</i>	nucleus spin
$\omega_{1/2}$	half width, Hz
VT	variable-temperature
EXSY	exchange spectroscopy
τ_m	mixing time
HSQC	heteronuclear single quantum correlation
HMBC	heteronuclear multiple-bond correlation spectroscopy

Cyclic Voltammetry

CV	Cyclic Voltammetry
$E_{1/2}$	half potential, V
i_{pf}	peak forward current, μA
i_{pr}	peak reverse current, μA
E_{pc}	peak cathodic potential, V
E_{pa}	peak anodic potential, V

Solvents

THF	tetrahydrofuran, C ₄ H ₈ O
Tol	toluene, C ₇ H ₈
NCMe	acetonitrile, CH ₃ CN
DME	1,2-dimethoxyethane, C ₄ H ₁₀ O ₂
Et ₂ O	diethylether, C ₄ H ₁₀ O
CH ₂ Cl ₂	dichloromethane

Mass Spectrometry

MS	Mass Spectrometry
[M] ⁺	molecular ion peak
<i>m/z</i>	mass to charge ratio
LIFDI	liquid injection field desorption ionization
ESI	electron spray ionization

SQUID and Evans Method

μ_{eff}	effective magnetic moment
μ_B	Bohr magneton
χ^P	molar paramagnetic susceptibility
χ^D	molar diamagnetic susceptibility
χ^M	molar measured magnetic susceptibility
Δf	chemical shift difference, Hz
<i>f</i>	operating frequency of NMR spectrometer in Hz

Mössbauer Spectroscopy

δ	isomer shift, mm·s ⁻¹
ΔE_Q	quadrupole splitting, mm·s ⁻¹

Raman Spectroscopy

$\tilde{\nu}$	wavenumber, cm ⁻¹
λ_{exc}	excitation wavelength, nm

Other

Å	Angstroem, 1 Å = 1·10 ⁻¹⁰ m
<i>T</i>	temperature, K or °C
<i>c</i>	concentration, mol · L ⁻¹
<i>M</i>	metal, specified in text
<i>d</i>	distance, Å
α	Angle, °
r.t.	room temperature
E	group 15 element

Ligands

nacnac	β -diketiminato, substituents specified in text
Ph*	aromatic substituent, specified in text
dipp	2,6-diisopropylphenyl
dmp	2,6-dimethylphenyl
R	organic substituent, specified in text
Me	Methyl, CH ₃
<i>t</i> Bu	<i>tert</i> -Butyl, -C ₄ H ₉
DAD	α -dialdimine, diazadiene
COD	1,5-cyclooctadiene
Cp	cyclopentadienyl, η^5 -C ₅ H ₅
Cp*	η^5 -C ₅ Me ₅
Cp ^{4Pr}	η^5 -C ₅ <i>i</i> Pr ₄ H
Cp ^{'''}	1,2,4-tris- <i>tert</i> -butylcyclopentadienyl, η^5 -C ₅ H ₂ <i>t</i> Bu ₃
Cp ^{Me}	η^5 -C ₅ H ₄ Me
Cp ^{BIG}	pentakis-4- <i>n</i> butylphenylcyclopentadienyl, η^5 -C ₅ (4- <i>n</i> BuC ₆ H ₄) ₅
triphos	1,1,1-tris(diphenylphosphinomethyl)ethane)
etriphos	(1,1,1-tris(diethylphosphinomethyl)ethane
dppe	1,2-bis(diphenylphosphino)ethane, Ph ₂ PCH ₂ CH ₂ PPh ₂
dppm	bis(diphenylphosphino)ethane)
np ₃	tris(2-diphenylphosphinoethyl)amine

10.2 Acknowledgements

Finally, I want to thank...

- Prof. Dr. Manfred Scheer for providing the interesting research topic and the supervision, for enabling visits to international conferences and my research stay in Canada. Additionally, for providing extraordinary and excellent working conditions and the freedom to pursue my own ideas in the lab.
- Dr. Gábor Balázs for all the encouraging discussions on chemistry and helpful, professional advice. Thanks for proofreading and the almost countless DFT calculations on the 'beloved' paramagnetic compounds!
- Dr. Michael Bodensteiner for the valuable advice in X-ray structure refinement, especially with the disordered central cores of the dinuclear E_n ligand complexes.
- Dr. Christian Marquardt and Dr. Eva-Maria Rummel for proofreading.
- Prof. Dr. Michael Fryzuk for giving me the opportunity to join this team in course of a research stay in Vancouver at UBC. Thanks to all group members for making it a pleasant stay.
- Prof. Dr. Karsten Meyer for the SQUID and Mössbauer experiments.
- Prof. Dr. Ruth Gschwind for the $^{75}\text{As}\{^1\text{H}\}$ NMR measurements.
- my former lab supervisors Dr. Sebastian Heinl, Dr. Christoph Schwarzmaier, Dr. Markus Stubenhofer and Dr. Christian Graßl for their encouragements.
- my present lab colleagues Moritz Modl, Julian Müller and Maria Haimerl for having debates on basic principles of preparative processes, e.g. filtrations(!).
- the staff of the Central Analytical Services of the University of Regensburg: X-ray, MS, EA and NMR department. Especially, Wolfgang Söllner for LIFDI-MS measurements. With special emphasis on Anette Schramm and Georgine Stühler for the countless ^1H NMR measurements.
- the staff of the glass blowing, electronics and mechanics facilities of the University of Regensburg for their valuable work.
- all present and former members of the Scheer group for the pleasant working atmosphere and an unforgettable time: Andi, Andrea, Barbara B., Barbara K., Barbara T., Bianca, Claudi, Claudia, Dani, David, Eric, Eva, Felix, Gábor, Helena, Hias, Jana, Jens, Julian, Kathl, Karin, Küken, Lena, Liese, Luigi, Luis, Maria, Martin P., Martina, Matthias H., Matthias L., Mehdi, Mia, Michi, Moartl, Mo, Moni, Musch, Muschine, Nase, Olli, Petra, Rebecca, Reini, Robert, Rudi, Schotti, Stubi, Susanne, Sµ, Thoms, Tobi, Vroni, Walter, Wast, Wurzl.
- Andi, Claudi, Eva, Moni and Sebi for having a good time (at work and in private) and having drinks after work.
- especially my family for their enduring support.
- above all Susi for her enduring support and patience. **I love you!** This work is dedicated to you.